

Electromagnetic Scattering and Induction Models for Spheroidal Geometries

by

Benjamin Earl Barrowes

B.S., Brigham Young University, Provo (1999)

M.S., Brigham Young University, Provo (1999)

Submitted to the Department of Electrical Engineering and Computer Science
in partial fulfillment of the requirements for the degree of

Doctor of Philosophy

at the

MASSACHUSETTS INSTITUTE OF TECHNOLOGY

January 2004

© Massachusetts Institute of Technology 2004. All rights reserved.

Author
Department of Electrical Engineering and Computer Science
January 22, 2004

Certified by
Jin Au Kong
Professor of Electrical Engineering and Computer Science
Thesis Supervisor

Accepted by
Arthur C. Smith
Chairman, Committee on Graduate Students
Department of Electrical Engineering and Computer Science

Electromagnetic Scattering and Induction Models for Spheroidal Geometries

by

Benjamin Earl Barrowes

Submitted to the Department of Electrical Engineering and Computer Science
on January 22, 2004, in partial fulfillment of the
requirements for the degree of
Doctor of Philosophy

Abstract

Electromagnetic scattering from a medium containing randomly distributed discrete dielectric spheroidal inclusions is studied. Also, the broadband magnetoquasistatic solution for the induced magnetic field from a conducting and permeable spheroid under time harmonic excitation is demonstrated. Analytical electromagnetic solutions for spheroidal geometries are desirable because of their versatility in modeling manmade and natural shapes including solid and hollow needles, spheres, and disks, while at the same time possessing analytic solutions.

Coherent scattering from a collection of small dielectric spheroids populating a dense medium is compared to scattering from a homogeneous sphere. A Method of Moments (MoM) solution is adopted which accounts for spheroid-spheroid interactions directly. Coherent scattering results from these collections are compared to Mie scattering and the effective permittivity of the dense medium is obtained. Results are in good agreement to the classical mixing formula and this lends credibility to both models.

In order to reduce memory requirements and computational complexity, the Sparse Matrix/Canonical Grid (SMCG) method is applied to 3-D dense media scattering. By approximating the dyadic Green's function about a canonical rectilinear grid, weak interaction between spheroid far apart may be quickly approximated. Strong interactions between dielectric spheroid in close proximity are still calculated directly. Weak interactions are quickly evaluated using a novel multilevel block-Toeplitz matrix vector multiply based on the Fast Fourier Transform.

Electromagnetic induction (EMI) models of conducting and permeable spheroids under time harmonic excitation are refined to produce the broadband response with high dependability. A hybrid method is constructed consisting of three different approaches: 1) at low frequencies, the formally exact (but truncated) solution is applied, 2) at moderate frequencies, asymptotic expansions of the spheroidal wave functions (SWFs) are employed, 3) and at high, but still magnetoquasistatic, frequencies, a Small Penetration Approximation is borrowed. The combined EMI response is accurate except near a switchover point where there is typically less than a two percent error. Results are compared to data from a set of 17 steel and aluminum machined spheroids taken by the GEM-3 instrument and found to be in excellent agreement.

Asymptotic expressions of the SWFs are found to depend on branch points and associated characteristic eigenvalues of the spheroidal wave equation. These branch points are found using polynomial estimation techniques and a quadruple precision Newton-Raphson

search method. Branch points for $(n - m) \leq 100$ are found in greater accuracy than previously available and many are tabulated in this thesis.

The solution for the induced magnetic field from multiple permeable and conducting spheroidal objects in close proximity under time harmonic excitation is presented. Interactions between spheroids is accounted for by a interspheroidal modal interaction matrix. This multibody solution may provide the basis for a forward model used by inversion routines designed to detect and discriminate UXO. Specifically, this multibody solution may help to isolate non-UXO clutter from actual UXO in the field.

Thesis Supervisor: Jin Au Kong

Title: Professor of Electrical Engineering and Computer Science

Acknowledgments

This thesis and this man are a culmination of years of effort on the part of many people. It is imperative to me to recognize and acknowledge key individuals and thank them for their help, support, encouragement, and examples.

I am deeply indebted to my parents and ancestors who deserve my utmost gratitude. In this academic context, it is appropriate to note that my father especially has had a profound influence on my academic career. He has played a crucial role in my intellectual development and is an exemplary scholar and a scientist. My mother has been a bastion of strength in my life. She has maintained a belief in my character and ability, even though there were times when no one else did. It seems impossible to appropriately exhaust one's gratitude to good parents. Thank you.

A turning point in my academic career occurred as an undergraduate when I decided to take a graduate class in remote sensing from Professor David G. Long at Brigham Young University (BYU). The excitement of discovery and the mutual respect encountered in that class was of significant importance in my immediate family's decision to further my education. Additionally, the example of character I perceived in Professor Long and the other Faculty at BYU still inspire me. I am very grateful for these experiences, these examples, and for the encouragement and advice given me while at BYU.

I have come to recognize a rare greatness in Professor Jin Au Kong, my Ph.D. advisor at the Massachusetts Institute of Technology (MIT). The specific aspect which I will notice here is his ability to elicit greatness in others, especially in his students, who often never recognize their own potential. Some people are hindered in discovering their ultimate best simply because there was no spark or catalyst to ignite them. Through his broad, extensive knowledge and skill, Professor Kong helped me uncover my latent abilities and then insist on their development. Though the abilities are mine in the end, the necessary spark for their ignition has been provided in many cases by Professor Kong. This merits gratitude, and I thank him.

Also deserving of special thanks is Kevin O'Neill and Chi Ao. Kevin has in many respects been a second advisor for this thesis specifically with reference to the conducting

and permeable spheroid chapters. Kevin has accomplished the difficult task of being a skilled mentor without being a micromanager. His help, patience, and respect were invaluable. Chi's work in spheroid scattering and induction models have had an important impact on the content of this thesis. I am indebted to him for his early tutoring and subsequent guidance as well as for his friendship.

I have had a chance to associate with many outstanding students in the course of my formal education. I make mention of two students in particular from the Microwave Earth Remote Sensing (MERS) Laboratory at BYU: Quinn Remund, whose integrity and character I admire, and James Bates who I hope will indeed be a friend for life. Also from BYU, Tom Stevens has been a genuine and straightforward friend. Thank you.

It is my pleasure to also recognize my colleagues at the Center for Electromagnetic Theory and Application (CETA) lab. To Chi Ao, Henning Braunisch, Jianbing Chen, Xudong Chen, Jie Lu, Christopher Moss, Joe Pacheco, Madhu Sudan, and Bae-Ian Wu, I thank you for your friendship and help during my educational experience. Sharing an education with such bright, interesting, and respectable people has helped make this a pleasurable, intellectually satisfying experience. I wish you the best in your personal and professional lives.

I would like to thank Professor Ronald R. Parker for his help and advice throughout my time at MIT. I also especially thank Fernando L. Teixeira and Tomasz M. Grzegorzczak for their skilled guidance, encouragement, and indefatigability as postdoctoral researchers in the CETA lab.

Financial assistance has been granted to me without which the academic path trodden would have been drastically more problematic. I am grateful for institutions interested in helping students achieve their potentials through financial assistance. I would like to thank BYU for a full-tuition, four year undergraduate scholarship. I am grateful for two Rocky Mountain Space Grant Consortium (RMSGC) grants. And I am grateful to the National Science Foundation for a fellowship which helped me explore more diverse topics as a graduate student. Student loans have come in quite handy at times as well.

A very personal recognition of influence is due. I am inescapably and profoundly thankful for the teachings and example of Jesus Christ. I believe that the theories and pronouncements on human existence from Jesus represent an interpersonally unprovable, yet intrapersonally self consistent, observable, and repeatable reality. His precepts have played

a periodic and central role in my inner dialogue, moral structure, and behavior decision tree. I would be remiss if I did not recognize this source of fulfillment, opportunity, and joy in my life.

Finally, I wish to express my deepest love, respect, and gratitude to my wife Masako. She has willingly sacrificed much comfort and convenience in order to uproot and be a family together with me in a country foreign to her. We have found that our love for each other and for our family is perhaps the only force powerful enough to enable these two disparate people to discard stubborn weaknesses and improve together. Our relationship has led us to be more honest, patient, loving, understanding, believing, excited, hopeful, empathetic, obedient, and the list continues. This thesis and this man would be much less were it not for my Masako. Thank you.

For my parents,

And especially for 雅子 (Masako)

Contents

1	Introduction	31
2	Monte Carlo Simulation of Electromagnetic Wave Propagation in Dense Random Media with Dielectric Spheroids	37
2.1	Introduction	37
2.2	Formulation	39
2.3	Characterization of Random Media	41
2.4	Numerical Results	43
2.5	Conclusions	47
3	Sparse Matrix/Canonical Grid Method Applied to 3-D Dense Medium Simulations	49
3.1	Introduction	49
3.2	Formulation	51
3.3	3-D SMCG Method	55
3.3.1	SMCG Model Parameters	57
3.3.2	Parameter Considerations	60
3.3.3	3-D Dyadic Green's Function Approximation	63
3.4	Results	66
3.5	Conclusions	70
4	On the Asymptotic Expansion of the Spheroidal Wave Function and its Eigenvalues for Complex Size Parameter	75

4.1	Introduction	75
4.2	Standard Formulation of the Prolate Angular Spheroidal Wave Function . .	78
4.3	Asymptotic Expansion of the Spheroidal Eigenvalues, λ_{mn}	80
4.3.1	<i>Prolate</i> -Type Asymptotic Expansion	81
4.3.2	<i>Oblate</i> -Type Asymptotic Expansion	82
4.3.3	Asymptotic Expansion of the Eigenvalues for Complex c	84
4.3.4	Computation of the Branch Points $c_{\sigma;r}^{mn}$	89
4.3.5	Eigenvalue Ordering for Complex c	91
4.4	Asymptotic Expansion of $S_{mn}(c, \eta)$	95
4.4.1	Normalizations of the Asymptotic Expansions	96
4.5	Discussion	100
4.6	Summary and Conclusion	106
5	Broadband Analytical Magnetoquasistatic Electromagnetic Induction So-	
	lution for a Conducting and Permeable Spheroid	109
5.1	Introduction	109
5.2	Exact Formulation	113
5.3	High Frequency Approximations	116
5.3.1	Asymptotic Expressions for the Spheroidal Wave Functions	116
5.3.2	Small Penetration Approximation	120
5.4	Validation and Results	121
5.4.1	Comparison with Simulation	121
5.4.2	Comparison with Measurements	125
5.5	Conclusion	144
6	Simultaneous Analytical Solution for the Broadband Magnetoquasistatic	
	Electromagnetic Induction (EMI) Response from Multiple Conducting	
	and Permeable Spheroids	147
6.1	Introduction	147
6.2	Formulation	150
6.3	Matrix Definitions and Dimensions	157

CONTENTS	13
6.4 Conclusion	159
7 Summary	161
A Fast Algorithm for Matrix-Vector Multiply of Asymmetric Multilevel Block-Toeplitz Matrices in 3-D Scattering	165
A.1 Introduction	165
A.2 Formulation	166
A.2.1 Definitions	166
A.2.2 Recursive Algorithms	167
A.2.3 \mathbf{T}_f^M Fast Multiply Example	172
A.3 Numerical Implementation and Example: 3-D Scattering	173
A.4 Discussion and Conclusion	178
B Magnetoquasistatic Solution for Conducting and Permeable Spheroidal Shells	179
B.1 Exact Formulation	179
B.2 Results	191
C Computational Elements in Spheroidal Wavefunction Expansions	197
C.1 Vector Spheroidal Wavefunctions	197
C.2 Coupling Matrices and System Matrices	200
D Reference Tables for the Spheroidal Wave Equation for Complex c	203
D.1 Branch points, $c_{o;r}^{m,n}$, and Associated Eigenvalues $\lambda_{o;r}^{m,n}$ of the SWE	203
D.1.1 $m = 0, n = [m..80]$	203
D.1.2 $m = 1, n = [m..80]$	210
D.1.3 $m = [2..8], n = [m..25 + m]$	218
D.1.4 $m = [8..50], n = [m..15 + m]$	224
D.2 $\lambda_{mn}^{(a)}, S_{mn}^{(a)}(c, \eta)$, and $S_{mn}^{(a)'}(c, \eta)$	240
D.2.1 Asymptotic expansions of the PASWF, $S_{mn}^{(a)}(c, \eta)$ and the corresponding characteristic eigenvalues, $\lambda_{mn}^{(a)}$, for $m = [0..1], n = [m..6]$	242

D.2.2	Asymptotic expansions of the derivative of the PASWF, $S_{mn}^{(a)'}(c, \eta)$ and the corresponding characteristic eigenvalues, $\lambda_{mn}^{(a)}$, for $m = [0..1]$, $n = [m..6]$	255
Publications		269
Bibliography		271
Biographical note		282

List of Figures

1-1	Electromagnetic induction (EMI) model flowchart.	33
2-1	N non-overlapping small dielectric spheroids in a spherical test volume. . .	40
2-2	Scattering from the spheroid test volume (solid line) compared to scattering from a homogeneous dielectric sphere with ϵ_{eff} obtained from using Eq. (2.8) as the search method error, and with ϵ_{eff} a classical mixing formula [1]. On average, 1571 particles were used in $N_r=50$ realizations.	44
2-3	ϵ_{eff} as a function of fractional volume and elongation as compared to the classical mixing formula for $e=1$ and $e=2.6$	46
2-4	$\Re\{\epsilon_{\text{eff}}\}$ and the error term δ_σ (subtracted from the final error ($\delta_{75} = \delta_\sigma(N_r = 75)$) and normalized for $N_a=39$) resulting from the Nelder Mead simplex search according to realization number. This is for the case of $f_v=0.2$, $e=2.6$, $\epsilon_p=3.2$, $ka=0.2$, and $N_r=1\dots 75$ realizations.	47
3-1	Densely packed medium consisting of 50 dielectric spheroids. Elongation=1.8, $f_v=0.1$	56
3-2	Strong interaction cloud with $r_d=1.1$. Spheroids S_1 and S_3 are closest to the same grid point and thus their interaction is included in $\overline{\overline{Z}}^s$. Spheroid S_2 is beyond r_d and thus its exact interactions with both S_1 ($\overline{\overline{G}}(R_{12})$ shown as a thick solid line between S_1 and S_2) and S_3 are approximated as $\overline{\overline{G}}^{\text{cg}}(\overline{\overline{r}}_g^{311}, \overline{\overline{r}}_g^{132})$ and included in $\overline{\overline{Z}}^w$	61
3-3	Computation times and Kullback-Leibler distances for SMCG method for $\gamma=0-5$ with $r_d=1.1\Delta r_g$ and $N_{\text{cube}}=10000$	68

3-4 Computation times and Kullback-Leibler distances for SMCG method for $r_d=0.1-2.1\Delta r_g$ with $\gamma=2$ and $N_g=8$ 69

3-5 Computation times and Kullback-Leibler distances for SMCG method for $N_g=6-14$ with $\gamma=2$ and $r_d=1.1\Delta r_g$ 71

3-6 Radar Cross Section (σ) for increasing accurate approximations. 72

4-1 Prolate Spheroidal Geometry: $1 \leq \xi < \infty$, $-1 \leq \eta \leq 1$, $0 \leq \phi \leq 2\pi$,
 $x = \frac{d}{2}[(1 - \eta^2)(\xi^2 - 1)]^{\frac{1}{2}} \cos(\phi)$, $y = \frac{d}{2}[(1 - \eta^2)(\xi^2 - 1)]^{\frac{1}{2}} \sin(\phi)$, $z = \frac{d}{2}\eta\xi$,
 $e = \frac{b}{a}$, $\xi = (1 - e^{-2})^{-\frac{1}{2}}$, $d = 2(b^2 - a^2)^{\frac{1}{2}}$ 79

4-2 Branch points, $c_{o;r}^{mn}$ for $m = 0$ and $n = 0(1)6$. Branch cuts associated with $n = 4$ are indicated by the dashed lines with the appropriate expansion type indicated for each resulting sector. The dash-dot line indicates $\arg(c) = \pi/4$. 84

4-3 λ_{mn} : Eigenvalues of the spheroidal wave equation. $m = 0$ and $n = 0(1)18$. Each curve tracks an eigenvalue as c ranges from $c = (1 + \frac{3}{4}i)1.6$ (lower end of each curve) to $c = (1 + \frac{3}{4}i)50$ (upper end of each curve). Dashed curves indicate coalescing oblate eigenvalue pairs. The “2” indicates $\lambda_{0,2}((1 + \frac{3}{4}i)50)$. 86

4-4 λ_{mn} : Eigenvalues of the spheroidal wave equation. $m = 0$ and $n = 0(1)18$. Each curve tracks an eigenvalue as c ranges from $c = (1 + i)1.7$ (lower end of each curve) to $c = (1 + i)50$ (upper end of each curve). Dashed curves indicate coalescing oblate eigenvalue pairs. 87

4-5 Branch point $c_{o;1}^{0,1} = c_{o;2}^{0,3} = 3.563644553545 + 2.887165344337i$ where $\lambda_{0,1}$ and $\lambda_{0,3}$ merge at $\lambda_{o;1}^{0,1} = \lambda_{o;2}^{0,3} = 10.1408387872326 + 11.1215866842249i$. Dashed curves indicate coalescing oblate eigenvalue pairs. 88

4-6 λ_{mn} : Eigenvalues of the spheroidal wave equation. $m = 0$ and $n = 0(1)58$ and $c = (1 + \frac{3}{4}i)50$. The solid line indicates the (incorrect) ordering returned from calculating λ_{mn} using Hodge’s [2] method, while the correct ordering is labeled by $\lambda_{m,n}$ 92

4-7 a) Spheroidal eigenvalues $\lambda_{0,0}$ for $c = (1 + i)\alpha$, $\alpha = [0, 7]$. b) Relative error between the prolate eigenvalue from Hodge’s method [2], $\lambda_{0,0}$, and its *prolate*-type asymptotic expansion [Eq. (4.12)], $\lambda_{0,0}^{(a)}$ 96

4-8 a) Spheroidal eigenvalues $\lambda_{0,1}$ for $c = (1 + i)\alpha$, $\alpha = [0, 7]$. b) Relative error between the prolate eigenvalue from Hogde’s method [2], $\lambda_{0,1}$, and its *oblate*-type asymptotic expansion [Eq. (4.19)], $\lambda_{0,1}^{(a)}$ 97

4-9 a) $S_{mn}(c, \eta)$ for $c = (1+i)20$, $m = 0$, $n = (0, 3, 4)$ (or $[n_p = 0, 1, 2]$), and $0 \leq \eta < 1$. b) Absolute error between Legendre expansion, $S_{mn}(c, \eta)$ from Eq. (4.5), and *prolate*-type asymptotic expansion, $S_{mn}^{(a)}(c, \eta)$ from Eqs. (4.7) and (4.11). 101

4-10 a) $S'_{mn}(c, \eta)$ for $c = (1+i)20$, $m = 0$, $n = (0, 3, 4)$ (or $[n_p = 0, 1, 2]$), and $0 \leq \eta < 1$. b) Absolute error between derivative of Legendre expansion, $S'_{mn}(c, \eta)$ from Eq. (4.5), and derivative of the *prolate*-type asymptotic expansion, $S_{mn}^{(a)'}(c, \eta)$ Eqs. (4.7) and (4.11). 102

4-11 a) $S_{mn}(c, \eta)$ for $c = (1+i)20$, $m = 0$, $n = (1, 2, 5)$ (or $[n_o = 0, 1, 2]$), and $0 \leq \eta \leq 1$. b) Relative error between Legendre expansion, $S_{mn}(c, \eta)$ from Eq. (4.5) and *oblate*-type asymptotic expansion, $S_{mn}^{(a)}(c, \eta)$ from Eqs. (4.13) and (4.18). 103

4-12 a) $S'_{mn}(c, \eta)$ for $c = (1+i)20$, $m = 0$, $n = (1, 2, 5)$ (or $[n_o = 0, 1, 2]$), and $0 \leq \eta \leq 1$. b) Relative error between derivative of Legendre expansion, $S'_{mn}(c, \eta)$ from Eq. (4.5)] and derivative of the *oblate*-type asymptotic expansion $S_{mn}^{(a)'}(c, \eta)$ from Eqs. (4.13) and (4.18). 104

4-13 $\Re\{S_{0,12}((1+i)400, \eta)\}$ and $\Im\{S_{0,12}((1+i)400, \eta)\}$ ($n_p = 6$), for $-1 \leq \eta \leq 1$. Legendre expansion [Eq. (4.5), black curves], *prolate*-type asymptotic expansion [Eqs. (4.7) and (4.11), blue curves], and Miles [3] Bessel-type asymptotic approximation (Equation (3.11) therein, red curves). $\lambda_{0,12}^{(a)} = 5178.20430071674 + 5200.04621007177i$ 106

5-1 Spheroidal Geometry: $1 \leq \xi < \infty$ (Oblate case: $0 \leq \xi < \infty$), $-1 \leq \eta \leq 1$, $0 \leq \phi \leq 2\pi$, $x = \frac{d}{2}[(1 \mp \eta^2)(\xi^2 \mp 1)]^{\frac{1}{2}} \cos(\phi)$, $y = \frac{d}{2}[(1 \mp \eta^2)(\xi^2 \mp 1)]^{\frac{1}{2}} \sin(\phi)$, $z = \frac{d}{2}\eta\xi$, $e = \frac{b}{a}$, $\xi = (\pm(1 - e^{-2}))^{-\frac{1}{2}}$, $d = 2(\pm(b^2 - a^2))^{\frac{1}{2}}$. Upper sign \rightarrow prolate, lower sign \rightarrow oblate. 110

5-2 Some examples of unexploded ordnance (UXO). 111

5-3 λ_{mn} : Eigenvalues of the spheroidal wave equation. $m = 0$ and $n = 0(1)18$. Each curve tracks an eigenvalue as c ranges from $c = (1 + i)1.7$ (lower end of each curve) to $c = (1 + i)50$ (upper end of each curve). Dashed curves indicate coalescing oblate eigenvalue pairs. 118

5-4 z -component of the induced secondary field, H_{sz} , from five different spheroids, aspect ratio $e = [6, 3, 1, 1/3, 1/6]$, with their longest dimension equal to 3cm, and axial excitation calculated by the combined method described in Sections 5.2 and 5.3. All spheroids were 30cm below the measurement point and under uniform excitation $\overline{H}_o = \hat{z}$ with $\sigma = 10^7$ and $\mu_r = 100$. Solid curves $\Rightarrow \Re\{H_{sz}\}$ (inphase component), while dashed curves $\Rightarrow \Im\{H_{sz}\}$ (quadrature component). Vertical dashed lines give a rough indication of the regions of validity for the exact, asymptotic-assisted, and SPA solutions, progressing from low to high frequency. Circles indicate the resonant peak of $\Im\{H_{sz}\}$. Squares indicate the frequency at which $|\Re\{H_{sz}\}| = |\Im\{H_{sz}\}|$. Dots indicate results from the corresponding numerical solution [4]. Note that H_{sz} for the sphere has been scaled by 1/3. 122

5-5 z -component of the induced secondary field, H_{sz} , from the same five spheroids as in Fig. 5-4 under transverse excitation. $\overline{H}_o = \hat{z}$ with spheroids' axes of revolution aligned along the x -axis. All spheroids were 30cm below the measurement point and under uniform excitation $\overline{H}_o = \hat{z}$ with $\sigma = 10^7$ and $\mu_r = 100$. Circles indicate the resonant peak of $\Im\{H_{sz}\}$. Squares indicate the frequency at which $|\Re\{H_{sz}\}| = |\Im\{H_{sz}\}|$. Dots indicate results from the corresponding numerical solution [4]. Again, the response for the sphere has been scaled by 1/3. 123

5-6 z -component of the induced secondary field, H_{sz} , from five spheroids under axial excitation with a similar configuration to that of Fig. 5-4, but with $\mu_r = [1, 5, 10, 50, 100]$ and aspect ratio $e = 3$ and $2a = 3\text{cm}$. All spheroids were 30cm below the measurement point and under uniform excitation $\overline{H}_o = \hat{z}$ with $\sigma = 10^7$. Circles indicate the resonant peak of $\Im\{H_{sz}\}$. Squares indicate the frequency at which $|\Re\{H_{sz}\}| = |\Im\{H_{sz}\}|$. Dots indicate results from the corresponding numerical solution [4]. $\overline{H}_o = \hat{z}$ 124

5-7 Geophex ultra-wideband GEM-3 instrument in various configurations [5]. 126

5-8 Geophex ultra-wideband GEM-3 instrument sensor head and measurement grid [6]. 127

5-9 Magnetic field produced by the Geophex ultra-wideband GEM-3 instrument [7]. 128

5-10 Primary field potential from the GEM-3, $U_o(\vec{r})$ (magnitudes marked on left), and the secondary potential induced by the spheroid, $U_s(\vec{r})$ (magnitudes marked in center) in the $x - z$ plane for the S2 spheroid (see Table 5.2), at low frequency, under axial excitation, and choosing $\mu_r = 100$ and $\sigma = 10^7$. Color of induced response has been adjusted for clarity. Axes are in meters. The white rectangle encompasses the GEM-3 instrument. 130

5-11 Primary field potential from the GEM-3, $U_o(\vec{r})$ (magnitudes marked on left), and the secondary potential induced by the spheroid, $U_s(\vec{r})$ (magnitudes marked in center) in the $x - z$ plane for the S2 spheroid (see Table 5.2), at high frequency, under axial excitation, and choosing $\mu_r = 100$ and $\sigma = 10^7$. Color of induced response has been adjusted for clarity. Axes are in meters. The white rectangle encompasses the GEM-3 instrument. 131

5-12 Primary field potential from the GEM-3, $U_o(\vec{r})$ (magnitudes marked on left), and the secondary potential induced by the spheroid, $U_s(\vec{r})$ (magnitudes marked in center) in the $x - z$ plane for the S2 spheroid (see Table 5.2), at low frequency, under transverse excitation, and choosing $\mu_r = 100$ and $\sigma = 10^7$. Color of induced response has been adjusted for clarity. Axes are in meters. The white rectangle encompasses the GEM-3 instrument. 132

- 5-13 Primary field potential from the GEM-3, $U_o(\vec{r})$ (magnitudes marked on left), and the secondary potential induced by the spheroid, $U_s(\vec{r})$ (magnitudes marked in center) in the $x - z$ plane for the S2 spheroid (see Table 5.2), at high frequency, under transverse excitation, and choosing $\mu_r = 100$ and $\sigma = 10^7$. Color of induced response has been adjusted for clarity. Axes are in meters. The white rectangle encompasses the GEM-3 instrument. . . . 133
- 5-14 Primary field potential from the GEM-3, $U_o(\vec{r})$ (magnitudes marked on left), and the secondary potential induced by the spheroid, $U_s(\vec{r})$ (magnitudes marked in center) in the $x - z$ plane for the S2 spheroid (see Table 5.2), at low frequency, under axial excitation, offcenter, and choosing $\mu_r = 100$ and $\sigma = 10^7$. Color of induced response has been adjusted for clarity. Axes are in meters. The white rectangle encompasses the GEM-3 instrument. . . 134
- 5-15 Primary field potential from the GEM-3, $U_o(\vec{r})$ (magnitudes marked on left), and the secondary potential induced by the spheroid, $U_s(\vec{r})$ (magnitudes marked in center) in the $x - z$ plane for the S2 spheroid (see Table 5.2), at high frequency, under axial excitation, offcenter, and choosing $\mu_r = 100$ and $\sigma = 10^7$. Color of induced response has been adjusted for clarity. Axes are in meters. The white rectangle encompasses the GEM-3 instrument. . . 135
- 5-16 Primary field potential from the GEM-3, $U_o(\vec{r})$ (magnitudes marked on left), and the secondary potential induced by the spheroid, $U_s(\vec{r})$ (magnitudes marked in center) in the $x - z$ plane for the S2 spheroid (see Table 5.2), at low frequency, under transverse excitation, offcenter, and choosing $\mu_r = 100$ and $\sigma = 10^7$. Color of induced response has been adjusted for clarity. Axes are in meters. The white rectangle encompasses the GEM-3 instrument. . . 136
- 5-17 Primary field potential from the GEM-3, $U_o(\vec{r})$ (magnitudes marked on left), and the secondary potential induced by the spheroid, $U_s(\vec{r})$ (magnitudes marked in center) in the $x - z$ plane for the S2 spheroid (see Table 5.2), at high frequency, under transverse excitation, offcenter, and choosing $\mu_r = 100$ and $\sigma = 10^7$. Color of induced response has been adjusted for clarity. Axes are in meters. The white rectangle encompasses the GEM-3 instrument. . . 137

5-18 Spheroid collection used for testing. Specifications are listed in Table 5.2. 138

5-19 GEM-3 experimental setup. 139

5-20 Comparison of GEM-3 induced magnetic field measurements, $H_{sz,d}$, from prolate steel spheroid S2 with combined model outlined in Sections 5.2 and 5.3. Both axial and transverse cases are shown. Orientations are similar to those shown in plots of $U_s(\bar{r})$ such as Fig. 5-11. Optimized permeability and conductivity were $\mu_r = 234.1$ and $\sigma = 4.315 \times 10^6 \text{U}/m$, respectively. 141

5-21 Comparison of $H_{sz,d}$ from prolate aluminum spheroid A1 with combined model outlined in Sections 5.2 and 5.3. Both axial and transverse cases. Optimized conductivity was $\sigma = 2.103 \times 10^7 \text{U}/m$ 142

5-22 Comparison of $H_{sz,d}$ from oblate steel spheroid S8 with combined model outlined in Sections 5.2 and 5.3. Both axial and transverse cases. Optimized permeability and conductivity were $\mu_r = 268.0$ and $\sigma = 1.939 \times 10^7 \text{U}/m$, respectively. 143

5-23 Comparison of $H_{sz,d}$ from oblate aluminum spheroid A7 with combined model outlined in Sections 5.2 and 5.3. Both axial and transverse cases. Optimized conductivity was $\sigma = 3.147 \times 10^7 \text{U}/m$ 144

6-1 Spheroidal Geometry: $1 \leq \xi < \infty$ (Oblate case: $0 \leq \xi < \infty$), $-1 \leq \eta \leq 1$, $0 \leq \phi \leq 2\pi$, $x = \frac{d}{2}[(1 \mp \eta^2)(\xi^2 \mp 1)]^{\frac{1}{2}} \cos(\phi)$, $y = \frac{d}{2}[(1 \mp \eta^2)(\xi^2 \mp 1)]^{\frac{1}{2}} \sin(\phi)$, $z = \frac{d}{2}\eta\xi$, $e = \frac{b}{a}$, $\xi = (\pm(1 - e^{-2}))^{-\frac{1}{2}}$, $d = 2(\pm(b^2 - a^2))^{\frac{1}{2}}$. Upper sign \rightarrow prolate, lower sign \rightarrow oblate. 148

6-2 Site cluttered with multiple potential targets in close proximity. 149

6-3 Example collection of 3 spheroids in close proximity. 150

A-1 Example of a $\mathbf{A} = \mathbf{T}_1^3(2, 2, 2)$ asymmetric MBT matrix. Unique entries are boxed with a solid line. In the upper left hand corner, \mathbf{a}_0^1 is enclosed by a dash-dot box, while at the lower left hand corner $\mathbf{a}_{-1}^1 | \mathbf{a}_{-1}^2$ is delineated by a dashed box. Thin solid lines delineate interaction between different rows of a 2x2x2 cubic mesh, while bold solid line delineate between planes. 168

A-2	$\mathbf{A}_u * \mathbf{x}_z$ step which yields the first term of \mathbf{b}_z . Note the insertion of zeros into \mathbf{x} yielding \mathbf{x}_z which causes proper alignment. Each entry in \mathbf{A}_u corresponds to an \mathbf{a}_i^M final level subblock where i is between $-n_M$ and n_M ; the thin vertical lines mark the separation between $\mathbf{a}_{-1}^2 \dots \mathbf{a}_1^2$ subblocks in $\mathbf{a}_{-1}^1 \dots \mathbf{a}_1^1$, and thicker vertical lines indicate the boundary between $\mathbf{a}_{-1}^1 \dots \mathbf{a}_1^1$ blocks.	171
A-3	Discrete Dipole Approximation of a homogeneous sphere using a 31x31x31 grid.	174
A-4	Effective permittivity (ϵ_{eff}) results for a spherical test volume having meshes with 7-31 grid points per axis, $\epsilon_p = 1.7688 + 0.0266i$, and $ka = 5$ for the test volume.	176
A-5	Effective permittivity (ϵ_{eff}) results for $\epsilon_p = 3.2 + 0.01i$, and $ka = 2.5$	177
B-1	A conducting and permeable prolate spheroidal shell is excited by a time-harmonic primary field $\overline{H}_o(\vec{r})e^{-i\omega t}$. The prolate spheroidal coordinate system is specified by (ξ, η, ϕ) with $-1 \leq \eta \leq 1$, $1 \leq \xi < \infty$, and $0 \leq \phi < 2\pi$. The outer (α) interface of the shell is given by $\xi = \xi_0 = 1/\sqrt{1 - (1/e)^2}$ and d_α with $e_\alpha = b_\alpha/a_\alpha = b_\beta/a_\beta$ is the elongation ratio. The inner (β) interface is specified by ξ_0 and d_β	180
B-2	Normalized dipole moment, m_z , from a nonmagnetic spherical shell with vanishing core size.	192
B-3	Normalized dipole moment, m_z , from a spherical shell with vanishing core size but high core contrast.	192
B-4	Normalized dipole moment, m_z , from a magnetic spherical shell with vanishing core size and high core contrast.	193
B-5	Normalized dipole moment, m_z , from a nonmagnetic spheroidal shell with vanishing core size but high core contrast.	193
B-6	Normalized dipole moment, m_z , from a nonmagnetic spherical shell with large core.	194
B-7	Normalized dipole moment, m_z , from a nonmagnetic spherical shell with moderate core size and contrast.	194

B-8 Normalized dipole moment, m_z , from a nonmagnetic spherical shell with large core size and contrast. 195

B-9 Normalized dipole moment, m_z , from a magnetic spherical shell with moderate core size and contrast. 195

B-10 Normalized dipole moment, m_z , from a magnetic spheroidal shell with moderate core size and contrast. 196

List of Tables

2.1	Summary of ϵ_{eff} results. For all cases presented, $ka=0.2$ and $\epsilon_p=3.2$	48
3.1	Number of surrounding gridpoints, g_{r_d} , included in the strong interaction cloud as a function of neighborhood distance r_d	60
3.2	Number of expansion terms and total number of FFTs (both forward and inverse) for expansion order γ	66
3.3	Computation times and relative speedup for the SMCG method compared to the full method. For all cases $N_{\text{cube}}=15000$	73
4.1	Solutions to Eq. (4.1): angular and radial, prolate and oblate spheroidal wave functions.	76
4.2	Branch points and eigenvalues for $m = 0(1)6$ and $n = 0(1)[6 - m]$. Accuracy was determined by the last correction of the Newton-Raphson method (in all cases $< 1 \times 10^{-15}$).	90
4.3	Pattern governing n_p , n_o and which type of asymptotic expansion, either the <i>prolate</i> -type (Pro. above) or the <i>oblate</i> -type (Obl. above), for different combinations of m and n . c is of the form $c = (1 + i)\alpha$. Normalizations for each case are also given (see Section 4.4.1).	94
4.4	Normalization table for both <i>prolate</i> -type or <i>oblate</i> -type asymptotic expansions with $(n - m)$ both <i>even</i> and <i>odd</i>	100
4.5	Some values for the PASWF and its derivative. $\eta = .5$ for all cases listed.	105

5.1	Pattern governing n_p , n_o and which type of asymptotic expansion, either the <i>prolate</i> -type (Pro. above) or the <i>oblate</i> -type (Obl. above), for different combinations of m and n . c is of the form $c = (1 + i)\alpha$	117
5.2	Physical dimensions of steel and aluminum spheroids. PS \Rightarrow Prolate Spheroid. OS \Rightarrow Oblate Spheroid.	140
A.1	Comparison of MBT fast method computation times with the full method for the case of Fig. A-4	178
D.1	Branch points and associated eigenvalues for $m = 0$	203
D.2	Branch points and associated eigenvalues for $m = 1$	210
D.3	Branch points and associated eigenvalues for $m = 2$	218
D.4	Branch points and associated eigenvalues for $m = 3$	219
D.5	Branch points and associated eigenvalues for $m = 4$	219
D.6	Branch points and associated eigenvalues for $m = 5$	220
D.7	Branch points and associated eigenvalues for $m = 6$	221
D.8	Branch points and associated eigenvalues for $m = 7$	222
D.9	Branch points and associated eigenvalues for $m = 8$	223
D.10	Branch points and associated eigenvalues for $m = 9$	224
D.11	Branch points and associated eigenvalues for $m = 10$	224
D.12	Branch points and associated eigenvalues for $m = 11$	224
D.13	Branch points and associated eigenvalues for $m = 12$	225
D.14	Branch points and associated eigenvalues for $m = 13$	225
D.15	Branch points and associated eigenvalues for $m = 14$	226
D.16	Branch points and associated eigenvalues for $m = 15$	226
D.17	Branch points and associated eigenvalues for $m = 16$	226
D.18	Branch points and associated eigenvalues for $m = 17$	227
D.19	Branch points and associated eigenvalues for $m = 18$	227
D.20	Branch points and associated eigenvalues for $m = 19$	228
D.21	Branch points and associated eigenvalues for $m = 20$	228
D.22	Branch points and associated eigenvalues for $m = 21$	228

D.23	Branch points and associated eigenvalues for $m = 22$.	229
D.24	Branch points and associated eigenvalues for $m = 23$.	229
D.25	Branch points and associated eigenvalues for $m = 24$.	230
D.26	Branch points and associated eigenvalues for $m = 25$.	230
D.27	Branch points and associated eigenvalues for $m = 26$.	230
D.28	Branch points and associated eigenvalues for $m = 27$.	231
D.29	Branch points and associated eigenvalues for $m = 28$.	231
D.30	Branch points and associated eigenvalues for $m = 29$.	232
D.31	Branch points and associated eigenvalues for $m = 30$.	232
D.32	Branch points and associated eigenvalues for $m = 31$.	232
D.33	Branch points and associated eigenvalues for $m = 32$.	233
D.34	Branch points and associated eigenvalues for $m = 33$.	233
D.35	Branch points and associated eigenvalues for $m = 34$.	233
D.36	Branch points and associated eigenvalues for $m = 35$.	234
D.37	Branch points and associated eigenvalues for $m = 36$.	234
D.38	Branch points and associated eigenvalues for $m = 37$.	235
D.39	Branch points and associated eigenvalues for $m = 38$.	235
D.40	Branch points and associated eigenvalues for $m = 39$.	235
D.41	Branch points and associated eigenvalues for $m = 40$.	236
D.42	Branch points and associated eigenvalues for $m = 41$.	236
D.43	Branch points and associated eigenvalues for $m = 42$.	237
D.44	Branch points and associated eigenvalues for $m = 43$.	237
D.45	Branch points and associated eigenvalues for $m = 44$.	237
D.46	Branch points and associated eigenvalues for $m = 45$.	238
D.47	Branch points and associated eigenvalues for $m = 46$.	238
D.48	Branch points and associated eigenvalues for $m = 47$.	239
D.49	Branch points and associated eigenvalues for $m = 48$.	239
D.50	Branch points and associated eigenvalues for $m = 49$.	239
D.51	Branch points and associated eigenvalues for $m = 50$.	240
D.52	$S_{0n}^{(a)}(c, \eta)$ for $n = [0..6]$.	242

D.53	$S_{1n}^{(a)}(c, \eta)$ for $n = [1..6]$.	249
D.54	$S_{0n}^{(a)'}(c, \eta)$ for $n = [0..6]$.	255
D.55	$S_{1n}^{(a)'}(c, \eta)$ for $n = [1..6]$.	262

List of Algorithms

1	Generation of full \mathbf{T}_f^M MBT matrices.	169
2	Π_{bt} : Direct assignment of \mathbf{A}_u	170
3	ζ_p : Generation of \mathbf{x}_z by inserting zeros into \mathbf{x}	171
4	ζ_a^{-1} : Reconstruction of \mathbf{b} from \mathbf{b}_z	172

Chapter 1

Introduction

Most human sensation of and interaction with the physical world has its basis in electromagnetic phenomena. Macroscopic electromagnetic phenomena are in turn completely described by Maxwell's equations combined with the constitutive relations. The ability to understand, explain, and predict physical phenomena is the first step in mastering and controlling the physical world rather than being powerless bystanders of it. Therefore, analytical and numerical solutions to Maxwell's equations are indispensable tools that enable man to direct the physical world to our advantage.

This thesis extends certain electromagnetic analytic and numerical solutions to Maxwell's equations enabling the accommodation of spheroidal geometries. Spheroidal geometries are desirable because of their versatility in modeling manmade and natural shapes including solid and hollow needles, spheres, and disks, while also possessing analytic solutions.

Beginning with Chapter 2, I study the electromagnetic wave propagation in three-dimensional (3-D) dense random discrete media containing dielectric spheroidal scatterers. I employ a Monte Carlo method in conjunction with the Method of Moments to solve the volume integral equation for the electric field. I calculate the effective permittivity of the random medium through a coherent-field approach and compare my results with a classical mixing formula. A parametric study on the dependence of the effective permittivity on particle elongation and fractional volume is included.

In Chapter 3, the Sparse Matrix/Canonical Grid (SMCG) method, which has been shown to be an efficient method for calculating the scattering from 1-D and 2-D random

rough surfaces, is extended to 3-D dense media scattering. In particular, I study the scattering properties of media containing randomly positioned and oriented dielectric spheroids. Mutual interactions between scatterers are formulated using a Method of Moments (MoM) solution of the volume integral equation. Iterative solvers for the resulting system matrix normally require $\mathcal{O}(N^2)$ operations for each matrix-vector multiply. The SMCG method reduces this complexity to $\mathcal{O}(N \log N)$ by defining a neighborhood distance, r_d , by which particle interactions are decomposed into “strong” and “weak”. Strong interaction terms are calculated directly requiring $\mathcal{O}(N)$ operations for each iteration. Weak interaction terms are approximated by a multivariate Taylor series expansion of the 3-D background dyadic Green’s function between any given pair of particles. Greater accuracy may be achieved by increasing r_d , using a higher order Taylor expansion, and/or increasing mesh density at the cost of more interaction terms, more FFTs, and longer FFTs, respectively. Scattering results, computation times, and accuracy for large-scale problems with r_d up to 2 grid points, $14 \times 14 \times 14$ canonical grid size, fifth order Taylor expansion, and 15000 discrete scatterers are presented and compared against full solutions.

The efficient calculations in Chapter 3 are accomplished using a new $\mathcal{O}(N \log N)$ FFT-based method to expedite matrix-vector multiplies involving multilevel block-Toeplitz (MBT) matrices. This new method is presented as Appendix A. The method is also a minimal memory method with $\mathcal{O}(N)$ memory requirements because only nonredundant entries of the MBT matrix are stored. The accuracy and convergence of the method are illustrated in the calculation of the scattered field and the effective permittivity of a sphere with size parameter ka up to 5 using a volume integral formulation akin to the discrete dipole approximation.

The detection and discrimination of subsurface unexploded ordnance (UXO) is of critical and timely importance to human populations and governments. Electromagnetic induction (EMI) models of canonical shapes are promising in this effort to detect and discriminate UXO. I develop a hybrid model including asymptotic expressions of the spheroidal wave functions (SWFs) to obtain a reliable, broadband solution for the electromagnetic induction (EMI) response from a conducting and permeable spheroid in Chapter 5. I obtain this broadband response, valid in the magnetoquasistatic regime from 0 Hz to 100’s of KHz, by

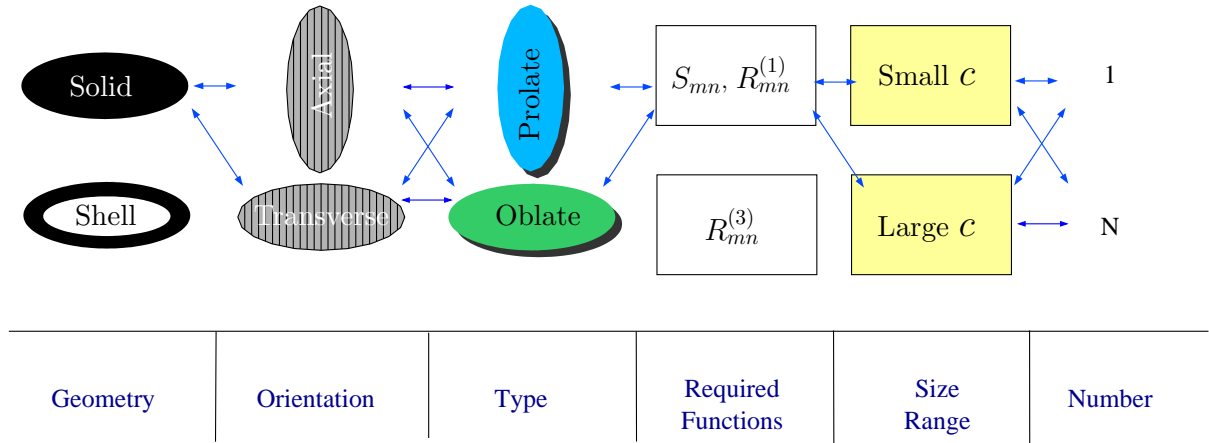


Figure 1-1: Electromagnetic induction (EMI) model flowchart.

combining three different techniques each applicable over a different frequency range. At low frequencies, the exact analytical solution is used. At mid-range frequencies, asymptotic expressions for the angular and radial SWFs, $S_{mn}(c, \eta)$ and $R_{mn}(c, \xi)$, are implemented to maintain a stable solution for the induced magnetic field. At higher frequencies, a Small Penetration Approximation (SPA) solution is used when the SPA solution approaches the asymptotic assisted solution to within some predefined tolerance. Validation of this combined technique is accomplished by comparison of the induced magnetic field predicted by my model to both a finite element method/boundary integral (FEM/BI) numerical solution and experimental data from various spheroids taken by an ultra-wideband EMI instrument. An outline of the various possibilities for spheroidal induction models is presented in Fig. 1-1.

This broadband EMI response is obtained through the use of asymptotic expansion of the SWFs for complex size parameters. In Chapter 4, I provide a rapid and accurate method for calculating the prolate and oblate spheroidal wave functions (PSWFs and OSWFs), $S_{mn}(c, \eta)$, and their eigenvalues, λ_{mn} , for arbitrary complex size parameter c in the asymptotic regime of large $|c|$, m and n fixed. The ability to calculate these SWFs for large and complex size parameters is important for many applications in mathematics, engineering, and physics. For arbitrary $\arg(c)$, the PSWFs and their eigenvalues are accurately

expressed by established *prolate*-type or *oblate*-type asymptotic expansions. However, determining the proper expansion type is dependent upon finding spheroidal branch points, $c_{o;r}^{mn}$, in the complex c -plane where the PSWF alternates expansion type due to analytic continuation. I implement a numerical search method for tabulating these branch points as a function of spheroidal parameters m , n , and $\arg(c)$. The resulting table allows rapid determination of the appropriate asymptotic expansion type of the SWFs. Normalizations, which are dependent on c , are derived for both the *prolate* and *oblate*-type asymptotic expansions and for both $(n - m)$ even and odd. The ordering for these expansions is different from the original ordering of the SWFs and is dictated by the location of $c_{o;r}^{mn}$. I document this ordering for the specific case of $\arg(c) = \pi/4$ which occurs for the diffusion equation in spheroidal coordinates. Some representative values of λ_{mn} and $S_{mn}(c, \eta)$ for large, complex c are also given while Appendix D contains a more complete listing of the branch points of the spheroidal wave equation, $c_{o;r}^{mn}$, along with their associated eigenvalues, $\lambda_{o;r}^{mn}$. Results are tabulated for a greater range of m and n than previously available as well as with greater accuracy. Also included in Section D.2 are tables containing the angular SWF for large and complex size parameter, c .

UXO discrimination is often hampered by multiple targets in close proximity corrupting individual induced field detection and processing. Exact calculation of the induced field produced by multiple spheroidal targets in close proximity may facilitate discrimination during inversion. Thus, I present the solution for the induced electromagnetic induction (EMI) response from multiple permeable and conducting spheroidal objects in close proximity under time harmonic excitation in Chapter 6. The exact formulation for the induced EMI response is based on magnetic field boundary conditions. The internal magnetic field of each spheroid is represented in terms of an infinite sum of the vector spheroidal wave functions. The external magnetic field is composed of the primary field and the induced secondary field from each spheroid, each expressed as an infinite sum of solutions of the first and second kinds of the Laplace equation in the spheroidal coordinate system. The total external secondary field summation coefficients are solved for simultaneously thus including all multiple body interactions.

In Appendix B, I present the exact formulation for the induced magnetic field from

a conducting and permeable spheroidal shell under time harmonic excitation. Some low frequency results are also presented.

Chapter 2

Monte Carlo Simulation of Electromagnetic Wave Propagation in Dense Random Media with Dielectric Spheroids

2.1 Introduction

In applications related to the remote sensing of the environment, the characterization of the electromagnetic wave interaction with natural media is of great importance. Natural media (e.g., snow, ice, and soil) often consist of a large number of densely packed, electrically small discrete scatterers that are randomly distributed in some background host medium.

The “classical” approach to study random discrete scatterers involves hypotheses such as the consideration of tenuous and/or sparse media. In sparse media, discrete scatterers occupy only a small volume fraction (typically less than 5%). In tenuous media, the constitutive parameters of discrete scatterers differ only slightly from that of the background medium. Such hypotheses allow for the solution of the problem through the independent scattering assumption, which neglects coherent interactions between the particles. However, in dense nontenuous media, the independent scattering assumption is no longer

valid [8,9,10]; hence the effects of multiple scattering and coherent wave mutual interactions must be taken into account. This is also true for media in which the scatterers occupy a low overall fractional volume but can be locally dense due to clustering properties (e.g., branches and leaves in vegetation canopies).

For such dense media, analytical wave theory and approximations such as Foldy's approximation [11], the quasicrystalline approximation (QCA) [12,13,14], and the QCA with coherent potential (QCA-CP) [12,8] are frequently employed. In QCA and QCA-CP, the pair distribution function, which constitutes a second-order spatial correlation among the scatterers, must be specified. Common approximations for the pair distribution function are the hole correction and the Percus-Yevick (PY) pair distribution function [8,15]. The use of such analytical techniques is adequate in the study of problems presenting configurational symmetries, such as media composed only of spherical particles. In many practical cases of interest, however, the adherence to spherical geometries is not able to capture the essential physics of the problem [16,17]. The need to incorporate nonspherical statistics into the analytical models makes such analytical treatments rather involved.

The alternative to deal with more complex problems in a systematic manner is to resort to numerical methods. In [16], the scattering problem involving dense dielectric scatterers is formulated using a volume integral equation, which may then be solved by the Method of Moments (MoM) [18]. This gives the complete solution for a given configuration of scatterers. For a random medium problem, the positions and properties of the scatterers are determined for different realizations according to some prescribed statistics using the Monte Carlo method. The MoM solution is sought for each realization so that statistical averages of the quantities of interest (e.g., effective permittivity, absorption rates, extinction rates, and phase functions of co-polarization and cross-polarization) can be determined.

In this work, we use the Monte Carlo method to characterize the effective permittivity of dense discrete random media composed of three-dimensional spheroidal dielectric scatterers as a function of the fractional volume of scatterers, particle elongation, the electromagnetic size of the particle (ka), and particle permittivity (media contrast). This extends previous studies (e.g. [19,20,21,15,22]) on the numerical calculation of effective permittivity which were limited to spherical particles and/or two-dimensional scattering.

2.2 Formulation

In this section, we briefly describe the volume integral formulation and the Monte Carlo methods used in our work. More detailed expositions of this MoM solution based on the volume integral formulation can be found in Chapter 3 and in [16].

Consider an incident electric field $\mathbf{E}_{inc}(\mathbf{r})$ impinging on N randomly positioned and oriented dielectric prolate spheroids (see Fig. 2-1). The total electric field $\mathbf{E}(\mathbf{r})$ can be expressed in terms of a volume integral equation as

$$\begin{aligned} \mathbf{E}(\mathbf{r}) = & \mathbf{E}_{inc}(\mathbf{r}) + k^2 \sum_{j=1}^N \int_{V_j} d\mathbf{r}' g(\mathbf{r}, \mathbf{r}') [\chi(\mathbf{r}') \mathbf{E}(\mathbf{r}')] \\ & - \sum_{j=1}^N \nabla \int_{V_j} d\mathbf{r}' \nabla' g(\mathbf{r}, \mathbf{r}') \cdot [\chi(\mathbf{r}') \mathbf{E}(\mathbf{r}')] \end{aligned} \quad (2.1)$$

where $k = \omega\sqrt{\mu\epsilon}$ is the background wavenumber and V_j is the volume of the spheroid j . The scalar Green's function $g(\mathbf{r}, \mathbf{r}')$ and electric susceptibility $\chi(\mathbf{r}')$ are given by

$$\begin{aligned} g(\mathbf{r}, \mathbf{r}') &= \frac{\exp(ik|\mathbf{r} - \mathbf{r}'|)}{4\pi|\mathbf{r} - \mathbf{r}'|} \\ \chi(\mathbf{r}') &= \frac{\epsilon_p(\mathbf{r}')}{\epsilon} - 1. \end{aligned}$$

with ϵ_p being the permittivity inside the spheroid.

To solve Eq. (2.1) using MoM, we assume that the spheroids are electrically small and choose the electrostatic solution of the Laplace equation to form a set of N_b basis functions. In this work, only the dipole basis functions are considered. The matrix equation that results for the internal field $\mathbf{E}(\mathbf{r})$ is solved iteratively using the biconjugate gradient stabilized method (Bi-CGSTAB). It should be pointed out that permittivities of the background medium and the spheroid must satisfy the conditions $ka \ll 1$ and $k_p a \ll 1$, where $k_p = \omega\sqrt{\mu\epsilon_p}$, in order for the small scatterer assumption to be valid.

To obtain the average fields, a Monte Carlo simulation is performed by creating multiple realizations of media consisting of thousands of discrete spheroids with random positions and orientations contained within some test volume. The Metropolis shuffling process [23, 24]

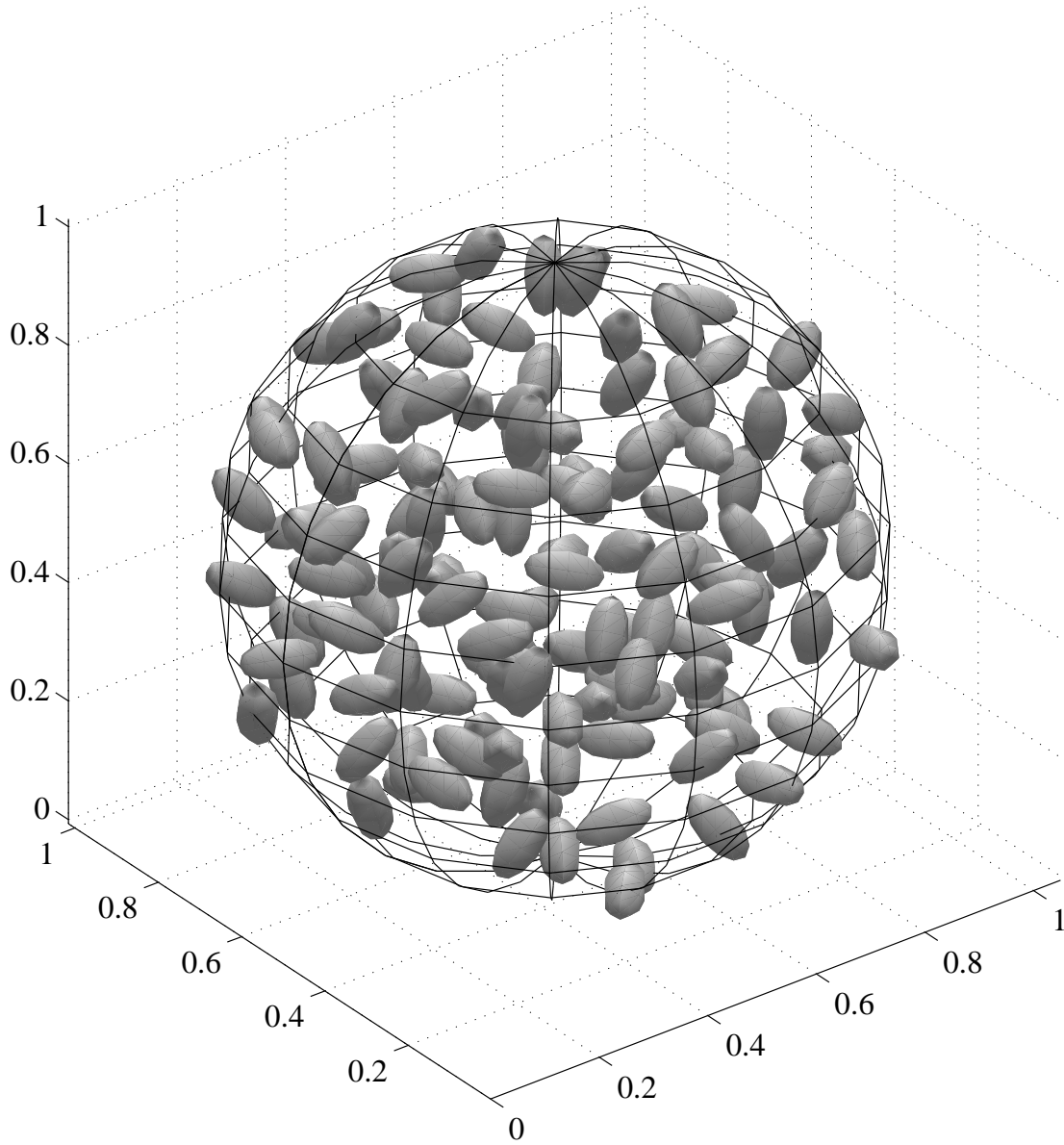


Figure 2-1: N non-overlapping small dielectric spheroids in a spherical test volume.

is used to generate the positions and orientations of a system of densely packed spheroids. Periodic boundary conditions [16] are employed for the test volume in order to minimize edge effects.

2.3 Characterization of Random Media

Generally speaking, the characterization of a random medium containing discrete scatterers can be studied from two different perspectives: the coherent and incoherent fields. The coherent scattered field is obtained by averaging the electric field solution over N_r realizations:

$$\langle \mathbf{E}_s \rangle = \frac{1}{N_r} \sum_{\sigma=1}^{N_r} \mathbf{E}_s^\sigma \quad (2.2)$$

The coherent field is closely related to the propagation characteristics of the random medium. On the other hand, the scattering of the coherent wave away from its forward propagation direction is related to the incoherent field, which is defined as

$$\mathcal{E}_s^\sigma = \mathbf{E}_s^\sigma - \langle \mathbf{E}_s \rangle \quad (2.3)$$

where $\sigma = 1, 2, \dots, N_r$ is the realization index. The incoherent intensity is then given by

$$\mathcal{I}_s = \frac{1}{N_r} \sum_{\sigma=1}^{N_r} |\mathcal{E}_s^\sigma|^2 \quad (2.4)$$

The incoherent intensity can be used to obtain the extinction coefficient and phase functions that are used in radiative transfer (RT) theory [16]. In contrast to “conventional” RT theory, the extinction coefficient and phase functions obtained through the Monte Carlo simulations outlined in Section 2.2 take into account of coherent multiple interactions among the scatterers.

In this work, we focus on the characterization of the propagation properties of the random medium. Thus the coherent field will be used to determine the effective propagation constant of the random medium (or equivalently the effective permittivity for a non-magnetic medium). In this “coherent-field approach,” the effective permittivity is obtained as the result of an inverse scattering problem. The coherent scattered fields from a collection of particles in a given finite test volume are compared to fields scattered from a homogeneous volume of the same size and shape. The permittivity of the homogeneous medium which yields scattered fields that best match the averaged scattered fields produced

by the random medium is considered to be the effective permittivity. This approach has the advantages of taking the size and shape of the test volume into account. It has been used for spheres contained in a cubic volume using the Born approximation for scattering from the cube [21], for 2-D rectangular regions [20], and for spheres contained in spherical volumes using Mie theory for scattering from the sphere [21, 25]. In the following, we apply this method to obtain the effective permittivity (ϵ_{eff}) of a dense discrete random medium containing many spheroids by comparing the coherent scattered fields from collections of spheroids contained in a spherical test volume (Fig. 2-1) to Mie scattering from the same size homogeneous sphere with permittivity equal to ϵ_{eff} . The bistatic radar cross section (RCS) will be used for the comparisons.

Let the incident electric field $\mathbf{E}_{\text{inc}}(\mathbf{r})$ be a plane wave

$$\mathbf{E}_{\text{inc}}(\mathbf{r}) = \mathbf{y} \exp(ikz) \quad (2.5)$$

The radar cross section (RCS) for the random spheroid medium (σ_{ran}) with the electromagnetic wavelength set to unity is then

$$\sigma_{\text{ran}} = 4\pi r^2 |\langle \mathbf{E}_s \rangle|^2. \quad (2.6)$$

The Mie scattering in the far field is computed using Wiscombe's code [26]. According to the notation in [26], the RCS of a Mie sphere σ_{mie} in the scattering plane is given by

$$\sigma_{\text{mie}} = \frac{4\pi}{k^2} |S_1(\theta)|^2 \quad (2.7)$$

where S_1 is the complex scattering amplitude, and θ is the scattering angle. The effective permittivity is calculated using a multistart Nelder-Mead simplex search method [27]. Only the real part of the effective permittivity is reported here. The error term used in this search method was chosen to be the absolute value of the cumulative difference between the spheroid medium RCS, σ_{ran} , and the Mie sphere RCS, σ_{mie} :

$$\text{error} = \delta_\sigma = \sum_{j=1}^{N_a} |(\sigma_{\text{mie},j}) - (\sigma_{\text{ran},j})|. \quad (2.8)$$

where $\sigma_{mie,j}$ and $\sigma_{ran,j}$ denote the RCS for the Mie sphere and the random spheroid medium respectively at the j^{th} angle. N_a represents the number of scattering angles used in the minimization process ($N_a=39$ for the results presented in this work).

A cumulative logarithmic error was also considered. However, the resulting ϵ_{eff} was slightly unstable. Using a logarithmic fit, even changes in scattering amplitude on the order of 10^{-4} would alter the resulting fit due to the emphasis placed on all scattering point. When using the linear error, the strong forward scattered field is fit best, and the behavior in the tails is accounted for automatically. In this work, only the real part of ϵ_{eff} is considered.

2.4 Numerical Results

The effective permittivity, ϵ_{eff} of dense random media containing discrete prolate spheroids was calculated for many combinations of f_v (fractional volume) and e (elongation, $c = ae$). For each ϵ_{eff} calculation, $N_r=50$ realizations were performed, and the results averaged according to Eq. (2.2) to yield the coherent scattered electric field $\langle \mathbf{E}_s \rangle$. The spherical test volume was first generated as a cubic test volume in order to employ periodic boundary conditions. After placement, the center of each spheroid was used to determine whether or not that spheroid would remain in the spherical test volume. $N=3000$ spheroids were placed in the cubic test volume, and therefore an average of $(N\pi/6) \approx 1571$ spheroids remained in the spherical test volume. The radius of the equivalent homogeneous sphere (R) used for Mie scattering was determined by

$$R = \left(\frac{N}{f_v} \left(\frac{\pi}{6} \right) a^3 e \right)^{\frac{1}{3}}. \quad (2.9)$$

The parameters for the simulations reported here were $f_v \Rightarrow [.05, .10, .15, .20, .25, .30, .35, .40]$, $e \Rightarrow [1.0, 1.8, 2.6]$, $\epsilon_p \Rightarrow 3.2$, and $ka \Rightarrow 0.2$. Both the random spheroid media scattering and the Mie sphere scattering were copolarized scattering with $\phi = 0^\circ$ and $\theta = 0^\circ$ to 180° . Typical scattering results for the case of $f_v=0.20$, $e=1.0$ (sphere case) and 2.6, $ka=0.2$, and $\epsilon_p=3.2+0.0i$ are shown in Fig. 2-2. As with previous results for spheres [21] and 2-D infinitely long cylinders [20], the coherent scattering from a homogeneous volume

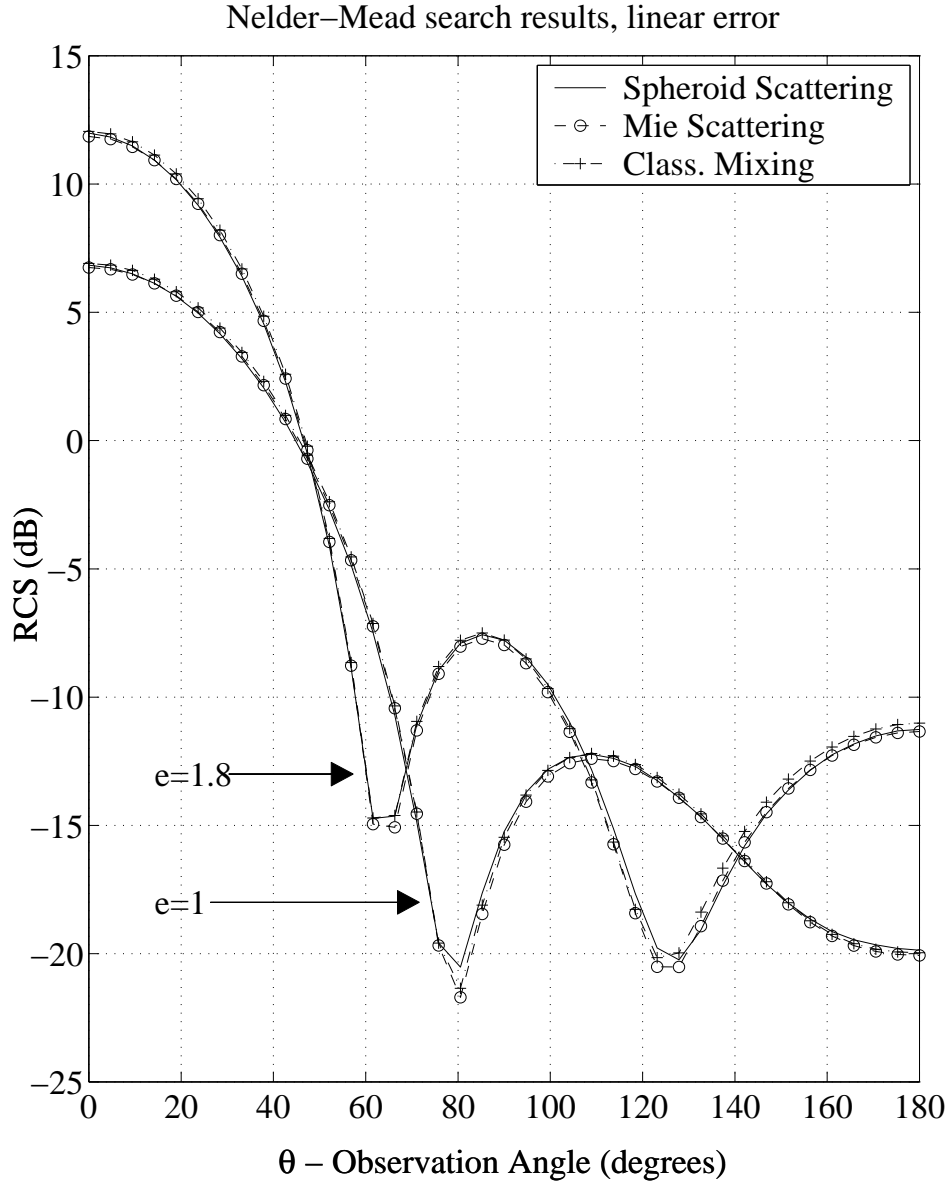


Figure 2-2: Scattering from the spheroid test volume (solid line) compared to scattering from a homogeneous dielectric sphere with ϵ_{eff} obtained from using Eq. (2.8) as the search method error, and with ϵ_{eff} a classical mixing formula [1]. On average, 1571 particles were used in $N_r=50$ realizations.

with permittivity ϵ_{eff} adequately model the coherent scattering from dense random media consisting of discrete spheroids.

The variation of ϵ_{eff} with f_v and e is depicted in Fig. 2-3. Also shown is the ϵ_{eff} predicted

by the classical mixing theory [1] for spheres (solid line) and for spheroids with $e=2.6$ (dash-dot line). This classical mixing formula for randomly oriented ellipsoids is expressed as

$$\epsilon_{\text{eff}} = \epsilon + \left(1 - \frac{f_v}{3} \sum_{i=1}^3 N_i \beta_i \right)^{-1} \frac{f_v}{3} \sum_{i=1}^3 \epsilon \beta_i \quad (2.10)$$

where

$$\beta_i = \frac{(\epsilon_p - \epsilon)}{\epsilon + N_i(\epsilon_p - \epsilon)}. \quad (2.11)$$

In the prolate spheroid case considered in this work, the depolarization factors N_i are given by [28]

$$N_z = \frac{1 - \varepsilon^2}{2\varepsilon^3} \left(\ln \frac{1 + \varepsilon}{1 - \varepsilon} - 2\varepsilon \right) \quad (2.12)$$

$$N_x = N_y = \frac{1}{2}(1 - N_z) \quad (2.13)$$

with the eccentricity $\varepsilon = \sqrt{1 - (1/e^2)}$.

For the case of a dense medium consisting of spheres ($e=1$), the results for effective permittivity are in excellent agreement the classical mixing formula except at higher fractional volumes where the results are slightly lower. For the case of a dense medium consisting of randomly oriented prolate spheroids ($e=2.6$), the results for effective permittivity are lower than that predicted by the classical mixing formula at f_v larger than about 0.2. These results are consistent with [21] for the spherical case. Note that as the fractional volume increases, the close proximity of the spheroids might necessitate the use of quadrupole terms to accurately model multiple scattering.

When interpreting numerical simulation results, accuracy and convergence of the computational method are important. A convergence criteria of residual error $\leq 10^{-6}$ was used in the iterative solver (Bi-CGSTAB) for Eq. (2.1). To ensure that the medium sample set was sufficiently random, many realizations were performed. Fig. 2-4 shows the calculated ϵ_{eff} and the final error term Eq. (2.8) resulting from the Nelder Mead simplex search as a function of the number of realizations performed. As the number of realizations increases the residual error decreases and ϵ_{eff} converges to its final value.

Table 2.1 lists the real part of ϵ_{eff} calculated from the method described in this work.

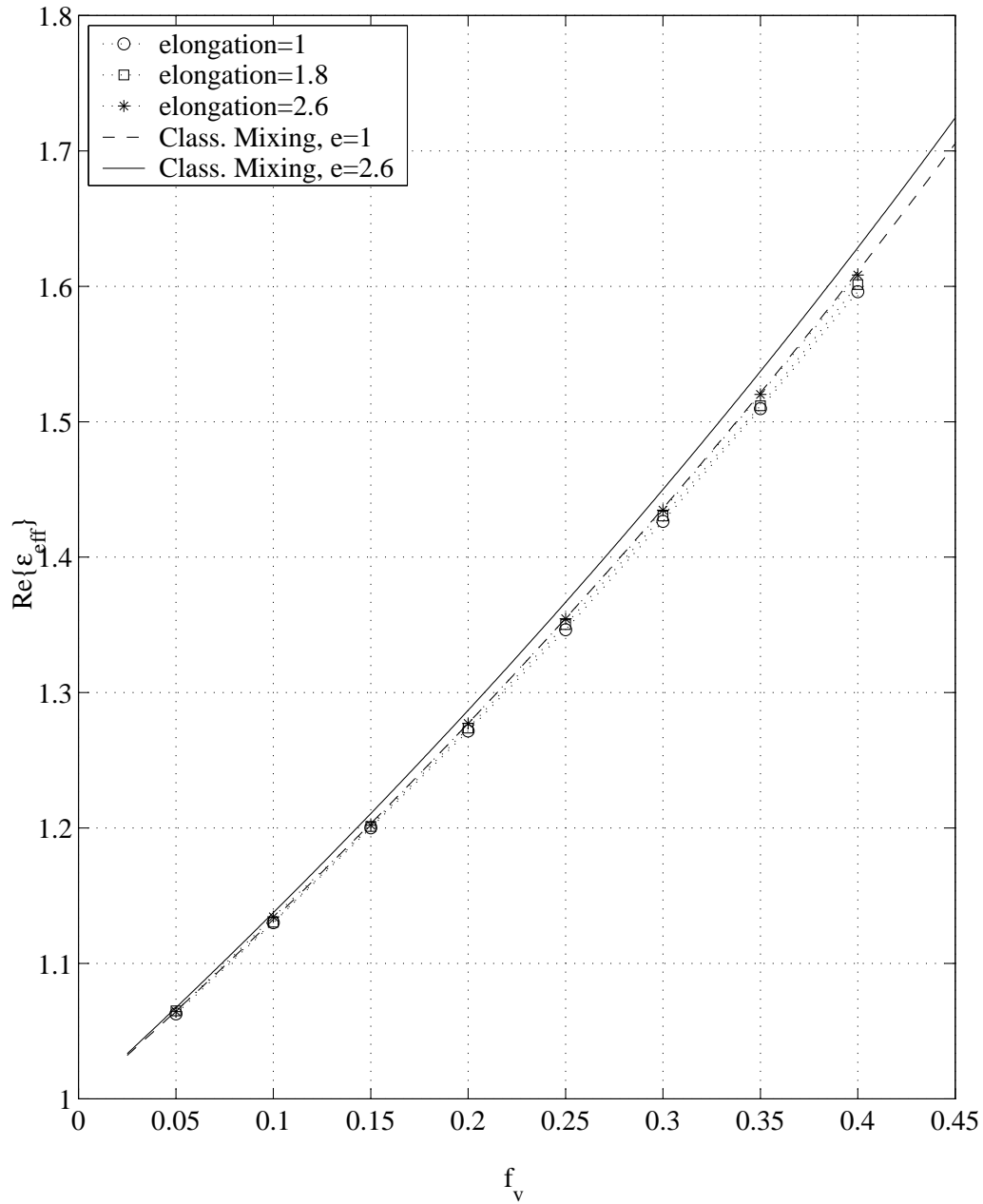


Figure 2-3: ϵ_{eff} as a function of fractional volume and elongation as compared to the classical mixing formula for $e=1$ and $e=2.6$.

These results provide numerical validation for the classical mixing formula for fractional volumes in the range of 0.05 to 0.4 for spheroids with elongations up to 2.6.

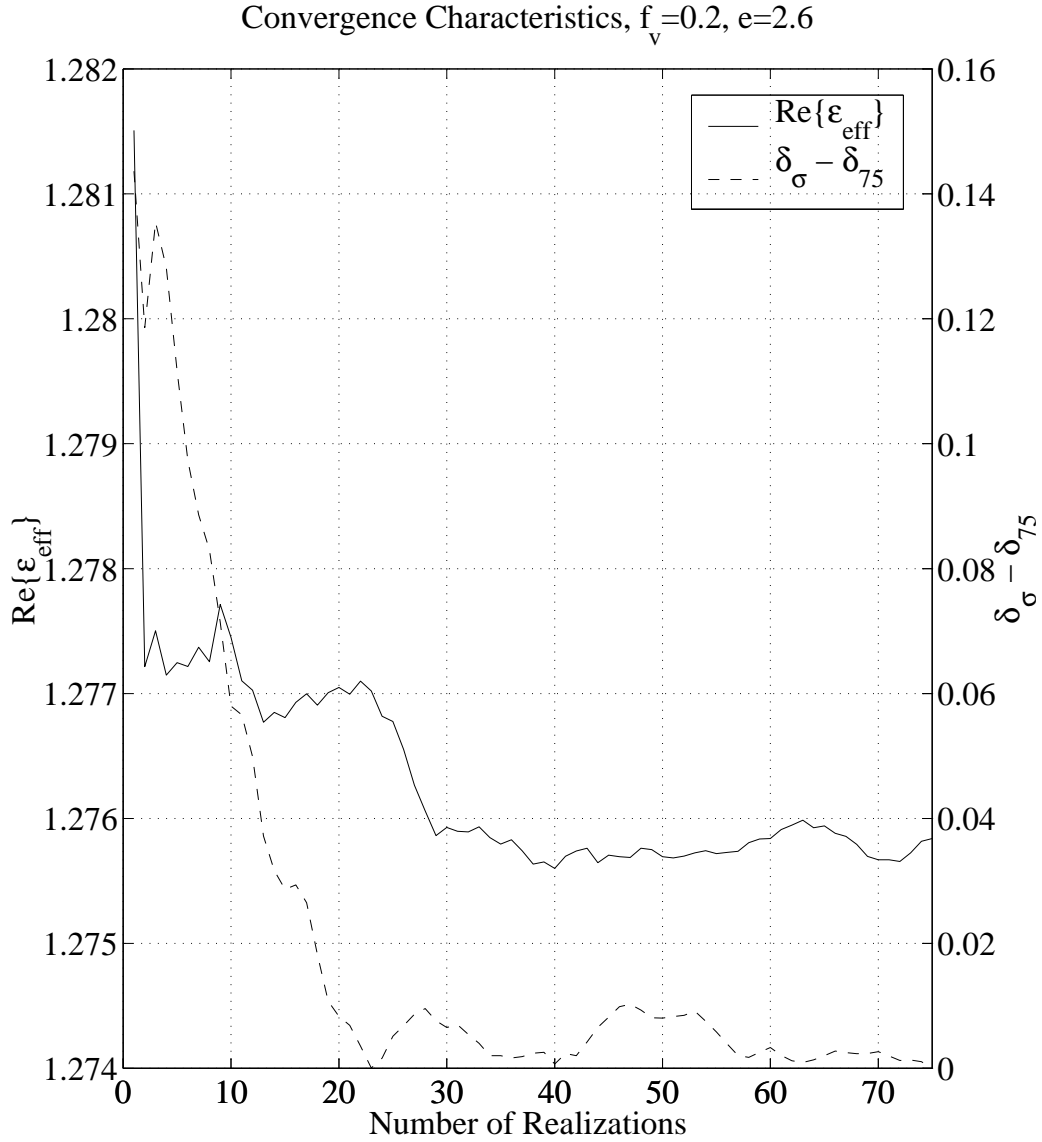


Figure 2-4: $\Re\{\epsilon_{\text{eff}}\}$ and the error term δ_σ (subtracted from the final error ($\delta_{75} = \delta_\sigma(N_r = 75)$) and normalized for $N_a=39$) resulting from the Nelder Mead simplex search according to realization number. This is for the case of $f_v=0.2$, $e=2.6$, $\epsilon_p=3.2$, $ka=0.2$, and $N_r=1 \dots 75$ realizations.

2.5 Conclusions

In this work, the effective permittivity (ϵ_{eff}) of dense random media was studied. The coherent scattered fields from a collection of particles in a given test volume were compared to fields scattered from a homogeneous volume of the same size and shape. The permittivity

	$e=1$	1.8	2.6
$f_v=0.05$	1.0628	1.0650	1.0645
0.10	1.1301	1.1304	1.1345
0.15	1.2001	1.2012	1.2021
0.20	1.2717	1.2738	1.2772
0.25	1.3465	1.3502	1.3546
0.30	1.4265	1.4304	1.4347
0.35	1.5097	1.5118	1.5202
0.40	1.5961	1.6014	1.6084

Table 2.1: Summary of ϵ_{eff} results. For all cases presented, $ka=0.2$ and $\epsilon_p=3.2$.

of the homogeneous medium which yielded scattered fields that best matched the averaged scattered fields produced by many configurations of particles was considered to be equal to ϵ_{eff} .

The effective permittivity of dense random media containing discrete spheroids was characterized through a Monte Carlo simulation employing the Method of Moments on the volume integral equation. The basis functions were chosen to be the electrostatic dipole solutions of a spheroid. Simulations with $N=3000$ particles, $N_r=50$ realizations and different fractional volumes ($f_v = 0.05-0.40$) and particle elongations ($e = 1.0-2.6$) were performed in a spherical test volume. The scattering from this volume was then compared to Mie scattering from a homogeneous sphere of the same size. Results indicate that ϵ_{eff} for a dense random medium containing randomly oriented discrete prolate spheroids agrees well with results from the classical mixing formula. This is consistent with previous studies considering spherical particles only.

Chapter 3

Sparse Matrix/Canonical Grid Method Applied to 3-D Dense Medium Simulations

3.1 Introduction

Electromagnetic scattering from and wave propagation in three-dimensional (3-D) discrete random media has been a topic of continued research due to its broad range of applications. For instance, in applications related to the remote sensing of the environment, the characterization of the electromagnetic wave interaction with natural media is of great importance. Natural media (e.g., snow, ice, and soil) often consist of a large number of densely packed, electrically small discrete scatterers that are randomly distributed in some background host medium (discrete random media). Moreover, many artificial materials (e.g., particulate composites) can also be characterized as being composed of randomly distributed scatterers in a host medium. Even some materials which can in principle be conceptualized and realized by regular, periodic arrangements, are often subject to random perturbations, both in terms of the positions, sizes and/or constitutive properties of the discrete scatterers.

For dense random media, several analytical methods based on wave theory, such as the quasi-crystalline approximation (QCA [12, 13]), the quasi-crystalline approximation with

coherent potential (QCA-CP [29]), or other approximations such as independent scattering and Foldy's approximation [11], are frequently employed. These analytical methods rely on basic simplifying assumptions about the media, such as tenuous media (low permittivity and permeability contrast), sparse media (low fractional volume of scatterers, typically less than 5%), or particle shape (*e.g.* spherical). These assumptions facilitate tractable analytical solutions but are not able to capture the essential physics of many real world problems. Moreover, it is often difficult to assess the range of validity of such analytical techniques *a priori*.

The alternative approach to deal with more complex media problems in a systematic manner is to resort to numerical techniques. Numerical methods such as the Method of Moments (MoM [18]), the finite difference time domain (FDTD [30, 31]), and related ones have allowed a partial relaxation of some of the limiting assumptions concerning the medium (Chapter 2 and [16]). In particular, the MoM provides a self-consistent solution which includes multiple interactions between discrete particles through an interaction (impedance) matrix $\overline{\overline{Z}}$. The main disadvantages of the MoM are the computation time required for solving the often large and dense resulting system of equations and the computer memory requirements for the storage of $\overline{\overline{Z}}$.

To help alleviate these bottlenecks, several so-called fast numerical methods have been developed in recent years for both 2-D and 3-D electromagnetic problems (*e.g.* [32, 33, 34, 35, 36, 37, 29, 38]). One of these fast methods, the Sparse Matrix/Canonical Grid (SMCG) method [39, 36, 40, 35, 41, 42], speeds up the solution of certain electromagnetic problems by decomposing the interaction matrix $\overline{\overline{Z}}$ into two separate matrices: a strong interaction matrix $\overline{\overline{Z}}^s$ which contains the interactions of nearby elements calculated exactly, and a weak interaction matrix $\overline{\overline{Z}}^w$ which contains an approximation of the weaker interaction terms from elements located farther apart. In contrast to Fast Multipole Methods (FMM), this procedure does not group interactions together, but rather approximates each individual weak interaction based on a canonical grid. The strong interaction matrix tends to be sparse while the vast majority of the interactions between elements are included in the weak interaction matrix. This latter matrix can be derived by a Taylor series expansion around a canonical grid [36, 42] or through the use of translation addition theorems [39, 29].

The advantage in doing this is that during the solution of $\overline{\overline{\mathbf{Z}}}$ using iterative solvers (as is frequently the case), the original full matrix-vector multiply $\overline{\overline{\mathbf{Z}}} \cdot \overline{\mathbf{x}}$ ($\mathcal{O}(N^2)$ complexity) may be replaced by a sparse matrix multiply, $\overline{\overline{\mathbf{Z}}}^s \cdot \overline{\mathbf{x}}$ ($\mathcal{O}(N)$) plus a Fast Fourier Transform (FFT) assisted multiply $\overline{\overline{\mathbf{Z}}}^w \cdot \overline{\mathbf{x}}$ ($\mathcal{O}(N \log N)$). This FFT assisted matrix-vector multiply is possible because of the multilevel block Toeplitz (MBT) structure inherent in $\overline{\overline{\mathbf{Z}}}^w$ as a result of the canonical grid expansion of the weak interactions.

In this work, we extend the SMCG method to 3-D case and consider its application to the scattering from complex media consisting of a collection of randomly positioned and oriented dielectric spheroids in a homogeneous host medium. In Section 3.2, we describe the MoM formulation of $\overline{\overline{\mathbf{Z}}}$ derived from a many-body volume integral equation. In Section 3.3, we describe the 3-D SMCG method in detail, including a discussion on the various tradeoffs associated with choosing the method parameters as well as the Taylor series expansion of the background dyadic Green's function around the canonical grid grid points. In Section 3.4, scattering results from these collections of spheroids calculated by the SMCG method are presented and compared to results obtained from the full MoM solution. Computation times, memory requirements, and accuracy for the approximated and full MoM solutions for cases of 500–15000 particles, varying neighborhood distances, Taylor series expansion orders of 0-5, and grids of $6 \times 6 \times 6$ to $14 \times 14 \times 14$ are also considered in Section 3.4. This is followed by conclusions in Section 3.5.

3.2 Formulation

The electric field $\overline{\mathbf{E}}(\overline{\mathbf{r}})$ in a random medium consisting of N arbitrary dielectric objects (discrete scatterers) with permittivity $\epsilon(\overline{\mathbf{r}}'_j)$ excited by an incident electric field $\overline{\mathbf{E}}_{inc}(\overline{\mathbf{r}})$ can be described by the volume integral equation (VIE) [43] through a summation over each scatterer, i.e.,

$$\overline{\mathbf{E}}(\overline{\mathbf{r}}) = \overline{\mathbf{E}}_{inc}(\overline{\mathbf{r}}) + \frac{k^2}{\epsilon} \sum_{j=1}^N \int_{V'_j} dV'_j (\epsilon(\overline{\mathbf{r}}'_j) - \epsilon) \overline{\overline{\mathbf{G}}}(\overline{\mathbf{r}}, \overline{\mathbf{r}}'_j) \cdot \overline{\mathbf{E}}(\overline{\mathbf{r}}'_j), \quad (3.1)$$

where V_j is the volume of scatterer j , k is the wavenumber of the homogeneous background medium, ϵ is the permittivity of the background medium, $\epsilon(\bar{r}'_j)$ is the permittivity inside the j^{th} scatterer. $\bar{\bar{G}}(\bar{r}, \bar{r}'_j)$ is the background generalized dyadic Green's function whose principal value is given by

$$\bar{\bar{G}}(\bar{r}, \bar{r}'_j) = \left[\bar{\bar{I}} + \frac{\nabla \nabla}{k^2} \right] g(\bar{r}, \bar{r}'_j), \quad (3.2)$$

which, to account for the singularity encountered when $\bar{r} = \bar{r}'_j$, should be written as [44, 29, 45]

$$\bar{\bar{G}}(\bar{r}, \bar{r}'_j) = P.V. \bar{\bar{G}}(\bar{r}, \bar{r}'_j) - \frac{\bar{\bar{L}} \delta(\bar{r} - \bar{r}'_j)}{k^2}. \quad (3.3)$$

where $P.V.$ stands for Principal Value. The exclusion volume dependent term in Eq. (3.3) becomes important when calculating the self interaction terms (see below). Finally, $g(\bar{r}, \bar{r}'_j)$ is the scalar Green's function,

$$g(\bar{r}, \bar{r}'_j) = \frac{e^{ik|\bar{r} - \bar{r}'_j|}}{4\pi|\bar{r} - \bar{r}'_j|}. \quad (3.4)$$

Primed variables indicate those variables pertaining to the scatterers while unprimed variables indicate quantities positioned outside the scatterers (background or host medium). The induced polarization inside each object due to the electric field at \bar{r}'_j is given by $\bar{P}(\bar{r}'_j) = (\epsilon(\bar{r}'_j) - \epsilon) \bar{E}(\bar{r}'_j)$ [from Eq. (3.1)].

To solve Eq. (3.1) using the Method of Moments (MoM), the electric field inside the each particle is expanded in a set of N_b basis functions, *e.g.* for the j^{th} particle,

$$\bar{E}(\bar{r}'_j) = \sum_{\alpha=1}^{N_b} c_{j\alpha} \bar{f}_{j\alpha}(\bar{r}'_j). \quad (3.5)$$

The basis functions $\bar{f}_{j\alpha}(\bar{r}'_j)$ for each particle can be chosen based on particle size and geometry as detailed later on. For our purposes, we will also assume that these basis functions are orthonormal:

$$\int_{V'_j} dV'_j \bar{f}_{j\alpha}(\bar{r}'_j) \cdot \bar{f}_{j\beta}(\bar{r}'_j) = \delta_{\alpha\beta}, \quad (3.6)$$

where $\delta_{\alpha\beta}$ is the Kronecker delta.

To find the field inside each object, we substitute Eq. (3.5) into Eq. (3.1) to arrive at

$$\left[\sum_{\beta=1}^{N_b} c_{i\beta} \bar{f}_{i\beta}(\bar{r}'_i) \right] = \bar{E}_{inc}(\bar{r}'_i) + \frac{k^2}{\epsilon} \sum_{j=1}^N \int_{V'_j} dV'_j (\epsilon(\bar{r}'_j) - \epsilon) \bar{G}(\bar{r}'_i, \bar{r}'_j) \cdot \left[\sum_{\alpha=1}^{N_b} c_{j\alpha} \bar{f}_{j\alpha}(\bar{r}'_j) \right]. \quad (3.7)$$

By invoking the orthonormality of the basis functions [Eq. (3.6)] and applying Galerkin's technique, Eq. (3.7) can be written as:

$$c_{i\beta} = \int_{V'_i} dV'_i \bar{f}_{i\beta}(\bar{r}'_i) \cdot \bar{E}_{inc}(\bar{r}'_i) + \sum_{j=1}^N \sum_{\alpha=1}^{N_b} c_{j\alpha} z_{ij,\alpha\beta}, \quad (3.8)$$

where

$$z_{ij,\alpha\beta} = B_j \int_{V'_i} dV'_i \int_{V'_j} dV'_j \bar{f}_{i\beta}(\bar{r}'_i) \cdot \bar{G}(\bar{r}'_i, \bar{r}'_j) \cdot \bar{f}_{j\alpha}(\bar{r}'_j), \quad (3.9)$$

with

$$B_j = \frac{k^2}{\epsilon} (\epsilon(\bar{r}'_j) - \epsilon). \quad (3.10)$$

The first term on the right hand side of Eq. (3.7) is determined by the incident field and is known for a given configuration while the other two terms describe the interaction matrix $\bar{\bar{Z}}$ with $c_{j\alpha}$ forming the unknown excitation vector \bar{x} . Suppose that the self term (that is, $i = j$, $\alpha = \beta$ term) in Eq. (3.8) is [16]

$$z_{ij,\alpha\beta}|_{i=j,\alpha=\beta} = C_{i\beta}, \quad (3.11)$$

then Eq. (3.8) can be recast into the matrix equation

$$\bar{\bar{Z}} \cdot \bar{x} = \bar{b}, \quad (3.12)$$

where

$$\bar{b} = \begin{bmatrix} \left[\begin{array}{c} \int_{V'_1} dV'_1 \bar{f}_{11}(\bar{r}'_1) \cdot \bar{E}_{inc}(\bar{r}'_1) \\ \int_{V'_1} dV'_1 \bar{f}_{12}(\bar{r}'_1) \cdot \bar{E}_{inc}(\bar{r}'_1) \\ \vdots \\ \int_{V'_1} dV'_1 \bar{f}_{1N_b}(\bar{r}'_1) \cdot \bar{E}_{inc}(\bar{r}'_1) \end{array} \right] \\ \vdots \\ \left[\begin{array}{c} \int_{V'_N} dV'_N \bar{f}_{N1}(\bar{r}'_N) \cdot \bar{E}_{inc}(\bar{r}'_N) \\ \int_{V'_N} dV'_N \bar{f}_{N2}(\bar{r}'_N) \cdot \bar{E}_{inc}(\bar{r}'_N) \\ \vdots \\ \int_{V'_N} dV'_N \bar{f}_{NN_b}(\bar{r}'_N) \cdot \bar{E}_{inc}(\bar{r}'_N) \end{array} \right] \end{bmatrix}. \quad (3.13)$$

Similarly

$$\bar{x} = \left[[c_{11}, c_{12}, \dots, c_{1N_b}], \dots, [c_{N1}, c_{N2}, \dots, c_{NN_b}] \right]^T, \quad (3.14)$$

and the $N_b \times N_b$ block of $\bar{\bar{Z}}$ which describes the interaction between particles i and j is given by

$$\bar{\bar{Z}}_{ij} = \begin{cases} \begin{bmatrix} z_{ij,11} & z_{ij,12} & \dots & z_{ij,1N_b} \\ z_{ij,21} & z_{ij,22} & & \\ \vdots & & \ddots & \vdots \\ z_{ij,N_b1} & & \dots & z_{ij,N_bN_b} \end{bmatrix} & i \neq j, \\ \begin{bmatrix} (1 - C_{i1}) & 0 & \dots & 0 \\ 0 & (1 - C_{i2}) & & \\ \vdots & & \ddots & \vdots \\ 0 & & \dots & (1 - C_{iN_b}) \end{bmatrix} & i = j, \end{cases} \quad (3.15)$$

where $\bar{\bar{Z}}$ is then understood to be

$$\bar{\bar{Z}} = \begin{bmatrix} \bar{\bar{Z}}_{11} & \bar{\bar{Z}}_{12} & \dots \\ \vdots & \ddots & \vdots \\ \bar{\bar{Z}}_{N_b1} & \dots & \bar{\bar{Z}}_{N_bN_b} \end{bmatrix}. \quad (3.16)$$

The size of $\bar{\bar{Z}}$ is $N_b N \times N_b N$, and the lengths of vectors \bar{x} and \bar{b} are $N_b N$. The calculation

of the self terms $C_{i\beta}$ are based on the electrostatic solution of spheroids and are described in detail in [16] Appendix A therein.

In this work, we consider identical prolate spheroidal particles at arbitrary locations and with arbitrary orientations. Assuming electrically small particles, we choose the basis functions to be the electrostatic solutions to the Laplace equation for a prolate spheroid. The interaction equation, Eq. (3.12), was derived above to show the generality of the method: for particles of different shapes, one need only choose appropriate basis functions (as many as needed) in order to calculate scattering from the collection. Also note that each individual particle need not be identical for the method described in Section 3.3 to be valid. Each particle may differ in shape, size, permittivity, *etc.* as long as the particle remains small enough compared to the wavelength (size parameter $ka \ll 1$) so that its response to $\bar{E}_{inc}(\bar{r})$ may be accurately modeled by a point response. For reference, the first three basis functions for the spheroid corresponding to the dipole solutions of the Laplace equation are given as

$$\bar{f}_{j1} = \hat{z}_{bj} \frac{1}{\sqrt{v_j}}, \quad (3.17a)$$

$$\bar{f}_{j2} = \hat{x}_{bj} \frac{1}{\sqrt{v_j}}, \quad (3.17b)$$

$$\bar{f}_{j3} = \hat{y}_{bj} \frac{1}{\sqrt{v_j}}. \quad (3.17c)$$

Here, \hat{x}_{bj} , \hat{y}_{bj} , and \hat{z}_{bj} are the principal axes of spheroid j . For the expressions of the higher order basis functions and further details concerning this MoM solution for the case of small prolate spheroids, the reader is referred to [16]. An example of one realization of a random medium filled with 30 spheroids with elongation $e = 1.8$, and fractional volume $f_v = 0.3$, contained a unit cube test volume is illustrated in Fig. 3-1.

3.3 3-D SMCG Method

Consider a medium filled with many discrete scatterers (*e.g.* spheroids, as in Fig. 3-1) at random positions and with random orientations contained in a cubic test volume. The

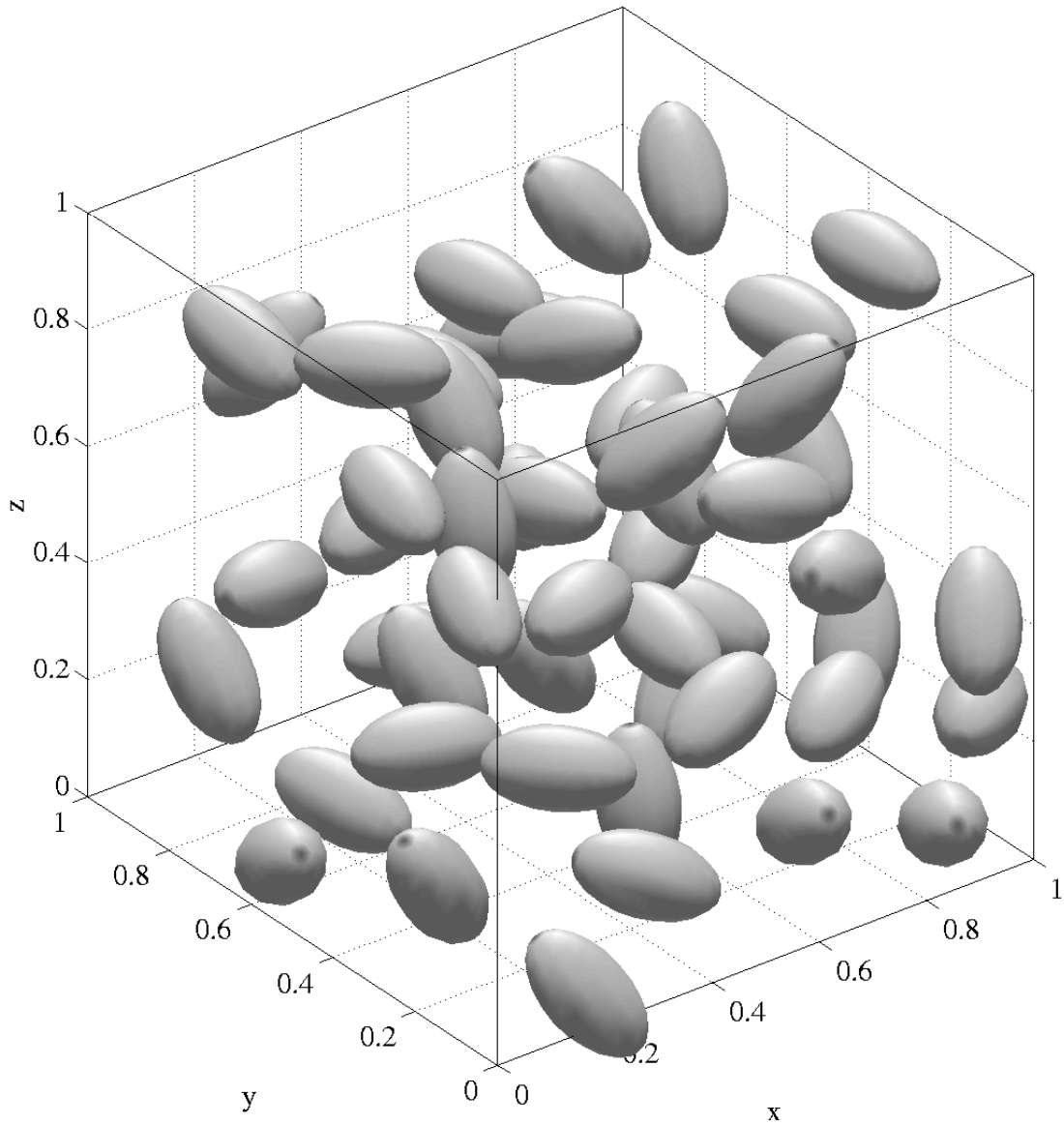


Figure 3-1: Densely packed medium consisting of 50 dielectric spheroids. Elongation=1.8, $f_v=0.1$.

dielectric spheroids have a statistical distribution realized by a shuffling process described in [16]. After a suitable distribution of N_{cube} particles is generated, the collection may be truncated to any shape. In our case we will truncate to a spherical test volume consisting of N_{sphere} particles.

3.3.1 SMCG Model Parameters

The Sparse Matrix/Canonical Grid (SMCG) method achieves reduced complexity and reduced memory requirements by assuming that scatterers are small enough so that accuracy is maintained though only point interactions are considered, and by decomposing the interaction matrix $\overline{\overline{Z}}$ into two separate matrices: the “strong” and “weak” interaction matrices. This decomposition is governed by a neighborhood distance, r_d , beyond which radius interactions are considered weak. The choice of the neighborhood distance is discussed in more detail in Section 3.3.2.

If the particles are small compared to the wavelength of the incident radiation, the induced electric field inside the particle can be considered constant and may therefore be accurately modeled by a dipole response located at the center of the particle. In this case, the integrals in Eqs. (3.7) and (3.13) may be replaced by the volume of that particle as:

$$\int_{V'_i} dV'_i \rightsquigarrow v_i = \frac{4}{3}\pi a_i^2 c_i, \quad (3.18)$$

where a_j is the length of the semiminor axis and $c_j = a_j e_j$ with e_j being the elongation or aspect ratio. The assumptions stated above allow the separation of $\overline{\overline{Z}}$ into three distinct matrices: 1) a pre-multiplying basis function matrix $\overline{\overline{f}}_i$ dependent on particle i , 2) the Green’s function kernel $\overline{\overline{G}}(\overline{\overline{r}}'_i, \overline{\overline{r}}'_j)$ (which now only depends on the distance separating the centers of particles i and j , R_{ij} [see Eq. (3.23)]), and 3) a post-multiplying basis function matrix $\overline{\overline{f}}_j$ dependent on j . In rectangular coordinates this becomes

$$\overline{\overline{Z}}_{ij} = \overline{\overline{f}}_i \cdot \overline{\overline{G}}(\overline{\overline{r}}'_i, \overline{\overline{r}}'_j) \cdot \overline{\overline{f}}_j \quad (3.19)$$

where

$$\bar{\bar{f}}_i = \begin{bmatrix} f_{i1,x} & f_{i1,y} & f_{i1,z} \\ \vdots & \vdots & \vdots \\ f_{iN_b,x} & f_{iN_b,y} & f_{iN_b,z} \end{bmatrix} \quad (3.20)$$

and

$$\bar{\bar{G}}(R_{ij}) = \begin{bmatrix} G_{xx}(R_{ij}) & G_{xy}(R_{ij}) & G_{xz}(R_{ij}) \\ G_{yx}(R_{ij}) & G_{yy}(R_{ij}) & G_{yz}(R_{ij}) \\ G_{zx}(R_{ij}) & G_{zy}(R_{ij}) & G_{zz}(R_{ij}) \end{bmatrix}. \quad (3.21)$$

Note that the pre-multiplying $\bar{\bar{f}}_j$ is the transpose of the post-multiplying $\bar{\bar{f}}_i$ if $i=j$. If ξ denotes x , y , or z , then the terms of Eq. (3.21) are

$$G_{\xi_1\xi_2}(R_{ij}) = g(R_{ij})\delta_{\xi_1\xi_2} + \frac{1}{k^2} \frac{\partial^2}{\partial\xi_1\partial\xi_2} g(R_{ij}), \quad (3.22)$$

where $g(R_{ij})$ is the scalar Green's function [Eq. (3.4)], again $\delta_{\xi_1\xi_2}$ is the Kronecker delta, and

$$R_{ij} = \sqrt{(x_i - x_j)^2 + (y_i - y_j)^2 + (z_i - z_j)^2}. \quad (3.23)$$

If $\bar{\bar{f}}$ is constructed by inserting $\bar{\bar{f}}_i$ into the appropriate columns (determined by grid point index) and rows (determined by particle index), then Eq. (3.19) can be expanded to include all particle interactions as

$$\bar{\bar{Z}} = \bar{\bar{f}} \cdot \bar{\bar{G}} \cdot \bar{\bar{f}}^T, \quad (3.24)$$

where $\bar{\bar{f}}^T$ denotes the transpose of $\bar{\bar{f}}$. Note that $\bar{\bar{f}}$ is sparse, while $\bar{\bar{G}}$ is a dense, $(NN_b) \times (NN_b)$ matrix containing the exact interactions between every pair of particles.

The next step in the SMCG method involves approximating the weak interaction between particles i and j in the interaction matrix $\bar{\bar{Z}}$ by a multivariate Taylor series expansion of $\bar{\bar{G}}(R_{ij})$ about the grid points nearest to the particles i and j , respectively. Let this approximated matrix be $\bar{\bar{Z}}^w$ defined according to the following. Let a cubic lattice be superimposed onto the test volume with $N_{g,x}$, $N_{g,y}$, and $N_{g,z}$ lattice points, or grid points, in the x , y ,

and z dimensions, respectively. For all of the simulations considered in this work,

$$N_{g,x} = N_{g,y} = N_{g,z} = N_g \quad (3.25)$$

with

$$N_{g,i} = \frac{(i-1) + \frac{1}{2}}{N_g} \quad (3.26)$$

for grid points located in a unit cube. The spacing between grid points is then $\Delta r_g = 1/N_g$. All those interactions located further apart than the predetermined neighborhood distance are considered “weak” interactions. Thus, decomposing $\overline{\overline{Z}}$ through the relation

$$\overline{\overline{G}} = \overline{\overline{G}}(\mathcal{R}_s) + \overline{\overline{G}}^{\text{cg}}(\mathcal{R}_w), \quad (3.27)$$

for all $i, j = 1 \dots N$ where \mathcal{R}_s denotes the set of distances between pairs of particles whose interactions are considered strong, and \mathcal{R}_w is a set containing all other pair interactions (considered weak), Eq. (3.19) can be written as

$$\begin{aligned} \overline{\overline{Z}} &= \overline{\overline{Z}}^s + \overline{\overline{Z}}^w \\ &= \underbrace{\overline{\overline{f}} \cdot \overline{\overline{G}}(\mathcal{R}_s) \cdot \overline{\overline{f}}^T}_{\overline{\overline{Z}}^s} + \underbrace{\overline{\overline{f}} \cdot \overline{\overline{G}}^{\text{cg}}(\mathcal{R}_w) \cdot \overline{\overline{f}}^T}_{\overline{\overline{Z}}^w} \end{aligned} \quad (3.28)$$

where the superscript “cg” denotes an approximation based on the distance between the particle and its associated canonical grid point located at \bar{r}_g . \mathcal{R}_s and \mathcal{R}_w are mutually exclusive sets with $\mathcal{R}_s \cup \mathcal{R}_w = R$. $\overline{\overline{G}}(\mathcal{R}_s)$ contains the exact Green’s function between particles only in close proximity (closer than r_d) while all other entries are set to 0. $\overline{\overline{G}}(\mathcal{R}_s)$ is the same size as $\overline{\overline{G}}$ from Eq. (3.24), but is sparse. $\overline{\overline{G}}^{\text{cg}}(\mathcal{R}_w)$ is also the same size as $\overline{\overline{G}}$ and contains an approximation of the remaining weak interactions. $\overline{\overline{G}}^{\text{cg}}(\mathcal{R}_w)$ is actually a sum of as many matrices as is required for the expansion (see Table 3.2). The derivation of $\overline{\overline{G}}^{\text{cg}}(\mathcal{R}_w)$ as well as fast methods for the subsequent matrix-vector multiply will be discussed below.

3.3.2 Parameter Considerations

A natural question at this point is: beyond what distance should interactions be considered “weak”? The distance at which the separation occurs is called the neighborhood distance (r_d) and is defined in terms of the number of grid points away from the grid point of interest. It is clear that the choice for r_d influences both the accuracy of the results using the SMCG method and the computation time required. On one hand, for small r_d (< 1 inter-grid point space Δr_g), approximation errors tend to accumulate and cause the iterative solver of Eq. (3.28) either to not converge or converge to incorrect values. On the other hand, a large r_d causes a greater number of interactions to be classified as “strong” and the SMCG method reverts to a full iterative approach. Reasonable r_d values from simulations are between 1 and 2 grid points.

The neighborhood distance must be defined in terms of grid points because for weak interactions, particles interact through the Green’s function matrix $\overline{\overline{G}}^{\text{cg}}(\mathcal{R}_w)$ which is defined only in terms of the number of grid points and their respective locations (see Section 3.3.3). Thus, all particles associated with grid points closer than r_d (measured with respect to the inter-grid point distance) will have strong interactions with the particle under consideration, while those particles associated with grid points which are located further away than r_d are classified as weak interactions. In this way, r_d defines the strong interaction cloud (or molecule) which is illustrated in Fig. 3-2 for three spheroids S_1 , S_2 , and S_3 with $N_g = 3$. Table 3.1 lists the number of grid points included in the strong interaction cloud (g_{r_d}) for the first few ranges of r_d .

Range of r_d (# of Δr_g)	g_{r_d}
$0 < r_d \leq 1$	1
$1 < r_d \leq \sqrt{2}$	7
$\sqrt{2} < r_d \leq 2$	19
$2 < r_d \leq \sqrt{5}$	33
\vdots	

Table 3.1: Number of surrounding gridpoints, g_{r_d} , included in the strong interaction cloud as a function of neighborhood distance r_d .

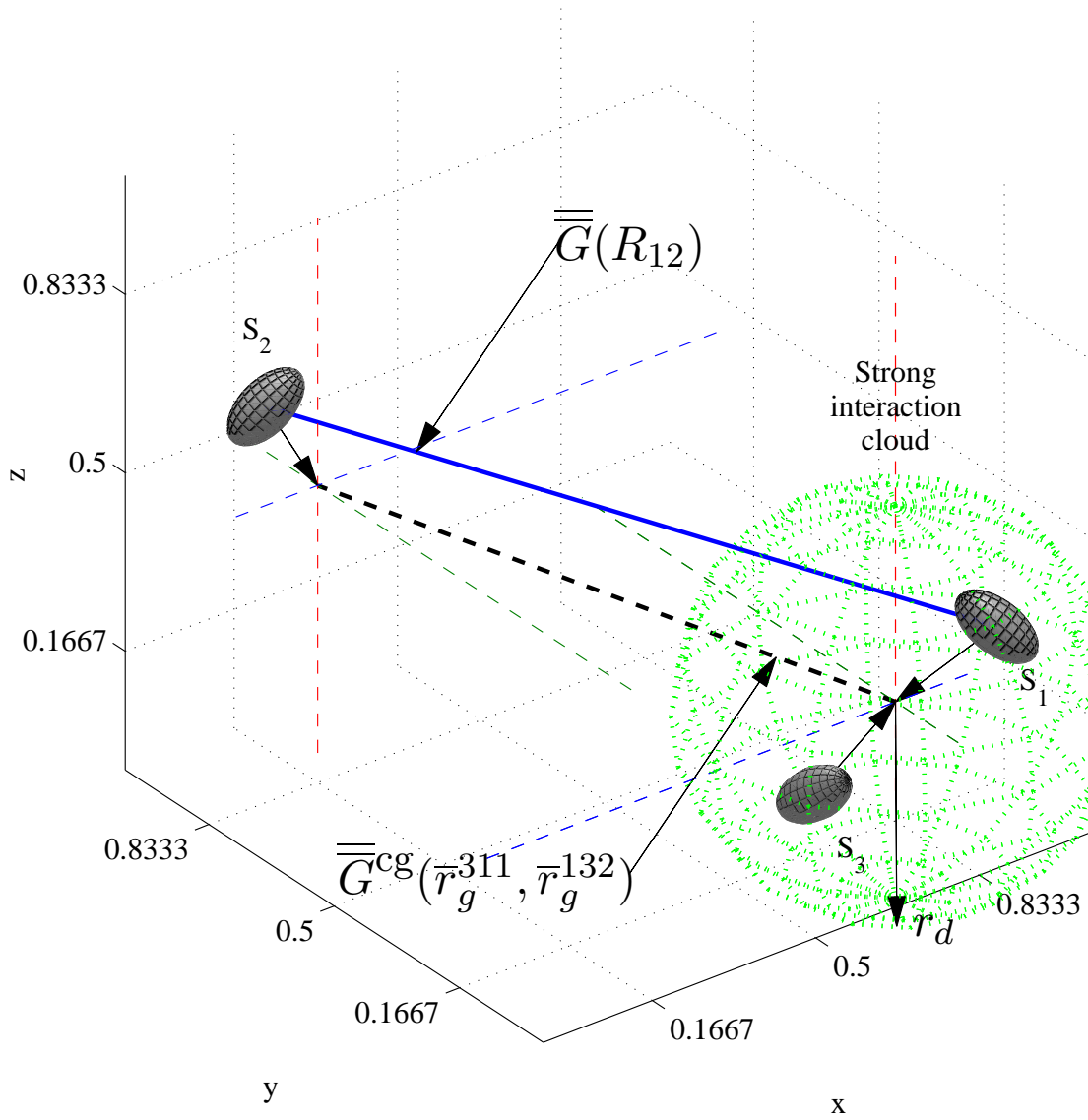


Figure 3-2: Strong interaction cloud with $r_d=1.1$. Spheroids S_1 and S_3 are closest to the same grid point and thus their interaction is included in $\bar{\bar{Z}}^s$. Spheroid S_2 is beyond r_d and thus its exact interactions with both S_1 ($\bar{\bar{G}}(R_{12})$) shown as a thick solid line between S_1 and S_2) and S_3 are approximated as $\bar{\bar{G}}^{cg}(\bar{r}_g^{311}, \bar{r}_g^{132})$ and included in $\bar{\bar{Z}}^w$.

One related question is, how fine or coarse of a grid is necessary or optimum for a given collection of scatterers? At the very least, there must be as many or fewer undulations (local extrema) in $\overline{\overline{G}}$ between gridpoints as the order of the Taylor series expansion (γ) for it to be possible for $\overline{\overline{G}}^{\text{cg}}$ to approximate $\overline{\overline{G}}$ adequately. In terms of computation time, the number of multiplies M^s required during each iteration of the iterative solver for $\overline{\overline{Z}}^s \cdot \overline{x}$ from Eq. (3.28) is $\mathcal{O}(N)$. M^s can be approximated as the average number of interactions with each particle from other particles associated with the same gridpoint, multiplied by the number of gridpoints in the strong interaction cloud, and multiplied again by the number of spheroids, *i.e.*

$$M^s = N \left(\frac{N}{N_g^3} \right) g_{rd}. \quad (3.29)$$

Because $1/N_g^3 \ll 1$, M^s is $\mathcal{O}(N)$ unless N_g is small and/or g_{rd} is large.

The number of multiplies M^w required during each iteration of the iterative solver for $\overline{\overline{Z}}^w \cdot \overline{x}$ in Eq. (3.28) depends on the FFT length ($\approx 8N_g^3$ for $\overline{\overline{G}}^{\text{cg}}(N_g)$, see Eq. (3.43)) and the number of expansion matrices (N_T , see Section 3.3.3 Table 3.2). Thus, if we estimate the number of multiplies required for an N -length FFT as $N \log_2 N$, M^w is

$$M^w = 8N_g^3 (\log_2(8N_g^3)) N_T. \quad (3.30)$$

Therefore, the total number of multiplies M for one iteration can be estimated by $M = M^w + M^s$. The N_g which minimizes this function can be found by solving the following transcendental equation for N_g given g_{rd} and N_T ,

$$\frac{-3N^2 g_{rd}}{N_g^4} + 24N_g^2 N_T \left(\log_2(8N_g^3) + \frac{1}{\ln 2} \right) = 0. \quad (3.31)$$

Equation (3.31) provides an estimate of the number of grid points which minimizes computation time as a function of the neighborhood distance and the expansion order.

The approximation error due to the SMCG method decreases if a larger r_d is chosen because more terms are being counted in the strong interaction cloud and computed exactly. This error will also decrease if N_g is chosen larger because a finer mesh implies that the Taylor series will estimate functions over smaller regions. In other words, the Taylor

approximation will have less error because it is fitted to a smoother function. The effect on computation time and accuracy of the expansion order, r_d , and N_g can be seen in the results listed in Table 3.3.

3.3.3 3-D Dyadic Green's Function Approximation

After the parameters of the 3-D SMCG method have been chosen, weak particle interactions are approximated by expanding the background dyadic Green's function about distance between the grid points nearest to each pair of particles. Let each particle located at \bar{r}_i be associated with its nearest grid point $g^{l_i m_i n_i}$ located at $\bar{r}_g^{l_i m_i n_i}$ where l_i , m_i , and n_i are grid point indices in the x , y , and z dimensions respectively and are integers in the range

$$1 \leq \{l_i, m_i, n_i\} \leq N_g, \quad \forall i = 1, \dots, N. \quad (3.32)$$

If particles i and j are associated with grid points $g^{l_i m_i n_i}$ and $g^{l_j m_j n_j}$ located at $\bar{r}_g^{l_i m_i n_i}$ and $\bar{r}_g^{l_j m_j n_j}$ respectively, $\bar{G}(R_{ij})$, defined in rectangular coordinates by Eq. (3.21), can be approximated by a γ^{th} order Taylor series expansion \bar{G}^{cg} as

$$\bar{G}_{ij}^{cg}(\mathcal{R}_w) = \sum_{\gamma=0}^{\infty} \left(\sum_{\xi=x,y,z} \Delta \xi_{ij} \frac{\partial}{\partial \xi} \right)^{\gamma} \frac{\bar{G}(\bar{r}_g^{l_i m_i n_i}, \bar{r}_g^{l_j m_j n_j})}{\gamma!}, \quad (3.33)$$

or via the trinomial theorem as

$$\bar{G}_{ij}^{cg}(\mathcal{R}_w) = \sum_{\gamma=0}^{\infty} \sum_{\gamma_x + \gamma_y + \gamma_z = \gamma} \left(\frac{1}{\gamma_x! \gamma_y! \gamma_z!} \right) \times \left\{ \prod_{\xi=x,y,z} (\Delta \xi_{ij})^{\gamma_{\xi}} \right\} \frac{\partial^{\gamma_x}}{\partial x^{\gamma_x}} \frac{\partial^{\gamma_y}}{\partial y^{\gamma_y}} \frac{\partial^{\gamma_z}}{\partial z^{\gamma_z}} \bar{G}(\bar{r}_g^{l_i m_i n_i}, \bar{r}_g^{l_j m_j n_j}) \quad (3.34)$$

where

$$\begin{aligned} \Delta \xi_{ij} &= \Delta \xi_i - \Delta \xi_j \\ &= (\bar{r}_{i,\xi} - \bar{r}_{g,\xi}^{l_i m_i n_i}) - (\bar{r}_{j,\xi} - \bar{r}_{g,\xi}^{l_j m_j n_j}), \end{aligned} \quad (3.35)$$

and again ξ is a placeholder for x , y , or z . $\overline{\overline{G}}^{\text{cg}}(\mathcal{R}_w)$ from Eq. (3.28) is realized by Eq. (3.33) over all values of i and j and depends only on grid point locations \overline{r}_g and the *relative* distance of each particle from its associated grid point.

Note that the relative distances $\Delta\xi_i$ in Eq. (3.33), are the only quantities which are particle specific and that they are scalars. Accordingly, we move these particle dependent quantities into \overline{f} by multiplying \overline{f}_i by $\Delta\xi_i$ over \overline{f} [*c.f.* Eqs. (3.19)–(3.24)], *i.e.*

$$\overline{f}_{\gamma_x\gamma_y\gamma_z} \equiv \left(\prod_{\xi=x,y,z} (\Delta\xi_i)^{\gamma_\xi} \right) \overline{f}_i, \quad \forall i = 1..N. \quad (3.36)$$

The remaining terms in Eq. (3.34) are dependent only upon the grid points, we define

$$\overline{\overline{G}}_{\gamma_x\gamma_y\gamma_z} \equiv \left(\frac{1}{\gamma_x!\gamma_y!\gamma_z!} \right) \frac{\partial^{\gamma_x}}{\partial x^{\gamma_x}} \frac{\partial^{\gamma_y}}{\partial y^{\gamma_y}} \frac{\partial^{\gamma_z}}{\partial z^{\gamma_z}} \overline{\overline{G}}(\overline{r}^{\Delta l \Delta m \Delta n}) \quad (3.37)$$

where $\overline{\overline{G}}(\overline{r}^{\Delta l \Delta m \Delta n})$ is an $3N \times 3N$ matrix defined by Eq. (3.21) with R_{ij} defined by Eq. (3.23) being the distance between grid points located at $\overline{r}_g^{l_i m_i n_i}$ and $\overline{r}_g^{l_j m_j n_j}$. Because of the translational invariance of the dyadic Green's function, the entries of $\overline{\overline{G}}(\overline{r}^{\Delta l \Delta m \Delta n})$ depend only on the differential number of grid points Δl , Δm , and Δn if the ordering of l , m , and n are sequential along the axes.

The i subscript in Eq. (3.36) corresponds to a pre-multiplication of $\overline{\overline{G}}_{\gamma_x\gamma_y\gamma_z}$ and can be thought of as a “source” particle from which radiation is being emitted, while the similar post-multiplication matrix corresponding to the j subscript would be $\overline{\overline{f}}_{\gamma_x\gamma_y\gamma_z}^{\text{T}}$ and is analogous to a “sink” particle with an induced electric field caused (in part) by particle i .

Using the definitions above, we can now expand the weak interaction matrix $\overline{\overline{Z}}^{\text{w}}$ as

$$\begin{aligned} \overline{\overline{Z}}^{\text{w}} &= \overline{f} \cdot \overline{\overline{G}}^{\text{cg}}(\mathcal{R}_w) \cdot \overline{\overline{f}}^{\text{T}} \\ &= \sum_{\gamma=0}^{\infty} \sum_{\gamma_x+\gamma_y+\gamma_z=\gamma} \overline{\overline{Z}}_{\gamma_x\gamma_y\gamma_z}^{\text{w}} \end{aligned} \quad (3.38)$$

where

$$\overline{\overline{Z}}_{\gamma_x \gamma_y \gamma_z}^w = \sum_{\left[\begin{array}{l} \gamma_{x_1} + \gamma_{x_2} = \gamma_x \\ \gamma_{y_1} + \gamma_{y_2} = \gamma_y \\ \gamma_{z_1} + \gamma_{z_2} = \gamma_z \end{array} \right]} \Lambda \overline{\overline{f}}_{\gamma_{x_1} \gamma_{y_1} \gamma_{z_1}} \overline{\overline{G}}_{\gamma_x \gamma_y \gamma_z} \overline{\overline{f}}_{\gamma_{x_2} \gamma_{y_2} \gamma_{z_2}}^T \quad (3.39)$$

and where

$$\Lambda = (-1)^{\gamma_{x_2} + \gamma_{y_2} + \gamma_{z_2}} \begin{pmatrix} \gamma_x \\ \gamma_{x_2} \end{pmatrix} \begin{pmatrix} \gamma_y \\ \gamma_{y_2} \end{pmatrix} \begin{pmatrix} \gamma_z \\ \gamma_{z_2} \end{pmatrix}. \quad (3.40)$$

The γ_{ξ_1} and γ_{ξ_2} in Eq. (3.39) are integers which take on all combinations in the interval $[0, \gamma_\xi]$ which satisfy $\gamma_{\xi_1} + \gamma_{\xi_2} = \gamma_\xi$. For example, in the second order ($\gamma=2$) Taylor series expansion, $\overline{\overline{Z}}^w$ would be approximated by 6 terms as

$$\overline{\overline{Z}}^w \approx \overline{\overline{Z}}_{200}^w + \overline{\overline{Z}}_{110}^w + \overline{\overline{Z}}_{101}^w + \overline{\overline{Z}}_{020}^w + \overline{\overline{Z}}_{011}^w + \overline{\overline{Z}}_{002}^w, \quad (3.41)$$

and, for example, the $\gamma_x=2, \gamma_y=0, \gamma_z=0$ ($\overline{\overline{Z}}_{200}^w$) term would be [from Eq. (3.39)]

$$\overline{\overline{Z}}_{200}^w = \overline{\overline{f}}_{200} \overline{\overline{G}}_{200} \overline{\overline{f}}_{000}^T - 2\overline{\overline{f}}_{100} \overline{\overline{G}}_{200} \overline{\overline{f}}_{100}^T + \overline{\overline{f}}_{000} \overline{\overline{G}}_{200} \overline{\overline{f}}_{200}^T \quad (3.42)$$

with $\overline{\overline{f}}_{000} = \overline{\overline{f}}$ from Eq. (3.36). Lastly, if $(\epsilon(\overline{\tau}'_j) - \epsilon)$ is particle dependent, $\frac{k^2}{\epsilon}(\epsilon(\overline{\tau}'_j) - \epsilon)$ from Eq. (3.10) should also be multiplied into either the pre- or post- $\overline{\overline{f}}$ multiplication in a fashion similar to that of Eq. (3.36).

The reduction in computational complexity and memory requirements is realized by exploiting the structure inherent to $\overline{\overline{G}}_{\gamma_x \gamma_y \gamma_z}$. As mentioned earlier, the Green's function matrix is highly redundant if the grid is ordered sequentially. In fact, $\overline{\overline{G}}_{\gamma_x \gamma_y \gamma_z}$ can be classified as a multilevel block Toeplitz (MBT) matrix with $M = 3$ levels, of size $N_{g,x}, N_{g,x}, N_{g,x}$ respectively, with the final level being a dense 3×3 block (Appendix A). Matrix-vector multiplies of MBT matrices can be achieved in $\mathcal{O}(N_{FFT} \log N_{FFT})$ operations, instead of $\mathcal{O}(N^2)$, where N_{FFT} is the FFT length defined as

$$N_{FFT} = 9 \left(\prod_{\xi=x,y,z} (2N_{g,\xi} - 1) \right). \quad (3.43)$$

For each unique vector, the matrix-vector multiply involving an MBT matrix requires another FFT with length given by Eq. (3.43). In terms of Eq. (3.39), because $\overline{\overline{G}}_{\gamma_x \gamma_y \gamma_z}$ remains unchanged for the same N_g and background wavenumber k , the FFT of the expansion matrices $\overline{\overline{G}}_{\gamma_x \gamma_y \gamma_z}$ may be performed once and stored. Then for each step in the iterative solution, one FFT must be performed for each unique combination of $\overline{\overline{f}}_{\gamma_{x_2} \gamma_{y_2} \gamma_{z_2}}^T$ and $\overline{\overline{x}}$, and likewise an inverse FFT must be calculated for each unique $\overline{\overline{f}}_{\gamma_{x_1} \gamma_{y_1} \gamma_{z_1}}$. Table 3.2 lists the total number of transforms performed for a single $\overline{\overline{Z}}^w \cdot \overline{\overline{x}}$ multiply using the canonical grid expansion (N_T).

Expansion order (γ)	Number of expansion terms ($\overline{\overline{G}}_{\gamma_x \gamma_y \gamma_z}$)	N_T
0	1	2
1	3	8
2	6	20
3	10	40
4	15	70
5	21	112

Table 3.2: Number of expansion terms and total number of FFTs (both forward and inverse) for expansion order γ .

Utilizing this 3-D SMCG method, the total complexity of solving Eq. (3.12) is reduced from $\mathcal{O}(KN^2)$ to $\mathcal{O}(KN_T N \log N)$ where K is the number of steps required for the iterative solver to converge. In Section 3.4, the 3-D SMCG method is shown to indeed realize results which require much less computation time while maintaining a desired tolerance.

3.4 Results

In this section, we apply the 3-D SMCG method to finding the scattering from a large collection of randomly distributed and oriented spheroids contained in a spherical test volume. Each of the $N_{cube}=500-15000$ spheroids considered are identical with respect to size, shape, and permittivity ($\epsilon(\overline{\overline{r}}'_j)$). The size parameter ka for each spheroid is 0.2. Likewise, the fractional volume of the spheroids in the test volume is 20%. Only the dipole basis functions of Eq. (3.17) are employed, i.e., $N_b = 3$. Thus, there are a maximum of 45000 unknown coefficients $c_{j\alpha}$ to solve for. For a given N_{cube} , the same randomly generated configuration

was used for all combinations of γ , r_d , and N_g . All results were computed on a Compaq Alphaserver DS20E with 4GB of RAM.

Four parameters dictate the resulting accuracy and computation time of the SMCG method as compared to the full MoM method. While the computation time of the full method depends only on the number of spheroids in the test volume N_{sphere} , the SMCG method additionally depends on the neighborhood distance r_d , the Taylor series expansion order γ , and the number of grid points N_g in each dimension. The relationship between expansion order and computation time and accuracy is illustrated in Fig. 3-3 where expansion orders from $\gamma=0$ to $\gamma=5$ were considered. Note that $\gamma=0$ corresponds physically to approximating all of the spheroids as actually being located at their respective (nearest) grid points.

As a measure of the “distance” of the approximated scattering results from those given by the full method, the Kullback-Leibler distance [46] is used, *i.e.*,

$$p(\sigma_T|\sigma) = \sum_{n=1}^{N_\theta} \left| \sigma_T(n) \log \frac{\sigma_T(n)}{\sigma(n)} \right| / N_\theta \quad (3.44)$$

where σ is the radar cross section (RCS) resulting from the full solution and σ_T is the approximated RCS calculated using the SMCG method. The RCSs are computed from the dipole excitation strengths [16] at $N_\theta=200$ distinct angles. An example can be seen in Fig. 3-6. As expected, for increasing expansion order and grid size, computation time increases dramatically until it approaches the computation time of the full solution. However, for $\gamma=2$, most grid sizes maintain a small Kullback-Leibler distance, while realizing an substantial reduction in computation time.

The effect of varying the neighborhood distance r_d is shown in Fig. 3-4. As the neighborhood distance increases from $0.1\Delta r_g$ to $2.1\Delta r_g$, the marginal speed of the SMCG method approaches the marginal speed of the full method (*i.e.* the slope of the curves are similar) due to many strong interactions being included in $\bar{\bar{Z}}^s$ instead of being approximated in $\bar{\bar{Z}}^w$. As a general trend, the Kullback-Leibler distance in Fig. 3-4 is smaller for larger r_d for the same reason.

Figure 3-5 shows computation times and Kullback-Leibler distances for the same set of

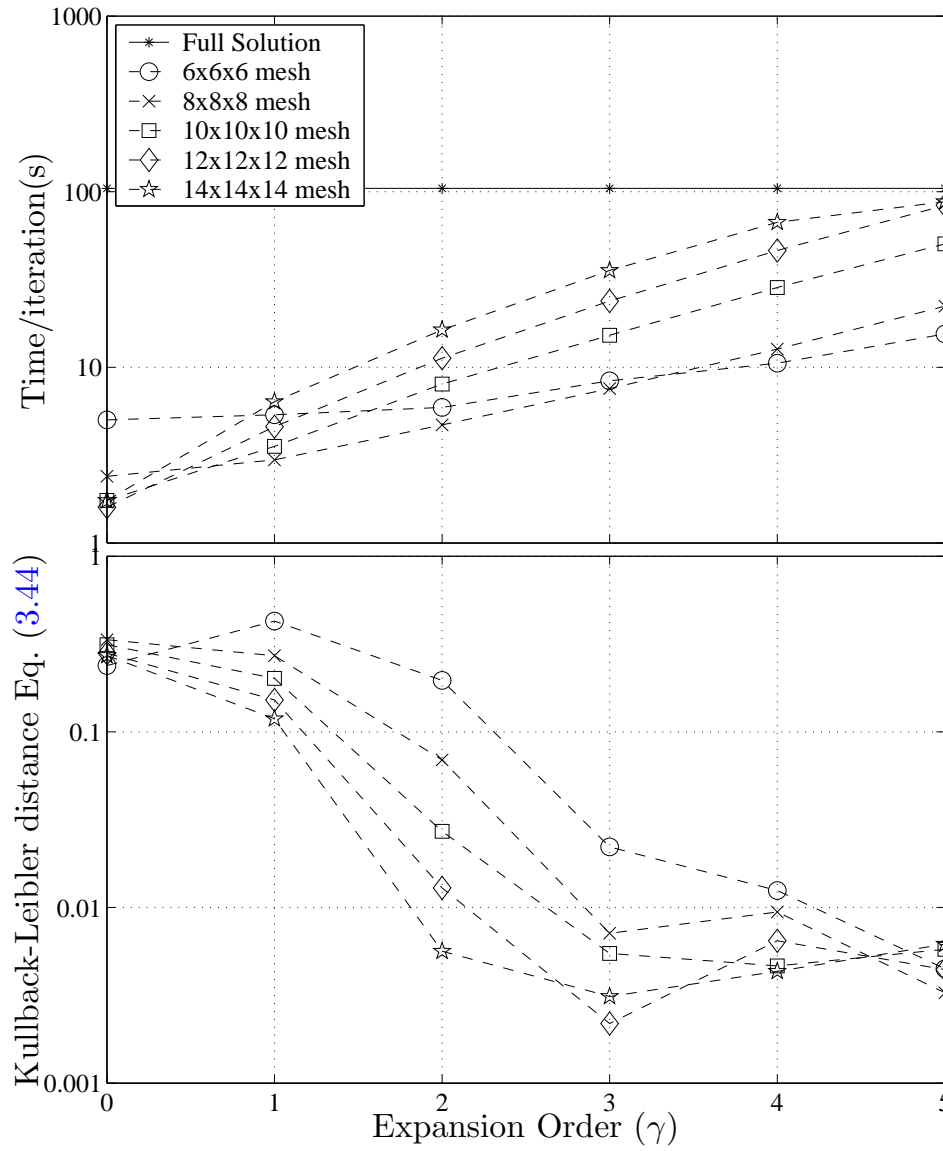


Figure 3-3: Computation times and Kullback-Leibler distances for SMCG method for $\gamma=0-5$ with $r_d=1.1\Delta r_g$ and $N_{cube}=10000$.

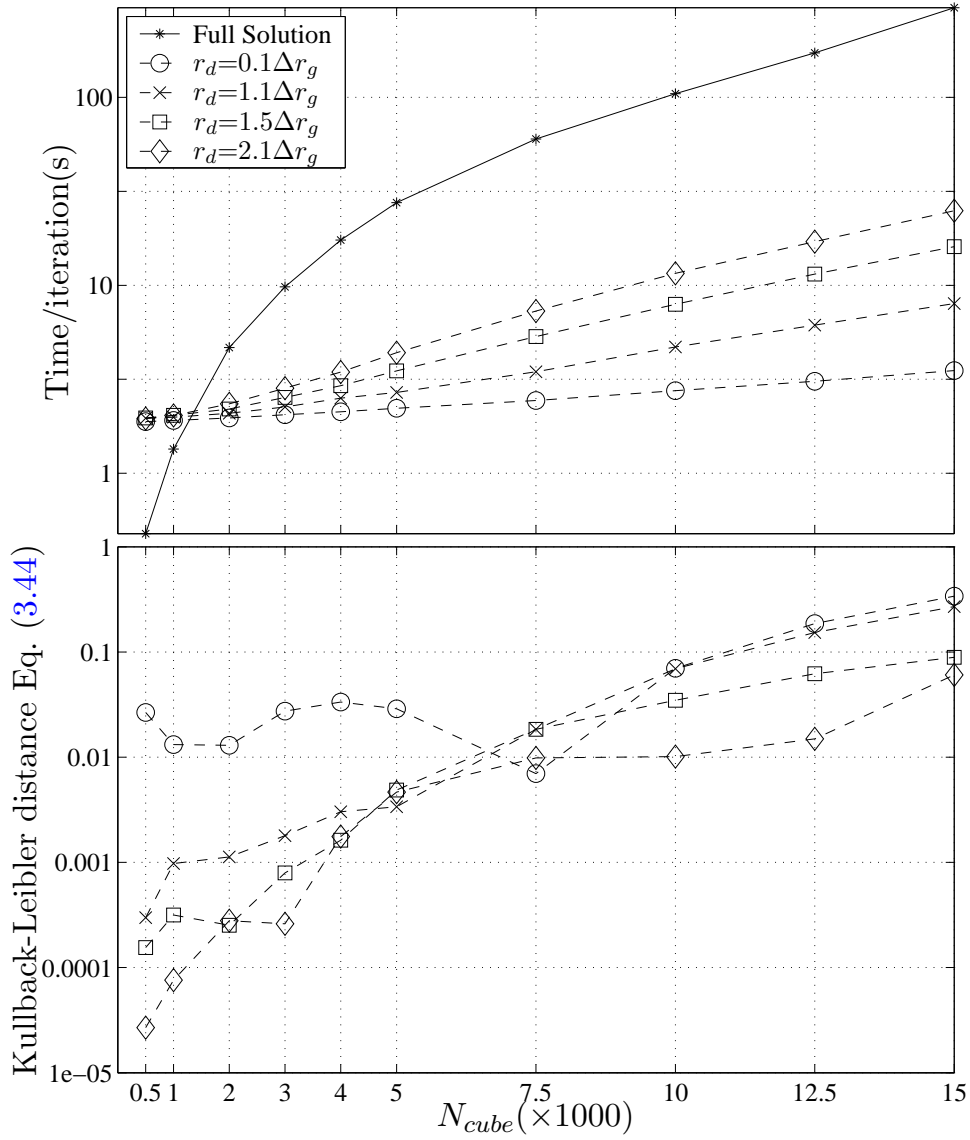


Figure 3-4: Computation times and Kullback-Leibler distances for SMCG method for $r_d=0.1-2.1\Delta r_g$ with $\gamma=2$ and $N_g=8$.

data as Fig. 3-4 except that r_d is kept at $r_d=1.1\Delta r_g$, while the number of grid points is varied from $N_g = 6$ to $N_g = 14$. Note that for finer meshes, the FFT computation time dominates the overall computation time, which results in very flat curves with respect to N_{cube} . This also illustrates the tradeoff between grid size and the neighborhood distance discussed in more detail in Section 3.3.2. The final figure, Fig. 3-6, shows the convergence of σ_T to σ for successively accurate model parameters, and Table 3.3 records pertinent computation times and Kullback-Leibler distances for a number of cases.

Memory requirements can be estimated by the number of expansion matrices $\overline{\overline{G}}_{\gamma_x\gamma_y\gamma_z}$ stored (times 2 including \overline{x}) multiplied by the length of each of those matrices given by Eq. (3.43). The memory required for the SMCG method is thus seen to be $\mathcal{O}(N)$ as compared to $\mathcal{O}(N^2)$ for the full method. As a final note, this SMCG algorithm is easily adapted to other types of particles such as spheres, crystals, dust grains, etc., for which the basis functions are known. This method may be used in a way which imitates the Discrete Dipole Approximation (DDA) (Appendix A and [47, 48]), and the author has used this method to find the effective permittivity of collections of randomly distributed spheroids (Chapter 2).

3.5 Conclusions

The sparse matrix canonical grid (SMCG) method has been extended to 3-D and illustrated by finding the scattering from random media filled with dielectric spheroids at random positions and orientations. The 3-D SMCG method achieves $\mathcal{O}(N \log N)$ complexity instead of $\mathcal{O}(N^2)$ for the matrix-vector multiply when using an iterative solver by decomposing the interaction matrix $\overline{\overline{Z}}$, generated by an MoM solution to the many-body volume integral equation, into strong and weak interaction matrices $\overline{\overline{Z}}^s$ and $\overline{\overline{Z}}^w$, respectively. The matrix $\overline{\overline{Z}}^s$ contains only those interactions which are between particles closer than the neighborhood distance r_d . Therefore, $\overline{\overline{Z}}^s$ is very sparse and the matrix-vector multiply $\overline{\overline{Z}}^s \cdot \overline{x}$ is accomplished in $\mathcal{O}(N)$ complexity. The matrix $\overline{\overline{Z}}^w$ is formed by expanding the dyadic Green's function between each pair of particles whose associated grid points are located further apart than r_d in a γ^{th} order multivariate Taylor series expansion around a canonical grid superim-

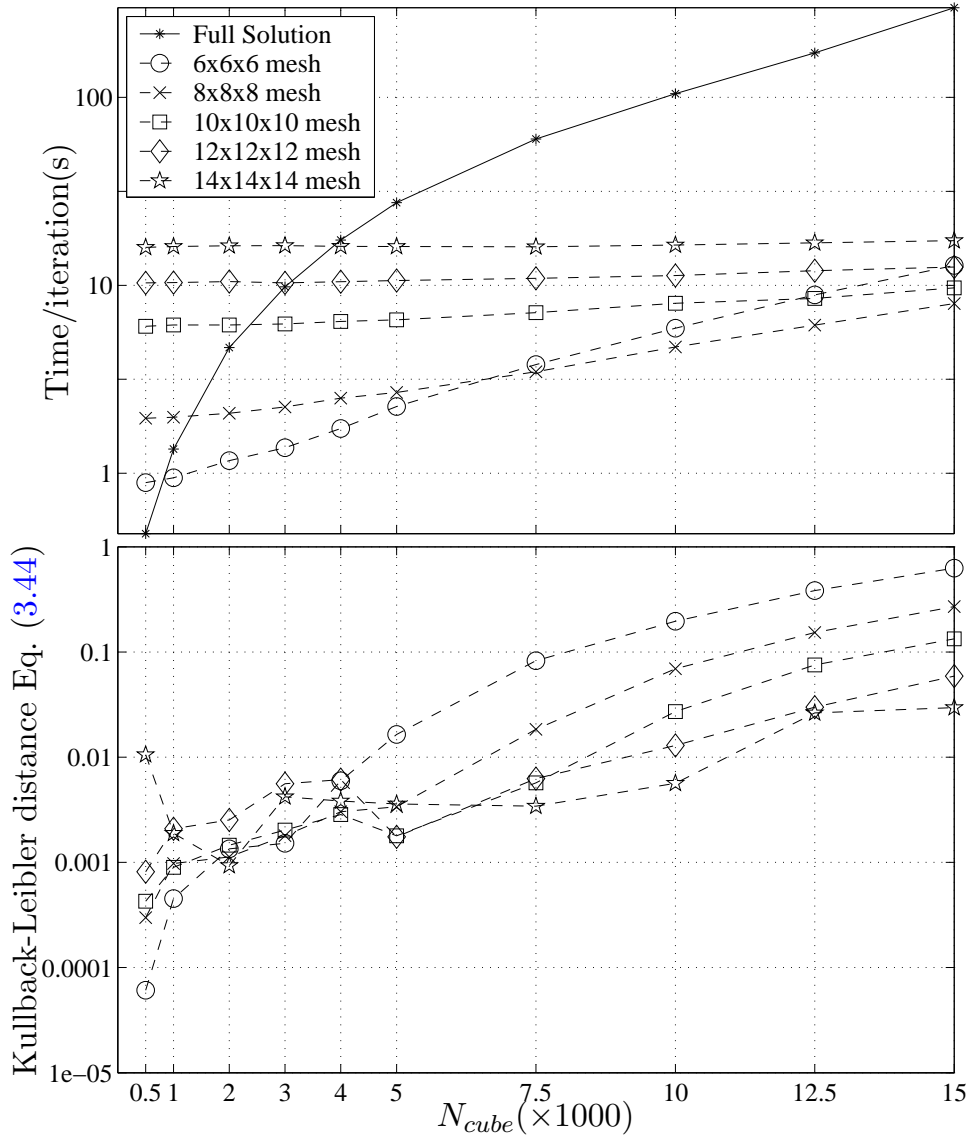
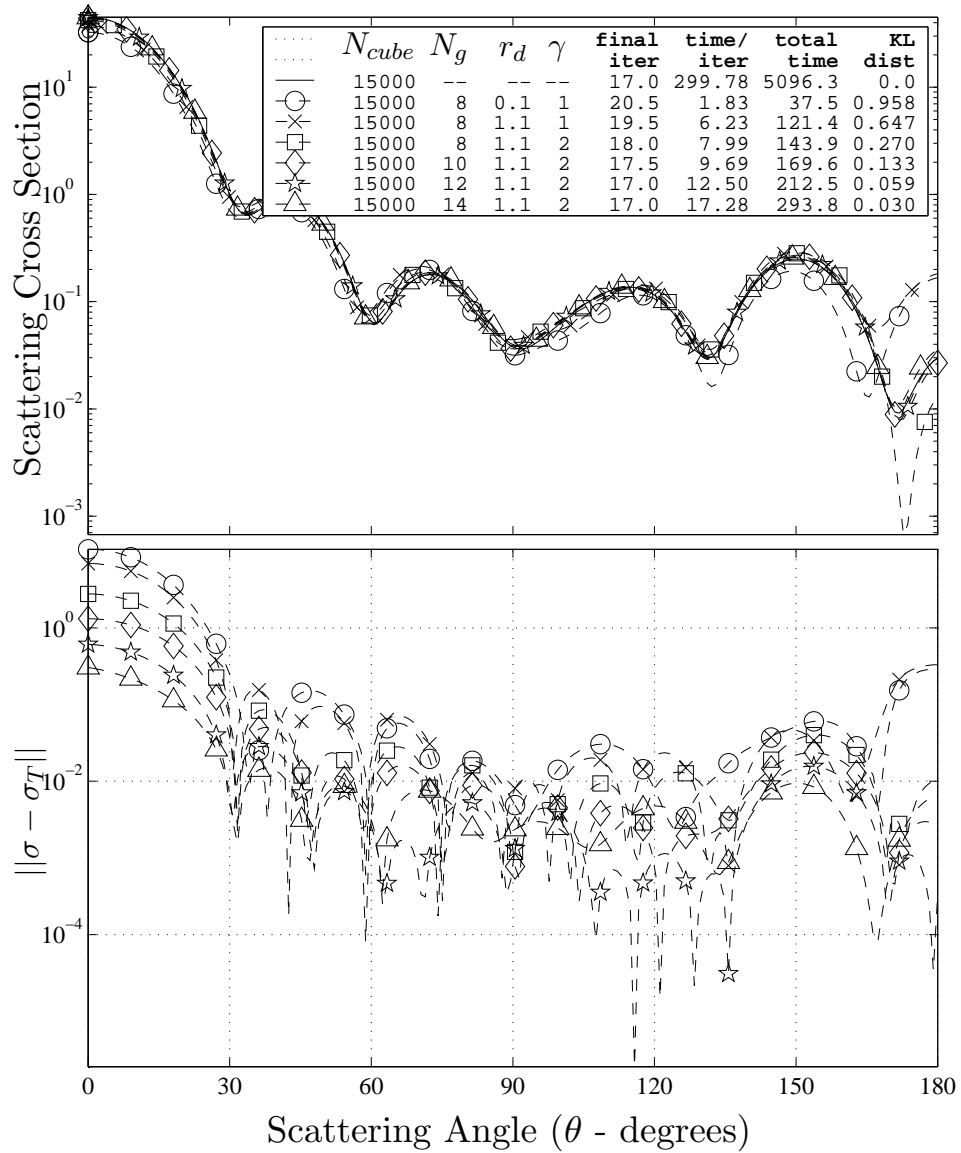


Figure 3-5: Computation times and Kullback-Leibler distances for SMCG method for $N_g=6-14$ with $\gamma=2$ and $r_d=1.1\Delta r_g$.

Figure 3-6: Radar Cross Section (σ) for increasing accurate approximations.

	N_q	N_{FFT}	total iters	time/ iter	Eq. (3.44)	speed up	
Neighborhood dist. $r_d = 0.1\Delta r_g$	$\gamma=1$	6	11979	28.0	2.4	2.485	124.45
		8	30375	20.5	1.8	0.958	163.88
		10	61731	19.5	2.9	0.708	103.04
		12	109503	18.0	4.3	0.507	70.40
		14	177147	17.5	6.2	0.380	48.38
	$\gamma=2$	6	11979	28.0	3.4	0.800	87.12
		8	30375	20.5	3.5	0.339	85.24
		10	61731	18.5	7.1	0.139	41.99
		12	109503	18.0	11.0	0.044	27.31
		14	177147	18.0	16.4	0.046	18.31
	$\gamma=3$	6	11979	20.0	7.3	0.080	41.15
		8	30375	18.0	6.8	0.085	44.09
10		61731	19.5	15.1	0.116	19.83	
12		109503	20.5	23.8	0.141	12.59	
14		177147	25.0	35.1	0.150	8.53	
Neighborhood dist. $r_d = 1.1\Delta r_g$	$\gamma=1$	6	11979	24.0	11.8	1.926	25.49
		8	30375	19.5	6.2	0.647	48.15
		10	61731	18.5	5.4	0.519	55.96
		12	109503	18.0	5.7	0.390	52.42
		14	177147	18.0	7.2	0.308	41.37
	$\gamma=2$	6	11979	20.5	12.8	0.628	23.50
		8	30375	18.0	8.0	0.270	37.51
		10	61731	17.5	9.7	0.133	30.92
		12	109503	17.0	12.5	0.059	23.98
		14	177147	17.0	17.3	0.030	17.35
	$\gamma=3$	6	11979	17.5	21.1	0.122	14.19
		8	30375	17.0	11.5	0.022	25.97
10		61731	16.0	17.4	0.018	17.25	
12		109503	16.0	26.5	0.015	11.31	
14		177147	15.0	36.4	0.009	8.23	
Neighborhood dist. $r_d = 1.5\Delta r_g$	$\gamma=1$	6	11979	19.5	29.4	1.177	10.21
		8	30375	20.5	14.9	0.467	20.14
		10	61731	18.5	9.8	0.372	30.44
		12	109503	17.5	8.5	0.296	35.40
		14	177147	17.5	9.0	0.247	33.33
	$\gamma=2$	6	11979	20.0	29.7	0.289	10.09
		8	30375	17.5	16.0	0.089	18.68
		10	61731	16.0	14.3	0.085	20.90
		12	109503	16.0	15.3	0.055	19.58
		14	177147	17.0	19.2	0.033	15.60
	$\gamma=3$	6	11979	17.5	31.5	0.155	9.52
		8	30375	16.0	20.1	0.018	14.94
10		61731	16.0	21.9	0.016	13.68	
12		109503	15.0	28.1	0.009	10.65	
14		177147	16.0	38.6	0.007	7.76	

Table 3.3: Computation times and relative speedup for the SMCG method compared to the full method. For all cases $N_{cube}=15000$

posed onto the test volume. The prolate spheroidal particles considered in this work were electrically small so that their response to electromagnetic excitation could be adequately approximated with a point response. Therefore, the Green's function interaction expansion

matrices $\overline{\overline{G}}_{\gamma_x \gamma_y \gamma_z}$ exhibit a multilevel block Toeplitz (MBT) structure. MBT matrices can be multiplied with an arbitrary vector using the only one forward and one inverse FFT. Thus $\overline{\overline{Z}}^w \cdot \overline{x}$ can be accomplished in $\mathcal{O}(N_T N \log N)$ complexity where N_T is the number of FFTs and depends on the expansion order γ . The 3-D SMCG method was demonstrated to indeed realize the predicted reduction in complexity and memory requirements through large-scale examples including up to 15000 discrete scatterers.

Chapter 4

On the Asymptotic Expansion of the Spheroidal Wave Function and its Eigenvalues for Complex Size Parameter

4.1 Introduction

Spheroidal wave functions (SWFs) have become increasingly important in the solution of a variety of different physical problems due to the flexibility afforded by the spheroid's nonspherical yet canonical geometry. The use of SWFs can be found in such diverse areas such as light scattering [49, 50, 51], nuclear modeling [52], signal processing and communication theory [53, 54, 55, 56], electromagnetic modeling [57, 58, 59, 60, 61], and in finding the electromagnetic induction (EMI) response of canonical objects at magnetoquasistatic frequencies [62, 63]. Three classic works on spheroidal wave functions are those by Stratton [64], Meixner [65], and Flammer [66], with tables of function values provided in [64, 66, 67].

Separation of variables of the wave equation in spheroidal coordinates results in a differential equation that is satisfied by both the angular and radial spheroidal wave functions

$$\frac{d}{d\zeta} \left[(1 - \zeta^2) \frac{d\chi_{mn}}{d\zeta} \right] + \left[\lambda_{mn} - c^2 \zeta^2 - \frac{m^2}{1 - \zeta^2} \right] \chi_{mn} = 0, \quad (4.1)$$

where c is the size parameter, m and n are integers with $m \geq 0$, $n \geq m$, and λ_{mn} are the separation, or characteristic, eigenvalues at which values the solution to Eq. (4.1) is bounded. Table 4.1 classifies the solutions of Eq. (4.1), χ_{mn} , into four cases according to the ranges of ζ and c (assumed purely real).

$\chi_{mn}(c, \zeta)$	c	ζ	range	name
$S_{mn}(c, \eta)$	c	η	$ \zeta < 1$	angular prolate
$R_{mn}^{(i)}(c, \xi)$	c	ξ	$ \zeta \geq 1$	radial prolate
$S_{mn}(-ic, \eta)$	$-ic$	η	$ \zeta < 1$	angular oblate
$R_{mn}^{(i)}(-ic, \xi)$	$-ic$	$i\xi$	$ \zeta \geq 1$	radial oblate

Table 4.1: Solutions to Eq. (4.1): angular and radial, prolate and oblate spheroidal wave functions.

Attempts to find rapid and accurate asymptotic expansions of the prolate angular and radial spheroidal wave functions (PASWF and PRSWF respectively) for large size parameter c (assumed real) have been ongoing. Flammer summarizes the work (up to 1957 [66]) and documents the asymptotic expansions of Eq. (4.1), for cases 1, 3, and 4 (see Table 4.1). The asymptotic expansion of Eq. (4.1), case 2, however, was unknown at the time of Flammer's work. Since that time, asymptotic approximations for this case have been developed by Slepian [68], for example, who built upon the asymptotic expansion of Eq. (4.1), case 1 found in Flammer (originally found by Meixner [65]) and extended the solution to five overlapping regions of validity. Miles [3, 69] provided compact, Bessel and Airy function expansions (used in part in Section 4.5) for the RSWFs in both the prolate and oblate cases. Streifer [70] (for the prolate case), and Cloizeaux and Mehta [71], also made strides in providing uniform asymptotic expansions for Eq. (4.1), and Sink and Eu [72] provided a WKB approximation for the angular SFW. More recently, asymptotic expansions of λ_{mn} for large c or n , $m = 0$ have been proposed in [73], expansions of Eq. (4.1) as they relate to the quantum shell model for both large n and large c have been proposed by [74, 75], and the work of Do-Nhat [76, 77] summarizes and provides more details of Flammer's expansions for Eq. (4.1) cases 1 and 3.

Evaluation of the SWFs for complex size parameter $c = c_r + c_i i$, where $c_r = \Re\{c\}$ and $c_i = \Im\{c\}$, has received less attention for both the standard and asymptotic regimes. Applications utilizing complex c include light scattering from spheroidal particles [49, 78] and spheroidal antennas enveloped in a plasma medium [79]. Schäfke and Groh [80] were the first to investigate the branch cuts associated with the SWFs (emanating radially outward from the branch points, $c_{o;r}^{mn}$ in the complex c -plane) although their results for $c_{o;r}^{mn}$ were not reported until [81]. Hunter and Guerrieri [82] provided one method for estimating then numerically solving for $c_{o;r}^{mn}$ while the first few were earlier recorded by Oguchi [83]. Existing routines for the computation of λ_{mn} and $S_{mn}(c, \eta)$ for complex c can be found in [84, 85], but these Mathematica routines are too slow to be used for anything but reference. In addition, it appears that these codes do not properly determine the expansion type for $\arg(c) \neq [0, \pi/4, \pi/2]$.

In this work, we implement a numerical method for first tabulating the branch points $c_{o;r}^{mn}$, then rapidly and accurately computing the asymptotic expansions of λ_{mn} and $S_{mn}(c, \eta)$ for arbitrary complex size parameter c in the asymptotic regime of $|c|$ large with n and m fixed. This regime corresponds to, for example, case (i) in [3] and the regime discussed in part I of [68]. To accomplish this, the branch points $c_{o;r}^{mn}$ are incorporated into a lookup table used to determine which asymptotic expansion is appropriate for a given c . Specifically, we elaborate on the solution for the specific case of $c_r = c_i$, and Table 4.3 lists which expansion type applies for a given m and n under this condition. This special case is encountered in the solution of the diffusion equation for spheroidal systems [63]. We also provide normalizations for the standard *prolate*-type and *oblate*-type asymptotic expansions for both $(n - m)$ even and odd. Expansions for the oblate SWFs are also discussed as a simple extension of the current investigation. All calculations in this work were performed in double precision except for the Newton-Raphson method, which was implemented in quadruple precision. The routines presented are rapid enough to be of practical use in applications requiring the calculation of many SWFs of varying orders, degrees, and arguments.

The structure of this work is as follows. Section 4.2 reviews the basic geometry and the definitions of the prolate SWFs. We describe the most common asymptotic expansions of the spheroidal eigenvalues λ_{mn} for purely real or imaginary c in Sections 4.3.1 and 4.3.2

respectively. The asymptotic expansion of λ_{mn} in the case of complex c depends on finding the branch, or double, points and our numerical method for finding these points is described in Section 4.3.3. The ordering of the eigenvalues λ_{mn} (and the SWFs) for the case of complex c is not as straightforward as the case of purely real (PSWFs) or purely imaginary c (Oblate SWFs) but instead depends on $\arg(c_{o;r}^{mn})$ as compared to $\arg(c)$. The first few of these branch points are listed in Table 4.2. Section 4.3.5 addresses the expansion ordering and describes how to incorporate this ordering into existing asymptotic expansions. In Section 4.4 the overall asymptotic expansion of the PASWF for complex c is shown to be comprised of the established expansions outlined in Section 4.3, where the choice of which type of asymptotic expansion to use is determined by m , n , and $\arg(c)$ via the same lookup table of branch points used in determining the correct expansion type for λ_{mn} . Proper normalizations for these asymptotic expansions are derived in Section 4.4.1. Section 4.5 contains a discussion of the expansions and patterns under consideration as well as some examples in graphical form of the real and imaginary parts of the complex PASWFs, $S_{mn}(c, \eta)$ and $S'_{mn}(c, \eta)$, as compared to the original Legendre expansion solutions. At the end of Section 4.5 we discuss briefly one asymptotic expansion of the PRSWFs $R_{mn}^{(i)}(c, \xi)$ for complex c , in light of the current discussion of the PASWFs. This is followed by a conclusion (Section 4.6) and information on how to obtain the computer programs implemented for this work.

4.2 Standard Formulation of the Prolate Angular Spheroidal Wave Function

The prolate and oblate spheroidal coordinate systems are two of the eleven coordinate systems in which the scalar wave equation

$$(\nabla^2 + k^2)\psi = 0 \tag{4.2}$$

is separable. The solution to Eq. (4.2) in prolate spheroidal coordinates is

$$\psi_{pmn}^{(i)} = S_{mn}(c, \eta) R_{mn}^{(i)}(c, \xi) T_{pm}(\phi), \tag{4.3}$$

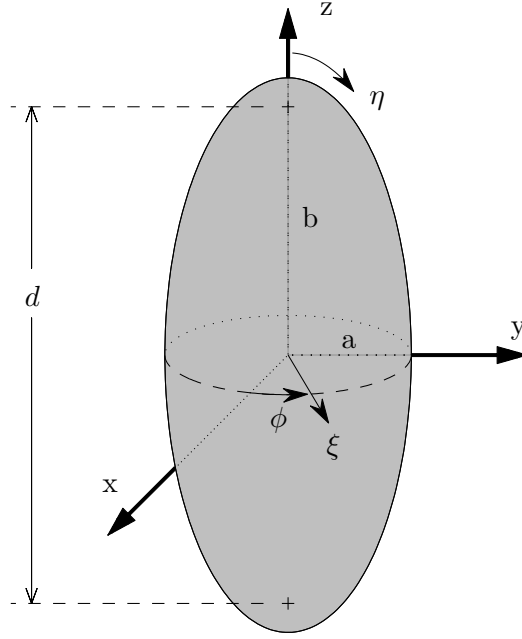


Figure 4-1: Prolate Spheroidal Geometry: $1 \leq \xi < \infty$, $-1 \leq \eta \leq 1$, $0 \leq \phi \leq 2\pi$, $x = \frac{d}{2}[(1-\eta^2)(\xi^2-1)]^{\frac{1}{2}} \cos(\phi)$, $y = \frac{d}{2}[(1-\eta^2)(\xi^2-1)]^{\frac{1}{2}} \sin(\phi)$, $z = \frac{d}{2}\eta\xi$, $e = \frac{b}{a}$, $\xi = (1-e^{-2})^{-\frac{1}{2}}$, $d = 2(b^2 - a^2)^{\frac{1}{2}}$.

where c is the size parameter ($c = kd/2$, where d is the interfocal distance as shown in Fig. 4-1), $S_{mn}(c, \eta)$ is the PASWF, $R_{mn}^{(i)}(c, \xi)$ is a the PRSWF of the i^{th} kind, and $T_{pm}(\phi)$ is the azimuthal function given by

$$T_{pm}(\phi) = \begin{cases} \cos(m\phi), & p = 0 \\ \sin(m\phi), & p = 1. \end{cases} \quad (4.4)$$

Flammer's notation [66] is used throughout except for the notation used for the harmonic functions [Eq. (4.4)] and some minor notational (but not formal) differences in the asymptotic expansions of Eqs. (4.7)–(4.12) and Eqs. (4.13)–(4.19) below. Expressions such as $n = 0(1)6$ indicate n equals [1..6] with an increment of 1.

Expressions for the prolate angular and radial functions have been studied for quite some time beginning with Lamé [86] and then Niven [87]. The most common form of the prolate

angular function is expressed as an expansion in terms of associated Legendre functions

$$S_{mn}(c, \eta) = \sum'_{r=0,1} d_r^{mn} P_{m+r}^m(\eta) \quad (4.5)$$

where the prime indicates summation from $\{0\}$ over $\{\text{even}\}$ indices when $(n-m)$ is $\{\text{even}\}$.

The radial function can be expressed as an expansion of spherical Bessel functions [88] as

$$R_{mn}^{(i)}(c, \xi) = \frac{\left(\frac{\xi^2-1}{\xi^2}\right)^{m/2}}{\sum'_{r=0,1} d_r^{mn} \frac{(2m+r)!}{r!}} \sum'_{r=0,1} d_r^{mn} \frac{(2m+r)!}{r!} i^{r+m-n} z_{m+r}^{(i)}(c\xi), \quad (4.6)$$

where $z_{m+r}^{(i)}(c\xi)$ represents the spherical Bessel functions $j_{m+r}(c\xi)$, $y_{m+r}(c\xi)$, $h_{m+r}^{(1)}(c\xi)$, and $h_{m+r}^{(2)}(c\xi)$, for $i = 1, 2, 3, 4$ respectively [88]. The expansion coefficients d_r^{mn} are determined by solving a three term recurrence relation obtained by substituting Eq. (4.5) into Eq. (4.1). These expansions are accurate for small size parameters up to $|c| \lesssim 30$, but encounter numerical difficulties leading to inaccuracy for larger $|c|$.

4.3 Asymptotic Expansion of the Spheroidal Eigenvalues, λ_{mn}

Eigenvalues of the spheroidal differential equation, λ_{mn} , are special values for which the equation's solutions are bounded at $\zeta = \pm 1$. We first review the two most common asymptotic expansions of the spheroidal eigenvalues and angular wavefunctions including both the *prolate*-type (c purely real) and *oblate*-type (c purely imaginary) before applying these expansions to the case of complex size parameter c .

A number of methods can be used to determine the eigenvalues, including the truncation and solution of the (transcendental) infinite continued fraction equation directly [66, 85]; successive approximations [66]; a power series representation for small $|c|$ [66, 88] followed by Bouwkamp's method of refinement [89]; the relaxation method [90, 91]; and an eigenvalue matrix approach [2] (see also [92, 93]). We prefer to use Hodge's [2] method because it is straightforward and rapidly computes the full set of λ_{mn} . When c is in the asymptotic regime considered here, the λ_{mn} produced by Hodge's method require a larger truncation size of the

eigenvalue matrix in order to maintain accuracy, at the cost of increased computation time. In this case, increased accuracy can be achieved instead by applying either Bouwkamp's method or using an asymptotic representation for λ_{mn} (see below). It should be noted that Bouwkamp's method converges very slowly near the branch points $c_{o;r}^{mn}$.

We use the Matlab codes found at [94], modified to accept complex c to calculate the spheroidal wave functions. These programs are based on those given in [95] and the results for the PSWF were compared to published tables [64, 66, 67] and found to be in agreement for purely real and purely imaginary values of small c . Results also matched values for the PSWFs and eigenvalues for complex c given in [84, 85].

4.3.1 Prolate-Type Asymptotic Expansion

The asymptotic expansion typically applied to the PASWF, $S_{mn}(c, \eta)$, and its characteristic eigenvalue, λ_{mn} , for the case of purely real c [Eq. (4.1) case 1] consists of an expansion of $S_{mn}(c, \eta)$ in terms of a series of parabolic cylinder, or Weber functions [66, 76]. We designate all asymptotic expansions typically applied to the PSWF for purely real c as *prolate*-type although as will be seen in Section 4.3.3, this expansion can also be applied to the OSWF in the case of arbitrary, complex c . We shall denote the asymptotic expansion by a superscript (*a*). The differential equation under these conditions becomes

$$\frac{d}{d\zeta} \left[(1 - \eta^2) \frac{dS_{mn}}{d\eta} \right] + \left[\lambda_{mn} - c^2 \eta^2 - \frac{m^2}{1 - \eta^2} \right] S_{mn} = 0. \quad (4.7)$$

If the following substitutions are made:

$$S_{mn}(c, \eta) \approx S_{mn}^{(a)}(c, \eta) = (1 - \eta^2)^{\frac{m}{2}} u_{mn}(c, \eta), \quad (4.8a)$$

$$\eta \Rightarrow \frac{x}{\sqrt{2c}} \quad (4.8b)$$

then in the limit as $c \uparrow \infty$, x fixed, Eq. (4.7) reduces to

$$\frac{d^2 u_{mn}}{dx^2} + \left(\frac{\lambda_{mn}}{2c} - \frac{x^2}{4} \right) u_{mn} = 0 \quad (4.9)$$

which is in the form of the parabolic cylinder differential equation. $u_{mn}(x)$ is therefore expanded in terms of an infinite series of parabolic cylinder functions

$$u_{mn}(x) = \sum'_{r=-\infty}^{\infty} C_r D_{n-m+r}(x) \quad (4.10)$$

where $D_{n-m+r}(x)$ is the parabolic cylinder function of order $n - m + r$ [88], the prime indicates summation over even r , and C_r are the expansion coefficients (unnormalized, see Section 4.4.1). Following this method, C_r and the eigenvalues λ_{mn} are further expanded as

$$C_r = \sum_{s=0}^{\infty} C_{rs} c^{-s} \quad (4.11)$$

and

$$\lambda_{mn} = \sum_{k=0}^{\infty} \Gamma_k c^{-k+1}. \quad (4.12)$$

Detailed description of the expansion coefficients, C_r and Γ_k , are given by Do-Nhat [76].

Slepian [68] states that the region of validity for this *prolate*-type expansion (Equation (1.6) in [68]) is $|\eta| \leq c^{-\frac{1}{2}}$. However, as noted by [70], if the infinite summations in equations Eqs. (4.10) and (4.11) are appropriately truncated, the approximation is remarkably accurate for a much larger range. Figures 4-9 and 4-10 show some examples of *prolate*-type $S_{mn}(c, \eta)$ and $S'_{mn}(c, \eta)$ as compared to $S_{mn}^{(a)}(c, \eta)$ and $S_{mn}^{(a)'}(c, \eta)$ respectively.

4.3.2 Oblate-Type Asymptotic Expansion

The asymptotic expansion typically applied to the oblate angular spheroidal wave function (OASWF) [case 3 of Eq. (4.1)] and its characteristic eigenvalue for the case of purely imaginary c , or $c \Rightarrow -ic$, consists of a similar method to that described by Eqs. (4.8)–(4.12) for the PSWF [66, 77]. Similar to the case above, we designate all asymptotic expansions typically applied to the OSWF for purely imaginary c as *oblate*-type although as will be seen in Section 4.3.3, this expansion can also be applied to the PSWF in the case of arbitrary, complex c . The original differential equation for the OASWF is

$$\frac{d}{d\zeta} \left[(1 - \eta^2) \frac{dS_{mn}}{d\eta} \right] + \left[\lambda_{mn} + c^2 \eta^2 - \frac{m^2}{1 - \eta^2} \right] S_{mn} = 0, \quad (4.13)$$

which, under the following substitutions

$$S_{mn}(-ic, \eta) \approx S_{mn}^{(a, \pm)}(-ic, \eta) = (1 - \eta^2)^{\frac{m}{2}} e^{-c(1 \mp \eta)} u_{mn}(-ic, \eta) \quad (4.14a)$$

$$\eta \Rightarrow \pm \left(\frac{x}{2c} - 1 \right), \quad (4.14b)$$

and in the limit as $c \uparrow \infty$, x fixed, becomes

$$\left[x \frac{d^2}{dx^2} + (m + 1 - x) \frac{d}{dx} + \nu \right] u_{mn}(x) = 0, \quad (4.15)$$

where $\nu = \left\{ \begin{array}{l} (n-m)/2 \\ (n-m-1)/2 \end{array} \right\}$ when $(n-m)$ is $\left\{ \begin{array}{l} \text{even} \\ \text{odd} \end{array} \right\}$. Equation (4.15) is satisfied by the associated Laguerre functions of degree m and order $\nu + r$, $L_{\nu+r}^{(m)}(x)$ [96, 88]. Accordingly, $u_{mn}(-ic, \eta)$ is expanded as

$$u_{mn}(-ic, \eta) = \sum_{r=-\nu}^{\infty} A_r \left\{ L_{\nu+r}^{(m)}[2c(1 \mp \eta)] + (-1)^{n-m} L_{\nu+r}^{(m)}[-i2c(1 + \eta)] \right\}, \quad (4.16)$$

so that $S_{mn}^{(a)}(-ic, \eta)$ becomes

$$S_{mn}^{(a)}(-ic, \eta) = (1 - \eta^2)^{\frac{m}{2}} \sum_{r=-\nu}^{\infty} A_r \left\{ e^{-c(1-\eta)} L_{\nu+r}^{(m)}[2c(1 - \eta)] + (-1)^{n-m} e^{-c(1+\eta)} L_{\nu+r}^{(m)}[2c(1 + \eta)] \right\}. \quad (4.17)$$

In a process similar to that for the prolate case, A_r and λ_{mn} are expanded in power series in c as

$$A_r = \sum_{s=0}^{\infty} A_{rs} (-ic)^{-s} \quad (4.18)$$

and

$$\lambda_{mn} = \sum_{k=0}^{\infty} \Gamma_k (-ic)^{-k+2}. \quad (4.19)$$

Detailed descriptions of the expansion coefficients, A_r and Γ_k , are given by Do-Nhat [77]. This *oblate*-type asymptotic expansion is found to be valid for all $|\eta| \leq 1$ and $|c| \gtrsim (n - m) + 20$. Figures 4-11 and 4-12 show some examples of *oblate*-type $S_{mn}(c, \eta)$ and $S'_{mn}(c, \eta)$ as compared to $S_{mn}^{(a)}(c, \eta)$ and $S_{mn}^{(a)'}(c, \eta)$ respectively.

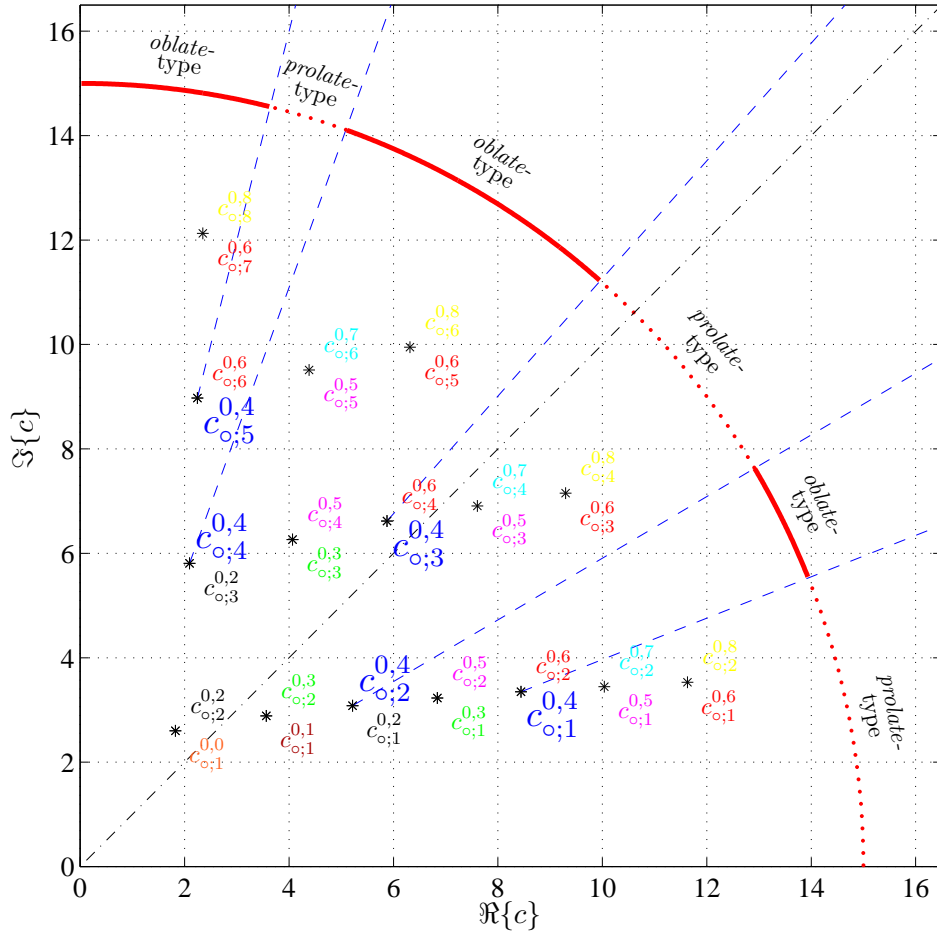


Figure 4-2: Branch points, $c_{o;r}^{mn}$ for $m = 0$ and $n = 0(1)6$. Branch cuts associated with $n = 4$ are indicated by the dashed lines with the appropriate expansion type indicated for each resulting sector. The dash-dot line indicates $\arg(c) = \pi/4$.

4.3.3 Asymptotic Expansion of the Eigenvalues for Complex c

When the size parameter c is complex, no new asymptotic expansions are necessary to determine the eigenvalues (and spheroidal wave functions) of the spheroidal wave equation. Instead, the expansions of λ_{mn} and $S_{mn}(c, \eta)$ for complex c are governed by a pattern, alternating between the aforementioned *prolate-type* (Section 4.3.1) and *oblate-type* (Section 4.3.2) expansions. This pattern is dictated solely by $\arg(c)$ for a given order m . The purpose of this Section is to provide a generally applicable numerical method for finding this asymptotic expansion pattern for the case of general complex c via a lookup table

consisting of the branch points, $c_{o;r}^{mn}$, for $0 \leq \arg(c) \leq \pi/2$. We also tabulate the pattern of correct asymptotic expansion types for the special case of $\arg(c) = \pi/4$ or $c = (1 + i)\alpha$, where $\alpha \in \mathfrak{R}^+$. We restrict our attention to c^2 in the upper half plane because the branch points are symmetric about the real axis [82]. Asymptotic expansions for the OSWFs follow the same pattern as that of the PSWFs with $c \Rightarrow -ic$ for the *prolate*-type expansions, and $c \not\Rightarrow -ic$ but remains unchanged for the *oblate*-type expansions.

The set of $S_{mn}(c, \eta)$, with their accompanying eigenvalues, is complete in the sense that an arbitrary square-integrable function $y(\eta)$ can be expanded in terms of an infinite linear combination

$$y(\eta) = \sum_{n=m}^{\infty} a_n S_{mn}(c, \eta). \quad (4.20)$$

Direct solutions of Eq. (4.1), either using the series defined by Eq. (4.5) or by numerical methods such as a Runge-Kutta method, are unambiguous and theoretically valid for any m , n , and c . However, the spheroidal eigenvalues develop square root branch cuts where the solution to the infinite continued fraction equation, or equivalently the characteristic eigenvalue equation (e.g from Hodge's method), becomes degenerate and possesses double roots [97].

At these branch points, $c_{o;r}^{mn}$, two spheroidal eigenvalues merge and become analytic continuations of each other [83, 82]. One consequence of this is that, as the eigenvalues exchange identities by level crossing onto each other's Riemann sheet, their respective asymptotic expansions are also interchanged. Thus λ_{mn} and $S_{mn}(c, \eta)$ are described alternately by a *prolate*-type asymptotic expansion then an *oblate*-type asymptotic expansion, as $\arg(c)$ (starting at $\arg(c) = 0$) crosses the branch cuts (emanating radially outward from $c_{o;r}^{mn}$) associated with a particular m and n . Given c , m , n , and $c_{o;r}^{mn}$ therefore, a simple lookup table determines which asymptotic expansion is appropriate by comparing $\arg(c)$ to $\arg(c_{o;r}^{mn})$. These transitions are depicted in Fig. 4-2, which shows the branch cuts and their appropriate asymptotic expansion regions for $m = 0$ and $n = 4$. As $\arg(c)$ progresses from 0 to $\pi/2$, each corresponding λ_{mn} crosses branch cuts (roughly proportional in number to $n + 1$) and alternates expansion type with each crossing. At $\arg(c) = 0$, all λ_{mn} are *prolate*-type, at $\arg(c) = \pi/2$, all λ_{mn} are *oblate*-type, while at $\arg(c) = \pi/4$, the λ_{mn} are divided evenly

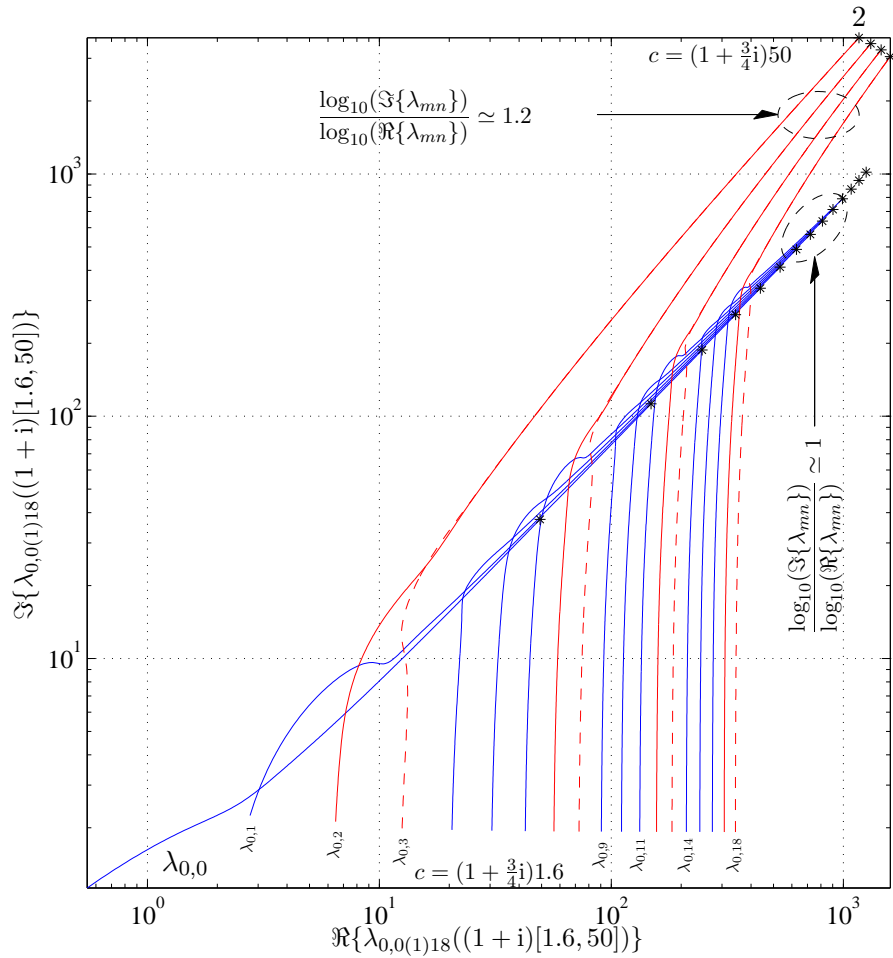


Figure 4-3: λ_{mn} : Eigenvalues of the spheroidal wave equation. $m = 0$ and $n = 0(1)18$. Each curve tracks an eigenvalue as c ranges from $c = (1 + \frac{3}{4}i)1.6$ (lower end of each curve) to $c = (1 + \frac{3}{4}i)50$ (upper end of each curve). Dashed curves indicate coalescing oblate eigenvalue pairs. The “2” indicates $\lambda_{0,2}((1 + \frac{3}{4}i)50)$.

between *prolate* and *oblate* types (see Fig. 4-4).

Further insight into the behavior of λ_{mn} for complex c can be obtained from Fig. 4-3 which shows λ_{mn} calculated by Hodge’s method for $m = 0$ and $n = 0(1)20$ with $c = (1 + \frac{3}{4}i)\alpha$, as $\alpha \approx [1, 50]$. A similar figure except with $c = (1 + i)\alpha$ is shown in Fig. 4-4. The eigenvalues in Figs. 4-3–4-4 display two distinct, alternating behaviors in the asymptotic regime, depending on $(n - m)$ for these $\arg(c)$. The first behavior is that of a linear relationship between $\Re\{\lambda_{mn}\}$ and $\Im\{\lambda_{mn}\}$ indicated by the lines with a slope of one for

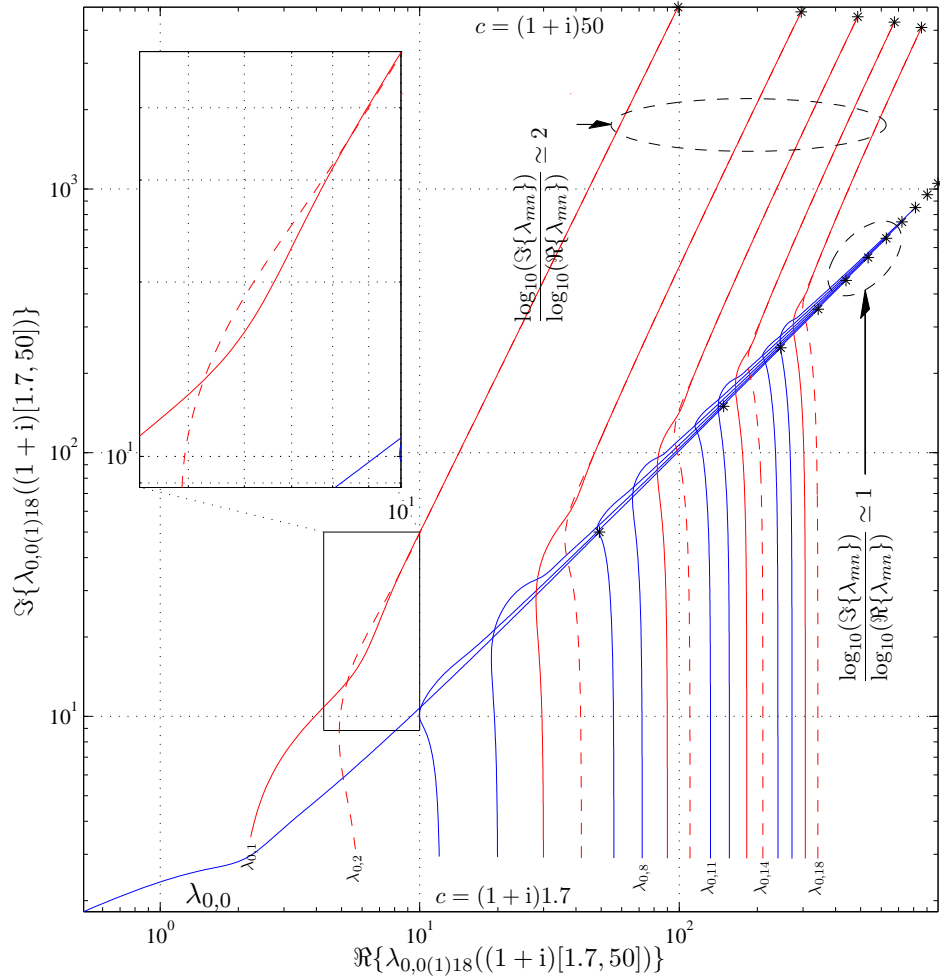


Figure 4-4: λ_{mn} : Eigenvalues of the spheroidal wave equation. $m = 0$ and $n = 0(1)18$. Each curve tracks an eigenvalue as c ranges from $c = (1+i)1.7$ (lower end of each curve) to $c = (1+i)50$ (upper end of each curve). Dashed curves indicate coalescing oblate eigenvalue pairs.

larger c (solid curves). This relationship can be seen more clearly in Fig. 4-7, in which the real and imaginary parts of $\lambda_{0,0}$ are shown explicitly as functions of c . This linear relationship is a consequence of the linear order term in the expansion of λ_{mn} in Eq. (4.12). The second behavior is a power law relationship between $\Re\{\lambda_{mn}\}$ and $\Im\{\lambda_{mn}\}$. Those eigenvalues that evince this type of behavior coalesce into pairs (dashed curves) and result from the *oblate*-type asymptotic expansion of λ_{mn} in Eq. (4.19). In the case of Fig. 4-3 with

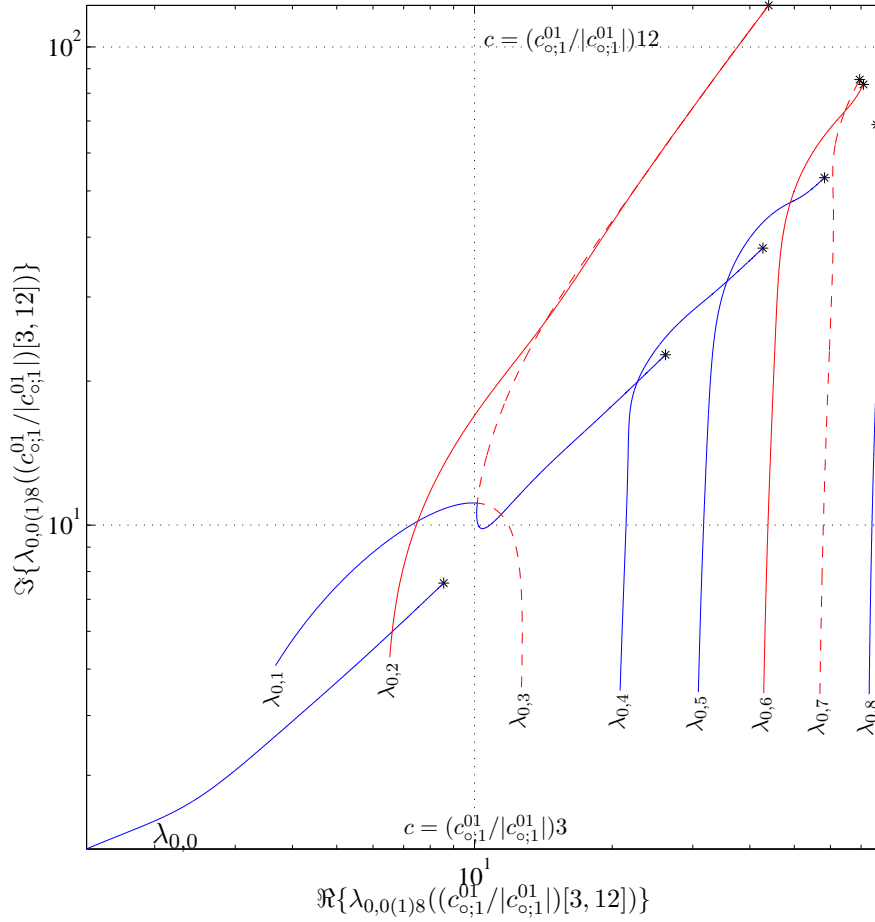


Figure 4-5: Branch point $c_{o;1}^{0,1} = c_{o;2}^{0,3} = 3.563644553545 + 2.887165344337i$ where $\lambda_{0,1}$ and $\lambda_{0,3}$ merge at $\lambda_{o;1}^{0,1} = \lambda_{o;2}^{0,3} = 10.1408387872326 + 11.1215866842249i$. Dashed curves indicate coalescing oblate eigenvalue pairs.

$c = (1 + \frac{3}{4}i) \alpha$, this pairing occurs after the first two unpaired eigenvalues, and thereafter after every 3 unpaired eigenvalues. When $c = (1 + i) \alpha$, oblate eigenvalue pairs occur after every two unpaired eigenvalues. This asymptotic behavior alternates with each level crossing, which occurs at the branch cuts associated with the branch points $c_{o;r}^{mn}$. At such points, two eigenvalues merge and become indistinguishable as shown for example in Fig. 4-5 where $\lambda_{0,1}$ and $\lambda_{0,3}$ merge at $c_{o;1}^{01} = 3.563644553545 + 2.887165344337i$.

4.3.4 Computation of the Branch Points $c_{o;r}^{mn}$

The computation of the branch points can be decomposed into two stages: finding a sufficiently accurate initial estimate for $c_{o;r}^{mn}$, then using a numerical root finding technique such as the Newton-Raphson (NR) method [98] to refine the estimate to the desired accuracy. Estimates for the first few branch points $c_{o;r}^{m,m}$ to $c_{o;r}^{m,m+3}$ for each m were found by a simple bisection technique utilizing the process described in 4.3.5 to determine the correct ordering and expansion type at a given c . The bisection technique tested successively narrower sectors of $\arg(c)$ in order to specify the approximate angle at which the asymptotic expansions for $\lambda_{m,n}$ and $\lambda_{m,n+2}$ interchanged. Once the initial guess for $\arg(c_{o;r}^{mn})$ was found to the desired accuracy, $|c_{o;r}^{mn}|$ was searched for between 0 and $n + 15$ (as an approximate upper bound) using a simplex search method [27] based on finding the minimum $|\lambda_{m,n} - \lambda_{m,n+2}|$ for the merging pair. After accurate $c_{o;r}^{m,m..m+1}$ were found in this manner, initial guesses for $\arg(c_{o;r}^{m,m+2..m+3})$ were obtained also via bisection by noting that $\arg(c_{o;r,\text{odd}}^{m,n+2})$ are interspersed with $\arg(c_{o;r,\text{even}}^{m,n})$, thus providing upper and lower bounds in $\arg(c)$ for the bisection method. An estimate for $|c_{o;r}^{m,m+2..m+3}|$ was obtained by noting that

$$\min \left(|c_{o;r,\text{odd}}^{m,n+2}| \right) > \max \left(|c_{o;r,\text{even}}^{m,n+2}| = |c_{o;r,\text{odd}}^{m,n}| \right) \quad (4.21)$$

and by observing the pattern which soon becomes apparent (see Fig. 4-2). Initial estimates for the remaining $c_{o;r}^{m,m+4..}$ were based on simple polynomial estimation techniques.

These initial guesses for $c_{o;r}^{mn}$ were then used as a starting point for a quadruple precision multivariate (in λ and c^2) NR root finding technique [82]. In most cases, these initial guesses were sufficiently accurate for the convergence of the NR method. Those that were not of sufficient accuracy were first refined using a simplex search method, which has a larger radius of convergence, prior to invoking the NR method. In all cases, this combined numerical procedure correctly and exhaustively identified the branch points for $m \leq n \leq 59$ as well as $m = 0(1)10, n \leq 100$. The accuracy as defined by the smallest correction of the NR method was less than 1×10^{-15} in the vast majority of cases. However, as n increased, the accuracy of the NR method decreased until, for example, of $c_{o;r}^{0,100} \approx 1 \times 10^{-8}$. This numerical procedure for finding initial guesses is an alternative to the WKBJ, or phase-

integral, method outlined in [82]. A brief table of these results is given as Table 4.2 while a more complete listing is provided in D. The programs used in this calculation may be obtained by contacting the author.

m	n	r	$c_{o;r}^{m,n} = c_{o;r+1}^{m,n+2}$	$\lambda_{o;r}^{m,n} = \lambda_{o;r+1}^{m,n+2}$
0	0	1	1.824770749208805 + 2.601670692890318i	1.705180091412460 + 4.220186348356370i
0	1	1	3.563644553545243 + 2.887165344336900i	10.140838787232552 + 11.121586684224873i
0	2	1	5.217093042404772 + 3.081362886557631i	23.915829574409656 + 18.743327216266508i
0	2	3	2.094267182395557 + 5.807965828216133i	1.998518598679208 + 8.578716573946885i
0	3	1	6.838151743509966 + 3.228540820485014i	42.839460829787278 + 26.892790566183677i
0	3	3	4.067274712533398 + 6.264358978587767i	11.780925838292136 + 22.541393207957562i
0	4	1	8.443063517943598 + 3.346896434708849i	66.833326753192964 + 35.456773864933439i
0	4	3	5.874514148328888 + 6.617314890038058i	27.516445359838094 + 37.764984283250755i
0	4	5	2.244329796261236 + 8.973752190228394i	2.156124860667898 + 12.810922196899876i
0	5	1	10.038665064092994 + 3.445770032753475i	95.856405565575329 + 44.361464108811766i
0	5	3	7.606334073445308 + 6.906465157219409i	48.806652414112627 + 54.0119898227262004i
0	5	5	4.383443826328900 + 9.509669337618593i	12.778186437528630 + 33.481761709843944i
0	6	1	11.628375737753831 + 3.530602623592430i	129.884250145370260 + 53.555053907976102i
0	6	3	9.295569705184056 + 7.151702724612575i	75.462208083813508 + 71.1126581786667672i
0	6	5	6.316233767329015 + 9.949229739353585i	29.846039092711770 + 55.689990108075811i
0	6	7	2.347893464857109 + 12.128185061133886i	2.263189447556893 + 16.978431740148483i
1	1	1	1.998555442181652 + 4.097453662365392i	2.915318658097470 + 6.133951063223160i
1	2	1	3.862833529248772 + 4.492300074953849i	12.201095993517072 + 16.244079086339937i
1	3	1	5.594491061915554 + 4.781582485576267i	27.134073085223168 + 27.423761751764438i
1	3	3	2.184204069300826 + 7.326156812534641i	3.102506602797785 + 10.539212581987126i
1	4	1	7.270040170458184 + 5.010809182556227i	47.410985357646396 + 39.426178765353157i
1	4	3	4.246372923512624 + 7.831360958311476i	13.386757375380991 + 27.641212328450003i
1	5	1	8.915451995089990 + 5.200792891998006i	72.896560506953961 + 52.09473392083313i
1	5	3	6.119087892218941 + 8.234638882858787i	29.880624051048471 + 46.181278766950726i
1	5	5	2.304084540373247 + 10.504790051881750i	3.223431021669091 + 14.784565087404808i
1	6	1	10.542501674387614 + 5.363017364859081i	103.515790242771686 + 65.322653293710630i
1	6	3	7.901814171761899 + 8.572100476598123i	52.112553092568930 + 65.921011346611721i
1	6	5	4.510843794687041 + 11.068777156965684i	14.199823500075389 + 38.585841097079758i
2	2	1	2.136987377094029 + 5.449457313914277i	6.102540356949614 + 7.684763813617406i
2	3	1	4.105156484215650 + 5.922750658440496i	16.136866268804905 + 20.406230631490939i
2	4	1	5.907125751703487 + 6.283464345814330i	32.087586148736847 + 34.487534677680138i
2	4	3	2.265822172027141 + 8.748077684520867i	6.207742694273197 + 12.250160879220145i
2	5	1	7.634658702877481 + 6.576768822063829i	53.561371101706115 + 49.638515941219318i
2	5	3	4.405746719793623 + 9.294389714166075i	16.974441589636069 + 32.109641041936442i
2	6	1	9.320494635222795 + 6.824432371374058i	80.376039435949536 + 65.668970414405067i
2	6	3	6.337223309080594 + 9.739915760209533i	34.182667033756140 + 53.573264399341902i
2	6	5	2.361167355756876 + 11.962429681198497i	6.294802569497238 + 16.568043718788960i
3	3	1	2.254441944326160 + 6.731940814252908i	11.273739025431583 + 9.046369132359118i
3	4	1	4.312789375877335 + 7.267942971679416i	21.989944786045928 + 24.064251342820775i
3	5	1	6.178462421804212 + 7.686866389128842i	38.868087480677623 + 40.699885683521551i
3	5	3	2.340324936128145 + 10.109946235283390i	11.310516001008940 + 13.800986115329859i
3	6	1	7.954733051349589 + 8.033437876318695i	61.436143112767034 + 58.624668698520892i
3	6	3	4.550052309842578 + 10.692087653052024i	22.538458584763827 + 36.168232895835459i
4	4	1	2.357663561227191 + 7.971913317957412i	18.433063143522340 + 10.285516884986537i
4	5	1	4.496463440238013 + 8.560827522001995i	29.782817773819936 + 27.394857362811521i
4	6	1	6.420513778117898 + 9.029346203504799i	47.523240440325630 + 46.358165420600599i
4	6	3	2.408979269086267 + 11.429969157729531i	18.410055957253928 + 15.237266195961114i
5	5	1	2.450444507315414 + 9.182664291501323i	27.583139404518864 + 11.436479619199886i
5	6	1	4.662342487692823 + 9.817718575239088i	39.529181751692839 + 30.489219805169245i
6	6	1	2.535162563188484 + 10.371846133322299i	38.725741591981532 + 12.519713968726423i

Table 4.2: Branch points and eigenvalues for $m = 0(1)6$ and $n = 0(1)[6 - m]$. Accuracy was determined by the last correction of the Newton-Raphson method (in all cases $< 1 \times 10^{-15}$).

4.3.5 Eigenvalue Ordering for Complex c

For purely real, purely imaginary, or sufficiently small complex c , the ordering (indexed by n) is determined by the absolute magnitude of λ_{mn} [2]. However, for larger complex c , the eigenvalues may no longer be sorted merely by $|\lambda_{mn}|$. The power law nature of the imaginary part of those coalescing eigenvalues, when compared to the real part, especially in the asymptotic regime (large c), soon dominates and disrupts ordering by $|\lambda_{mn}|$ (see Fig. 4-6). A better choice for deciding the ordering of λ_{mn} seems to be $\Re\{\lambda_{mn}\}$ due to its linear increase in the asymptotic regime, for both types of behaviors noted above. Yet this choice of ordering is also not correct as coalescing oblate pairs of eigenvalues often reverse order, according to this measure, before becoming indistinguishable (see Fig 4-4 and inset therein). Additionally, ordering by $\Re\{\lambda_{mn}\}$ fails for cases of general c such as $c = (1 + \frac{3}{4}i)\alpha$, as can be seen by comparing Fig. 4-3 with Fig. 4-6. To illustrate the difficulty associated with eigenvalue ordering, note the eigenvalue corresponding to the asterisk labeled “ $\lambda_{0,2}$ ” in Figs. 4-3 and 4-6. This eigenvalue is assigned order $n = 7$ by an eigenvalue solver in Hodge’s method, $n = 12$ when arranged according to increasing $|\Re\{\lambda_{mn}\}|$, $n = 52$ when arranged according to $|\lambda_{mn}|$, while inspection of Fig. 4-3 reveals that this eigenvalue should in fact correspond to order $n = 2$.

At least it can be said that the eigenvalue ordering and expansion patterns for general, complex c should follow the ordering for λ_{mn} when $c = 0$. At that point, the eigenvalues reduce to

$$\lambda_{mn}(c = 0) = n(n + 1), \quad n \geq m, \quad (4.22)$$

and the spheroidal wave equation (4.1) reduces to the equation satisfied by the associated Legendre functions of the first kind of integral order and degree, $P_n^m(\eta)$. This fact is sufficient to suggest a brute force method for finding λ_{mn} ordering and expansion type for large, complex values of c . The method consists of simply computing λ_{mn} in sufficient density in the range

$$c = \frac{(c_r + c_i)\alpha}{|c|}, \quad \alpha \in [0, \text{large}) \quad (4.23)$$

so that the ordering may be determined by tracing each eigenvalue back to its corresponding value (and order) at $c = 0$ ((c.f. Figs 4-3-4-5). “Large” in this case is to be interpreted as

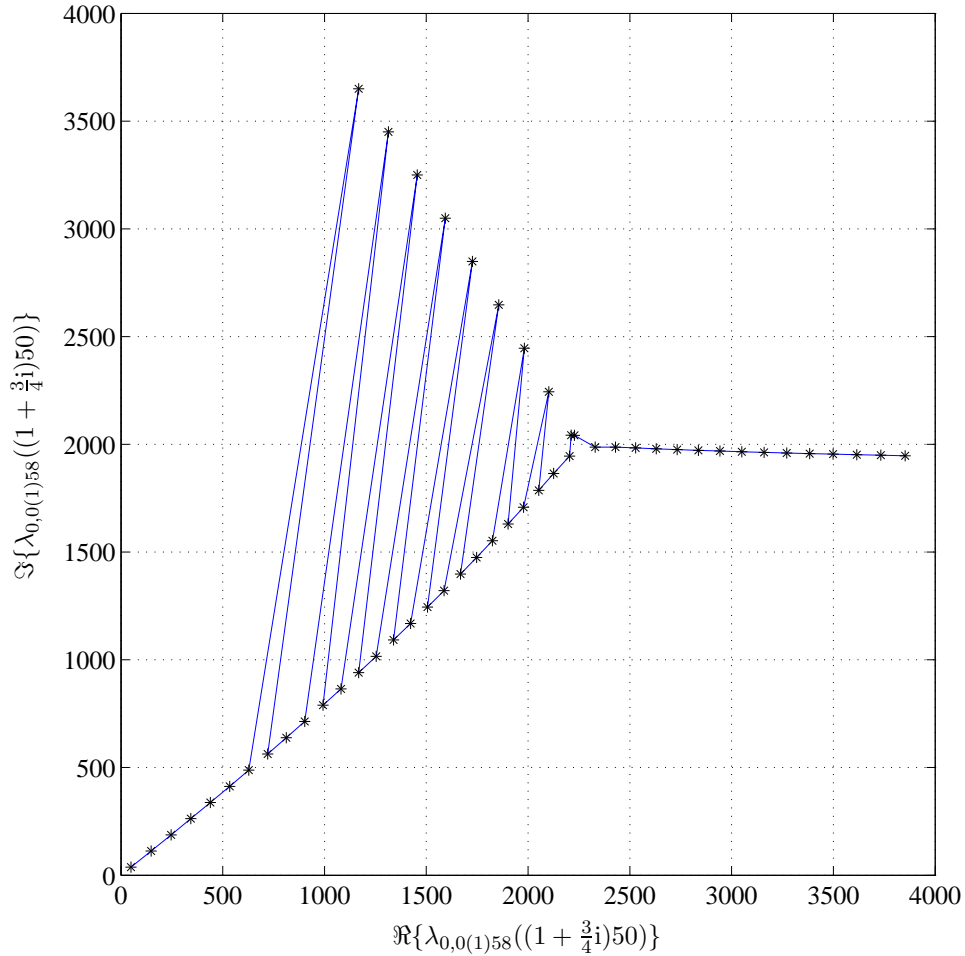


Figure 4-6: λ_{mn} : Eigenvalues of the spheroidal wave equation. $m = 0$ and $n = 0(1)58$ and $c = (1 + \frac{3}{4}i)50$. The solid line indicates the (incorrect) ordering returned from calculating λ_{mn} using Hodge's [2] method, while the correct ordering is labeled by $\lambda_{m,n}$.

any α large enough to satisfy the assumptions that $|c|$ is large compared to fixed m and n . As a rule of thumb, $|c| \gtrsim (n - m) + 20$, although this has not been investigated thoroughly.

In practical application, a set of λ_{mn} is often obtained simultaneously using a method such as Hodge's method. Ordering for the entire set of eigenvalues can be determined uniquely by first making use of the fact that the *prolate* and *oblate*-type eigenvalues can be sorted as *separate* sets according to $\Re\{\lambda_{mn}\}$ and then by consulting the lookup table to determine which $n - m$ correspond to each type of expansion. Eigenvalues described by an

oblate-type asymptotic expansion can be identified according to $\Im\{\lambda_{mn}\} > c^2/2$ for c in the asymptotic regime.

The ordering of the *prolate*-type and *oblate*-type asymptotic expansions of λ_{mn} (denoted $\lambda_{mn}^{(a)}$) for general, complex c , is different from the ordering, according to n , of the eigenvalues themselves. While the n indicates λ_{mn} ordering for each m , the $\lambda_{mn}^{(a)}$ are ordered according to m , but independently, corresponding to the sequential ordering for each type of expansion separately. Let n_p be the number of *prolate*-type expansions of λ_{mn} necessary up to but excluding n , and n_o be the number of *oblate*-type expansions of λ_{mn} necessary up to but excluding n . λ_{mn} can then be approximated by *prolate*-type $\lambda_{mn}^{(a)}$ ordered according to n_p beginning at $n_p = m$, and *oblate*-type $\lambda_{mn}^{(a)}$ ordered according to n_o beginning at $n_o = m$, interspersed in a pattern determined by $\arg(c)$ via the lookup table described in Section 4.3.3.

As an illustration, for the case of c of the form $c = (1 + i)\alpha$, $\lambda_{0,0}$ would correspond to the zeroth ($n_p = 0$) *prolate*-type asymptotic expansion. On the other hand, the second eigenvalue for $m = 0$, $\lambda_{0,1}$, coalesces with the third eigenvalue, $\lambda_{0,2}$ (see Fig. 4-4), and these correspond to the zeroth ($n_o = 0$) and first ($n_o = 1$) *oblate*-type asymptotic expansions respectively. To be specific, we explicitly show the dependence of Γ_k on m and n , and express the *prolate*-type expansion of $\lambda_{0,0}^{(a)}$ from Eq. (4.12) as

$$\lambda_{0,0} \approx \lambda_{0,0}^{(a)} = \sum_{k=0}^{\infty} \Gamma_k(m=0, n \Rightarrow n_p=0) c^{-k+1}. \quad (4.24)$$

For completeness, we also show the *oblate*-type expansion of $\lambda_{0,1}^{(a)}$ and $\lambda_{0,2}^{(a)}$ from Eq. (4.19) as

$$\lambda_{0,1} \approx \lambda_{0,1}^{(a)} = \sum_{k=0}^{\infty} \Gamma_k(m=0, n \Rightarrow n_o=0) (-ic)^{-k+2}. \quad (4.25a)$$

$$\lambda_{0,2} \approx \lambda_{0,2}^{(a)} = \sum_{k=0}^{\infty} \Gamma_k(m=0, n \Rightarrow n_o=1) (-ic)^{-k+2}. \quad (4.25b)$$

In turn the fourth eigenvalue, $\lambda_{0,3}$, corresponds to the first ($n_p = 1$) *prolate*-type asymptotic expansion, and so on (c.f. Fig. 4-4). The oblate spheroidal eigenvalues are also expressed in terms of either the *prolate*-type and *oblate*-type asymptotic expansions, however, $c \Rightarrow (-ic)$

$(n-m)$	$m=0$				$m=1$				$m=2$			
	type	n_p	n_o	norm.	type	n_p	n_o	norm.	type	n_p	n_o	norm.
0	Pro.	0	-	C_{Pe}	Pro.	1	-	C_{Pe}	Pro.	2	-	C_{Pe}
1	Obl.	-	0	C_{Oo}	Pro.	2	-	C_{Po}	Pro.	3	-	C_{Po}
2	Obl.	-	1	C_{Oe}	Obl.	-	1	C_{Oe}	Pro.	4	-	C_{Pe}
3	Pro.	1	-	C_{Po}	Obl.	-	2	C_{Oo}	Obl.	-	2	C_{Oo}
4	Pro.	2	-	C_{Pe}	Pro.	3	-	C_{Pe}	Obl.	-	3	C_{Oe}
5	Obl.	-	2	C_{Oo}	Pro.	4	-	C_{Po}	Pro.	5	-	C_{Po}
6	Obl.	-	3	C_{Oe}	Obl.	-	3	C_{Oe}	Pro.	6	-	C_{Pe}
7	Pro.	3	-	C_{Po}	Obl.	-	4	C_{Oo}	Obl.	-	4	C_{Oo}
8	Pro.	4	-	C_{Pe}	Pro.	5	-	C_{Pe}	Obl.	-	5	C_{Pe}
\vdots		\vdots				\vdots				\vdots		

Table 4.3: Pattern governing n_p , n_o and which type of asymptotic expansion, either the *prolate*-type (Pro. above) or the *oblate*-type (Obl. above), for different combinations of m and n . c is of the form $c = (1 + i)\alpha$. Normalizations for each case are also given (see Section 4.4.1).

in Eq. (4.24) while $(-ic) \Rightarrow c$ in Eq. (4.25a). The ordering of the *prolate*-type and *oblate*-type asymptotic expansions in Section 4.3 as applied to the OSWFs also adhere to this alternating pattern according to n_p and n_o .

Table 4.3 details which type of asymptotic expansion of the prolate spheroidal eigenvalue λ_{mn} is appropriate for a given m and n and indicates the ordering aspects of these expansions for the specific cases of $m = 0(1)2$, $(n-m) = 0(1)8$, and c of the form $c = (1 + i)\alpha$. For this case, the first $m + 1$ expansions of λ_{mn} are *prolate*-type expansions after which alternating pairs of *oblate*-type and *prolate*-type asymptotic expansions develop. The relationship between m , n , n_p , and n_o , again only for c of the form $c = (1 + i)\alpha$, may be expressed compactly as

$$n_p = \begin{cases} n, & (n-m) \leq m \\ \left\lfloor \frac{(n-m)-m}{2} \right\rfloor + m + m, & (n-m) > m \end{cases} \quad (4.26)$$

and

$$n_o = \left\lfloor \frac{(n-m)-m}{2} \right\rfloor + m, \quad (4.27)$$

where $\lfloor \cdot \rfloor$ denotes the floor function.

The infinite summations for the asymptotic expansion of the eigenvalues and PASWFs,

either the *prolate*-type Eq. (4.12) or the *oblate*-type Eq. (4.19), must be truncated at some point or they will eventually diverge. The index, k_T , at which the summation is truncated is decided in the usual manner [97] by finding the minimum value in the series, truncating the summation at this index, and assuming the remaining error is less than this term. This truncation index is approximately proportional to $|c|$ as shown in Figs. 4-7b and 4-8b. We calculated the expansion coefficients C_r and A_r from Eqs. (4.11) and (4.18), respectively, for $r \leq 120$, $m = 0(1)5$, and $n = 0(1)100$. Thereafter, the eigenvalues themselves were calculated for both types of asymptotic expansions. These asymptotic values for λ_{mn} were compared to those eigenvalues obtained using other methods and found to be in excellent agreement in overlapping regions of high accuracy. Table 4.5 contains a few values for $\lambda_{mn}^{(a)}$ in the asymptotic regime, calculated using the methods described here.

4.4 Asymptotic Expansion of $S_{mn}(c, \eta)$

We now turn our attention to the asymptotic expansion of the PASWF, $S_{mn}(c, \eta)$, for complex argument c . The pattern governing which asymptotic expansion type is appropriate for obtaining the prolate spheroidal eigenvalues, λ_{mn} , for a given c , m , and n , can be applied directly to finding an appropriate asymptotic expansion of the PSWFs. This statement not only applies to the expansions summarized in Section 4.3, but also applies to all other known expansions in the literature that are typically applied to the PSWFs (*prolate*-type expansions) or the OSWFs (*oblate*-type expansions). This seems natural due to the fact that each of the respective asymptotic expansion types from Secs. 4.3 applies to its accompanying angular function as well as to the eigenvalue itself. Extending the example of $c = (1 + i)\alpha$ and following the pattern given in Section 4.3.5, the asymptotic expansion of $S_{0,0}(c, \eta)$ is of the *prolate*-type given by Eq. (4.8), with $n_p = 0$, while $S_{0,1}(-ic, \eta)$ and $S_{0,2}(-ic, \eta)$ are of the *oblate*-type given by Eq. (4.14), i.e. $S_{m, n_o=1}^{(a)}(-ic, \eta)$ and $S_{m, n_o=2}^{(a)}(-ic, \eta)$, and so on. The same accounting for $(-i)$ must be done when finding the *oblate*-type asymptotic expansion for the PASWF as in the case of the *oblate*-type asymptotic expansion for the prolate eigenvalue (see Section 4.3.3). For the OSWFs this accounting is reversed, as noted in the previous Section.

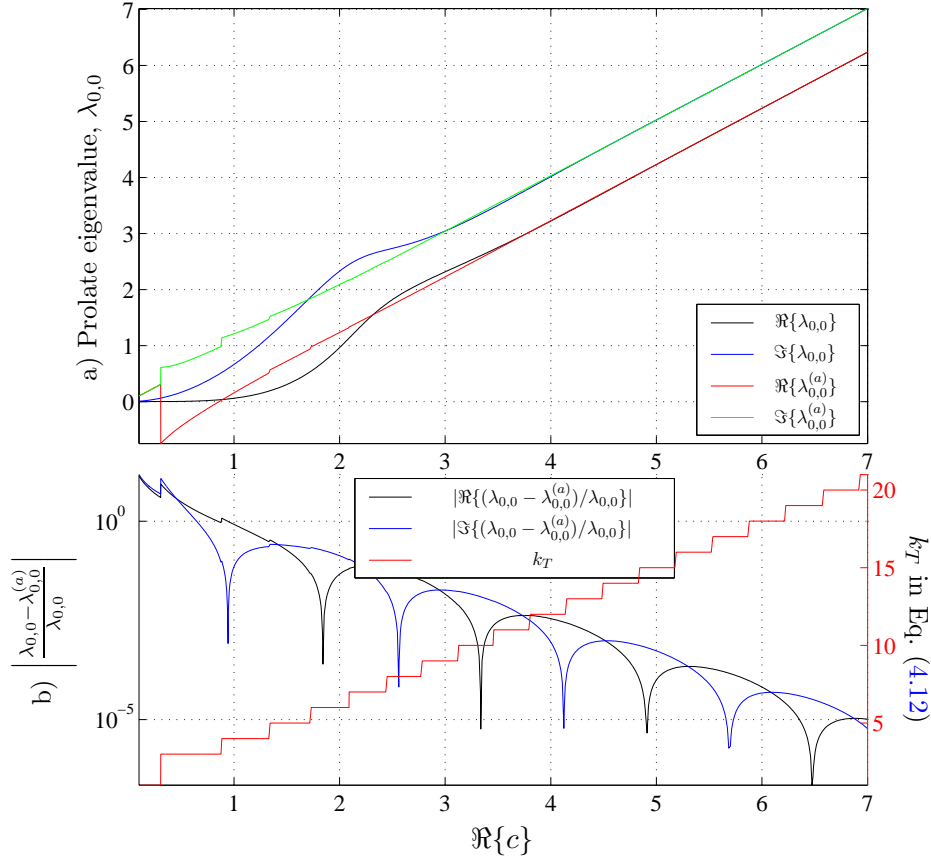


Figure 4-7: a) Spheroidal eigenvalues $\lambda_{0,0}$ for $c = (1 + i)\alpha$, $\alpha = [0, 7]$. b) Relative error between the prolate eigenvalue from Hodge's method [2], $\lambda_{0,0}$, and its *prolate*-type asymptotic expansion [Eq. (4.12)], $\lambda_{0,0}^{(a)}$.

4.4.1 Normalizations of the Asymptotic Expansions

Both the *prolate*-type and *oblate*-type asymptotic expansions for the prolate angular functions are correct to within a constant. This discrepancy is due to the fact that a suitable normalization must be adopted in order for these asymptotic expansions to match with the Legendre expansion of Eq. (4.5). This normalization is dependent on the parameters m , n , and c as well as n_p or n_o . To find suitable normalizations for both the $(n - m) \Rightarrow \text{even}$ and $(n - m) \Rightarrow \text{odd}$ cases, we follow a procedure similar to that of Stratton [64] and Flammer [66].

For the *prolate*-type asymptotic expansion and in the $(n - m) \Rightarrow \text{even}$ case we constrain the value of the asymptotic expansion at $\eta = 0$ to be equal to the associated Legendre

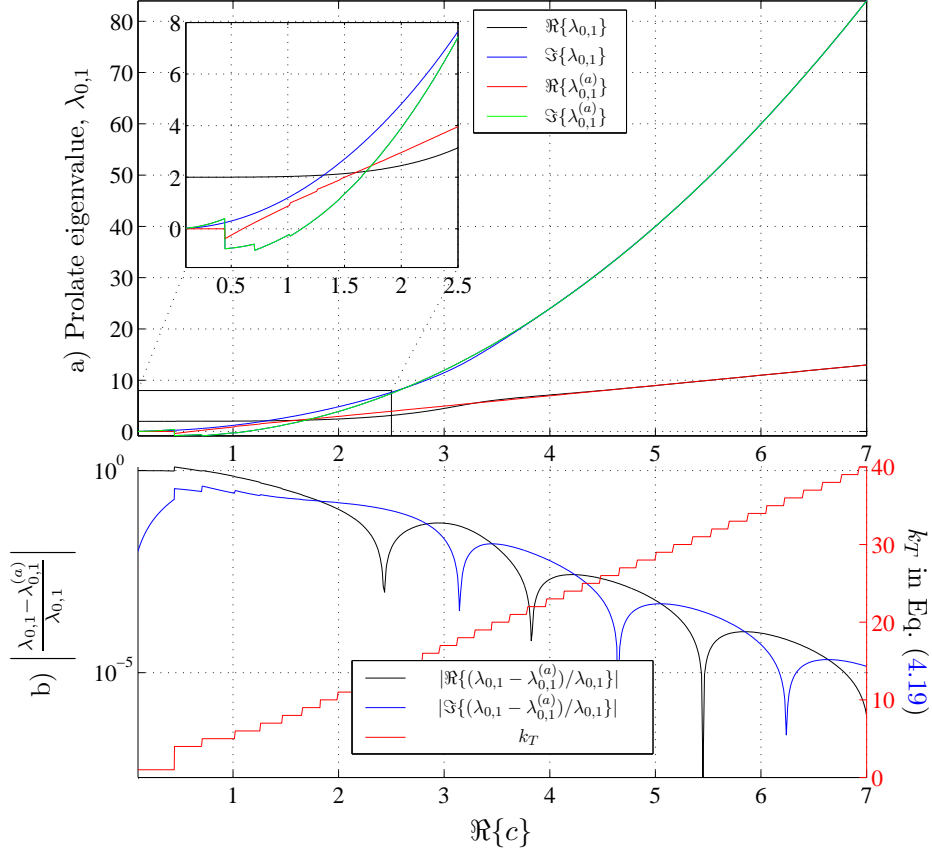


Figure 4-8: a) Spheroidal eigenvalues $\lambda_{0,1}$ for $c = (1 + i)\alpha$, $\alpha = [0, 7]$. b) Relative error between the prolate eigenvalue from Hogde's method [2], $\lambda_{0,1}$, and its *oblate*-type asymptotic expansion [Eq. (4.19)], $\lambda_{0,1}^{(a)}$.

function of degree n and order m ,

$$S_{mn}(c, 0) \approx C_{Pe} \left[\sum_{r=-\infty}^{\infty} C_r D_{n_p - m + r}(0) \right] = P_n^m(0) \quad (4.28)$$

where we have extracted the normalizing constant C_{Pe} . Note that n_p has been inserted into the parabolic cylinder expansion reflecting the fact that this is only for *prolate*-type asymptotic expansions and therefore ordering must be according to n_p instead of n . The associated Legendre function $P_n^m(\eta)$ retains n as the order because this index is specified by the n of $S_{mn}(c, \eta)$. Based on the expressions for the Legendre and parabolic cylinder

functions of zero argument [88], C_{Pe} becomes

$$C_{Pe} = \frac{\left[(-1)^{\frac{n-m}{2}}(n+m)!\right] / \left[2^n \left(\frac{n-m}{2}\right)! \left(\frac{n+m}{2}\right)!\right]}{\sum'_{r=-\infty}^{\infty} C_r \frac{\sqrt{\pi}}{2^{\frac{-(n_p-m+r)}{2}} \Gamma\left(\frac{1-(n_p-m+r)}{2}\right)}} \quad (4.29)$$

where Γ refers to the Gamma function [88].

When $(n-m) \Rightarrow \text{odd}$, we constrain the value of the first derivative of the asymptotic expansion at $\eta = 0$ to be equal to the derivative of the associated Legendre function of degree n and order m ,

$$S'_{mn}(c, 0) \approx C_{Po} \frac{\partial}{\partial \eta} \left[(1 - \eta^2)^{\frac{m}{2}} \sum'_{r=-\infty}^{\infty} C_r D_{n_p-m+r}(\eta\sqrt{2c}) \right] \Big|_{\eta=0} = P_n^{m'}(0) \quad (4.30)$$

having extracted the normalizing constant C_{Po} . The derivative of the left side of Eq. (4.30) can be expressed as

$$(1 - \eta^2)^{\frac{m}{2}} \left[\sum'_{r=-\infty}^{\infty} C_r \left[D'_{n_p-m+r}(\eta\sqrt{2c}) \right] \sqrt{2c} \right] + \left[\sum'_{r=-\infty}^{\infty} C_r D_{n_p-m+r}(\eta\sqrt{2c}) \right] \frac{m}{2} (1 - \eta^2)^{\frac{m}{2}-1} (-2\eta). \quad (4.31)$$

When $\eta = 0$ in Eq. (4.31), the normalization constant for the *prolate*-type asymptotic expansion for $(n-m) \Rightarrow \text{odd}$ becomes

$$C_{Po} = \frac{\left[(-1)^{\frac{n-m-1}{2}}(n+m+1)!\right] / \left[2^n \left(\frac{n-m-1}{2}\right)! \left(\frac{n+m+1}{2}\right)!\right]}{- \sum'_{r=-\infty}^{\infty} C_r \frac{\sqrt{2c\pi}}{2^{\frac{-(n_p-m+r+1)}{2}} \Gamma\left(\frac{-(n_p-m+r)}{2}\right)}}. \quad (4.32)$$

The *oblate*-type asymptotic expansions of the PASWF require similar normalizations. When $(n-m) \Rightarrow \text{even}$, we constrain the value of the *oblate*-type asymptotic expansion at

$\eta = 0$ to be equal to the associated Legendre function of degree n and order m ,

$$S_{mn}(-ic, 0) \approx C_{Oe} \left[\sum_{r=-\nu}^{\infty} A_r \left\{ e^{ic} L_{\nu+r}^{(m)}(-i2c) + (-1)^{n-m} e^{ic} L_{\nu+r}^{(m)}(-i2c) \right\} \right] = P_n^m(0). \quad (4.33)$$

where ν is now defined as

$$\nu = \begin{cases} \frac{n_o - m}{2}, & (n - m) \text{ even} \\ \frac{n_o - m - 1}{2}, & (n - m) \text{ odd.} \end{cases} \quad (4.34)$$

It is important to note that the n in the factor $(-1)^{n-m}$ in Eqs. (4.33) and (4.37) remains the n of the prolate angular function, $S_{mn}(-ic, \eta)$ (as opposed to being replaced by n_o), because it is introduced to assure the symmetry or antisymmetry of the prolate angular functions. Therefore it remains associated with them rather than with the *oblate*-type asymptotic expansion. In this case, since $(n - m) \Rightarrow \text{even}$, Eq. (4.33) reduces to

$$S_{mn}(-ic, \eta) \approx C_{Oe} \left[\sum_{r=-\nu}^{\infty} A_r 2 e^{ic} L_{\nu+r}^{(m)}(-i2c) \right] = P_n^m(0). \quad (4.35)$$

Thus, the normalization constant, C_{Oe} , for the *oblate*-type asymptotic expansion, $(n - m) \Rightarrow \text{even}$, is

$$C_{Oe} = \frac{\left[(-1)^{\frac{n-m}{2}} (n+m)! \right] / \left[2^n \left(\frac{n-m}{2} \right)! \left(\frac{n+m}{2} \right)! \right]}{2e^{ic} \sum_{r=-\nu}^{\infty} A_r L_{\nu+r}^{(m)}(-i2c)} \quad (4.36)$$

Finally, the normalization constant for the *oblate*-type asymptotic expansion when $(n - m) \Rightarrow \text{odd}$ can be found by constraining the value of the first derivative of the asymptotic expansion at $\eta = 0$ to be equal to the derivative of the associated Legendre function of degree n and order m ,

$$\begin{aligned} S'_{mn}(-ic, 0) &\approx \\ C_{Oo} \frac{\partial}{\partial \eta} \left[(1 - \eta^2)^{\frac{m}{2}} \sum_{r=-\nu}^{\infty} A_r \left\{ \frac{L_{\nu+r}^{(m)}[-i2c(1 - \eta)]}{e^{-ic(1 - \eta)}} + (-1)^{n-m} \frac{L_{\nu+r}^{(m)}[-i2c(1 + \eta)]}{e^{-ic(1 + \eta)}} \right\} \right] \Big|_{\eta=0} \\ &= P_n^{m'}(0). \quad (4.37) \end{aligned}$$

Expansion Type	$(n - m)$	Normalization Constant
Prolate	even	$C_{Pe} = \frac{[(-1)^{\frac{n-m}{2}}(n+m)!]}{[2^n (\frac{n-m}{2})! (\frac{n+m}{2})!]} \frac{\sqrt{\pi}}{\sum_{r=-\infty}^{\infty} C_r \frac{2^{-(n_p-m+r)}}{\Gamma(\frac{1-(n_p-m+r)}{2})}}$
	odd	$C_{Po} = \frac{[(-1)^{\frac{n-m-1}{2}}(n+m+1)!]}{[2^n (\frac{n-m-1}{2})! (\frac{n+m+1}{2})!]} \frac{\sqrt{2c\pi}}{-\sum_{r=-\infty}^{\infty} C_r \frac{2^{-(n_p-m+r+1)}}{\Gamma(\frac{-(n_p-m+r)}{2})}}$
Oblate	even	$C_{Oe} = \frac{[(-1)^{\frac{n-m}{2}}(n+m)!]}{[2^n (\frac{n-m}{2})! (\frac{n+m}{2})!]} \frac{1}{2e^{ic} \sum_{r=-\nu}^{\infty} A_r L_{\nu+r}^{(m)}(-i2c)}$
	odd	$C_{Oo} = \frac{[(-1)^{\frac{n-m-1}{2}}(n+m+1)!]}{[2^n (\frac{n-m-1}{2})! (\frac{n+m+1}{2})!]} \frac{1}{-i2c e^{ic} \sum_{r=-\nu}^{\infty} A_r \{L_{\nu+r}^{(m)}(-i2c) - 2L_{\nu+r}^{(m)'}(-i2c)\}}$

Table 4.4: Normalization table for both *prolate*-type or *oblate*-type asymptotic expansions with $(n - m)$ both *even* and *odd*.

After taking the derivative of the left side of Eq. (4.37) and letting $\eta = 0$, one obtains the normalization constant for the *oblate*-type asymptotic expansion for $(n - m) \Rightarrow$ *odd* as

$$C_{Oo} = \frac{[(-1)^{\frac{n-m-1}{2}}(n+m+1)!]}{[2^n (\frac{n-m-1}{2})! (\frac{n+m+1}{2})!]} \frac{1}{-i2c e^{ic} \sum_{r=-\nu}^{\infty} A_r \{L_{\nu+r}^{(m)}(-i2c) - 2L_{\nu+r}^{(m)'}(-i2c)\}}. \quad (4.38)$$

Table 4.4 summarizes the normalization constants required in order to calculate the asymptotic expansion of the prolate angular function for any combination of n and m and either the *prolate*-type or *oblate*-type asymptotic expansion.

4.5 Discussion

$S_{0,0}(c, \eta)$, $S_{0,3}(c, \eta)$, and $S_{0,4}(c, \eta)$ for $c = (1 + i)20$ and $\eta = [0, 1]$ with their asymptotic expansions (all *prolate*-type) are shown in Fig. 4-9. Their first derivatives for the same c

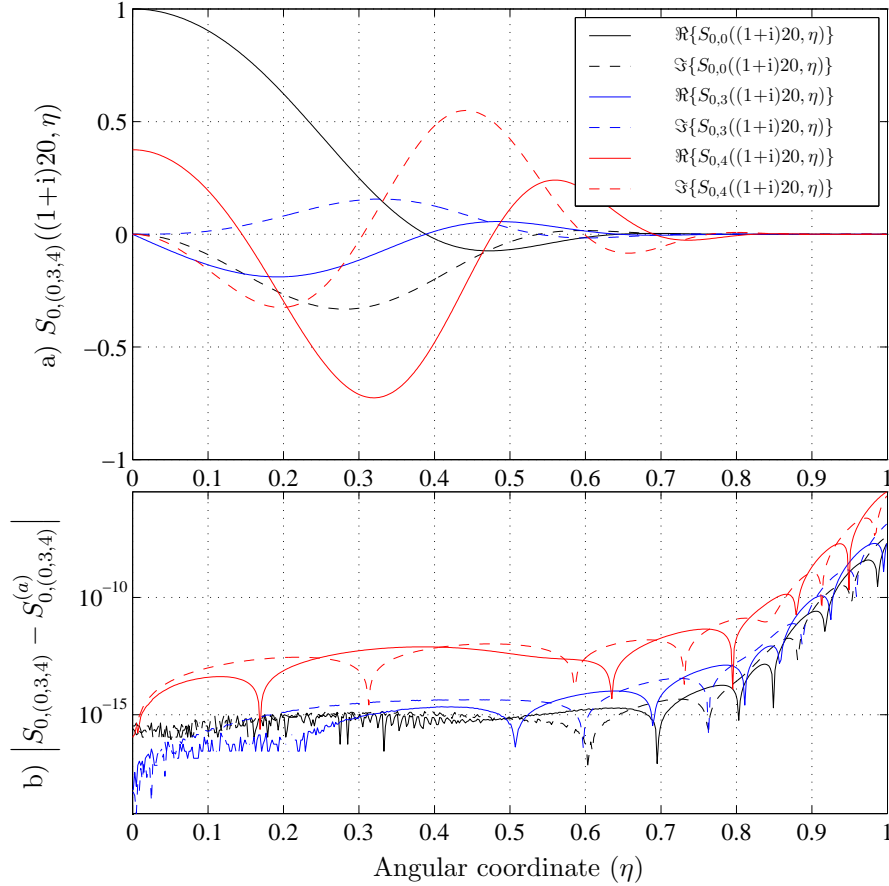


Figure 4-9: a) $S_{mn}(c, \eta)$ for $c = (1+i)20$, $m = 0$, $n = (0, 3, 4)$ (or $[n_p = 0, 1, 2]$), and $0 \leq \eta < 1$. b) Absolute error between Legendre expansion, $S_{mn}(c, \eta)$ from Eq. (4.5), and *prolate*-type asymptotic expansion, $S_{mn}^{(a)}(c, \eta)$ from Eqs. (4.7) and (4.11).

are shown in Fig. 4-10. For this size parameter c and range of n , both the original Legendre expansion, Eq. (4.5), and its *prolate*-type asymptotic expansion, Eqs. (4.7) and (4.11), are accurate expansions to at least 5 or 6 decimal places. This is not always the case. In fact, the *prolate*-type expansion of the PASWF described in Section 4.3.1 merely extends the region of accuracy for $S_{mn}(c, \eta)$ further toward $|\eta| \Rightarrow 1$ (see Fig. 4-13). This has been noticed by Slepian [68] and others, who provide other expansions in an effort to extend the region of applicability of the *prolate*-type asymptotic expansion to all values of η (and ξ). We do not implement or elaborate on these expansions here. However, it should be noted that all other *prolate*-type and *oblate*-type asymptotic expansions found in the literature

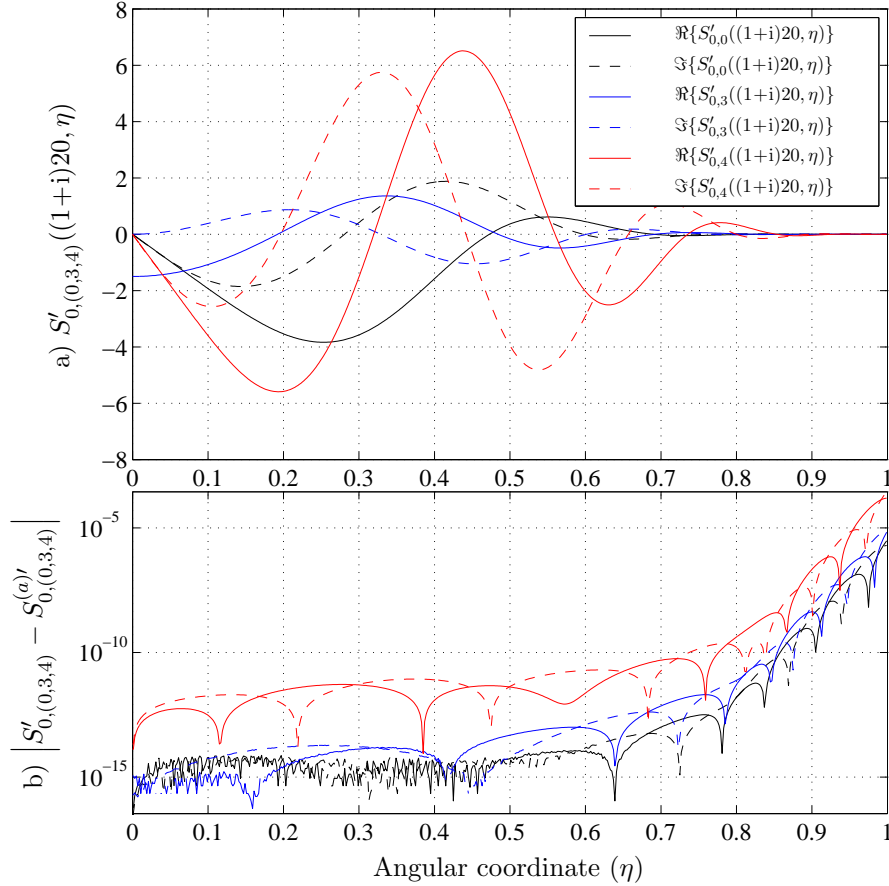


Figure 4-10: a) $S'_{mn}(c, \eta)$ for $c = (1+i)20$, $m = 0$, $n = (0, 3, 4)$ (or $[n_p = 0, 1, 2]$), and $0 \leq \eta < 1$. b) Absolute error between derivative of Legendre expansion, $S'_{mn}(c, \eta)$ from Eq. (4.5), and derivative of the *prolate*-type asymptotic expansion, $S^{(a)'}_{mn}(c, \eta)$ Eqs. (4.7) and (4.11).

adhere to the pattern dictated by the branch points, $c_{o;r}^{mn}$.

Some remarks about the behavior of these asymptotic expansions of the PASWFs for complex c are in order. To begin with, the magnitudes of the *oblate*-type functions increase with increasing $|\eta|$, whereas those functions approximated by *prolate* expansions [Eqs. (4.7) and (4.11)] decrease for increasing $|\eta|$. $S_{0,1}(c, \eta)$, $S_{0,2}(c, \eta)$, and $S_{0,5}(c, \eta)$ for $c = 20 + 20i$ and $\eta = [0, 1]$ with their asymptotic expansions (all *oblate*-type) are shown in Fig. 4-11. Their first derivatives for the same c are shown in Fig. 4-12. Furthermore, important differences are evident in the applicability of the expansions in Section 4.3 to the case of

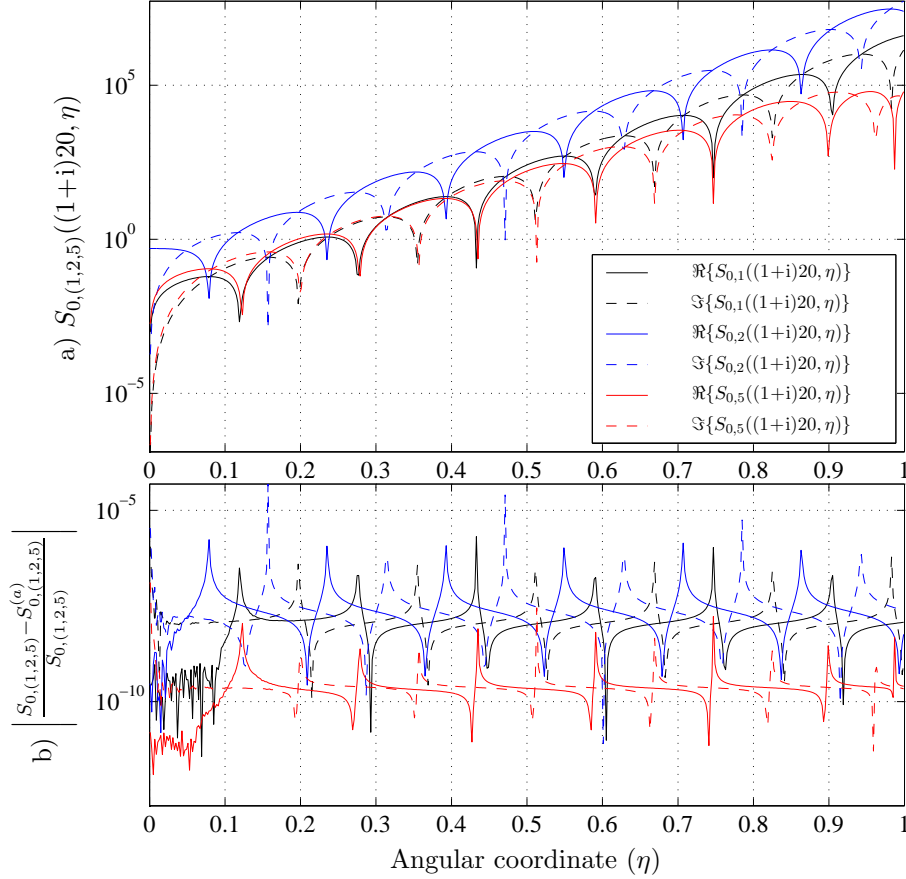


Figure 4-11: a) $S_{mn}(c, \eta)$ for $c = (1+i)20$, $m = 0$, $n = (1, 2, 5)$ (or $[n_o = 0, 1, 2]$), and $0 \leq \eta \leq 1$. b) Relative error between Legendre expansion, $S_{mn}(c, \eta)$ from Eq. (4.5) and *oblate*-type asymptotic expansion, $S_{mn}^{(a)}(c, \eta)$ from Eqs. (4.13) and (4.18).

$\eta > 1$, or in other words, to the PRSWF. For the case of the *prolate*-type expansions, the continued presence of singularities at $\eta = \pm 1$, even under transformation [Eq. (4.8)], causes increasing error as η approaches ± 1 . Letting η become greater than 1 in Eq. (4.1) case 1 does not lead to Eq. (4.9), but leads instead to

$$\frac{d^2 u_{mn}}{dx^2} + \left(- \left((n-m) + \frac{1}{2} \right) - \frac{x^2}{4} \right) = 0, \quad (4.39)$$

for which the solutions are functionally different from those for Eq. (4.9).

The *oblate*-type asymptotic expansion, however, has no such difficulty and in fact, the resulting differential equation Eq. (4.15) remains unchanged as η becomes > 1 . Letting η

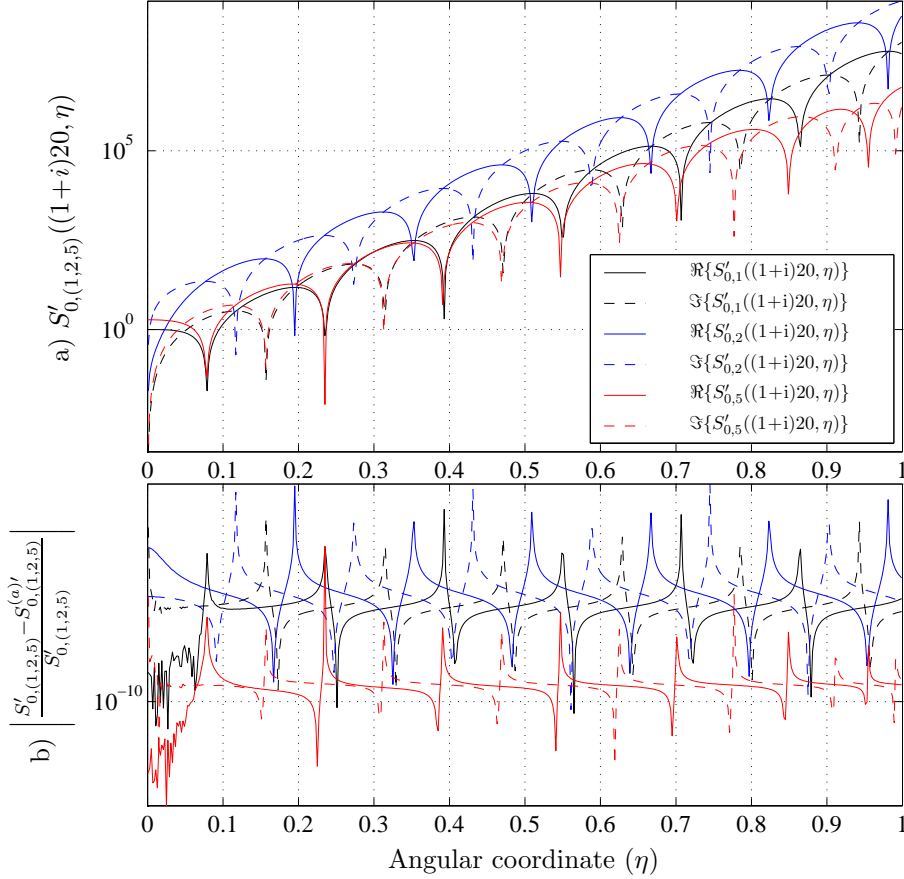


Figure 4-12: a) $S'_{mn}(c, \eta)$ for $c = (1+i)20$, $m = 0$, $n = (1, 2, 5)$ (or $[n_o = 0, 1, 2]$), and $0 \leq \eta \leq 1$. b) Relative error between derivative of Legendre expansion, $S'_{mn}(c, \eta)$ from Eq. (4.5) and derivative of the *oblate*-type asymptotic expansion $S_{mn}^{(a)'}(c, \eta)$ from Eqs. (4.13) and (4.18).

become greater than 1 is equivalent to transforming Eq. (4.1) case 1 to case 2 (or similarly case 3 to case 4) and assuming $\eta \Rightarrow \xi$ (or $\eta \Rightarrow i\xi$). In this case, the associated Laguerre functions of the second kind are useful for finding asymptotic solutions of Eq. (4.1) case 4, the solution to which is the ORSWFs [66, 77]. Both types of expansions for the radial functions obey the same pattern as described in Section 4.3.5 and summarized for c of the form $c = (1+i)\alpha$ in Table 4.3 for the PASWFs. Normalizations for the prolate radial functions for complex c need to properly account for the altered ordering based on n_p and n_o as determined via the lookup table.

Figure 4-13 shows the limits of the original Legendre function expansions as compared

to the asymptotic expansions. The *prolate*-type functions are incorrect for large $|\eta|$ while the asymptotic expansion is accurate for a larger range. We can obtain accurate $S_{mn}(c, \eta)$ over the entire domain ($-1 \leq \eta \leq 1$) by using a number of different expansions, for example the expansion Equation (3.11) in [3]. This expansion becomes more accurate for smaller ξ (or η) as $c \uparrow \infty$, and applies to η beyond the region where the expansion in Eq. (4.10) fails. To use this expansion the proportionality constant between $S_{mn}(c, \eta)$ and $R_{mn}(c, \xi)$, i.e. the joining factor κ_{mn} , must be calculated using values for the angular and radial spheroidal wave functions in the overlapping region of accuracy. Note also that for this *prolate*-type asymptotic expansion $R_{mn}^{(a)}(c, \xi)$, n should be replaced by n_p , i.e. $R_{mn}(c, \xi) \approx R_{mn_p}^{(a)}(c, \xi)$. *Oblate*-type expansions for the PRSWF would naturally be approximated by $R_{mn}(c, \xi) \approx R_{mn_o}^{(a)}(c, \xi)$. As with the case of the ASWFs, the expansion pattern governing the RSWFs can be extracted from the lookup table of branch points obtained in Section 4.3.4.

Some representative values for the PSWFs, based on the expansion of Section 4.3 and in the asymptotic regime considered here, are given in Table 4.5. More extensive tables cataloging the spheroidal eigenvalues, λ_{mn} , and the prolate spheroidal wave functions and their derivatives, $S_{mn}(c, \eta)$, $S'_{mn}(c, \eta)$, are given in D.

m	n	c or		exp. type	$\lambda_{mn}^{(a)}$	$S_{mn}^{(a)}(c, \eta)$	$S_{mn}^{(a)'}(c, \eta)$
		c	arg(c)				
0	0	(1+i)	20	Pro	1.92453281e+01 + 2.00049941e+01i	-6.83836700e-02 - 3.39951350e-02i	3.63351070e-01 + 1.16571397e+00i
0	1	(1+i)	20	Obl	3.89937623e+01 + 7.59993426e+02i	-2.57938462e+02 - 6.09345190e+01i	-6.20443272e+03 + 3.98256577e+03i
0	2	(1+i)	20	Obl	3.89937623e+01 + 7.59993426e+02i	3.05857460e+03 - 2.00264676e+03i	1.90507143e+04 - 9.98963377e+04i
0	3	(1+i)	20	Pro	5.82267144e+01 + 6.00256155e+01i	5.50084037e-02 + 2.73108705e-02i	-1.65474256e-01 - 8.74325313e-01i
0	0	(1+3/4i)	20	Pro	2.18720402e+01 + 1.69748407e+01i	-3.47455676e-02 - 4.09615124e-02i	3.53508024e-02 + 8.55512159e-01i
0	1	(1+3/4i)	20	Pro	6.61052450e+01 + 5.09337263e+01i	-1.86395360e-02 - 2.19543826e-02i	-2.39785921e-02 + 4.07982154e-01i
0	2	(1+3/4i)	20	Obl	2.56935925e+02 + 7.22737790e+02i	-2.55445410e+02 - 7.62763344e+02i	-2.14280028e+04 - 6.65075161e+03i
0	3	(1+3/4i)	20	Obl	2.56935925e+02 + 7.22737790e+02i	5.15777934e+01 - 7.02010195e+01i	-7.48251071e+02 - 2.31164090e+03i
1	1	20 $\sqrt{2}$	82.5 $^\circ$	Obl	-6.62608483e+02 + 1.92282723e+02i	-6.38183239e+04 - 2.24521930e+05i	-2.49033999e+06 - 5.60757007e+06i
1	2	200 $\sqrt{2}$	75 $^\circ$	Obl	-6.81912154e+04 + 3.97071788e+04i	9.09767490e+55 + 4.24988282e+56i	5.57846942e+58 + 1.08598335e+59i
1	3	20 $\sqrt{2}$	67.5 $^\circ$	Pro	1.10776528e+01 + 2.61206172e+01i	3.66399689e-01 - 1.36935639e-01i	-4.17673071e+00 - 4.73542913e+00i
1	4	200 $\sqrt{2}$	60 $^\circ$	Pro	4.23515050e+02 + 7.34845178e+02i	-4.46622017e-09 + 2.60371439e-08i	4.03463760e-06 - 1.42147750e-06i
1	5	20 $\sqrt{2}$	52.5 $^\circ$	Pro	8.33329846e+01 + 1.12201499e+02i	1.37884345e+00 + 2.88997048e+00i	3.17195438e+01 - 3.17033885e+01i
3	3	200 $\sqrt{2}$	45 $^\circ$	Pro	2.08260781e+02 + 1.99989137e+02i	-3.44330629e-12 - 3.82844150e-11i	-4.02443549e-09 + 4.79990764e-09i
3	4	200 $\sqrt{2}$	37.5 $^\circ$	Pro	6.80467972e+02 + 5.16523773e+02i	-2.60817965e-12 + 4.83013584e-12i	8.10759895e-10 - 3.53034286e-10i
3	5	200 $\sqrt{2}$	30 $^\circ$	Pro	1.23005566e+03 + 7.07071083e+02i	4.77547059e-11 + 2.20057916e-11i	-4.71197888e-09 - 6.89895126e-09i
3	3	20 $\sqrt{2}$	45 $^\circ$	Pro	2.83577369e+01 + 1.98839189e+01i	-9.98471665e-01 - 5.19994344e-01i	5.16758633e+00 + 1.72331507e+01i
3	4	20 $\sqrt{2}$	37.5 $^\circ$	Pro	7.49297681e+01 + 5.13430059e+01i	-2.00381999e+00 - 2.28550597e+00i	-1.99261253e+00 + 4.31871548e+01i
3	5	20 $\sqrt{2}$	30 $^\circ$	Pro	1.28377385e+02 + 7.02592909e+01i	8.18626749e+00 - 3.13154480e+01i	-3.31331032e+02 + 2.10442556e+02i
4	4	200 $\sqrt{2}$	22.5 $^\circ$	Pro	2.76588216e+02 + 1.08228546e+02i	-2.57734140e-14 - 6.79600600e-14i	-3.70059261e-13 + 1.18316534e-11i
4	5	200 $\sqrt{2}$	15 $^\circ$	Pro	8.33944637e+02 + 2.19593771e+02i	-6.61149570e-14 + 2.65401397e-14i	1.13666158e-11 - 1.31862709e-12i
4	6	200 $\sqrt{2}$	7.5 $^\circ$	Pro	1.41449695e+03 + 1.84574257e+02i	4.11004645e-13 + 4.04943129e-12i	2.18766576e-11 - 6.43661714e-10i
4	5	20 $\sqrt{2}$	7.5 $^\circ$	Pro	9.92587462e+01 + 1.09491032e+01i	1.11029103e+01 - 5.89455918e+00i	-1.63601043e+02 + 5.69861065e+01i

Table 4.5: Some values for the PASWF and its derivative. $\eta = .5$ for all cases listed.

The computer codes used for evaluating the PSWFs in this work are available for educational and research use. Interested readers may contact the author or go to [99].

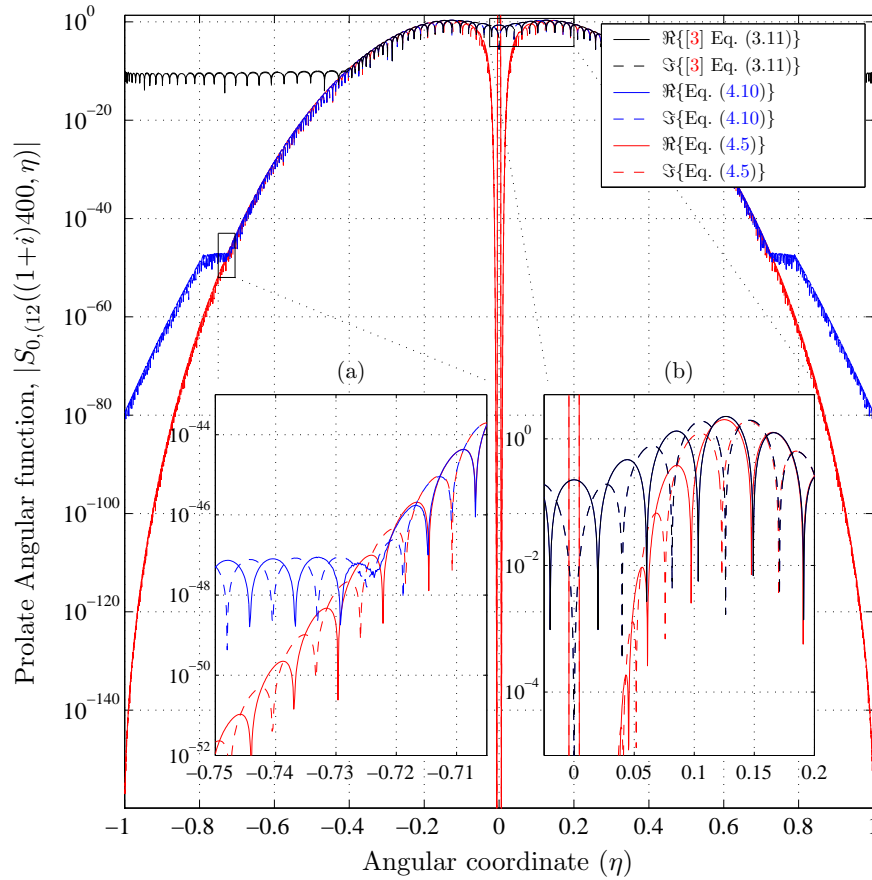


Figure 4-13: $\Re\{S_{0,12}((1+i)400, \eta)\}$ and $\Im\{S_{0,12}((1+i)400, \eta)\}$ ($n_p = 6$), for $-1 \leq \eta \leq 1$. Legendre expansion [Eq. (4.5), black curves], *prolate*-type asymptotic expansion [Eqs. (4.7) and (4.11), blue curves], and Miles [3] Bessel-type asymptotic approximation (Equation (3.11) therein, red curves). $\lambda_{0,12}^{(a)} = 5178.20430071674 + 5200.04621007177i$.

4.6 Summary and Conclusion

The asymptotic expansion of the spheroidal wave function (SWF) and its eigenvalues have been investigated for complex size parameter c . No fundamentally new asymptotic expansions are required, but instead, established *prolate*-type and *oblate*-type asymptotic expansions are directly applicable to finding the asymptotic expansion of the SWF for complex size parameter c . A rapid and accurate method for calculating the SWFs for complex c in the asymptotic regime has been presented based on a lookup table consisting of branch

points, $c_{o;r}^{mn}$. Through a brute force numerical method, this lookup table, based on the number of branch cuts (emanating from $c_{o;r}^{mn}$) traversed according to $\arg(c)$, is calculated once and recorded. This allows the assignment of any SWF to either a *prolate*-type or *oblate*-type expansion (ordered by n_p and n_o respectively) for any general complex size parameter c . The ordering for these expansions was found to be different than the original ordering of the spheroidal wave functions, with Table 4.3 documenting the ordering for the special case when $\arg(c) = \pi/4$. Normalizations, dependent on c , were derived for both the *prolate* and *oblate*-type asymptotic expansions and for both $(n - m)$ even and odd. These normalized asymptotic expansions for the PASWFs $S_{mn}(c, \eta)$ and $S'_{mn}(c, \eta)$, together with established asymptotic expansions for the prolate radial spheroidal wave functions $R_{mn}(c, \eta)$ and $R'_{mn}(c, \eta)$, allow the rapid calculation of the vector spheroidal wave functions for significantly larger (complex) size parameter c than previously possible.

Chapter 5

Broadband Analytical Magnetoquasistatic Electromagnetic Induction Solution for a Conducting and Permeable Spheroid

5.1 Introduction

Electromagnetic induction (EMI) techniques have long been important in geophysical surveying [100,101,102]. In the past ten years or so, intense interest has focused on small ultra-wide band (UWB) electromagnetic induction (EMI) (10's of Hz up to 100's of kHz) sensors used for shallow surveying to detect and discriminate metallic objects with one principal application being the detection and discrimination of unexploded ordnance (UXO) [103, 104, 105, 106, 107]. UXO contaminate wide regions of the globe and render those regions dangerous at best and uninhabitable at worst [108,109,110]. Typical UXO are nonspherical, however, thus complicating the detection and discrimination process. Some examples of UXO are pictured in Fig. 5-2.

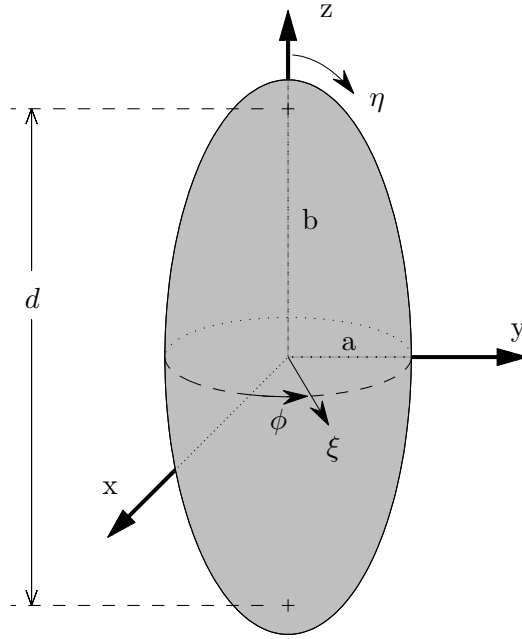


Figure 5-1: Spheroidal Geometry: $1 \leq \xi < \infty$ (Oblate case: $0 \leq \xi < \infty$), $-1 \leq \eta \leq 1$, $0 \leq \phi \leq 2\pi$, $x = \frac{d}{2}[(1 \mp \eta^2)(\xi^2 \mp 1)]^{\frac{1}{2}} \cos(\phi)$, $y = \frac{d}{2}[(1 \mp \eta^2)(\xi^2 \mp 1)]^{\frac{1}{2}} \sin(\phi)$, $z = \frac{d}{2}\eta\xi$, $e = \frac{b}{a}$, $\xi = (\pm(1 - e^{-2}))^{-\frac{1}{2}}$, $d = 2(\pm(b^2 - a^2))^{\frac{1}{2}}$. Upper sign \rightarrow prolate, lower sign \rightarrow oblate.

While the solution for the induced magnetic field and potential within and around a conducting and permeable sphere under time harmonic excitation were first proposed by Wait [111, 112] over fifty years ago, lack of an analytical magnetoquasistatic solution for nonspherical shapes has hampered development of appropriate signal processing, inversion, and even instrument calibration. Recently some important progress has been made in formulating and evaluating spheroidal EMI solutions [63, 62]. While special approximations resolved evaluation problems at high EMI frequencies, and the full analytical formulation worked well at low EMI frequencies, stability problems persisted in the mid-frequency range, depending on the geometrical and material properties of the spheroid. To remedy this, we construct a combined solution for the induced magnetic field from metallic spheroids that applicable over the entire EMI band, for both oblate and prolate spheroidal shapes.

Our combined system incorporates asymptotic approximations of the angular and radial spheroidal wave functions (ASWFs and RSFWs) (see Chapter 4) into these existing low and

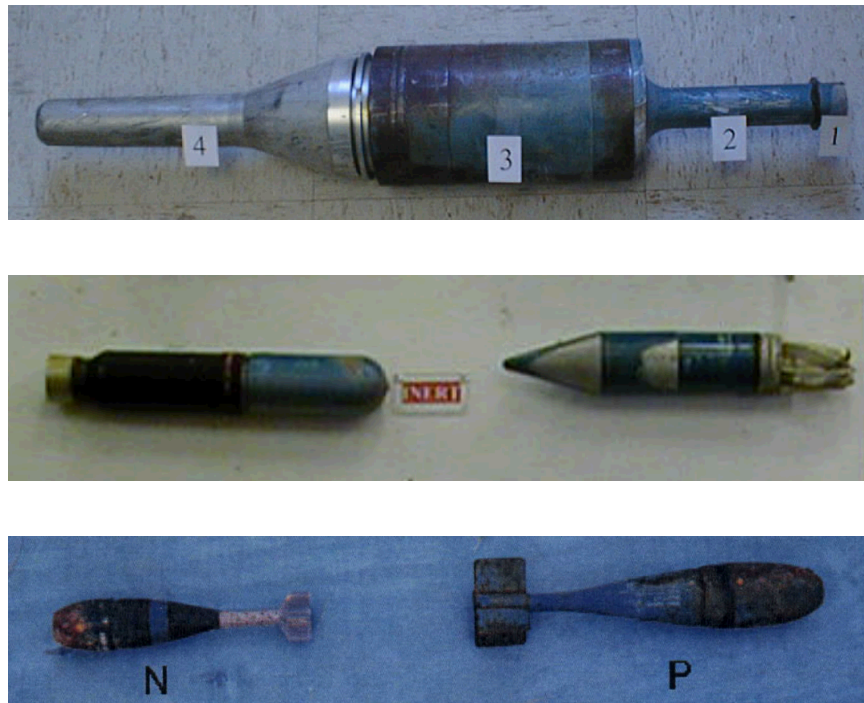


Figure 5-2: Some examples of unexploded ordnance (UXO).

high frequency solutions [63] for the induced magnetic field. This extends the frequency range over which the induced magnetic field external to the spheroid may be obtained to cover the problematical mid-frequency range. To be more specific, “low” frequency generally refers to frequencies ranging from static to frequencies below the resonant peak of the phase quadrature response of the induced magnetic field. “High” EMI frequencies are those at which the skin depth of the metallic object is very small relative to its dimensions. As frequency increases further into this “high” frequency range, the EMI response asymptotically approaches the high frequency limit of vanishing internal magnetic field and the object acts as a perfect (EMI) reflector.

Section 5.2 contains a brief review of the formulation for the exact solution for the magnetic field within and around a conducting and permeable spheroid under time harmonic excitation, valid at small size parameters (or frequencies). Section 5.3.1 presents an asymptotic-assisted analytical solution based on known asymptotic expansions (Chapter 4) of the spheroidal wave functions (SWFs). One other approach proposed in the literature to bridge this frequency gap is to implement a rational function approximation [62] which is based on the singular expansion method (SEM) [113]. However, this solution is neither rigorous nor exact, and can yield incorrect results for underdetermined systems. Our asymptotic-assisted solution realizes all higher order terms for mid-frequencies until it too encounters numerical difficulties for higher frequencies. A small penetration approximation (SPA) is then used to find the solution for the external induced magnetic field at high frequencies for which the exact and asymptotic-assisted solutions do not converge. This SPA solution is summarized in Section 5.3.2.

Results for the induced magnetic field from a conducting and permeable spheroid are compared to both Wait’s solution (in the particular case of the sphere) as well as to a finite element/boundary integral (FE-BI) numerical solution [4] in the case of a spheroid, in Section 5.4.1. In Section 5.4.2, the induced fields predicted by our combined method are compared to ultrawide band (UWB) data obtained with the Geophex GEM-3 [114] instrument, for prolate and oblate, permeable (magnetic) and non-permeable machined spheroids. Model and data are found to be in excellent agreement if the permeability and conductivity of the spheroids are allowed to vary within acceptable physical ranges. Results

illustrate that solutions are distinct based on spheroid characteristics and orientation. On this basis, our method could become the forward problem component on which inversion schemes may be based.

5.2 Exact Formulation

The formulation for the exact analytical solution for the induced magnetic field from a conducting and permeable spheroid under time harmonic excitation in the magnetoquasistatic regime is given in [63] and will only be summarized here.

Let a spheroid with high conductivity σ and relative permeability μ_r (as compared to the background medium) be excited by a time harmonic primary field $\overline{H}_o(\vec{r})e^{-i\omega t}$ (time dependence expression $e^{-i\omega t}$ is suppressed below). We assume the background medium is homogeneous, only weakly magnetic, and poorly conducting so that the wavenumber, k_o , of the host medium may be approximated by $k_o \approx 0$. As a result of this magnetoquasistatic approximation [102], the primary magnetic field, $\overline{H}_o(\vec{r})$, and the induced (or secondary) external magnetic field, $\overline{H}_s(\vec{r})$, are irrotational and can be described by scalar potentials, $U_o(\vec{r})$ and $U_s(\vec{r})$ respectively which both satisfy the Laplace equation in spheroidal coordinates. The known primary field potential can be expanded in terms of solutions of the first kind of the Laplace equation in spheroidal coordinates

$$U_o(\vec{r}) = H_o \frac{d}{2} \sum_{m=0}^{\infty} \sum_{n=m}^{\infty} \sum_{p=0}^1 b_{pmn} P_n^m(\eta) P_n^m(\xi) T_{pm}(\phi), \quad (5.1)$$

where $P_n^m(\beta)$ represents the associated Legendre function of the first kind of degree n and order m [88]. Similarly, the secondary field potential can be expanded in terms of Laplace solutions of the second kind as

$$U_s(\vec{r}) = H_o \frac{d}{2} \sum_{m=0}^{\infty} \sum_{n=m}^{\infty} \sum_{p=0}^1 B_{pmn} P_n^m(\eta) Q_n^m(\xi) T_{pm}(\phi), \quad (5.2)$$

where $Q_n^m(\beta)$ represents the associated Legendre function of the second kind of degree n and order m [88] and B_{pmn} are unknown secondary induced field expansion coefficients.

The total external magnetic field is the sum of the primary and secondary fields

$$\overline{H}_2 = \overline{H}_o + \overline{H}_s = -\nabla U_o - \nabla U_s. \quad (5.3)$$

Within the highly conducting object, the internal magnetic field of the spheroid, $\overline{H}_1(\vec{r})$, can be found by solving the vector wave equation in spheroidal coordinates

$$\nabla \times \nabla \times \overline{H}_1(\vec{r}) - k_1^2 \overline{H}_1(\vec{r}) = 0 \quad (5.4)$$

where $k_1^2 = i\omega\sigma_1\mu_1$. Under these assumptions, the Helmholtz equation above becomes a diffusion equation. $\overline{H}_1(\vec{r})$ can be expressed as an infinite series of vector spheroidal wave functions (VSWFs) \overline{M} and \overline{N} as

$$\overline{H}_1 = H_o \sum_{m=0}^{\infty} \sum_{n=m}^{\infty} \sum_{p=0}^1 \left[A_{pmn}^{(M)} \overline{M}_{pmn}^{r(1)}(c_1; \eta, \xi, \phi) + A_{pmn}^{(N)} \overline{N}_{pmn}^{r(1)}(c_1; \eta, \xi, \phi) \right] \quad (5.5)$$

where the size parameter, c , of a spheroid is defined as

$$c = \frac{k_1 d}{2}, \quad (5.6)$$

k_1 is the wavenumber inside the spheroid, and d is the interfocal distance.

$\overline{M}_{pmn}^{r(1)}(c_1; \eta, \xi, \phi)$ and $\overline{N}_{pmn}^{r(1)}(c_1; \eta, \xi, \phi)$ are in turn composed of the angular and radial SWFs, $S_{mn}(c, \eta)$ and $R_{mn}(c, \xi)$ [66] as well as the harmonic functions $T_{pm}(\phi)$ defined as

$$T_{pm}(\phi) = \begin{cases} \cos(m\phi) & p=0, \\ \sin(m\phi) & p=1. \end{cases} \quad (5.7)$$

The exact solution for \overline{H}_s can be obtained by matching the tangential magnetic fields, \overline{H}_η and \overline{H}_ϕ , and the normal component of the magnetic flux density, \overline{B}_ξ , at the surface of

the spheroid, i.e.

$$H_{1\eta} = H_{2\eta} \quad (5.8a)$$

$$\mu_r H_{1\xi} = H_{2\xi} \quad (5.8b)$$

$$H_{1\phi} = H_{2\phi} \quad (5.8c)$$

where $\mu_r = \mu_1/\mu_2$ is the relative permeability of the spheroid compared to the surrounding medium. Substituting Eqs. (5.1)–(5.6) into Eq. (5.8) results in an infinite set of equations which must be massaged, truncated, and then cast into matrix form in order to be solved [63].

Even though this solution for the induced magnetic field from a conducting and permeable spheroid is theoretically applicable for any frequency satisfying the magnetoquasistatic assumptions, two problems limit the practical applicability of this solution. The first is that the basis functions used to express the magnetic field internal to the spheroid, in this case the angular (ASWF) and radial (RSWF) spheroidal wave functions, $S_{mn}(c, \eta)$ and $R_{mn}(c, \xi)$ respectively, are in general not orthogonal to each other for different m , n , and c as are the spherical wave functions. Because of this, the complexity of the solution is increased due to the infinite sets of equations arise when matching the boundary conditions at the spheroidal surface.

The second, more challenging difficulty is that the angular and radial SWFs, which must be evaluated as part of $\overline{M}_{pmn}^{r(1)}(c_1; \eta, \xi, \phi)$ and $\overline{N}_{pmn}^{r(1)}(c_1; \eta, \xi, \phi)$, become unstable at moderate size parameters (or frequencies) on the order of $|c| \approx 30$ [66, 63]. This tendency to diverge is shown qualitatively in Section 5.4.1 Fig. 5-4 where the frequencies to the left of the first dashed vertical line indicate the limited region of stability of the exact method. This numerical difficulty is typically encountered at frequencies lower than that where the resonant peak of the response is fully developed. Some other method is therefore desirable, to extend the range of frequencies over which solutions for the induced magnetic field are tractable. In the next section, we implement asymptotic expansions of the SWFs in order to extend the solution's range of stability to higher frequencies. However, the size parameter c for the wave (in this case, diffusion) equation is complex (see Section 5.2), and asymptotic

expansions of the SWFs for the case of complex size parameter have not been treated extensively in the literature (for a summary, see [115]).

5.3 High Frequency Approximations

5.3.1 Asymptotic Expressions for the Spheroidal Wave Functions

We use asymptotic expansions of the spheroidal wave function for complex size parameter c [115, 82] to extend the range over which the full analytical solution is stable to larger c than previously possible. Through the use of these asymptotic expansions, the maximum c for which the full analytic solutions is stable is increased closer to the size parameter for which the small penetration approximation (SPA [63], see Section 5.3.2) is valid. Accordingly, the accuracy of the induced field solution for this mid-frequency range is on the same order as the accuracy of the asymptotic expansions. Unfortunately, some aspect of this asymptotic-assisted solution also becomes numerically unstable at a frequency that is a function of the relative permeability, μ_r , the overall dimensions a and b of the spheroid, and the aspect ratio $e = b/a$.

The original Legendre and Bessel function expansions for the ASWF and RSWF respectively become unstable in double precision for size parameters larger than $|c| \approx 30$ [63, 66]. Consequently, the full analytic solution outlined in Section 5.2 fails to converge for spheroidal size parameters beyond this range. For these larger c , asymptotic expansions of the SWFs do exist which remain stable. However, these established asymptotic expansions traditionally treat only the cases of purely real (for the case of the prolate SWFs) or purely imaginary (oblate SWFs) size parameter [66, 76, 77, 115].

When c is complex, asymptotic representations of the prolate SWFs (for prolate spheroids) and the oblate SWFs (for oblate spheroids) consist of either the *prolate*-type or *oblate*-type asymptotic expansions (Chapter 4). The choice of which type of asymptotic expansion is appropriate is determined by the spheroidal parameters m , n , and the size parameter c through a comparison of $\arg(c)$ to a look up table containing the branch points, $c_{\sigma;r}^{mn}$ of the spheroidal wave equation. These branch points are found once through polynomial estimation techniques followed by a Newton-Raphson multivariable root finding method and

$(n - m)$	exp. $m=0$		exp. $m=1$		exp. $m=2$	
	type	n_p n_o	type	n_p n_o	type	n_p n_o
0	Pro.	0 -	Pro.	1 -	Pro.	2 -
1	Obl.	- 0	Pro.	2 -	Pro.	3 -
2	Obl.	- 1	Obl.	- 1	Pro.	4 -
3	Pro.	1 -	Obl.	- 2	Obl.	- 2
4	Pro.	2 -	Pro.	3 -	Obl.	- 3
5	Obl.	- 2	Pro.	4 -	Pro.	5 -
6	Obl.	- 3	Obl.	- 3	Pro.	6 -
7	Pro.	3 -	Obl.	- 4	Obl.	- 4
8	Pro.	4 -	Pro.	5 -	Obl.	- 5
\vdots	\vdots		\vdots		\vdots	

Table 5.1: Pattern governing n_p , n_o and which type of asymptotic expansion, either the *prolate*-type (Pro. above) or the *oblate*-type (Obl. above), for different combinations of m and n . c is of the form $c = (1 + i)\alpha$.

stored for reference (see Chapter 4). $c_{o;r}^{mn}$ for $0 \leq m \leq n \leq 110$ have been found, but for the purposes of this work, only $m \leq 1$, $n \leq 60$ are used. The diffusion equation, Eq. (5.4), dictates $\arg(c) = \pi/4$, for which a simple pattern, alternating between the *prolate* and *oblate* expansion types soon develops. Beginning at $n = m$, this pattern consists of $m + 1$ *prolate*-type expansions followed by alternating pairs of *oblate* then *prolate*-type expansions.

When computing the *prolate*-type and *oblate*-type asymptotic expansions of the spheroidal eigenvalues, λ_{mn} , (and $S_{mn}(c, \eta)$, denoted $\lambda_{mn}^{(a)}$ and $S_{mn}^{(a)}(c, \eta)$ respectively) for complex c , the ordering is different from the ordering, according to n , of the eigenvalues themselves. While the n indicates λ_{mn} ordering for each m , the $\lambda_{mn}^{(a)}$ are ordered according to m , but independently, corresponding to the sequential ordering for each type of expansion separately. Let n_p be the number of *prolate*-type expansions of λ_{mn} necessary, up to but excluding n , and n_o be the number of *oblate*-type expansions of λ_{mn} necessary, up to but excluding n . λ_{mn} can then be approximated by *prolate*-type $\lambda_{mn}^{(a)}$ ordered according to n_p beginning at $n_p = m$, and *oblate*-type $\lambda_{mn}^{(a)}$ ordered according to n_o beginning at $n_o = m$. This behavior can clearly be seen in Fig. 5-3, is summarized in Table 5.1, and can be succinctly written as (Chapter 4)

$$n_p = \begin{cases} n, & (n - m) \leq m \\ \left\lfloor \frac{(n-m)-m}{2} \right\rfloor + m + m, & (n - m) > m \end{cases} \quad (5.9)$$

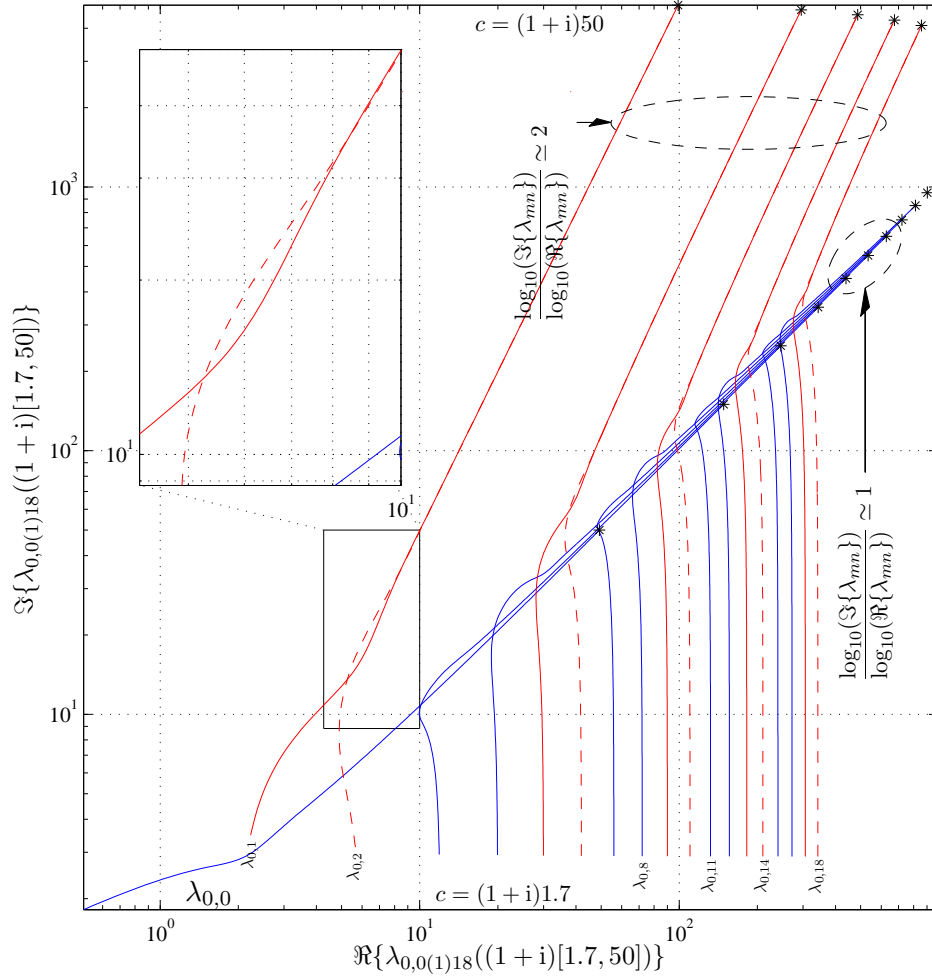


Figure 5-3: λ_{mn} : Eigenvalues of the spheroidal wave equation. $m = 0$ and $n = 0(1)18$. Each curve tracks an eigenvalue as c ranges from $c = (1+i)1.7$ (lower end of each curve) to $c = (1+i)50$ (upper end of each curve). Dashed curves indicate coalescing oblate eigenvalue pairs.

and

$$n_o = \left\lfloor \frac{(n-m) - m}{2} \right\rfloor + m, \tag{5.10}$$

where $\lfloor \cdot \rfloor$ denotes the floor function.

The *prolate*-type asymptotic expansion of the angular SWF, $S_{mn}^{(a)}(c, \eta)$, used in this work

is found by expanding $S_{mn}(c, \eta)$ in terms of an infinite series of the form,

$$S_{mn}(c, \eta) \approx S_{mn}^{(a)}(c, \eta) = (1 - \eta^2)^{\frac{m}{2}} \sum'_{r=-\infty}^{\infty} C_r D_{n_p-m+r}(x) \quad (5.11)$$

where $D_{n_p-m+r}(x)$ is the parabolic cylinder function of order $(n_p - m + r)$ [88] (note the dependence on n_p), the prime indicates summation over even r , and C_r are expansion coefficients (Chapter 4 and [66, 76]). The eigenvalues in this case are expanded in an inverse power series as

$$\lambda_{mn} \approx \lambda_{mn}^{(a)} = \sum_{k=0}^{\infty} \Gamma_k(m, n_p) c^{-k+1} \quad (5.12)$$

where the functional dependence of the expansion coefficients Γ_k has been made explicit. C_r and $\Gamma_k(m, n_p)$ are found by substituting Eqs. (5.11) and (5.12) into the spheroidal wave equation [76].

If a given combination of m , n , and $\arg(c)$ requires an *oblate*-type asymptotic expansion for $S_{mn}(c, \eta)$, it is expressed as an infinite series of associated Laguerre polynomials, $L_{\nu+r}^{(m)}(x)$ [96, 88],

$$S_{mn}^{(a)}(-ic, \eta) = (1 - \eta^2)^{\frac{m}{2}} \sum_{r=-\nu}^{\infty} A_r \left\{ e^{-c(1-\eta)} L_{\nu+r}^{(m)} [2c(1-\eta)] \right. \\ \left. + (-1)^{n-m} e^{-c(1+\eta)} L_{\nu+r}^{(m)} [2c(1+\eta)] \right\}, \quad (5.13)$$

where A_r are expansion coefficients and $\nu = \begin{cases} (n_o - m)/2 \\ (n_o - m - 1)/2 \end{cases}$ when $(n_o - m)$ is $\begin{cases} \text{even} \\ \text{odd} \end{cases}$ (Chapter 4 and [66, 77]). The inverse power series representation for λ_{mn} now becomes

$$\lambda_{mn} = \sum_{k=0}^{\infty} \Gamma_k(m, n_o) (-ic)^{-k+2}. \quad (5.14)$$

where $\Gamma_k(m, n_o)$ are expansion coefficients. In a manner similar to that used in the case of the *prolate*-type asymptotic expansion, A_r and $\Gamma_k(m, n_o)$ for the *oblate*-type asymptotic expansion can be found by substituting Eqs. (5.13) and (5.14) into the spheroidal wave equation [77].

The original expansion for radial SWFs in terms of an infinite series of spherical Bessel

functions also becomes inaccurate for large c [66]. Fortunately, the RSWFs adhere to the same pattern of asymptotic expansion types as in the case of the ASWFs. Additionally, $S_{mn}(c, \eta)$ and $R_{mn}(c, \xi)$ are proportional for a given c , i.e.

$$S_{mn}^{(i)}(c, \eta) = \kappa_{mn}^{(i)}(c)R_{mn}^{(i)}(c, \eta) \quad (5.15)$$

where the superscript (i) indicates the *kind* of the SWF [66]. For the *prolate*-type asymptotic expansion of $R_{mn}(c, \xi)$, we use Equation (3.11) in Miles [3]. For the *oblate*-type asymptotic expansion of the RSWF, we use Eq. (5.15) because $S_{mn}^{(a)}(-ic, \eta)$ is much better behaved and suffers from fewer numerical problems for $|\eta| > 1$.

5.3.2 Small Penetration Approximation

For much higher frequencies which approach the limit of vanishing internal magnetic field, a small penetration approximation (SPA) for the internal magnetic field, $\overline{H}_1(\overline{r})$, has been developed [63, 7]. According to the SPA, the ξ -dependence of the azimuthal component of the internal magnetic field, $H_{1\phi}$, is approximated as a decaying exponential, $e^{-ik_1 h \xi}$, leading to a self-consistent equation relating the internal fields of the spheroid at the boundary. Using the boundary conditions of Eq. (5.8), \overline{H}_1 can then be expressed in terms of the components of $\overline{H}_2(\overline{r})$, thus avoiding any reference to the SWFs and the accompanying computational difficulty. This approach yields stable solutions for very large c , up into the frequency range in which the magnetic field inside the spheroid becomes negligible as it approaches the high frequency limit of zero field. In this frequency range, and the induced field can be well modeled as a dipole response from a perfect EMI reflector.

This SPA solution applies at very high frequencies, but has also been found to be moderately accurate for lower frequencies, especially for highly permeable objects. In anticipation of the non-convergence of the asymptotic-assisted solution, both solutions are calculated over the entire frequency range. If the asymptotic-assisted solution remains convergent for frequencies at which the SPA solution is sufficiently accurate (arbitrarily set to some predefined tolerance), a seamless switchover to the SPA solution occurs. If instead the asymptotic-assisted solution fails to converge before some suitable switchover criterion is

satisfied, the asymptotic-assisted solution is abandoned and the SPA solution is adopted regardless. We choose the switchover frequency to be the frequency at which the dipole term of the asymptotic-assisted solution of the induced field is within some small error, B_{0m1}^δ , of the dipole term of the corresponding SPA solution in the asymptotic regime,

$$B_{0m1}^\delta = \left| \frac{B_{0m1} - B_{0m1}^{spa}}{B_{0m1}^{spa}} \right| \quad (5.16)$$

where $m = 0$ for axial excitation, and $m = 1$ for transverse excitation. For spheroids with $1 \leq \mu_r \leq \infty$ and $\frac{1}{8} \leq \mu_r \leq 8$, the asymptotic-assisted solution switches over to the SPA solution when B_{0m1}^δ is less than 5%. In the vast majority of cases, B_{0m1}^δ is less than 2% with only more extreme aspect ratios and slightly magnetic objects posing the most difficulty.

5.4 Validation and Results

5.4.1 Comparison with Simulation

The induced magnetic field potential and hence the magnetic field can be calculated anywhere external to the spheroid through Eq. (5.2) after the induced potential expansion coefficients B_{pmn} are found from the combined solution outlined in the previous sections. In this section, we compare this solution with results from both Wait's solution for a conducting and permeable sphere [111] and to results obtained from a hybrid solution based on a finite element/boundary integral method (FE-BI) combined with a thin skin approximation [4]. We compare both the axial ($m = 0$) and transverse ($m = 1$) excitations of prolate and oblate spheroids. For axial excitation, the primary field is aligned with the laboratory z -axis $\overline{H}_o(\vec{r}) = \hat{z}$, the axis of rotation of the spheroid is aligned with the z -axis, and $b_{001} = -1$ in Eq. (5.1) with all other $b_{00n} = 0$. In the case of transverse excitation, we choose to rotate the spheroid (as opposed to the laboratory reference frame) so that the spheroid is aligned with the x -axis while the primary magnetic field is still $\overline{H}_o(\vec{r}) = \hat{z}$ mandating $b_{011} = 1$ with all other $b_{01n} = 0$. Following this convention, the Cartesian coordinates refer to the laboratory reference frame. The spheroid's location is then expressed in terms of this Cartesian system, while its orientation relative to the laboratory is referenced

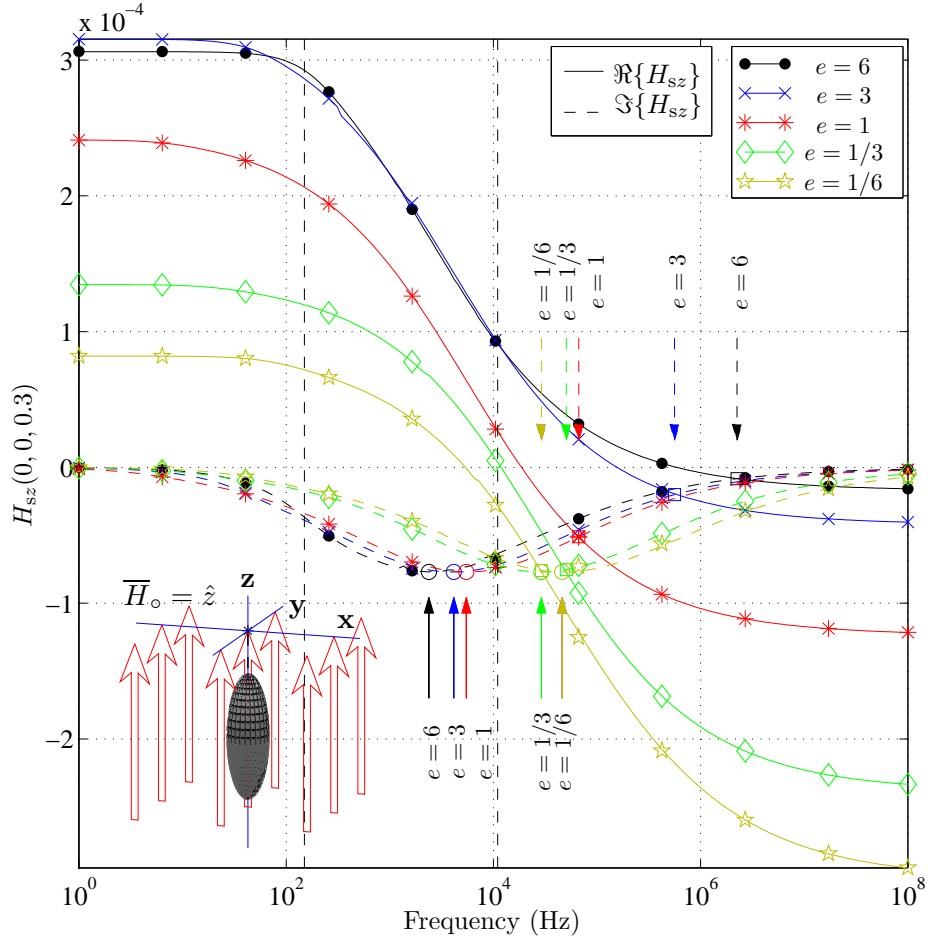


Figure 5-4: z -component of the induced secondary field, H_{sz} , from five different spheroids, aspect ratio $e = [6, 3, 1, 1/3, 1/6]$, with their longest dimension equal to 3cm, and axial excitation calculated by the combined method described in Sections 5.2 and 5.3. All spheroids were 30cm below the measurement point and under uniform excitation $\vec{H}_o = \hat{z}$ with $\sigma = 10^7$ and $\mu_r = 100$. Solid curves $\Rightarrow \Re\{H_{sz}\}$ (inphase component), while dashed curves $\Rightarrow \Im\{H_{sz}\}$ (quadrature component). Vertical dashed lines give a rough indication of the regions of validity for the exact, asymptotic-assisted, and SPA solutions, progressing from low to high frequency. Circles indicate the resonant peak of $\Im\{H_{sz}\}$. Squares indicate the frequency at which $|\Re\{H_{sz}\}| = |\Im\{H_{sz}\}|$. Dots indicate results from the corresponding numerical solution [4]. Note that H_{sz} for the sphere has been scaled by 1/3.

using the three Euler angles $\{\alpha, \beta, \gamma\}$ [43].

In all cases considered here, even at the “high” frequencies, we assume that electromagnetic phenomena are magnetoquasistatic in the sense that displacement currents are negli-

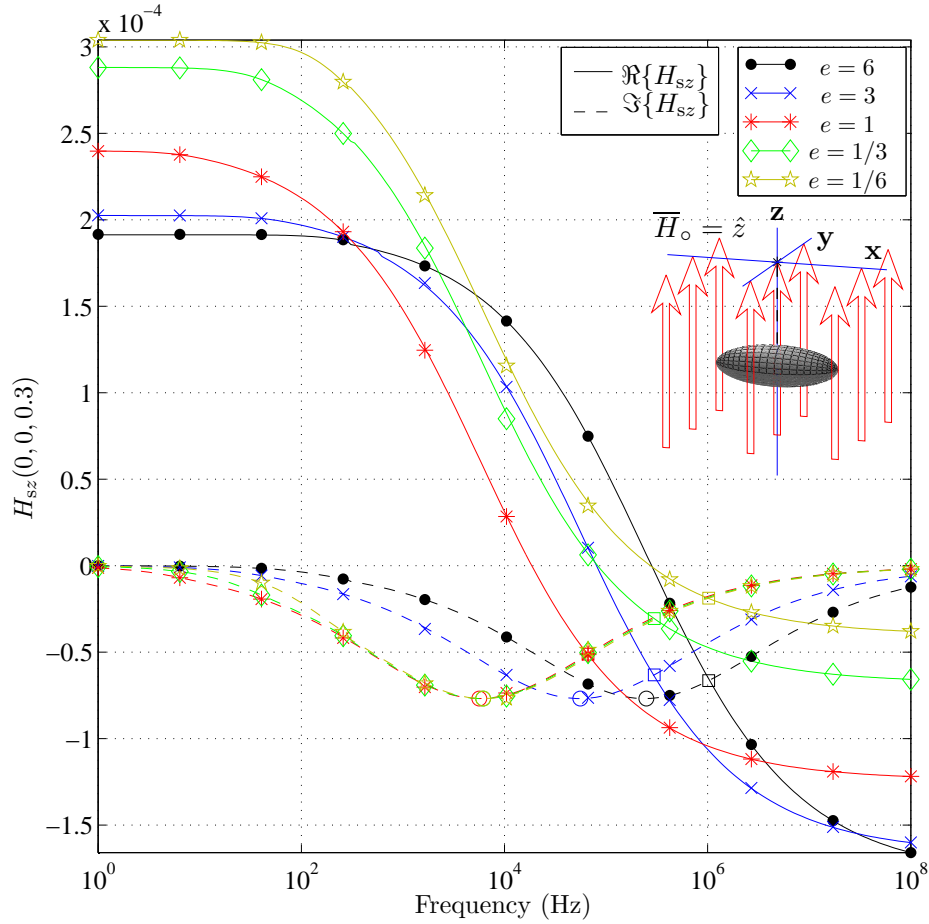


Figure 5-5: z -component of the induced secondary field, H_{sz} , from the same five spheroids as in Fig. 5-4 under transverse excitation. $\bar{H}_o = \hat{z}$ with spheroids' axes of revolution aligned along the x -axis. All spheroids were 30cm below the measurement point and under uniform excitation $\bar{H}_o = \hat{z}$ with $\sigma = 10^7$ and $\mu_r = 100$. Circles indicate the resonant peak of $\Im\{H_{sz}\}$. Squares indicate the frequency at which $|\Re\{H_{sz}\}| = |\Im\{H_{sz}\}|$. Dots indicate results from the corresponding numerical solution [4]. Again, the response for the sphere has been scaled by 1/3.

ble. Within the metallic object, the ratio of conduction to displacement currents is $\sigma/(\omega\epsilon)$. Even at a frequency of 100 MHz (as shown in Figs. 5-4-5-6), this is $\approx 10^7/(10^8 \cdot 10^{-11})$, so that conduction currents dominate by orders of magnitude [116, 117]. Accordingly, even at EMI frequencies above 1 MHz, there is essentially no phase difference between one observation point and another within the length scale of interest (meters). External fields appear

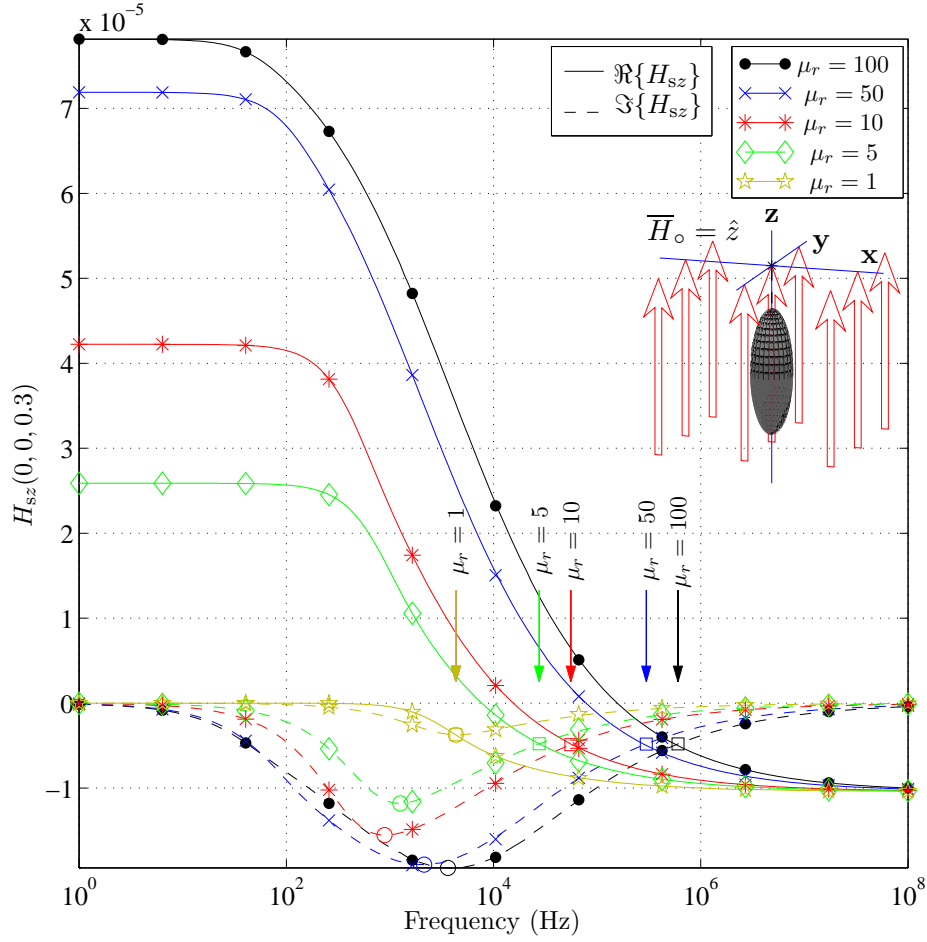


Figure 5-6: z -component of the induced secondary field, H_{sz} , from five spheroids under axial excitation with a similar configuration to that of Fig. 5-4, but with $\mu_r = [1, 5, 10, 50, 100]$ and aspect ratio $e = 3$ and $2a = 3\text{cm}$. All spheroids were 30cm below the measurement point and under uniform excitation $\bar{H}_o = \hat{z}$ with $\sigma = 10^7$. Circles indicate the resonant peak of $\Im\{H_{sz}\}$. Squares indicate the frequency at which $|\Re\{H_{sz}\}| = |\Im\{H_{sz}\}|$. Dots indicate results from the corresponding numerical solution [4]. $\bar{H}_o = \hat{z}$

static, being time dependent only as they follow imposed boundary conditions.

When the asymptotic representations of the SWFs outlined in Section 5.3 are utilized to find $\bar{H}_2(\bar{\tau})$, the solution is indeed stable for higher frequencies, as can be seen in Fig. 5-4, which shows combined results calculated by all three techniques outlined in this paper, viz. original exact solution, asymptotic-assisted solution, and the SPA solution. This

combined solution is capable of finding the induced secondary magnetic field over a broad EMI frequency range from static to very high frequencies.

Important characteristics of the broadband EMI response are illustrated in Figs. 5-4–5-6. For all the results reported in this work, our choice of sign convention follows the convention common in the geophysics field in that the conjugate of the magnetic field is shown. In Fig. 5-4, as the aspect ratio decreases from $e = 6$ (prolate) to $e = 1/6$ (oblate), the resonant peak of the induced field shifts to higher frequencies under axial excitation. Simultaneously, the frequency at which $|\Re\{H_{sz}\}| = |\Im\{H_{sz}\}|$ shifts from higher to lower frequencies.

Figure 5-5 shows $\overline{H}_2(\bar{r})$ for the same five spheroids considered in Fig. 5-4 except that they are under transverse excitation, i.e. the spheroids' axes of revolution are aligned with the x -axis, with the same primary field, $\overline{H}_o(\bar{r}) = \hat{z}$. Both Wait's solution ($e = 1$) and the numerical solution are included for reference. Figure 5-6 compares the combined analytical solution to solutions from the same numerical method for spheroids with aspect ratio $e = 3$ and $\mu_r = [1, 5, 10, 50, 100]$. Note that the high frequency limits of all the spheroids in Fig. 5-6 are identical because the spheroids' dimensions are equal, whereas the static limit and the peak and crossover points are characteristic of each spheroid. The distinct progression of the crossover point to lower frequencies as the permeability decreases is noteworthy.

For the spherical cases shown, the aspect ratio used for the combined method is slightly different from 1.0 (in this case 1.005) because $R_{mn}(c, \xi)$ possesses a singularity at $e = 1$ ($\xi = \infty$). Wait's solution is obscured by our analytical model. Results from our combined model, Wait's solution, and the FE-BI numerical method are essentially equal.

5.4.2 Comparison with Measurements

In this section we compare our results from the combined broadband method to measurements taken in the frequency domain using the UWB GEM-3 instrument [114]. The GEM-3 instrument is a monostatic, broadband, electromagnetic sensor used for subsurface geomagnetic sensing at magnetoquasistatic frequencies. The instrument is constructed as two large coils of 32cm and approximately 16cm diameters. The currents in these two concentric loops are in opposing directions thus creating a “magnetic cavity” region of near zero

primary field magnitude at the common center where the pickup coil(s) are located. The induced secondary response from metallic objects at 10 or more programmable frequencies are simultaneously recorded for later analysis. The frequency range of the GEM-3 is roughly 30Hz–100KHz (but with decreasing accuracy at the upper frequency range, see page 142) as in Figs. 5-20–5-23. Examples of the GEM-3 instrument are shown in Fig. 5-7 [5].



Figure 5-7: Geophex ultra-wideband GEM-3 instrument in various configurations [5].

The experimental setup used is pictured in Fig. 5-19. To minimize variance due to sensor position, the GEM-3's position and orientation was fixed relative to the laboratory. Test objects (see Table 5.2 and Fig. 5-18) were placed upon a supporting wooden platform built around the instrument. These objects were placed in various locations (e.g., a grid) relative to the instrument and their induced field responses were measured. The sensor head and grid are pictured in more detail in Fig. 5-8, while a qualitative representation of the magnetic field produced by the instrument is shown in Fig. 5-9 [7]. All of the measurements reported in this thesis (c.f. Figs. 5-20–5-23) were taken by my colleague Dr. Kevin O'Neill at Hanover, NH in October, 2003 [6].

For nonuniform primary fields such as those produced by the GEM-3 that still satisfy the

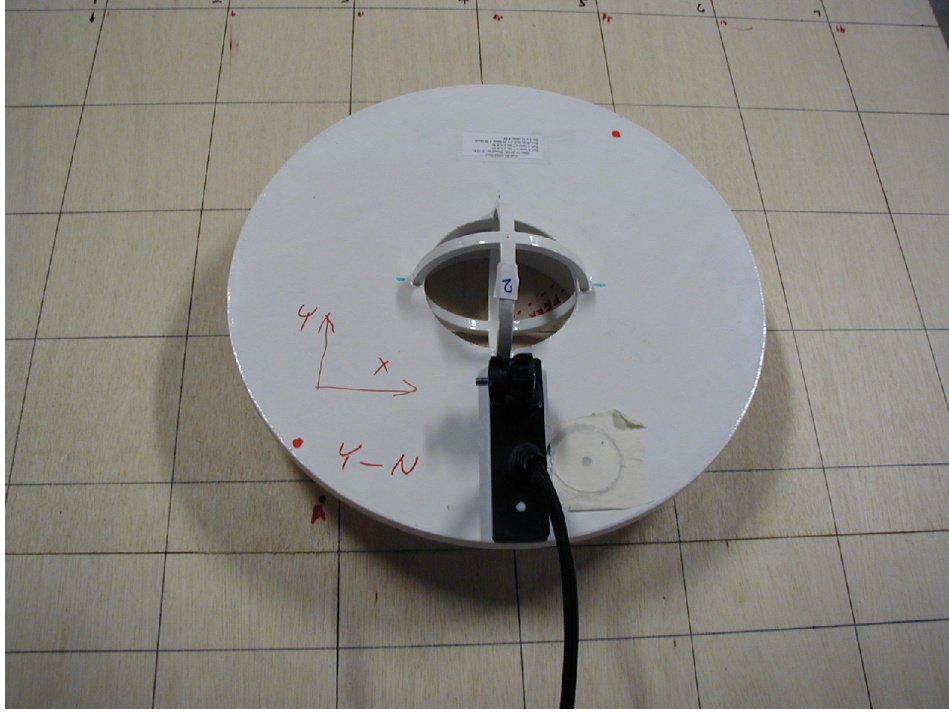


Figure 5-8: Geophex ultra-wideband GEM-3 instrument sensor head and measurement grid [6].

magnetoquasistatic assumptions, $b_{0mn} \neq 0$ for $n \neq 1$. In order to find the induced external magnetic field from Eqs. (5.2) and (5.3), the primary field from the GEM-3 must be expressed in terms of excitation coefficients b_{0mn} . The b_{0mn} are dependent upon the particular spheroidal coordinate system, (η, ξ, ϕ, d) , and its orientation with respect to $\overline{H}_o(\vec{r})$.

One way to find these excitation coefficients is to utilize the orthogonality of the associated Legendre and harmonic functions in Eq. (5.1) in order to find an expression for b_{pmn} [88], i.e.

$$b_{pmn} = \frac{\int_0^{2\pi} T_{pm}(\phi) \int_{-1}^1 P_n^m(\eta) U_o(\vec{r}) d\eta d\phi}{\ell \pi H_o \frac{d}{2} \frac{P_n^m(\xi)}{(n+\frac{1}{2})} \frac{(n+m)!}{(n-m)!}}, \quad (5.17)$$

where

$$\ell = \begin{cases} 2\pi \tilde{p} m=0, \\ \pi \text{ otherwise} \end{cases} \quad (5.18)$$

with $\tilde{p} = 1$ for $p = 0$ and vice versa. This assumes that the potential for the primary field

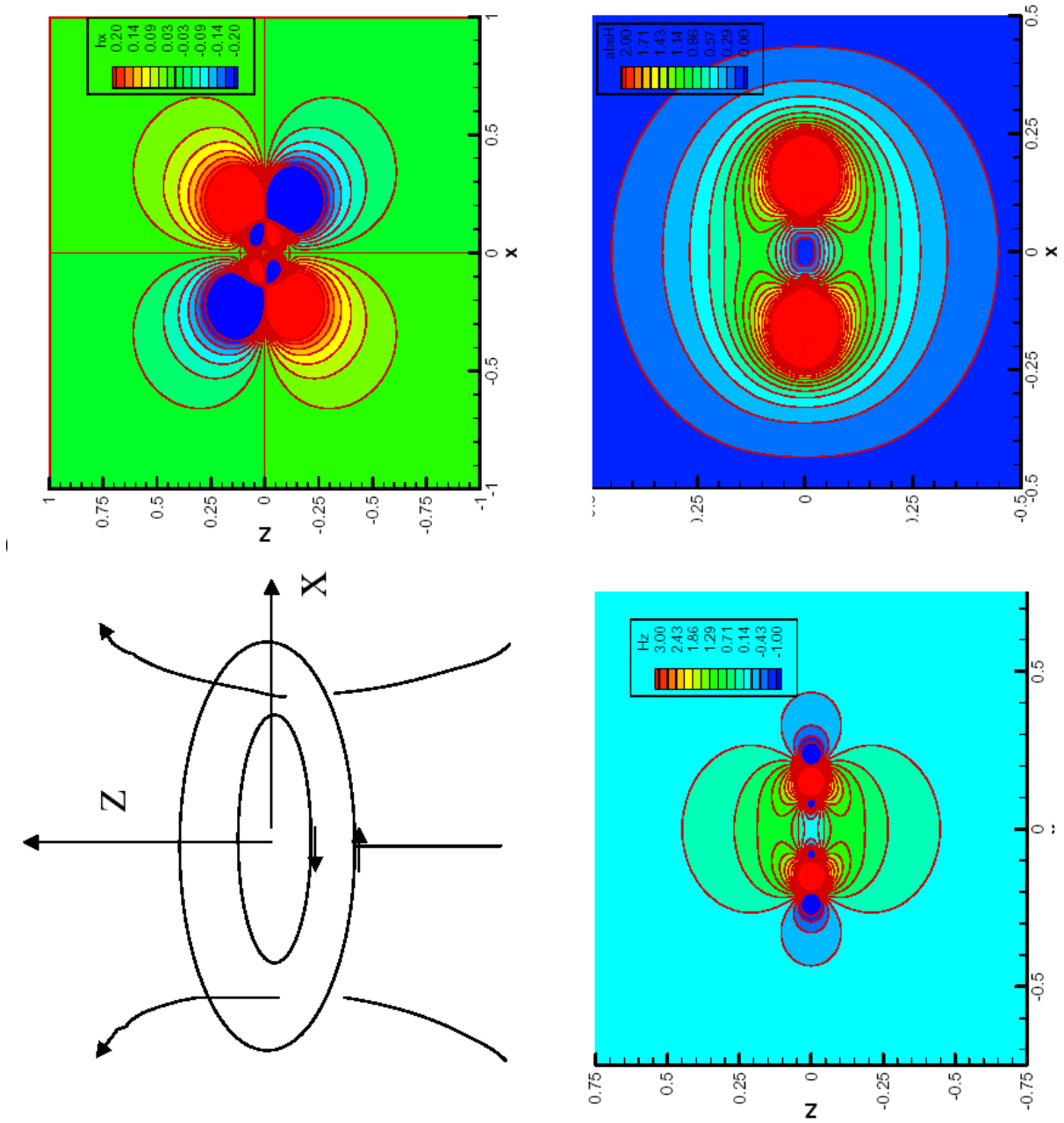


Figure 5-9: Magnetic field produced by the Geopex ultra-wideband GEM-3 instrument [7].

is known at the surface of the spheroid. If $U_o(\bar{r})$ is unknown, $\overline{H}_o(\bar{r})$ may be used instead by taking $-\nabla$ of both sides of (5.1) and performing the same procedure as shown in (5.17). These expressions involve multiple integrals which must be performed numerically unless some convenient analytical representation of $U_o(\bar{r})$ or $\overline{H}_o(\bar{r})$ is known.

A simpler method, which avoids time consuming numerical integrations, for obtaining b_{pmn} is to use point matching in (5.1) at $N_p > 2(\max(m) + 1)(\max(n) + 1)$ points on the surface of the spheroid defined by $\xi = \xi_o$. The resulting system of equations resolves up to $N \leq N_p$ expansion coefficients again assuming some convenient expression for $U_o(\bar{r})$ or $\overline{H}_o(\bar{r})$ is known. This system of equations can be expressed as

$$\begin{bmatrix} U_o(\bar{r}_1) \\ U_o(\bar{r}_2) \\ \vdots \\ U_o(\bar{r}_{N_p}) \end{bmatrix} = \begin{bmatrix} \Phi_1(\bar{r}_1) & \Phi_2(\bar{r}_1) & \cdots & \Phi_N(\bar{r}_1) \\ \Phi_1(\bar{r}_2) & \Phi_2(\bar{r}_2) & \cdots & \Phi_N(\bar{r}_2) \\ \vdots & \ddots & \ddots & \vdots \\ \Phi_1(\bar{r}_{N_p}) & \Phi_2(\bar{r}_{N_p}) & \cdots & \Phi_N(\bar{r}_{N_p}) \end{bmatrix} \begin{bmatrix} b_1 \\ b_2 \\ \vdots \\ b_N \end{bmatrix} \quad (5.19)$$

where the potential at the i^{th} point on the surface is

$$\Phi_j(\bar{r}_i) = P_n^m(\eta_i)P_n^m(\xi_o)T_{pm}(\phi_i) \quad (5.20)$$

given some suitable mapping of $[p, m, n] \rightarrow j$. Equation (5.19) can easily be solved via (pseudo-) inversion or conjugate gradient techniques, yielding b_{pmn} in terms of the object's coordinates system. We adopt this approach, using an approximate representation of the GEM-3 primary field modeled as rings of magnetic sources [7]. Figure 5-11 depicts the primary and secondary induced potentials in the x - z plane which includes both the center of the GEM-3 (assigned to be the origin) and a spheroid located at $\bar{r} = [0.0, 0.0, -0.25]$ meters. The spheroid's axis of symmetry is aligned with the z -axis in this case. Figures 5-11 and 5-16 illustrate the dramatic falloff in magnitude of the induced field as compared to the primary field. For these realistic cases, the induced field at the sensor is five orders of magnitude smaller than the primary field even though the object is at a relatively shallow depth.

For high but still magnetoquasistatic frequencies (see Fig. 5-11), the induced magnetic

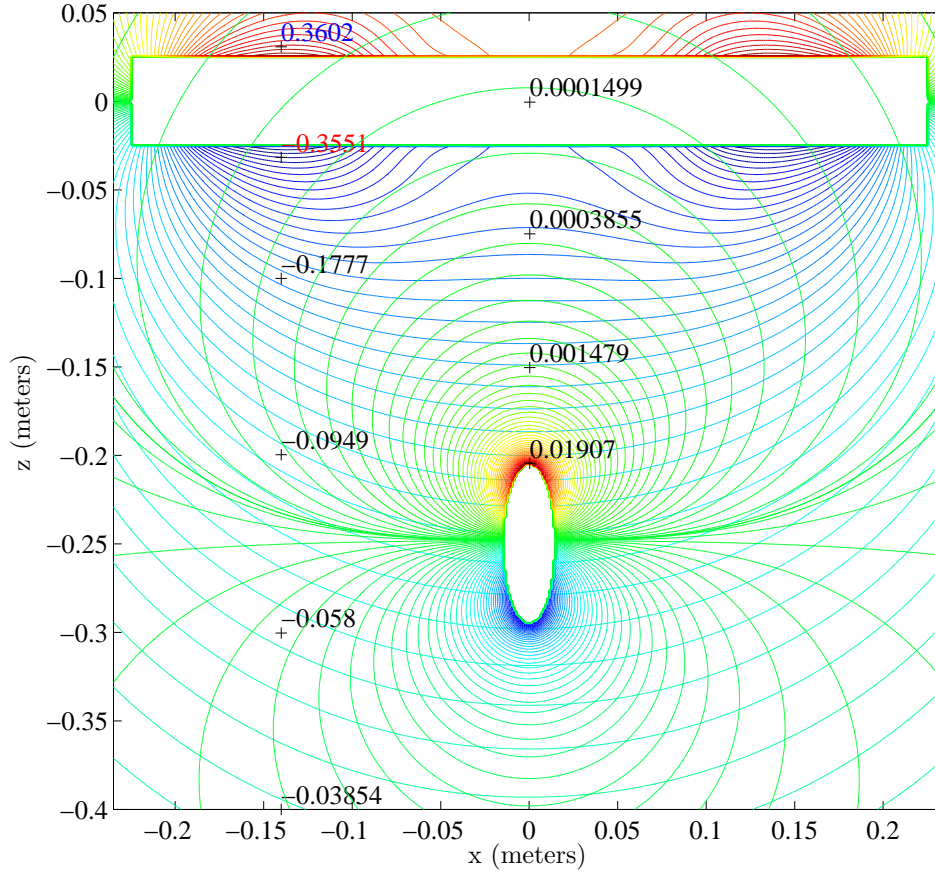


Figure 5-10: Primary field potential from the GEM-3, $U_o(\vec{r})$ (magnitudes marked on left), and the secondary potential induced by the spheroid, $U_s(\vec{r})$ (magnitudes marked in center) in the $x-z$ plane for the S2 spheroid (see Table 5.2), at low frequency, under axial excitation, and choosing $\mu_r = 100$ and $\sigma = 10^7$. Color of induced response has been adjusted for clarity. Axes are in meters. The white rectangle encompasses the GEM-3 instrument.

field will be out of phase with the primary field due to Lenz's law. Figure 5-16 shows $U_o(\vec{r})$ and $U_s(\vec{r})$ for a low (near static) frequency case with the spheroid removed from the z -axis. In this case, the induced response is in phase with the primary field.

We now compare the theoretical induced external magnetic field predicted by our combined broadband technique with the induced field measured by the GEM-3 instrument. The primary field and potential, $\vec{H}_o(\vec{r})$ and $U_o(\vec{r})$ respectively, at the surface of the spheroid are described by 12 rings of dipoles whose location and magnitudes are given by the method found in [7]. The primary field potential expansion coefficients, b_{pmn} , are then found via

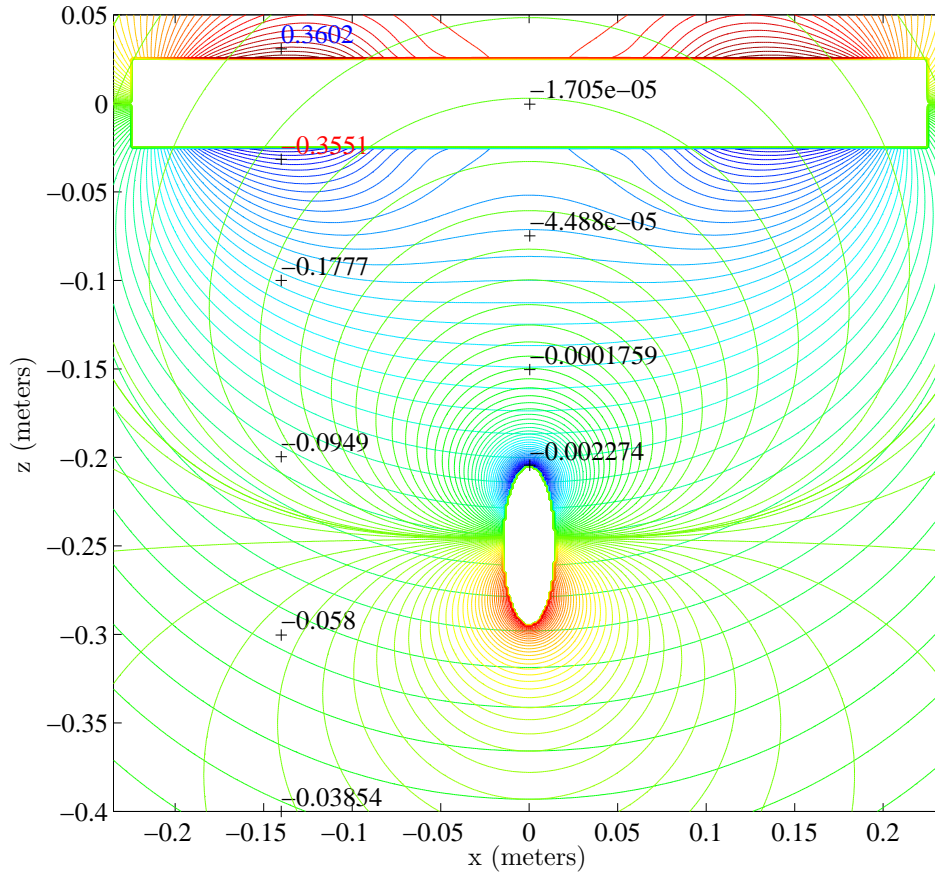


Figure 5-11: Primary field potential from the GEM-3, $U_o(\vec{r})$ (magnitudes marked on left), and the secondary potential induced by the spheroid, $U_s(\vec{r})$ (magnitudes marked in center) in the $x-z$ plane for the S2 spheroid (see Table 5.2), at high frequency, under axial excitation, and choosing $\mu_r = 100$ and $\sigma = 10^7$. Color of induced response has been adjusted for clarity. Axes are in meters. The white rectangle encompasses the GEM-3 instrument.

Eq. (5.19).

I machined a set of 17 spheroids for test objects: three spheres, six prolate spheroids, and eight oblate spheroids machined from aluminum and mild steel. Table 5.2 summarizes the spheroids' designations and characteristics, and they are pictured in Fig. 5-18. The induced magnetic fields for prolate steel spheroid S2 for both axial and transverse orientations are shown in Fig. 5-20. Figure 5-21 shows similar results for the aluminum spheroid A1 and Figs. 5-22 and 5-23 show similar comparisons for oblate spheroids S8 and A7 respectively. The measurements were taken from a position directly above each object.

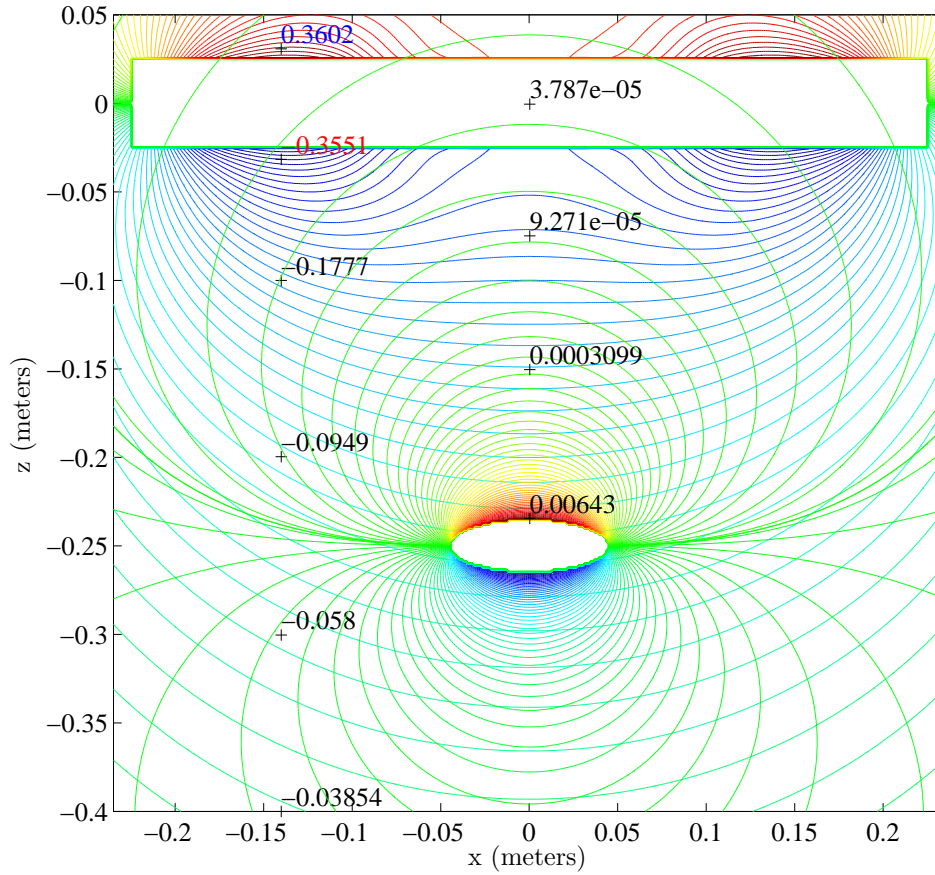


Figure 5-12: Primary field potential from the GEM-3, $U_o(\vec{r})$ (magnitudes marked on left), and the secondary potential induced by the spheroid, $U_s(\vec{r})$ (magnitudes marked in center) in the $x - z$ plane for the S2 spheroid (see Table 5.2), at low frequency, under transverse excitation, and choosing $\mu_r = 100$ and $\sigma = 10^7$. Color of induced response has been adjusted for clarity. Axes are in meters. The white rectangle encompasses the GEM-3 instrument.

The distance from the center of the receiver to the closest edge of each object was 25cm in the case of the steel objects, and 15cm in the case of the aluminum objects. The experimental setup is shown in Fig. 5-19.

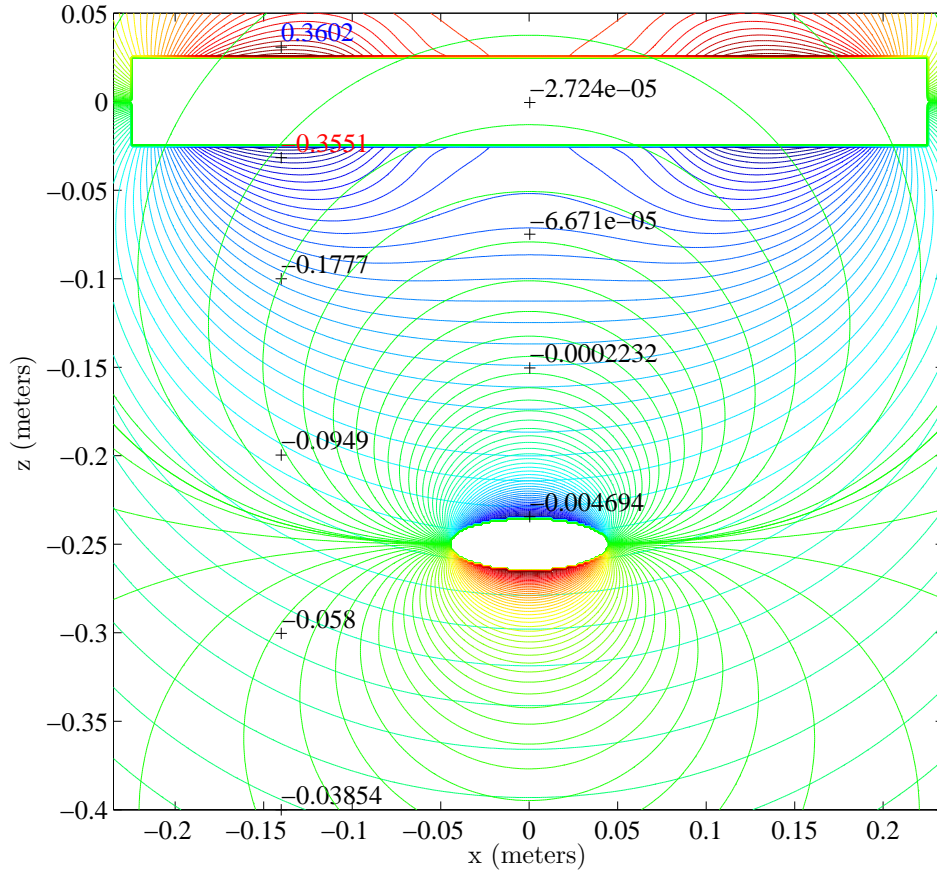


Figure 5-13: Primary field potential from the GEM-3, $U_o(\vec{r})$ (magnitudes marked on left), and the secondary potential induced by the spheroid, $U_s(\vec{r})$ (magnitudes marked in center) in the $x - z$ plane for the S2 spheroid (see Table 5.2), at high frequency, under transverse excitation, and choosing $\mu_r = 100$ and $\sigma = 10^7$. Color of induced response has been adjusted for clarity. Axes are in meters. The white rectangle encompasses the GEM-3 instrument.

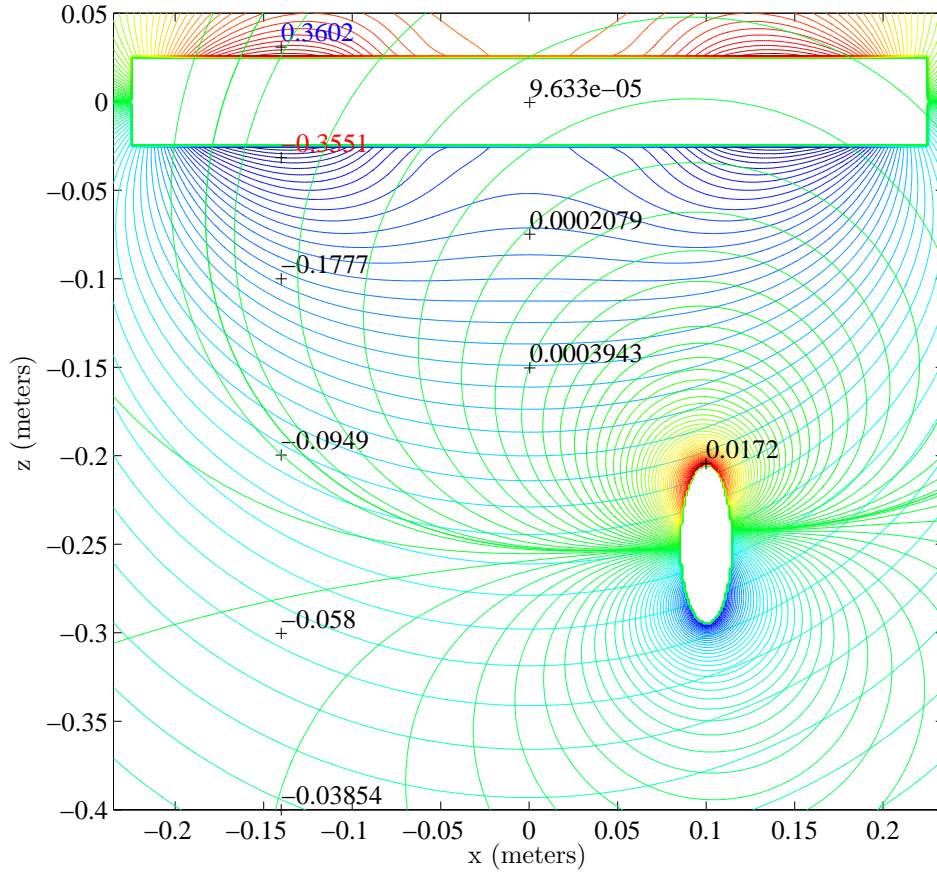


Figure 5-14: Primary field potential from the GEM-3, $U_o(\vec{r})$ (magnitudes marked on left), and the secondary potential induced by the spheroid, $U_s(\vec{r})$ (magnitudes marked in center) in the $x-z$ plane for the S2 spheroid (see Table 5.2), at low frequency, under axial excitation, offcenter, and choosing $\mu_r = 100$ and $\sigma = 10^7$. Color of induced response has been adjusted for clarity. Axes are in meters. The white rectangle encompasses the GEM-3 instrument.

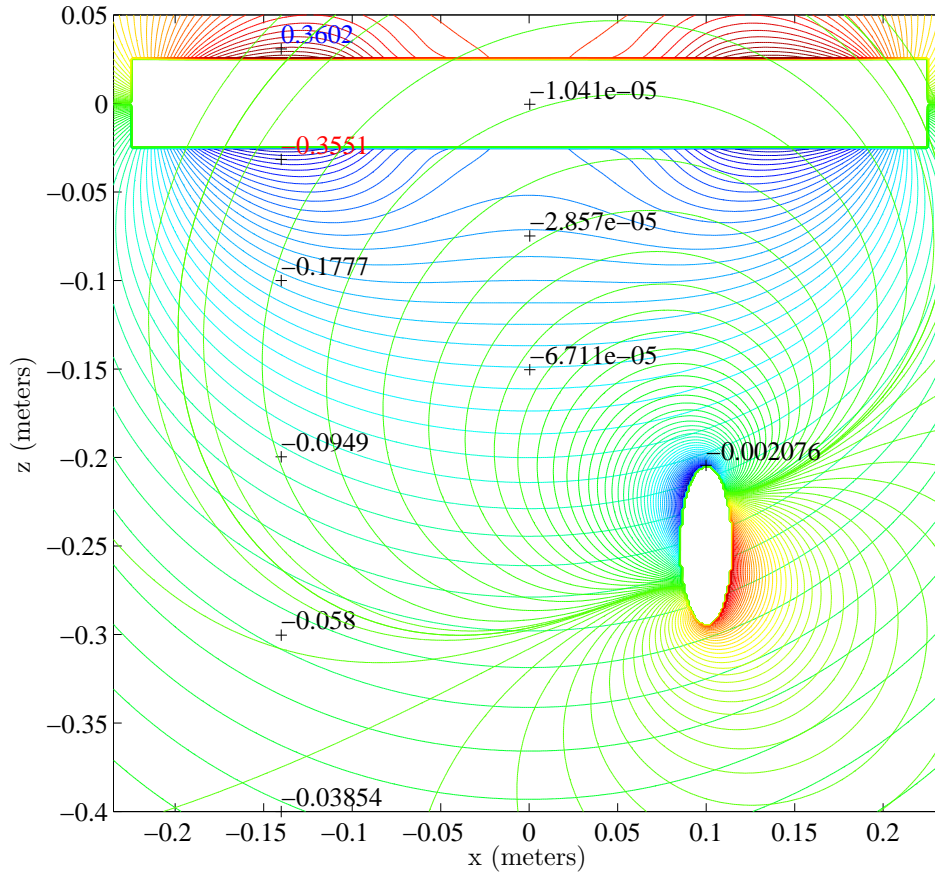


Figure 5-15: Primary field potential from the GEM-3, $U_o(\bar{r})$ (magnitudes marked on left), and the secondary potential induced by the spheroid, $U_s(\bar{r})$ (magnitudes marked in center) in the $x - z$ plane for the S2 spheroid (see Table 5.2), at high frequency, under axial excitation, offcenter, and choosing $\mu_r = 100$ and $\sigma = 10^7$. Color of induced response has been adjusted for clarity. Axes are in meters. The white rectangle encompasses the GEM-3 instrument.

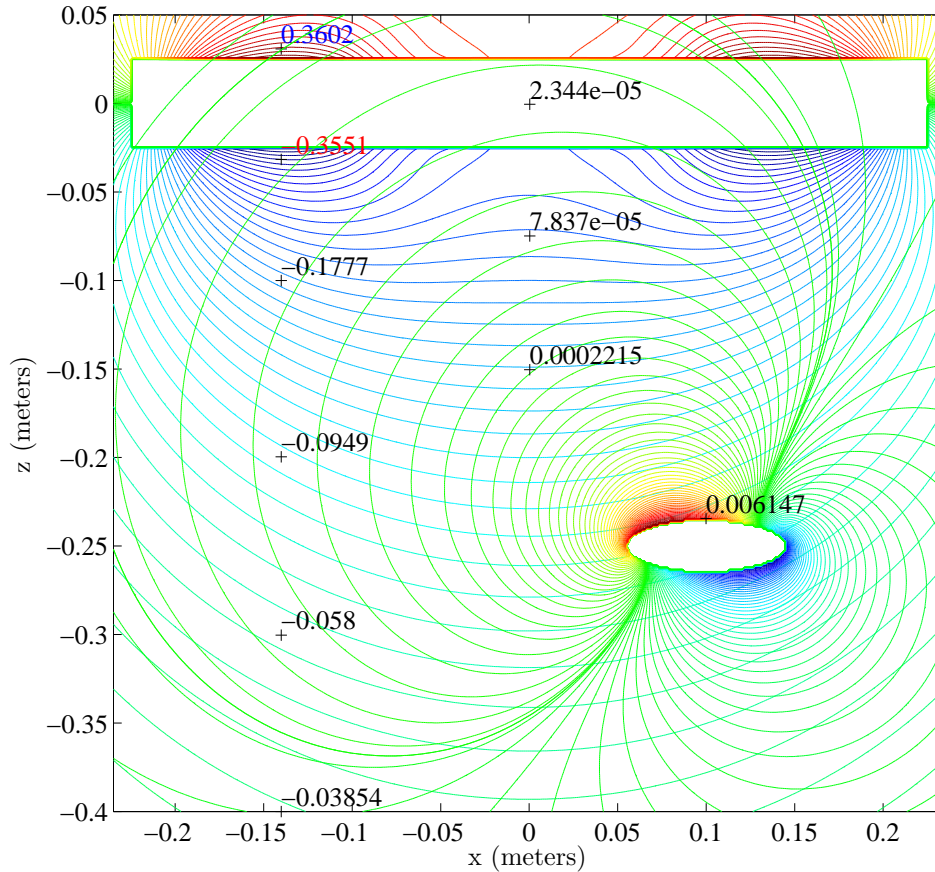


Figure 5-16: Primary field potential from the GEM-3, $U_o(\vec{r})$ (magnitudes marked on left), and the secondary potential induced by the spheroid, $U_s(\vec{r})$ (magnitudes marked in center) in the $x - z$ plane for the S2 spheroid (see Table 5.2), at low frequency, under transverse excitation, offcenter, and choosing $\mu_r = 100$ and $\sigma = 10^7$. Color of induced response has been adjusted for clarity. Axes are in meters. The white rectangle encompasses the GEM-3 instrument.

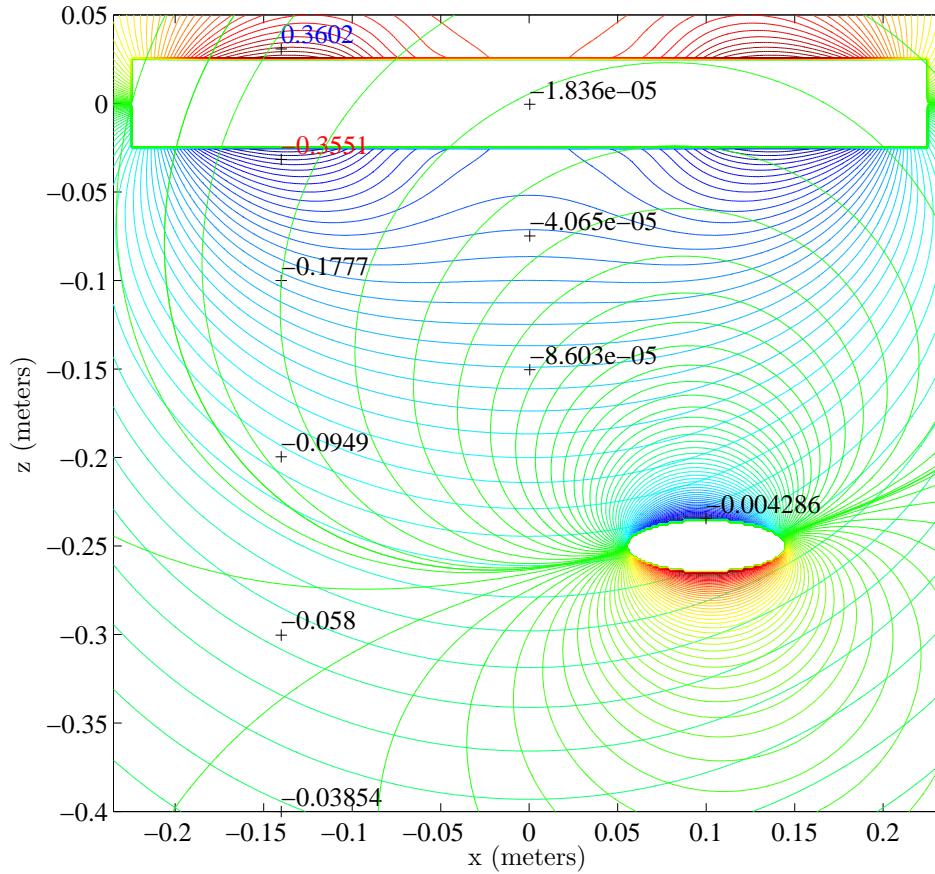


Figure 5-17: Primary field potential from the GEM-3, $U_o(\bar{r})$ (magnitudes marked on left), and the secondary potential induced by the spheroid, $U_s(\bar{r})$ (magnitudes marked in center) in the $x - z$ plane for the S2 spheroid (see Table 5.2), at high frequency, under transverse excitation, offcenter, and choosing $\mu_r = 100$ and $\sigma = 10^7$. Color of induced response has been adjusted for clarity. Axes are in meters. The white rectangle encompasses the GEM-3 instrument.



Figure 5-18: Spheroid collection used for testing. Specifications are listed in Table 5.2.



Figure 5-19: GEM-3 experimental setup.

Therefore, the distance to the center of S2 under axial orientation was $z = -34\text{cm}$, while the depth to the center under transverse orientation was $z = -26.5\text{cm}$, etc.

	comp.	type	semiaxis (a)	semiaxis (b)	nominal $e = b/a$
S1	Iron	sphere	90.62mm	90.62mm	1
S2	Steel	PS	30.02mm	182.19mm	6
S3	Steel	PS	29.94mm	90.28mm	3
S4	Steel	PS	14.97mm	90.76mm	6
S5	Steel	OS	29.32mm	4.56mm	1/6
S6	Steel	OS	29.59mm	9.65mm	1/3
S7	Steel	sphere	29.87mm	29.87mm	1
S8	Steel	OS	89.85mm	28.39mm	1/3
S9	Steel	OS	89.95mm	15.32mm	1/6
A1	Al	PS	30.17mm	180.23mm	6
A2	Al	PS	29.9mm	91.29mm	3
A3	Al	PS	15.04mm	91.14mm	6
A4	Al	OS	29.36mm	4.34mm	1/6
A5	Al	OS	29.36mm	8.88mm	1/3
A6	Al	sphere	29.91mm	29.91mm	1
A7	Al	OS	89.92mm	30.38mm	1/3
A8	Al	OS	89.98mm	15.94mm	1/6

Table 5.2: Physical dimensions of steel and aluminum spheroids. PS \Rightarrow Prolate Spheroid. OS \Rightarrow Oblate Spheroid.

Our implementation truncates the infinite sets of equations resulting from Eq. (5.8) at $m = 1$. This is partially due to the fact that at remote points in the “far field”, or farther than one or two characteristic lengths (i.e. longest dimension of the object), the lower order, or $m = 0, 1$, terms of the induced magnetic field tend to dominate. Consequently, our solution includes effects for $m = 0$ and $m = 1$ only, which correspond to the axial and transverse excitations respectively [63]. Even with this limitation, the primary and secondary fields may be spatially nonuniform, however, because all n in the range $n \leq 60$ are considered. With reference to the GEM-3 primary field (see Section 5.4.2), objects closer than one or two characteristic lengths from the instrument may have important interaction with $m \geq 2$ orders of the primary field. For objects this close, our model may not accurately predict the induced field response unless the response due to higher order terms are included.

The exact permeability (for the steel) and conductivity of the spheroids were not known

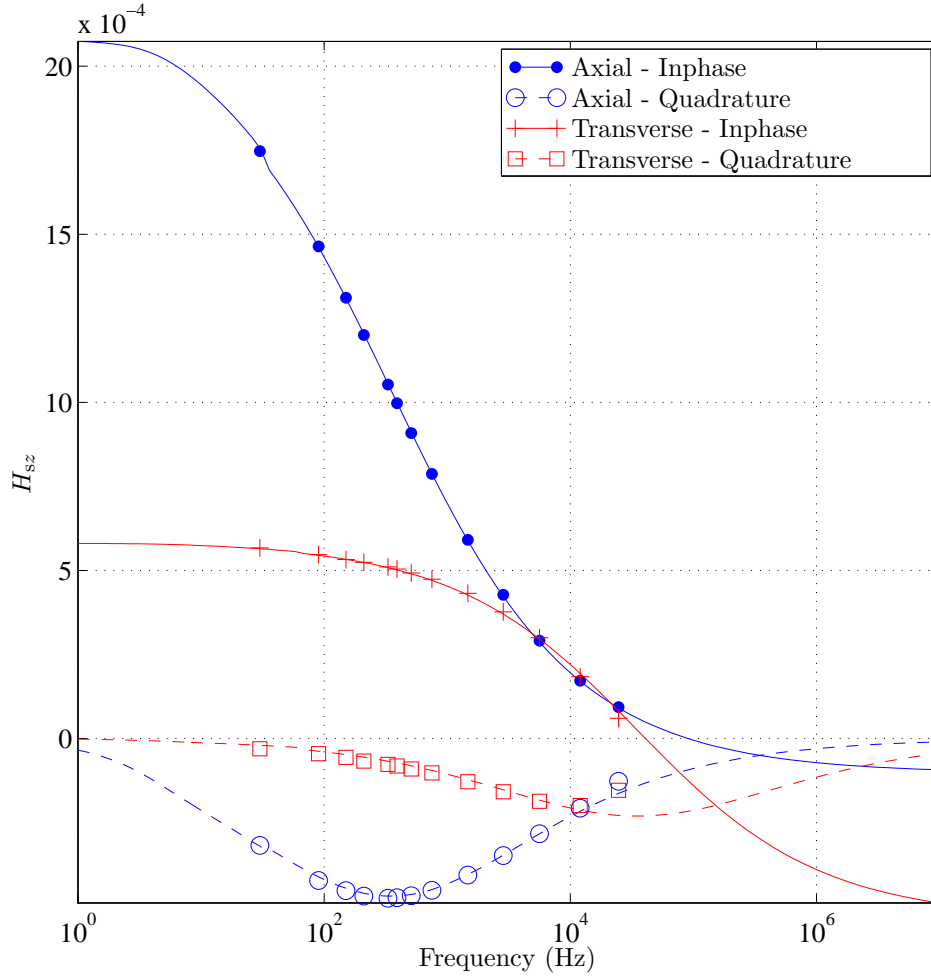


Figure 5-20: Comparison of GEM-3 induced magnetic field measurements, $H_{sz,d}$, from prolate steel spheroid S2 with combined model outlined in Sections 5.2 and 5.3. Both axial and transverse cases are shown. Orientations are similar to those shown in plots of $U_s(\vec{r})$ such as Fig. 5-11. Optimized permeability and conductivity were $\mu_r = 234.1$ and $\sigma = 4.315 \times 10^6 \mathcal{U}/m$, respectively.

or measured beforehand. We sidestepped this lack of information by obtaining these parameters via inversion of the measurements. In other words, we extracted σ and μ_r using a simple search routine by fitting out model to the axial measurements first. We then used these extracted parameters for the transverse measurements from the same object and found them to deliver reasonable results. The resulting conductivity and permeability are within acceptable ranges for these metals.

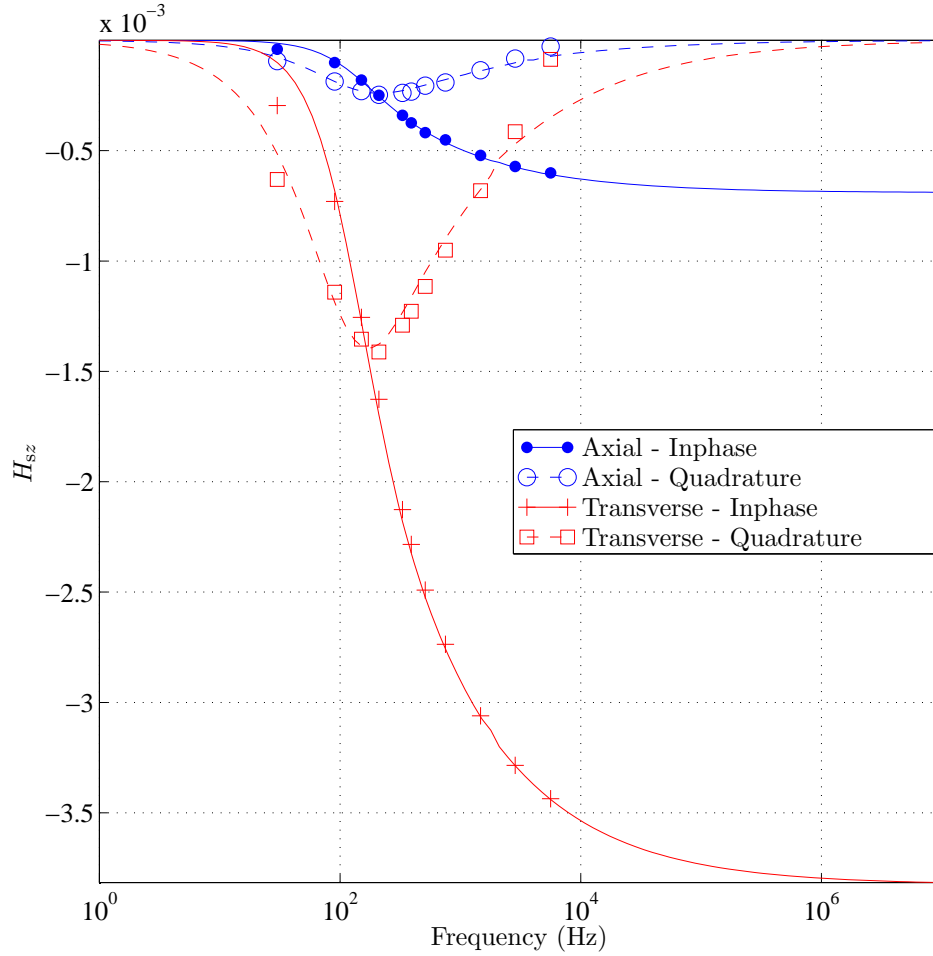


Figure 5-21: Comparison of $H_{sz,d}$ from prolate aluminum spheroid A1 with combined model outlined in Sections 5.2 and 5.3. Both axial and transverse cases. Optimized conductivity was $\sigma = 2.103 \times 10^7 \text{U/m}$.

The experimental GEM-3 we used for these measurements records reliable data at frequencies up to about 12kHz [118]. Measurements are not absolutely calibrated with respect to the primary field. Therefore, the following procedure to normalize and remove any possible constant offset was adopted. Let $H_{sz,d}$ be the z -component of the induced magnetic field measured with the GEM-3 and let H_z be the z -component of the induced magnetic field predicted by our model. In order to compare $H_{sz,d}$ and H_{sz} (as in Figs. 5-20–5-23), we

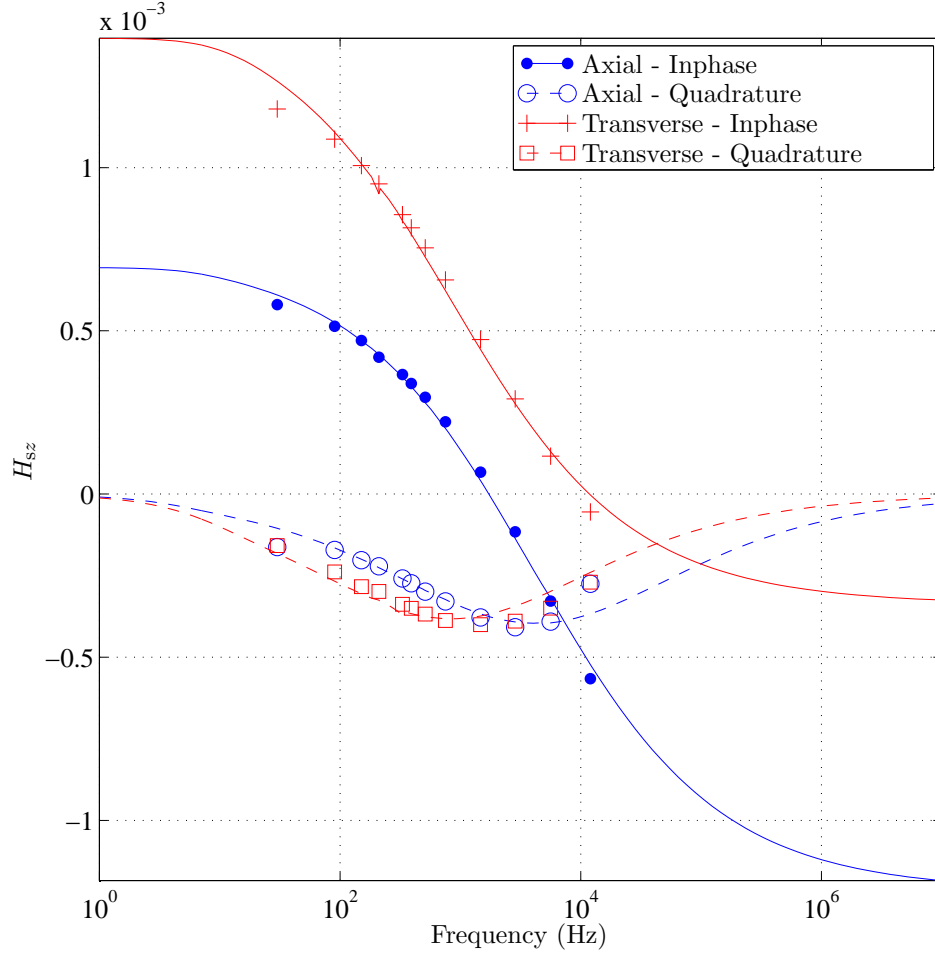


Figure 5-22: Comparison of $H_{sz,d}$ from oblate steel spheroid S8 with combined model outlined in Sections 5.2 and 5.3. Both axial and transverse cases. Optimized permeability and conductivity were $\mu_r = 268.0$ and $\sigma = 1.939 \times 10^7 \text{U}/m$, respectively.

set

$$H_{sz,d} = \left[(H_{sz,d} - \overline{H_{sz,d}}) \frac{\sum_f (|H_{sz} - \overline{H_{sz}}|)}{\sum_f (|H_{sz,dat} - \overline{H_{sz,dat}}|)} \right] + \overline{H_{sz}} \quad (5.21)$$

where the overline implies an average over frequency, and the summation is over all data frequencies used.

Data and model predictions are seen to agree quite well under all conditions except possibly for high frequencies where the accuracy of the data may be suspect [118]. The agreement is not as good for the cases comparing oblate spheroids. This may be due to not

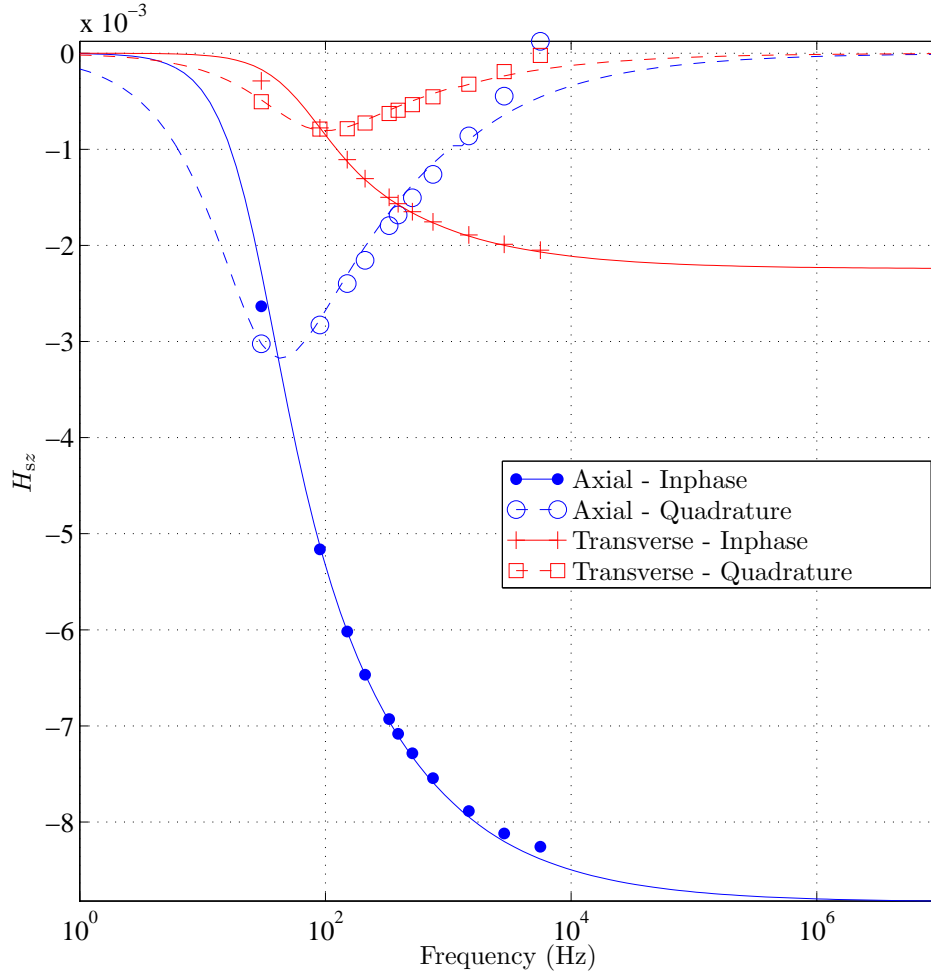


Figure 5-23: Comparison of $H_{sz,d}$ from oblate aluminum spheroid A7 with combined model outlined in Sections 5.2 and 5.3. Both axial and transverse cases. Optimized conductivity was $\sigma = 3.147 \times 10^7 \text{ U/m}$.

having the globally optimal σ and/or μ_r for these spheroids or due to our truncation of Eqs. (5.1) and (5.6) at $m = 1$.

5.5 Conclusion

We have constructed a broadband solution for the induced magnetic field from conducting and permeable prolate and oblate spheroids under time harmonic excitation in the magnetoquasistatic regime. Our combined method consists of the exact analytical solution,

an asymptotic-assisted analytical solution, and a small penetration approximation (SPA). This combined solution is accurate to within 5% error for most spheroids with aspect ratio $\frac{1}{8} < e < 8$. Results produced by this combined method were compared to results from a finite element/boundary integral numerical method and found to be in excellent agreement. Results were also compared to induced magnetic field measurements taken by the UWB GEM-3 instrument from metal prolate and oblate spheroids. If the permeability and conductivity of the spheroids is allowed to vary within accepted physical ranges, results were seen to match very well with measurements. Using this model, one can calculate the broadband induced magnetic field response from a flexible set of canonical shapes such as spheres, spheroids, plates, and needles is now possible. The results indicate that solutions from our model display distinct, systematic response patterns based on the spheroidal characteristics and orientation. On this basis, our method could become a forward model upon which inversions schemes may be based.

Chapter 6

Simultaneous Analytical Solution for the Broadband Magnetoquasistatic Electromagnetic Induction (EMI) Response from Multiple Conducting and Permeable Spheroids

6.1 Introduction

Electromagnetic induction (EMI) response techniques at low frequencies (0-100's kHz) comprise a promising method for the detection and discrimination of unexploded ordnance (UXO). The broadband analytical magnetoquasistatic solution for the induced EMI response from a conducting and permeable spheroid under time harmonic excitation has recently been theoretically and experimentally demonstrated [63, 119] and Chapter 5. This

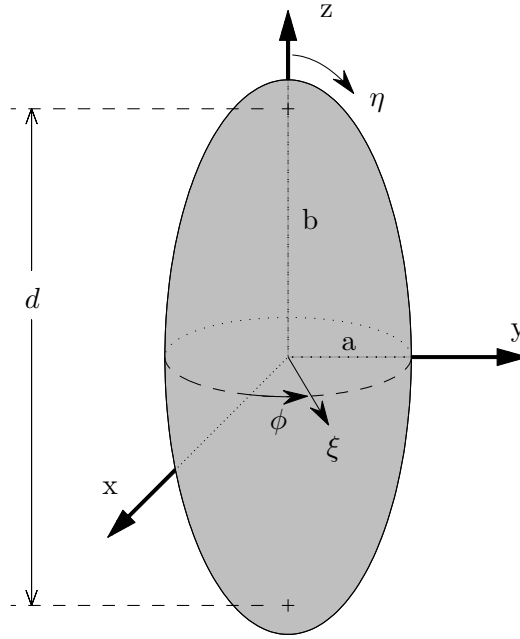


Figure 6-1: Spheroidal Geometry: $1 \leq \xi < \infty$ (Oblate case: $0 \leq \xi < \infty$), $-1 \leq \eta \leq 1$, $0 \leq \phi \leq 2\pi$, $x = \frac{d}{2}[(1 \mp \eta^2)(\xi^2 \mp 1)]^{\frac{1}{2}} \cos(\phi)$, $y = \frac{d}{2}[(1 \mp \eta^2)(\xi^2 \mp 1)]^{\frac{1}{2}} \sin(\phi)$, $z = \frac{d}{2}\eta\xi$, $e = \frac{b}{a}$, $\xi = (\pm(1 - e^{-2}))^{-\frac{1}{2}}$, $d = 2(\pm(b^2 - a^2))^{\frac{1}{2}}$. Upper sign \rightarrow prolate, lower sign \rightarrow oblate.

model gives the induced secondary magnetic field from multiple spheroidal objects in close proximity and is based on a boundary condition formulation similar to the formulation for spherical objects given by the Wait [111, 112].

EMI models of canonical shapes are promising in the detection and discrimination of metallic UXO. As a practical matter, however, many field sites are littered with copious amounts of metallic debris (see Fig. 6-2). This clutter can be anything from other UXO, spent shell casings, old cutlery, coins, or any other highly conductive remnant of civilization. Distinguishing these non-hazardous targets from actual UXO, and along the same lines, detecting UXOs amid these minutiae has been an ongoing topic of research [120, 121, 122, 123, 110]. Previously, we have studied the case of a single, larger spheroidal target surrounded by a cloud of smaller spheroids [119]. However, this treatment did not account for the interactions between spheroids that do occur when multiple targets are in close proximity. This paper rigorously treats the case of multiple metallic spheroidal targets in close proximity



Figure 6-2: Site cluttered with multiple potential targets in close proximity.

and in so doing includes all interactions that occur between objects.

When multiple conducting and permeable spheroidal targets are in close proximity (e.g. Fig. 6-3), their respective induced secondary magnetic fields interact and form a nonlinear system. The separate responses may not be simply superposed to find the total induced field from the collection. Instead, the induced response of any individual spheroid is a result of both the primary magnetic field and the secondary field emanating from all the other spheroids. Our formulation accounts for these multiple interaction terms through the construction of an interaction matrix which couples excitation modes of one spheroid to those of each of the other spheroids. This interaction matrix scales in both memory and complexity as L^2 as compared to the case of a single isolated spheroid where L is the number of spheroids present.

We present the formulation of our model, including the use of asymptotic representations of the spheroidal wave functions in Section 6.2.

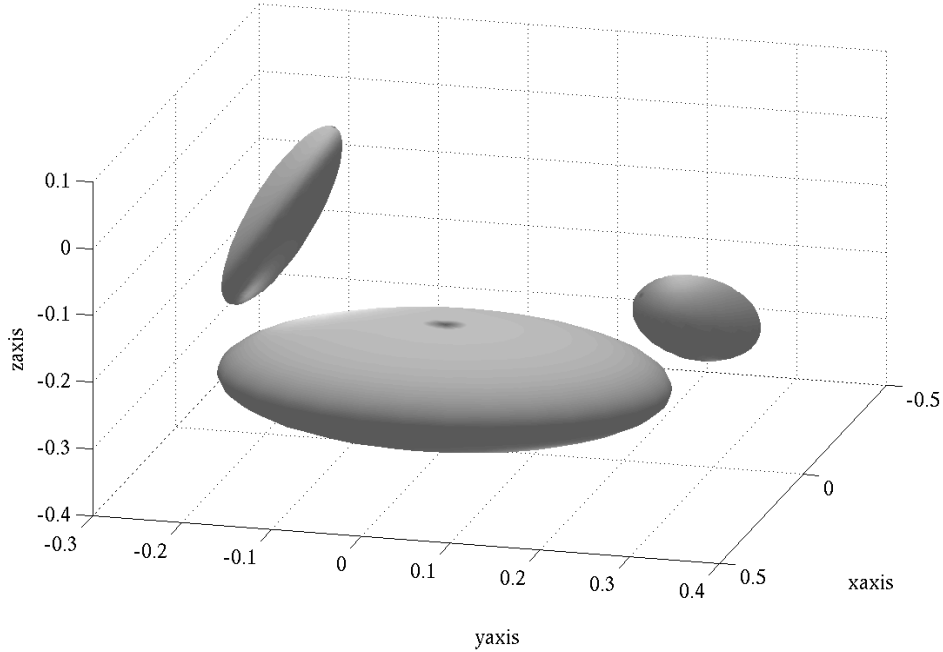


Figure 6-3: Example collection of 3 spheroids in close proximity.

6.2 Formulation

This formulation for the induced secondary magnetic field external to multiple spheroidal targets in close proximity has many similarities with the solution for a single isolated spheroid (Chapter 5 and [63]). In turn, these solutions follow a similar method based on boundary conditions used by Wait [112, 124] in the solution for the induced field from a spherical target. These solutions are exact except for the truncation of the infinite sets of resulting equations.

Let a time harmonic primary magnetic field, $\overline{H}_o(\overline{r}, t) = \overline{H}_o(\overline{r})e^{-i\omega t}$ ($e^{-i\omega t}$ suppressed below), excite a collection of permeable and conducting spheroidal targets in close proximity. Spheroid ℓ is defined by its permeability relative to the host medium, $\mu_r^{(\ell)}$, conductivity, $\sigma^{(\ell)}$, semi-axis of revolution $a^{(\ell)}$, interfocal distance $d^{(\ell)}$, wavenumber

$$\left(k^{(\ell)}\right)^2 = i\omega\sigma^{(\ell)}\mu_r^{(\ell)} \quad (6.1)$$

and size parameter

$$c^{(\ell)} = \frac{k^{(\ell)} d^{(\ell)}}{2} \quad (6.2)$$

(see Fig. 6-1). Each spheroid possesses its own local coordinate system defined by $(d^{(\ell)}, \eta, \xi, \phi)$ with

$$d^{(\ell)} = 2\sqrt{\pm \left((b^{(\ell)})^2 - (a^{(\ell)})^2 \right)} \quad (6.3)$$

where the upper sign applies to prolate spheroids and the lower sign applies to oblate spheroids. The orientation of each spheroid with reference to some laboratory Cartesian system is expressed by the three Euler angles, $\{\alpha^{(\ell)}, \beta^{(\ell)}, \gamma^{(\ell)}\}$ [43].

For frequencies low enough to satisfy the magnetoquasistatic assumptions, the magnetic field inside spheroid ℓ , $\overline{H}^{(\ell)}(\overline{r})$, satisfies the vector wave equation (in this case, the diffusion equation)

$$\nabla \times \nabla \times \overline{H}^{(\ell)} - \left(k^{(\ell)} \right)^2 \overline{H}^{(\ell)} = 0 \quad (6.4)$$

$H^{(\ell)}$ can naturally be expressed in terms of an infinite sum of r -type vector spheroidal wave functions of the first kind, $\overline{M}_{pmn}(c; \eta, \xi, \phi)$ and $\overline{N}_{pmn}(c; \eta, \xi, \phi)$ [66], as

$$\begin{aligned} \overline{H}^{(\ell)} = H_o \sum_{m=0}^{\infty} \sum_{n=m}^{\infty} \sum_{p=0}^1 \left[A_{pmn}^{(M)(\ell)} \overline{M}_{pmn}(c^{(\ell)}; \beta_{\ell\ell}) \right. \\ \left. + A_{pmn}^{(N)(\ell)} \overline{N}_{pmn}(c^{(\ell)}; \beta_{\ell\ell}) \right] \end{aligned} \quad (6.5)$$

where $A_{pmn}^{(M)(\ell)}$ and $A_{pmn}^{(N)(\ell)}$ are expansion coefficients and H_o is the relative magnitude of the primary field. Subscripts such as in $\beta_{\ell q} \equiv [\eta_{\ell q}, \xi_{\ell q}, \phi_{\ell q}]$ are interpreted as indicating locations in the coordinate system of spheroid ℓ expressed in the coordinate system of spheroid q . The azimuthal dependence of $\overline{M}_{pmn}(c^{(\ell)}; \beta_{\ell\ell})$ and $\overline{N}_{pmn}(c^{(\ell)}; \beta_{\ell\ell})$ can be compactly expressed as

$$T_{pm}(\phi) = \begin{cases} \cos(m\phi) & p=0, \\ \sin(m\phi) & p=1. \end{cases} \quad (6.6)$$

The background host medium is assumed to be homogeneous, only weakly magnetic and poorly conducting so that the wavenumber in the background medium, k_o , can be approximated as 0, or $k_{\text{sec}}^2 \approx 0$. In this case, the primary magnetic field becomes irrotational

and can be therefore represented by a scalar potential which satisfies the Laplace equation. Let U_o be the primary magnetic field potential with

$$\overline{H}_o = -\nabla U_o. \quad (6.7)$$

At spheroid ℓ , U_o can be decomposed into an infinite summation of solutions of the first kind of the Laplace equation in spheroidal coordinates which are regular at the origin,

$$U_o(\overline{r}) = H_o \frac{d^{(\ell)}}{2} \sum_{m=0}^{\infty} \sum_{n=m}^{\infty} \sum_{p=0}^1 b_{pmn}^{(\ell)} P_n^m(\eta) P_n^m(\xi) T_{pm}(\phi). \quad (6.8)$$

The primary field expansion coefficients, $b_{pmn}^{(\ell)}$, are specific to each spheroid and are assumed to be known *a priori*.

The induced secondary magnetic field from spheroid ℓ may also be represented by a potential, $U_s^{(\ell)}$, and can be expressed as

$$U_s^{(\ell)}(\overline{r}) = H_o \frac{d^{(\ell)}}{2} \sum_{m=0}^{\infty} \sum_{n=m}^{\infty} \sum_{p=0}^1 B_{pmn}^{(\ell)} P_n^m(\eta) Q_n^m(\xi) T_{pm}(\phi) \quad (6.9)$$

which consists of Laplace solutions of the second kind in spheroidal coordinates. The secondary field expansion coefficients, $B_{pmn}^{(\ell)}$, contain all multiple interaction effects and must be solved for. Once the $B_{pmn}^{(\ell)}$ are known, the total induced magnetic field potential can be found.

The total magnetic field on the surface of spheroid ℓ is a combination of the primary field, the self induced secondary field, and the contribution from the induced fields emanating from all the other spheroids. Thus, the total magnetic field in terms of spheroid ℓ 's coordinate

system, $\overline{H}_{\text{tot}}^{(\ell)}$, is

$$\begin{aligned}
\overline{H}_{\text{tot}}^{(\ell)} &= \overline{H}_{\circ} + \overline{H}_{\text{s}} = -\nabla U_{\circ} - \sum_{\ell=1}^L \nabla U_{\text{s}}^{(\ell)} \\
&= -H_{\circ} \sum_{m=0}^{\infty} \sum_{n=m}^{\infty} \sum_{p=0}^1 \frac{d^{(\ell)}}{2} b_{pmn}^{(\ell)} \nabla \Psi_{pmn}(\beta_{\ell\ell}) \\
&\quad - H_{\circ} \sum_{m'=0}^{\infty} \sum_{n'=m'}^{\infty} \sum_{p'=0}^1 \sum_{q=1}^L \frac{d^{(q)}}{2} B_{p'm'n'}^{(q)} \overline{\overline{R}}_{\ell q} \cdot \nabla \Phi_{p'm'n'}(\beta_{\ell q}) \quad (6.10)
\end{aligned}$$

where $\overline{\overline{R}}_{\ell q}$ is a rotation matrix based on the three Euler angles that rotates the vector magnetic field from the coordinate system of spheroid q to that of spheroid ℓ . Note that when $q = \ell$, $\overline{\overline{R}}_{\ell q} = \overline{\overline{I}}$, or the identity dyad, which case corresponds to the self induced magnetic field of spheroid ℓ .

The total induced magnetic field, \overline{H}_{s} , may be solved for by utilizing the boundary conditions at the surface of each of the L spheroids. At the surface of every spheroid, the normal component of the magnetic flux density and the tangential components of the magnetic field must be equal. Thus there are $3L$ sets of boundary conditions we use to solve for the unknowns $A_{pmn}^{(M)(\ell)}$, $A_{pmn}^{(N)(\ell)}$, and $B_{pmn}^{(\ell)}$. For spheroid ℓ , these boundary conditions are written

$$H_{\eta}^{(\ell)} = H_{\text{tot};\eta}^{(\ell)} \quad (6.11a)$$

$$\mu_r^{(\ell)} H_{\xi}^{(\ell)} = H_{\text{tot};\xi}^{(\ell)} \quad (6.11b)$$

$$H_{\phi}^{(\ell)} = H_{\text{tot};\phi}^{(\ell)}. \quad (6.11c)$$

Considering Eqs. (6.5) and (6.10), Eq. (6.11b), for example, can now be written as

$$\begin{aligned}
\mu_r^{(\ell)} H_o \sum_{m=0}^{\infty} \sum_{n=m}^{\infty} \sum_{p=0}^1 & \left[A_{pmn}^{(M)(\ell)} \overline{M}_{pmn;\xi}(c^{(\ell)}; \beta_{\ell\ell}) \right. \\
& \left. + A_{pmn}^{(N)(\ell)} \overline{N}_{pmn;\xi}(c^{(\ell)}; \beta_{\ell\ell}) \right] \\
= -H_o \sum_{m=0}^{\infty} \sum_{n=m}^{\infty} \sum_{p=0}^1 & \frac{d^{(\ell)}}{2} b_{pmn}^{(\ell)} [\nabla \Psi_{pmn}(\beta_{\ell\ell})]_{\xi} \\
- H_o \sum_{m'=0}^{\infty} \sum_{n'=m'}^{\infty} \sum_{p'=0}^1 & \sum_{q=1}^L \frac{d^{(q)}}{2} B_{p'm'n'}^{(q)} \left[\overline{\overline{R}}_{\ell q} \cdot \nabla \Phi_{p'm'n'}(\beta_{\ell q}) \right]_{\xi} \quad (6.12)
\end{aligned}$$

In order to reduce the complexity of Eq. (6.12) and its counterparts from Eqs. (6.11a) and (6.11c), we use a similar procedure as used in [63] and exploit the orthogonality among the azimuthal and Associated Legendre functions between different p , m , and n . We first define an inner product for the azimuthal functions:

$$\langle T_{pm}(\phi), (\cdot) \rangle = \int_{-\pi}^{\pi} T_{pm}(\phi), (\cdot) d\phi. \quad (6.13)$$

Taking $\langle T_{pm}(\phi_{\ell\ell}), (\text{Eq. (6.12)}) \rangle$ isolates m and p from the summations on the internal and primary magnetic field terms due to the orthogonality of the azimuthal functions and gives

$$\begin{aligned}
\mu_r^{(\ell)} \sum_{n=m}^{\infty} & \left[A_{pmn}^{(M)(\ell)} \langle T_{pm}(\phi_{\ell\ell}), \overline{M}_{pmn;\xi}(c^{(\ell)}; \beta_{\ell\ell}) \rangle \right. \\
& \left. + A_{pmn}^{(N)(\ell)} \langle T_{pm}(\phi_{\ell\ell}), \overline{N}_{pmn;\xi}(c^{(\ell)}; \beta_{\ell\ell}) \rangle \right] \\
= - \sum_{n=m}^{\infty} \frac{d^{(\ell)}}{2} b_{pmn}^{(\ell)} & \langle T_{pm}(\phi_{\ell\ell}), [\nabla \Psi_{pmn}(\beta_{\ell\ell})]_{\xi} \rangle \\
& - \sum_{m'=0}^{\infty} \sum_{n'=m'}^{\infty} \sum_{p'=0}^1 \sum_{q=1}^L \frac{d^{(q)}}{2} B_{p'm'n'}^{(q)} \\
& \left\langle T_{pm}(\phi_{\ell\ell}), \left[\overline{\overline{R}}_{\ell q} \cdot \nabla \Phi_{p'm'n'}(\beta_{\ell q}) \right]_{\xi} \right\rangle. \quad (6.14)
\end{aligned}$$

The summations over m' and p' must be retained for the terms involving $\ell \neq q$ spheroids because

$$\left\langle T_{pm}(\phi_{\ell\ell}), \left[\overline{\overline{R}}_{\ell q} \cdot \nabla \Phi_{p'm'n'}(\beta_{\ell q}) \right]_{\xi} \right\rangle \neq 0 \quad (6.15)$$

in general due to coordinate systems of spheroids ℓ and q being non-located.

We define another inner product of the associated Legendre functions:

$$\langle P_n^m(\eta), (\cdot) \rangle = \int_{-1}^1 P_n^m(\eta), (\cdot) d\eta. \quad (6.16)$$

$\langle P_{n''}^m(\eta_{\ell\ell}), (\text{Eq. (6.14)}) \rangle$ results in

$$\begin{aligned} & \mu_r^{(\ell)} \sum_{n=m}^{\infty} \left[A_{pmn}^{(M)(\ell)} I_{pmnn'';\xi}^{(\ell)} + A_{pmn}^{(N)(\ell)} J_{pmnn'';\xi}^{(\ell)} \right] \\ &= - \sum_{n=m}^{\infty} \frac{d^{(\ell)}}{2} b_{pmn}^{(\ell)} F_{pmnn'';\xi}^{(\ell)} \\ & - \sum_{m'=0}^{\infty} \sum_{n'=m'}^{\infty} \sum_{p'=0}^1 \sum_{q=1}^L \frac{d^{(q)}}{2} B_{p'm'n'}^{(q)} G_{p'm'n'n'';\xi}^{(\ell)(q)}. \end{aligned} \quad (6.17)$$

where

$$I_{pmnn'';\xi}^{(\ell)} \equiv \left\langle P_{n''}^m(\eta_{\ell\ell}), \left\langle T_{pm}(\phi_{\ell\ell}), \overline{M}_{pmn;\xi}(c^{(\ell)}; \beta_{\ell\ell}) \right\rangle \right\rangle \quad (6.18)$$

$$J_{pmnn'';\xi}^{(\ell)} \equiv \left\langle P_{n''}^m(\eta_{\ell\ell}), \left\langle T_{pm}(\phi_{\ell\ell}), \overline{N}_{pmn;\xi}(c^{(\ell)}; \beta_{\ell\ell}) \right\rangle \right\rangle \quad (6.19)$$

$$F_{pmnn'';\xi}^{(\ell)} \equiv \left\langle P_{n''}^m(\eta_{\ell\ell}), \left\langle T_{pm}(\phi_{\ell\ell}), [\nabla \Psi_{pmn}(\beta_{\ell\ell})]_{\xi} \right\rangle \right\rangle \quad (6.20)$$

and

$$G_{p'm'n'n'';\xi}^{(\ell)(q)} \equiv \left\langle P_{n''}^m(\eta_{\ell\ell}), \left\langle T_{pm}(\phi_{\ell\ell}), \left[\overline{\mathbf{R}}_{\ell q} \cdot \nabla \Phi_{p'm'n'}(\beta_{\ell q}) \right]_{\xi} \right\rangle \right\rangle. \quad (6.21)$$

The equations are very similar for the boundary condition on the η and ϕ components of the magnetic field [Eqs. (6.11a) and (6.11c), respectively].

Because the functional dependence on η of $[\nabla \Psi_{pmn}(\beta_{\ell\ell})]_{\xi}$ or ϕ is $P_{n''}^m(\eta_{\ell\ell})$, the only nonzero $F_{pmnn'';\xi}^{(\ell)}$ or ϕ occurs when $n = n''$. The η dependence of $[\nabla \Psi_{pmn}(\beta_{\ell\ell})]_{\eta}$ is $dP_{n''}^m(\eta_{\ell\ell})/d\eta_{\ell\ell}$ resulting in two nonzero modes, $n - 1 = n''$ and $n + 1 = n''$ [63, 88].

When $\ell = q$ in Eq. (6.17), the primed summation indices are equivalent to their unprimed counterparts. In this case, $B_{pmn}^{(\ell)}$ are the expansion coefficients for the self induced magnetic field potential, and the inner products in $G_{p'm'n'n''}^{(\ell)(q)}$ are again over an orthogonal set and

reduce to one or two terms in the same way as described above for the $F_{pmnn}^{(\ell)}$.

The solution to this system, i.e. finding the expansion coefficients $A_{pmn}^{(M)(\ell)}$, $A_{pmn}^{(N)(\ell)}$, and $B_{pmn}^{(\ell)}$, requires the truncation of these infinite sets of equations. The total number of boundary conditions, N_{BC} , is

$$N_{BC} = 3L2(m_{\max} + 1)(n_{\max,0} + 1) \quad (6.22)$$

where m_{\max} indicates the truncation order for the m index, and $n_{\max,0}$ indicates the truncation order for the n index when $m = 0$. These boundary conditions, one for each distinct mode on each spheroid, from Eq. (6.11) may then be cast into 3 matrix equations which we write as

$$\overline{\overline{Z}}_{\eta}^M \overline{A}^M + \overline{\overline{Z}}_{\eta}^N \overline{A}^N = -\overline{\overline{W}}_{\eta} \overline{b} - \overline{\overline{Y}}_{\eta} \overline{B} \quad (6.23a)$$

$$\overline{\overline{Z}}_{\xi}^M \overline{A}^M + \overline{\overline{Z}}_{\xi}^N \overline{A}^N = -\overline{\overline{W}}_{\xi} \overline{b} - \overline{\overline{Y}}_{\xi} \overline{B} \quad (6.23b)$$

$$\overline{\overline{Z}}_{\phi}^M \overline{A}^M + \overline{\overline{Z}}_{\phi}^N \overline{A}^N = -\overline{\overline{W}}_{\phi} \overline{b} - \overline{\overline{Y}}_{\phi} \overline{B}. \quad (6.23c)$$

The definitions and dimensions for $\overline{\overline{Z}}_{\zeta}^M$, $\overline{\overline{Z}}_{\zeta}^N$, $\overline{\overline{W}}_{\zeta}$, $\overline{\overline{Y}}_{\zeta}$, \overline{b} , and \overline{B} where $\zeta = \eta, \xi, \text{ or } \phi$ are found in Section 6.3.

Equation (6.23) includes all multiple body interaction effects and provides a simultaneous solution for the internal and induced, secondary external magnetic fields. In particular, the secondary induced magnetic field, \overline{H}_s , may be calculated from the expansion coefficients \overline{B} and compared to frequency domain measurements made with instruments such as the ultrawide band GEM-3 [114] instrument

The formulation for the induced electromagnetic induction (EMI) response from multiple permeable and conducting spheroidal objects in close proximity under time harmonic excitation presented here is formally exact except for the truncation of the infinite sets of equations. However, as the size parameters, $c^{(\ell)}$, become larger, the vector spheroidal wave functions $\overline{M}_{pmn}(c^{(\ell)}; \beta_{\ell\ell})$ and $\overline{N}_{pmn}(c^{(\ell)}; \beta_{\ell\ell})$ become numerically unstable preventing calculation of the expansion coefficients $A_{pmn}^{(M)(\ell)}$, $A_{pmn}^{(N)(\ell)}$, and $B_{pmn}^{(\ell)}$. To extend the range of c over which solutions can be calculated, we can use asymptotic forms of the angular

and radial spheroidal wave functions in the internal modal field matrices $\overline{\overline{Z}}_\zeta^M$, and $\overline{\overline{Z}}_\zeta^N$ (see Chapters 4 and 5). As these representations also become inaccurate for even larger size parameters, it is expected that the small penetration approximation (SPA) [63, 7] in the spheroidal modal interaction matrix $\overline{\overline{Y}}_\zeta$ can be used at these frequencies.

This multibody solution may provide the basis for a forward model used by inversion routines designed to detect and discriminate UXO. Specifically, this multibody solution may help to isolate non-UXO clutter from actual UXO in the field.

6.3 Matrix Definitions and Dimensions

The matrices $\overline{\overline{Z}}_\zeta^M$, $\overline{\overline{Z}}_\zeta^N$, and $\overline{\overline{W}}_\zeta$, where $\zeta = \eta, \xi, \text{ or } \phi$, are coefficient matrices describing the relative magnitude of the various spheroidal modes internal and external to the spheroids. The size of these matrices are prescribed by the truncation values used. Given m_{max} and n_{max} as described in Section 6.2, then the size of $\overline{\overline{Z}}_\zeta^M$, $\overline{\overline{Z}}_\zeta^N$, and $\overline{\overline{W}}_\zeta$ are

$$2L(m_{max} + 1)(n_{max,o} + 1) \quad (6.24)$$

where the 2 accounts for the p index.

The entries of $\overline{\overline{Z}}_\zeta^M$, $\overline{\overline{Z}}_\zeta^N$, and $\overline{\overline{W}}_\zeta$ are arranged in blocks according to, first, spheroid index ℓ , then m , then p , and finally n (or n'). Defining matrix indices

$$\begin{aligned} i &= 1 + (\ell - 1)(m_{max} + 1)2(n_{max,o} + 1) \\ &\quad + m2(n_{max,o} + 1) \\ &\quad + p(n_{max,o} + 1) \\ &\quad + (n'' - m) \end{aligned} \quad (6.25)$$

$$\begin{aligned} j &= 1 + (\ell - 1)(m_{max} + 1)2(n_{max,o} + 1) \\ &\quad + m2(n_{max,o} + 1) \\ &\quad + p(n_{max,o} + 1) \\ &\quad + (n - m), \end{aligned} \quad (6.26)$$

then

$$\overline{\overline{Z}}_{\zeta}^M(i, j) = I_{pmnn''; \zeta}^{(\ell)}, \quad (6.27)$$

$$\overline{\overline{Z}}_{\zeta}^N(i, j) = J_{pmnn''; \zeta}^{(\ell)}, \quad (6.28)$$

and

$$\overline{\overline{W}}_{\zeta}(i, j) = F_{pmnn''}^{(\ell)}. \quad (6.29)$$

Using index j , we also define the order of the spheroidal expansion coefficients \bar{b} and $\overline{\overline{B}}$ as,

$$b_{pmn}^{(\ell)} = \bar{b}(j) \quad (6.30)$$

and

$$B_{pmn}^{(\ell)} = \overline{\overline{B}}(j). \quad (6.31)$$

The spheroidal modal interaction matrix $\overline{\overline{Y}}_{\zeta}$ has the same size as $\overline{\overline{Z}}_{\zeta}^M$, $\overline{\overline{Z}}_{\zeta}^N$, and $\overline{\overline{W}}_{\zeta}$ (assuming $m'_{\max} = m_{\max}$ and $n'_{\max, o} = n_{\max, o}$), but has nonzero terms which account for the interspheroidal interactions in addition to the self induced terms. We define different matrix indices such that

$$\begin{aligned} i' &= 1 + (\ell - 1)(m_{\max} + 1)2(n_{\max, o} + 1) \\ &\quad + m2(n_{\max, o} + 1) \\ &\quad + p(n_{\max, o} + 1) \\ &\quad + (n'' - m) \end{aligned} \quad (6.32)$$

$$\begin{aligned} j' &= 1 + (q - 1)(m_{\max} + 1)2(n_{\max, o} + 1) \\ &\quad + m'2(n_{\max, o} + 1) \\ &\quad + p'(n_{\max, o} + 1) \\ &\quad + (n' - m'). \end{aligned} \quad (6.33)$$

Now, the entries of $\overline{\overline{Y}}_\zeta$ can be specified as

$$\overline{\overline{Y}}_\zeta(i', j') = G_{p'm'n'n''; \zeta}^{(\ell)(q)}. \quad (6.34)$$

6.4 Conclusion

We have constructed a solution for the induced magnetic field from multiple conducting and permeable prolate and oblate spheroids in close proximity and under time harmonic excitation in the magnetoquasistatic regime. This solution solves for the induced field expansion coefficients for all spheroids in the collection simultaneously and includes all intertarget interactions and effects.

Chapter 7

Summary

In this thesis, I have studied electromagnetic scattering and induction models with regard to spheroidal geometries. Principal results recorded in this thesis include advances in finding the asymptotic expressions of the spheroidal wave functions, obtaining a broadband electromagnetic induction (EMI) response for realistic conducting and permeable spheroids and showing agreement of my model with data, formulating and implementing a simultaneous solution for the induced magnetic field from multiple permeable and conducting spheroidal objects in close proximity under time harmonic excitation, and the first application of the Sparse Matrix/Canonical Grid (SMCG) method to three dimensions as applied to scattering from dense random discrete media containing dielectric spheroidal scatterers.

These models advance our ability to calculate the scattered fields and the induced secondary magnetic fields from more realistic canonical shapes such as spheroids, plates, and needles.

First in Chapter 2, the effective permittivity (ϵ_{eff}) of dense random media was studied. The coherent scattered fields from a collection of particles in a given test volume were compared to fields scattered from a homogeneous volume of the same size and shape. The permittivity of the homogeneous medium which yielded scattered fields that best matched the averaged scattered fields produced by many configurations of particles was considered to be equal to ϵ_{eff} . The effective permittivity of dense random media containing discrete spheroids was characterized through a Monte Carlo simulation employing the Method of Moments on the volume integral equation. The basis functions were chosen to be the

electrostatic dipole solutions of a spheroid. Simulations with $N=3000$ particles, $N_r=50$ realizations and different fractional volumes ($f_v = 0.05-0.40$) and particle elongations ($e = 1.0-2.6$) were performed in a spherical test volume. The scattering from this volume was then compared to Mie scattering from a homogeneous sphere of the same size. Results indicate that ϵ_{eff} for a dense random media containing randomly oriented discrete prolate spheroids agrees well with results from the classical mixing formula. This is consistent with previous studies considering spherical particles only.

The sparse matrix canonical grid (SMCG) method has been extended to 3-D and illustrated by finding the scattering from random media filled with dielectric spheroids at random positions and orientations in Chapter 3. The 3-D SMCG method achieves $\mathcal{O}(N \log N)$ complexity instead of $\mathcal{O}(N^2)$ for the matrix-vector multiply when using an iterative solver by decomposing the interaction matrix $\overline{\overline{Z}}$, generated by an MoM solution to the many-body volume integral equation, into strong and weak interaction matrices $\overline{\overline{Z}}^s$ and $\overline{\overline{Z}}^w$, respectively. The matrix $\overline{\overline{Z}}^s$ contains only those interactions which are between particles closer than the neighborhood distance r_d . Therefore, $\overline{\overline{Z}}^s$ is very sparse and the matrix-vector multiply $\overline{\overline{Z}}^s \cdot \overline{x}$ is accomplished in $\mathcal{O}(N)$ complexity. The matrix $\overline{\overline{Z}}^w$ is formed by expanding the dyadic Green's function between each pair of particles whose associated grid points are located further apart than r_d in a γ^{th} order multivariate Taylor series expansion around a canonical grid superimposed onto the test volume. The prolate spheroidal particles considered in this paper were electrically small so that their response to electromagnetic excitation could be adequately approximated with a point response. Therefore, the Green's function interaction expansion matrices $\overline{\overline{G}}_{\gamma_x \gamma_y \gamma_z}$ exhibit a multilevel block Toeplitz (MBT) structure. MBT matrices can be multiplied with an arbitrary vector using the only one forward and one inverse FFT. Thus $\overline{\overline{Z}}^w \cdot \overline{x}$ can be accomplished in $\mathcal{O}(N_T N \log N)$ complexity where N_T is the number of FFTs and depends on the expansion order γ . The 3-D SMCG method was demonstrated to indeed realize the predicted reduction in complexity and memory requirements through large-scale examples including up to 15000 discrete scatterers.

The procedure for expediting a matrix-vector multiply involving \mathbf{T}_f^M multilevel block-Toeplitz (MBT) matrices outlined in Appendix A is efficient both in terms of memory and computational complexity. It can be easily applied to 3-D scattering from arbitrary shaped

targets using a discretized integral formulation. This was illustrated in Section A.3, where a comparison between the scattering from a spherical volume containing many small dielectric spheres and the scattering from a homogeneous sphere of the same size and shape of the spherical volume was presented. The effective permittivity ϵ_{eff} of the medium composed by the small particles was calculated and shown to converge to the permittivity of the Mie sphere for sufficiently fine grid spacings. In contrast to previously proposed algorithms, this fast matrix-vector multiply may be accurately described as a minimal memory method due to the fact that only the unique information from a \mathbf{T}_f^M matrix is stored in memory. Also, the reduced complexity is achieved in a fashion similar, but not identical to those described in [125] and [126] with a speed improvement (due to the 1-D FFT length of $\prod_{i=1}^M (2n_i - 1)$) in the present method.

The asymptotic expansion of the spheroidal wave function (SWF) and its eigenvalues have been investigated for complex size parameter c in Chapter 4. No fundamentally new asymptotic expansions are required, but instead, established *prolate*-type and *oblate*-type asymptotic expansions are directly applicable to finding the asymptotic expansion of the SWF for complex size parameter c . A rapid and accurate method for calculating the SWFs for complex c in the asymptotic regime has been presented based on a lookup table consisting of branch points, $c_{o;r}^{mn}$. Through a brute force numerical method, this lookup table, based on the number of branch cuts (emanating from $c_{o;r}^{mn}$) traversed according to $\arg(c)$, is calculated once and recorded. This allows the assignment of any SWF to either a *prolate*-type or *oblate*-type expansion (ordered by n_p and n_o respectively) for any general complex size parameter c . The ordering for these expansions was found to be different than the original ordering of the spheroidal wave functions, with Table 4.3 documenting the ordering for the special case when $\arg(c) = \pi/4$. Normalizations, dependent on c , were derived for both the *prolate* and *oblate*-type asymptotic expansions and for both $(n - m)$ even and odd. These normalized asymptotic expansions for the PASWFs $S_{mn}(c, \eta)$ and $S'_{mn}(c, \eta)$, together with established asymptotic expansions for the prolate radial spheroidal wave functions $R_{mn}(c, \eta)$ and $R'_{mn}(c, \eta)$, allow the rapid calculation of the vector spheroidal wave functions for significantly larger (complex) size parameter c than previously possible. In Appendix D, I provided some of the branch points of the spheroidal wave equation,

$c_{o;r}^{mn}$, with their associated eigenvalues, $\lambda_{o;r}^{mn}$ for a greater range of m and n than previously available as well as with greater accuracy. Also included are tables containing the angular SWF for large and complex size parameter, c .

Chapter 5 discusses my broadband solution for the induced magnetic field from conducting and permeable prolate and oblate spheroids under time harmonic excitation in the magnetoquasistatic regime. My combined method consists of the exact analytical solution, asymptotic assisted analytical solution, and a small penetration approximation (SPA). This combined solution is accurate to within 2% error for most spheroids with aspect ratio $\frac{1}{8} < e < 8$. Results produced by this combined method were compared to results from a method of moments/boundary integral method and found to be in excellent agreement. Results were also compared to induced magnetic field measurements taken by the GEM-3 instrument from metal prolate and oblate spheroids. If the permeability and conductivity of the spheroids is allowed to vary within accepted physical ranges, results were seen to match exceptionally well with measurements. Using this model, calculation of the broadband induced magnetic field response from more realistic canonical shapes such as spheroids, plates, and needles is now possible. The results indicate that solutions from my model are indeed unique for a given spheroid and orientation. On this basis, my method could become a forward model upon which inversions schemes may be based.

Finally in Chapter 6, I have constructed a broadband solution for the induced magnetic field from multiple conducting and permeable prolate and oblate spheroids in close proximity and under time harmonic excitation in the magnetoquasistatic regime. This solution solves for the induced field expansion coefficients for all spheroids in the collection simultaneously and includes all intertarget interactions and effects. My combined method consists of the exact analytical solution at low frequencies, asymptotic assisted analytical solution at mid-range frequencies, and a small penetration approximation (SPA) for high frequencies in the MQS regime.

Appendix A

Fast Algorithm for Matrix-Vector Multiply of Asymmetric Multilevel Block-Toeplitz Matrices in 3-D Scattering

A.1 Introduction

Multilevel block-Toeplitz (MBT) matrices often arise in the solution of electromagnetic scattering problems due to the translational invariance and convolutional nature of the free-space Green's function. For example, a three-level MBT matrix arises in connection with the solution of the scattering from arbitrarily shaped targets using either the Discrete Dipole Approximation (DDA) [47, 127, 128] or, similarly, using a (volumetric) discretized integral formulation [48, 129, 16]. In other contexts, MBT matrices are also generated as the result of the autocorrelation of a two dimensional (2-D) discrete random process [130], and in many problems involving symmetries based on cubic meshes [131, 132].

In this communication, we describe a new fast Fourier transform (FFT)-based method to expedite matrix-vector multiplies involving MBT matrices with minimal memory requirements. This method applies to MBT matrices with blocks and subblocks which are

themselves MBT and in general asymmetric, and provides for the last, M^{th} , level subblock to be a square, possibly asymmetric, arbitrary matrix (*i.e.*, not necessarily Toeplitz). The method has a similar purpose to the FFT-based method of [125], but it is more general in implementation due to its ability to multiply arbitrary MBT matrices. Moreover, it is based on 1-D FFTs implementations directly (as opposed to 2-D and 3-D FFTs [42]), and can be classified as a truly minimal memory method because it stores only nonredundant matrix entries. The computational complexity is $O(N \log N)$ and the memory requirement is $O(2^M N) \approx O(N)$. The convergence and accuracy of the method are assessed in the calculation of the scattering and effective permittivity of a dielectric sphere.

A.2 Formulation

A.2.1 Definitions

Let \mathbf{A} be a square matrix in the matrix equation $\mathbf{A} \cdot \mathbf{x} = \mathbf{b}$ which consists of block-Toeplitz (BT) matrices each containing BT subblocks continuing for $M - 1$ levels with the last M^{th} level containing a possibly asymmetric, square matrix, *i.e.*,

$$\mathbf{A} = \begin{bmatrix} \mathbf{a}_0^1 & \mathbf{a}_1^1 & \cdots & \mathbf{a}_{n_1}^1 \\ \mathbf{a}_{-1}^1 & \mathbf{a}_0^1 & & \\ \vdots & \ddots & \ddots & \\ \mathbf{a}_{-n_1}^1 & \cdots & \mathbf{a}_0^1 \end{bmatrix}, \quad (\text{A.1})$$

where

$$\mathbf{a}_{-n_1}^1, \dots, \mathbf{a}_{n_1}^1 = \begin{bmatrix} \mathbf{a}_0^2 & \mathbf{a}_1^2 & \cdots & \mathbf{a}_{n_2}^2 \\ \mathbf{a}_{-1}^2 & \mathbf{a}_0^2 & & \\ \vdots & \ddots & \ddots & \\ \mathbf{a}_{-n_2}^2 & \cdots & \mathbf{a}_0^2 \end{bmatrix}, \quad (\text{A.2})$$

continuing until the $(M - 1)^{\text{st}}$ level

$$\mathbf{a}_{-n_{(M-1)}}^{M-1}, \dots, \mathbf{a}_{n_{(M-1)}}^{M-1} = \begin{bmatrix} \mathbf{a}_0^M & \mathbf{a}_1^M & \dots & \mathbf{a}_{n_M}^M \\ \mathbf{a}_{-1}^M & \mathbf{a}_0^M & & \\ \vdots & & \ddots & \vdots \\ \mathbf{a}_{-n_M}^M & & \dots & \mathbf{a}_0^M \end{bmatrix}, \quad (\text{A.3})$$

with $\mathbf{a}_{-n_M}^M, \dots, \mathbf{a}_{n_M}^M$ being arbitrary $f \times f$ matrices. Furthermore, let $\mathbf{a}^{1\dots(M-1)}$ be asymmetric and let \mathbf{A} be referred to as $\mathbf{T}_f^M(n_1, n_2, \dots, n_M)$ or simply \mathbf{T}_f^M where M denotes the number of BT levels, f denotes the size of the final dense matrix, and n_1, n_2, \dots, n_M denote the number of BT blocks at each level. As an example, a typical $\mathbf{T}_1^3(2, 2, 2)$ matrix is shown in Fig. A-1. A $\mathbf{T}_3^3(2, 2, 2)$ matrix (the type produced in the solution to the example in Section A.3) would be similar except that each unique integer depicted in Fig. A-1 is replaced by a corresponding 3×3 dense matrix.

A.2.2 Recursive Algorithms

In order to illustrate the fast matrix-vector multiply method, we divided the method into parts 1–4 which are briefly described below. For brevity and ease of use, each step is also separately cast in terms of Matlab codes in the Appendix, and can be easily ported into other programming languages.

In part 1, full \mathbf{T}_f^M matrices, which will be generically referred to as \mathbf{A} , are defined recursively. The definition is described in Algorithm 1, which steps through each of the first level of subblocks $(\mathbf{a}_{-n_1}^1, \dots, \mathbf{a}_{n_1}^1)$ recursively defining each level and then assigning that subblock along its diagonal when completed.

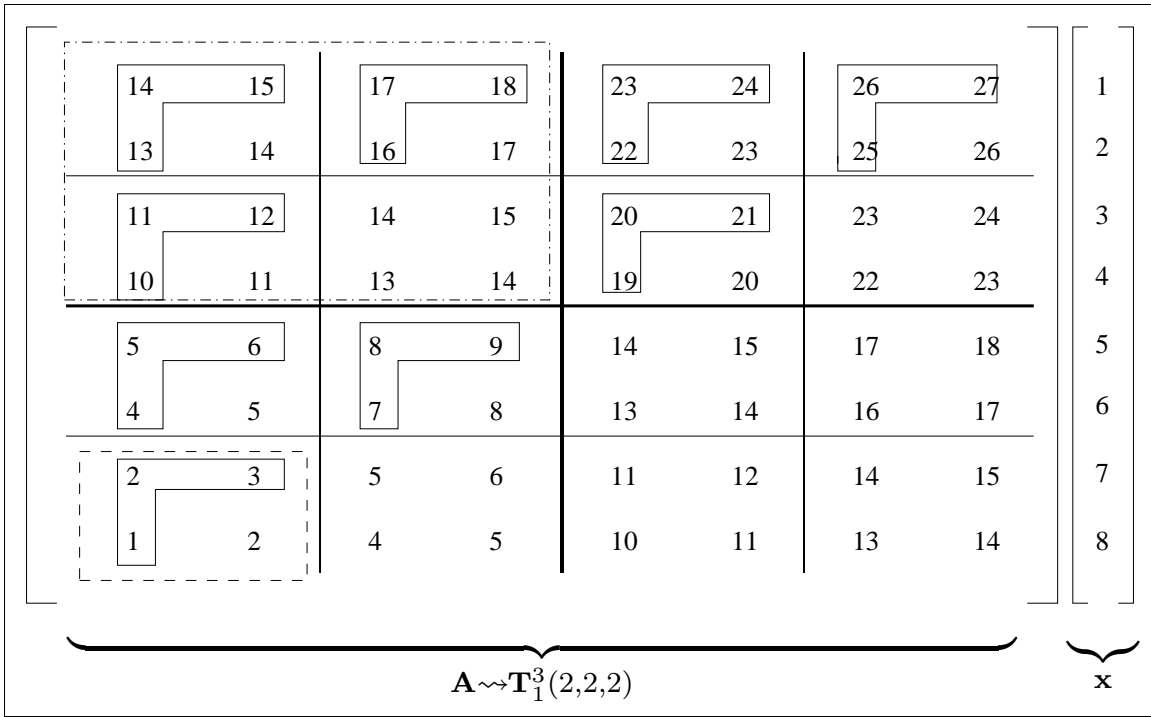


Figure A-1: Example of a $\mathbf{A} = \mathbf{T}_1^3(2, 2, 2)$ asymmetric MBT matrix. Unique entries are boxed with a solid line. In the upper left hand corner, \mathbf{a}_0^1 is enclosed by a dash-dot box, while at the lower left hand corner $\mathbf{a}_{-1}^1 | \mathbf{a}_{-1}^2$ is delineated by a dashed box. Thin solid lines delineate interaction between different rows of a 2x2x2 cubic mesh, while bold solid line delineate between planes.

Algorithm 1: Generation of full \mathbf{T}_f^M MBT matrices.

```

1 function [A]=BT_full(n,f,n_ind,level)
2 % [A]=BT_full(n,f,n_ind,level)
3 % Recursive multilevel block Toeplitz (MBT) matrix generator.
4 % n=[n1 n2 ... nM] is the number of BT blocks at each level.
5 % f is the size of the final dense fxf block.
6 % n_ind is size 2xn and indicates the current block index.
7 % Row 1 => down, Row 2 => across,
8 % level indicates which level is current.
9 % BT_full is initially called with only n and f as arguments.
10 if nargin<3, n_ind=ones(2,length(n)); level=1; end
11 if level==length(n)+1
12 A=application_function(n,f,n_ind,level); %fxf block assignment.
13 else
14 this_n=n(level);
15 for i=1:this_n %Lower triangle and diagonal assignment.
16 b_edge=prod(n(level+1:length(n)))*f;
17 n_ind(1,level)=i;
18 blk=BT_full(n,f,n_ind,level+1);
19 for j=1:(this_n-i+1)
20 A(b_edge*(i-1)+[b_edge*(j-1)+1:b_edge*j],...
21 [b_edge*(j-1)+1:b_edge*j])=blk;
22 end
23 end
24 for i=2:this_n %Upper triangle assignment.
25 n_ind(2,level)=i;
26 blk=BT_full(n,f,n_ind,level+1);
27 for j=1:this_n-i+1
28 A([b_edge*(j-1)+1:b_edge*j],...
29 b_edge*(i-1)+[b_edge*(j-1)+1:b_edge*j])=blk;
30 end
31 end
32 end

```

The application function in line 12 of Algorithm 1 assigns the final $f \times f$ block and should be replaced by appropriate statements involving the physical parameters and relationships of the system as a function of the current indices n_1, n_2, \dots, n_M (represented by n_ind).

Storing the entire matrix \mathbf{A} in computer memory would be inefficient due to the many repeated entries in MBT matrices. Indeed, for many large scale problems, storing \mathbf{A} is impractical if not impossible. Part 2 is designed to circumvent the matrix filling process by assigning only the nonredundant information from \mathbf{A} to an associated *vector* \mathbf{A}_u . We call this a MBT projection, denoted by

$$\mathbf{A}_u = \Pi_{bt}(\mathbf{A}). \quad (\text{A.4})$$

This projection is performed by Algorithm 2.

Algorithm 2: Π_{bt} : Direct assignment of \mathbf{A}_u .

```

1 function [Au]=BT_fft(n,f,n_ind,level)
2 if nargin<3, n_ind=ones(2,length(n));level=1; end
3 if level==(length(n)+1)
4 Au=flipud(application_function(f)).'; Au=Au(:)';
5 else
6 this_n=n(level);
7 for i=this_n:-1:1
8 b_edge=f^2*prod(2*n(level+1:length(n))-1);
9 n_ind(1,level)=i;
10 blk=BT_fft(n,f,n_ind,level+1);
11 Au(1+b_edge*(this_n-i):b_edge*(this_n-i+1))=blk;
12 end
13 for i=2:(this_n)
14 n_ind(2,level)=i;
15 blk=BT_fft(n,f,n_ind,level+1);
16 Au(1+b_edge*(i+this_n-2):b_edge*(i+this_n-1))=blk;
17 end
18 end

```

Algorithm 2 proceeds in the same block order convention as Algorithm 1 assigning only the left column and top row of each subblock to \mathbf{A}_u . The final $f \times f$ block is assigned in line 4 of Algorithm 2 from left to right, bottom to top, i.e.,

$$\begin{bmatrix} f_1 & f_2 & f_3 \\ f_4 & f_5 & f_6 \\ f_7 & f_8 & f_9 \end{bmatrix} \rightarrow [f_7, f_8, f_9, f_4, f_5, f_6, f_1, f_2, f_3]. \quad (\text{A.5})$$

For example, applying Algorithm 2 to achieve a MBT projection from the matrix \mathbf{A} of Fig. A-1 would result in $\Pi_{bt}(\mathbf{A}) = \mathbf{A}_u = [1:27]$. The memory requirement for storing MBT matrices in this way is reduced substantially from

$$f^2 \left(\prod_{i=1}^M n_i \right)^2 = f^2 N^2 \quad (\text{A.6})$$

stored elements for the full MBT matrix \mathbf{A} to

$$f^2 \prod_{i=1}^M (2n_i - 1) \approx f^2 2^M N \quad (\text{A.7})$$

stored elements for \mathbf{A}_u . If \mathbf{T}_f^M possessed any symmetry (as in the case of the DDA approximation, see [125]), this requirement could be reduced even further.

In part 3, zeros are inserted at appropriate locations into \mathbf{x} according to the BT structure, in order to obtain an auxiliary vector denoted by $\mathbf{x}_z = \zeta_p(\mathbf{x})$, suitable for the direct

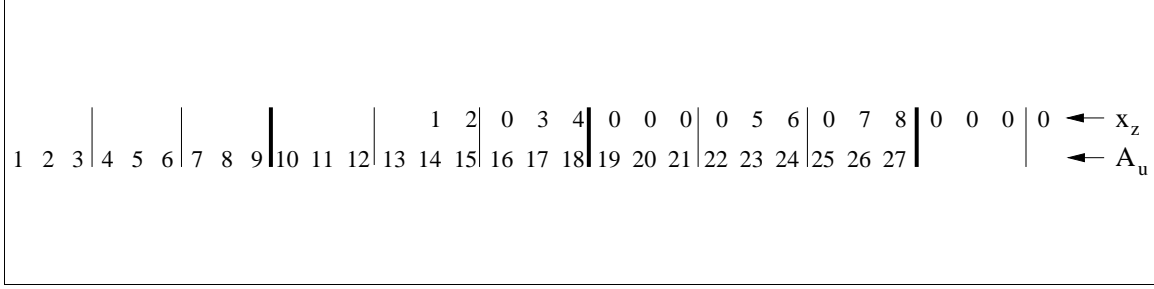


Figure A-2: $\mathbf{A}_u * \mathbf{x}_z$ step which yields the first term of \mathbf{b}_z . Note the insertion of zeros into \mathbf{x} yielding \mathbf{x}_z which causes proper alignment. Each entry in \mathbf{A}_u corresponds to an \mathbf{a}_i^M final level subblock where i is between $-n_M$ and n_M ; the thin vertical lines mark the separation between $\mathbf{a}_{-1}^2 \dots \mathbf{a}_1^2$ subblocks in $\mathbf{a}_{-1}^1 \dots \mathbf{a}_1^1$, and thicker vertical lines indicate the boundary between $\mathbf{a}_{-1}^1 \dots \mathbf{a}_1^1$ blocks.

convolution with $\Pi_{bt}(\mathbf{A})$.

Algorithm 3: ζ_p : Generation of \mathbf{x}_z by inserting zeros into \mathbf{x} .

```

1 function xz=BT_pad(n,f,x)
2 xz=[];
3 if isempty(n)
4   xz=[x zeros(1,f^2-f)];
5 else
6   b_edge=prod(n(2:length(n)))*f;
7   this_n=n(1);
8   for i=1:this_n
9     if length(n)>1
10      xz=[xz BT_pad(n(2:length(n)),f,x(1+(i-1)*b_edge:i*b_edge))...
11          zeros(1,(n(2)-1)*prod(2*(n(3:length(n)))-1)*f^2)]
12     else
13      xz=[xz BT_pad(n(2:length(n)),f,x(1+(i-1)*b_edge:i*b_edge))]
14     end
15   end
16 end

```

These projections are done because the full matrix-vector multiply $\mathbf{A} \cdot \mathbf{x}$, which requires $O(N^2)$ complexity, may be replaced with a convolution, or outer product, in the Fourier domain. Rather than multiplying the full MBT matrix \mathbf{A} with \mathbf{x} , the vector $\Pi_{bt}(\mathbf{A})$ is convolved with $\zeta_p(\mathbf{x})$. Algorithm 3 in Appendix performs the ζ_p operation which depends on n_1, n_2, \dots, n_M . This is also depicted graphically in Fig. A-2. Note that \mathbf{x}_z must be zero-padded to the length of \mathbf{A}_u before the FFT and subsequent multiplication in the Fourier domain (see example in next Section).

The convolution is easily accomplished in $O(N \log N)$ complexity by multiplying $\tilde{\mathbf{A}}_u$ and $\tilde{\mathbf{x}}_z$ (the tildes denote Fourier transformed quantities: $\mathbf{A}_u \xleftrightarrow{\mathcal{F}} \tilde{\mathbf{A}}_u$) in the Fourier domain

to obtain $\tilde{\mathbf{b}}_z$. In the final step, the vector \mathbf{b} is recovered after the multiplication in the Fourier domain. This is done in a process similar to Algorithm 3, through the suppression of extra terms in \mathbf{b}_z , where

$$\mathbf{b}_z = \mathcal{F}^{-1}(\tilde{\mathbf{A}}_u \cdot \tilde{\mathbf{x}}_z), \quad (\text{A.8})$$

to reconstruct \mathbf{b} . For completeness, this is illustrated in the last algorithm, Algorithm 4, which performs this reconstruction of \mathbf{b} from the IFFT of $\tilde{\mathbf{b}}_z$.

Algorithm 4: ζ_a^{-1} : Reconstruction of \mathbf{b} from \mathbf{b}_z .

```

1 function b=BT_reconstruct(n,f,bz)
2 b=[];
3 if isempty(n)
4 b=bz(f:f:f^2);
5 else
6 b_edge=prod(2*n(2:length(n))-1)*f^2;
7 this_n=n(1);
8 for i=this_n:2*this_n-1
9 b=[b BT_reconstruct(n(2:length(n)),f,...
10 bz(1+(i-1)*b_edge:i*b_edge));
11 end
12 end

```

If we denote this last operation by ζ_a^{-1} , then the fast matrix-vector multiply can be concisely written as

$$\mathbf{b} = \zeta_a^{-1} \left[\mathcal{F}^{-1} \left(\widetilde{\Pi_{bf}(\mathbf{A})} \cdot \widetilde{\zeta_p(\mathbf{x})} \right) \right] \quad (\text{A.9})$$

A.2.3 \mathbf{T}_f^M Fast Multiply Example

As an example, consider the $\mathbf{T}_1^3(2,2,2)$ matrix shown in Fig. A-1. Here, $\Pi_{bf}(\mathbf{A}) = \mathbf{A}_u = [1:27]$ and if $\mathbf{x}=[1:8]$ as in Fig. A-1, The operator ζ_p implemented by algorithm 3 in the Appendix yields $\zeta_p(\mathbf{x}) = \mathbf{x}_z = [1 \ 2 \ 0 \ 3 \ 4 \ 0 \ 0 \ 0 \ 0 \ 0 \ 5 \ 6 \ 0 \ 7 \ 8 \ 0 \ 0 \ 0 \ 0]$. A graphical representation of the step in the convolution $\mathbf{A}_u * \mathbf{x}_z$ that yields the first term of \mathbf{b}_z (and \mathbf{b}) is provided as Fig. A-2.

The following Matlab commands perform the FFT on \mathbf{A}_u and \mathbf{x}_z to yield $\tilde{\mathbf{A}}_u$ and $\tilde{\mathbf{x}}_z$ respectively, the multiplication of $\tilde{\mathbf{A}}_u$ and $\tilde{\mathbf{x}}_z$ which yields $\tilde{\mathbf{b}}_z$, and the reconstruction of \mathbf{b} from the IFFT of $\tilde{\mathbf{b}}_z$ using Algorithm 4. Here, $\mathbf{A}_u = [1:27]$, $\mathbf{x} = [1:8]$, $n=[2 \ 2 \ 2]$, $f=1$, and `fft_length=27`.

```

x_z=BT_pad(n,f,x);
A_u_tilde=fft(fliplr(A_u),fft_length);
x_z_tilde=fft(x_z,fft_length);

```

```

b_z_tilde=A_u_tilde.*x_z_tilde;
b_z=ifft(b_z_tilde);
b=BT_reconstruct(n,f,b_z);

```

A.3 Numerical Implementation and Example: 3-D Scattering

We study the electromagnetic scattering from an arbitrarily shaped dielectric target inscribed in a cube which has a mesh having N_x , N_y , and N_z grid points in the x , y , and z directions respectively superimposed upon it. At each grid point, a small (electric field assumed constant or $ka \ll 1$) sphere with permittivity ϵ_p and volume $V = d_x d_y d_z$ (where d_x , d_y , and d_z are the lattice spacings) is placed and allowed to exhibit only an electric dipole response (see Fig. A-3). This method can be shown to be equivalent to the DDA ([48], [129]) and in fact the fast method presented in this work may also be applied to matrix-vector multiplications used for iterative solutions in the DDA.

The scattered electric field from a small dielectric scatterer is [43]

$$\bar{E}_s(\bar{r}) = \frac{-k^2}{\epsilon} \bar{G}(\bar{r}, \bar{r}') \bar{p}, \quad (\text{A.10})$$

where

$$\bar{G}(\bar{r}, \bar{r}') = \left[\bar{I} + \frac{\nabla \nabla}{k^2} \right] g(\bar{r}, \bar{r}'), \quad (\text{A.11})$$

$$\bar{p} = v_0(\epsilon_p - \epsilon) \bar{E}(\bar{r}'), \quad (\text{A.12})$$

$g(\bar{r}, \bar{r}')$ is the scalar Green's function, v_0 is the volume of the particle, ϵ_p is the permittivity of the particle, k is the background wavenumber, and ϵ is the permittivity of the host medium. Accordingly, the scattering from a collection of small scatterers excited by an incident electric field \bar{E}_{inc} leads to the discretized volume integral equation (VIE), *i.e.*

$$\bar{E}(\bar{r}) = \bar{E}_{inc}(\bar{r}) + \frac{k^2}{\epsilon} \sum_{j=1}^N v_j(\epsilon_j - \epsilon) \bar{G}(\bar{r}, \bar{r}_j) \bar{E}(\bar{r}_j). \quad (\text{A.13})$$

Thus the electric field at each scatterer caused by both the incident electric field and the

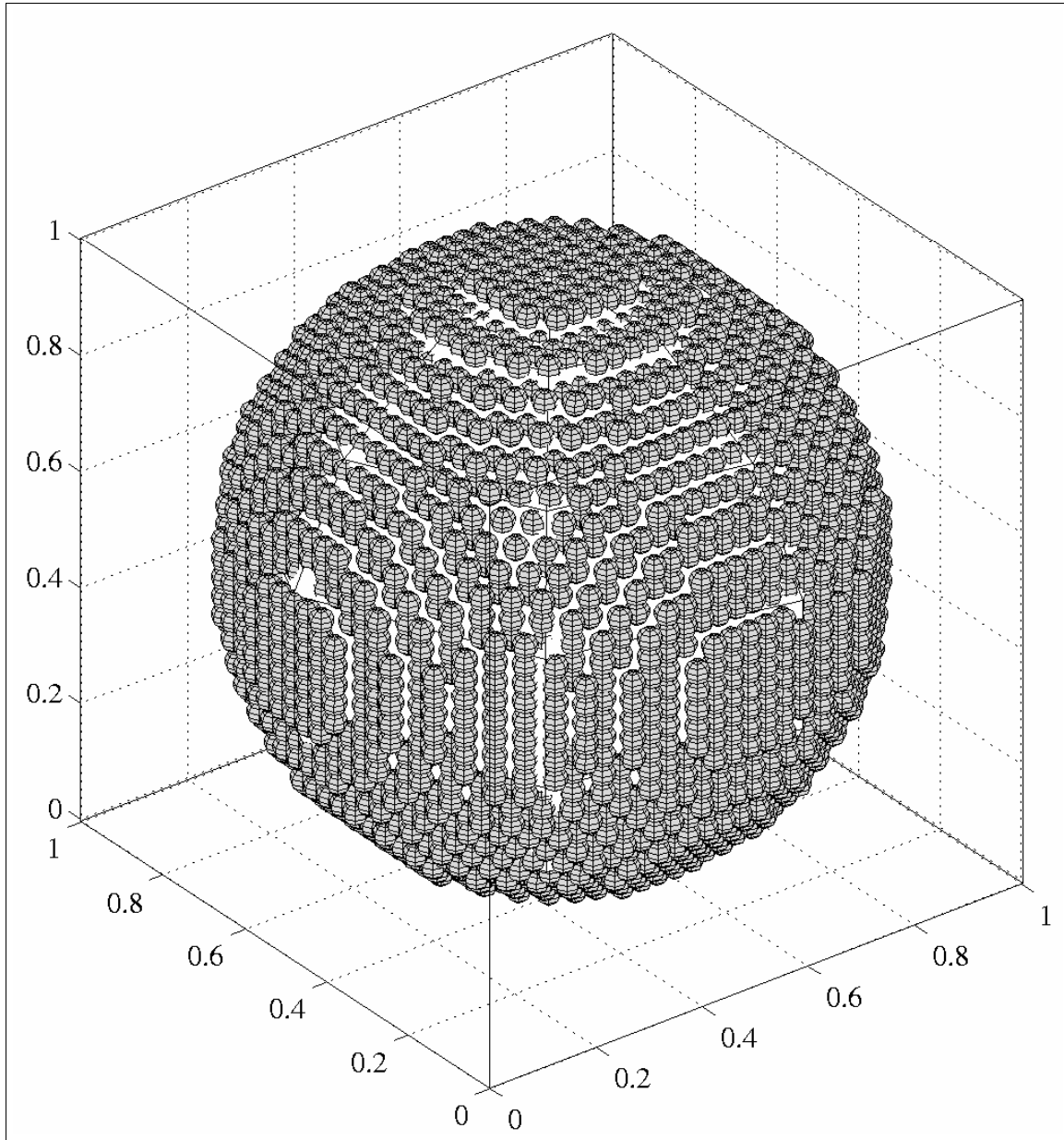


Figure A-3: Discrete Dipole Approximation of a homogeneous sphere using a 31x31x31 grid.

field radiated from each of the other dipoles can be expressed as

$$\bar{\mathbf{E}}(\bar{\mathbf{r}}_i) = \bar{\mathbf{E}}_{inc}(\bar{\mathbf{r}}_i) + \frac{k^2}{\epsilon} \sum_{j=1}^N v_j (\epsilon_j - \epsilon) \bar{\bar{\mathbf{G}}}(\bar{\mathbf{r}}_i, \bar{\mathbf{r}}_j) \bar{\mathbf{E}}(\bar{\mathbf{r}}_j). \quad (\text{A.14})$$

For otherwise similar spheres on lattice points, the interaction between particles i and j can be seen to depend only on $\bar{\bar{\mathbf{G}}}(\bar{\mathbf{r}}_i, \bar{\mathbf{r}}_j)$ which is translationally invariant.

Using a method of moments (MoM) procedure [16], induced dipole strengths are computed using the electrostatic solution to the Laplace equation for a sphere as the basis functions. This model incorporates multiple scattering effects into an interaction (impedance) matrix \mathbf{Z} based on Eq. A.14. The entries of \mathbf{Z} constitute a MBT ($\mathbf{T}_3^3(N_x, N_y, N_z)$) due to the translationally invariant Green's function kernel. The scattered electric field in the far-field can be approximated using these induced dipole moments. The resulting system of equations is often ill-conditioned in the case of large scatterers. Therefore, the solution is usually sought through iterative techniques requiring (fast) matrix-vector multiplies.

The inverse problem of finding the effective permittivity (ϵ_{eff}) of the target – defined as the permittivity of a homogeneous solid of the same size and shape as the test volume which reacts to electromagnetic excitation in the most similar manner as the test volume – may be calculated through comparison of the scattered field to Mie scattering (Chapter 2 and [16, 21]) in the case that the target is a sphere, as illustrated in Fig. A-3. As the discretization size is decreased, or equivalently, as the number of grid points in each dimension increases, the result is expected to converge to the scattering from a homogeneous sphere with uniform permittivity ϵ_{eff} . Figures. A-4 and A-5 illustrate results of this comparison for two different sizes and contrasts with increasingly fine grid spacings. The %error column included on the table accompanying each plot is calculated according to

$$\%error = \text{rms} \left(\frac{\sigma_{vie}}{\sigma_{Mie}} - 1 \right) \times 100, \quad (\text{A.15})$$

where σ_{Mie} is the radar cross section (RCS) of a homogeneous dielectric sphere according Mie scattering, and σ_{VIE} is the RCS computed using the discrete volume integral equation (Eq. A.14). Table A.1 shows the total number of iterations used by the iterative solver (in

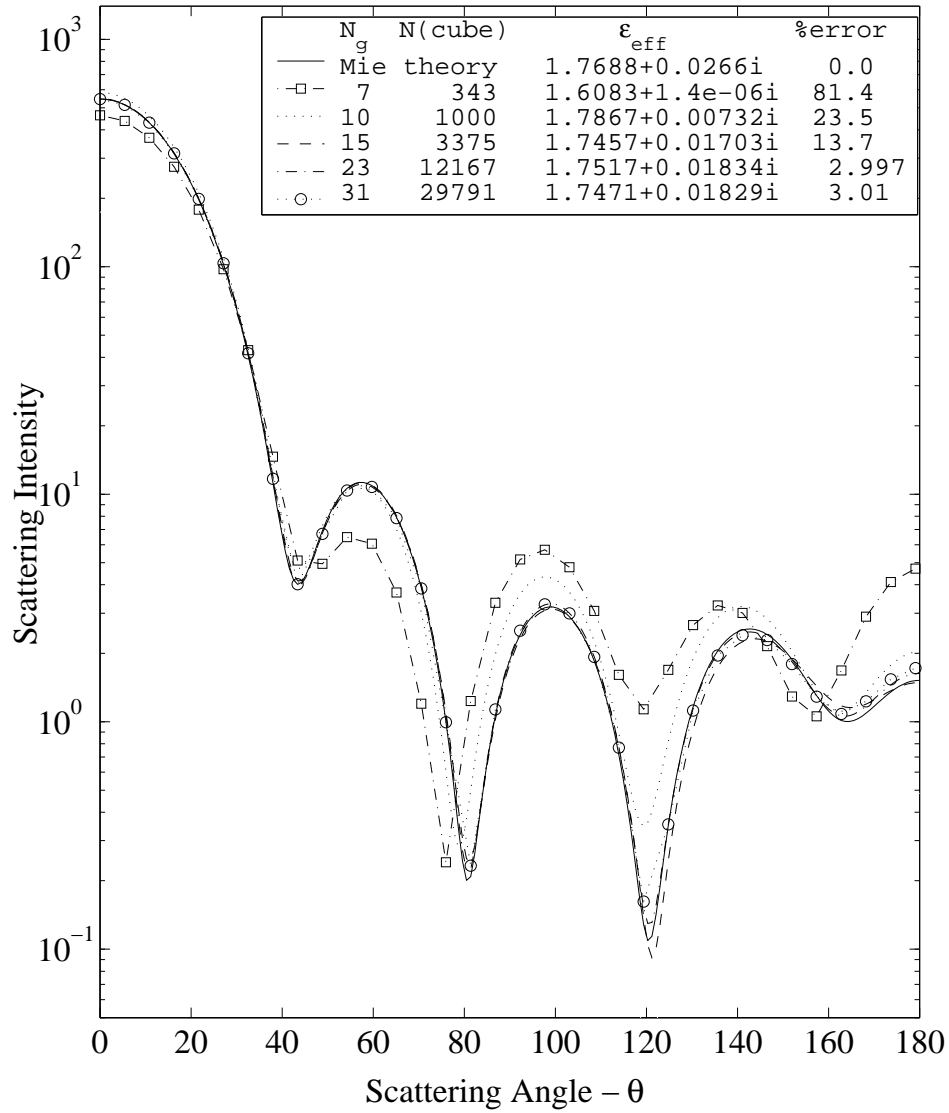


Figure A-4: Effective permittivity (ϵ_{eff}) results for a spherical test volume having meshes with 7-31 grid points per axis, $\epsilon_p = 1.7688 + 0.0266i$, and $ka = 5$ for the test volume.

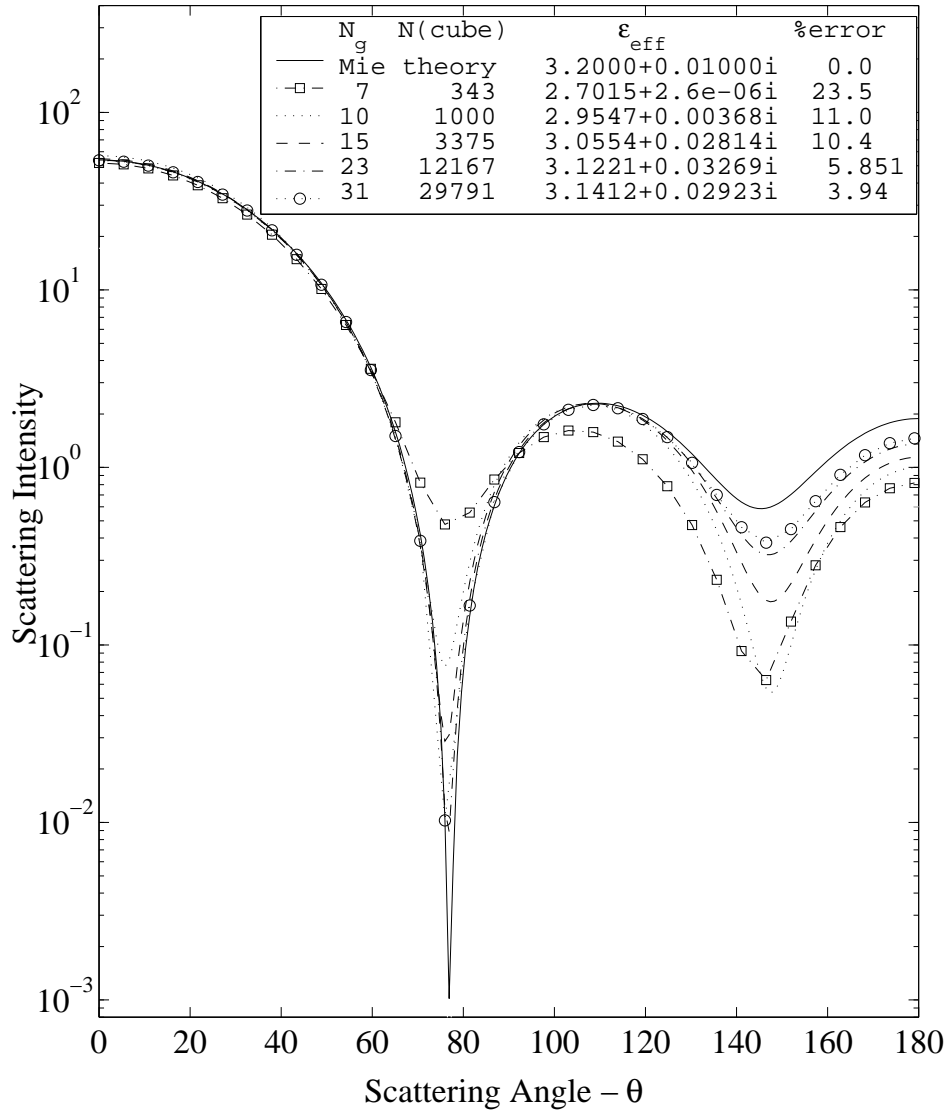


Figure A-5: Effective permittivity (ϵ_{eff}) results for $\epsilon_p = 3.2 + 0.01i$, and $ka = 2.5$.

this case the biconjugate gradient stabilized solver) and the total computational time for each solution on a Compaq Alphaserer DS20E with 4GB of RAM.

The far field scattering results for the collection of spheres contained in a spherical boundary approaches the Mie scattering results given a sufficiently fine grid spacing. As ka and ϵ_p increase the grid needs to be more densely spaced in order to maintain the validity of the previously mentioned assumptions.

N_g	length of \mathbf{A}_u (FFT length) (Eq. A.7)	MBT Fast Method Time (s)	Full Method Time (s)	%error (Eq A.15)
7	19773	1.33	5.85	124.0
10	61731	5.98	25.5	37.2
15	219501	19.25	190.7	9.41
23	820125	87.9	2544.0	2.904
31	2042829	363.3	14295.3	3.06

Table A.1: Comparison of MBT fast method computation times with the full method for the case of Fig. A-4.

A.4 Discussion and Conclusion

The procedure for expediting a matrix-vector multiply involving \mathbf{T}_f^M multilevel block-Toeplitz (MBT) matrices outlined in this communication is efficient both in terms of memory and computational complexity. It can be easily applied to 3-D scattering from arbitrary shaped targets using a discretized integral formulation. This was illustrated in Section A.3, where a comparison between the scattering from a spherical volume containing many small dielectric spheres and the scattering from a homogeneous sphere of the same size and shape of the spherical volume was presented. The effective permittivity ϵ_{eff} of the medium composed by the small particles was calculated and shown to converge to the permittivity of the Mie sphere for sufficiently fine grid spacings. In contrast to previously proposed algorithms, this fast matrix-vector multiply may be accurately described as a minimal memory method due to the fact that only the unique information from a \mathbf{T}_f^M matrix is stored in memory. Also, the reduced complexity is achieved in a fashion similar, but not identical to those described in [125] and [126] with a speed improvement due to the 1-D FFT length of $\prod_{i=1}^M (2n_i - 1)$ in the present method.

Appendix B

Magnetoquasistatic Solution for Conducting and Permeable Spheroidal Shells

B.1 Exact Formulation

A conducting and permeable prolate spheroidal shell of uniform thickness is placed in a nonpermeable and weakly conducting homogeneous background and excited by a time-harmonic primary magnetic field $\overline{H}_o(\overline{r})e^{-i\omega t}$ (Fig. B-1). The time dependence expression of $e^{-i\omega t}$ is suppressed below. In the quasi-magnetostatic regime, we assume that the displacement current can be neglected in comparison to the conduction current. The magnetic fields in the spheroidal shell and in the core satisfy the vector wave equation [134]

$$\nabla \times \nabla \times \overline{H}_1 - k^2 \overline{H}_1 = 0 \tag{B.1}$$

with the wavenumber k being either $k_1^2 = i\omega\sigma_1\mu_1$ for the shell layer, or $k_3^2 = i\omega\sigma_3\mu_3$ for the core. Thus the magnetic field inside the shell layer ($\xi = \xi_0$, $d_\beta < d < d_\alpha$ [region 1]) can be expanded using the (divergence-free) vector spheroidal wavefunctions of first kind (which

¹This Appendix, as well as Appendix C, borrows heavily from [133], Chapter 2 therein.

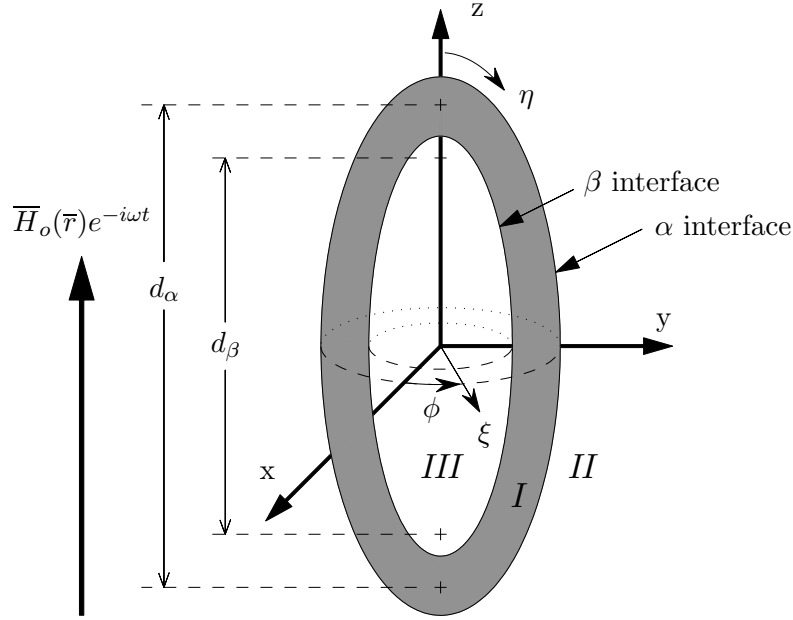


Figure B-1: A conducting and permeable prolate spheroidal shell is excited by a time-harmonic primary field $\overline{H}_o(\vec{r})e^{-i\omega t}$. The prolate spheroidal coordinate system is specified by (ξ, η, ϕ) with $-1 \leq \eta \leq 1$, $1 \leq \xi < \infty$, and $0 \leq \phi < 2\pi$. The outer (α) interface of the shell is given by $\xi = \xi_0 = 1/\sqrt{1 - (1/e)^2}$ and d_α with $e_\alpha = b_\alpha/a_\alpha = b_\beta/a_\beta$ is the elongation ratio. The inner (β) interface is specified by ξ_0 and d_β .

are regular at the origin) and third kind (which are regular at infinity) [66]:

$$\begin{aligned} \overline{H}_1 = H_o \sum_{m=0}^{\infty} \sum_{n=m}^{\infty} \sum_{p=0}^1 & \left[A_{pmn}^{(M)} \overline{M}_{pmn}^{r(1)}(c; \xi, \eta, \phi) + A_{pmn}^{(N)} \overline{N}_{pmn}^{r(1)}(c; \xi, \eta, \phi) \right. \\ & \left. + C_{pmn}^{(M)} \overline{M}_{pmn}^{r(3)}(c; \xi, \eta, \phi) + C_{pmn}^{(N)} \overline{N}_{pmn}^{r(3)}(c; \xi, \eta, \phi) \right] \end{aligned} \quad (\text{B.2})$$

while the field inside the core of the spheroid (region 3), is expanded in terms of spheroidal wavefunctions of the first kind only:

$$\overline{H}_3 = H_o \sum_{m=0}^{\infty} \sum_{n=m}^{\infty} \sum_{p=0}^1 \left[D_{pmn}^{(M)} \overline{M}_{pmn}^{r(1)}(c; \xi, \eta, \phi) + D_{pmn}^{(N)} \overline{N}_{pmn}^{r(1)}(c; \xi, \eta, \phi) \right] \quad (\text{B.3})$$

In Eqs. (B.2) and (B.3), H_o is a constant and the dimensionless spheroidal frequency parameter c is defined as

$$c = k \frac{d}{2} \quad (\text{B.4})$$

with $d = 2\sqrt{b^2 - a^2}$ being the interfocal distance for either the inner or outer layer.

The vector spheroidal wavefunctions of the third kind must be included in the description of the field in the shell layer due to the presence of the inner boundary of the shell layer. Using an analogy to microwave scattering, the spheroidal wavefunctions of the first kind represent the “ingoing” wave, while the spheroidal wavefunctions of the third kind represent the “outgoing” wave. This corresponds to the case of a layered sphere under the excitation of a standing wave [44]. The angular function is an infinite sum of associated Legendre functions, radial function of the first kind is an infinite sum of spherical Bessel functions, while the radial function of the third kind is an infinite sum of spherical Hankel functions of the first kind.

The vector wavefunctions can be generated from the scalar wavefunction as follows [66]:

$$\overline{M}_{pmn}^{r(i)} = \nabla \psi_{pmn}^{(i)} \times \bar{r} \quad (\text{B.5})$$

$$\overline{N}_{pmn}^{r(i)} = \frac{1}{k_1} \nabla \times \overline{M}_{pmn}^{r(i)} \quad (\text{B.6})$$

with $i=1, 2, 3,$ or 4 and

$$\psi_{pmn}^{(i)} = S_{mn}(c_1, \eta) R_{mn}^{(i)}(c_1, \xi) T_{pm}(\phi) \quad (\text{B.7})$$

where $S_{mn}(c_1, \eta)$ and $R_{mn}^{(i)}(c_1, \xi)$ are the spheroidal angle and radial functions, respectively, while the azimuthal function $T_{pm}(\phi)$ is simply

$$T_{pm}(\phi) = \begin{cases} \cos m\phi, & p=0 \\ \sin m\phi, & p=1 \end{cases} \quad (\text{B.8})$$

Note that other choices for generating the vector wavefunctions are possible besides (B.5) and (B.6), (cf. [50, 66]). The r -vector wavefunctions used here represent a common choice

for scattering problems [49, 59]. To simplify notation, we will dispense with the superscript r and the explicit dependence on x_{i_0} of the spheroidal wavefunctions.

Outside the spheroid (region 2) the medium is assumed to be poorly conducting and weakly magnetic. Thus $k_2 \rightarrow 0$ in the quasi-static limit, and the magnetic fields can be obtained from their scalar potentials, which satisfy the Laplace equation. We define a scalar potential $U_2(\bar{r})$ such that the external magnetic field is $\bar{H}_2 = -\nabla U_2$. The total external magnetic field can be written as a sum of the primary and secondary fields, i.e.,

$$\bar{H}_2 = \bar{H}_o + \bar{H}_s = -\nabla U_o - \nabla U_s \quad (\text{B.9})$$

The primary field potential $U_o(\bar{r})$ is expanded as

$$U_o(\bar{r}) = \frac{H_o d_\alpha}{2} \sum_{m=0}^{\infty} \sum_{n=m}^{\infty} \sum_{p=0}^1 b_{pmn} \Phi_{pmn}^{(1)}(\xi, \eta, \phi) \quad (\text{B.10})$$

where

$$\Phi_{pmn}^{(1)}(\xi, \eta, \phi) = P_n^m(\xi) P_n^m(\eta) T_{pm}(\phi) \quad (\text{B.11})$$

is the spheroidal Laplace solution of first kind which is regular at the origin ($\xi \rightarrow 1$). The source coefficients b_{pmn} are determined from the primary field. The functions $P_n^m(\eta)$ and $P_n^m(\xi)$ are the associated Legendre functions of first kind. The associated Legendre functions used here follow the convention of Abramowitz and Stegun [88] (Eqs. 8.6.6 and 8.6.7), which is slightly different from that of Flammer [66].

Similarly, the secondary magnetic field potential $U_s(\bar{r})$ can be expanded as

$$U_s(\bar{r}) = \frac{H_o d}{2} \sum_{m=0}^{\infty} \sum_{n=m}^{\infty} \sum_{p=0}^1 B_{pmn} \Phi_{pmn}(\xi, \eta, \phi) \quad (\text{B.12})$$

where

$$\Phi_{pmn}(\xi, \eta, \phi) = Q_n^m(\xi) P_n^m(\eta) T_{pm}(\phi) \quad (\text{B.13})$$

is the spheroidal Laplace solution of second kind which is regular at infinity ($\xi \rightarrow \infty$). The function $Q_n^m(\xi)$ is the associated Legendre function of second kind.

The boundary conditions are specified by the continuity of tangential components of \overline{H} and normal component of \overline{B} [134] at the outer surface of the spheroidal shell (ξ_0, d_α)

$$H_{1\eta} = H_{2\eta} \quad (\text{B.14a})$$

$$H_{1\phi} = H_{2\phi} \quad (\text{B.14b})$$

$$\mu_{r1}H_{1\xi} = H_{2\xi} \quad (\text{B.14c})$$

and at the inner surface (ξ_0, d_β)

$$H_{1\eta} = H_{3\eta} \quad (\text{B.15a})$$

$$H_{1\phi} = H_{3\phi} \quad (\text{B.15b})$$

$$\mu_{r1}H_{1\xi} = \mu_{r3}H_{3\xi} \quad (\text{B.15c})$$

where $\mu_{r1} = \mu_1/\mu_0$ and $\mu_{r3} = \mu_3/\mu_0$ are the relative permeabilities of the spheroidal shell and core with respect to their surrounding respectively.

The vector spheroidal wavefunctions in component forms are given in Appendix C.1. In matching the boundary conditions, first note that from (B.8),

$$\frac{dT_{pmn}}{d\phi} = (-1)^{\tilde{p}}mT_{\tilde{p}mn}(\phi) \quad (\text{B.16})$$

where $\tilde{p} = 0$ for $p = 1$ and vice versa. Now, matching the angular component H_η according

to (B.14a) gives

$$\begin{aligned}
& \sum_{n=m}^{\infty} \left\{ \left[(-1)^p m A_{\tilde{p}mn}^{(M)} \widetilde{M}_{\eta;mn}^{(1)}(c_{1\alpha}, \eta) + \frac{1}{c_{1\alpha}} A_{\tilde{p}mn}^{(N)} \widetilde{N}_{\eta;mn}^{(1)}(c_{1\alpha}, \eta) \right] + \right. \\
& \quad \left. \left[(-1)^p m C_{\tilde{p}mn}^{(M)} \widetilde{M}_{\eta;mn}^{(3)}(c_{1\alpha}, \eta) + \frac{1}{c_{1\alpha}} C_{\tilde{p}mn}^{(N)} \widetilde{N}_{\eta;mn}^{(3)}(c_{1\alpha}, \eta) \right] \right\} \\
& = - \sum_{n=m}^{\infty} [b_{pmn} P_n^m(\xi_0) + B_{pmn} Q_n^m(\xi_0)] \frac{dP_n^m}{d\eta}
\end{aligned} \tag{B.17}$$

where

$$c_{1\alpha} = k_1 \frac{d_\alpha}{2} \tag{B.18}$$

and we have made use of the orthogonality property of $\cos m\phi$ and $\sin m\phi$ to eliminate the sum over the indices m and p and However, the sum over n must be retained because no such orthogonality condition exists between the angular functions $S_{mn}(c, \eta)$ and $P_n^m(\eta) = S_{mn}(c=0, \eta)$. In general, $S_{mn}(c, \eta)$ and $S_{mn}(c', \eta)$ are orthogonal only when $c = c'$. This accounts for the complexity of the multi-media spheroidal boundary value problem. $\widetilde{M}_{mn}^{(i)}$ and $\widetilde{N}_{mn}^{(i)}$ are “reduced” vector spheroidal wavefunctions whose definitions can be found in Appendix C.

Similarly, matching H_ϕ and H_ξ according to Eqs. (B.14c)–(B.14b) yields

$$\begin{aligned}
& \mu_{r1} \sum_{n=m}^{\infty} \left\{ \left[(-1)^p m A_{\tilde{p}mn}^{(M)} \widetilde{M}_{\xi;mn}^{(1)}(c_{1\alpha}, \eta) + \frac{1}{c_{1\alpha}} A_{\tilde{p}mn}^{(N)} \widetilde{N}_{\xi;mn}^{(1)}(c_{1\alpha}, \eta) \right] + \right. \\
& \quad \left. \left[(-1)^p m C_{\tilde{p}mn}^{(M)} \widetilde{M}_{\xi;mn}^{(3)}(c_{1\alpha}, \eta) + \frac{1}{c_{1\alpha}} C_{\tilde{p}mn}^{(N)} \widetilde{N}_{\xi;mn}^{(3)}(c_{1\alpha}, \eta) \right] \right\} \\
& = - \sum_{n=m}^{\infty} \left[b_{pmn} \frac{dP_n^m}{d\xi_0} + B_{pmn} \frac{dQ_n^m}{d\xi_0} \right] P_n^m(\eta).
\end{aligned} \tag{B.19}$$

$$\begin{aligned}
& \sum_{n=m}^{\infty} \left\{ \left[(-1)^{p+1} A_{\tilde{p}mn}^{(M)} \widetilde{M}_{\phi;mn}^{(1)}(c_{1\alpha}, \eta) + \frac{m}{c_{1\alpha}} A_{\tilde{p}mn}^{(N)} \widetilde{N}_{\phi;mn}^{(1)}(c_{1\alpha}, \eta) \right] + \right. \\
& \quad \left. \left[(-1)^{p+1} C_{\tilde{p}mn}^{(M)} \widetilde{M}_{\phi;mn}^{(3)}(c_{1\alpha}, \eta) + \frac{m}{c_{1\alpha}} C_{\tilde{p}mn}^{(N)} \widetilde{N}_{\phi;mn}^{(3)}(c_{1\alpha}, \eta) \right] \right\} \\
& = - \sum_{n=m}^{\infty} m [b_{pmn} P_n^m(\xi_0) + B_{pmn} Q_n^m(\xi_0)] P_n^m(\eta)
\end{aligned} \tag{B.20}$$

For the inner boundary, we have respectively for the H_η , H_ξ , and H_ϕ boundary conditions:

$$\begin{aligned} & \sum_{n=m}^{\infty} \left\{ \left[(-1)^p m A_{\tilde{p}mn}^{(M)} \widetilde{M}_{\eta;mn}^{(1)}(c_{1\beta}, \eta) + \frac{1}{c_{1\beta}} A_{pmn}^{(N)} \widetilde{N}_{\eta;mn}^{(1)}(c_{1\beta}, \eta) \right] + \right. \\ & \quad \left. \left[(-1)^p m C_{\tilde{p}mn}^{(M)} \widetilde{M}_{\eta;mn}^{(3)}(c_{1\beta}, \eta) + \frac{1}{c_{1\beta}} C_{pmn}^{(N)} \widetilde{N}_{\eta;mn}^{(3)}(c_{1\beta}, \eta) \right] \right\} \\ &= \sum_{n=m}^{\infty} \left\{ \left[(-1)^p m D_{\tilde{p}mn}^{(M)} \widetilde{M}_{\eta;mn}^{(1)}(c_{3\beta}, \eta) + \frac{1}{c_{3\beta}} D_{pmn}^{(N)} \widetilde{N}_{\eta;mn}^{(1)}(c_{3\beta}, \eta) \right] \right\} \end{aligned} \quad (\text{B.21})$$

$$\begin{aligned} & \mu_{r1} \sum_{n=m}^{\infty} \left\{ \left[(-1)^p m A_{\tilde{p}mn}^{(M)} \widetilde{M}_{\xi;mn}^{(1)}(c_{1\beta}, \eta) + \frac{1}{c_{1\beta}} A_{pmn}^{(N)} \widetilde{N}_{\xi;mn}^{(1)}(c_{1\beta}, \eta) \right] + \right. \\ & \quad \left. \left[(-1)^p m C_{\tilde{p}mn}^{(M)} \widetilde{M}_{\xi;mn}^{(3)}(c_{1\beta}, \eta) + \frac{1}{c_{1\beta}} C_{pmn}^{(N)} \widetilde{N}_{\xi;mn}^{(3)}(c_{1\beta}, \eta) \right] \right\} \\ &= \mu_{r3} \sum_{n=m}^{\infty} \left\{ \left[(-1)^p m D_{\tilde{p}mn}^{(M)} \widetilde{M}_{\xi;mn}^{(1)}(c_{3\beta}, \eta) + \frac{1}{c_{3\beta}} D_{pmn}^{(N)} \widetilde{N}_{\xi;mn}^{(1)}(c_{3\beta}, \eta) \right] \right\} \end{aligned} \quad (\text{B.22})$$

$$\begin{aligned} & \sum_{n=m}^{\infty} \left\{ \left[(-1)^{p+1} A_{\tilde{p}mn}^{(M)} \widetilde{M}_{\phi;mn}^{(1)}(c_{1\beta}, \eta) + \frac{m}{c_{1\beta}} A_{pmn}^{(N)} \widetilde{N}_{\phi;mn}^{(1)}(c_{1\beta}, \eta) \right] + \right. \\ & \quad \left. \left[(-1)^{p+1} C_{\tilde{p}mn}^{(M)} \widetilde{M}_{\phi;mn}^{(3)}(c_{1\beta}, \eta) + \frac{m}{c_{1\beta}} C_{pmn}^{(N)} \widetilde{N}_{\phi;mn}^{(3)}(c_{1\beta}, \eta) \right] \right\} \\ &= \sum_{n=m}^{\infty} \left\{ \left[(-1)^{p+1} D_{\tilde{p}mn}^{(M)} \widetilde{M}_{\phi;mn}^{(1)}(c_{3\beta}, \eta) + \frac{m}{c_{3\beta}} D_{pmn}^{(N)} \widetilde{N}_{\phi;mn}^{(1)}(c_{3\beta}, \eta) \right] \right\} \end{aligned} \quad (\text{B.23})$$

where

$$c_{1\beta} = k_1 \frac{d_\beta}{2} \quad \text{and} \quad c_{3\beta} = k_3 \frac{d_\beta}{2}. \quad (\text{B.24})$$

Equations (B.14) and (B.15) are used to determine the field expansion coefficients $A_{\tilde{p}mn}^{(M)}$, $A_{pmn}^{(N)}$, $C_{\tilde{p}mn}^{(M)}$, $C_{pmn}^{(N)}$, $D_{\tilde{p}mn}^{(M)}$, $D_{pmn}^{(N)}$, and $B_{\tilde{p}mn}$. Further simplifications can be made by considering the parity of the η dependence on the left- and right-hand sides of these equations. Take (B.19), for example. Under the parity transformation $\eta \rightarrow -\eta$, the n th term of its right-hand side, due to the functional form of $P_n^m(\eta)$, gives a factor of $(-1)^{n-m}$. On the other hand, $\widetilde{M}_{\xi;mn}^{r(i)}(\xi_0, \eta)$ and $\widetilde{N}_{\xi;mn}^{r(i)}(\xi_0, \eta)$ give $(-1)^{n-m+1}$ and $(-1)^{n-m}$, respectively. These can be deduced from their expressions in Appendix C and the fact that $S_{mn}(\eta)$ has

the same parity property as $P_n^m(\eta)$ [66]. These considerations imply that excitations b_{pmn} with $n-m$ even and $n-m$ odd are decoupled and can be treated separately. If $b_{pmn} \neq 0$ for $n-m$ even, then $B_{pmn'}$, $A_{pmn'}^{(N)}$, $A_{pm(n'+1)}^{(M)}$, $C_{pmn'}^{(N)}$, $C_{pm(n'+1)}^{(M)}$, $D_{pmn'}^{(N)}$, and $D_{pm(n'+1)}^{(M)}$ can be nonzero only for $n' = m, m+2, \dots$. This will be referred to as the case of *even* excitation. If $b_{pmn} \neq 0$ for $n-m$ odd, then $B_{pmn'}$, $A_{pmn'}^{(N)}$, $A_{pm(n'-1)}^{(M)}$, $C_{pmn'}^{(N)}$, $C_{pm(n'-1)}^{(M)}$, $D_{pmn'}^{(N)}$, and $D_{pm(n'-1)}^{(M)}$ can be nonzero only for $n' = m+1, m+3, \dots$. This will be referred to as the case of *odd* excitation.

Note that Eqs. (B.17)-(B.23) must hold for all η on the surface of the spheroid. A common procedure to solve such equations is to expand the left-hand sides, which are regular functions of η , in terms of an infinite series of $P_n^m(\eta)$. This can be accomplished by multiplying both sides of the equations by $P_{n'}^m(\eta)$, $n' = m, m+1, \dots$, and integrating over η from -1 to 1 . Applying this “testing” procedure to (B.19), (B.20), (B.22), (B.23), and (B.21) yield respectively,

$$\begin{aligned} \mu_{r1} \sum_{n=m}^{\infty} \left\{ \left[(-1)^p m A_{\tilde{p}mn}^{(M)} I_{\xi;n'n}^{(1)}(c_{1\alpha}, \eta) + \frac{1}{c_{1\alpha}} A_{pmn}^{(N)} J_{\xi;n'n}^{(1)}(c_{1\alpha}, \eta) \right] + \right. \\ \left. \left[(-1)^p m C_{\tilde{p}mn}^{(M)} I_{\xi;n'n}^{(3)}(c_{1\alpha}, \eta) + \frac{1}{c_{1\alpha}} C_{pmn}^{(N)} J_{\xi;n'n}^{(3)}(c_{1\alpha}, \eta) \right] \right\} \\ = - \left[b_{pmn'} \frac{dP_{n'}^m}{d\xi_0} + B_{pmn'} \frac{dQ_{n'}^m}{d\xi_0} \right] \end{aligned} \quad (\text{B.25})$$

$$\begin{aligned} \sum_{n=m}^{\infty} \left\{ \left[(-1)^{p+1} A_{\tilde{p}mn}^{(M)} I_{\phi;n'n}^{(1)}(c_{1\alpha}, \eta) + \frac{m}{c_{1\alpha}} A_{pmn}^{(N)} J_{\phi;n'n}^{(1)}(c_{1\alpha}, \eta) \right] + \right. \\ \left. \left[(-1)^{p+1} C_{\tilde{p}mn}^{(M)} I_{\phi;n'n}^{(3)}(c_{1\alpha}, \eta) + \frac{m}{c_{1\alpha}} C_{pmn}^{(N)} J_{\phi;n'n}^{(3)}(c_{1\alpha}, \eta) \right] \right\} \\ = -m \left[b_{pmn'} P_{n'}^m(\xi_0) + B_{pmn'} Q_{n'}^m(\xi_0) \right] \end{aligned} \quad (\text{B.26})$$

$$\begin{aligned} \mu_{r1} \sum_{n=m}^{\infty} \left\{ \left[(-1)^p m A_{\tilde{p}mn}^{(M)} I_{\xi;n'n}^{(1)}(c_{1\beta}, \eta) + \frac{1}{c_{1\beta}} A_{pmn}^{(N)} J_{\xi;n'n}^{(1)}(c_{1\beta}, \eta) \right] + \right. \\ \left. \left[(-1)^p m C_{\tilde{p}mn}^{(M)} I_{\xi;n'n}^{(3)}(c_{1\beta}, \eta) + \frac{1}{c_{1\beta}} C_{pmn}^{(N)} J_{\xi;n'n}^{(3)}(c_{1\beta}, \eta) \right] \right\} \\ = \mu_{r3} \sum_{n=m}^{\infty} \left[(-1)^p m D_{\tilde{p}mn}^{(M)} I_{\xi;n'n}^{(1)}(c_{3\beta}, \eta) + \frac{1}{c_{3\beta}} D_{pmn}^{(N)} J_{\xi;n'n}^{(1)}(c_{3\beta}, \eta) \right] \end{aligned} \quad (\text{B.27})$$

$$\begin{aligned}
& \sum_{n=m}^{\infty} \left\{ \left[(-1)^{p+1} A_{\tilde{p}mn}^{(M)} I_{\phi;n'n}^{(1)}(c_{1\beta}, \eta) + \frac{m}{c_{1\beta}} A_{\tilde{p}mn}^{(N)} J_{\phi;n'n}^{(1)}(c_{1\beta}, \eta) \right] + \right. \\
& \quad \left. \left[(-1)^{p+1} C_{\tilde{p}mn}^{(M)} I_{\phi;n'n}^{(3)}(c_{1\beta}, \eta) + \frac{m}{c_{1\beta}} C_{\tilde{p}mn}^{(N)} J_{\phi;n'n}^{(3)}(c_{1\beta}, \eta) \right] \right\} \\
&= \sum_{n=m}^{\infty} \left[(-1)^{p+1} D_{\tilde{p}mn}^{(M)} I_{\phi;n'n}^{(1)}(c_{3\beta}, \eta) + \frac{m}{c_{3\beta}} D_{\tilde{p}mn}^{(N)} J_{\phi;n'n}^{(1)}(c_{3\beta}, \eta) \right] \tag{B.28}
\end{aligned}$$

$$\begin{aligned}
& \sum_{n=m}^{\infty} \left\{ \left[(-1)^p m A_{\tilde{p}mn}^{(M)} I_{\eta;n'n}^{(1)}(c_{1\beta}, \eta) + \frac{1}{c_{1\beta}} A_{\tilde{p}mn}^{(N)} J_{\eta;n'n}^{(1)}(c_{1\beta}, \eta) \right] + \right. \\
& \quad \left. \left[(-1)^p m C_{\tilde{p}mn}^{(M)} I_{\eta;n'n}^{(3)}(c_{1\beta}, \eta) + \frac{1}{c_{1\beta}} C_{\tilde{p}mn}^{(N)} J_{\eta;n'n}^{(3)}(c_{1\beta}, \eta) \right] \right\} \\
&= \sum_{n=m}^{\infty} \left[(-1)^p m D_{\tilde{p}mn}^{(M)} I_{\eta;n'n}^{(1)}(c_{3\beta}, \eta) + \frac{1}{c_{3\beta}} D_{\tilde{p}mn}^{(N)} J_{\eta;n'n}^{(1)}(c_{3\beta}, \eta) \right]. \tag{B.29}
\end{aligned}$$

The integrals $I_{\gamma;n'n}^{(i)}(c, \eta)$ and $J_{\gamma;n'n}^{(i)}(c, \eta)$ for $i = 1, 3$ and $(\beta = \xi, \eta, \phi)$ are matrices that couple different angular modes as a result of the non-orthogonality of the angular wavefunctions. They are defined in Appendix C.2.

For the angular component at the outer (α) layer, the angular dependence of the right-hand side of Eq. (B.17) is $dP_n^m/d\eta$. Multiplying with $P_n^m(\eta)$ and integrating would result in somewhat complicated expressions on the right-hand side. We prefer therefore to multiply both sides of Eq. (B.17) by the factor $(1 - \eta^2)$ before applying the testing procedure. Since

$$(1 - \eta^2) \frac{dP_n^m}{d\eta} = \gamma_{1m}(n) P_{n-1}^m(\eta) - \gamma_{2m}(n) P_{n+1}^m(\eta) \tag{B.30}$$

with

$$\gamma_{1m}(n) = \frac{(n+1)(n+m)}{2n+1}, \quad \gamma_{2m}(n) = \frac{n(n-m+1)}{2n+1} \tag{B.31}$$

we get, from (B.17),

$$\begin{aligned}
& \sum_{n=m}^{\infty} \left\{ \left[(-1)^p m A_{\tilde{p}mn}^{(M)} I_{\eta;n'n}^{(1)}(c_{1\alpha}, \eta) + \frac{1}{c_{1\alpha}} A_{pmn}^{(N)} J_{\eta;n'n}^{(1)}(c_{1\alpha}, \eta) \right] + \right. \\
& \quad \left. \left[(-1)^p m C_{\tilde{p}mn}^{(M)} I_{\eta;n'n}^{(3)}(c_{1\alpha}, \eta) + \frac{1}{c_{1\alpha}} C_{pmn}^{(N)} J_{\eta;n'n}^{(3)}(c_{1\alpha}, \eta) \right] \right\} \\
& = -\gamma_{1m}(n'+1) [b_{pm(n'+1)} P_{n'+1}^m(\xi_0) + B_{pm(n'+1)} Q_{n'+1}^m(\xi_0)] \\
& \quad + \gamma_{2m}(n'-1) [b_{pm(n'-1)} P_{n'-1}^m(\xi_0) + B_{pm(n'-1)} Q_{n'-1}^m(\xi_0)] \tag{B.32}
\end{aligned}$$

Equations (B.25)–(B.28), (B.29), and (B.32), are the master equations with which the unknown expansion coefficients can be solved. Using (B.25), we can solve for $B_{pmn'}$ in terms of $A_{\tilde{p}mn}^{(M)}$, $A_{pmn}^{(N)}$, $C_{\tilde{p}mn}^{(M)}$ and $C_{pmn}^{(N)}$:

$$\begin{aligned}
B_{pmn'} & = - \left[\frac{dQ_{n'}^m}{d\xi_0} \right]^{-1} \left\{ b_{pmn'} \frac{dP_{n'}^m}{d\xi_0} \right. \\
& \quad + \mu_{r1} \sum_{n=m}^{\infty} \left\{ \left[(-1)^p m A_{\tilde{p}mn}^{(M)} I_{\xi;n'n}^{(1)}(c_{1\alpha}, \eta) + \frac{1}{c_{1\alpha}} A_{pmn}^{(N)} J_{\xi;n'n}^{(1)}(c_{1\alpha}, \eta) \right] \right. \\
& \quad \left. \left. + \left[(-1)^p m C_{\tilde{p}mn}^{(M)} I_{\xi;n'n}^{(3)}(c_{1\alpha}, \eta) + \frac{1}{c_{1\alpha}} C_{pmn}^{(N)} J_{\xi;n'n}^{(3)}(c_{1\alpha}, \eta) \right] \right\} \right\} \tag{B.33}
\end{aligned}$$

Incidentally, Eq. (B.33) can be used to obtain the high-frequency limit for $B_{pmn'}$. In this limit, only surface currents exist; therefore, the internal field must vanish. Thus setting $A_{\tilde{p}mn}^{(M)} = A_{pmn}^{(N)} = C_{\tilde{p}mn}^{(M)} = C_{pmn}^{(N)} = 0$ in (B.33) gives

$$B_{pmn'} \rightarrow - \left[\frac{dQ_{n'}^m}{d\xi_0} \right]^{-1} \frac{dP_{n'}^m}{d\xi_0} b_{pmn'} \quad \text{as } |c_{1\alpha}| \rightarrow \infty \tag{B.34}$$

which is only a function of ξ_0 (or equivalently elongation ratio $e = b/a$) and the source vector $b_{pmn'}$.

To obtain numerical results, the infinite system of equations must be truncated. Let N_T be the maximum order of coefficients considered, i.e.,

$$A_{\tilde{p}m(n+1)}^{(M)} = A_{pmn}^{(N)} = C_{\tilde{p}m(n+1)}^{(M)} = C_{pmn}^{(N)} = D_{\tilde{p}m(n+1)}^{(M)} = D_{pmn}^{(N)} = B_{pmn} = 0 \tag{B.35}$$

(even excitation) or

$$A_{\tilde{p}mn}^{(M)} = A_{pm(n+1)}^{(N)} = C_{\tilde{p}mn}^{(M)} = C_{pm(n+1)}^{(N)} = D_{\tilde{p}mn}^{(M)} = D_{pm(n+1)}^{(N)} = B_{pm(n+1)} = 0 \quad (\text{B.36})$$

(odd excitation) for $n > N_T$. We choose N_T such that $N_T - m$ is even. Then the total number for each set of coefficients is $L_T = (N_T - m)/2 + 1$.

To cast the system of equations in matrix form, we let, for even excitation,

$$\bar{B} = [B_{pmm}, B_{pm(m+2)}, \dots, B_{pmN_T}]^t \quad (\text{B.37a})$$

$$\bar{b} = [b_{pmm}, b_{pm(m+2)}, \dots, b_{pmN_T}]^t \quad (\text{B.37b})$$

$$\bar{A} = \left[A_{pmm}^{(N)}, A_{pm(m+2)}^{(N)}, \dots, A_{pmN_T}^{(N)}, \right. \\ \left. (-1)^p A_{\tilde{p}m(m+1)}^{(M)}, (-1)^p A_{\tilde{p}m(m+3)}^{(M)}, \dots, (-1)^p A_{\tilde{p}m(N_T+1)}^{(M)} \right]^t \quad (\text{B.37c})$$

$$\bar{C} = \left[C_{pmm}^{(N)}, C_{pm(m+2)}^{(N)}, \dots, C_{pmN_T}^{(N)}, \right. \\ \left. (-1)^p C_{\tilde{p}m(m+1)}^{(M)}, (-1)^p C_{\tilde{p}m(m+3)}^{(M)}, \dots, (-1)^p C_{\tilde{p}m(N_T+1)}^{(M)} \right]^t \quad (\text{B.37d})$$

$$\bar{D} = \left[D_{pmm}^{(N)}, D_{pm(m+2)}^{(N)}, \dots, D_{pmN_T}^{(N)}, \right. \\ \left. (-1)^p D_{\tilde{p}m(m+1)}^{(M)}, (-1)^p D_{\tilde{p}m(m+3)}^{(M)}, \dots, (-1)^p D_{\tilde{p}m(N_T+1)}^{(M)} \right]^t \quad (\text{B.37e})$$

where b and B are column vectors with length L_T and A , C , and D are column vectors with length $2L_T$. The superscript t denotes matrix transpose. Similarly, for odd excitation,

$$\bar{B} = [B_{pm(m+1)}, B_{pm(m+3)}, \dots, B_{pm(N_T+1)}]^t \quad (\text{B.38a})$$

$$\bar{D} = [D_{pm(m+1)}, D_{pm(m+3)}, \dots, D_{pm(N_T+1)}]^t \quad (\text{B.38b})$$

$$\bar{b} = [b_{pm(m+1)}, b_{pm(m+3)}, \dots, b_{pm(N_T+1)}]^t \quad (\text{B.38c})$$

$$\bar{A} = \left[A_{pm(m+1)}^{(N)}, A_{pm(m+3)}^{(N)}, \dots, A_{pm(N_T+1)}^{(N)}, \right. \\ \left. (-1)^p A_{\tilde{p}mm}^{(M)}, (-1)^p A_{\tilde{p}m(m+2)}^{(M)}, \dots, (-1)^p A_{\tilde{p}mN_T}^{(M)} \right]^t \quad (\text{B.38d})$$

$$\bar{C} = \left[C_{pm(m+1)}^{(N)}, C_{pm(m+3)}^{(N)}, \dots, C_{pm(N_T+1)}^{(N)}, \right. \\ \left. (-1)^p C_{\tilde{p}mm}^{(M)}, (-1)^p C_{\tilde{p}m(m+2)}^{(M)}, \dots, (-1)^p C_{\tilde{p}mN_T}^{(M)} \right]^t \quad (\text{B.38e})$$

$$\bar{D} = \left[D_{pm(m+1)}^{(N)}, D_{pm(m+3)}^{(N)}, \dots, D_{pm(N_T+1)}^{(N)}, \right. \\ \left. (-1)^p D_{\tilde{p}mm}^{(M)}, (-1)^p D_{\tilde{p}m(m+2)}^{(M)}, \dots, (-1)^p D_{\tilde{p}mN_T}^{(M)} \right]^t \quad (\text{B.38f})$$

$$(\text{B.38g})$$

Then (B.32), (B.26), (B.33), (B.29), (B.28), and (B.27) can be rewritten in matrix notation

a

$$\bar{\bar{Z}}_{\xi}^{(1)}(c_{1\alpha}, \eta) \cdot \bar{A} + \bar{\bar{Z}}_{\xi}^{(3)}(c_{1\alpha}, \eta) \cdot \bar{C} = \bar{\bar{W}}_{\xi}^{(p)} \cdot \bar{b} + \bar{\bar{W}}_{\xi}^{(q)} \cdot \bar{B} \quad (\text{B.39a})$$

$$\bar{\bar{Z}}_{\phi}^{(1)}(c_{1\alpha}, \eta) \cdot \bar{A} + \bar{\bar{Z}}_{\phi}^{(3)}(c_{1\alpha}, \eta) \cdot \bar{C} = \bar{\bar{W}}_{\phi}^{(p)} \cdot \bar{b} + \bar{\bar{W}}_{\phi}^{(q)} \cdot \bar{B} \quad (\text{B.39b})$$

$$\bar{\bar{Z}}_{\eta}^{(1)}(c_{1\alpha}, \eta) \cdot \bar{A} + \bar{\bar{Z}}_{\eta}^{(3)}(c_{1\alpha}, \eta) \cdot \bar{C} = \bar{\bar{W}}_{\eta}^{(p)} \cdot \bar{b} + \bar{\bar{W}}_{\eta}^{(q)} \cdot \bar{B} \quad (\text{B.39c})$$

$$\bar{\bar{Z}}_{\xi}^{(1)}(c_{1\beta}, \eta) \cdot \bar{A} + \bar{\bar{Z}}_{\xi}^{(3)}(c_{1\beta}, \eta) \cdot \bar{C} = \bar{\bar{Z}}_{\xi}^{(1)}(c_{3\beta}, \eta) \cdot \bar{D} \quad (\text{B.39d})$$

$$\bar{\bar{Z}}_{\phi}^{(1)}(c_{1\beta}, \eta) \cdot \bar{A} + \bar{\bar{Z}}_{\phi}^{(3)}(c_{1\beta}, \eta) \cdot \bar{C} = \bar{\bar{Z}}_{\phi}^{(1)}(c_{3\beta}, \eta) \cdot \bar{D} \quad (\text{B.39e})$$

$$\bar{\bar{Z}}_{\eta}^{(1)}(c_{1\beta}, \eta) \cdot \bar{A} + \bar{\bar{Z}}_{\eta}^{(3)}(c_{1\beta}, \eta) \cdot \bar{C} = \bar{\bar{Z}}_{\eta}^{(1)}(c_{3\beta}, \eta) \cdot \bar{D} \quad (\text{B.39f})$$

where $\bar{\bar{Z}}_{\gamma}^{(i)}(c, \eta)$ are $L_T \times 2L_T$ matrices and $\bar{\bar{W}}_{\gamma}^{(p,q)}$ are $L_T \times L_T$ matrices, respectively ($\gamma = \xi, \eta, \phi$). Their expressions can be found in Appendix C. Equations (B.39), can be

applied independently for even and odd excitations due to decoupling. Thus, Eqs. (B.39) provide $12L_T$ linear equations for the $2L_T$ unknowns each in \bar{A} , \bar{C} , and \bar{D} , and the L_T unknowns in \bar{B} . Once \bar{B} is determined, it can then be used to obtain the secondary magnetic field \bar{H}_s .

It should be remarked that for the special axisymmetric case of $m = 0$ ($p = 0$), it follows from (B.26) and (B.28) that

$$\begin{aligned} A_{10n}^{(M)} &= 0, & \text{for } n = 0, 1, 2, \dots \\ C_{10n}^{(M)} &= 0, & \text{for } n = 0, 1, 2, \dots \\ D_{10n}^{(M)} &= 0, & \text{for } n = 0, 1, 2, \dots \end{aligned} \tag{B.40}$$

Thus we only need to solve for $A_{00n}^{(N)}$, $C_{00n}^{(N)}$, $D_{00n}^{(N)}$, and B_{00n} , using (B.39a), (B.39c), (B.39d), and (B.39f). The size of the truncated system of equations in this case is reduced to $4L_T \times 4L_T$ (for either even or odd excitation).

B.2 Results

We show some preliminary low frequency results in Figures B-2–B-10.

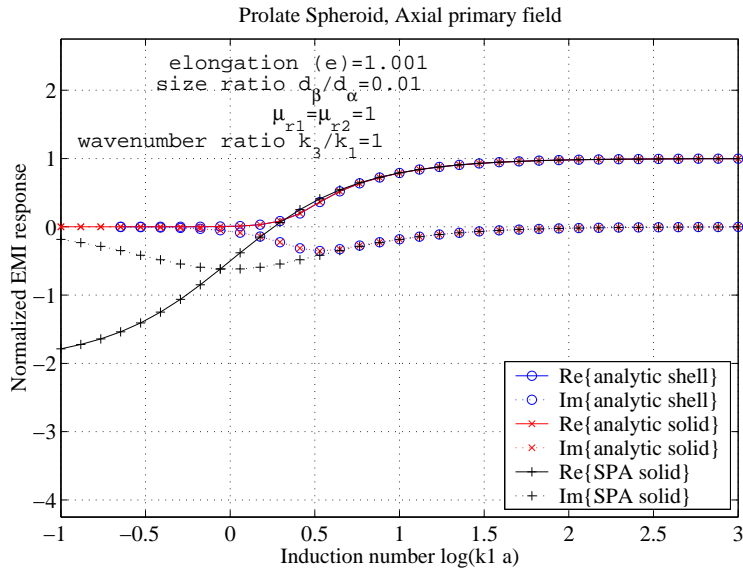


Figure B-2: Normalized dipole moment, m_z , from a nonmagnetic spherical shell with vanishing core size.

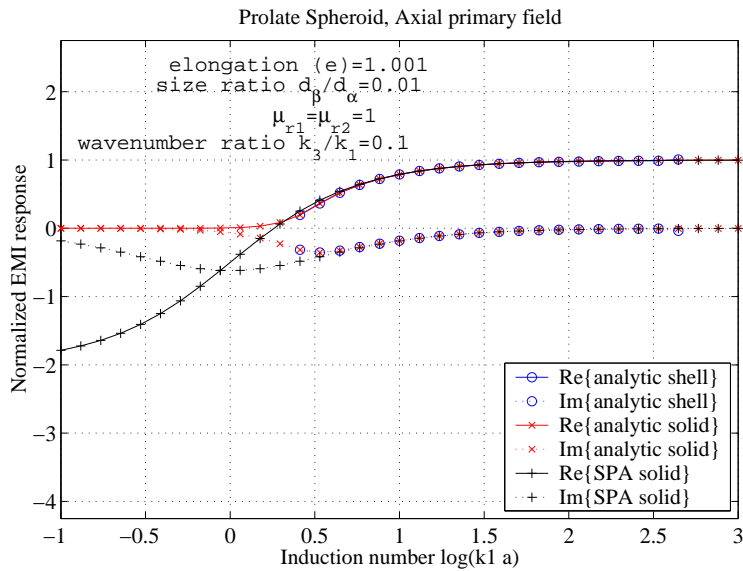


Figure B-3: Normalized dipole moment, m_z , from a spherical shell with vanishing core size but high core contrast.

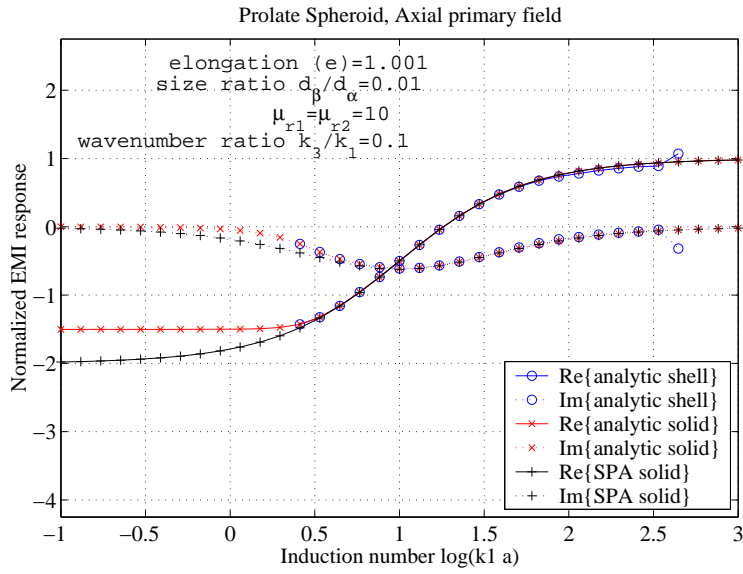


Figure B-4: Normalized dipole moment, m_z , from a magnetic spherical shell with vanishing core size and high core contrast.

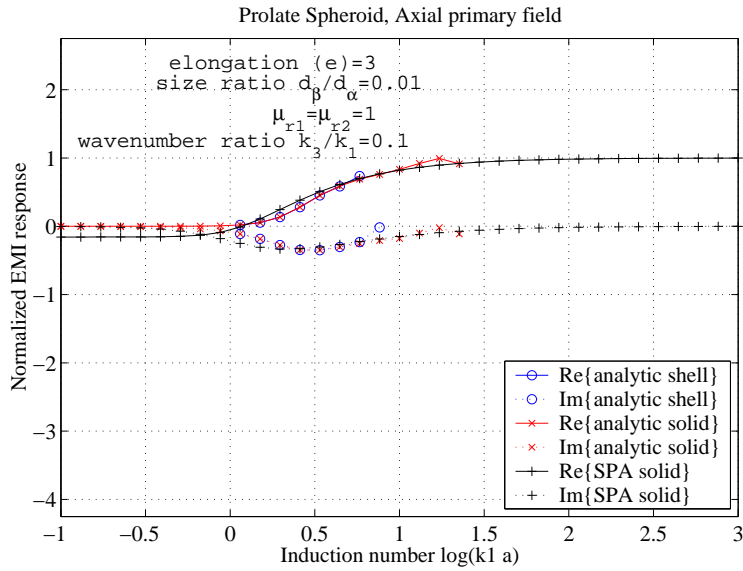


Figure B-5: Normalized dipole moment, m_z , from a nonmagnetic spheroidal shell with vanishing core size but high core contrast.

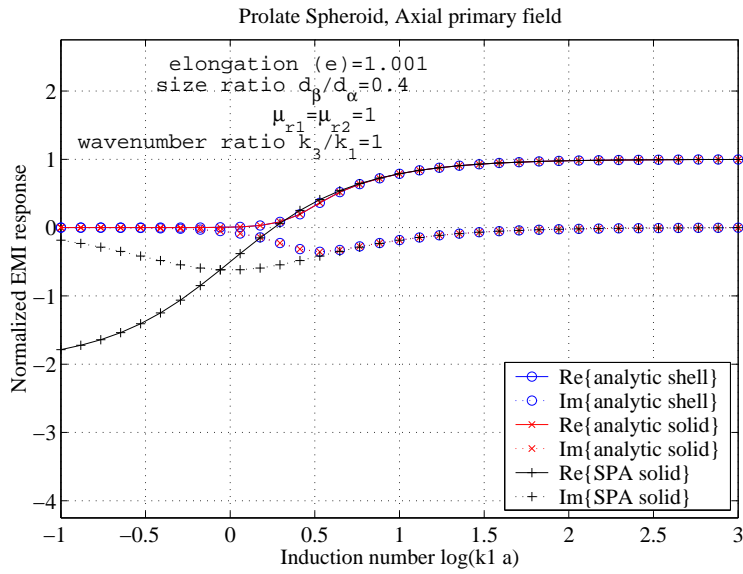


Figure B-6: Normalized dipole moment, m_z , from a nonmagnetic spherical shell with large core.

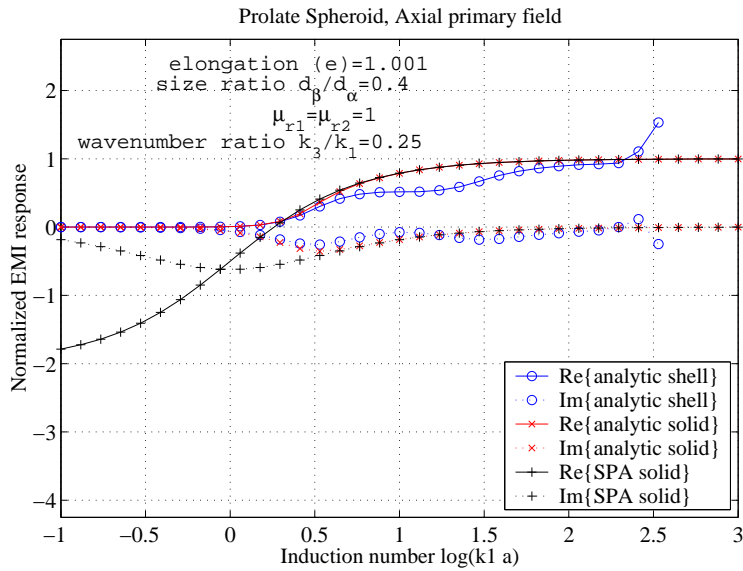


Figure B-7: Normalized dipole moment, m_z , from a nonmagnetic spherical shell with moderate core size and contrast.

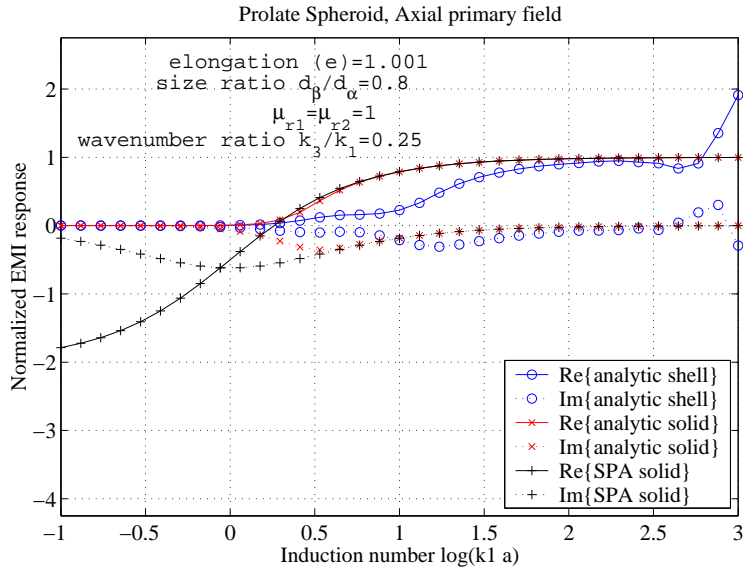


Figure B-8: Normalized dipole moment, m_z , from a nonmagnetic spherical shell with large core size and contrast.

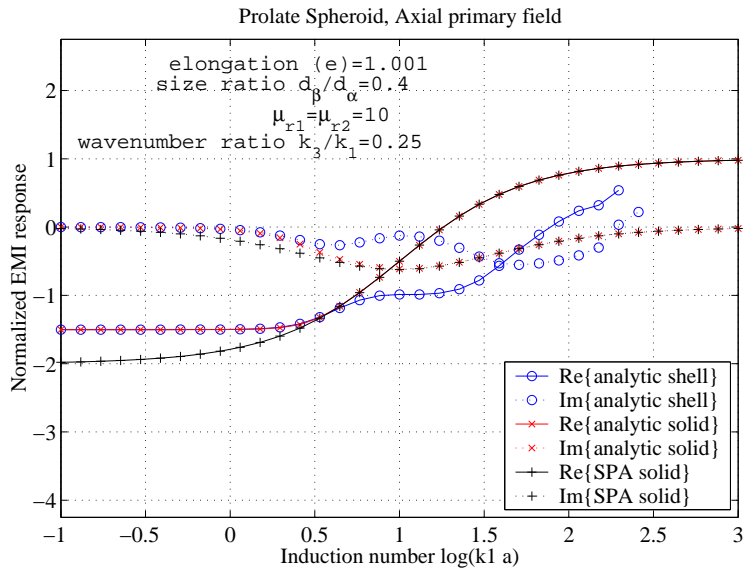


Figure B-9: Normalized dipole moment, m_z , from a magnetic spherical shell with moderate core size and contrast.

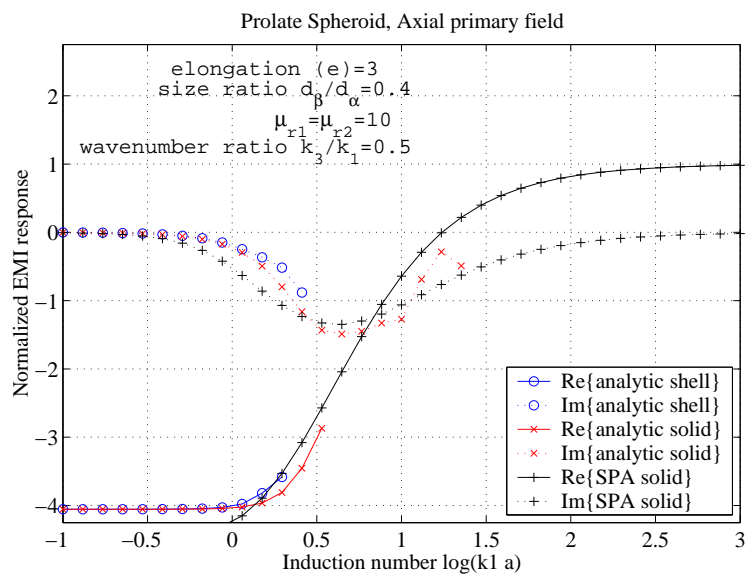


Figure B-10: Normalized dipole moment, m_z , from a magnetic spheroidal shell with moderate core size and contrast.

Appendix C

Computational Elements in Vector Spheroidal Wavefunction Expansions

C.1 Vector Spheroidal Wavefunctions

For computational purposes, it is convenient to express the vector spheroidal wavefunctions of (B.5) and (B.6) in partially separable forms. Explicit expressions of \overline{M} and \overline{N} in component forms can be found in Flammer's monograph on spheroidal wavefunctions [66]. They can be manipulated to yield

$$M_{\gamma;pmn}^{(i)}(c, \eta) = \frac{d}{2h_\gamma} \frac{dT_{pmn}}{d\phi} \widetilde{M}_{\gamma;mn}^{(i)}(c, \eta) \quad (\text{C.1a})$$

$$M_{\phi;pmn}^{(i)}(c, \eta) = \frac{d}{2h_\phi} T_{pmn}(\phi) \widetilde{M}_{\phi;mn}^{(i)}(c, \eta) \quad (\text{C.1b})$$

$$N_{\gamma;pmn}^{(i)}(c, \eta) = \frac{1}{c} \frac{d}{2h_\gamma} T_{pmn}(\phi) \widetilde{N}_{\gamma;mn}^{(i)}(c, \eta) \quad (\text{C.1c})$$

$$N_{\phi;pmn}^{(i)}(c, \eta) = \frac{1}{c} \frac{d}{2h_\phi} \frac{dT_{pmn}}{d\phi} \widetilde{N}_{\phi;mn}^{(i)}(c, \eta) \quad (\text{C.1d})$$

²This Appendix, as well as Appendix B, borrows heavily from [133], Appendix B therein.

where $\gamma = \eta, \xi$ and h_γ, h_ϕ are the metric coefficients for the prolate spheroidal coordinates:

$$h_\eta = \frac{d}{2} \sqrt{\frac{\xi^2 - \eta^2}{1 - \eta^2}}, \quad h_\xi = \frac{d}{2} \sqrt{\frac{\xi^2 - \eta^2}{\xi^2 - 1}}, \quad h_\phi = \frac{d}{2} \sqrt{(1 - \eta^2)(\xi^2 - 1)} \quad (\text{C.2})$$

It is important to note that d in Eqs. (C.1) and (C.2) is implicitly decided by the choice of c through Eq. (B.18) or (B.24). The modified vector wavefunctions in (C.1) can be written as:

$$\widetilde{M}_{\gamma;mn}^{(i)}(c, \eta) = F_{\gamma;mn}^{(M)(1)(i)}(\xi) G_{\gamma;mn}^{(M)(1)}(\eta) \quad (\text{C.3})$$

$$\widetilde{M}_{\phi;mn}^{(i)}(c, \eta) = \frac{1}{(\xi^2 - \eta^2)} \sum_{t=1}^2 F_{\phi;mn}^{(M)(t)(i)}(\xi) G_{\phi;mn}^{(M)(t)}(\eta) \quad (\text{C.4})$$

$$\widetilde{N}_{\gamma;mn}^{(i)}(c, \eta) = \frac{1}{(\xi^2 - \eta^2)^2} \sum_{t=1}^5 F_{\gamma;mn}^{(N)(t)(i)}(c, \xi) G_{\gamma;mn}^{(N)(t)}(\eta) \quad (\text{C.5})$$

$$\widetilde{N}_{\phi;mn}^{(i)}(c, \eta) = \frac{1}{(\xi^2 - \eta^2)} \sum_{t=1}^2 F_{\phi;mn}^{(N)(t)(i)}(c, \xi) G_{\phi;mn}^{(N)(t)}(\eta) \quad (\text{C.6})$$

The functions $F_{mn}^{(t)(i)}(c, \xi)$ and $G_{mn}^{(t)}(\eta)$ represent the separable parts of the vector spheroidal wavefunctions. They are listed below.

For the \overline{M} wavefunctions:

$$F_{\eta;mn}^{(M)(1)(i)}(\xi) = -\xi R_{mn}^{(i)}(\xi) \quad (\text{C.7a})$$

$$G_{\eta;mn}^{(M)(1)}(\eta) = \frac{1}{(1 - \eta^2)} S_{mn}(\eta) \quad (\text{C.7b})$$

$$F_{\xi;mn}^{(M)(1)(i)}(\xi) = \frac{1}{(\xi^2 - 1)} R_{mn}^{(i)}(\xi) \quad (\text{C.7c})$$

$$G_{\xi;mn}^{(M)(1)}(\eta) = \eta S_{mn}(\eta) \quad (\text{C.7d})$$

$$F_{\phi;mn}^{(M)(1)(i)}(\xi) = (\xi^2 - 1) \xi R_{mn}^{(i)}(\xi) \quad (\text{C.7e})$$

$$G_{\phi;mn}^{(M)(1)}(\eta) = (1 - \eta^2) \frac{dS_{mn}}{d\eta} \quad (\text{C.7f})$$

$$F_{\phi;mn}^{(M)(2)(i)}(\xi) = -(\xi^2 - 1) \frac{dR_{mn}^{(i)}}{d\xi} \quad (\text{C.7g})$$

$$G_{\phi;mn}^{(M)(2)}(\eta) = (1 - \eta^2) \eta S_{mn}(\eta) \quad (\text{C.7h})$$

For the \overline{N} wavefunctions:

$$F_{\eta;mn}^{(N)(1)(i)}(c, \xi) = 2\xi(\xi^2 - 1) \frac{dR_{mn}^{(i)}}{d\xi} - (\xi^2 - 1)(\lambda_{mn} - c^2\xi^2)R_{mn}^{(i)}(\xi) + m^2 R_{mn}^{(i)}(\xi) \quad (\text{C.8a})$$

$$G_{\eta;mn}^{(N)(1)}(\eta) = \eta S_{mn}(\eta) \quad (\text{C.8b})$$

$$F_{\eta;mn}^{(N)(2)(i)}(c, \xi) = -(\lambda_{mn} - c^2\xi^2)R_{mn}^{(i)}(\xi) \quad (\text{C.8c})$$

$$G_{\eta;mn}^{(N)(2)}(\eta) = (1 - \eta^2)\eta S_{mn}(\eta) \quad (\text{C.8d})$$

$$F_{\eta;mn}^{(N)(3)(i)}(\xi) = m^2(\xi^2 - 1)R_{mn}^{(i)}(\xi) \quad (\text{C.8e})$$

$$G_{\eta;mn}^{(N)(3)}(\eta) = \frac{1}{(1 - \eta^2)}\eta S_{mn}(\eta) \quad (\text{C.8f})$$

$$F_{\eta;mn}^{(N)(4)(i)}(\xi) = (\xi^2 - 1)^2 \left[\xi \frac{dR_{mn}^{(i)}}{d\xi} + R_{mn}^{(i)}(\xi) \right] \quad (\text{C.8g})$$

$$G_{\eta;mn}^{(N)(4)}(\eta) = \frac{dS_{mn}}{d\eta} \quad (\text{C.8h})$$

$$F_{\eta;mn}^{(N)(5)(i)}(\xi) = \xi(\xi^2 - 1) \frac{dR_{mn}^{(i)}}{d\xi} + (3\xi^2 - 1)R_{mn}^{(i)}(\xi) \quad (\text{C.8i})$$

$$G_{\eta;mn}^{(N)(5)}(\eta) = (1 - \eta^2) \frac{dS_{mn}}{d\eta} \quad (\text{C.8j})$$

$$F_{\xi;mn}^{(N)(1)(i)}(c, \xi) = (\xi^2 - 1) \left[-2 \frac{dR_{mn}^{(i)}}{d\xi} + \left(\lambda_{mn} - c^2 + \frac{m^2}{\xi^2 - 1} \right) \xi R_{mn}^{(i)}(\xi) \right] \quad (\text{C.8k})$$

$$G_{\xi;mn}^{(N)(1)}(\eta) = S_{mn}(\eta) \quad (\text{C.8l})$$

$$F_{\xi;mn}^{(N)(2)(i)}(c, \xi) = 3(\xi^2 - 1) \frac{dR_{mn}^{(i)}}{d\xi} + \left[(\xi^2 - 2)c^2 + \lambda_{mn} + \frac{m^2}{\xi^2 - 1} \right] \xi R_{mn}^{(i)}(\xi) \quad (\text{C.8m})$$

$$G_{\xi;mn}^{(N)(2)}(\eta) = (1 - \eta^2)S_{mn}(\eta) \quad (\text{C.8n})$$

$$F_{\xi;mn}^{(N)(3)(i)}(c, \xi) = \frac{dR_{mn}^{(i)}}{d\xi} + c^2\xi R_{mn}^{(i)}(\xi) \quad (\text{C.8o})$$

$$G_{\xi;mn}^{(N)(3)}(\eta) = (1 - \eta^2)^2 S_{mn}(\eta) \quad (\text{C.8p})$$

$$F_{\xi;mn}^{(N)(4)(i)}(\xi) = (\xi^2 - 1) \frac{dR_{mn}^{(i)}}{d\xi} - 2\xi R_{mn}^{(i)}(\xi) \quad (\text{C.8q})$$

$$G_{\xi;mn}^{(N)(4)}(\eta) = (1 - \eta^2)\eta \frac{dS_{mn}}{d\eta} \quad (\text{C.8r})$$

$$F_{\xi;mn}^{(N)(5)(i)}(\xi) = \frac{dR_{mn}^{(i)}}{d\xi} \quad (\text{C.8s})$$

$$G_{\xi;mn}^{(N)(5)}(\eta) = (1 - \eta^2)^2 \eta \frac{dS_{mn}}{d\eta} \quad (\text{C.8t})$$

$$F_{\phi;mn}^{(N)(1)(i)}(\xi) = (\xi^2 - 1) \left[\xi \frac{dR_{mn}^{(i)}}{d\xi} + R_{mn}^{(i)}(\xi) \right] \quad (\text{C.8u})$$

$$G_{\phi;mn}^{(N)(1)}(\eta) = S_{mn}(\eta) \quad (\text{C.8v})$$

$$F_{\phi;mn}^{(N)(2)(i)}(\xi) = R_{mn}^{(i)}(\xi) \quad (\text{C.8w})$$

$$G_{\phi;mn}^{(N)(2)}(\eta) = (1 - \eta^2) \frac{dS_{mn}}{d\eta} \quad (\text{C.8x})$$

C.2 Coupling Matrices and System Matrices

The definitions for the coupling matrices are given below:

$$I_{\xi;n',n}^{(i)}(c, \eta) = \frac{2n' + 1}{2} \frac{(n' - m)!}{(n' + m)!} \int_{-1}^1 d\eta P_{n'}^m(\eta) \widetilde{M}_{\xi;mn}^{(i)}(c, \eta) \quad (\text{C.9a})$$

$$I_{\eta;n',n}^{(i)}(c, \eta) = \frac{2n' + 1}{2} \frac{(n' - m)!}{(n' + m)!} \int_{-1}^1 d\eta P_{n'}^m(\eta) (1 - \eta^2) \widetilde{M}_{\eta;mn}^{(i)}(c, \eta) \quad (\text{C.9b})$$

$$I_{\phi;n',n}^{(i)}(c, \eta) = \frac{2n' + 1}{2} \frac{(n' - m)!}{(n' + m)!} \int_{-1}^1 d\eta P_{n'}^m(\eta) \widetilde{M}_{\phi;mn}^{(i)}(c, \eta) \quad (\text{C.9c})$$

$$J_{\xi;n',n}^{(i)}(c, \eta) = \frac{1}{c} \frac{2n' + 1}{2} \frac{(n' - m)!}{(n' + m)!} \int_{-1}^1 d\eta P_{n'}^m(\eta) \widetilde{N}_{\xi;mn}^{(i)}(c, \eta) \quad (\text{C.10a})$$

$$J_{\eta;n',n}^{(i)}(c, \eta) = \frac{1}{c} \frac{2n' + 1}{2} \frac{(n' - m)!}{(n' + m)!} \int_{-1}^1 d\eta P_{n'}^m(\eta) (1 - \eta^2) \widetilde{N}_{\eta;mn}^{(i)}(c, \eta) \quad (\text{C.10b})$$

$$J_{\phi;n',n}^{(i)}(c, \eta) = \frac{1}{c} \frac{2n' + 1}{2} \frac{(n' - m)!}{(n' + m)!} \int_{-1}^1 d\eta P_{n'}^m(\eta) \widetilde{N}_{\phi;mn}^{(i)}(c, \eta) \quad (\text{C.10c})$$

The explicit expressions of $\widetilde{M}_{\gamma;mn}^{(i)}(c, \eta)$ and $\widetilde{N}_{\gamma;mn}^{(i)}(c, \eta)$ for $\gamma = \eta, \xi, \phi$ are given in Appendix C.1. Once they are determined, the integrals can be easily evaluated numerically by Gaussian quadrature.

The system matrices $\overline{\overline{Z}}_{\gamma}^{(i)}(c, \eta)$ and $\overline{\overline{W}}_{\gamma}^{(p,q)}$ are given as follows. We distinguish the cases of even and odd excitations by defining

$$r_j = \begin{cases} 2j + m - 2 & \text{for even excitation} \\ 2j + m - 1 & \text{for odd excitation} \end{cases} \quad (\text{C.11})$$

The matrices $\overline{\overline{Z}}_\gamma^{(i)}(c, \eta)$ are of size $L_T \times 2L_T$. For $j, k = 1, \dots, L_T$,

$$Z_{\xi;j,k}^{(i)}(c, \eta) = \mu_r J_{\xi;r_j, r_k}^{(i)}(c, \eta) \quad (\text{C.12a})$$

$$Z_{\xi;j,k+L_T}^{(i)}(c, \eta) = \mu_r m I_{\xi;r_j, r_{k\pm 1}}^{(i)}(c, \eta) \quad (\text{C.12b})$$

$$Z_{\eta;j,k}^{(i)}(c, \eta) = J_{\eta;r_j+1, r_k}^{(i)}(c, \eta) \quad (\text{C.12c})$$

$$Z_{\eta;j,k+L_T}^{(i)}(c, \eta) = m I_{\eta;r_j+1, r_{k\pm 1}}^{(i)}(c, \eta) \quad (\text{C.12d})$$

$$Z_{\phi;j,k}^{(i)}(c, \eta) = m J_{\phi;r_j, r_k}^{(i)}(c, \eta) \quad (\text{C.12e})$$

$$Z_{\phi;j,k+L_T}^{(i)}(c, \eta) = -I_{\phi;r_j, r_{k\pm 1}}^{(i)}(c, \eta) \quad (\text{C.12f})$$

In (C.12b), (C.12d), and (C.12f), the upper sign is for even excitation and the lower sign is for odd excitation.

The matrices $\overline{\overline{W}}_\gamma$ are of size $L_T \times L_T$. For $j, k = 1, \dots, L_T$,

$$W_{\xi;j,k}^{(p)} = -\frac{dP_{r_j}^m}{d\xi} \delta_{jk} \quad (\text{C.13a})$$

$$W_{\xi;j,k}^{(q)} = -\frac{dQ_{r_j}^m}{d\xi} \delta_{jk} \quad (\text{C.13b})$$

$$W_{\eta;j,k}^{(p)} = -\gamma_{1m}(r_j) P_{r_j}^m(\xi) \delta_{(j+1)k} + \gamma_{2m}(r_j + 2) P_{r_j+2}^m(\xi) \delta_{(j-1)k} \quad (\text{C.13c})$$

$$W_{\eta;j,k}^{(q)} = -\gamma_{1m}(r_j) Q_{r_j}^m(\xi) \delta_{(j+1)k} + \gamma_{2m}(r_j + 2) Q_{r_j+2}^m(\xi) \delta_{(j-1)k} \quad (\text{C.13d})$$

$$W_{\phi;j,k}^{(p)} = -m P_{r_j}^m(\xi) \delta_{jk} \quad (\text{C.13e})$$

$$W_{\phi;j,k}^{(q)} = -m Q_{r_j}^m(\xi) \delta_{jk} \quad (\text{C.13f})$$

where δ_{jk} is the Kronecker delta.

Appendix D

Reference Tables for the Spheroidal Wave Equation for Complex c

D.1 Branch points, $c_{o;r}^{m,n}$, and Associated Eigenvalues $\lambda_{o;r}^{m,n}$ of the SWE

These branch points and associated eigenvalues for a greater range of m and n can be reproduced by software written by the author. Tables in this section are included because no other source has published tables of branch points for this range of parameter and at this level of accuracy. Contact the author for access to these programs.

D.1.1 $m = 0, n = [m..80]$

Accuracy was determined by the last correction of the Newton-Raphson method.

Table D.1: Branch points and associated eigenvalues for $m = 0$.

m, n, r	$c_{o;r}^{m,n} = c_{o;r+1}^{m,n+2}$	$\lambda_{o;r}^{m,n} = \lambda_{o;r+1}^{m,n+2}$	m, n, r	$c_{o;r}^{m,n} = c_{o;r+1}^{m,n+2}$	$\lambda_{o;r}^{m,n} = \lambda_{o;r+1}^{m,n+2}$
0, 0, 1	1.824770749208805 + 2.6016706928903181i	1.705180091412460 + 4.220186348356370i	0, 1, 1	3.563644553545243 + 2.887165344336900i	10.140838787232552 + 11.121586684224873i
0, 2, 1	5.217093042404772 + 3.081362886557631i	23.915829574409656 + 18.743327216266508i	0, 2, 3	2.094267182395557 + 5.807965828216133i	1.99851859867921 + 8.57871657394688i
0, 3, 1	6.838151743509966 + 3.228540820485014i	42.839460829787278 + 26.892790566183677i	0, 3, 3	4.067274712533398 + 6.264358978587767i	11.780925838292136 + 22.541393207957562i
0, 4, 1	8.443063517943598 + 3.346896434708849i	66.83332575192964 + 35.456773864933339i	0, 4, 3	5.874514148328888 + 6.617314890038058i	27.516445359838094 + 37.764984283250755i
0, 4, 5	2.244329796261236 + 8.973752190228394i	2.156124860667898 + 12.810922196899876i	0, 5, 1	10.038665064092994 + 3.445770032733475i	95.85640556575329 + 44.361464108811766i
0, 5, 3	7.606334073445308 + 6.906465157219409i	48.806652414112627 + 54.011989822762004i	0, 5, 5	4.383443826328900 + 9.50669337618593i	12.778186437528630 + 33.481761709843944i
0, 6, 1	11.62837573753831 + 3.530602623592430i	129.884250145370260 + 53.55053907976102i	0, 6, 3	9.29569705184056 + 7.151702724612575i	75.46220808313508 + 71.112658178667672i
0, 6, 5	6.316233767329015 + 9.949229739353585i	29.846039092711770 + 55.68990108075811i	0, 6, 7	2.347893464857109 + 12.128185061133886i	2.263189447556893 + 16.978431740148483i
0, 7, 1	13.214108021867665 + 3.604842114031867i	168.901012550649369 + 62.999226446425368i	0, 7, 3	10.957870542891056 + 7.364707014831354i	107.373656814110845 + 88.944615504739886i
0, 7, 5	8.147467516661960 + 10.323899301379097i	52.831395893010438 + 79.222018475547969i	0, 7, 7	4.613983308387243 + 12.710935561838975i	13.496424361795992 + 44.232604764077692i
0, 8, 1	14.797019945736288 + 3.670810179656952i	212.895788730994781 + 72.664518377383786i	0, 8, 3	12.601853656860371 + 7.552989106884000i	144.470630704203188 + 107.415994842966938i
0, 8, 5	9.917892969755632 + 10.651089858500113i	81.465390714716307 + 103.897214349459944i	0, 8, 7	6.649722635876492 + 13.206057605249066i	31.579166145618920 + 73.187499640071934i
0, 8, 9	2.426755266724711 + 15.277799057286881i	2.343980783624102 + 21.103815837875132i	0, 9, 1	16.377855800081942 + 3.730143922754754i	261.860733447250368 + 82.52758389596282i
0, 9, 3	14.232725426889811 + 7.721687504996004i	186.704669933275369 + 126.455376010690060i	0, 9, 5	11.648031656826387 + 10.941780718183141i	115.584894994604014 + 129.57872480192004i
0, 9, 7	8.566807794592391 + 13.638874465481070i	55.895670794459470 + 103.670385974408049i	0, 9, 9	4.795233775398997 + 15.891693671884648i	14.057386209297746 + 54.879985036694711i
0, 10, 1	17.957116787021921 + 3.784040426698697i	315.79001871496999 + 92.569477952059643i	0, 10, 3	15.83845319218598 + 7.874480991123857i	234.040731693069716 + 146.005634344901444i
0, 10, 5	13.349712997597559 + 11.203435277353591i	155.081025165167944 + 156.148368174552417i	0, 10, 7	10.410251940624978 + 14.024247058616169i	86.118562824385393 + 135.50569619167808i
0, 10, 9	6.917582942451463 + 16.425839365768446i	32.960499851131885 + 90.459854620068782i	0, 10, 11	2.490327262437059 + 18.424904659115747i	2.408721597834776 + 25.198509979662479i
0, 11, 1	19.535153320240660 + 3.833401137717104i	374.679115756393969 + 102.774525241977997i	0, 11, 3	17.467490992090958 + 8.014097371116032i	286.452526568988958 + 166.020127896453602i
0, 11, 5	15.030367143915981 + 11.441392537803358i	199.87646246007843 + 183.526690015259589i	0, 11, 7	12.203452288695585 + 14.371989749736837i	122.042803329388377 + 168.549078518222814i
0, 11, 9	8.909332180700922 + 16.901125867449363i	58.375129164312511 + 127.715473425074194i	0, 11, 11	4.944445545948445 + 19.061129762281226i	14.517281031107508 + 65.460946543531545i
0, 12, 1	21.112218078841369 + 3.878921577406139i	438.52456371006440 + 113.12954516530115i	0, 12, 3	19.075267730064859 + 8.142616883703791i	343.919755416526698 + 186.459890248030973i
0, 12, 5	16.694951390324288 + 11.659619367791977i	249.913830458837651 + 211.638677650511283i	0, 12, 7	13.960273952682158 + 14.689027894000139i	163.528082012527875 + 202.683151467007804i
0, 12, 9	10.818019546945614 + 17.330295405580152i	89.929406582396609 + 166.482831755741131i	0, 12, 11	7.141319713525860 + 19.624346718372887i	34.108834335464920 + 107.593796180195483i

Table D.1. (continued)

m, n, r	$c_{0,r} = \frac{m, n-2}{c_{0,r+1}}$	$\lambda_{0,r} = \lambda_{0,r+1}$	m, n, r	$c_{0,r} = \frac{m, n-2}{c_{0,r+1}}$	$\lambda_{0,r} = \lambda_{0,r+1}$
0.12,13	2.54351835446380	21.5705324751554991	2.462661335970665	29.2693517097868221	0.151
0.13,3	20.678342962879118	8.216629013696561	406.426375302075428	207.292027886879033	0.15
0.15,7	15.689639674099469	14.980741804610651	210.472702790300791	237.811279835347441	0.159
0.15,11	9.198821610189677	20.1321858167126661	60.45857049139088	151.5137267861872041	0.15,13
0.19,1	24.264134691677103	3.960523726292934	581.07760141115948	134.24673195444621	0.14,7
0.14,5	19.988793917311303	12.048364758091291	365.547666091260356	269.831891436271064	0.15
0.14,14	14.477056541232737	18.0826623697673731	1705.57620876289207	248.004294031771010	0.14,11
0.19,15	7.333341616356575	22.809411118445475	35.091269269676218	124.634010860626484	0.14,15
0.15,1	25.832275175106841	3.9974014205309688	659.773347558225055	144.989531669067475	0.15,3
0.15,5	17.902415054670839	12.223160918517681	438.08160312226666	299.818239434997984	0.15,7
0.15,9	16.252801090666024	18.4169212913846979	219.379095965306874	290.457461986475648	0.15,11
0.15,13	9.4495495467191	23.340832668249511	62.255361539978637	175.146497927910931	0.15,15
0.16,1	27.4189901408814	4.03207683178031	743.420732857636814	155.86419297666624	0.16,3
0.16,5	23.249209268514452	12.387081660956988	501.728141365965063	330.345095961266168	0.16,7
0.16,9	18.00231661748597	18.7285195774240381	273.701829967417382	334.132958353474781	0.16,11
0.16,13	12.9376136823892	23.8312901845011	95.9480947342280	227.397818192079875	0.16,15
0.16,17	6.29229023914731	27.859250742326031	2.54919969151395	37.355977677037764	0.17,1
0.17,1	27.058287902712471	8.6655763181762931	706.6202607188069	294.032586594024471	0.17,3
0.17,5	22.141289423011670	15.956875308241884	451.53596702228844	386.81663021371394	0.17,9
0.17,9	16.74415963252558	21.787991446405044	227.07735539684940	342.27628800171333	0.17,13
0.18,1	9.670386647074043	26.44012812698641	63.834827607906852	198.6610953583436	0.18,3
0.18,5	30.562110508378850	4.095746088586221	925.5537962292423	177.873242594149651	0.18,7
0.18,9	26.48649194627669	12.687169786510331	658.28629564236031	392.8908531802177	0.18,11
0.18,13	21.443041605601852	19.2949714565305011	398.624626816785792	424.226014713129271	0.18,15
0.18,17	15.32125752053804	24.715310219911824	181.948999084427413	336.60382439778241	0.19,1
0.19,1	7.65987971431295	29.15843011644251	36.71131070393888	158.5271448014844	0.19,5
0.19,5	36.8542334307291	4.12513834130242	1024.037079851818731	209.437497808518731	0.19,9
0.19,9	28.08549740839150	12.8252653045472	744.6884983908394	424.8540809030651	0.19,13
0.19,13	23.14056235698121	19.554818907013801	469.116547007323845	470.602716395206801	0.19,17
0.19,17	17.180594246186434	25.1142916684145621	233.863488859081735	393.338663554370051	0.20,1
0.20,1	9.86787614454309	29.727040515056661	65.245769753912702	222.087248107604751	0.20,5
0.20,5	37.9219766738975	4.12513834130242	112.96490452716056	200.28319728128987	0.20,9
0.20,9	29.707018768146455	12.956517008515272	835.103242636504547	457.24529204577376	0.20,13
0.20,13	24.82600803206616	19.799702273230171	544.905245064517885	517.798760188386268	0.20,17
0.20,17	19.0073124666665	25.490176512053761	291.55416477539052	451.37117371657791	0.21,1
0.21,1	11.98079955732012	30.260668715498071	100.66333984411224	287.539886476961771	0.21,5
0.21,5	2.698552949059518	34.7806979426363921	7.61785498821204	45.386491521266461	0.21,9
0.21,9	34.0633308920556	4.12513834130242	1086.727530751469430	385.332396627554931	0.21,13
0.21,13	29.01106303733646	16.72621630711974	775.972270781619045	546.9592854858053	0.21,17
0.21,17	23.722833820288579	23.06930618801489	484.577926446458857	552.29632411857198	0.22,1
0.21,19	23.79399396898119	28.408324621754489	239.934848841559301	443.91232691781836	0.22,5
0.22,1	10.04639413076345	32.90847680518773	66.515318096136204	245.44472653359870	0.22,9
0.22,5	36.8542334307291	4.12513834130242	134.1421911980198	246.281239761780931	0.22,13
0.22,9	32.91497464378460	13.20814111864016	1032.091721700944210	523.22898893039261	0.22,17
0.22,13	28.167359263681654	20.2549757109332771	712.240643087345210	614.47582990168839	0.23,1
0.22,17	22.584891074027819	26.18276990366091	423.8956260837826	571.02384238243562	0.23,5
0.23,1	9.60776207392785	31.232327313459745	190.963030839574704	423.6060550101107	0.23,9
0.23,5	35.958155976239	4.12513834130242	355.4827672669161	535.4827672669161	0.23,13
0.23,9	38.428275601970007	4.229718917881131	1467.40024866491718	234.53800449718463	0.23,17
0.23,13	34.5157144861968	13.314937632410001	1138.128973801862685	556.7848374986557	0.24,1
0.23,17	29.8258440746527	20.46694038611849	803.732729068565959	663.881337289422959	0.24,5
0.23,19	24.33588185771894	26.5035127910107461	498.397540402630682	632.512752248614741	0.24,9
0.24,1	17.92964999010213	31.6782680636639501	245.4294919654227	494.11811749288921	0.24,5
0.24,5	36.8542334307291	4.12513834130242	67.8737869308808	200.5232368184591	0.24,9
0.24,9	40.0097962914073	4.2314039439884	150.59947732532120	246.1125877221420	0.24,13
0.24,13	36.113239097491018	13.24304169092089	1249.185547194198534	590.694916122959801	0.24,17
0.24,17	31.477536448562849	20.669680830051401	901.01605681757602	713.954259889770501	0.25,1
0.24,19	26.80690569450432	26.8094015931517831	578.380241414240459	695.03408202265611	0.25,5
0.25,1	19.8249589019935	32.1015646450951	305.9041757656547055	566.05281916831724	0.25,9
0.25,5	42.0093236194793	4.2314039439884	1054.1181962398463	347.243244125334002	0.25,13
0.25,9	27.5624006459813	14.0431829106927671	2.673107766574164	53.373941562088135	0.25,17
0.25,13	39.7362596243216	9.2563762492657701	1546.45672121660626	480.364113033558197	0.26,1
0.25,17	35.504301369347928	17.3612425691204501	1022.338864715545499	716.047301262823482	0.26,5
0.26,1	30.56280130851295	24.09852748268095	828.44536206890406	777.33410651584191	0.26,9
0.26,5	34.4281605527923	3.995819269154908	535.4827672669161	535.4827672669161	0.26,13
0.26,9	38.428275601970007	4.229718917881131	1467.40024866491718	234.53800449718463	0.26,17
0.26,13	34.5157144861968	13.314937632410001	1138.128973801862685	556.7848374986557	0.27,1
0.26,17	29.8258440746527	20.46694038611849	803.732729068565959	663.881337289422959	0.27,5
0.26,19	24.33588185771894	26.5035127910107461	498.397540402630682	632.512752248614741	0.27,9
0.27,1	17.92964999010213	31.6782680636639501	245.4294919654227	494.11811749288921	0.27,5
0.27,5	36.8542334307291	4.12513834130242	67.8737869308808	200.5232368184591	0.27,9
0.27,9	40.0097962914073	4.2314039439884	150.59947732532120	246.1125877221420	0.27,13
0.27,13	36.113239097491018	13.24304169092089	1249.185547194198534	590.694916122959801	0.27,17
0.27,17	31.477536448562849	20.669680830051401	901.01605681757602	713.954259889770501	0.28,1
0.27,19	26.80690569450432	26.8094015931517831	578.380241414240459	695.03408202265611	0.28,5
0.28,1	19.8249589019935	32.1015646450951	305.9041757656547055	566.05281916831724	0.28,9
0.28,5	42.0093236194793	4.2314039439884	1054.1181962398463	347.243244125334002	0.28,13
0.28,9	27.5624006459813	14.0431829106927671	2.673107766574164	53.373941562088135	0.28,17
0.28,13	39.7362596243216	9.2563762492657701	1546.45672121660626	480.364113033558197	0.29,1
0.28,17	35.504301369347928	17.3612425691204501	1022.338864715545499	716.047301262823482	0.29,5
0.28,19	30.56280130851295	24.09852748268095	828.44536206890406	777.33410651584191	0.29,9
0.29,1	34.4281605527923	3.995819269154908	535.4827672669161	535.4827672669161	0.29,13
0.29,5	38.428275601970007	4.229718917881131	1467.40024866491718	234.53800449718463	0.29,17
0.29,9	34.5157144861968	13.314937632410001	1138.128973801862685	556.7848374986557	0.30,1
0.29,13	29.8258440746527	20.46694038611849	803.732729068565959	663.881337289422959	0.30,5
0.29,17	24.33588185771894	26.5035127910107461	498.397540402630682	632.512752248614741	0.30,9
0.29,19	17.92964999010213	31.6782680636639501	245.4294919654227	494.11811749288921	0.30,13
0.30,1	36.8542334307291	4.12513834130242	67.8737869308808	200.5232368184591	0.30,17
0.30,5	40.0097962914073	4.2314039439884	150.59947732532120	246.1125877221420	0.31,1
0.30,9	36.113239097491018	13.24304169092089	1249.185547194198534	590.694916122959801	0.31,5
0.30,13	31.477536448562849	20.669680830051401	901.01605681757602	713.954259889770501	0.31,9
0.30,17	26.80690569450432	26.8094015931517831	578.380241414240459	695.03408202265611	0.31,13
0.31,1	19.8249589019935	32.1015646450951	305.9041757656547055	566.05281916831724	0.31,17
0.31,5	42.0093236194793	4.2314039439884	1054.1181962398463	347.243244125334002	0.32,1
0.31,9	27.5624006459813	14.0431829106927671	2.673107766574164	53.373941562088135	0.32,5
0.31,13	39.7362				

D.1. Branch points, $c_{0,r}^n$, and Associated Eigenvalues $\lambda_{0,r}^n$ of the SWE

Table D.1. (continued)

m, n, r	$c_{0,r}^n = c_{0,r+1}^{m,n+2}$	$\lambda_{0,r}^n = \lambda_{0,r+1}^{m,n+2}$	m, n, r	$c_{0,r}^n = c_{0,r+1}^{m,n+2}$	$\lambda_{0,r}^n = \lambda_{0,r+1}^{m,n+2}$
0.32,33	2.84130336485150 + 53.00162830519471i	2.76176135384854 + 69.2506198185212161i	0.33,1	54.150669800708876 + 4.4295544468544911i	2921.631725806150380 + 553.254015850423117i
0.33,3	52.366035342002837 + 9.686654252151243i	2704.149782644520056 + 679.347794357167659i	0.33,5	50.429294735594772 + 14.245153121211846i	2473.7410012863474 + 909.739454122537386i
0.33,7	48.35152094798280 + 18.372524313932601i	2237.923744863245049 + 1075.533482792930032i	0.33,9	46.173261608581781 + 22.18133394404365i	2031.307298860137664 + 1190.4843103764726i
0.33,11	43.78738515303697 + 25.373675565878451i	1767.298441608223740 + 1462.602145211665179i	0.33,13	41.300457962513083 + 29.068576833550139i	1538.404132623225552 + 1297.2556769313482675i
0.33,15	38.62398740892221 + 32.12461021024299i	1407.6889806017020 + 1298.3804649253777i	0.33,17	37.9764243866222 + 35.18481338979913i	1106.5765797944182 + 269.037251375730734i
0.33,19	32.966481495760554 + 37.9967467368217i	907.235956807119464 + 1211.720514448857877i	0.33,21	29.86665425231750 + 40.668013612559361i	721.645769741988829 + 128.588007064978511i
0.33,23	26.580887032015550 + 43.181883134492191i	551.178661065013521 + 1021.466103070270191i	0.33,25	25.004949806595931 + 45.565668207068291i	399.44665925270029 + 892.035718901835594i
0.33,27	19.34258486368268 + 47.81359059346949i	267.061872486308744 + 741.83258298119402i	0.33,29	21.3859921194629 + 49.92563391623929i	156.992108174357838 + 572.268581121243785i
0.33,31	10.89786253238449 + 51.899219256493540i	72.290256615439745 + 384.714521532494700i	0.33,33	9.84091043485394 + 53.722477139082216i	71.147831064127779 + 1180.11969425306349i
0.33,35	55.22963271622980 + 4.446178964232807i	3004.224404093941624 + 65.450223179729221i	0.34,3	53.94296888524283 + 19.730966411783301i	2871.1063597321455874 + 740.945278497076981i
0.33,37	52.01477323467742 + 14.322280007376364i	2634.74801675088156 + 946.54171356642226i	0.34,5	5.0492917190401504 + 18.48124678088312i	2392.501380827697176 + 112.17259135838831i
0.34,1	47.9308431144167 + 22.322611310445804i	2149.06675145944828 + 1245.941387369702953i	0.34,11	45.1975626800287 + 25.908545057879596i	1907.84662361029020 + 1326.04360031949012i
0.34,3	42.95696363050100 + 29.278179223561401i	1671.57767249619701 + 1367.96581665404574i	0.34,15	40.375802309951222 + 32.45807206907632i	1442.599852507567267 + 1375.715956046960202i
0.34,17	31.6727412834542 + 35.467078906095922i	1223.009208068124963 + 1352.409885925932423i	0.34,19	34.7258446485572 + 38.181941202609541i	1014.75647801865935 + 1300.585755030811451i
0.34,21	21.573098347080009 + 41.02360870513021i	819.7201644648621 + 1222.388842973692212i	0.34,23	28.44915279370558 + 43.588351258384897i	639.76903774971498 + 1119.69088649128510i
0.34,25	25.02441037620207 + 46.006807264894101i	476.8249319395405 + 994.16684789384382i	0.34,27	21.2111871692312784 + 48.312543064747241i	314.29217295193040 + 190.46450738377691i
0.34,29	17.4469504398915 + 50.480855821166721i	210.390929851376086 + 680.608007967836502i	0.34,31	13.280288311939858 + 52.51266233573321i	172.90216037816562 + 49.2053274885302676i
0.34,33	7.14947732638530 + 54.40498396166722i	40.87270881817954 + 292.8783474052113671i	0.34,35	2.80070383211779 + 56.14385312058399i	1.87842051095884 + 73.423127688570761i
0.35,1	57.29424682711528 + 4.623321161630981i	3271.749663168061943 + 377.698273126458814i	0.35,3	55.51947350664510 + 9.778219964131301i	3043.133717349467218 + 169.13574004923684i
0.35,5	53.5992556853601 + 14.397193242907501i	2800.726453540848524 + 983.584149545218906i	0.35,7	51.54520084570266 + 18.58680967701252i	2552.09128079984944 + 110.671523993979488i
0.35,9	49.361359856653308 + 22.459728480897070i	2301.8873636678525 + 1301.841661915118771i	0.35,11	47.049297971221641 + 26.078186910076151i	2055.307758491501590 + 130.036437999645821i
0.35,13	44.60821426186953 + 29.48107986276181i	1809.6955768069230 + 1439.3398505883882i	0.35,15	42.03551325508687 + 32.69606901636816i	1527.7711549237808 + 1453.83359494334141i
0.35,17	39.26290296562698 + 35.741175025301917i	1344.825474599713743 + 1436.69400178300814i	0.35,19	36.23797952497065 + 38.630622145061317i	1127.763249792403707 + 1390.4857625643400i
0.35,21	33.468241373087525 + 41.37466896465499i	923.430427930481300 + 1317.38259914848479i	0.35,23	30.29697288043531 + 43.980794820209597i	733.64043579041338 + 1219.266078905848001i
0.35,25	26.94229361842810 + 46.454236144014970i	560.240633007648285 + 1097.81958166027010i	0.35,27	23.7967310393423 + 48.79823224020997i	485.17451896607100 + 954.57479058710911i
0.35,29	21.573098347080009 + 51.01068280820494i	270.5671195950004 + 790.95583512943631i	0.35,31	15.46804605329761 + 53.100942869787471i	158.85732991568766 + 608.298145837026141i
0.35,33	10.96647648029000 + 55.50680651545152i	74.04585816978546 + 401.81172301078231i	0.35,35	8.58297298376164 + 56.86769761316169i	57.29217295193040 + 190.46450738377691i
0.36,1	85.8659796916461 + 4.780490780249424i	3454.21274373854521 + 389.996712500981i	0.36,3	5.09756062850126 + 82.0296060420240i	3220.053861686115852 + 756.56965558126431i
0.36,5	55.1838809755799 + 14.470015341603515i	2971.680324608593310 + 1020.859029975711020i	0.36,7	51.140192781005055 + 18.689391762176523i	1764.689251200137998 + 1216.46239919388221i
0.36,9	50.970315782506687 + 22.59222559818511i	2459.750251341149578 + 1358.171423625593661i	0.36,11	48.675617529059863 + 26.242903631426259i	2204.27470663024931 + 1284.554569636096176i
0.36,13	46.2559888055767 + 29.67860464942956i	1952.9834199337117 + 1511.380010751312349i	0.36,15	43.70797838968047 + 32.96915750452828i	1708.2001463789261 + 1532.71682128529778i
0.36,17	41.16241037620207 + 46.006807264894101i	1471.9810831935624 + 1092.8868049384382i	0.36,19	38.2111871692312784 + 48.312543064747241i	1246.2211871692312784 + 48.312543064747241i
0.36,21	35.2476730386530 + 47.174410034971735i	1032.730225884195761 + 1413.52715573010030i	0.36,23	32.126651984645598 + 44.32601844330909i	833.269839126569877 + 1320.14253460071724i
0.36,25	28.8235910786013 + 46.875454857297882i	649.6247268287303 + 1029.934599047781i	0.36,27	25.34563019529215 + 49.26383978601702i	483.6496850874057 + 1063.43716548497644i
0.36,29	21.63508879025409 + 51.527233211207701i	337.338213130203542 + 903.07156637576223i	0.36,31	17.65766648024971 + 53.66563576375210i	212.93211907208477 + 273.1639927103154i
0.36,33	13.34191793577964 + 59.287037356590614i	113.089397705935355 + 524.981024008927307i	0.36,35	8.546517731335694 + 54.5475359828637i	41.25573399421478 + 309.594752160469544i
0.37,1	2.8777795976811 + 55.66035118138302i	27.98139975720676 + 717.499273599353271i	0.37,1	60.437666873303880 + 1.53452386895900488i	3647.6139982732390 + 402.344346091701357i
0.37,3	58.67178631839040 + 30.876631577266731i	3401.92501202883517 + 782.58858947309644i	0.37,5	56.67020535795403 + 14.54089241716856i	3147.6076279618780 + 382.6256406692044i
0.37,7	54.73936643671984 + 18.789155392492489i	2886.29223754685892 + 1264.09261025184352i	0.37,9	52.77460997637667 + 22.722410917048364i	2622.662439529478234 + 1414.918918082532628i
0.37,11	50.29917935525157 + 26.401975765845361i	2360.132179308961440 + 1519.60960140588801i	0.37,13	47.899021488499514 + 29.870221835612522i	2140.26066557843839 + 1584.000855118988581i
0.37,15	45.37509557844031 + 33.151031057015304i	1848.852034860141885 + 1612.33055874227966i	0.37,17	42.2335744714044 + 36.264652250784116i	1604.45236819465196 + 1607.88076491522777i
0.37,19	39.9824969999647 + 39.22528725776763i	170.04152754254387 + 1573.29109624946037i	0.37,21	37.0147534213943 + 42.04356604792204i	1147.57818909506163 + 1510.78267496632507i
0.37,23	33.9403124283331 + 46.006807264894101i	912.68015644744942 + 1030.247149319166991i	0.37,25	32.2111871692312784 + 48.312543064747241i	742.942195194131 + 190.46450738377691i
0.37,27	27.8292733659937 + 49.713438224585051i	568.25844500344438 + 1173.87305721029261i	0.37,29	23.62722908530843 + 52.02193023626237i	410.55290269740974 + 110.6440317536059038i
0.37,31	19.79070061497155 + 54.208878599291851i	273.873120955023239 + 839.967123622232i	0.37,33	15.26624689566061 + 56.273026691265271i	160.618379277680615 + 96.276597492506510i
0.37,35	11.067023502129928 + 58.214068702991851i	73.757868943603725 + 430.93046289376176i	0.37,37	5.89693939982721 + 60.012572253002060i	17.4277545200625 + 200.8017544564306i
0.38,1	60.300409069993 + 4.5082170609179501i	3833.951790581837486 + 414.73909867861761i	0.38,3	60.47570080668990 + 9.90657105029060i	3588.74641299916872 + 800.74035773490507i
0.38,5	58.34985486586861 + 13.68149814454001952i	3350.6683831681444 + 1088.85317648571088i	0.38,7	56.75618756781832 + 18.884834571096991i	3147.6076279618780 + 382.6256406692044i
0.38,9	54.1827725426140 + 22.848393230499831i	2790.6143949000737 + 1474.072281758310965i	0.38,11	51.92016984094053 + 26.58565130317010i	2552.09128079984944 + 110.671523993979488i
0.38,13	49.53884691893780 + 30.056467027013579i	2255.013231134959824 + 1657.25015241796474i	0.38,15	45.17702172720505 + 33.36879953235251i	1994.7173197667020 + 1692.661179923023525i
0.38,17	44.21206750930601 + 36.510035378285401i	1742.2209342581119 + 1694.722726157590951i	0.38,19	41.65873872225575 + 39.50946082609540i	1499.3787614984989 + 1666.129156257832941i
0.38,21	38.77065619518699 + 42.362794368498967i	1267.937180419961578 + 1609.11279633049171i	0.38,23	35.79960465528297 + 45.083054812668030i	1049.586100474787647 + 1525.621315951933101i
0.38,25	32.5523585867778 + 47.676995132386047i	846.004254310393662 + 1417.335821303048505i	0.38,27	29.19507014564126 + 50.148175028795919i	658.9042743698697 + 1285.82409126269931i
0.38,29	25.8382616667406 + 52.033750320387201i	515.444393725012538 + 122.49494917451022i	0.38,31	23.480683291398761 + 53.880573891695901i	414.93120510291364 + 931.6730531837515i
0.38,33	17.9436868295999 + 56.84635782662881i	215.33480873932121 + 765.610480549842292i	0.38,35	13.66997836899040 + 58.838722496136261i	114.249398387979376 + 554.6958868438187i
0.38,37	8.617135574160638 + 60.703693629504596i	41.61360809872215 + 326.30145010196121i	0.38,39	2.89451193035209 + 62.42812388975506i	2.818485354621380 + 81.051196525698375i
0.39,1	63.8090286346978 + 4.522726265294291i	4031.227493281765874 + 427.18160350117089i	0.39,3	61.32128736470821 + 9.946887020302325i	3780.51735252816328 + 835.02136625852570i
0.39,5	59.93216478266870 + 14.677020354525551i	3514.37672723123444 + 1134.02431731478446i	0.39,7	57.91831397931850 + 18.980815123831000i	3240.4991268430731 + 1360.27095168842150i
0.39,9	55.78653710326407 + 22.9771083806207751i	2963.6096378710476 + 1529.63048560080085i	0.39,11	53.53880248068048 + 26.710170646991577i	2687

Table D.1. (continued)

Table with 10 columns: m1, n1, m2, n2, m1+n2, m1-n2, m1+n2, m1-n2, m1+n2, m1-n2. The table contains numerical values for various combinations of m and n, organized in a grid-like structure.

D.1. Branch points, $c_{\alpha;r}^{m,n}$, and Associated Eigenvalues $\lambda_{\alpha;r}^{m,n}$ of the SWE 207

Table D.1. (continued)

m, n, r	$\lambda_{\alpha;r}^{m,n} = c_{\alpha;r}^{m,n} + i$	$\lambda_{\alpha;r}^{m,n} = c_{\alpha;r}^{m,n} + i$	m, n, r	$\lambda_{\alpha;r}^{m,n} = c_{\alpha;r}^{m,n} + i$	$\lambda_{\alpha;r}^{m,n} = c_{\alpha;r}^{m,n} + i$
0.54,25	60.61272488047488 + 52.720381114158741i	32.2169562707/8346 + 32.9715708288540711i	57,82/2388949903550 + 55.677095195870261i	2885.93407117215452 + 3247.6994340285109501i	
0.54,29	54.945297124276308 + 58.5350891175808211i	2561.773159972394751 + 3169.9183085201054i	55.66207934453658 + 61.296697667774474i	2520.358954682905527 + 3065.35967186209691i	
0.54,33	48.872268735432677 + 63.965930857623249i	1952.907738043977815 + 2395.285390940209930i	55.660991817252345 + 66.545503993997031i	1670.621799179376467 + 2780.8774831131242775i	
0.54,37	42.34531094855193 + 69.037529426682381i	1404.726139993549850 + 2603.215682340880460i	55.6590079129513040 + 71.4435454317937231i	1156.481715617164264 + 3339.944467620201i	
0.54,41	35.290931928191728 + 76.54647174043134i	927.23511096620882 + 2182.212163887235293i	55.653153543711907 + 61.000698840286663i	718.39263497979952 + 1940.7907833078211i	
0.54,45	27.90011534121778 + 78.15624535953959i	531.514080656368228 + 1679.97830145258167i	55.647234364557075737 + 80.21866811858279i	368.341763527292424 + 1400.60533705217334i	
0.54,49	19.025885891422588 + 82.197278850603801i	230.905637959465808 + 1103.663607161081700i	55.6412438918406183521 + 84.085384863983931i	121.67634370278178 + 789.7953588880401i	
0.54,53	9.077589762188355 + 85.8779074024399761i	43.940423197549445 + 459.637984410322851i	55.63510067934453658 + 61.296697667774474i	2.9234258961942 + 112.464734691477844i	
0.55,1	88.72864483241932 + 4.71529662190197961i	7859.04972954150528 + 631.772020417121529i	55.62781074793976049 + 10.484437290352730i	7521.565123143959198 + 1270.87260746880001i	
0.55,2	88.197413377663574 + 15.466700117983461i	7163.157587894878350 + 656.47827055950207i	55.625823292774066235 + 20.2313196987900771i	6792.05789306069377 + 2148.017135904459291i	
0.55,3	88.226460743273922 + 24.889978087820831i	6413.160577276766162 + 2496.92795854798103i	55.62379217108337860012 + 28.705848621662110i	6030.02901621483981 + 2765.445856281489031i	
0.55,13	77.053303185206249 + 32.6187821549330931i	5645.42896819153579 + 2981.571362283386861i	55.62170.0628809216054 + 36.35639615471039i	562.638389052572165 + 3151.0332292385803661i	
0.55,17	72.476151505139659 + 39.938873874309141i	4880.60625125223218 + 3278.148826269013625i	55.61974.062413687071967 + 43.38140024446244i	4504.0512554397027 + 3366.330514358480761i	
0.55,21	67.564066352740949 + 46.690200928149551i	4133.521345406684304 + 3418.363519623592010i	55.61664.97958037681483 + 49.892208419077967i	3770.441599113109987 + 3436.58273309665701i	
0.55,25	62.306880823634636 + 52.9776588673078451i	3416.144759973002328 + 3422.98920359359771i	55.61459.534202535896 + 56.95864379534834i	3107.8966319085857 + 3379.33025760962450i	
0.55,29	56.6854789043399 + 58.840329022272081i	2738.914276255318037 + 2907.15640581244371i	55.6127.101824767216402 + 43.56740620832962i	4727.5268865064087 + 3472.47856281489031i	
0.55,33	50.67084166726555 + 64.3219764129229221i	2111.50539175472362 + 3082.72448890855456i	55.61540.802710240839896 + 66.928203509594780i	4180.42879722587725 + 2932.91253809402849i	
0.55,37	44.218244646243599 + 69.4478382559279341i	1543.358971990740292 + 2759.521982098279750i	55.6139.4007326719750610 + 71.882540115228929i	1284.52869948731293 + 5623.7882768043951i	
0.55,41	37.261705015401262 + 74.233445913846231i	1044.209397543984323 + 2346.07288300338607i	55.6126.33698515540899 + 76.501168744308799i	827.73215109184079 + 2107.929500383913924i	
0.55,45	29.696363083603654 + 78.6857672120929741i	642.692703447370718 + 1850.056200782487394i	55.6116.75369944257169 + 84.731201840229403i	448.99684699598771 + 1573.32653153539324i	
0.55,49	21.38426893005710 + 82.8025498517915681i	297.349274636822031 + 1278.594757682229767i	55.616.71451922644292 + 88.3066626207767i	18.400874232698477 + 293.5576564019181i	
0.55,53	11.78476273518159 + 86.568099039504051i	78.85178824030150 + 638.23012178652816i	55.6158.84037707444836 + 51.021666076091808i	7797.4028093982574 + 1298.9571146994751i	
0.56,1	90.294608080892547 + 4.725411229324424i	1404.248203769134307 + 64.862892604525811i	55.6148.72990771014165 + 20.296809052475969i	7056.31236356518816 + 2220.465863227784666i	
0.56,5	86.774431071556500 + 15.6137881653174551i	733.358889135653044 + 4807.404284030042845i	55.6148.01249665368263 + 28.80997862075885i	6281.66680458738483 + 2838.2281998271770442i	
0.56,9	82.882849516324239 + 24.674674253530711i	6671.231341813093422 + 2559.9316844525269i	55.61674.20376738028427 + 36.50069415185251i	5498.68026236695853 + 3241.519182871325444i	
0.56,13	78.657542102715027 + 32.742815438855451i	589.38696981038469 + 3063.490981761320700i	55.6147.101824767216402 + 43.56740620832962i	4727.5268865064087 + 3472.47856281489031i	
0.56,17	74.103687280995797 + 40.1038018813911921i	511.49675263814087 + 2377.69881497197864i	55.6136.205096375684643 + 50.121831501780604i	3978.35883866531153 + 5568.682486429252i	
0.56,21	69.81379262108769 + 46.90361858028511i	439.343374297676746 + 3531.4088386871539i	55.6126.51289934935663 + 56.23392423266500i	3263.19949474381537 + 3511.872639229651i	
0.56,25	63.996581460923785 + 53.2298261650723391i	361.589234443166060 + 3549.491408155848072i	55.6156.2593735853348 + 61.950344082747044i	2591.945891282106599 + 3351.45529629260511672i	
0.56,29	58.1951726238894 + 59.1393231001479461i	2921.493435161132124 + 3445.39144196780856i	55.6149.324828671611953 + 67.302645967297735i	935.936530104910371 + 3086.229393368083161i	
0.56,33	52.46003001510431 + 64.709407259245661i	2275.715105520794198 + 3231.338052208174304i	55.6135.818259758214445 + 43.56740620832962i	4148.35966413910989 + 3107.8966319085857i	
0.56,37	46.07716269955257 + 70.347054719682381i	1689.837318882611077 + 2807.15640581244371i	55.6135.7198478094405 + 76.989431586706601i	1148.35966413910989 + 3107.8966319085857i	
0.56,41	39.2126338096975 + 74.691479565395221i	1167.344952779071881 + 2511.537204380347248i	55.6127.190492526423574 + 81.340100914471762i	555.76920415831958 + 1747.96917375702721i	
0.56,45	31.77184445787807 + 79.205740518183347i	724.8263338430816 + 2202.990120863671881i	55.6127.190492526423574 + 81.340100914471762i	555.76920415831958 + 1747.96917375702721i	
0.56,49	23.97755460952865 + 83.9315417332470241i	371.10870468389130 + 1455.68571875795891i	55.6159.264313016358469 + 91.449756893484505i	174.2944112253987610 + 1145.97192317933431i	
0.56,53	13.407707184572511 + 87.2371029476310301i	222.4642582656999 + 819.14661723474493i	55.6191.862525890627200 + 74.735482683567061i	44.181623149997340 + 476.27444809318927i	
0.57,3	90.15724942698882 + 10.5447299116438644i	8078.184724154674980 + 1327.13039606518833i	55.6188.5086442366612 + 15.65964216050164i	8426.382787817885858 + 657.985329668758771i	
0.57,7	86.45434513209506 + 20.361116167124499i	7325.535356416637114 + 2273.11939218200774i	55.6187.42191941538554 + 24.75752906856791i	7708.4049008721987 + 348.47616386656211i	
0.57,11	82.407108831740572 + 28.91226496908931i	6538.31068770109587 + 2911.342177832889774i	55.6180.26706997621540 + 32.8648623060875i	6130.2867559024271 + 2623.201160281210792i	
0.57,15	78.03829119207689 + 36.6423364388217861i	4752.78367573430245 + 3332.46055412937808i	55.6175.726760350699387 + 40.2657009414328i	5374.46389656511065 + 3475.675196981973558i	
0.57,19	73.33894907080707 + 45.75001674828809i	4956.13651239037205 + 3295.71820277236781i	55.6170.8968016326379 + 47.107274240006427i	4540.34966656448013 + 3645.67398395316441i	
0.57,23	68.21591923111411 + 54.40574741480311i	4210.49675263814087 + 2377.69881497197864i	55.6170.8968016326379 + 47.107274240006427i	4540.34966656448013 + 3645.67398395316441i	
0.57,27	62.95980724137851 + 56.5037786747358981i	3459.846510869454050 + 3645.30720612599384i	55.6170.41303312184462 + 59.43235615030557i	2105.4084805156638 + 3384.6011815862389i	
0.57,31	57.24205194718781 + 62.67163796930131i	2770.991715967251821 + 3496.10423292974351i	55.6154.240537701884321 + 65.011797296170769i	3449.5030745698884 + 3584.30112444036014i	
0.57,35	51.59677108224607 + 67.669197334073829i	2134.169783215182197 + 3248.701520734201987i	55.6147.924783964884412 + 70.21736410224473i	3188.11892618349430 + 3076.23196762030004i	
0.57,39	44.39774824217593 + 72.7312714166673801i	1558.520549475266098 + 2889.50773184127371i	55.6141.14255996326379 + 51.193911862649443i	1296.5736763471322194 + 3596.5999984016522i	
0.57,43	38.5570219836750 + 78.662496265515101i	1053.52052595215743 + 2351.99385867067417i	55.6133.818259758214445 + 43.56740620832962i	4727.5268865064087 + 3472.47856281489031i	
0.57,47	32.9526809716377 + 81.87979215521521i	729.72589589692290 + 1924.6008412006771i	55.6132.40710674717397 + 83.965287436789671i	452.0012138044708 + 1634.7969510959202i	
0.57,51	21.97763596437337 + 85.98633101459094i	499.456298071576555 + 1327.12227669473929i	55.6116.857457969574828 + 87.886564820789971i	174.2944112253987610 + 1145.97192317933431i	
0.57,55	11.852516552325210 + 89.716023198426931i	79.31134694055497 + 661.21561360658482i	55.616.246413016358469 + 91.449756893484505i	18.488711149997340 + 303.8607122672322i	
0.58,1	93.43646362838367 + 7.451138224849281i	8717.453412145539914 + 671.1389601182710451i	55.6191.70386614229944 + 10.36765345891874i	8363.906353149913311 + 3355.3903712286671i	
0.58,5	89.92714704480480 + 15.7046995140740931i	7398.582214607600690 + 1889.69134687032296i	55.6189.63571454903085 + 20.424305921412110i	7799.723183215349309 + 2325.97408840788281i	
0.58,9	84.2132540232321 + 23.965232514180631i	6232.3265420325114 + 2493.83192086208992i	55.6187.3265254055089 + 26.82819729052031i	6799.858720878769 + 2178.7378424087834i	
0.58,13	81.862850948414319 + 32.984175260344931i	5395.4078773939758 + 3228.4937189828671i	55.6186.0453281956741 + 36.7818162688001i	5990.9240432323731 + 3423.84872923938584i	
0.58,17	77.349282824951544 + 40.424646433211681i	5888.53044889432294 + 3575.347088490452529i	55.6185.9473881910895244 + 43.92921553687701i	5189.87347861748848 + 3686.537527326928931i	
0.58,21	72.518630331955535 + 47.307139553406871i	4796.511842602886030 + 3760.31028162156507i	55.6184.99283646691888 + 50.56801858632366i	4490.854157743122541 + 3799.0184106395172i	
0.58,25	67.36358219732028 + 53.719655768662831i	4031.211636426953646 + 3804.91771246855893i	55.6183.66007971840909 + 56.768419924860403i	3661.82265813530375 + 3779.6	

Table D.1. (continued)

m, n, r	$c_{0:r}^m = \frac{m \cdot n + 2}{c_{0:r+1}^m}$	$\lambda_{0:r}^m = \lambda_{0:r+1}^m$	m, n, r	$c_{0:r}^m = \frac{m \cdot n + 2}{c_{0:r+1}^m}$	$\lambda_{0:r}^m = \lambda_{0:r+1}^m$				
0.62,33	63.03107201969830	66.620146289480301	337.35354260886834	441.466.337065378402521	0.62,35	60.0628289425275	69.3942289436202401	3019.4756374594391	4031.303913005706361
0.62,34	57.002136901821508	72.0789429190132731	265.308101132093270	389.0520402460102284	0.62,36	53.84468143165277	74.7019983631480071	10.401476015281878	3725.031273764089881
0.62,35	50.58462999948381	77.23868523499611	2032.317456781427381	355.85.81726996576576	0.62,37	47.11540410076906	79.699405050073242	1735.642517357695851	3523.180668486624088
0.62,36	42.752789683949577	82.085187565459611	1457.001384112179721	3089.885001359003295	0.62,38	40.112654085056846	84.396696974849211	1197.5717684782909	2834.9024949660115451
0.62,37	40.6560173321597	86.63631375570775	958.611739419502555	2309.68079331479093	0.62,39	32.443104909092618	88.79763106683894	741.4744010433188	2265.01815911883851
0.62,38	28.35039470272232	90.8863513768173451	547.65072555247402	1597.62735664957671	0.62,40	24.048107693664338	92.8992273403030	378.83704048179035	1620.462002915140361
0.62,39	19.491533101845067	94.834359329369691	237.00992500869711	1272.056198198840641	0.62,41	13.608240821835885	96.688741315456909	124.6012426479464	907.139057688250297
0.62,40	15.29219329883777	98.457404505262161	44.856912356142089	526.152051917269631	0.62,42	10.44630247305028	100.13102119420143	2.966061914695728	128.06599182850247
0.63,1	10.129220913604978	4.791561791468704	10246.846164025519101	737.356942574669531	0.63,3	99.950971186422444	10.697282943150984	9866.6519138822089	1497.940279034400882
0.63,2	97.807144136031093	15.918938837256021	1457.001384112179721	3089.885001359003295	0.63,4	95.154191625700029	10.697282943150984	9866.6519138822089	1497.940279034400882
0.63,3	93.986292507861563	25.2273684144486871	8617.21480770447528	300.1352750557156	0.63,11	91.96031179010229	29.48980574326960	8183.189263324630701	3356.571732004169081
0.63,10	89.85982976908594	33.55193770520947	7745.845476284125652	3647.4718491791304713	0.63,15	87.16860228794248	37.44144261876351	7307.48110824298437	3887.21925518179051
0.63,11	85.43929599704730	41.178584994789489	6870.049531388035575	4080.622952349698579	0.63,19	83.698742231473	44.778801249194089	6435.25862208957098	4221.46056291312951
0.63,20	80.726750347493365	48.254198002370705	6004.635124371245183	4432.8173116737525656	0.63,23	80.0003464307381	51.61449144229248	5579.57091040942555	4747.212100892226601
0.63,25	75.71840252491211	54.875968760010061	5161.345789908526708	4546.88485386033562	0.63,27	73.120526955010857	58.020059969196931	4571.170311955734427	4463.66428433559621
0.63,29	70.40705227375032	61.073731299372381	4350.186519618718020	4439.230683213106294	0.63,31	67.62826960823468	64.04400865013179	3959.490647869144257	4585.66008619152801
0.63,33	64.76975753304461	66.92329182616845	3580.148298218690398	4052.508662189703500	0.63,35	61.62498705153791	69.720344876724121	3252.2018982805087	4127.7804952626788
0.63,34	58.79061796775140	72.4359781878195	2859.683251087244116	4057.00900662513271	0.63,39	55.662260426887720	75.073092432156599	2520.62308312707286	3896.23864296896246
0.63,41	52.434688071003947	77.633538971878195	2197.062459468047109	3171.455542903429452	0.63,43	49.10464259565534	80.118790454960461	1890.065119295293003	3503.5874564007875
0.63,45	45.6557475285658	82.529661351226888	1600.713989053872865	3273.519740931023534	0.63,47	42.087245717010033	84.86781634468517	1330.16048984202573	3022.100195149617801
0.63,49	38.3819677924570	87.13262652107151	1079.606383879407127	2750.147324261851264	0.63,51	34.534895690326579	89.2248435224073631	907.346039470412393	2458.45572183888760
0.63,53	30.517405710527637	91.436666551363031	643.791968865389663	2147.799404349661176	0.63,55	26.107116885365743	93.48835627431966	641.52292959792495	1819.337408173450001
0.63,57	21.80755652527038	95.457403968452255	305.35376379696128	1472.591586231775001	0.63,59	17.42653109145588	97.348422571574901	477.455290051265	1119.838700370060000
0.63,61	12.80432097357800	99.1576311293151921	80.59835439138365	730.12885232423847	0.63,63	10.62761945250795	100.878512547880216	18.734907867806533	334.656118248039344
0.64,1	102.8633122460466	4.800410380056041	10567.53292870336480	750.687118349099594	0.64,3	101.67827965769519	10.712978031278981	10182.0227979449838	1526.69987870961281
0.64,5	99.38279158213207	15.957400411888778	9770.72640751739527	2139.885833048320309	0.64,7	95.154191625700029	20.78183713906808	9349.08077420743642	2647.138362896191201
0.64,9	90.98010829739216	23.3012812665193732	8975.623651107328221	3073.131479819146604	0.64,11	92.50387265140878	29.58057180963137	8474.820319439562	3431.820513094228799
0.64,13	87.45683734714273	33.65911273811329	8030.98287213051844	3722.6531558475721	0.64,15	89.29088287951379	37.566912911562700	7585.91137383693180	3981.125811633103104
0.64,17	83.05102667929797	41.32184684917815	7141.560463088080724	4183.091124629860956	0.64,19	84.793561143608389	44.940163571684721	6699.637811320590663	4342.050286360757251
0.64,21	82.3620131258068	48.43396735393148	6261.66864409538671	4461.1058712591259606	0.64,23	79.00785602283694	51.81304499299999	5829.0402310379876	4542.84323993692002
0.64,25	77.38014299071826	55.805279401495818	5403.03902736236996	4459.461417371471513	0.64,27	74.77604452766617	58.25725125126245	4984.84942401464307	4602.865128719919067
0.64,29	72.6845205783032	61.073731299372381	4575.623651107328221	3073.131479819146604	0.64,31	69.43151213219575	64.04400865013179	3959.490647869144257	4585.66008619152801
0.64,33	66.50280804002802	67.222265601420409	3788.37967894809387	4459.461417371471513	0.64,35	63.8008690161119	70.04003804059782	3412.2903850888182	4355.3278111232831
0.64,37	60.5136688091388	72.7758393439552	3049.64075917534302	4424.67967596176019	0.64,39	57.47079332368600	75.43721540730217	2701.01804364788016	4068.681995913286671
0.64,41	54.27411057760598	78.020839925437485	2367.58257157336345	3888.41813701995571	0.64,43	50.5762717917503	80.529995140432156	2050.371696317418382	3684.78851255670141
0.64,45	47.568423944568124	82.96587171159121	1750.4505256668797	3458.6685675235760	0.64,47	44.044160226112936	85.329259001179728	1468.92499401612657	3210.9143412689901
0.64,49	40.592530879599857	87.628087021866242	1206.9578012548061	2942.338562038640588	0.64,51	36.607105285889801	89.62940271801566	965.787435591308003	2625.7339796717805
0.64,53	32.6312762777328	91.40545665822211	746.7568633886969	2345.8645890177850	0.64,55	28.52487124235974	94.06365848537681	551.349076699144257	2019.4881763198245
0.64,57	24.18834898414390	96.065343139971858	381.24435757543548	1675.33598499175011	0.64,59	19.50852488254943	97.99114803203621	238.414113374911	1314.11096978293496
0.64,61	14.68237293148450	99.838245516327252	125.27372471028099	936.45116049586000	0.64,63	9.39867948056487	101.60192201218416	45.06759867517683	542.7681821952065
0.64,65	3.056498714871942	103.277811156844710	2.975854244473967	311.99580541890319	0.64,65	1.04334441175189796	104.80912355680590	10893.1544206933053	7644.05099518837160
0.65,1	102.740536959198186	4.746292377271525	10502.33516904724682	1555.518694298543911	0.65,1	100.85801850111270	15.99908826534966	10893.10594997434849	2182.01224474775861
0.65,5	98.733010829739216	15.957400411888778	9770.72640751739527	2139.885833048320309	0.65,5	95.154191625700029	20.78183713906808	9349.08077420743642	2647.138362896191201
0.65,9	90.98010829739216	23.3012812665193732	8975.623651107328221	3073.131479819146604	0.65,9	92.50387265140878	29.58057180963137	8474.820319439562	3431.820513094228799
0.65,13	87.45683734714273	33.65911273811329	8030.98287213051844	3722.6531558475721	0.65,13	89.29088287951379	37.566912911562700	7585.91137383693180	3981.125811633103104
0.65,17	83.05102667929797	41.32184684917815	7141.560463088080724	4183.091124629860956	0.65,17	84.793561143608389	44.940163571684721	6699.637811320590663	4342.050286360757251
0.65,21	82.3620131258068	48.43396735393148	6261.66864409538671	4461.1058712591259606	0.65,21	79.00785602283694	51.81304499299999	5829.0402310379876	4542.84323993692002
0.65,25	77.38014299071826	55.805279401495818	5403.03902736236996	4459.461417371471513	0.65,25	74.77604452766617	58.25725125126245	4984.84942401464307	4602.865128719919067
0.65,29	72.6845205783032	61.073731299372381	4575.623651107328221	3073.131479819146604	0.65,29	69.43151213219575	64.04400865013179	3959.490647869144257	4585.66008619152801
0.65,33	66.50280804002802	67.222265601420409	3788.37967894809387	4459.461417371471513	0.65,33	63.8008690161119	70.04003804059782	3412.2903850888182	4355.3278111232831
0.65,37	60.5136688091388	72.7758393439552	3049.64075917534302	4424.67967596176019	0.65,37	57.47079332368600	75.43721540730217	2701.01804364788016	4068.681995913286671
0.65,41	54.27411057760598	78.020839925437485	2367.58257157336345	3888.41813701995571	0.65,41	50.5762717917503	80.529995140432156	2050.371696317418382	3684.78851255670141
0.65,45	47.568423944568124	82.96587171159121	1750.4505256668797	3458.6685675235760	0.65,45	44.044160226112936	85.329259001179728	1468.92499401612657	3210.9143412689901
0.65,49	40.592530879599857	87.628087021866242	1206.9578012548061	2942.338562038640588	0.65,49	36.607105285889801	89.62940271801566	965.787435591308003	2625.7339796717805
0.65,53	32.6312762777328	91.40545665822211	746.7568633886969	2345.8645890177850	0.65,53	28.52487124235974	94.06365848537681	551.349076699144257	2019.4881763198245
0.65,57	24.18834898414390	96.065343139971858	381.24435757543548	1675.33598499175011	0.65,57	19.50852488254943	97.99114803203621	238.414113374911	1314.11096978293496
0.65,61	14.6823729314								

Table D.1. (continued)

m, n, r	$\frac{m, n}{c_{0;r}^m} = \frac{m, n+2}{c_{0;r+1}^m}$	$\frac{m, n}{\lambda_{0;r}^m} = \frac{m, n+2}{\lambda_{0;r+1}^m}$	m, n, r	$\frac{m, n}{c_{0;r}^m} = \frac{m, n+2}{c_{0;r+1}^m}$	$\frac{m, n}{\lambda_{0;r}^m} = \frac{m, n+2}{\lambda_{0;r+1}^m}$
0.69, 47	53.056843725104+8.7506322118648981i	225.53869338122420+71.79954000460311361i	0.69, 49	50.164598211562975+89.9202204064792911i	1936.789974206899387+3927.8046363167127317i
0.69, 51	46.612200296398797+9.22669469352976351i	1638.734750771009099+3056.202834460571921i	0.69, 53	42.93944245377335+94.546892758789710i	1360.464715916743211+3363.9434469475704651i
0.69, 55	39.134486888192491+9.7670159976948661i	1103.153257813096521+351.75928508594400i	0.69, 57	35.83029478965935+98.90635666278700i	860.048451581067074+270.3660917332528581i
0.69, 59	31.66598192477493+10.985442290796791i	635.53446784120883+2370.4646788561813081i	0.69, 61	27.74810575899884+102.959518363499721i	470.156888393883426+2002.749618099259211i
0.69, 63	22.1674747435892+10.94363728852673891i	310.70633428294682+1617.899739750553299i	0.69, 65	17.40442239545022+104.80471692209091i	180.82927654972077+12.16442861525207981i
0.69, 67	12.0062135415859+10.9896606657678041i	81.768435110026218+78.987009009475514i	0.69, 69	6.40147647919890+110.306369804097831i	98.57654682621027+365.44411166697951i
0.70, 1	112.28988465231034+4.8507134096075371i	12595.301040724010818+81.2375391469164741i	0.70, 3	110.60307835750891+10.862358797525221i	12177.000161915238203+1700.776539070210921i
0.70, 5	108.8332122073149+16.1919061230744571i	11735.721843087594607+2394.626400722875901i	0.70, 7	106.987407627814299+21.107100634018381i	11277.00047690383018+2974.753570110890461i
0.70, 9	105.06852113820321+25.721035886362643i	10806.99205378247432+3467.871379257227090i	0.70, 11	103.08331354514612+30.096498069810666i	10392.366535602799599+3889.131917205029921i
0.70, 13	101.02420398728090+34.27342328578361i	9846.968146937787501+4588.398359017509392i	0.70, 15	98.90121822237399+38.279546963001631i	9362.110877781928689+4552.652808356888411i
0.70, 17	96.71222033693995+42.1351889689476461i	8876.765231323170156+4807.15678177950386i	0.70, 19	94.5735257932256+45.85585784542060i	8329.6387732639997+5010.001165991039831i
0.70, 21	92.136748851112173+49.453746635129661i	7911.251617744498617+5182.513642601713654i	0.70, 23	89.750075411545959+52.938678023029446i	7433.97936822107041+5309.45210586534501i
0.70, 25	87.29682551677242+56.318682038248461i	6962.08541991385437+5399.154822464471731i	0.70, 27	84.776211987991999+59.60044018494879i	6496.745063947443880+5453.63825875285251i
0.70, 29	82.187189497086308+62.7895611192798741i	6039.06493810449776+5474.670876799076069i	0.70, 31	79.52844341558454+65.89079473739017i	5590.093619942816076+5463.821168447580931i
0.70, 33	76.7983739519439295+68.9081878818217461i	5150.84223841612448+5422.497859326524063i	0.70, 35	73.95017325362090+71.845201250097361i	4722.286278772312427+5351.979228192151691i
0.70, 37	71.448262080840931+74.7049701783398941i	4303.3789719620511952+4855.69059518111631i	0.70, 39	68.9316809289839+77.48973279613975i	3941.088167018006406+5127.946707197373261i
0.70, 41	65.1264101821802+80.201520623067609i	3510.254688137364610+4976.52106837783201i	0.70, 43	61.998309746649106+82.84263491459657i	3123.89116287810462+4800.890830451811061i
0.70, 45	58.18285952402752+85.414385771197901i	2772.92969313342098+4599.57246944765890i	0.70, 47	55.84014430528526+87.918019413550240i	2448.300290786366077+4375.787596393728829i
0.70, 49	52.07463947681627+90.35451510690331i	2100.98917339468935+4129.552387947324201i	0.70, 51	50.86209220334323+92.72459545565052i	1723.9014702534338+3861.64416489960471i
0.70, 53	44.93413201701805+95.02872408640711i	1502.41973225685803+3572.814097370171323i	0.70, 55	41.180582510396451+97.267099058652661i	1292.341861759274934+3263.791937074951715i
0.70, 57	37.28843781186405+99.43963219702891i	985.97497969751254+2935.289714500011771i	0.70, 59	33.241097312524017+101.54591439351865i	761.635584783477952+2588.00498993163145i
0.70, 61	29.0166096387829+103.585154694655851i	561.769124489185401+2222.6114274323871i	0.70, 63	24.8461112722688+105.55699725701471i	388.030343397089389+1839.8009441885112149i
0.70, 65	19.9003914173431+107.4568246040111771i	242.364607211324198+1440.18681260855310i	0.70, 67	15.89445263946508+109.284462809738301i	172.16988709136714+1024.343829548121269i
0.70, 69	14.86746374999097+111.0344393741669591i	45.662357910661832+592.59043890402152i	0.70, 71	3.084348112778115+112.6981182768607i	3.003477599692051+104.623759616999261i
0.71, 1	113.80095179532054+4.8587407206282221i	12950.53748558652824+844.75381207136868i	0.71, 3	115.7279457085396+10.884793003432529i	12527.954837529706567+1730.044263456544383i
0.71, 5	110.46864631566085+16.2286504326325981i	12080.145520934569504+2437.50660700950861i	0.71, 7	108.5644464249011+21.1585670233570871i	11615.67206964281130+3029.942429713019864i
0.71, 9	106.6032813305151+25.78465119767611i	11319.69769854075677+3534.41892007197881i	0.71, 11	104.0780983838363+30.17807854344343i	10655.9051523808909+3966.28680136216611i
0.71, 13	102.616627905387403+34.703799679562415i	10167.13873404466620+4535.62056910693450i	0.71, 15	100.50019750904502+38.392149281412635i	9675.7237982710684+4639.2059916931320661i
0.71, 17	98.178025720737300+42.26635435303551i	9183.626127543848270+4912.645782164711819i	0.71, 19	96.07189498379222+46.000428283993962i	8925.55604459458103+5129.994617509087221i
0.71, 21	93.76020316467470+49.164792563002029i	8204.0335943053891+5304.6114642852011093i	0.71, 23	91.38364431344222+53.1162312700317901i	7719.4344116979215452+5439.28327387697751i
0.71, 25	88.94172355194307+56.313164127031621i	7240.014415659181399+5556.37104473335562i	0.71, 27	86.43332953844527+59.812087752043588i	6765.951577573270653+5597.912313508071861i
0.71, 29	83.87196805313015+63.745419268398941i	6301.344196805313015+63.745419268398941i	0.71, 31	81.213105002535383+67.37731737309146981i	5844.28283817737302+5782.6458979184321i
0.71, 33	78.499373442496989+69.173348308745869i	5396.6456047042934+5856.12001099574002i	0.71, 35	75.713404928657061+72.128905402326661i	4959.5231875177588+5521.478021318142351i
0.71, 37	72.8536727984834+75.004733027036881i	4533.8202666715034+5428.53794631763645i	0.71, 39	70.197153481653976+77.811537226932921i	4102.46500425624262+5308.38628946502861i
0.71, 41	66.90216348470180+80.543367953067076i	3720.37646065524359+5162.03391109438491i	0.71, 43	63.804205801589660+83.20480318068567i	3334.47176073327025+4909.245630724103030i
0.71, 45	60.917946598883740+85.797411365365363i	2963.7332902634546+4794.455382732717915i	0.71, 47	57.34420159316282+88.322483312206641i	2698.91635312689735+4546.994875657428824i
0.71, 49	55.97210725588227+90.780525517200811i	2175.7025424366820+4352.768049042170881i	0.71, 51	50.4972235702541+93.179060654528901i	1851.388178062103052+40685652610760321i
0.71, 53	46.91127351233203+94.8666623231427391i	1650.61812595927464+3783.24668493981261i	0.71, 55	43.20627470706487+97.6436262694571i	1369.94796913773302+3477.865782210199131i
0.71, 57	39.369320712668302+99.9622742320716641i	1110.52437753076351+3152.80060484839861i	0.71, 59	35.38624977941914+102.095042828047875i	873.5931051475817+8002.52095770966171i
0.71, 61	31.2808587281174632+106.1620880325536451i	660.52734232195029+2444.588842625513735i	0.71, 63	26.9900907254174+106.162296804075595i	472.864845365327369+2063.94921601362551i
0.71, 65	22.32842865124604+108.994197657417453i	312.386015688326154+1666.246856067834451i	0.71, 67	17.48323998919756+109.95533204398702i	181.202734984000661+1252.082948594293181i
0.71, 69	12.252705201343067+111.742445399668661i	132.13593994542091+821.9288755460629841i	0.71, 71	4.26468496712908+113.449234804619095i	19.029073323020990+73.7007292858605481i
0.72, 1	149.927015199869205+14.324761599069761i	1310.7001498216283791+1386.62227364060131i	0.72, 3	106.25446025389508+30.258495961452318i	10957.423994913122733+10463.699364776048023i
0.72, 5	111.982674187352628+16.264874000251171i	12429.51564132927872+2480.50074745888002i	0.72, 7	100.4267416346680+21.209390605272232i	10989.2466863971006+3085.292407078991421i
0.72, 9	108.232071844692329+25.8528129271309281i	11477.30748074610674+3601.176465561952275i	0.72, 11	106.25446025389508+30.258495961452318i	11957.423994913122733+10463.699364776048023i
0.72, 13	104.208850484380314+34.659841445774621i	10492.30920795627265+4422.94762549507171i	0.72, 15	102.698407450194586+38.30312414885396i	9994.355247868154329+5244.445365885121601i
0.72, 17	99.238741302473147+42.390249143088461i	9595.52505345248755+5018.540070661442769i	0.72, 19	97.025487434559005+46.142880403858479i	8981.030456289513825+5516.658165829497931i
0.72, 21	95.28217238388525+49.267327221881011i	8723.9939946272281801+5674.208921657384053i	0.72, 23	88.888103157182858+60.02053058738493i	8042.34814912588238+4782.865102627656971i
0.72, 25	90.592662640527+56.704672433666763i	7528.053087218472865+5746.45878207327548i	0.72, 27	82.09532347730753+66.38093184252344i	7103.66117246380931+5779.54585165187261i
0.72, 29	85.25382629872353+63.244357258396541i	6547.7658055488224+5750.601653298140261i	0.72, 31	71.62754145391786+72.40813252065121i	5202.1290795645350+5691.900094221442941i
0.72, 33	80.196640769051129+69.434362734564441i	4767.68813748699492+5706.631134822151631i	0.72, 35	61.6995666020806+78.128349255190661i	4345.3616242530746+5489.8853759737221i
0.72, 37	76.67678103813608+80.974094709015701i	3946.05820985444239+5348.677168917949873i	0.72, 39	52.621488194023624+83.560946573853670i	3540.08201294870750+5181.95761427378131i
0.72, 41	72.419556467567789+84.6666623231427391i	3127.004964527315942+4842.80850301078561i	0.72, 43	45.0218815892452035+93.051200720691238i	2716.805065754853331+4977.195296428704751i
0.72, 45	68.3356930594405+95.965819887283721i	1805.006294708728774+3995.506182501234434i	0.72, 45	41.513124749083207+89.25235258863950i	1512.903601719029439+3460.10446070562781i
0.72, 49	64.42773673110075+100.474916386145892i	1241.0664107560520592+3730.695612918036691i	0.72, 49	37.504223632777247+102.6335929049025i	926.03184804272293+3028.969292512658571i
0.72, 53	61.425980275369291+104.772239455202451i	766.302381999563181+2668.60136384839298i	0.72, 53	34.21107069312043+105.7656908565	

Table D.1: (continued)

Table with columns for m, n, r and associated eigenvalues. The table is organized into four quadrants based on the parity of m, n, and r. Each quadrant has a header defining the relationship between the indices and the eigenvalue. The data consists of numerical values for each combination of m, n, r.

Table D.1: Branch points and associated eigenvalues for m = 0.

D.1.2 m = 1, n = [m..80]

Accuracy was determined by the last correction of the Newton-Raphson method.

Table D.2: Branch points and associated eigenvalues for m = 1.

Table with columns for m, n, r and associated eigenvalues. The table is organized into four quadrants based on the parity of m, n, and r. Each quadrant has a header defining the relationship between the indices and the eigenvalue. The data consists of numerical values for each combination of m, n, r.

D.1. Branch points, $c_{\sigma;r}^{m,n}$, and Associated Eigenvalues $\lambda_{\sigma;r}^{m,n}$ of the SWE 211

Table D.2. (continued)

m, n, r	$c_{\sigma;r}^{m,n} = c_{\sigma;r+1}^{m,n+2}$	$\lambda_{\sigma;r}^{m,n} = \lambda_{\sigma;r+1}^{m,n+2}$	m, n, r	$c_{\sigma;r}^{m,n} = c_{\sigma;r+1}^{m,n+2}$	$\lambda_{\sigma;r}^{m,n} = \lambda_{\sigma;r+1}^{m,n+2}$
1.3, 1	5.59491061915554 + 4.781582485762671i	27.134073085223168 + 27.423761571644381i	1.3, 3	2.184204069300826 + 7.326156812534641i	3.10256060797785 + 10.539212881981126i
1.4, 1	7.20040170458184 + 5.0108091825662271i	47.41098557646396 + 39.4240718765353157i	1.4, 3	4.24672923512624 + 7.831360958311476i	13.86757405380991 + 27.642112872540003i
1.5, 1	8.91545199508990 + 5.207928919980661i	72.89656036953961 + 52.09473920833313i	1.5, 3	6.1908789218941 + 8.27468882858778i	29.88062450108477 + 46.18127766959076i
1.5, 5	2.30408340373247 + 10.540790051881750i	3.22345112166909 + 14.78456568704811i	1.6, 3	1.52350167438761 + 5.363017364859081i	65.322653297106301 + 105.51790242771686 + 65.322653297106301i
1.6, 3	7.90184171761789 + 8.572100476668989i	52.1112833092568930 + 65.921011346611721i	1.7, 3	5.41083474687041 + 11.06871516965604i	14.9886250535389 + 38.58841409779759i
1.7, 1	12.5742551872748 + 5.504539534898089i	29.22192302143287 + 79.0325713310344433i	1.7, 3	6.924074824342478 + 8.862803308220407i	74.1996519538421772 + 86.6784170737916i
1.7, 5	6.497378520948285 + 11.540048903871105i	31.83374549876009 + 64.029483325071382i	1.7, 7	3.29232650572686 + 13.667125470943089i	3.12353326245665 + 18.95959364310853i
1.8, 1	13.763874711921164 + 5.630024308478101i	179.983540743798642 + 93.165884343630244i	1.8, 3	11.39289694262133 + 9.118350208514050i	108.3173449883304749 + 108.3173449883304749i
1.8, 5	8.32857881069370 + 11.947103162705321i	55.547115833727254 + 90.91865684544613i	1.8, 7	4.71288908410366 + 14.268247694128767i	14.818382803263212 + 49.34207107855510i
1.9, 1	15.364144468012046 + 5.742727343885289i	225.77874983608704 + 67.076529019960242i	1.9, 3	13.0089290948708 + 9.3464616392199919i	151.343076053641511 + 130.738820970417352i
1.9, 5	10.1806379695939 + 12.306198702934776i	85.03918060224113 + 119.06293528610698i	1.9, 7	6.79347465093069 + 14.785378425843306i	33.352512036252448 + 81.494598435999708i
1.9, 9	2.46198752467070 + 16.822045374262045i	3.38245769554427 + 23.08175627203863i	1.10, 1	16.9597688923902 + 5.849491740557074i	22.526899642288888 + 122.52758046736241i
1.10, 3	14.65627569602667 + 5.52373733926231i	194.94427689049020 + 153.848777963964721i	1.10, 5	11.94263654404307 + 12.627831816288797i	120.125066815811548 + 132.125066815811548i
1.10, 7	8.79027039897156 + 15.241610918357121i	58.26331927138862 + 115.263410679382951i	1.10, 9	4.87511879261963 + 17.448960842939921i	13.31707805947175 + 59.99348725671252i
1.11, 1	18.55176580589899 + 5.938490783135454i	332.40599055150289 + 137.688566848597294i	1.11, 3	16.28683997932507 + 9.740141886979372i	243.71485444447166 + 177.59310268146587i
1.11, 5	13.67212407838859 + 12.91273290788901i	160.67919914291962 + 178.88985701828479i	1.11, 5	10.62832789715593 + 15.680083076169292i	89.109129488819362 + 150.47240125871592i
1.11, 9	7.036579565300370 + 17.999591990490915i	34.59250471277656 + 98.753300589341109i	1.11, 9	2.19494898084327 + 19.97294939823424i	3.44020570332667 + 27.17536891312683i
1.12, 1	20.14092533079789 + 6.024700935856217i	393.21634772648978 + 153.134011701354349i	1.12, 1	6.92792400309869 + 9.912674095212714i	297.6189197363051 + 201.91286351201892i
1.12, 5	15.37719798621701 + 13.185060596025644i	206.611687570376508 + 209.76061852395408i	1.12, 5	12.448411897296973 + 16.02243129736466i	125.937152863100550 + 186.97756889038784i
1.12, 9	9.06220724999535 + 18.492458162374121i	60.6119987367100 + 139.25328415235210i	1.12, 9	10.2107467457113 + 20.61891680783224i	15.74494384282545 + 50.77545345584554i
1.13, 1	21.72778657047993 + 6.104630638373134i	459.013538130049369 + 168.84228330428970i	1.13, 1	19.5556920747562 + 10.07225407343612i	356.65169913907510 + 226.76293982185083i
1.13, 5	17.063442736915551 + 13.431409424175248i	257.855444145423007 + 241.760821147452134i	1.13, 5	14.01263443422278 + 16.36257995713196i	168.323896047642 + 264.6589569249001i
1.13, 9	11.00089587022626 + 18.94018319479134i	92.676523819663501 + 181.33496733953951i	1.13, 9	7.242780446626386 + 21.194664090490219i	35.64654052953452 + 115.87912795495487i
1.13, 13	2.568300292315928 + 23.121427531129123i	3.489236429700662 + 31.244427740543561i	1.14, 1	13.1276117318234 + 6.179125414274073i	529.79117046303959 + 184.7945403064194i
1.14, 1	17.8037298718918 + 10.22068524099801i	420.72864651279149 + 252.102483501750015i	1.14, 5	18.374793289598922 + 13.659160057042378i	134.35840466757359 + 274.52525742814352i
1.14, 5	15.49235161063713 + 16.67727534519416i	216.245888823473909 + 263.416532843769575i	1.14, 9	12.878594212361513 + 19.53075501609978i	224.856182829617621 + 324.856182829617621i
1.14, 9	9.330439063738341 + 21.710563850276861i	62.43094766365691 + 163.01846826324909i	1.14, 13	5.29554584043660 + 3.278091783669927i	16.093204598373720 + 81.112789160339864i
1.14, 13	2.8967174619145 + 2.648871216060073i	605.544064799664056 + 200.9753614821308i	1.15, 2	22.785579087509738 + 10.359418740290204i	489.892921131206833 + 277.89983173851531i
1.15, 5	20.399119945131 + 13.871494281619029i	376.079339618917572 + 307.998311781125551i	1.15, 7	17.12912286300956 + 16.96868591674522i	269.618829229189828 + 306.167209540021603i
1.15, 9	14.170275366808509 + 24.37782406012361i	174.812812633243453 + 269.69710619695274i	1.15, 11	11.32483990235599 + 22.194980627990206i	95.66574817545551 + 211.8508647863197i
1.15, 13	7.4221173256808509 + 24.37782406012361i	36.55731660897702 + 132.9146078186091i	1.15, 15	5.26107533403184 + 26.268235538818395i	3.53179695225998 + 35.29736264001924i
1.16, 1	22.04354833555521 + 14.07037521642998i	642.98489237048545 + 342.13198784612001i	1.16, 1	12.82858042369517 + 17.212436752872162i	568.37546020966810 + 343.88311569714404i
1.16, 5	16.50836792182958 + 20.08364524460742i	224.475648587231092 + 315.7559692282221i	1.16, 11	13.32827887252669 + 22.63722818716101i	162.316323088408510 + 92.212435990242294i
1.16, 9	9.5649629519458 + 24.92295420540041i	6.104505264001375 + 186.6292510266677i	1.16, 15	5.25257349523292 + 26.94700137094073i	16.40753457042004 + 61.261215890455042i
1.17, 1	28.05927860818817 + 6.376278315290989i	771.95897868273979 + 233.96518784811031i	1.17, 3	25.99793285486185 + 10.61231185933116i	463.36726408317059 + 39.749548710270363i
1.17, 5	22.79888844488920 + 17.737803753475124i	515.04761590329737 + 376.88418914903187i	1.17, 5	11.117348550987550 + 17.409662135827737i	392.46213903607510 + 385.36652118099319i
1.17, 9	18.27809453946806 + 20.41001762180922i	279.723410720493501 + 362.94286837999538i	1.17, 11	15.10736822506620 + 23.048724720788967i	180.45728878871767 + 110.07056923294854i
1.17, 13	11.609922651340975 + 25.426468750545723i	98.287608917575938 + 242.12916698291274i	1.17, 15	7.57974174656437 + 25.52747191916115i	37.360814824936652 + 149.88930044679876i
1.17, 17	2.648270598403898 + 29.414135460952782i	3.569372107334297 + 39.326818867030951i	1.18, 1	19.932325398202242 + 6.434804309050247i	86.216425409236105 + 250.75183126783134i
1.18, 1	27.99088273906524 + 10.728290686285843i	727.654270692997397 + 357.75405909515577i	1.18, 5	21.8396723621769 + 9.339030849093494i	592.24464366285216 + 412.218761752423899i
1.18, 5	22.79888844488920 + 17.737803753475124i	641.835027192791057 + 427.70303752652760i	1.18, 9	10.02533914690252 + 20.72287826565978i	340.4761391151516 + 491.18379154166959i
1.18, 9	14.07212407838859 + 12.91273290788901i	267.017823736971937 + 407.328302707800369i	1.18, 13	6.0023329207506 + 28.80407210069584i	138.90228283041662 + 252.8283041662i
1.18, 13	9.73267447529681 + 28.11693946952981i	65.58820118059196 + 120.12899992566760i	1.18, 17	5.32429883357478 + 30.0960777818858i	16.687188868371296 + 102.0882879707252i
1.19, 1	31.21855197437158 + 6.490345716684749i	958.231013597469424 + 267.718198061057306i	1.19, 3	29.197486235912713 + 10.838292693944201i	816.96348257263290 + 385.7116787309815957i
1.19, 5	26.947331712313896 + 14.610056861366935i	674.656508302782959 + 448.102335969841941i	1.19, 7	24.766518879879342 + 17.95641956891296i	556.545689198115986 + 470.795491422146778i
1.19, 9	21.7540174720204 + 21.01500213260698i	406.69132698773581 + 402.12726004441253i	1.19, 11	18.46963465330968 + 23.79656147235931i	288.59425362918230 + 441.69749232660502i
1.19, 13	15.49235161063713 + 26.333475175234104i	185.47060836937306 + 351.981034842265075i	1.19, 15	10.09809299181995 + 28.641613845812619i	100.626604277830162 + 351.02251483530306i
1.19, 17	7.721177736803752 + 31.61208285334104i	38.07881123989373 + 66.80256240403329i	1.19, 19	6.28186490794784 + 5.95163510807171i	67.020948975695900 + 45.34592447616294i
1.20, 1	32.79706542387272 + 6.54318974560377i	1058.80697125493837 + 284.85541971378673i	1.20, 3	30.79320186823034 + 10.94275184864958i	91.12857619416576 + 412.81935296617204i
1.20, 5	28.57057623009113 + 14.759735867943657i	761.96680926925441 + 484.50951538866782i	1.20, 7	26.31089929257755 + 18.18196193611043i	16.62994961863736 + 51.60423457405301i
1.20, 9	23.46713635786374 + 21.294700419919034i	478.249077451358232 + 510.57024195918961i	1.20, 11	20.56148110010765 + 24.13714494062102i	351.14409914567248 + 477.226374651620051i
1.20, 13	17.38484661537075 + 26.75650179745127i	238.60429488999221 + 418.115171928915345i	1.20, 15	11.381394817881253 + 29.132043647867378i	142.14928250210429 + 336.08158033925045i
1.20, 17	9.01592120570078 + 32.84837157338616i	114.00895989978346 + 444.87228890358959i	1.20, 19	6.43096348211076 + 32.81086430249071i	59.1091261877783106 + 301.02251483530306i
1.21, 1	34.7495515887518 + 6.59358424978377i	1104.3001342789018 + 302.156554303854421i	1.21, 3	32.38748594741077 + 11.042342047056653i	1016.1050607619219 + 940.54037121620357i
1.21, 5	30.18904472633456 + 14.91077867397268i	854.461277910156468 + 521.403374181271261i	1.21, 7	27.8446549979300 + 18.38631028835190i	701.23346087998551 + 592.87240861878286i
1.21, 9	25.10763237692124 + 21.553776208465788i	555.171375944207512 + 561.060166370418691i	1.21, 11	22.32093277987649 + 24.460468634060411i	419.325979786427379 + 535.95909110696251i
1.21, 13	19.22873625922523 + 27.134768194690991i	296.57019438681712 + 479.59644504436944i	1.21, 15	14.516242839989702 + 29.693360397949949i	189.939627465692411 + 401.455744012912910i
1.21, 17	12.07158166951997 + 35.70310474643841i	107.32731315338704702 + 677.879502508			

Table D.2. (continued)

m, n	$m, n = \begin{matrix} m, n-1 \\ c_{0:r} \end{matrix}$	$m, n = \begin{matrix} m, n+2 \\ c_{0:r+1} \end{matrix}$	$m, n = \begin{matrix} m, n-1 \\ \lambda_{0:r} \end{matrix}$	$m, n = \begin{matrix} m, n+2 \\ \lambda_{0:r+1} \end{matrix}$	m, n, r	$m, n, r = \begin{matrix} m, n+2 \\ c_{0:r+1} \end{matrix}$	$m, n, r = \begin{matrix} m, n+2 \\ \lambda_{0:r+1} \end{matrix}$
1.31,1	46.2283758926040+...	16.193409933664111	2056.91851714814497+...	913.208575180055541	1.31,1	44.046934695673855+...	201198225261882291
1.31,1	47.762727589026396+...	23.607380696173581	1611.9592165064115+...	1111.9959128234245331	1.31,1	39.26100026613088+...	27.00182243223333
1.31,1	36.64762322659907+...	30.1671435293844021	1186.03289539840096+...	1154.631918068191141	1.31,1	33.87808604175103+...	33.1472250362474981
1.31,1	30.94293094354700+...	35.958250135966041	798.73321440734746+...	1073.651313974916751	1.31,1	27.8794295700570+...	38.6112725721964211
1.31,2	24.51324312653201+...	41.113880782974461	466.81935445787064+...	889.20850071878261	1.31,2	22.96483198098954+...	43.470662602404525
1.31,2	17.54171028598004+...	45.683576805470711	207.31418186203308+...	616.4951005402427881	1.31,2	10.99997195715912+...	47.7513960652652681
1.31,2	8.52244178319348+...	49.66864671550451+...	41.276705018487256+...	267.64038559648061+...	1.31,2	2.8317749139496+...	51.4207761161598451
1.32,1	51.705769882808021+...	7.30328081045927631	2651.987963127629428+...	501.4831793457196341	1.32,1	49.85766824736922+...	11.9077935823734991
1.32,1	47.81673892081387+...	16.2180116876193271	2204.76856604224816+...	954.344024390794511	1.32,1	45.655774328484320+...	20.1527178105884991
1.32,1	43.5525235039363+...	23.7994894256113191	1745.97255664998900+...	1170.419882419366691	1.32,1	40.914579126659185+...	27.207226736976241
1.32,1	38.29665756213987+...	30.4100116775258621	1304.523176734874824+...	1227.147991751574531	1.32,1	35.96175582796000+...	33.4297144675821441
1.32,1	32.70433767001415+...	36.2822145997550721	899.840858156785771+...	1157.71686036940181	1.32,1	29.642186055004576+...	39.788806938596371
1.32,1	26.39261609477965+...	41.527900247611601	548.32744922358713+...	982.60023641935621	1.32,1	22.931644228338278+...	43.9328437961179911
1.32,2	19.223806384617891+...	46.2000173151373021	266.297710496490666+...	716.9054338939419041	1.32,2	15.213840883813641+...	48.326251536530441
1.32,2	10.804796476345988+...	50.309257759511311	252.908215216858153+...	375.005270246610251	1.32,2	7.80655148152087+...	52.1401478999712481
1.33,1	35.27907872848881+...	7.06521736904112921	2816.91171765876879+...	520.302157848188601	1.33,1	51.417015785790475+...	11.971327447179451
1.33,1	44.0898164596608+...	16.3136801445317481	2357.6188202623836+...	955.77991048885701	1.33,1	47.262542414106854+...	20.2814873356709281
1.33,1	49.805161128487+...	23.9619258831525671	1885.09162240478953+...	1229.3731446711101401	1.33,1	42.624609535856964+...	27.405504278853271
1.33,1	40.05705560429419+...	30.6449267713232491	1428.271027161584698+...	1300.4395506270161601	1.33,1	37.305280123926796+...	33.7027939166183301
1.33,1	34.45542462096359+...	36.5950372110205611	1066.440351812107565+...	1242.835219470529401	1.33,1	31.8971872570529+...	39.334593824570791
1.33,1	28.294046474982995+...	41.926305189080041	635.689757403219801+...	1077.321378656975491	1.33,2	24.862076844192533+...	44.379039059737441
1.33,2	21.24857511549818+...	46.6957033493188551	331.683858002614564+...	819.074252079992801	1.33,2	17.3650719194488+...	48.8764902375904891
1.33,2	13.1396358315982911+...	50.9199350198295311	112.26474218658551+...	480.48017478720001	1.33,2	10.8339615319796+...	52.820352832909021
1.33,3	2.85107779043231+...	54.563594864768471	3.771860591637443+...	71.2054424672789571	1.34,1	5.4562621218106+...	7.0966078158885051
1.33,3	5.299726236592840+...	10.229947812193101	2755.60155633710050+...	829.177049142561241	1.34,1	50.99994695050331+...	16.4064949138537721
1.34,1	48.06480198627879+...	24.4063745764468061	488.06480198627879+...	635.0382582929921	1.34,1	42.06480198627879+...	21.009279096649471
1.34,1	44.206283346209943+...	27.5976171975804941	1790.19611578690477+...	1349.74002627832441	1.34,1	41.674553473716216+...	30.872397669251531
1.34,1	39.0604838847696+...	33.966293860156561	132.68587813782550+...	366.61545391774911	1.34,1	36.1947629107073+...	36.897478194093651
1.34,1	33.22240383194232+...	39.6759348666817571	91.6590087172084054+...	1263.879996227565671	1.34,1	30.086210688196701+...	42.3109150824437991
1.34,2	26.76535499477198+...	44.808620249920941	55.120631672673198+...	1059.11712367434261	1.34,2	25.2542251751696+...	47.172402018934661
1.34,2	19.46906890958405+...	49.404449954753651	269.878195012068900+...	766.1015077486415861	1.34,2	15.38636654614870+...	51.5040193861872951
1.34,2	13.7105306801355+...	53.517497951189261	75.6842917165876879+...	520.302157848188601	1.34,2	8.523195119824878+...	55.261962447179451
1.34,2	56.427318706833107+...	7.12711092211849+...	3161.591595125851200+...	558.23986068838111	1.35,1	54.70739984533702+...	12.09290134280259261
1.35,1	52.58997107818108+...	16.4966292025510981	2678.305740852693361+...	5448.8636994198751	1.35,1	50.45051380327706+...	20.5276143857840761
1.35,1	48.22513577323390+...	24.27310535551671	2178.59642377375476+...	1348.8011096156385521	1.35,1	45.86186437139039+...	27.7839376234178101
1.35,1	43.33974675424096+...	31.029885062002141	1691.46330704777692+...	1449.243957101939941	1.35,1	40.69949114307651+...	34.2228300118360881
1.35,1	37.919549159137333+...	37.54425803991	1235.97206664537901+...	1416.080058885895401	1.35,2	34.99187752208878+...	40.007123609385311
1.35,1	31.90534158666705+...	42.68244800302631	827.706129347851162+...	1270.663692371106331	1.35,2	28.64894471102965+...	45.22533064497861
1.35,2	25.18981536070888+...	47.631645703528161	481.34934317534639+...	1028.390265987535261	1.35,2	21.10715016261613+...	49.9120954881932801
1.35,2	17.6537464585223+...	52.0641771527713291	212.708383436509138+...	701.6749290746142831	1.35,2	13.67348341823823+...	54.08572581636791
1.35,3	8.510254457270735+...	55.9710372894433381	42.07600139436587+...	301.145230280669651	1.35,3	2.86923892164964+...	57.706289001248421
1.35,3	58.00087006616267+...	7.1567732096576851	3341.346793491121844+...	577.351207702104101	1.36,1	55.1769455200007521	12.151445426287831
1.36,1	54.1765178359141+...	16.58835843029951	341.5746175905907441+...	741.8531937949921	1.36,1	47.8250070917179+...	27.9648052251536931
1.36,1	49.893687126671372+...	24.220118120204721	2332.96609510637245+...	1049.24511783074261	1.36,1	42.486104811579676+...	34.470961515859361
1.36,1	44.99904720101517+...	31.3068071671258381	1830.84642157300641+...	1524.2094912998118161	1.36,1	37.49390396135929+...	40.327791918760091
1.36,1	33.708718561780831+...	37.4738781160971111	1358.84254666226488+...	1504.1378691683200941	1.36,2	30.50393001665275+...	45.6226088526426061
1.36,1	26.35300912670801+...	43.041824040659101	925.245032218976235+...	1399.1948190161347161	1.36,2	24.5726072965120871	50.8761319087615861
1.36,2	19.028381522490028+...	52.620670871006711	573.2757366542771540+...	1155.195318895861761	1.36,3	15.48941494431858+...	54.678219519720101
1.36,2	11.07925158071442+...	56.241250137979101	741.6534443053024+...	419.256113828521561	1.36,3	10.5752859140388+...	58.4316321639710431
1.37,1	59.574290365371855+...	7.1856415973778041	3526.044939173310468+...	596.556023826334751	1.37,1	57.3702371391359+...	12.2078132419488171
1.37,1	55.76725480600231+...	16.66944247584021	3018.95490323067853+...	1164.4346926060434661	1.37,1	53.672062524084069+...	20.759832689782921
1.37,1	51.45457357437653+...	24.566697124729161	2492.40430967928478+...	1470.156849249887051	1.37,1	49.11513854164725+...	28.30030046101101
1.37,1	47.064769696959771+...	31.51479796959771	1975.4769696959771+...	1089.69036909721	1.37,1	44.826107296512078+...	36.198448186490471
1.37,1	41.34940663690463+...	37.74900949569171	1487.07917948419538+...	1593.110868909132671	1.37,1	39.485614732959200+...	40.638592192188851
1.37,1	35.497952617005254+...	43.3898440519518831	1042.40513933489546+...	1468.907401179747601	1.37,2	32.43520448108151+...	46.0096538510192231
1.37,1	29.01741848006344+...	48.520959589514821	655.40595904893644+...	1243.905840138170331	1.37,2	25.98862185376776+...	50.872937969280201
1.37,1	21.75811411247643+...	53.121167259643701	340.84850989178610+...	930.566948842825241	1.37,1	17.310726461313531+...	55.24741634081311
1.37,2	13.33081808188435+...	57.42534672534671	116.48167162534671+...	574.25819796301	1.37,2	10.357670324670324+...	58.916703246703241
1.37,2	8.86483555080955+...	60.84856270080321	3.807079522089604+...	99.10454801472621	1.38,1	6.114789122089864+...	7.213756305958681
1.38,1	59.31597957599132+...	12.262990417065041	3461.49815823926659+...	955.914315025425481	1.38,1	57.354647814934296+...	16.752385429973261
1.38,1	55.27040887055206+...	20.8713892175048131	2927.24832014430044+...	1395.09493171929291	1.38,1	53.067345407346309+...	24.70746302234171
1.38,1	50.745481183966700+...	28.31397235378251	2388.74563062522686+...	1624.00228582416791	1.38,1	48.304280732981873+...	31.716452017000531
1.38,1	45.741367832148370+...	34.9457473558490431	1868.582549598473861+...	1696.315491323029541	1.38,1	43.5025824212171687+...	38.016120247904071
1.38,1	40.38196360842901+...	40.940126135908071	1383.274511030623207+...	1640.089855461675791	1.38,2	37.27435958046473+...	43.727291416873671
1.38,2	34.166915679690466+...	46.3845319234034581	946.943719958549082+...	1473.804757653380781	1.38,2	30.891713963024349+...	48.917227316695541
1.38,2	27.44705027443981+...	51.3288615858496101	573.153614140673540+...	1211.35472735092231	1.38,2	23.94820448108151+...	53.6214466584718201
1.38,1	19.895702003007324+...	55.7954186174265351	276.48906088260120+...	864.2011313000543601	1.38,3	15.70283486888836+...	

D.1. Branch points, $c_{\alpha, r}^{m, n}$, and Associated Eigenvalues $\lambda_{\alpha, r}^{m, n}$ of the SWE

Table D.2. (continued)

m, n, r	$\frac{m, n}{c_{\alpha, r}^{m, n}} = \frac{m, n+2}{c_{\alpha, r+1}^{m, n+2}}$	$\lambda_{\alpha, r}^{m, n} = \lambda_{\alpha, r+1}^{m, n+2}$	m, n, r	$\frac{m, n}{c_{\alpha, r}^{m, n}} = \frac{m, n+2}{c_{\alpha, r+1}^{m, n+2}}$	$\lambda_{\alpha, r}^{m, n} = \lambda_{\alpha, r+1}^{m, n+2}$
1.43.1	8.71921986348976 + 68.56191801102065i	43.435467296672210 + 367.9469362466694521i	1.43.43	2.93301146671074 + 70.276095880104194i	3.853428997480489 + 90.9066787499169927i
1.44.1	70.585252315288587 + 7.368570682398195i	4957.305536446239785 + 733.385419258819414i	1.44.3	6.828625215498538 + 12.56661536888027i	4669.083855066493925 + 111.152026959163656i
1.44.5	66.88483530028889 + 17.204808163486308i	4368.15369853978757 + 1469.78665542072368i	1.44.7	64.383546707834347 + 21.483570402069631i	4600.425813670378830 + 175.485334491717811i
1.44.9	62.70729267917501 + 25.47969348950205i	3749.898774823266438 + 1908.610444840805518i	1.44.11	60.47270327588165 + 29.247876992685299i	4339.610521378659541 + 2051.322964579875886i
1.44.13	58.135076410321102 + 32.821609701979355i	3132.03339231094578 + 1251.80067467994450i	1.44.15	55.693611783310713 + 36.224291831000575i	4285.276874674239861 + 2212.9213190723211i
1.44.17	53.146505379106095 + 39.47368067535401i	2533.20625862330007 + 2239.31761896063201i	1.44.19	50.94094672435698 + 42.58240710055219i	2829.511404135591522 + 2325.25390760193252i
1.44.21	47.723046439984714 + 45.568084978656548i	1967.798715397626665 + 2196.92553117021023i	1.44.23	47.637689697169502 + 48.416933187053992i	2170.55450730160425 + 132.270082249039953i
1.44.25	41.828302117715694 + 51.156854245450077i	1448.255066897561072 + 2040.7839189595948i	1.44.27	38.686493990030371 + 53.78540363680377i	1209.353745484993523 + 1924.65521757919931i
1.44.29	35.401523331033097 + 56.306706456425297i	986.337525269287691 + 1784.40099397826005i	1.44.31	31.959467306582450 + 58.7219904711994262i	780.17977807657301 + 1621.78313165538333i
1.44.33	28.341891317240277 + 61.034106160358261i	594.47471113543881 + 1477.891724699219193i	1.44.35	24.5238591594466777 + 63.243178624982875i	428.28219510134997 + 1233.86707531630685i
1.44.37	20.48335766182936 + 65.34861256645012i	285.181257186801361 + 1010.79656047229547i	1.44.39	16.21034374225746 + 67.343831610793510i	225.121426928760561 + 769.711859759860317i
1.44.41	11.3819710995511 + 69.238359710137861i	76.990582734842221 + 511.552077667014474i	1.44.43	6.03970171628403 + 71.0105011079017168i	18.85454224212713 + 236.8802495576880i
1.45.1	72.15778990155366 + 7.392337009589151i	5181.53503817996689 + 753.250737929671373i	1.45.3	70.5740182629707 + 12.61397123041070i	4887.6866046955433 + 184.174533739807851i
1.45.5	68.44780276415208 + 17.27815654943260i	4580.797852536713835 + 1514.108324058047322i	1.45.7	66.28860076679991 + 21.57733606116984i	4626.793738543972752 + 1772.31129149965617i
1.45.9	64.308871461326272 + 25.59786669811649i	3949.6802541262858 + 1972.842877268461791i	1.45.11	62.09858694355557 + 29.391052298744157i	4360.571288898938324 + 2124.228113276622381i
1.45.13	59.76331547150263 + 32.890369406388661i	3317.60073808537463 + 2322.29556091833760i	1.45.15	57.301862715338639 + 36.41942309360547i	3007.520348243004264 + 301.34469598760440i
1.45.17	54.81168169683238 + 39.69601215332822i	2703.65639425393283 + 2334.720750820387i	1.45.19	52.17862709241646 + 42.83208946531114i	2407.8552150122054 + 2335.133120422667616i
1.45.21	49.43662384864170 + 45.83912325386218i	2121.68567685633973 + 2304.84676374369559i	1.45.23	46.580945554280717 + 48.724733341668212i	1846.38085192126726 + 2325.805001716220886i
1.45.25	43.60568714601941 + 51.495241993871375i	1584.157425372164425 + 2159.71232283847200i	1.45.27	40.5033597367193 + 54.155592848157710i	1335.66942483125671 + 2048.0293210070221i
1.45.29	37.26432122409112 + 56.7095705713781096i	1102.60987279964911 + 1912.330077453269951i	1.45.31	33.76734659163311 + 59.159939388341414i	886.452232032817282 + 1757.70389317157189i
1.45.33	30.32460291484546 + 61.508515321493881i	688.741535021247610 + 1573.40933434398759i	1.45.35	26.584103764340412 + 63.76173865880191i	511.13656849690275 + 1372.57364677116160i
1.45.37	22.62825467842419 + 65.902777135520253i	355.472400698175363 + 1152.291926752470545i	1.45.39	18.1433253595886 + 67.94698000489536i	223.8354894599672 + 913.58495771322886i
1.45.41	13.86125296174848 + 69.88579562503917i	118.82579417362162 + 657.42927911433992i	1.45.43	8.838741250923450 + 71.13549016680270i	43.7361967045772 + 384.6237074835446i
1.45.45	5.947179043242463 + 73.418378031605311i	3.8674500689745445 + 94.8326265321180i	1.45.45	7.730474031432905 + 74.1558925535897i	54.407057441969076 + 773.190270913398185i
1.45.47	1.93605641638870 + 12.65876393216276i	511.124673072887021 + 1217.39229372933180i	1.46.1	70.37047328525515 + 17.364686321095035i	4798.12568145885283 + 1558.85629642379857i
1.46.1	1.96736726740857 + 21.66902135747002i	4478.15026874024252 + 1827.43070020016906i	1.46.3	68.61098705153526 + 21.735815355040053i	4694.510389747504696 + 1882.837101523331285i
1.46.11	6.69890767044126 + 29.530944456164072i	3830.48375025718889 + 2197.58390400387910i	1.46.13	61.898424137367562 + 33.155233930256010i	3508.58860824968681 + 1331.77452971806678i
1.46.15	58.98162193765919 + 36.609890425408341i	3190.915085934792387 + 2390.387446691758225i	1.46.17	56.27862124293393 + 39.91232696829273i	2879.31513939933823 + 2430.818556876980892i
1.46.19	53.86118310551209 + 43.075804172202073i	2575.46633119262378 + 2347.8147880713571i	1.46.21	51.14382970468665 + 46.110627940516327i	2280.244861966211546 + 2344.667899941733104i
1.46.23	48.31621901361295 + 49.21499126612117511i	1997.163046987826874 + 2360.32652992968397i	1.46.25	45.37135712402685 + 51.825079033422469i	1725.60447661915919 + 2247.9551278891395065i
1.46.27	42.30785378820426 + 54.51161879403739501i	1467.647369734248969 + 2172.847380360600737i	1.46.29	39.11669876040757 + 57.102165212031956i	1224.691937711434548 + 2041.602088474515153i
1.46.31	36.34541646461 + 59.6620949057074701i	924.76623427863252 + 1827.43070020016906i	1.46.33	32.781640515338639 + 62.713291273709819i	789.5595512430638 + 1852.837101523331285i
1.46.35	30.22460748986493 + 64.251481829359463i	600.44082971230718 + 1513.0565046696441i	1.46.37	24.74507308505959 + 66.40032912072049i	432.545169987423074 + 1295.712872069771001i
1.46.39	20.64187701056565 + 68.5263925313217i	287.811953661750351 + 1059.547698900130045i	1.46.41	16.246939043856710 + 70.510872446296972i	168.2573881283033 + 805.54845625651868i
1.46.43	11.627406765088079 + 72.389594488770939i	77.561320219903010 + 534.59238184852711i	1.46.45	6.072993603571454 + 74.15460421850777i	18.63658131399354 + 247.189802691629414i
1.47.1	75.0298186441663 + 7.438348424137253i	5644.816138511327154 + 793.20249365194348i	1.47.3	73.51244422171280 + 12.7358140074148i	4533.50648418057641 + 1250.75223322230495i
1.47.5	71.61210657049544 + 21.66902135747002i	4848.15026874024252 + 1827.43070020016906i	1.47.7	68.61098705153526 + 21.735815355040053i	4694.510389747504696 + 1882.837101523331285i
1.47.9	67.50846358348649 + 25.82638905571602i	4368.328986187582362 + 2102.41175377142917i	1.47.11	63.69505626027575 + 29.66077680072599i	5039.75029496843675 + 2271.38028873713723i
1.47.13	63.10385269290382 + 33.16421236234331i	3704.51238036162096 + 2395.74543692760744i	1.47.15	60.21184405875418 + 36.79603695968672i	3739.452146070120954 + 2480.03484800936044i
1.47.17	58.13031023473962 + 40.124069857608601i	3060.170870676449795 + 2527.60790552294665i	1.47.19	55.539230730494275 + 43.313825250703680i	2748.3375527043546 + 2541.2788089467748i
1.47.21	52.84508883375408 + 46.375695254804043i	2445.49622843651319 + 2523.365986179872843i	1.47.23	50.04101178374234 + 43.67817865334940i	2153.104855763415799 + 2475.85666492450631i
1.47.25	47.13148835766681 + 52.146799921300214i	1872.566114714725927 + 2400.48457682943838i	1.47.27	44.100923247190863 + 55.667717416834950i	1605.23565970885347 + 2298.79482070368671i
1.47.29	42.09549395118 + 57.466581311295502i	1307.103267540943327 + 2127.183044709871083i	1.47.31	38.01594238091283 + 60.00092308700551i	1021.954470312831 + 1925.847403101283i
1.47.33	34.21490816014295 + 62.418061931686367i	896.481364829280210 + 1489.24657641620744i	1.47.35	30.61237891424535 + 64.738154069104482i	606.089670351295240 + 1655.242455147571813i
1.47.37	26.824527631292050 + 66.961524678937536i	516.256279252521474 + 1440.95013596525222i	1.47.39	22.81284943081215 + 69.087805826528866i	358.79141765243425 + 2107.532252761624116i
1.47.41	18.58807148847252 + 71.115508171923977i	225.779138493152686 + 955.840838410595084i	1.47.43	13.962687080890800 + 73.031594482331602i	191.84601050896646 + 686.845293408200611i
1.47.45	11.595718458841768 + 74.860467991804043i	44.023980847727998 + 401.292441996162020i	1.47.47	9.266577786193669 + 76.560591756092959i	113.780602078969761 + 98.754428718298768i
1.48.1	76.8731394045627 + 7.460861896763666i	5825.868835809653566 + 2049.6845800000000i	1.48.3	73.51244422171280 + 12.7358140074148i	5578.164014287266178 + 127.920307019614771i
1.48.5	73.1943773521336 + 17.479079947908978i	5248.548314619990379 + 1648.98848902441118i	1.48.7	71.199156770851618 + 12.7358140074148i	4915.856272914416369 + 1938.5260528628674i
1.48.9	69.106622649231923 + 25.93699277766585i	4579.177962208709687 + 1677.731880251776147i	1.48.11	66.91860383386817 + 29.801602966210123i	4241.57614724250429 + 2360.6709735296277i
1.48.13	64.635805385305267 + 33.47037202664307i	3905.524941685834165 + 2478.283705107052523i	1.48.15	62.258032975014886 + 36.978054679794341i	3573.123163400714826 + 2570.278253299189881i
1.48.17	59.784268835575766 + 40.310550171501921i	3246.212742094314763 + 2625.072411721325352i	1.48.19	57.12724686149521 + 43.5644674341381i	2926.42555015226067 + 2645.504718291978182i
1.48.21	54.540820819962384 + 46.634627828384161i	2615.38356071692311 + 2633.919176504005001i	1.48.23	51.765112218987580 + 49.603887599471985i	2314.441658085602090 + 2592.322624674896901i
1.48.25	49.37857547474077 + 51.684528913624077i	2070.5697497972713 + 2745.36627252597126i	1.48.27	46.818866512515618 + 55.667717416834950i	1605.23565970885347 + 2298.79482070368671i
1.48.29	42.76527154657654 + 57.87562350255253i	1486.09760442053826 + 2304.03616014013773i	1.48.31	40.917581276101666 + 60.04478953882225i	1029.299501897937490 + 1928.6302465441101i
1.48.33	36.12951409937328 + 62.854711064353552i	1009.446596116296746 + 1988.46850872870548i	1.48.35	32.58692726906517 + 65.208929017090497i	

Table D.2. (continued)

m, n, r	$m, n = c_{0:r} + m, n + 1$	$m, n = c_{0:r} + m, n + 1$	$m, n = c_{0:r} + m, n + 1$	m, n, r	$m, n = c_{0:r} + m, n + 1$	$m, n = c_{0:r} + m, n + 1$
1.53,41	31.40894901159463 + 71.390194463122131	716.300207648542823 + 1899.814552861247071	367.94352575162304 + 1372.9175929838171	1.53,42	27.48762012343805 + 76.3511873569578261	530.356674508675837 + 1645.6679876754510591
1.53,43	23.54087263621690 + 68.25081818661954	122.28871778466954 + 775.004206633129781	107.862325932149753 + 80.6102117410837021	1.53,44	18.963259532149753 + 80.6102117410837021	231.093732643240344 + 1082.42838152217311
1.53,44	14.242675049204225 + 82.503232410366671	391.79155543491625 + 110.49700226015946191	9.053305476473979 + 84.299053445795361	1.53,45	86.308941470186355 + 73.5834316972390981	44.819673921516120 + 451.2556941027293831
1.53,45	2.997990546471317 + 85.986988212131941	7077.924628691157523 + 1488.017482121195964	84.541828054232695 + 12.991405256684901	1.54,41	82.676016189228927 + 17.84537357263491	7421.89600300835252 + 935.2003914035730081
1.54,41	80.720638235515679 + 22.337291364235959	6348.602560348399493 + 2278.23228752625861	6348.602560348399493 + 2278.23228752625861	1.54,42	82.676016189228927 + 17.84537357263491	1781.12231344360401 + 1924.165809881585801
1.54,42	76.54784670851305 + 30.5489604492083141	5595.828337448727277 + 2799.509397909915491	4842.5505693633687 + 3123.393596830031551	1.54,43	73.30452734350899 + 34.3536412396361331	5973.473841596825877 + 2566.6904719257683801
1.54,43	72.030548889422050 + 37.9927467265589061	4842.5505693633687 + 3123.393596830031551	4842.5505693633687 + 3123.393596830031551	1.54,44	64.617691101870349 + 48.07388993512095701	1258.15684801620291 + 4983.430253404791071
1.54,44	67.1753006874048 + 44.8407338899726711	4104.662675852091525 + 3285.9365234557390071	3394.70713215259841 + 499.8450526604241491	1.54,45	47.231623689774021 + 54.201846723177331	4470.841797445496276 + 3223.20117413059446741
1.54,45	83.97099116309060 + 51.1919467157800911	2723.49118162794321 + 3231.27625197319511	2100.926567268438248 + 3002.690027513803541	1.54,46	47.231623689774021 + 54.201846723177331	3745.488958958905167 + 3314.1005109349882851
1.54,46	56.9994116366650875 + 57.109260190120181	1536.63051628684655 + 2694.3148845498130871	4104.662675852091525 + 3285.9365234557390071	1.54,47	40.23646914554320 + 70.2439637455107401	3053.624025869117304 + 3275.024858480849661
1.54,47	50.43154807283031 + 62.634341679590521	1536.63051628684655 + 2694.3148845498130871	1536.63051628684655 + 2694.3148845498130871	1.54,48	33.433025745888894 + 74.886599440169231	1810.89106005182740 + 2860.400411730194861
1.54,48	44.023747245129670 + 67.794786732670644	4104.662675852091525 + 3285.9365234557390071	4104.662675852091525 + 3285.9365234557390071	1.54,49	25.542660490774071 + 79.21047075959281	1279.388057202070 + 2505.494338841180451
1.54,49	37.11002766932374 + 72.607061587178741	623.3979413990320 + 2294.94336105640701	623.3979413990320 + 2294.94336105640701	1.54,50	19.73263972023639 + 81.50030314021321	821.21518358280163 + 2063.6219351452679991
1.54,50	29.5875658562521 + 77.0802931506454001	297.084373669923786 + 1254.344764819818791	297.084373669923786 + 1254.344764819818791	1.54,51	6.120279323653254 + 86.729324537817711	47.82766366959046 + 7542.3348377078931
1.54,51	21.267332932388621 + 81.2129062033999911	79.621144488991468 + 626.649961823324701	79.621144488991468 + 626.649961823324701	1.54,52	86.116829456750139 + 13.0294924713669801	173.836242737291040 + 948.660308644632761
1.54,52	11.754373319473688 + 84.988108526314281	690.41904327900760 + 1970.68542634699141	690.41904327900760 + 1970.68542634699141	1.54,53	82.30570782288130 + 22.4137003688766041	10.357140238346842 + 288.3754851740330671
1.54,53	87.88102782547800 + 7.604488306565771	6223.366119239523869 + 2634.2947862386918131	6223.366119239523869 + 2634.2947862386918131	1.54,54	73.6537260293639 + 38.150030314021321	6846.825290167517778 + 2335.720938421791241
1.54,54	84.25636879017054 + 17.908423265696221	4692.94057462984461 + 3335.001102273940891	4692.94057462984461 + 3335.001102273940891	1.54,55	88.164386280792925 + 30.66510966384331	5839.14113695250355 + 2876.570480968231521
1.54,55	80.2683538072005 + 26.508427099938551	5454.643121000954125 + 3069.712151956733901	5454.643121000954125 + 3069.712151956733901	1.54,56	89.84263730541628 + 51.437322550990631	5071.96871697419378 + 3217.421832688893931
1.54,56	75.94925094466337 + 34.4903158447823021	3952.18257253442447 + 3340.110270650103901	3952.18257253442447 + 3340.110270650103901	1.54,57	88.62563730541628 + 51.437322550990631	4931.8465441887539 + 3395.043396601226581
1.54,57	71.28052563452244 + 41.662784330189211	3243.860361727103282 + 3403.68814105608981	3243.860361727103282 + 3403.68814105608981	1.54,58	82.12726048237131 + 57.402280651081121	2965.06729351023864 + 3345.720527578939951
1.54,58	66.283538072005 + 26.508427099938551	2578.15916317898979 + 3259.93790074457441	2578.15916317898979 + 3259.93790074457441	1.54,59	75.6357260293639 + 38.150030314021321	2204.28999723244423 + 3147.673317521581831
1.54,59	49.1014730601049 + 65.43217552617011	4164.08759750093395 + 3546.83732643585351	4164.08759750093395 + 3546.83732643585351	1.54,60	89.84263730541628 + 51.437322550990631	3797.17642816093957 + 3555.68602349420491
1.54,60	42.5367108736266 + 70.665001382026701	492.546787822542391 + 2269.139849202678131	492.546787822542391 + 2269.139849202678131	1.54,61	73.6537260293639 + 38.150030314021321	1163.01060094715713 + 2457.0152137348995801
1.54,61	35.43367425547304 + 75.3709931413313261	932.46787822542391 + 2269.139849202678131	932.46787822542391 + 2269.139849202678131	1.54,62	23.51201208922477 + 81.799249378782571	72.25061711243409 + 1981.082706032053131
1.54,62	27.69172769797969 + 79.7404631138536451	534.691571670157563 + 1713.31763343732921	534.691571670157563 + 1713.31763343732921	1.54,63	14.29060060431797 + 85.653994897792451	123.072614005294888 + 1427.95171671516161
1.55,49	19.10193695815250 + 87.4446462261989721	45.065135571926270 + 467.8972642088379531	45.065135571926270 + 467.8972642088379531	1.55,55	8.009497668007619 + 89.129046689776621	9.32937505976385 + 114.404179066724401
1.55,53	89.243232388621 + 81.2129062033999911	7247.67572774017169 + 201.38386276201981	7247.67572774017169 + 201.38386276201981	1.55,56	89.84263730541628 + 51.437322550990631	6866.0224737936636 + 2393.4573342528391
1.55,55	85.8344312438139 + 19.58528788195511	6478.255677513145201 + 202.200545214054271	6478.255677513145201 + 202.200545214054271	1.55,57	79.746018130395935 + 30.7491579869808991	6807.47528313699122 + 9953.80565878149191
1.55,56	81.85991490688303 + 26.7451669854716491	5696.17928903962409 + 3155.42485948726261	5696.17928903962409 + 3155.42485948726261	1.55,58	70.47127457608196 + 45.2381506864098171	5306.46514341913657 + 331.948348094347841
1.55,57	77.550092018160314 + 34.624439736002751	4920.15427325806505 + 3427.3783507679481	4920.15427325806505 + 3427.3783507679481	1.55,59	85.3352177002656 + 51.6784754761761751	4538.8693029248889 + 3041.7498449021976891
1.55,58	72.91310367629528 + 41.838248940993311	1049.9789044072849 + 2396.231837006516381	1049.9789044072849 + 2396.231837006516381	1.55,60	89.84263730541628 + 51.437322550990631	2092.0752563385783 + 3841.122447120307751
1.55,59	66.23627062387054 + 54.723557705530361	628.2669936209499 + 1487.0521194612421	628.2669936209499 + 1487.0521194612421	1.55,61	82.12726048237131 + 57.402280651081121	1021.6566800214806 + 2620.33270958966041
1.55,60	62.623627062387054 + 54.723557705530361	2756.268027113908 + 3400.86213901608381	2756.268027113908 + 3400.86213901608381	1.55,62	85.3352177002656 + 51.6784754761761751	1293.756166800214806 + 2620.33270958966041
1.55,61	56.96749687711685 + 60.547321034653271	2124.061026353316907 + 3161.126120295904741	2124.061026353316907 + 3161.126120295904741	1.55,63	47.198435998920103 + 63.312883017951191	1823.96180796756234 + 3235.30041393799542051
1.55,62	50.9666657390485 + 65.9895318331976881	1552.09325904219025 + 2823.514853271787301	1552.09325904219025 + 2823.514853271787301	1.55,64	51.68232425425579 + 68.5789483597792921	1291.6566800214806 + 2620.33270958966041
1.55,63	44.410266596595207 + 71.083569387495281	1049.9789044072849 + 2396.231837006516381	1049.9789044072849 + 2396.231837006516381	1.55,65	89.84263730541628 + 51.437322550990631	1291.6566800214806 + 2620.33270958966041
1.55,64	37.111919712300 + 75.8439997970240681	628.2669936209499 + 1487.0521194612421	628.2669936209499 + 1487.0521194612421	1.55,66	82.12726048237131 + 57.402280651081121	1291.6566800214806 + 2620.33270958966041
1.55,65	30.979993901687 + 80.6999939016871	299.42933098530321 + 1302.687699168814561	299.42933098530321 + 1302.687699168814561	1.55,67	16.07383743286522 + 86.303121352931791	174.74530871961201 + 934.904544111752621
1.55,66	21.400993709377824 + 84.3797186441211411	80.088518648781726 + 649.61942895942271	80.088518648781726 + 649.61942895942271	1.55,68	6.23224039041958 + 89.872665013983451	19.446487385278285 + 298.606139582698241
1.55,67	11.82051716560569 + 88.1364484508078551	82.58634915369475 + 997.011558386919181	82.58634915369475 + 997.011558386919181	1.55,69	89.266447464189750 + 13.1036424182018261	7897.0768290646093 + 5591.56524637040451
1.55,68	91.025078784505041 + 7.642751131896621	7519.89149600338943 + 2064.2572662200127521	7519.89149600338943 + 2064.2572662200127521	1.55,70	87.47448877359792 + 25.2629280265018261	7132.198791730453195 + 2451.429455397847051
1.55,69	87.41426114117125 + 18.013569980373641	1566.64851847818210 + 3010.149752704664041	1566.64851847818210 + 3010.149752704664041	1.55,71	89.84263730541628 + 51.437322550990631	6340.464281609330587 + 3048.5052674805678471
1.55,70	85.15052105618753 + 26.837087456336361	599.76179417318989 + 3242.0601283793502671	599.76179417318989 + 3242.0601283793502671	1.55,72	80.1047768758466 + 30.891137339027801	546.03941122757378 + 406.9649627326882161
1.55,71	79.158019723032950 + 47.610638526621071	5152.48201458120367 + 3530.27226808109541	5152.48201458120367 + 3530.27226808109541	1.55,73	72.11534770466310 + 45.431215339913721	4763.70944567839165 + 3615.163913401081671
1.55,72	74.5363171693140 + 44.05436536557371	4381.193933713307160 + 3664.256012574000321	4381.193933713307160 + 3664.256012574000321	1.55,74	71.1407403203852 + 51.94649988951881	3291.99129008793445 + 3679.7677125314059261
1.55,73	69.605127176682847 + 48.7297361439947921	3640.298443086278439 + 3663.680009794664991	3640.298443086278439 + 3663.680009794664991	1.55,7		

D.1. Branch points, $c_{0,r}^n$, and Associated Eigenvalues $\lambda_{0,r}^n$ of the SWE

Table D.2. (continued)

m, n, r	$c_{0,r}^n = c_{0,r+1}^{n+2}$	$\lambda_{0,r}^n = \lambda_{0,r+1}^{n+2}$	m, n, r	$c_{0,r}^n = c_{0,r+1}^{n+2}$	$\lambda_{0,r}^n = \lambda_{0,r+1}^{n+2}$				
1.62,3	97.13842860900241	13.2782406379113441	9361.257426673853843	+1.7662421716426745411	1.62,3	95.304869149117110	18.2150102356693601	8955.33152216700729	+2.01174258295857627
1.62,7	93.389558684003731	+22.912214346105849	8537.655594931080486	+2744.6681343540511821	1.62,9	91.395878347300403	+27.277549167851177	8112.23295761343441	+31.16576624959392981
1.62,11	89.325945732708969	+31.422403708062260	7682.78153772100333	+3245.356169700467490	1.62,13	87.181091519876844	+35.380519689930455	7251.24621025667468	+3681.313112183597241
1.62,15	84.962024862096612	+39.1758259206135761	6819.92388876919039	+3889.066477181977491	1.62,17	82.668951557156004	+42.826208645838918	6390.64110710767345	+4052.8376786989497961
1.62,19	80.30175502679805	+46.345404758342991	5964.987745613836523	+4176.021095718197749	1.62,21	77.859788251809974	+49.773340300418349	5594.4403501375788	+4261.399167103184972
1.62,23	75.42139930196765	+53.031701348384791	5130.329290421955533	+411.294840982095911	1.62,25	72.747500160795525	+56.214803826263566	4723.901897414637437	+4327.7325037389746761
1.62,27	70.07417102335947	+59.295881926130161	4326.33637161097953	+4312.464326347817131	1.62,29	67.00637606602251	+62.29103382245761	3938.75911224866314	+4267.8040601464241
1.62,31	64.28621516265957	+65.193339131799121	3562.2589207997367	+4192.882976538684109	1.62,33	61.558751234963083	+68.009934942252717	3197.8993838661961	+4091.24072387476431
1.62,35	58.54487596964473	+70.743959624674361	2846.730097143729836	+3963.288882998725967	1.62,37	55.36452018916164	+73.397673661376317	2509.7973268871398	+3811.109780871490329
1.62,39	52.228461959421609	+75.973137942060431	2188.15497480850786	+4122.715890853521781	1.62,41	48.914614676017045	+78.479497897743101	1882.875358345704399	+3432.066300770445371
1.62,43	45.44877714912574	+80.895327499866198	1595.0622793521542795	+3209.051598700125641	1.62,45	41.93535858569649	+83.244121542975128	1238.8653871085693	+2964.5561490327146
1.62,47	38.25365136841745	+85.518811972052859	1076.498276519523870	+2699.410083949726881	1.62,49	34.24198388852808	+87.19489095816826	848.261724081354714	+2414.42339046410561
1.62,51	30.421253481568785	+89.8458114653043791	642.5735529625357	+2110.384217420765181	1.62,53	26.22821407569053	+91.896929321805928	461.0234453972624	+1788.061590843643464
1.62,55	21.805610633660565	+93.87134880145246491	305.42598302283466	+1448.201551364693159	1.62,57	17.09737945173130	+95.766680270735625	177.95992731672265	+1091.508627300772521
1.62,59	12.00592309667887	+97.579116207464511	131.396790997043595	+718.373466835495474	1.62,61	8.31479694292599	+99.20070542717801	19.696638324248660	+739.489410067277601
1.63,1	107.456386276159317	+7.490014012878011	100.8023158148418380	+112.193393053694291	1.63,3	90.1281973831502	+13.314712445693161	96.982909620963402	+1801.7168921476891231
1.63,5	96.88236589408084	+18.32475325726301	9257.287198122432528	+2349.010369120546021	1.63,7	94.97152496265709	+22.978478171949707	883.65638426439181	+2803.965520170297441
1.63,9	92.9833262908214	+27.361183383956851	8402.241548429505606	+1858.538541021501712	1.63,11	90.019982040013352	+31.523371067702071	7966.1962111815245	+3055.0987945260521881
1.63,13	88.7284156485645	+35.499121119529409	7528.036100839733990	+3770.329137345261329	1.63,15	86.72389567225529	+39.312973345261329	7080.875362982849279	+3986.826664318602981
1.63,17	84.28918523675516	+42.981045599670210	6653.5160246028077	+4158.881672943630292	1.63,19	81.93301028977415	+46.518835512766159	6229.614609854034910	+4289.916284596129891
1.63,21	79.50333622908212	+49.936678450300801	5792.577763303068422	+4382.7411529219313	1.63,23	76.99937949241903	+53.2433781801913001	5370.7546229082914	+4439.721402180398521
1.63,25	74.419802420743210	+56.446179695528900	4956.3879362307038	+4462.887612145256626	1.63,27	71.76316437593812	+59.55107156022499	4550.64800757626089	+4484.011272108191596
1.63,29	69.02746884101441	+62.5630783108584	4154.6549428269446	+4414.6167597988542184	1.63,31	66.102343565339557	+65.486417239451811	3769.48744695375639	+4346.262083081036981
1.63,33	63.398938692908467	+68.3246375917603791	3396.197639052824798	+4250.075798305232638	1.63,35	60.51961883374740	+71.08072462580896	3035.821446871008447	+4127.282704701768301
1.63,37	57.2320344256876	+73.757172102028164	2689.388895934973746	+3978.609562964774468	1.63,39	54.018619844208884	+76.356038955348551	2357.93271686367509	+3806.151403002626581
1.63,41	50.7823334256876	+78.87897797018891	2042.506702349620127	+3609.7834026204316	1.63,43	47.3938168592287	+81.32731628599404	1744.181646492454547	+3359.773875698381621
1.63,45	43.887878493816449	+83.701964937865191	1464.074167465792016	+3149.98755312778892	1.63,47	40.54268732112133	+86.0033434054347	1203.354887605712141	+2888.25846502828651
1.63,49	36.48011249315815	+88.232225958954387	963.27009808686154	+2606.392368820403221	1.63,51	32.54891227667401	+90.38790866972321	745.16843587937412	+2305.174102357661021
1.63,53	28.438727378991592	+92.469946671921511	550.53912740213454	+1958.386612509784891	1.63,55	24.119266105747474	+94.47173224749208	381.067623669045458	+1647.721455988105331
1.63,57	19.548027619149205	+96.407684292023673	238.72464261901190	+1292.94926884197181	1.63,59	14.64858134001243	+98.258489698417243	125.964619907902453	+921.702847171004261
1.63,61	9.280375796192298	+100.027416412305641	45.965490357298876	+54.408466453551881	1.63,63	6.051689418701653	+101.697002844744034	3.971119390077420	+1300.017428424765051
1.63,65	102.3701310073917	+6.790014012878011	100.8023158148418380	+112.193393053694291	1.63,67	90.1281973831502	+13.314712445693161	96.982909620963402	+1801.7168921476891231
1.64,1	98.45967504189397	+18.32475325726301	9257.287198122432528	+2349.010369120546021	1.64,3	94.97152496265709	+22.978478171949707	883.65638426439181	+2803.965520170297441
1.64,3	94.570361608727261	+27.361183383956851	8402.241548429505606	+1858.538541021501712	1.64,5	90.019982040013352	+31.523371067702071	7966.1962111815245	+3055.0987945260521881
1.64,5	89.38351758473501	+35.499121119529409	7528.036100839733990	+3770.329137345261329	1.64,7	86.72389567225529	+39.312973345261329	7080.875362982849279	+3986.826664318602981
1.64,7	85.907950478191509	+42.981045599670210	6653.5160246028077	+4158.881672943630292	1.64,9	81.93301028977415	+46.518835512766159	6229.614609854034910	+4289.916284596129891
1.64,9	81.14469824043617	+49.936678450300801	5792.577763303068422	+4382.7411529219313	1.64,11	76.99937949241903	+53.2433781801913001	5370.7546229082914	+4439.721402180398521
1.64,11	76.08895065133653	+56.473577727381	4694.074167465792016	+3149.98755312778892	1.64,13	71.76316437593812	+59.55107156022499	4550.64800757626089	+4484.011272108191596
1.64,13	70.0448762658668	+62.830245019167161	3757.8862093098022	+4463.169426195232512	1.64,15	66.102343565339557	+65.486417239451811	3769.48744695375639	+4346.262083081036981
1.64,15	65.05206860875717	+68.3246375917603791	2874.6065626094947	+4149.022769037710532	1.64,17	60.51961883374740	+71.08072462580896	3035.821446871008447	+4127.282704701768301
1.64,17	59.3330400857228	+74.10997406381194	2027.9692622994216	+3788.87398251842806	1.64,19	54.018619844208884	+76.356038955348551	2357.93271686367509	+3806.151403002626581
1.64,19	52.63855389090854	+79.278164362153781	1468.3964010909873	+3363.9838018416892	1.64,21	47.3938168592287	+81.32731628599404	1744.181646492454547	+3359.773875698381621
1.64,21	45.931576729523310	+83.701964937865191	1084.735619008446520	+2845.132513997160222	1.64,23	40.54268732112133	+86.0033434054347	1203.354887605712141	+2888.25846502828651
1.64,23	36.1280729363414	+87.402931959178591	647.021754180684397	+2184.69624621250081	1.64,25	34.347680554097896	+90.91813225742698	464.03599158530012	+2501.86204907532822
1.64,25	30.61287969363414	+93.02995919378591	307.294590898482227	+1496.659004719578871	1.64,27	26.3855270612961	+95.0866004533961	248.45899175808932	+1849.3882519080241
1.64,27	21.92927397959179	+97.023217233046824	131.804923508984227	+741.53712820530491	1.64,29	17.48822789011094	+98.91974823032768	178.96224090362064	+1127.18769593140249
1.64,29	12.0637988174328	+100.027416412305641	45.965490357298876	+54.408466453551881	1.64,31	6.3715413263015	+101.697002844744034	3.971119390077420	+1300.017428424765051
1.65,1	102.3701310073917	+6.790014012878011	100.8023158148418380	+112.193393053694291	1.65,3	90.1281973831502	+13.314712445693161	96.982909620963402	+1801.7168921476891231
1.65,3	100.03686565471078	+18.32475325726301	9257.287198122432528	+2349.010369120546021	1.65,5	94.97152496265709	+22.978478171949707	883.65638426439181	+2803.965520170297441
1.65,5	96.15692075048446	+27.361183383956851	8402.241548429505606	+1858.538541021501712	1.65,7	90.019982040013352	+31.523371067702071	7966.1962111815245	+3055.0987945260521881
1.65,7	91.92344749336286	+35.499121119529409	7528.036100839733990	+3770.329137345261329	1.65,9	86.72389567225529	+39.312973345261329	7080.875362982849279	+3986.826664318602981
1.65,9	87.3833633635318	+42.981045599670210	6653.5160246028077	+4158.881672943630292	1.65,11	81.93301028977415	+46.518835512766159	6229.614609854034910	+4289.916284596129891
1.65,11	82.783976810881748	+49.936678450300801	5792.577763303068422	+4382.7411529219313	1.65,13	76.99937949241903	+53.2433781801913001		

Table D.2. (continued)

m, n	$m, n+1$ $c_{0,r}$	$m, n+2$ $c_{0,r+1}$	m, n $c_{0,r}$	$m, n+1$ $c_{0,r+1}$	$m, n+2$ $c_{0,r+2}$				
1.69,25	84.39244212465993	+ 57.753486576888744	6460.8391406291716	+ 5288.9778536465107	1.69,27	81.824598246909915	+ 60.932812110153251	6007.03607462828426	+ 5319.8498509101531
1.69,29	79.18647592756064	+ 64.100501873561740	5561.634082459020647	+ 5318.36020574272338	1.69,31	76.76522031164307	+ 67.141508906166390	5126.627329894467082	+ 5285.992610285497725
1.69,33	73.692858921536272	+ 70.100036299860258	4700.133992024125276	+ 5224.0781727456517	1.69,35	70.832374454743105	+ 72.979272766212492	4508.005964007156763	+ 5133.83301792578747
1.69,37	67.09514826341965	+ 75.781939535002621	3884.23755194536852	+ 5016.7643772260335	1.69,39	64.875434581656680	+ 78.103526772774499	3495.73543775105748	+ 4872.74805834926086
1.69,41	61.0943646019293	+ 81.166470315524061	3121.5570038035126	+ 4703.9151099448336	1.69,43	58.576323719185674	+ 83.751938582071939	2762.5711549997463	+ 4510.7965680084782
1.69,45	55.287682037282	+ 86.2680817316141	2419.6774115103359	+ 4294.25518275028198	1.69,47	51.899112436088465	+ 88.715968490579090	2093.9647109154875	+ 4055.120534447276843
1.69,49	48.40331613787796	+ 91.0966333696560	1786.419692363705963	+ 3794.18259957732140	1.69,51	44.91960230054144	+ 93.409847886603858	1498.1084771408032	+ 3511.25151001223942
1.69,53	41.05493158978054	+ 95.65606134621472	1230.158311169367320	+ 3209.9331364534879	1.69,55	37.178572743356590	+ 97.83660929853431	938.776689471222922	+ 2888.123953498512675
1.69,57	33.14704953881872	+ 99.94496404508250	760.2776058971952	+ 2547.445371643839828	1.69,59	28.380969397286405	+ 101.99424755656880	561.11865008122131	+ 2188.5817946163437
1.69,61	24.52137574698810	+ 103.920218625138187	387.95686969203923	+ 112.249017330047975	1.69,63	19.83221739907804	+ 105.874940412133551	242.73974274192758	+ 1419.0581089491519
1.69,65	14.85811331903978	+ 107.70569678618360	127.87072396357175	+ 109.61379636145721	1.69,67	9.3999486868576	+ 109.4578450842960	46.58910862849245	+ 511.92653461338440
1.69,69	3.079950078135794	+ 111.22741971515453	3.999210686272515	+ 141.670551483625271	1.70,1	111.458294654210692	+ 7.860919477622121	12392.47480529184608	+ 1270.65135860300328
1.70,3	109.7287843939095	+ 13.53207170962301	11961.0639392099605	+ 2051.605060002492571	1.70,5	107.92001714402162	+ 18.652229294919688	11509.67045306239359	+ 2688.27613657005390
1.70,7	106.0371253320977	+ 23.4165987394737561	1044.70368097776497	+ 3224.701366624909951	1.70,9	104.08361634993331	+ 27.911165123396316	9006.429988623276945	+ 3681.78818489560234
1.70,11	101.06126842529557	+ 32.187256254359061	10090.05082581551746	+ 4017.9001867885289	1.70,13	97.671627035452568	+ 36.278133318463351	9076.11768984730070	+ 4403.5713454708397
1.70,15	93.85737135899470	+ 40.209546643119584	9120.7520717317228	+ 4682.87054161030073	1.70,17	85.9360350100263	+ 43.997666751706184	8638.38487876339314	+ 4914.0446675260788
1.70,19	93.305882603443877	+ 47.656923209213053	8152.81973086626682	+ 5102.09100537453257	1.70,21	90.95228089184631	+ 51.198319288596480	7673.3001724728629	+ 5428.7606860965475
1.70,23	88.5329920874462	+ 54.63078004250642	7198.54180937805059	+ 5357.02830716142081	1.70,25	86.04579141550377	+ 57.96166346036303	6726.7609930928570	+ 5429.027561269118
1.70,27	83.49090512491544	+ 61.197112584502712	6268.09597058129931	+ 5466.784612415723202	1.70,29	80.867198613512542	+ 64.34236041990749	5814.62310384192101	+ 5411.8728067329304
1.70,31	78.1730049747699	+ 67.40164132799019	5370.37130674711760	+ 5445.703260389585921	1.70,33	75.406572941401109	+ 70.378876406221355	4936.33110863795084	+ 5389.741240276292922
1.70,35	72.54480170097668	+ 73.89067445393679	4513.4662711524978	+ 5305.16994391275116	1.70,37	69.6483236150972	+ 76.09942183202424	4102.721441755296635	+ 5193.11471316743524
1.70,39	66.651212352447658	+ 78.84739476205739	3705.02964408844116	+ 5054.61879866406587	1.70,41	63.71160203451484	+ 81.5244528455069	3321.308282512627274	+ 4809.656624932369
1.70,43	60.40427319202326	+ 84.130954260263863	2952.528310991460785	+ 4702.14483897896587	1.70,45	57.14598540078186	+ 86.66872589789148	2599.59078880523985	+ 4489.9513853182164
1.70,45	55.7909143622561978	+ 89.13888143727263	2263.491993883678788	+ 4254.9302437999604	1.70,49	50.332664009339389	+ 91.542273635410865	1945.20721591206826	+ 3997.7925289617796
1.70,47	51.73004973694500	+ 93.87949807910959	1664.777218655080560	+ 3791.385313317317468	1.70,53	43.7425420399072	+ 96.150889749738583	1366.20010481260782	+ 3410.49886475746621
1.70,49	39.251402149334553	+ 98.35650644459379	1072.86868214097364	+ 3566.0831995054547	1.70,57	37.865570713205	+ 101.496108463267913	5630.373092804456	+ 5406.25601319656747
1.70,51	31.153024916755992	+ 102.56910623379916	659.568701037646747	+ 2407.3071007196283	1.70,61	26.8294948759995	+ 104.57449092970854	472.53890617242032	+ 2033.16593646679482
1.70,53	22.77964536565712	+ 106.51070262389411	312.56410625329271	+ 1641.9132109110848	1.70,65	17.42491257353558	+ 108.37546099879800	181.790204671688	+ 1528.12367468519250
1.70,67	12.227049041810	+ 110.16501767370471	82.95695570587249	+ 100.39311732800885	1.70,69	6.413286819050765	+ 111.87347635810488	19.99505210905701	+ 70.543873402771396
1.71,1	113.0290638043990	+ 7.87592990924759	12745.10422870158023	+ 1292.057015910134169	1.71,3	111.3002318296782	+ 13.559795485472268	12308.280265120954	+ 2087.6887600507607
1.71,5	109.49621607495839	+ 18.696307096475131	11851.25171180574261	+ 2273.391544878541446	1.71,7	107.1018947537730	+ 23.475510187781065	11340.41606902488747	+ 3285.578023788416294
1.71,11	105.6577184734527	+ 30.80826619539584	10900.0845701734327	+ 3452.870543382184829	1.71,11	103.0473091491493	+ 33.997666751706184	9801.87236933431291	+ 4764.046675260788
1.71,15	101.56718818485435	+ 34.383479200707676	9923.0375186693853	+ 4495.5142076738009	1.71,15	99.4180607265100	+ 40.330054157963232	9101.071640692725510	+ 5783.8922060260290
1.71,17	97.20884174874233	+ 44.134157959961361	8929.201603620749665	+ 5024.23383692013563	1.71,19	94.8245483382004	+ 47.80964385236874	8449.1969332611877	+ 5220.14660392809677
1.71,21	92.58088504061978	+ 51.376532972162628	7622.4455307084631	+ 5374.73259100405591	1.71,23	90.17164184127733	+ 54.816755024236599	7480.2611167624454	+ 5490.5054030393636
1.71,25	87.69645174470261	+ 58.164684315535934	6073.8874864960328	+ 5569.82667274072681	1.71,27	85.3456932516041	+ 61.41749524054578	6534.36931307674867	+ 5614.4462046990453215
1.71,29	82.54480170097668	+ 65.851372105971501	4702.86868214097364	+ 5856.3127643787161	1.71,31	78.29352021944585	+ 67.657675124083255	4746.33828293682765	+ 5446.25601319656747
1.71,33	77.11671284006178	+ 70.653288606211587	3571.88295955349658	+ 6252.3978405787614	1.71,35	74.25430657124488	+ 73.570354553271909	3419.82963130441734	+ 5237.6058879330957
1.71,37	71.39586372110474	+ 76.41171272329298	4326.67963108151456	+ 5703.895971082045435	1.71,39	68.22048582757858	+ 79.1797209064354	3198.22607206871328	+ 4894.7611932955680
1.71,41	65.36426879243090	+ 81.87641009232465	3526.705551681635110	+ 5078.7857324546019	1.71,43	62.23578370662288	+ 84.50349623451744	2438.9290063038105	+ 4456.11867812849037
1.71,45	58.99418560018594	+ 87.062409970004893	2785.3102739930740	+ 4686.99560517584116	1.71,47	56.07118264528403	+ 89.554315401606672	1799.61562894930230	+ 3928.1694341671875
1.71,49	52.24858693081011	+ 91.98012347888524	2110.92604973727388	+ 4020.922393471120813	1.71,51	48.179317048020230	+ 94.9849800819086	1138.75047804766188	+ 3416.9253458668681
1.71,53	45.10745315007142	+ 95.8584562547021	1505.75394706736818	+ 3562.978404571614	1.71,59	33.33458934015650	+ 103.13197004224311	760.102355191608208	+ 2628.67063349709076
1.71,57	37.3972525918249	+ 101.03186713973364	990.1985895874662	+ 2891.85288339236639	1.71,63	24.647858749690460	+ 107.132525288214261	390.118237582890786	+ 1816.03194251171039
1.71,69	19.94835183694983	+ 109.029256258033769	243.999182719297077	+ 1461.0672447395803	1.71,67	14.24786491626218	+ 110.85400284854760	126.07598132231949	+ 1038.90254810129355
1.71,71	9.43757126805010	+ 112.60197530300918	46.75847185641542	+ 600.84426784517864	1.71,71	3.08824997690218	+ 114.26402994479688	4.00806308132231949	+ 145.55101239158395
1.72,1	114.0472810596578	+ 3.89086754975721	13163.7281058448296	+ 1480.6075180729178	1.72,3	110.857823734023	+ 13.53868076421291	12660.460679268280	+ 2087.6887600507607
1.72,5	110.07280469460215	+ 18.7397663249202	12197.780096794800556	+ 2786.50051294538878	1.72,7	106.9693837000116	+ 23.33389280074066	11721.0099082326010	+ 3346.6591874286928
1.72,9	104.5715775656642	+ 28.08502220828483	11234.70500860802526	+ 3825.694676107613	1.72,11	105.239755918832628	+ 32.6448458544783	10741.8069383625696	+ 4236.46936191741205
1.72,13	103.16211589636636	+ 36.486731797786813	10244.965801897124037	+ 4857.58659409651177	1.72,15	101.9173816905790	+ 40.448814625155358	9340.60903996825846	+ 4885.3041606651496
1.72,17	98.81346857878962	+ 44.268656361013591	9247.66792726394884	+ 5134.40347083054664	1.72,19	96.54257174095218	+ 47.960213234895320	8750.6490720972519	+ 5338.6818670793926
1.72,21	94.2079598964079	+ 51.534238438616832	8256.695757164166527	+ 5501.2425160965541	1.72,23	91.89090471091829	+ 54.99950661277766	8077.1429348941494	+ 5624.8524973954786
1.72,25	89.1473208292597	+ 58.806729379848521	7169.61801309784901	+ 5708.64310612667783	1.72,27	85.1850254433477	+ 61.35860739907016	7185.84726406210621	+ 5957.6054698193061
1.72,29	84.2199529184163	+ 64.814711365197397	6336.36089290157626	+ 5781.1012239419068	1.72,31	81.5524281186289	+ 67.909733209632961	6575.7162932515159	+ 5767.638917295306
1.72,33	78.82155537521573	+ 70.92335519108554	5424.770623608454	+ 5273.725371598598	1.72,35	76.0163032061336	+ 73.85883809441693	4984.6073008017809	+ 5650.74811963718224
1.72,37	73.13805710447276	+ 76.718984188798643	4556.0953179208242	+ 5549.701881251905	1.72,39	70.18308408674615	+		

D.1. Branch points, $c_{\sigma,r}^{m,n}$, and Associated Eigenvalues $\lambda_{\sigma,r}^{m,n}$ of the SWE 217

Table D.2. (continued)

m, n, r	m, n, σ $c_{\sigma,r}^{m,n} = c_{\sigma,r+1}^{m,n+2}$	m, n, σ $\lambda_{\sigma,r}^{m,n} = \lambda_{\sigma,r+1}^{m,n+2}$	m, n, r	m, n, σ $c_{\sigma,r}^{m,n} = c_{\sigma,r+1}^{m,n+2}$	m, n, σ $\lambda_{\sigma,r}^{m,n} = \lambda_{\sigma,r+1}^{m,n+2}$
1.75,7	9.50686049269559+11.88981218652941i	47.1221109004058+9.6340378683966044951i	1.75,7	-3.105845696563446-120.3483535956506131i	-4.024871159995857+153.317133689786901i
1.76,1	120.88757704436720+7.948327208589531i	14582.31865960148484+1399.781130287518181i	1.76,1	19.1685666470143+13.701183029867301i	14118.527261007284324-2269.465431608365634i
1.76,5	110.735291398588203+18.9077422057285623i	13633.3927599660606+2984.566775695765045i	1.76,5	115.2106262136978+23.758029777258269i	13133.41367941303957+3592.67275066880829i
1.76,9	113.58416171970797+28.397762354745499i	12622.92511181533107+114.3065865760451i	1.76,9	111.59433580798016+32.70451268345212i	12105.164684878732529-4568.8915775884459i
1.76,13	109.53608468680859+26.885492106477081i	11582.70929557932389+4059.47738611404921i	1.76,13	107.41896642401585+30.907349010829864i	11057.7010133825863304-5294.61171081514544i
1.76,17	105.24079599499383+44.787830210009908i	10531.972127184124474+5579.311326011209377i	1.76,17	103.001801677878879+48.54082690774313i	10007.135388995726316-5817.52581855883234i
1.76,21	100.720248012726798+52.177396376156665i	9484.62968497568181+2160.469681662350663i	1.76,21	98.341780505256921+55.706526407132628i	8965.76272031063630+1666.9309758063787i
1.76,25	95.20102858430356+9.1356466999136801i	8451.73782327590743+6283.13427217605633i	1.76,25	93.436647529327558-62.47098117858018i	7943.67514689380441+6363.105138215572879i
1.76,29	90.8964497836902+65.717799927701719i	7442.62942560212014+6086.59918435345753i	1.76,29	88.28119676875099-68.88002651525274i	6949.5964598989478-6421.17700212187241i
1.76,33	85.60881245920789+1.79632548310413881i	6465.54280473928+6402.2441221099922i	1.76,33	82.866502675122512-74.969095151654486i	5991.38423635782601+6533.07211512123831i
1.76,37	80.05834123575998+77.901013102485621i	5528.019570264005+6274.8725743483101i	1.76,37	77.180433362503251-80.761512963252926i	5076.3279151704810-6168.5862250267244i
1.76,41	74.23054282519199+83.552763667117151i	4637.17510387301081+6035.347667139487381i	1.76,41	71.20607473802828-86.276636834600213i	4211.42032264130839-5876.0742117554664i
1.76,45	68.10404597591310+88.947376681178921i	3799.92196958497016+5691.5650022149047i	1.76,45	64.921004912809749+91.528428612546918i	3403.5437505411318+5482.7350307653245i
1.76,49	61.65293988877757+94.058846938132191i	3023.1599674517808+5250.35114459419331i	1.76,49	58.295190049002564-96.56291753687015i	2659.66399073809278-4995.173261711945997i
1.76,53	54.82283406011790+98.9335660249198061i	2315.97585027299757+4777.932119875628591i	1.76,53	51.287748305644776+107.286944043273767i	1984.02089812879794-4441.91356424125414872i
1.76,57	47.6238295130836+103.563216873670221i	1679.86561409565560+4800.071011083561475i	1.76,57	44.1454237681334-105.781073623998771i	1393.40871628422514-3760.806161881993870i
1.76,61	39.928073942460884+107.950089286383641i	1129.069501188425647+3042.197509291143433i	1.76,61	36.8997616336412+110.051890933239903i	887.18018464471353+3024.88753452540673i
1.76,65	31.64780333060453+112.09178534926651i	671.045774202304983+2629.512534506839071i	1.76,65	27.235912246174006+114.068705466465887i	480.3224686964413+2216.68771377808971i
1.76,69	22.59770469782725+115.981079622747431i	313.94057529816678+1787.01646434651534i	1.76,69	17.677037532330925+117.826659689892935i	184.38410195682336+141.306494849744681i
1.76,73	12.37694079557204+119.60189926518424i	84.014201501160755+879.20187032425541i	1.76,73	6.480081666672810+121.301393139039092i	20.19732604726017+401.3011839239751431i
1.77,1	12.49515253375428+7.9622244626972721i	14964.572521241739522+1421.4607885735214423i	1.77,1	120.741647554709203+13.728343727463236i	14495.401726771614385+2386.0897959469434i
1.77,5	118.950754965272495+18.948348588386941i	14004.66966274728267+3034.40979359170843i	1.77,5	117.091372876442449+23.812271088116266i	13498.88907592470430+3654.62374070958774i
1.77,9	115.166550749906264+28.480738818674414i	12982.40621749999636+4189.506891152478554i	1.77,9	113.178347108629652-32.786417282345927i	12458.4467575920531+4625.65925257565865i
1.77,13	111.128186665819822+36.981809350214135i	11929.64597234031657+5053.228145280749231i	1.77,13	109.107402628526880+41.01808074390979i	11398.930453331607907+5397.84125335908304i
1.77,17	106.845540710221812+44.91317570692805i	10865.644594045857957+5551.5854792522919i	1.77,17	104.104202510732737+41.680993815931750i	10393.91004592770467+5938.37671512021040i
1.77,21	100.322585412698477+42.32598047807317i	9804.329497036896946+6414.57650114558671i	1.77,21	99.1071077181961616-75.876982493438861i	9278.20974747567130+6038.8868643957928i
1.77,25	97.589263758603251+59.321954497098121i	8756.57279317806417+6047.63678635171661i	1.77,25	95.08653166882611-69.67262108387882i	8241.07665579046035+14.8419623269883i
1.77,29	92.55219536545624+65.934608153962921i	7732.23205803153698+6567.27346655042907i	1.77,29	91.54320315876099+122.0336692951272i	7231.21533030605106+6586.5049605376636i
1.77,33	87.29485222446004+72.213713835061668i	6738.97925001165640+6573.95047009328961i	1.77,33	84.56939236835336-75.23639870184231i	6256.4419044141291+6530.8922902417581i
1.77,37	81.77139073181159+78.185475630919481i	5784.4945283476970+6458.5032545080611i	1.77,37	78.917028972463986-81.063473861615662i	5324.008205547217343+6357.8679910200531i
1.77,41	75.958189297281769+83.872584738557563i	4875.8406803849321+6292.984044676115846i	1.77,41	72.98244144419142+86.417050667827335i	4440.84105701985842+6075.79664716583102i
1.77,45	69.928501521698306+84.32058072605315i	4079.86561409565560+4800.071011083561475i	1.77,45	66.44858810012061+105.781073623998771i	3687.38330681711+5691.907708618617i
1.77,49	63.505117020794277+94.454276110216256i	3223.34474284607173+3544.02485942710800i	1.77,49	60.72544926555535+96.94424892710800i	2849.55172722539842+5212.98368318761i
1.77,53	56.753309938100522+99.369582187071217i	2493.257191539187716+4939.6638263979208i	1.77,53	55.237516468187855+101.736217316450649i	2155.38878612517950+4644.749043702809104i
1.77,57	49.13903460115231+104.024740484196781i	1836.91410178308882+4328.92365768008771i	1.77,57	49.538052582337808+106.289326147241615i	1538.851823765492704+3992.852596116140232i
1.77,61	42.016096753472866+108.475934785817261i	1262.2863198071039+2637.196437284349086i	1.77,61	38.018112757120406+110.602288189027416i	1008.38557490486463+3262.586579999198420i
1.77,65	33.86644055014133+132.88827296260481i	778.42869262326206-2869.65416304498431i	1.77,65	31.64780333060453+112.09178534926651i	573.8406892649816-2459.02116321841407i
1.77,69	25.067393708675295+156.61293844040101i	596.2488276676287+3031.268588045988809i	1.77,69	20.21251258061862+114.671706329230901i	247.82799607770103+1827.02830319756422i
1.77,73	15.114088815194492+120.29704712742355i	310.190743052134167+1126.79502921958271i	1.77,73	9.54420315876099+122.0336692951272i	47.296730951480576+60.62917217203341i
1.77,77	3.114017007398344+123.691734222166051i	4.03269503826777+157.194769027169059i	1.77,77	124.030636255411481+7.975943222959544i	15351.76338909285206+1443.184016163069132i
1.78,1	122.3146895622612019+13.7551534898922961i	14877.217812044699603+2342.78741564066301i	1.78,1	120.526111104084805-19.98842863223366i	14340.894697921121406+3084.37824543486393i
1.78,5	114.60776393992210+23.865813551859671i	13869.321211190663987+3716.739046236045312i	1.78,5	116.74876372645129-28.47629292999664i	13386.856066997991314-4202.92134569254870i
1.78,9	114.78811148979711589793+32.86741721015123578i	12762.9456701720151+4736.6846366570764i	1.78,9	117.9825951203162+105.781073623998771i	12381.5919263360104-3760.806161881993870i
1.78,13	106.42477432983335+41.1273377887308924i	11743.5010059379887+5501.416683971152954i	1.78,13	108.449477623848836+45.036837732620548i	11204.33066462492480-5804.19445812281345i
1.78,17	100.11555036993503+48.819265574052621i	10665.39812184987386+6059.671261945270181i	1.78,17	103.941727585275601+52.485686010125081i	10218.10821251251178-6271.148202595929509i
1.78,21	91.599007822519326+56.0451078892173481i	9595.761891408968683+6444.38177475242340i	1.78,21	99.196738744461294-59.50497486612171i	9066.90176401594991+6572.763185145160971i
1.78,25	96.734402449959632+62.871533842634321i	8543.64309127000706+6667.23734737595015i	1.78,25	94.21134776188538-66.150078592325130i	8027.03432634759907+6726.64631925359953i
1.78,29	91.1278501524196878+84.98098478053151i	7538.068714811726+662.38270819216161i	1.78,29	90.761640623505961-72.86760285657070i	7017.6356836561671+6746.8467467561i
1.78,33	86.268763235795191+75.499840323569245i	7268.82221160340627+607.97888052031671i	1.78,33	87.492429424121677-78.465784924934666i	6046.3480807.950656+1067.381755611i
1.78,37	80.94901624619988+81.360976742523261i	5577.113230001249+6548.13456484844i	1.78,37	84.23921938801841+84.18762621925089i	5119.9894973926788-6425.627803603025i
1.78,41	74.52860104949404+86.9476937823105521i	4675.8082627396088+6276.6642732104151i	1.78,41	71.69514452322687-89.624730677410398i	4245.3081879150708+6100.9915719542955i
1.78,45	68.5054523477738+92.274263994921371i	3829.62587368763116+5926.30240080144261i	1.78,45	65.34528207490319+94.84346513041866i	3429.3071661604046+5678.9842759103007i
1.78,49	62.045619665708279+13.513364944072781i	3045.315303824529562+5432.200398965417662i	1.78,49	60.76667848137257+99.79866859922302i	2676.520341922344623+5162.8807479863172i
1.78,53	55.785293404231808+15.127938115619015i	2339.83404337942919+6421.609645090959754i	1.78,53	55.237516468187855+101.736217316450649i	2147.28314437720170+4861.901179343720201i
1.78,57	47.894859876329748+106.782871676729840i	1690.590656960698516+4226.651287069393571i	1.78,57	44.082843178425584-108.992440746098126i	1407.066483206551117-3874.03685144711031i
1.78,61	40.14089558096150+111.142645906620371i	1135.736614838405785+3202.2530830721065i	1.78,61	36.54219079509828+113.233061943671188i	892.228650673666838+3111.842576987516622i
1.78,65	31.80915067682145+115.262972030190753i	674.664915040929372+2703.504817731423749i			

Table D.2. (continued)

m, n, r	$\lambda_{0;r}^{m,n} = \lambda_{0;r+1}^{m,n+2}$	m, n, r	$\lambda_{0;r}^{m,n} = \lambda_{0;r+1}^{m,n+2}$
2, 2, 1	6.102540356949614 + i.6847638136174061	2, 3, 1	4.105156484215650 + 5.9227350658440496i
2, 2, 2	32.0875861487368474 + 34.487534676801381i	2, 3, 2	2.26582712027141 + 8.74807768453067i
2, 2, 3	53.56137110170611 + 49.638515941219321i	2, 3, 3	4.40574479793623 + 9.294389714166075i
2, 2, 4	80.376039435949536 + 65.668070414405067i	2, 6, 3	6.33722309080594 + 9.739915760209533i
2, 2, 5	109.649461249734259 + 99.874080075743143i	2, 7, 1	10.980074056517031 + 7.03893055722324i
2, 2, 6	149.649461249734259 + 99.874080075743143i	2, 7, 2	4.629138586623777 + 12.552028695435473i
2, 2, 7	204.75441220447553 + 178.043025829063822i	2, 7, 3	9.93556181902666 + 10.44808878158699i
2, 2, 8	279.2805718343691 + 492.152865189961861i	2, 8, 7	2.4358705380044652 + 15.146579362179107i
2, 2, 9	374.446011209116184 + 18.316234296956101i	2, 9, 3	11.866348566585869 + 10.740571478359586i
2, 2, 10	500.69169854608070 + 117.876711993110590i	2, 9, 7	4.606341649488908 + 15.765290336173946i
2, 2, 11	662.1777629190639 + 126.012736403749801i	2, 10, 3	13.364818667036719 + 11.00353250197448i
2, 2, 12	871.525710630890151 + 14.542695936779409i	2, 10, 7	6.29144665851361 + 16.30279491673473i
2, 2, 13	1150.78078089148 + 19.521857266786085i	2, 11, 1	17.482820216659340 + 7.690583126361104i
2, 2, 14	1509.28078089148 + 19.521857266786085i	2, 11, 5	12.21643900459271 + 14.224396063855474i
2, 2, 15	2019.585686041580 + 79.9331768083366i	2, 11, 9	4.95299695013199 + 18.956019363165186i
2, 2, 16	2671.178302395029 + 14.851253732078784i	2, 12, 3	16.70802697381598 + 11.461446441695077i
2, 2, 17	3519.2081435184197 + 20.03168168607726i	2, 12, 7	10.2799345047075 + 12.33583788759058i
2, 2, 18	4603.228982489857405 + 8.04922959312671i	2, 13, 1	16.811825124377230 + 199.00519216368476i
2, 2, 19	6039.29095014855 + 15.105661852017079i	2, 13, 5	2.548584923292930 + 21.447767913975164i
2, 2, 20	8010.25932951752294 + 24.63279466012309i	2, 13, 9	12.379130440845256 + 11.663561552198820i
2, 2, 21	10593.62035706280397 + 18.301669596034067i	2, 13, 13	12.69542571894926 + 17.604732464963025i
2, 2, 22	14059.222581493300 + 23.256794015108071i	2, 13, 17	5.077990345047075 + 12.33583788759058i
2, 2, 23	18510.74738637452137 + 15.9281898327381763i	2, 14, 1	14.487287283714512 + 17.96649247382285i
2, 2, 24	24451.09847965486846 + 7.81920288893248i	2, 14, 5	13.740857167654913 + 22.721475484744366i
2, 2, 25	32289.2489857405 + 8.04922959312671i	2, 14, 9	12.69542571894926 + 17.604732464963025i
2, 2, 26	42500.69169854608070 + 117.876711993110590i	2, 14, 13	5.077990345047075 + 12.33583788759058i
2, 2, 27	55913.2081435184197 + 20.03168168607726i	2, 14, 17	14.487287283714512 + 17.96649247382285i
2, 2, 28	73639.29095014855 + 15.105661852017079i	2, 14, 21	13.740857167654913 + 22.721475484744366i
2, 2, 29	9790.25932951752294 + 24.63279466012309i	2, 15, 1	15.86838833094567 + 25.302736926542226i
2, 2, 30	13016.62035706280397 + 18.301669596034067i	2, 15, 5	23.2593714630083 + 12.19068131659769i
2, 2, 31	17451.09847965486846 + 7.81920288893248i	2, 15, 9	18.101655622457983 + 18.614020149983862i
2, 2, 32	23121.50078089148 + 19.521857266786085i	2, 15, 13	13.078549421581902 + 20.924871737688786i
2, 2, 33	30509.29095014855 + 15.105661852017079i	2, 15, 17	15.86838833094567 + 25.302736926542226i
2, 2, 34	40167.62035706280397 + 18.301669596034067i	2, 16, 1	23.2593714630083 + 12.19068131659769i
2, 2, 35	52566.222581493300 + 23.256794015108071i	2, 16, 5	18.101655622457983 + 18.614020149983862i
2, 2, 36	69009.74738637452137 + 15.9281898327381763i	2, 16, 9	13.078549421581902 + 20.924871737688786i
2, 2, 37	90639.29095014855 + 15.105661852017079i	2, 16, 13	15.86838833094567 + 25.302736926542226i
2, 2, 38	11900.25932951752294 + 24.63279466012309i	2, 16, 17	23.2593714630083 + 12.19068131659769i
2, 2, 39	15721.50078089148 + 19.521857266786085i	2, 17, 1	17.41751546283125 + 23.74934719181533i
2, 2, 40	20721.50078089148 + 19.521857266786085i	2, 17, 5	2.623563457359253 + 27.784764128401766i
2, 2, 41	27871.50078089148 + 19.521857266786085i	2, 17, 9	8.4279927978056429 + 12.345176217180304i
2, 2, 42	37041.50078089148 + 19.521857266786085i	2, 17, 13	19.740166697747100 + 18.906530469171756i
2, 2, 43	49491.50078089148 + 19.521857266786085i	2, 17, 17	13.42908942040983 + 24.206102734761365i
2, 2, 44	65641.50078089148 + 19.521857266786085i	2, 18, 1	5.28319824060583 + 28.466167412298066i
2, 2, 45	86141.50078089148 + 19.521857266786085i	2, 18, 5	6.648753076434426 + 12.49114539589862i
2, 2, 46	111741.50078089148 + 19.521857266786085i	2, 18, 9	13.078549421581902 + 20.924871737688786i
2, 2, 47	145591.50078089148 + 19.521857266786085i	2, 18, 13	15.86838833094567 + 25.302736926542226i
2, 2, 48	191141.50078089148 + 19.521857266786085i	2, 18, 17	23.2593714630083 + 12.19068131659769i
2, 2, 49	252191.50078089148 + 19.521857266786085i	2, 19, 1	17.41751546283125 + 23.74934719181533i
2, 2, 50	334241.50078089148 + 19.521857266786085i	2, 19, 5	2.623563457359253 + 27.784764128401766i
2, 2, 51	443291.50078089148 + 19.521857266786085i	2, 19, 9	8.4279927978056429 + 12.345176217180304i
2, 2, 52	594341.50078089148 + 19.521857266786085i	2, 19, 13	19.740166697747100 + 18.906530469171756i
2, 2, 53	794391.50078089148 + 19.521857266786085i	2, 19, 17	13.42908942040983 + 24.206102734761365i
2, 2, 54	105444.50078089148 + 19.521857266786085i	2, 20, 1	5.28319824060583 + 28.466167412298066i
2, 2, 55	139549.50078089148 + 19.521857266786085i	2, 20, 5	6.648753076434426 + 12.49114539589862i
2, 2, 56	185654.50078089148 + 19.521857266786085i	2, 20, 9	13.078549421581902 + 20.924871737688786i
2, 2, 57	248709.50078089148 + 19.521857266786085i	2, 20, 13	15.86838833094567 + 25.302736926542226i
2, 2, 58	336764.50078089148 + 19.521857266786085i	2, 20, 17	23.2593714630083 + 12.19068131659769i
2, 2, 59	459819.50078089148 + 19.521857266786085i	2, 21, 1	17.41751546283125 + 23.74934719181533i
2, 2, 60	629874.50078089148 + 19.521857266786085i	2, 21, 5	2.623563457359253 + 27.784764128401766i
2, 2, 61	86141.50078089148 + 19.521857266786085i	2, 21, 9	8.4279927978056429 + 12.345176217180304i
2, 2, 62	114591.50078089148 + 19.521857266786085i	2, 21, 13	19.740166697747100 + 18.906530469171756i
2, 2, 63	155041.50078089148 + 19.521857266786085i	2, 21, 17	13.42908942040983 + 24.206102734761365i
2, 2, 64	208091.50078089148 + 19.521857266786085i	2, 22, 1	5.28319824060583 + 28.466167412298066i
2, 2, 65	280141.50078089148 + 19.521857266786085i	2, 22, 5	6.648753076434426 + 12.49114539589862i
2, 2, 66	370691.50078089148 + 19.521857266786085i	2, 22, 9	13.078549421581902 + 20.924871737688786i
2, 2, 67	49491.50078089148 + 19.521857266786085i	2, 22, 13	15.86838833094567 + 25.302736926542226i
2, 2, 68	65641.50078089148 + 19.521857266786085i	2, 22, 17	23.2593714630083 + 12.19068131659769i
2, 2, 69	86141.50078089148 + 19.521857266786085i	2, 23, 1	17.41751546283125 + 23.74934719181533i
2, 2, 70	114591.50078089148 + 19.521857266786085i	2, 23, 5	2.623563457359253 + 27.784764128401766i
2, 2, 71	155041.50078089148 + 19.521857266786085i	2, 23, 9	8.4279927978056429 + 12.345176217180304i
2, 2, 72	208091.50078089148 + 19.521857266786085i	2, 23, 13	19.740166697747100 + 18.906530469171756i
2, 2, 73	280141.50078089148 + 19.521857266786085i	2, 23, 17	13.42908942040983 + 24.206102734761365i
2, 2, 74	370691.50078089148 + 19.521857266786085i	2, 24, 1	5.28319824060583 + 28.466167412298066i
2, 2, 75	49491.50078089148 + 19.521857266786085i	2, 24, 5	6.648753076434426 + 12.49114539589862i
2, 2, 76	65641.50078089148 + 19.521857266786085i	2, 24, 9	13.078549421581902 + 20.924871737688786i
2, 2, 77	86141.50078089148 + 19.521857266786085i	2, 24, 13	15.86838833094567 + 25.302736926542226i
2, 2, 78	114591.50078089148 + 19.521857266786085i	2, 24, 17	23.2593714630083 + 12.19068131659769i
2, 2, 79	155041.50078089148 + 19.521857266786085i	2, 25, 1	17.41751546283125 + 23.74934719181533i
2, 2, 80	208091.50078089148 + 19.521857266786085i	2, 25, 5	2.623563457359253 + 27.784764128401766i
2, 2, 81	280141.50078089148 + 19.521857266786085i	2, 25, 9	8.4279927978056429 + 12.345176217180304i
2, 2, 82	370691.50078089148 + 19.521857266786085i	2, 25, 13	19.740166697747100 + 18.906530469171756i
2, 2, 83	49491.50078089148 + 19.521857266786085i	2, 25, 17	13.42908942040983 + 24.206102734761365i
2, 2, 84	65641.50078089148 + 19.521857266786085i	2, 26, 1	5.28319824060583 + 28.466167412298066i
2, 2, 85	86141.50078089148 + 19.521857266786085i	2, 26, 5	6.648753076434426 + 12.49114539589862i
2, 2, 86	114591.50078089148 + 19.521857266786085i	2, 26, 9	13.078549421581902 + 20.924871737688786i
2, 2, 87	155041.50078089148 + 19.521857266786085i	2, 26, 13	15.86838833094567 + 25.302736926542226i
2, 2, 88	208091.50078089148 + 19.521857266786085i	2, 26, 17	23.2593714630083 + 12.19068131659769i
2, 2, 89	280141.50078089148 + 19.521857266786085i	2, 27, 1	17.41751546283125 + 23.74934719181533i
2, 2, 90	370691.50078089148 + 19.521857266786085i	2, 27, 5	2.623563457359253 + 27.784764128401766i
2, 2, 91	49491.50078089148 + 19.521857266786085i	2, 27, 9	8.4279927978056429 + 12.345176217180304i
2, 2, 92	65641.50078089148 + 19.521857266786085i	2, 27, 13	19.740166697747100 + 18.906530469171756i
2, 2, 93	86141.50078089148 + 19.521857266786085i	2, 27, 17	13.42908942040983 + 24.206102734761365i
2, 2, 94	114591.50078089148 + 19.521857266786085i	2, 28, 1	5.28319824060583 + 28.466167412298066i
2, 2, 95	155041.50078089148 + 19.521857266786085i	2, 28, 5	6.648753076434426 + 12.49114539589862i
2, 2, 96	208091.50078089148 + 19.521857266786085i	2, 28, 9	13.078549421581902 + 20.924871737688786i
2, 2, 97	280141.50078089148 + 19.521857266786085i	2, 28, 13	15.86838833094567 + 25.302736926542226i
2, 2, 98	370691.50078089148 + 19.521857266786085i	2, 28, 17	23.2593714630083 + 12.190681316

D.1. Branch points, $c_{0;r}^{m,n}$, and Associated Eigenvalues $\lambda_{0;r}^{m,n}$ of the SWE

Table D.4: Branch points and associated eigenvalues for $m = 3$.

m, n, r	$\frac{m, n}{c_{0;r}} = \frac{m, n+2}{c_{0;r+1}}$	$\frac{\lambda_{0;r}^{m, n}}{c_{0;r}} = \frac{\lambda_{0;r+1}^{m, n+2}}{c_{0;r+1}}$	m, n, r	$\frac{m, n}{c_{0;r}} = \frac{m, n+2}{c_{0;r+1}}$	$\frac{\lambda_{0;r}^{m, n}}{c_{0;r}} = \frac{\lambda_{0;r+1}^{m, n+2}}{c_{0;r+1}}$
3, 1, 1	2.25344194326160	- 6.119408142529081	11, 273	29925431583	- 47046569123591181
3, 1, 2	6.178462421804212	- 6.038666389128842	38, 868	8047967762623	- 40.699885683521511
3, 1, 3	7.954373031349589	+ 8.0734378618186951	61, 436	43112767034	+ 58.62466689520892
3, 1, 4	9.679537838481016	+ 8.32995857322275	89, 470	6070015046380	+ 77.619039007122961
3, 1, 5	2.1524551817370	- 13.6858709792547	11, 366	7844813620	+ 18.216098734546031
3, 1, 6	8.408413761373746	- 11.586690629808351	64, 372	50041226623	- 89.585133654764031
3, 1, 7	13.9990880485291	- 8.20008939822151	75, 466	125749971762	- 118.2412081558443621
3, 1, 8	6.8206246032426	+ 14.50687833697131	41, 769	18170557318	+ 78.62645641100531
3, 1, 9	14.69213166051157	+ 9.027864573426063	205, 284	176825622268	+ 139.665659403400156
3, 1, 10	8.75744701101597	- 14.9687927964529	66, 851	1325907066851	- 111.423995118616021
3, 1, 11	16.331761264312494	+ 9.380581505776191	254, 255	255269969606	+ 161.732450878841320
3, 1, 12	10.651470589674066	- 15.3821429668019501	97, 958	36886175313	- 145.699374966281624
3, 1, 13	23.4088424711793	- 19.717007607942952	11, 468	839867538773	- 27.667835568886348
3, 1, 14	15.40405708979813	+ 12.840807767839081	216, 209	795302860556	+ 20.1235754270491
3, 1, 15	9.083360089359133	- 18.270880620834731	68, 959	1997293197	+ 136.1116245246454
3, 1, 16	15.383908575131731	+ 9.550912817537837	367, 523	29983385074	+ 207.572171900797979
3, 1, 17	14.254386548225456	- 16.099572729390915	177, 396	78399393586	- 218.091256512405001
3, 1, 18	27.5686065821556	- 21.038721162042791	45, 884	39094702897	- 111.892736378449733
3, 1, 19	21.199007417432726	+ 9.69991838953617	43, 779	959373553026	+ 231.25643718763091
3, 1, 20	16.005863704601872	- 16.41574425405843	225, 462	924717398596	- 255.977101184420690
3, 1, 21	9.34745484742751	- 21.529461495595625	70, 868	30230277900	+ 160.35185532555489
3, 1, 22	20.10792404351979	+ 9.83980413894421	501, 092	57860357829	+ 255.40417872085531
3, 1, 23	17.733742704855722	- 16.709220354417767	278, 971	184891743083	- 294.866951097862001
3, 1, 24	13.1594574940676	+ 22.010797095334071	104, 139	21181918749	+ 205.25482700281800
3, 1, 25	2.61821985508352	- 26.115380693490717	11, 549	285448236096	- 34.919026168321625
3, 1, 26	20.6646235821890	- 13.70232590122780	453, 163	48305812248	- 328.06227151262694
3, 1, 27	16.52692455017808	- 19.87767961832869	233, 451	175330312083	- 309.64914257139391
3, 1, 28	9.594571036937599	+ 24.76076480367952	172, 395	76994693250	+ 184.311602313464161
3, 1, 29	26.102455482028076	- 22.010797095334071	654, 866	7616616603	- 27.667835568886348
3, 1, 30	21.13620089065717	- 17.23991175935753	402, 063	388960998030	- 375.376651090624700
3, 1, 31	15.1748030133920	- 22.86846513266631	189, 158	4607233987	+ 309.485122495448802
3, 1, 32	7.591431619691627	- 27.406896208371	45, 519	845230527917	- 148.363748952478121
3, 1, 33	27.62043928941434	- 10.20870253359998	739, 251	109719876676	+ 330.23068676469871
3, 1, 34	22.818531646989381	- 17.481691509389120	471, 551	79057343606	- 216.634605553801
3, 1, 35	16.9864824497177	+ 23.25547641928022	240, 477	6660297511	+ 362.034878972292311
3, 1, 36	9.78562560778719	- 27.973656274302934	73, 819	1935682762	- 208.0733251998906
3, 1, 37	29.21779732231306	+ 10.31767974824171	828, 678	920974671739	+ 356.042473355490017
3, 1, 38	24.486732052770879	- 17.710057280120996	546, 284	10822249618	- 449.13873563560178
3, 1, 39	18.794498785357729	- 23.618715093389120	507, 669	3917767166	- 415.8448784595116601
3, 1, 40	11.87008718574221	- 28.500344651815869	108, 953	3385206345	- 269.66624359186471
3, 1, 41	2.687016083134644	- 32.453985118016546	11, 619	491625644629	- 43.04512570698527
3, 1, 42	28.58787363238888	- 14.4218114713472722	772, 607	604459018943	- 466.09428973745780
3, 1, 43	23.48281992020630	- 21.084737461286267	487, 665	1099325316	- 691.593283969525569
3, 1, 44	17.397525408298136	+ 19.59105925239738	246, 748	143006252178	+ 415.74468600241261
3, 1, 45	9.018745749842923	- 27.30922347908881	75, 125	7437439482	- 239.6790880881
3, 1, 46	32.40598380513610	- 10.532027413349433	1022, 553	3955004709	- 408.493488844832319
3, 1, 47	27.80020049011515	- 18.132173108484039	711, 364	98226761713	- 545.7853457229136
3, 1, 48	23.32590490019906	+ 24.285648341513340	428, 344	300909597109	+ 526.925575395872566
3, 1, 49	18.554231881410881	- 29.454862103473073	196, 448	4505744052219	- 397.997428895526031
3, 1, 50	7.857810152929134	- 33.767460162090888	46, 843	3007439758502	- 182.6643837387597
3, 1, 51	30.97344129620349	- 10.61816503439814	118, 974	6246548018	- 192.16696663321
3, 1, 52	29.44614733698992	- 18.32811716512542	601, 665	2256156718	- 590.970621204458
3, 1, 53	24.00834251032829	+ 24.593549954146767	502, 016	6788185042969	+ 584.06427265957542
3, 1, 54	17.76940045330273	- 29.8923645060282	252, 410	409080815721	- 464.519006004786661
3, 1, 55	10.10411624985835	+ 34.3635707705969	76, 308	1191020466	+ 255.2207000905972
3, 1, 56	35.87166324615822	- 10.7918414862929	1236, 408	98941994203	- 462.183144656104281
3, 1, 57	31.08611012777221	- 18.51223369754008	897, 114	107182513210	- 635.0230089341590
3, 1, 58	25.80882687763050	+ 24.8866646858036	581, 119	2515740466	+ 642.1926529722037
3, 1, 59	19.64802506543600	+ 30.36242457397994	312, 366	65808057745	+ 532.48604720659641
3, 1, 60	12.313591862792206	+ 34.922735764388662	112, 890	21639258083	+ 329.98029924421345
3, 2, 1	2.743823191317114	- 38.74486903257601	11, 669	951817636687	+ 31.098157868269240
3, 2, 2	35.0915072120773	- 14.98785124877942	1173, 356	2654693106	- 4612.13328969531024
3, 2, 3	20.21821429601070	- 22.664743026217172	827, 429	15448495932	- 707.98980060746987
3, 2, 4	14.623578118605163	- 28.03695492089685	514, 964	408637494330	- 664.77703302672291
3, 2, 5	11.08912519644773	- 33.168221270909125	257, 572	26313852553	- 515.02281648762636
3, 2, 6	10.294896714617739	+ 37.54630011789289	177, 392	62617380458	+ 278.63864025240904
3, 2, 7	36.76289701871307	- 10.880180349574021	1490, 216	2183212280490	- 462.66107874827576
3, 2, 8	34.5091326119335	- 18.665849878816281	1103, 387	755667431	- 726.61764849870063
3, 2, 9	29.27067082690959	- 25.4393844678954	755, 444	1710193044	+ 761.22518611435749
3, 2, 10	23.3197472693198	+ 31.074364814474020	449, 587	76260132159	+ 672.441570882310254
3, 2, 11	16.438891179640027	- 35.94975789763124	206, 117	7057871148035	- 485.07506236161494
3, 2, 12	8.080201719353126	+ 40.105702004215871	47, 952	2801603423701	+ 216.3053801497881
3, 2, 13	40.34904164535600	+ 10.96972513380022	1594, 596	603043232197	+ 544.81152746281831
3, 2, 14	35.97885280425008	- 19.03605308645107	1214, 184	5809685550	- 773.234274483317080
3, 2, 15	30.92042551782913	- 25.69234091709183	890, 555	48635128466	- 822.04399504813547
3, 2, 16	25.12057898156810	- 34.432962391241249	526, 764	19126527211	+ 744.293993993154521
3, 2, 17	18.4212407067480	+ 36.4254590530797	262, 315	412519849	+ 565.18936216733960
3, 2, 18	10.37771937232160	- 42.93204040331	47, 523	404040331	- 46.358102784622250
3, 2, 19	19.16344702048843	- 11.0382915006547	1723, 950	2544565822	- 572.86869849213390
3, 2, 20	17.39906981622698	- 19.1891208368345	1330, 073	136513124609	- 820.367953148223819
3, 2, 21	32.604931286532596	- 25.963123290390819	951, 033	6007809044	- 883.6807878382460
3, 2, 22	26.90304669324530	+ 31.775149941115946	609, 547	6976649604	+ 817.133680294344863
3, 2, 23	10.363055831108198	- 36.8771499840534951	324, 683	305412246928	- 646.8992956903669
3, 2, 24	25.64976803924405	- 21.193737532932804	1851, 324	483533670	- 28.3419367451287
3, 2, 25	27.92132705486251	- 45.405919036014432	11, 716	6949703115751	- 59.098981725351921
3, 2, 26	41.44746506631286	- 15.46948561743267	1654, 754	589616125350	- 764.79864005993072
3, 2, 27	36.83043028569717	- 22.88710537628529	1250, 710	2046350780838	- 925.90969808918285
3, 2, 28	31.564745349102875	- 29.23666215477105	871, 678	3087399522657	+ 933.44021387474297
3, 2, 29	12.68211404815072	+ 41.30712601778573	57, 608	68823984875	+ 822.900737329962
3, 2, 30	28.191406158745391	- 39.665547450190089	266, 702	272751403093	- 615.09326166500620
3, 2, 31	10.5702091569630	- 45.89560849158088	79, 324	247171917009	+ 325.349116257786307
3, 2, 32	21.00436943931866	+ 11.846633071752501	386, 753	584081812050	+ 237.48745636163971
3, 2, 33	14.50426860716576	- 17.605703074277401	188, 574	29273413957	+ 236.00881945172348
3, 2, 34	7.36492622716822	- 24.52764398382886	51, 526	3072709583	+ 120.92286357853906
3, 2, 35	2.571663561227191	+ 79.7931319574124	18, 435	306314352740	- 85.38827522019955
3, 2, 36	6.42051377817898	- 9.029246303504799	47, 523	404040331	- 46.358102784622250
3, 2, 37	8.24246345110581	+ 9.42183626464764	71, 108	1823129688	- 10.6811509306571054
3, 2, 38	10.00449270374917	+ 9.76083110144660	100, 284	262190451	+ 10.85922810344552
3, 2, 39	2.466495386168887	- 14.736164316478286	18, 438	67761859122	+ 78.76017740637572
3, 2, 40	8.63141242464210	- 13.00527322111146	73, 354	409696312831	+ 94.79336060987813
3, 2, 41	14.4268069633217	- 15.12937319656606	174, 831	1972134855647	- 134.98856835994037
3, 2, 42	6.9672064900502	+ 15.91929723324128	49, 681	9422405292	+ 85.2325169653851
3, 2, 43	15.097865049058187	+ 10.569708924714181	202, 034	243193300256	+ 159.53886791723499

Table D.5: (continued)

Table D.5: (continued) - A large table with columns for m, n, r and lambda values. It contains numerical data for various combinations of m, n, and r.

Table D.6: Branch points and associated eigenvalues for m = 5.

Table D.6: Branch points and associated eigenvalues for m = 5. - A table with columns for m, n, r and lambda values, providing branch points and eigenvalues for m=5.

D.1. Branch points, $c_{\sigma;r}^n$, and Associated Eigenvalues $\lambda_{\sigma;r}^n$ of the SWE

Table D.6: (continued)

m, n, r	$m, n = c_{\sigma;r}^n = c_{\sigma;r+1}^{n+2}$	$\lambda_{\sigma;r}^n = \lambda_{\sigma;r+1}^{n+2}$	m, n, r	$m, n = c_{\sigma;r}^n = c_{\sigma;r+1}^{n+2}$	$\lambda_{\sigma;r}^n = \lambda_{\sigma;r+1}^{n+2}$
5.21.1	30.2488701588577/0 + 15.7983734816303191	888.060604119624031 + 457.345364932912201	5.21.3	27.836389190530998 + 17.587395609765451	751.96608069566741 + 517.284403029297781
5.21.5	25.215333678637723 + 20.6917814833808254	583.981043816452939 + 532.10167772803121	5.21.7	22.36856106561527 + 23.2954832199167571	464.706780340184594 + 512.532792422552571
5.21.9	19.27068349288981 + 26.667973936007621	322.92260932287198 + 644.158927745804841	5.21.11	15.88053618141161 + 29.1748949956780571	215.50011913892912 + 590.74877660536151
5.21.13	12.128264931957355 + 31.4607415371723071	127.60254723759700 + 295.2110514734288461	5.21.15	7.87658724872873 + 35.5282594158795821	63.08094886104897 + 179.942630211240861
5.21.17	2.76731178659007 + 36.364285120648191	27.66471851275822 + 46.524369662180481	5.21.19	31.8631315851781400 + 94.943458725084041	985.9518860048266 + 91.19420267977021
5.22.1	29.40842568571308 + 17.84423040828361	822.47714629691675 + 559.4894965615691	5.22.23	26.902070865227909 + 21.694947531327031	666.50129725824794 + 581.9002947767781
5.22.7	14.11072923780424 + 24.235178958919651	520.57223874630313 + 568.4812212082661	5.22.27	11.086035061354639 + 27.0399002011241121	387.7682797033291 + 525.32914385259341
5.22.11	77.955123106668203 + 29.61444819699191	269.642465495980218 + 546.2991995610179861	5.22.31	21.18547476094945 + 31.975143238921551	170.28307408994177 + 34.3206832886656241
5.22.15	10.1594235672821 + 31.12793673670611651	92.67977452777440 + 251.829034358075521	5.22.35	5.50174194295163 + 36.0678852051342031	41.318005702755867 + 120.80867839949291
5.23.1	33.4057493986842 + 14.038679435365001	1088.8921704232933 + 525.477881545661481	5.23.39	31.19433867391832 + 17.792461855812691	918.1170910522210 + 603.0327339315691
5.23.5	28.57912951183737 + 21.409546878784483	754.28157493230524 + 632.50465686740211	5.23.43	25.837697738146211 + 24.290856903005201	599.86025765397742 + 625.429929870707841
5.23.9	22.877984861498387 + 27.390331218450901	457.472784143872843 + 557.7285800242760421	5.23.47	19.73484091754947 + 30.036304131354521	329.73041296855005 + 523.312656741468231
5.23.13	16.182304900794864 + 32.40355106865635971	219.35789680555121 + 435.166923536264201	5.23.51	12.333692101505729 + 34.6904550066051131	129.4003974128429 + 325.738014370776341
5.23.17	7.9891162099564954 + 36.7204494401261951	63.6256619582632 + 197.113699029589331	5.23.55	2.75159811844244 + 38.5326367914184601	27.68802479230981 + 50.59038280956351
5.24.1	5.07700017901208 + 14.215755911927321	196.86720739421571 + 560.205933467859711	5.23.59	35.75287304663996 + 18.152297059417901	1018.8910680386625 + 646.8154566675579391
5.24.5	30.0475171787974 + 21.6385115409758941	847.29057639972861 + 683.87021084229461	5.24.1	35.51562564391639 + 24.810937427066821	684.527161260421735 + 683.28425727176881
5.24.9	24.650025169041058 + 27.729253564295401	533.141182310680733 + 501.272079310092191	5.24.15	12.12333863155565 + 30.4259486463313561	395.65371604380197 + 591.705624218729691
5.24.13	18.13919290042371 + 32.91890424624641	274.64032664116329 + 657.6443563089534901	5.24.19	41.462724027798448 + 35.2027409531106931	172.89718917048759 + 401.55876697699041
5.24.17	10.311876260770899 + 37.3312341192923721	93.71508970075695 + 275.559696149470401	5.24.23	5.68817525373316 + 39.2446202924889891	41.507944553636438 + 131.3939162562711111
5.25.1	36.68092490114634 + 14.3420074216205041	1309.875423218156584 + 595.34930533848011	5.25.3	34.587156005197516 + 18.3246257095167061	1124.76878616515748 + 961.166828348401921
5.25.5	31.908966423250721 + 21.8578584161328171	945.51800226309960 + 735.965904737983271	5.25.7	29.254032747038629 + 25.0796492042994541	774.5342083393573 + 742.1306313024379051
5.25.9	26.404985721876759 + 28.050119819412081	614.32354801070067 + 515.912880802178021	5.25.11	34.236834074466209 + 30.7022502998238801	467.32087447113351 + 661.4037949071655481
5.25.13	20.0427745875856 + 33.3563116348765821	335.98283820666473 + 878.61660292079461	5.25.15	16.45952072460390 + 38.82253724215231	222.91310534737661 + 479.17291216181911
5.25.17	12.52283076374669 + 37.9064382216756291	131.065215407318931 + 356.0703532893606391	5.25.19	8.09914778353785 + 39.9048516322304961	642.93211949076630 + 214.204744803280211
5.25.21	2.775638858302242 + 41.7035525796830701	27.09995666169380 + 54.6358819531837271	5.26.1	38.28267543138305 + 14.4642514662330671	1427.10821731068301 + 650.89195873794081
5.26.1	36.060587162783008 + 18.4904425285734071	1235.74279150873628 + 736.058270652678261	5.26.5	33.563635063487271 + 22.0682078190867021	1048.92977052056023 + 788.7582626232107201
5.26.5	30.946518052849278 + 23.437053780004141	869.8524686937611 + 801.7949991262860401	5.26.9	28.145149291401289 + 28.31766567683001	700.969903844745859 + 873.79511653582091
5.26.9	25.14429542750073 + 31.1620744868625451	544.65536888691333 + 732.340679387514871	5.26.13	21.921280472352947 + 33.772212297914301	403.26601217235041 + 657.136079986038681
5.26.13	18.448380413636794 + 36.1997201282820151	279.25327060201955 + 558.488668051572341	5.26.17	14.621313117281513 + 38.450673594348181	175.318117721378513 + 438.540224982806181
5.26.17	10.452845157517734 + 40.5253511025797961	94.67745328660221 + 299.177434168038921	5.26.21	5.69937628268529 + 42.4161702788562291	41.685526899736688 + 141.93866172036261
5.27.1	39.88278708967767 + 14.5818668904062201	1550.95973380647333 + 668.87170316739411871	5.27.3	37.62796803500971 + 18.649090377866961	637.809204411375803 + 781.4769739043147371
5.27.5	31.99333083576568 + 23.702286202758941	157.23263676392861 + 683.87021084229461	5.27.7	32.1213849897240594 + 33.2868583824291	159.130297242579797 + 873.77591957338691
5.27.9	29.872383996145700 + 28.61539998433151	793.07315465880733 + 848.218562734383201	5.27.11	22.61656668480000 + 31.206719297126851	6251.80020373257269 + 804.455492420526201
5.27.13	23.727564565872482 + 34.16947593442011	476.39089393388724 + 733.992767988369501	5.27.15	12.383490753414627 + 36.654188820780771	341.76123963266269 + 649.4120581737199701
5.27.17	16.715849348383017 + 38.9675581612716761	226.209450314057250 + 522.865394300200231	5.27.19	12.69804604930430 + 41.111803702486811	132.61291392769712 + 386.25081864436311
5.27.21	8.19117624362630 + 43.0837116053898361	64.60497416237446 + 231.2138856910194461	5.27.23	2.798061957604203 + 44.8672242353252771	27.730725281290297 + 58.6644082574621771
5.28.1	41.80136357240632 + 14.665921591282821	1679.02456783832159 + 703.110330549454351	5.28.3	40.80776698454927 + 18.94999891882491	1472.9386184339882 + 827.186998731587351
5.28.5	36.856125684266482 + 24.647202990166971	1271.24864228708569 + 896.11886604098551	5.28.7	34.30645246760350 + 25.86073398017867661	1076.30258277491125 + 923.56227520406021
5.28.9	31.58827629944148 + 28.933881798644071	890.48774379069938 + 915.898780438169411	5.28.11	22.6911738255105783 + 31.8361734735160451	716.0703371851847 + 897.699641613034611
5.28.13	20.00496048889987 + 34.54939819260381	555.27450352886066 + 812.162601236549081	5.28.15	12.291176942124544 + 37.088364826734341	410.31029238981096 + 721.8614716082411
5.28.17	18.728939217718720 + 39.4600227505181871	283.53487471845756 + 608.944830556791351	5.28.19	14.8896707417463 + 41.6683763488600651	177.57145619362052 + 475.328445595396531
5.28.21	10.58391744155555 + 43.712275080424681	95.57595678469174 + 322.704612141904331	5.28.23	5.687224399316383 + 45.5836177886040661	41.85219425808575 + 152.4496768691915351
5.29.1	43.061291889477829 + 23.22484178109671	1812.0977571222847 + 801.7949991262860401	5.29.3	40.30761697658743 + 18.94999891882491	159.130297242579797 + 873.77591957338691
5.29.5	38.495118491402645 + 22.6520703604370681	1390.1250046450941 + 951.403257326140871	5.29.7	35.974914763460575 + 26.0501594286842141	1187.38841234788053 + 955.598972732901921
5.29.9	33.2940648407505 + 29.065130356531951	993.28871223917270 + 984.436296038884261	5.29.11	34.0030064407395 + 32.1531732984651431	1103.08531629940991 + 952.103219642178301
5.29.13	27.408217186287287 + 39.19462461927481	639.846150591271225 + 891.5924637832512391	5.29.15	24.170026980303682 + 37.9041046994294591	648.7905260712795 + 805.763273959267041
5.29.17	20.698846501010683 + 39.930466164053021	347.13094165807574 + 696.700694681456591	5.29.19	16.954196735565681 + 42.39841308916811	229.2805701709862 + 566.3111538194482361
5.29.21	12.86123696659265 + 38.591372360185231	134.08512346981352 + 416.269381687654101	5.29.23	8.28149335420525 + 38.591372360185231	104.88449133916837 + 273.9352846646461
5.30.1	10.0939133112371 + 48.0276854414770231	27.75031340910482 + 478.3781342233861	5.30.3	10.9719368734908 + 14.9101427212453661	1950.17544990671066 + 776.748616596298201
5.30.5	42.4731500837809 + 19.09247554515531	1730.39032581944813 + 307.6709823253171	5.30.7	41.029892082069340 + 22.828366237623671	1514.218117127118230 + 106.344307165932921
5.30.9	37.67351929234705 + 26.2705782259336531	1303.68729985082648 + 1048.3651555914941	5.30.11	9.0978651769426 + 29.467363800329441	110.410928546613974 + 1053.84180055103331
5.30.13	32.48102666574972 + 32.45822058112591	909.497180354465627 + 1027.359675248176721	5.30.13	29.198281146571301 + 35.265223754891241	730.04496889533844 + 972.191977250403361
5.30.15	26.204901185338980 + 39.300353807095271	565.12658293412521 + 891.050268248483271	5.30.17	22.635216864784805 + 40.3810256861978941	416.864312954891299 + 786.904157647604461
5.30.19	18.592414900118 + 46.8934265198919041	287.5924126918018 + 391.85016379292921	5.30.19	6.51091412691061 + 47.185816379190941	622.44907242579797 + 873.77591957338691
5.30.23	10.70631459102390 + 46.8934265198919041	96.41813493928344 + 346.158134939283441	5.30.25	5.130985926269984 + 48.74761033927941	42.00904305991462 + 196.33416773647821

Table D.6: Branch points and associated eigenvalues for $m = 5$.

Table D.7: Branch points and associated eigenvalues for $m = 6$.

m, n, r	$m, n = c_{\sigma;r}^n = c_{\sigma;r+1}^{n+2}$	$\lambda_{\sigma;r}^n = \lambda_{\sigma;r+1}^{n+2}$	m, n, r	$m, n = c_{\sigma;r}^n = c_{\sigma;r+1}^{n+2}$	$\lambda_{\sigma;r}^n = \lambda_{\sigma;r+1}^{n+2}$
6. 6. 1	2.535162563188484				

Table D.7: (continued)

Table with 4 columns: m, n, r; c_0:r; m, n+2; lambda_0:r; m, n+1; m, n, r; c_0:r; m, n+2; lambda_0:r; m, n+1. It contains numerical data for various combinations of m, n, and r.

Table D.7: Branch points and associated eigenvalues for m = 6.

Table with 4 columns: m, n, r; c_0:r; m, n+2; lambda_0:r; m, n, r; c_0:r; m, n+2; lambda_0:r; m, n+1. It contains numerical data for various combinations of m, n, and r.

Table D.8: Branch points and associated eigenvalues for m = 7.

Table with 4 columns: m, n, r; c_0:r; m, n+2; lambda_0:r; m, n, r; c_0:r; m, n+2; lambda_0:r; m, n+1. It contains numerical data for various combinations of m, n, and r.

D.1. Branch points, $c_{\alpha,r}^{m,n}$, and Associated Eigenvalues $\lambda_{\alpha,r}^{m,n}$ of the SWE 223

Table D.8: (continued)

m, n, r	$c_{\alpha,r}^{m,n} = c_{\alpha,r+1}^{m,n+2}$	$\lambda_{\alpha,r}^{m,n} = \lambda_{\alpha,r+1}^{m,n+2}$	m, n, r	$c_{\alpha,r}^{m,n} = c_{\alpha,r+1}^{m,n+2}$	$\lambda_{\alpha,r}^{m,n} = \lambda_{\alpha,r+1}^{m,n+2}$
7.30.1	42.52420212253506 + 18.149187128239983i	1766.288128678755356 + 843.76548090586060i	7.30.3	40.17286420034854 + 22.14512862672263i	1546.50314407262780 + 953.28112072178419i
7.30.5	37.62023251622247 + 25.716663674548052i	1334.091172463971425 + 1009.07340513057320i	7.30.7	35.026844029192674 + 28.99823468117785i	1130.43070512392626 + 1023.41325724374880i
7.30.9	32.215801163919404 + 32.048028979339762i	937.4421626452960 + 4003.3774144986291i	7.30.11	29.3704863073718 + 34.898361996013083i	757.110893445950182 + 953.2313252150767i
7.30.13	26.0547927397811 + 37.5691124612076659i	591.45252206238708 + 876.108611718596762i	7.30.15	22.63879849899176 + 40.072818271055331i	442.55960441685677 + 774.48894333306475i
7.30.17	19.02692927385259 + 42.416904498044993i	312.686466827295135 + 650.470798612154066i	7.30.19	15.075702113615350 + 44.60454577184732i	240.36401823987076 + 505.8960883191784i
7.30.21	10.725155403758452 + 46.634472831616269i	120.766361736270028 + 342.41664420304831i	7.30.23	7.5537253282776 + 48.49891110863134i	66.102517451659398 + 161.32261023815747i
7.31.1	44.13605672838189 + 18.287601196423665i	1902.8598628928248 + 888.99004734848482i	7.31.3	41.80240818302877 + 22.32083582743165i	166.857403495038852 + 1007.416231103136922i
7.31.5	39.31842029794203 + 25.930458774656465i	1455.810146170304279 + 1070.772306933873846i	7.31.7	37.161455644747789 + 29.25191176472941i	124.458077370624379 + 1092.14106843004625i
7.31.9	33.942290290436233 + 32.343369184405895i	1042.512368720404885 + 1078.360232032737581i	7.31.11	31.004523031587617 + 35.27445522042869i	853.09086571195354 + 1033.78543403767345i
7.31.13	27.86675289408997 + 37.95459870225892i	677.754847309188425 + 965.88143273755775i	7.31.15	24.56870646622109 + 40.507266160192600i	518.511379520213723 + 864.28073742208919i
7.31.17	21.021263327919467 + 42.901459374139110i	374.4843512049325 + 743.9733617099961i	7.31.19	17.200632300775896 + 45.1492625838347876i	287.022879870983008 + 602.5114547096748856i
7.31.21	13.033966151094678 + 47.242977808383199i	159.903697547961286 + 441.56795841632940i	7.31.23	8.32920001935827 + 49.180919586376703i	89.659769064415016 + 262.56978005128600i
7.31.25	2.846023544986199 + 50.949434048841563i	51.785639202163480 + 66.10420121136340i	7.32.1	4.397307430938176 + 18.421498920652365i	204.467062415156989 + 932.85909714565437i
7.32.1	43.428321291495983 + 22.490224039232111i	1810.308589840527702 + 1061.600872686235173i	7.32.3	40.982611716069577 + 26.137046017654793i	1582.701623881239584 + 1133.141648282651470i
7.32.3	38.595065804099154 + 29.440685620203522i	1362.966616608442337 + 161.68503443800826i	7.32.5	35.65875585158098 + 32.62829478627531i	1152.962774506628421 + 1154.306822708079180i
7.32.5	32.6452362303097 + 35.64232980241819i	954.59308669881245 + 115.45291856563641i	7.32.7	29.69938082086612 + 38.32328383478761i	769.738842733774031 + 1048.34836691557646i
7.32.7	26.44706417096335 + 40.924812926138507i	600.391262561239273 + 955.35352605951645i	7.32.9	22.9828603715152 + 43.371583786690911i	448.511013721726161 + 939.13805212609396i
7.32.9	19.27666818750390 + 45.67058460390970i	316.30932341880793 + 501.02761739890761i	7.32.11	15.255055612240680 + 47.82333448210246i	260.292056118413163 + 542.814622562926878i
7.32.13	10.838243104527786 + 49.82778053311645i	121.522990232159671 + 366.051999964260119i	7.32.15	5.80270265628584 + 51.675833167056069i	66.24066959686847 + 171.882394067892250i

Table D.8: Branch points and associated eigenvalues for $m = 7$.

Table D.9: Branch points and associated eigenvalues for $m = 8$.

m, n, r	$c_{\alpha,r}^{m,n} = c_{\alpha,r+1}^{m,n+2}$	$\lambda_{\alpha,r}^{m,n} = \lambda_{\alpha,r+1}^{m,n+2}$	m, n, r	$c_{\alpha,r}^{m,n} = c_{\alpha,r+1}^{m,n+2}$	$\lambda_{\alpha,r}^{m,n} = \lambda_{\alpha,r+1}^{m,n+2}$
8. 8. 1	2.686505191832351 + 12.703398412561352i	66.993245738841736 + 14.5326216092174331i	8. 9. 1	5.086727408730243 + 13.451056164498548i	80.567627929013113 + 38.81506457453207i
8.10.1	7.207364983300353 + 14.066948948945089i	101.340216207095068 + 65.766223667610130i	8.10.3	6.1622843177086 + 16.45653784926519i	67.77998393517430 + 20.25891504717704i
8.11.1	9.197890646464675 + 14.602962864047828i	128.522722130864963 + 94.899324485307898i	8.11.3	5.130653917000092 + 17.173781932324100i	80.06170887241893 + 53.10860520355289i
8.12.1	11.082883634074511 + 15.072360020462711i	161.726950735166668 + 125.8783715059231i	8.12.3	7.33640256045397 + 17.793604564948524i	100.94436557587927 + 88.40677236951815i
8.12.5	2.648997050830888 + 19.954127675883806i	66.71366286548207 + 25.247894941448976i	8.13.1	12.91964383153202 + 15.497700068989700i	200.71964441506948 + 158.46259210625482i
8.13.3	9.39321626102360 + 15.94297673309506i	128.57439362162930 + 125.865574183449439i	8.13.5	10.502924917914 + 20.66327189146196i	202.902982941798 + 65.8154221173645i
8.14.1	14.714357224497717 + 15.882941176778051i	245.34487414969641 + 192.477404846955398i	8.14.3	11.355888778922630 + 18.83821462332072i	162.517037090700676 + 165.224544026045045i
8.15.1	7.480028708021058 + 21.290771799394305i	101.164718122245958 + 107.71250102401181i	8.15.3	2.6672448183596690 + 23.336346803622273i	66.4945277611534 + 206.9275826412426i
8.15.5	46.72791703973868 + 16.236740472558493i	295.491099296849825 + 227.762008113667946i	8.16.3	12.35059414464374 + 19.289931080719271i	202.6883288936653 + 90.27715821628371i
8.16.5	9.595987262318898 + 21.856380288546061i	129.33668665341482 + 153.78454938926954i	8.16.7	5.286142778641089 + 24.044294788123473i	100.56449522884476 + 77.78765382732573i
8.17.1	18.254115046506968 + 16.654184081199931i	264.22117596603107i	8.17.9	18.254115046506968 + 16.654184081199931i	204.30222474460199 + 248.8686330231079i
8.17.5	11.61897114463731 + 22.372844772426141i	164.044821121289888 + 200.803120573818916i	8.18.7	7.61808261980930 + 24.640671769992900i	101.5725312123336 + 127.97316969491760i
8.17.9	2.69038485439107 + 26.65376027394877i	66.6938533572408 + 34.38534908425837i	8.17.1	19.93668200885446 + 16.86898867998269i	412.030711274006340 + 301.75415396821539i
8.17.13	16.91375299174141 + 20.0914514754595479i	299.8191728175124 + 292.83982886828872i	8.17.5	13.93783288126854 + 22.84885158911326i	204.9849219186374 + 249.5919161007557i
8.17.17	9.971876117121825 + 25.260816789187256i	130.27466486816618 + 180.250181785734309i	8.17.9	5.363132841463818 + 27.36309536297796i	80.207069714621142 + 89.338116706807259i
8.18.1	21.655695065644166 + 17.154355708890265i	478.307402394404789 + 340.28139441754201i	8.18.3	12.289738305884589 + 32.464220503032067i	356.95420441303555 + 338.09497757280897i
8.18.5	15.46419617000770 + 23.290829721052607i	251.943326739023377 + 299.99072445325297i	8.18.7	11.86174113880957 + 25.795716258303666i	163.716735352152921 + 234.56851873919362i
8.18.9	7.746927409672943 + 28.0077411966272045i	102.018436787741862 + 146.50626952504064i	8.19.1	2.71436933189171 + 29.93034183868791i	66.701671203196710 + 38.742589884619377i
8.19.1	23.242426584057509 + 17.4226165625729417i	549.86258870411882 + 379.73527167091156i	8.19.3	20.454980024631048 + 20.78866730632130i	419.565014834361545 + 384.5544368066240622i
8.19.5	17.31938431426253 + 23.703671654358644i	304.763498152322313 + 351.897041152535163i	8.19.7	13.81719884592136 + 26.29256913203268i	207.56514669485188 + 190.72823784216717i
8.19.9	9.69938473174328 + 28.601628925507103i	131.244674792519760 + 205.862832008575836i	8.19.11	5.435804651148969 + 30.642080367505031i	80.35416648787683 + 105.615185616960407i
8.20.1	25.00145406056968 + 17.6992092169193148i	626.601321608940049 + 425.8620908372567i	8.20.3	22.194135961623092 + 42.3654419556748i	487.64545761154065 + 234.23039361522i
8.20.5	19.14177783693019 + 24.091228357208841i	363.32456322783697 + 405.17768015095439i	8.20.7	11.766167533440268 + 26.756939563151786i	255.93749881860091 + 348.574826825131709i
8.20.9	12.084616870538531 + 29.1915972502605696i	167.376572917540554 + 267.26180727674277i	8.20.11	7.89604355493071 + 31.29456970848368i	102.48309501370979 + 164.666114903982244i
8.21.3	23.973907473753154 + 33.179246050107972i	66.713704538414959 + 403.3718371290700i	8.21.1	6.68999522679158 + 17.91560374999301i	708.6742142887418 + 491.19430752325191i
8.21.5	23.916887850895428 + 21.406717969808706i	561.12240866060769 + 480.7013833964800i	8.21.5	20.93737459363470 + 24.45659103624436i	427.52986751951107 + 446.19430752325191i
8.21.7	17.691023261228491 + 27.193157795399546i	309.626190319399967 + 408.000037974481586i	8.21.9	14.22221865424626 + 29.66684221923695i	210.07489978413876 + 330.556230404833536i
8.21.9	10.133040388758468 + 31.89936660845949i	132.197081925731169 + 235.97187210884167i	8.21.13	6.25723364975968 + 21.691503311916922i	63.947188908136995 + 59.27896111045438i
8.22.1	28.32823650497455 + 18.143530901774159i	795.876253342801760 + 503.10263767304782i	8.22.3	19.55025202507862 + 27.604681959529067i	399.530083562460849 + 468.84940085430078i
8.22.5	27.102688024345007 + 24.80228470168011i	497.30270548586056 + 515.528531869416611i	8.22.7	12.289738305884589 + 32.464220503032067i	168.974654914036801 + 299.24995590512328i
8.22.9	16.00611818088343 + 30.150606593122613i	259.09588971650272 + 395.614079697212428i	8.22.11	2.76075608675959 + 36.408403549718123i	66.72826273750253 + 47.23156007171527i
8.22.13	7.977242823046248 + 34.553734454798679i	102.940204475336131 + 182.537020525412743i	8.22.15	37.23223443849957 + 21.96330018486530i	72.128058586884813 + 880.7884745323350i
8.22.17	24.465201879944420 + 25.1304402972189750i	779.578729180874850 + 572.44727395690170i	8.22.19	23.80154216614983 + 37.9433216450822i	485.19852762879874 + 353.166989168294663i
8.23.1	10.823185469156396 + 30.607146182815040i	314.254106401518015 + 462.31936196655740i	8.23.1	5.366213854190370 + 32.994809837734415i	212.644158665691220 + 369.59121300683321i
8.23.5	10.28440081442511 + 35.1683191921242128i	133.113595495013868 + 255.582459218385457i	8.23.5	14.5676719755927 + 37.125745257653413i	80.660313971997949 + 122.658867741387724i
8.23.9	31.625960458739254 + 18.567277344579079i	985.76455220516528 + 589.0732675436285i	8.23.9	29.009190153451350 + 22.200549392872657i	813.50217702789590 + 632.159166681134236i
8.24.1	20.30662182566463 + 25.442075530339131i	653.304188354554412 + 670.44678162256998i	8.24.3	23.1850545642515	

Table D.9: (continued)

m, n, r	$c_{0;r}^{m,n} = c_{0;r-1}^{m,n+2}$	$\lambda_{0;r}^{m,n} = \lambda_{0;r+1}^{m,n+2}$	m, n, r	$c_{0;r}^{m,n} = c_{0;r+1}^{m,n+2}$	$\lambda_{0;r}^{m,n} = \lambda_{0;r-1}^{m,n+2}$
-----------	-------------------------------------	---	-----------	-------------------------------------	---

Table D.9: Branch points and associated eigenvalues for $m = 8$.

D.1.4 $m = [8..50]$, $n = [m..15 + m]$

Accuracy was determined by the last correction of the Newton-Raphson method.

Table D.10: Branch points and associated eigenvalues for $m = 9$.

m, n, r	$c_{0;r}^{m,n} = c_{0;r-1}^{m,n+2}$	$\lambda_{0;r}^{m,n} = \lambda_{0;r+1}^{m,n+2}$	m, n, r	$c_{0;r}^{m,n} = c_{0;r+1}^{m,n+2}$	$\lambda_{0;r}^{m,n} = \lambda_{0;r-1}^{m,n+2}$
9, 9, 1	2.754837260868474 - 13.851441882694608i	84.119800179347351 + 15.47850220681031i	9, 10, 1	5.210456108591401 + 14.630754035290515i	98.196512712728453 + 41.359057139269964i
9, 10, 1	7.373579112214387 - 15.79926027621195i	119.65453715103877 + 70.09027491511756i	9, 11, 1	2.692813452216789 + 17.67128615248811i	83.8659222163584 + 21.38977159761660i
9, 12, 1	9.58190345506693 - 15.841057462384994i	147.65108905635530 - 101.15728601845260i	9, 12, 2	5.27939150566409 + 18.410130978007146i	97.52058995202127 - 56.07838928372878i
9, 13, 1	11.31394140682295 + 16.33919987165150i	181.769654631620227 + 134.20543110708605i	9, 13, 3	7.471125229994036 + 19.051816341368784i	118.942833053701179 + 93.339048563992165i
9, 13, 5	2.688782760124380 + 21.214600446608813i	83.779187331570777 + 26.495206916215878i	9, 14, 1	13.176717485589499 + 16.7882056390200443i	172.759276963529771 + 168.977641584379853i
9, 14, 3	9.559790268618221 + 19.622777889799718i	147.242660310175921 + 132.876348174122342i	9, 14, 5	5.287389515541451 + 21.939901617171888i	97.366793973099292 + 69.069218344212857i
9, 15, 1	14.994456153865672 + 17.197762482699861i	267.451716717069132 + 205.28203862482336i	9, 15, 3	11.550144886446424 + 20.138976194955255i	181.950800232922006 + 174.41987314305481i
9, 15, 5	7.594241543688684 - 22.584516130873159i	118.98310071020294 - 114.068714275871287i	9, 15, 7	2.701281260524641 + 24.63108955965184i	83.747683717417019 + 31.2399495686711424i
9, 16, 1	16.778003329413085 + 17.57477516935406i	318.726324914900772 + 242.967901700277963i	9, 16, 3	13.471840665281809 + 20.61108864125819i	222.77352326925672 + 174.354399081250995i
9, 16, 5	9.7424342017080 + 23.167141115334193i	147.724220148075659 + 161.322795888526271i	9, 16, 7	3.555514134990377 + 25.35137458927147i	97.384500414317761 + 81.251390270202549i
9, 17, 1	18.534744623462007 + 19.24381594180911i	375.492412132602283 + 281.91355790063217i	9, 17, 3	15.342720624711641 + 21.046724753905067i	269.509182520370801 + 262.70855943544981i
9, 17, 5	11.787543467909179 + 23.700683394833629i	183.096891240541026 + 210.615754921269456i	9, 17, 7	7.717382672985513 + 26.001592868531940i	119.252809124262464 + 133.59643525510032i
9, 17, 9	2.719005174867769 + 27.975465290228627i	83.7384054193766985 + 35.79653228164864i	9, 18, 1	20.269942871047590 + 18.250526613001256i	437.6704344894913 - 322.018436877198837i
9, 18, 3	17.17449160305657 + 21.451551152690350i	322.01070070721383 + 340.140016962897846i	9, 18, 5	13.759445012148502 + 24.193545673214071i	224.78219187884413 - 92.160444102422525i
9, 18, 7	9.917471711642445 + 26.596045204652878i	148.465862132364887 + 188.189902511613383i	9, 18, 9	5.42877629875380 + 28.69511609787345i	97.468387724759335 + 92.65164091937783i
9, 19, 1	21.987482186654743 + 18.556321829702764i	505.2308918470976 - 363.1923981649891i	9, 19, 3	18.975103874711298 + 21.829931341050252i	380.16201692931338 + 356.934395259121629i
9, 19, 5	15.676415785615609 + 24.652074528061501i	272.55644467181741 + 314.6001230681089282i	9, 19, 7	12.010896909517948 + 27.145189694502765i	184.495383926896303 + 224.85543444993151i
9, 19, 9	7.834792881718449 - 29.351087813263448i	119.620941881890616 + 152.419004661368461i	9, 19, 11	2.739937855783677 + 31.27294895532327i	83.739930272890060 + 48.18738332698218i
9, 20, 1	23.690310523443514 - 18.844271210664809i	578.100827937273807 + 405.379251701642602i	9, 20, 3	20.75052258337754 + 22.185312635962728i	443.887799024734774 + 405.9928077329443i
9, 20, 5	17.55057343257917 + 25.081130888078707i	326.25480059222340 + 369.0030618923832i	9, 20, 7	14.027630253167510 + 27.656273586326343i	227.0111020757727 - 303.4274052869605i
9, 20, 9	10.08138307202973 + 29.962572732330207i	149.288794760749596 + 214.122173863183605i	9, 20, 11	5.489813951463718 + 31.994267153277639i	97.58249677286451 + 104.37539832799020i
9, 21, 1	25.38071175767305 + 19.116425031822093i	656.250963518649314 + 448.49999111131280i	9, 21, 3	22.50566043610945 + 22.520476053349569i	513.104722555356489 + 456.23023494458048i
9, 21, 5	19.390412735981403 + 25.445441506710271i	385.74927330551554 + 424.85737679283921i	9, 21, 7	15.986211660957119 + 28.134767266896988i	275.770393845243177 + 363.76139555688701i
9, 21, 9	12.18446216151028 + 30.519273062289063i	185.947298594631206 + 277.929136347105612i	9, 21, 11	7.945194650478268 + 32.656314579657554i	120.051117653486465 + 170.7807197304147546i
9, 22, 1	27.60636011705558 + 34.541063718384030i	83.747136517737246 + 44.303826428497277i	9, 22, 1	27.060514166967828 + 19.374486686601553i	739.6700433377059 + 492.5048389818081i
9, 22, 3	24.242079165660015 + 22.837703967177355i	587.758839434639413 + 507.574181559044007i	9, 22, 5	21.202139083781262 + 25.865398452687291i	450.93904540685842 + 348.6067273869661i
9, 22, 7	17.899054227448719 + 28.584942887396490i	330.59652877001386 + 425.73288541930852i	9, 22, 9	14.276010445454745 + 31.046359930915763i	229.246137817034054 + 434.69179879578731i
9, 22, 11	10.234101780288519 + 33.271235999597086i	150.126191030258610 + 239.439190358464287i	9, 22, 13	5.552495315039050 + 35.262835012556764i	97.709798017536571 + 115.574347442686321i
9, 23, 1	28.731195260883095 + 19.619889235886351i	828.267661711721874 + 537.345404356800467i	9, 23, 3	25.964183634740748 + 23.13896765311959i	667.801611217680147 + 559.96073562288421i
9, 23, 5	22.990432004419410 + 26.226232509533494i	521.742109270653169 + 540.54796459398377i	9, 23, 7	19.774939308991193 + 30.00224413213373i	391.34886611383829 + 489.23421624326604i
9, 23, 9	16.272788637976650 + 31.342352252156217i	278.932801266700608 + 411.275243345611269i	9, 23, 11	12.41113053930583 + 33.84653195248444i	187.380919897353436 + 310.251069894779353i
9, 23, 13	8.048636047265848 + 35.930654329700565i	120.416085015561407 + 188.819582006161699i	9, 23, 15	2.871163604753508 + 37.785634885437076i	87.167167630415975 + 48.751947128917678i
9, 24, 1	30.393841654887513 + 17.875340300200879i	922.08304898527967 - 582.978290223741851i	9, 24, 3	27.633471956574417 + 23.425656397794155i	753.191953103744341 + 61.33155549040510i
9, 24, 5	24.758911383487526 + 26.569123729512356i	598.090676698486618 + 600.227329009479111i	9, 24, 7	21.620334186416763 + 29.413401856723670i	457.9155760812730 + 554.171505508762951i
9, 24, 9	18.221404122735609 + 32.011065738905651i	334.816064306616449 + 480.562381436657404i	9, 24, 11	14.50291274364679 + 34.38774709193175i	231.417898926524373 + 383.032179967624538i
9, 24, 13	10.37645450773650 + 36.55435994893179i	150.90025120520621 + 264.323651251739705i	9, 24, 15	5.61177068347723 + 38.50921969275071i	97.84190521748348 + 126.618640052519382i

Table D.10: Branch points and associated eigenvalues for $m = 9$.

Table D.11: Branch points and associated eigenvalues for $m = 10$.

m, n, r	$c_{0;r}^{m,n} = c_{0;r-1}^{m,n+2}$	$\lambda_{0;r}^{m,n} = \lambda_{0;r+1}^{m,n+2}$	m, n, r	$c_{0;r}^{m,n} = c_{0;r+1}^{m,n+2}$	$\lambda_{0;r}^{m,n} = \lambda_{0;r-1}^{m,n+2}$
10, 10, 1	2.81948507565682 + 14.990209607367479i	103.24235891816643 + 16.391683445935321i	10, 11, 1	5.321463550267296 + 15.799055606477189i	117.805507012199811 + 43.814865986473905i
10, 12, 1	7.531075603313457 + 16.475682283040410i	139.927485038865967 + 74.264535271178221i	10, 12, 3	2.741193306016878 + 18.874227379496350i	102.947078388647057 + 22.484191708419950i
10, 13, 1	9.580214373016309 + 17.063890194677363i	168.712887961199812 + 107.199795253734711i	10, 13, 5	5.320828223919550 + 19.633473961894863i	116.967664663069556 + 58.52785996838779i
10, 14, 1	11.533697900323475 + 17.857189694302932i	203.71939659863049 + 142.24420366390933i	10, 14, 3	7.59987812107518 + 20.295775310695054i	138.91799663356466 + 98.11359814173479i
10, 15, 1	13.533697900323475 + 17.857189694302932i	203.71939659863049 + 142.24420366390933i	10, 15, 1	13.421630220845062 + 18.060152891012372i	244.67457060736544 + 19.128638504466778i
10, 15, 3	9.19088684478374 + 20.887048665512200i	167.867441937917420 + 139.66601070484501i	10, 15, 5	5.365124724158615 + 23.202881185941066i	116.727156382017967 + 72.225099776044147i
10, 16, 1	15.261723909386927 + 18.49256626220623i	291.402713863630709 + 217.649509390694907i	10, 16, 3	11.736136249012668 + 21.42307362931252i	203.3246394829881 + 183.32946004624782i
10, 16, 5	7.704026910883870 + 23.665468387021181i	138.784049313074673 + 119.260386941438981i	10, 16, 7	2.734251578588265 + 25.912491803406724i	102.800079823345492 + 32.332012881862271i
10, 17, 1	17.06535915225751 + 18.891442694493417i	343.72793287313177 + 257.64705022269366i	10, 17, 3	13.68158043204477 + 21.944723008226411i	244.97438313240102 + 282.8676716673719i
10, 17, 5	9.880024574418687 + 24.46257976633967i	168.08171565918377 + 168.63847866119616i	10, 17, 7	5.42255521956821 + 26.645361714273491i	116.684523202292675 + 84.618431212976035i
10, 18, 1	18.840310767808059 + 19.26007703330692i	401.687744634006094 + 298.9393554709126954i	10, 18, 3	15.57384428395973 + 22.368827472164783i	292.60742307466927 + 276.118142785971i
10, 18, 5	11.94793453785180 + 25.102353402970790i	204.104155779745729 + 220.139902531725709i	10, 18, 7	7.813311632017969 + 27.308330345049526i	138.940186591375323 + 139.10441880060898i
10, 19, 1	27.48074475170671 + 29.287493982701744i	102.7825541804646 + 37.137151956870869i	10, 19, 3	20.92123585880896 + 25.602278309200825i	465.071130466539976 + 334.51454754924386i
10, 19, 5	17.424896423769244 + 22.791814066765816i	346.068761939624665 + 324.92985784863063i	10, 19, 7	13.948387983751492 + 25.521245400167999i	246.5183782294851 - 273.57241380014292i
10, 19, 9	10.038835292572902 + 27.916276585871766i	168.63575762105278 + 195.91123895398888i	10, 19, 11	5.482850437506527 + 30.013400523564101i	116.726479538457752 + 96.49741678006657i
10, 20, 1	22.324940049120521 + 19.934394336324881i	533.862212438753318 + 385.321337859691994i	10, 20, 3	19.243281602994298 + 23.18710520123232i	405.23905108119564 - 375.19528764551947i
10, 20, 5	15.881010502806063 + 25.995531945176928i	295.090607358207819 + 328.77476			

D.1. Branch points, $c_{o;r}^{m,n}$, and Associated Eigenvalues $\lambda_{o;r}^{m,n}$ of the SWE

Table D.12: (continued)

m, n, r	$\lambda_{o;r}^{m,n} = \lambda_{o;r+1}^{m,n+2}$	$\lambda_{o;r}^{m,n} = \lambda_{o;r+1}^{m,n+2}$	m, n, r	$\lambda_{o;r}^{m,n} = \lambda_{o;r+1}^{m,n+2}$	$\lambda_{o;r}^{m,n} = \lambda_{o;r+1}^{m,n+2}$
11,15.1	11.74394408568887 + 18.82067095041478i	227.58239683052037 + 151.03048585471420i	11,15.3	11.725251144001322 + 21.52735043259707i	160.8695323121305 - 102.748525625780672i
11,15.5	2.765702550697174 + 23.69830356115600i	123.906628235540055 + 28.881292524927652i	11,16.1	13.6550878667717575 + 19.16203555083614i	269.479380192609599 + 188.960789732558374i
11,16.3	9.871892164775630 + 21.37845386532565i	190.452791202714678 + 146.251346390969776i	11,16.5	14.0007121888860 + 24.453826920965565i	138.07846780856494 + 75.29584061411964i
11,17.1	15.517599013054131 + 19.770201183588594i	317.215074915491186 + 229.628490378400045i	11,17.3	11.914729713646317 + 22.692670926492042i	226.63671009826358 + 191.96708568272232i
11,17.5	7.808862205744 + 25.1297928494998i	160.568839901336474 + 124.310189761662290i	11,17.7	2.766231055546819 + 27.182019422701668i	123.85764053638902 + 33.792815419616630i
11,18.1	17.340818171827522 + 20.189759237600740i	370.651577406959461 + 271.8657179523165129i	11,18.3	13.883140737884853 + 23.202633964309122i	269.096110892501737 + 239.658382939437274i
11,18.5	10.012669232080280 + 25.744484894557188i	190.411398035704849 + 175.755719909517267i	11,18.7	5.487456803844618 + 27.926673542452552i	337.979818804904720 + 89.849643084387015i
11,19.1	19.133576208284734 + 20.5801812362008420i	429.684830196503638 + 315.53379381092959i	11,19.3	15.796105844100689 + 23.674501514024758i	137.607108362999740 + 271.109567190848244i
11,19.5	12.106316265578933 + 26.309749639589866i	227.070013244907187 + 249.4006003016133667i	11,19.7	7.906156745916614 + 28.602240179933943i	160.6107207268602 + 144.471203069259143i
11,19.9	2.75817560102565 + 30.5799830113851600i	123.826281209471233 + 38.461389641815018i	11,20.1	20.901702169768214 + 20.945604283161281i	494.2355173958767 + 360.529961060885141i
11,20.3	17.66609786657805 + 24.11475994788805i	372.005793210289141 + 340.26282519494865i	11,20.5	14.12192258927844 + 26.833937514005281i	270.17995040262356 + 285.0655118248132i
11,20.7	10.156321422872574 + 29.2231311051089892i	90.78551993057616 + 203.43532933914686i	11,20.9	5.540173848927354 + 31.319338900136184i	137.981350604031974 + 99.947813328130274i
11,21.1	22.64952085998802 + 21.28912908309171i	564.23254029816913 + 406.749993061591188i	11,21.3	19.501794637957246 + 24.5275312868466987i	432.1670971482869855 + 392.874521981362191i
11,21.5	16.078666194078302 + 27.323270601565767i	319.551401991364173 + 342.567697488667623i	11,21.7	12.29471753605731 + 29.798962189337725i	227.957085653157066 + 264.612684640579630i
11,21.9	8.002845716734798 + 31.9799106039891i	160.801194210817158 + 163.798849435552525i	11,21.11	2.789448776724601 + 33.922517625418912i	123.81582321420072 + 42.972637936995511i
11,22.1	24.380331350664784 + 21.613501513086572i	639.62837515834813 + 454.116063587178661i	11,21.13	21.309496670383330 + 24.916380926913983i	497.992488414634181 + 446.923712823967781i
11,22.5	19.89278942674966 + 27.782541146325528i	374.949319766536291 + 401.722556028321581i	11,22.7	1.552330206305054 + 30.336708180481445i	271.764354033073756 + 327.83045214708122i
11,22.9	10.29556516983466 + 32.624368177278505i	191.331659435590126 + 230.02259073708674i	11,22.11	5.93978331558379 + 34.65974279152537i	103.823284357348 + 111.624100263245408i
11,23.3	26.09670800892586 + 21.920824534190871i	720.376541130967667 + 502.557862197032534i	11,23.3	23.093903997170130 + 25.283891906203093i	569.40239946150404 + 502.2917974564611784i
11,23.5	19.86275784221590 + 28.215544291598544i	436.25192174274082 + 462.56084043539477i	11,23.7	16.348409654129579 + 30.841676290530962i	321.94939580516698 + 392.938578004915823i
11,23.9	12.44400186186878 + 33.210220444134311i	229.0180578798630 + 298.46983638388531i	11,23.11	8.09665260954512 + 35.336989686256691i	161.061840039701318 + 182.575198196914606i
11,24.3	2.80486808775927 + 37.226363342513909i	123.813774028085527 + 47.37965591496311i	11,24.1	27.80698015670008 + 22.12887366495202i	806.43909695757976 + 452.01374216756484i
11,24.5	24.85873842762070 + 25.62629378909726i	646.331291393496485 + 558.87936433373487i	11,24.5	15.6474555406627 + 28.625500853445001i	303.84006072386032 + 524.829842413799696i
11,24.9	18.29586807697173 + 31.31806373374100i	378.13299582747045 + 459.80676800321216i	11,24.9	4.570313474359873 + 33.760355227335091i	273.48854524552483 + 368.9891279838571i
11,24.11	10.42828242147879 + 35.973886461951395i	191.951440027978094 + 255.88157423794547i	11,24.13	16.348409654129579 + 37.96252426557124i	138.110748780959042 + 123.04841574384695i
11,25.1	25.1816517199642 + 22.491199631276101i	897.78477976883110 + 602.429170426104861i	11,24.15	26.6084072063050 + 23.59911209758520i	728.7249648014713 + 616.636116442589601i
11,25.3	25.323016255153873 + 29.0144892330196774i	576.14734313270793 + 588.49015614250991i	11,25.7	20.20887416874753 + 31.769147266697981i	440.7198734646566 + 429.82190850291813i
11,25.5	16.02460230764848 + 34.279416550703162i	324.4725969627211 + 441.4427614930811i	11,25.11	12.64316882247539 + 36.56902719789290i	230.140772084066026 + 379.26248483737081i
11,25.13	8.18646618071750 + 38.64612493866377i	161.355877509241196 + 200.9639515768321i	11,25.15	2.821029524417447 + 40.502809702612651i	123.81670628201155 + 67.6943328987421i
11,25.15	31.177836061882324 + 22.757048649013246i	994.3846845537986 + 653.7540632510561i	11,26.3	30.24036345551138 + 26.28101798572579i	816.53485251020636 + 45.68560497491935i
11,26.5	25.318651100700719 + 29.385072266808228i	654.57478964518004 + 653.46206253210046i	11,26.7	22.079245716804582 + 32.19776868621325i	509.03291885503460 + 598.385149613808721i
11,26.9	10.83591181785901 + 26.60762318593664i	1245.8695613280494 + 39.75344019413572i	11,26.11	14.754584584383330 + 22.64087230817212i	275.2452791315761 + 409.6932831991961i
11,26.13	10.5540526853859 + 39.286618085931460i	192.599005308255386 + 281.22351742110280i	11,26.15	5.69727267979202 + 41.23861234620701i	138.202821731130769 + 184.2416310582875i

Table D.12: Branch points and associated eigenvalues for $m = 11$.

m, n, r	$\lambda_{o;r}^{m,n} = \lambda_{o;r+1}^{m,n+2}$	$\lambda_{o;r}^{m,n} = \lambda_{o;r+1}^{m,n+2}$	m, n, r	$\lambda_{o;r}^{m,n} = \lambda_{o;r+1}^{m,n+2}$	$\lambda_{o;r}^{m,n} = \lambda_{o;r+1}^{m,n+2}$
12,21.1	2.9325385156778 + 17.24501390600442i	147.47722005336200 + 18.13505239200206i	12,21.5	5.544632105740728 + 18.107759709994960i	162.97247182574631 + 48.30569472121527i
12,21.4	7.824098120010937 + 18.835504866723756i	186.36719880726083 + 82.235527907017001i	12,21.9	6.232007398772770 + 21.250536974781532i	147.108386499700941 + 24.579402471413691i
12,21.5	9.536451102430660 + 19.472170117524460i	216.66550260834895 + 18.173536996382852i	12,22.3	5.495037562576078 + 22.047504963861562i	161.83049681651616 + 64.457397546556479i
12,21.6	11.944429186178885 + 20.041555312320618i	253.37107104606429 + 105.793109409663961i	12,22.6	7.841807714301229 + 22.747971929051783i	184.799474931301518 + 107.03661372968598i
12,21.11	2.802192542820323 + 24.94442755943893i	146.968662837596725 + 30.42758002085917i	12,22.7	13.880323913730085 + 20.558466134503007i	296.180504249002121 + 198.5102630254685826i
12,21.13	10.018853070703202 + 23.376784229192499i	215.002158312580235 + 152.661618732907121i	12,22.15	15.29229894858958 + 25.694064509660619i	161.423205743885774 + 78.28764178678403i
12,21.17	15.763273052868891 + 21.032924750927891i	344.902949361299534 + 241.263140534474811i	12,22.18	12.086652524305665 + 23.948494212562289i	251.898447281367344 + 200.379540743341380i
12,21.18	7.911948323049684 + 26.384740466999574i	184.33853136141754 + 179.232144944899061i	12,22.19	2.797288728242561 + 28.40897492315591i	146.602747176993935 + 53.021961137017280i
12,21.19	17.60559237061158 + 21.472118126364872i	399.3926874971873 + 285.6738154861215i	12,22.19	10.36739979117545 + 24.47669075545347i	295.148253098879920 + 425.10687621540877i
12,21.21	10.40814074815598 + 27.014359637901395i	214.715248329652184 + 182.69426512659375i	12,22.19	5.57033636867012 + 29.196928960857647i	161.207553190882545 + 0.1999910105468553i
12,22.1	19.4157653693742 + 21.88142168875424i	459.503587055380251 + 331.60480884922994i	12,22.20	16.010507361445761 + 24.965695304313495i	344.51686717682149 + 301.81353594831489i
12,22.5	12.57616297481558 + 27.594432084205035i	251.997479721806428 + 238.4934329902987i	12,22.27	7.996163781757708 + 29.884625249853961i	251.898447281367344 + 200.379540743341380i
12,22.9	2.802874117110447 + 31.86523218593664i	146.8695613280494 + 39.75344019413572i	12,22.11	21.199875861214316 + 22.64087230817212i	525.1895216226295 + 378.6368214042404i
12,22.13	17.60559237061158 + 21.472118126364872i	399.3926874971873 + 285.6738154861215i	12,22.15	14.29414863971391 + 28.133257034438078i	295.820829115268 + 296.20718847258624i
12,22.15	10.40814074815598 + 27.014359637901395i	214.715248329652184 + 182.69426512659375i	12,22.19	5.59598586790958 + 32.61405918021394i	161.233044979651964 + 103.317180484182625i
12,22.17	19.4157653693742 + 21.88142168875424i	459.503587055380251 + 331.60480884922994i	12,22.23	12.5140988619173 + 28.85122416275450i	460.96338418601722 + 40.1434713106600801i
12,22.20	12.57616297481558 + 27.594432084205035i	251.997479721806428 + 238.4934329902987i	12,22.27	19.730159486704998 + 31.106305096400263i	252.64835282195909 + 274.13386750058188i
12,22.23	24.70694177595909 + 22.967431666750898i	672.98112455136241 + 477.406326132693101i	12,22.31	8.134741137424572 + 35.22983245715379i	146.85332667138703 + 44.319043416271533i
12,22.25	18.198139950154552 + 29.1104133705104580i	402.167038813747752 + 447.531438018034276i	12,22.37	14.70399009796056 + 31.656639976604605i	297.0803113161442227 + 339.59226062250877i
12,22.29	10.39821874311034 + 33.99966819746608i	215.31487132753409 + 237.70008849921320i	12,23.11	5.64897006164220 + 35.974664515442740i	161.25427374171953 + 115.129107691288951i
12,23.1	26.46309535711747 + 23.291195158963360i	754.982341914687936 + 528.391186623115250i	12,23.13	23.3797551355164 + 26.63832085897146i	620.27098906016465 + 524.382132931911896i
12,23.4	20.087849786308198 + 25.597287261781042i	464.34708569088558 + 480.693962677295513i	12,23.17	16.521495475021929 + 32.174068856159082i	347.95891036901864 + 407.003218906408222i
12,23.9	12.5716541				

Table D.14: (continued)

Table with 5 columns: m, n, r; m, n, r; m, n, r; m, n, r; m, n, r. Each column contains mathematical expressions for lambda and c, followed by numerical values for various m, n, r combinations.

Table D.14: Branch points and associated eigenvalues for m = 13.

Table with 5 columns: m, n, r; m, n, r; m, n, r; m, n, r; m, n, r. Each column contains mathematical expressions for lambda and c, followed by numerical values for various m, n, r combinations.

Table D.15: Branch points and associated eigenvalues for m = 14.

Table with 5 columns: m, n, r; m, n, r; m, n, r; m, n, r; m, n, r. Each column contains mathematical expressions for lambda and c, followed by numerical values for various m, n, r combinations.

Table D.16: Branch points and associated eigenvalues for m = 15.

Table with 5 columns: m, n, r; m, n, r; m, n, r; m, n, r; m, n, r. Each column contains mathematical expressions for lambda and c, followed by numerical values for various m, n, r combinations.

Table D.17: Branch points and associated eigenvalues for m = 16.

Table with 5 columns: m, n, r; m, n, r; m, n, r; m, n, r; m, n, r. Each column contains mathematical expressions for lambda and c, followed by numerical values for various m, n, r combinations.

Table D.17: (continued)

m, n, r	$c_{\sigma;r}^{m,n} = c_{\sigma;r+1}^{m,n+2}$	$\lambda_{\sigma;r}^{m,n} = \lambda_{\sigma;r+1}^{m,n+2}$	m, n, r	$c_{\sigma;r}^{m,n} = c_{\sigma;r+1}^{m,n+2}$	$\lambda_{\sigma;r}^{m,n} = \lambda_{\sigma;r+1}^{m,n+2}$
16,22,5	8.28913929265447 + 31.31191163453021i	299.285119651720958 + i47.852910396260086i	16,22,7	2.913466888730951 + 33.388293456599025i	259.10004764804518 + 39.6822747685512901i
16,23,1	18.037267058345890 + 26.475886644153102i	533.0347511889540 + 337.583675808229827i	16,23,3	14.792782560639520 + 29.463978371685997i	418.757214260452379 + 289.783041216200502i
16,23,5	10.61526733986064 + 31.99547594963936i	331.705005280873820 + 208.943059639543719i	16,23,7	5.785084328058061 + 34.186424981977783i	274.39185761624126 + 103.241654486194944i
16,24,1	20.45238427059115 + 26.952788647995895i	597.29368252963168 + 392.000425085107311i	16,24,3	16.80013206711877 + 30.014045326957590i	471.390827346419190 + 349.474921846677143i
16,24,5	12.81851125782787 + 36.629258832724289i	71.37367112545798 + 272.672171450602498i	16,24,7	8.35771015368110 + 34.9186932997454082i	298.81679858236785 + 169.584060167711431i
16,24,9	2.9045255779039 + 36.915531290820248i	259.03827346937365 + 44.673548797618842i	16,25,1	12.29740862737578 + 27.401638421070100i	667.291921300147448 + 448.10848058882193i
16,25,3	18.759403172423152 + 30.530201266558075i	500.19827213248315 + 411.500661375253077i	16,25,5	14.93341965447259 + 33.221190192296568i	417.877029307289263 + 138.684279142152140i
16,25,7	10.695201426689010 + 35.597629539528817i	331.268486549409147 + 238.6755021724858i	16,25,9	5.805575324876602 + 37.69583598453188i	274.290590279571033 + 116.11826768717696i
16,26,1	24.11646570305927 + 27.82590444644355i	742.944554965336238 + 505.790850088950127i	16,26,3	20.67048404684117 + 31.0168680566592928i	595.0243582554603 + 475.22127191494086i
16,26,5	16.981052529064846 + 33.772527372974521i	470.927316974284054 + 406.927660872626581i	16,26,7	12.953058148481869 + 36.231997067006362i	371.1352677225818 + 310.271458373808855i
16,26,9	6.82881189462633 + 32.625162289045728i	298.6186186626096 + 190.1870951762891i	16,26,11	2.994478595251654 + 40.366507678937952i	299.06066366635875 + 140.49506251326742i
16,27,1	25.913580521416087 + 28.22839784814812i	824.18129682214790 + 564.94202426329644i	16,27,3	12.58880699790639 + 31.47611198042670i	665.7462409084607 + 540.6740046649980i
16,27,5	18.975482174864343 + 34.302111328885507i	530.30648399569730 + 477.195213666539644i	16,27,7	5.83242033867149 + 41.141483068973834i	417.98860858723284 + 384.21894356978094i
16,27,9	10.78631850449005 + 39.10263292513883i	331.1997642367344 + 266.90889495463231i	16,27,11	5.8342033867149 + 41.141483068973834i	274.12020884131025 + 128.478262513045944i
16,28,1	27.69190998385522 + 28.611447605829355i	103.9454811684638 + 625.490390800650581i	16,28,3	24.4131672669228 + 31.915330469839752i	742.264262167070342 + 607.74938150171141i
16,28,5	26.586673110106 + 36.1547669464683i	828.20953941216246 + 776.0503454965321i	16,28,5	17.68897276148900 + 37.39129587561365i	471.5328117823952 + 460.40317613368234i
16,28,9	13.058116518936938 + 39.739269283282525i	71.327351534061393 + 346.138106326307536i	16,28,11	8.44498373597461 + 41.863348543089927i	298.59744414918954 + 210.02921386549184i
16,28,13	2.908554954956998 + 43.763259419669297i	258.977483349588624 + 54.07135888924581i	16,29,1	12.84104377290596 + 35.27240596735472i	1003.17187890426913767 + 687.343854427092586i
16,29,3	26.243375832232978 + 32.33249145466107i	824.495966969089994 + 676.3523153445817004i	16,29,5	25.249120365581436 + 40.340562902899885i	667.41197590700607 + 623.28304441634486i
16,29,7	19.196166014504348 + 37.92514590113193i	531.54050547921474 + 538.61108284179043i	16,29,9	5.864942832168929 + 44.5322641279365i	474.08004115888398 + 140.49506251326742i
16,29,11	10.87459303314657 + 42.541019964643271i	331.3220437493355 + 294.167898454965321i	16,29,13	8.205820328251723 + 32.73026905267971i	312.37202310794456 + 746.39967444515544i
16,30,1	31.201861049313882 + 29.32668404299277i	1100.85146505483110 + 750.43984109276051i	16,30,3	28.05201802804650 + 38.433093409925156i	597.832455973582228 + 618.73968368213843i
16,30,5	24.727295691495748 + 35.723499860231151i	744.894031804849885 + 698.8818469116923995i	16,30,5	21.178610820084650 + 38.73093409925156i	371.755173104588919 + 380.790580823004848i
16,30,9	17.355567252685187 + 40.910825348024260i	472.64148864502924 + 511.493250767101621i	16,30,11	13.180363639346227 + 43.18078524838838i	258.9634310965699 + 58.580771542215496i
16,30,13	8.50598959561931 + 45.25218004948191i	298.631999415257894 + 229.325232639455974i	16,30,15	2.91536748113825 + 47.119997114470934i	100.833341382929782 + 817.18111367356029i
16,31,1	32.937241001408964 + 29.661933732680575i	1203.91700882132868 + 814.71767479264017i	16,31,3	15.844166283718110 + 33.12540768666261i	308.06125737882664 + 92.29445013893720i
16,31,5	26.868811310106 + 36.1547669464683i	828.20953941216246 + 776.0503454965321i	16,31,5	8.395435398109856 + 38.97179811125514i	507.544287044872056 + 174.3214717948949i
16,31,9	19.41301165938748 + 41.455337999682944i	533.29758838147399 + 597.3394734285047i	16,31,11	25.255166331576367 + 28.657387185893521i	705.4351203097398 + 464.47986762570137i
16,31,13	10.965297210179159 + 49.93100432755521i	331.582287133054535 + 320.709588646783970i	16,31,15	5.89819654718546 + 47.884733037378489i	274.086535902157379 + 152.23366796549952i

Table D.17: Branch points and associated eigenvalues for $m = 16$.

m, n, r	$c_{\sigma;r}^{m,n} = c_{\sigma;r+1}^{m,n+2}$	$\lambda_{\sigma;r}^{m,n} = \lambda_{\sigma;r+1}^{m,n+2}$	m, n, r	$c_{\sigma;r}^{m,n} = c_{\sigma;r+1}^{m,n+2}$	$\lambda_{\sigma;r}^{m,n} = \lambda_{\sigma;r+1}^{m,n+2}$
17,11,1	1.197512982593725 + 22.78664690209216i	293.018167585218305 + 2.128063940071181i	17,11,1	6.014574080227733 + 23.762872908768973i	10.6601117688001 + 59.242090904253928i
17,11,9	8.460731647192855 + 24.977031054352479i	336.988062490769721 + 100.489885798006100i	17,11,9	3.032234896764332 + 27.063878584858558i	292.448769529020885 + 29.399057426588977i
17,20,1	10.713476809257828 + 25.336288145441414i	370.57948686713662 + 45.158175419390403i	17,20,3	3.879238093833929 + 27.41873983515103i	330.840069373780238 + 17.7228811518258084i
17,21,1	12.843676929898904 + 26.02835006871514i	411.409013710472607 + 192.749197604645190i	17,21,3	5.37634498080343 + 28.723868477038732i	384.18003498080343 + 128.30044136289974i
17,21,5	2.96873784881393 + 30.9347366018357712i	292.26421455156884 + 35.391860102655751i	17,21,5	14.888165369574903 + 26.612740116108998i	458.512342269010674 + 242.90006236832801i
17,22,1	10.68281411815851 + 29.43312065066321i	367.300587768626315 + 58.924969360701468i	17,22,3	12.865041366933672 + 30.0103294948706725i	308.06125737882664 + 92.29445013893720i
17,22,5	16.889269062388387 + 27.1764749236401912i	511.832186363228285 + 295.347627923451157i	17,22,7	9.460743812026563 + 34.606678726226600i	292.4782947252932 + 40.79266403693929i
17,23,1	8.377615878011665 + 32.5244549155596029i	332.992617062012812 + 152.28034736839429i	17,23,7	2.9587069225991699 + 30.688416645679879i	454.53098067259831 + 299.18750466339766i
17,23,5	18.80028562206427 + 27.701589627853029i	571.183427663701850 + 349.8696973132425i	17,23,9	5.840060595016042 + 35.414594005627877i	307.6626291368611036 + 106.135415198841802i
17,23,9	10.725729152562609 + 33.220351501150112i	365.902805762832944 + 215.187995701512865i	17,23,11	6.985027628929055 + 31.252334291751122i	507.944583262397858 + 360.98872603031216i
17,25,1	26.092135531428708 + 28.19375919018031i	406.17967682230425 + 406.291599257073862i	17,25,3	10.624942280711472 + 280.76135947977589i	332.42487044872056 + 174.3214717948949i
17,25,5	12.9492371017774 + 33.826640734601912i	406.17967682230425 + 406.291599257073862i	17,25,5	15.55166331576367 + 28.657387185893521i	705.4351203097398 + 464.47986762570137i
17,25,9	2.920904336875818 + 38.158780317137811i	292.079314423046469 + 45.84779912952587i	17,26,1	25.082596185438309 + 34.470477848218124i	455.289801144233699 + 348.77969602687355i
17,26,3	18.95453083117374 + 31.781984130447581i	567.587177095789343 + 424.86744080475183i	17,26,9	5.854992430014150 + 38.951109664677148i	307.44626638486195 + 19.176510866923834i
17,26,7	10.794776051288457 + 36.846639764315604i	365.318167160039081 + 245.303241151429391i	17,27,3	20.891288768099209 + 32.281825456260044i	633.297343907216828 + 490.669687296469306i
17,27,1	24.38423625381265 + 29.095976378303022i	784.17252170880709 + 524.304234095461361i	17,27,7	12.084364348751630 + 37.49157269556737i	405.69826952754467 + 138.89918580635979i
17,27,5	17.147163101355055 + 35.038580065215719i	507.043736053147256 + 419.042378078503361i	17,27,11	9.29615238292890 + 41.630891215770816i	292.056716441878058 + 50.675762785628699i
17,27,9	8.47062154573725 + 39.68529147562485i	332.16140522401696 + 195.17820490468281i	17,28,3	7.358196700465274 + 32.75542691660474i	704.947866290214897 + 558.269490643254190i
17,28,1	26.193990755428448 + 29.51237681662452i	866.512171632186210 + 585.6662816906321i	17,28,7	15.227949361820023 + 38.098355813664192i	453.136162608014598 + 93.68904147039447i
17,28,5	19.157276045491496 + 35.575145879494937i	567.180918614102438 + 491.395060183946498i	17,28,11	5.87833036685606 + 42.413002685780882i	307.331212060335897 + 331.803041680481819i
17,28,9	10.87442728684672 + 40.371212730718370i	365.136711712095904 + 273.88755139499870i	17,29,3	24.655789931407760 + 33.205700977161935i	782.434779930562250 + 627.540731783145930i
17,29,1	27.984183938756249 + 29.908935303511665i	954.410693245248581 + 648.469690960125995i	17,29,7	17.230949632764879 + 38.71925129893637i	407.322302652206110 + 473.140814924449588i
17,29,5	21.12310701652854 + 36.084191300475889i	635.52760481404400 + 565.695264062936431i	17,29,11	8.610207731986978 + 43.142573483321988i	332.06731696112510 + 215.2341754503634i
17,29,9	13.166766503968965 + 41.018037302511665i	405.733294423899679 + 355.158697803128860i	17,30,1	29.57428513009984 + 30.28762346982389i	1047.5187698002988 + 712.64043391753301i
17,29,13	2.928227054061864 + 45.040626718027478i	292.00959962990535 + 55.34311511979033i	17,30,5	20.05217270052415 + 36.568438321603701i	705.4949782886242 + 641.821631722801i
17,30,3	26.490826549993290 + 33.63065912715283i	865.6740089071268 + 698.39932601083759i	17,30,9	15.367021028526235 + 41.628665528863237i	453.51899024396007 + 438.830816548987173i
17,30,7	19.3611922116261				

Table D.19: (continued)

Table with 4 columns: m, n, r; c_{0:r}^{m,n} = c_{0:r-1}^{m,n+2}; lambda_{0:r}^{m,n} = lambda_{0:r-1}^{m,n+2}; m, n, r; c_{0:r}^{m,n} = c_{0:r-1}^{m,n+2}; lambda_{0:r}^{m,n} = lambda_{0:r-1}^{m,n+2}. Rows contain numerical data for various m, n, r values.

Table D.19: Branch points and associated eigenvalues for m = 18.

Table with 4 columns: m, n, r; c_{0:r}^{m,n} = c_{0:r-1}^{m,n+2}; lambda_{0:r}^{m,n} = lambda_{0:r-1}^{m,n+2}; m, n, r; c_{0:r}^{m,n} = c_{0:r-1}^{m,n+2}; lambda_{0:r}^{m,n} = lambda_{0:r-1}^{m,n+2}. Rows contain numerical data for various m, n, r values.

Table D.20: Branch points and associated eigenvalues for m = 19.

Table with 4 columns: m, n, r; c_{0:r}^{m,n} = c_{0:r-1}^{m,n+2}; lambda_{0:r}^{m,n} = lambda_{0:r-1}^{m,n+2}; m, n, r; c_{0:r}^{m,n} = c_{0:r-1}^{m,n+2}; lambda_{0:r}^{m,n} = lambda_{0:r-1}^{m,n+2}. Rows contain numerical data for various m, n, r values.

Table D.20: Branch points and associated eigenvalues for m = 19.

Table with 4 columns: m, n, r; c_{0:r}^{m,n} = c_{0:r-1}^{m,n+2}; lambda_{0:r}^{m,n} = lambda_{0:r-1}^{m,n+2}; m, n, r; c_{0:r}^{m,n} = c_{0:r-1}^{m,n+2}; lambda_{0:r}^{m,n} = lambda_{0:r-1}^{m,n+2}. Rows contain numerical data for various m, n, r values.

Table D.21: Branch points and associated eigenvalues for m = 20.

Table with 4 columns: m, n, r; c_{0:r}^{m,n} = c_{0:r-1}^{m,n+2}; lambda_{0:r}^{m,n} = lambda_{0:r-1}^{m,n+2}; m, n, r; c_{0:r}^{m,n} = c_{0:r-1}^{m,n+2}; lambda_{0:r}^{m,n} = lambda_{0:r-1}^{m,n+2}. Rows contain numerical data for various m, n, r values.

Table D.21: Branch points and associated eigenvalues for m = 20.

Table with 4 columns: m, n, r; c_{0:r}^{m,n} = c_{0:r-1}^{m,n+2}; lambda_{0:r}^{m,n} = lambda_{0:r-1}^{m,n+2}; m, n, r; c_{0:r}^{m,n} = c_{0:r-1}^{m,n+2}; lambda_{0:r}^{m,n} = lambda_{0:r-1}^{m,n+2}. Rows contain numerical data for various m, n, r values.

Table D.22: Branch points and associated eigenvalues for m = 21.

Table with 4 columns: m, n, r; c_{0:r}^{m,n} = c_{0:r-1}^{m,n+2}; lambda_{0:r}^{m,n} = lambda_{0:r-1}^{m,n+2}; m, n, r; c_{0:r}^{m,n} = c_{0:r-1}^{m,n+2}; lambda_{0:r}^{m,n} = lambda_{0:r-1}^{m,n+2}. Rows contain numerical data for various m, n, r values.

D.1. Branch points $c_{0;r}^n$, and Associated Eigenvalues $\lambda_{0;r}^n$ of the SWE

Table D.22: (continued)

m, n, r	$c_{0;r}^n = c_{0;r-1}^{n+2}$	$\lambda_{0;r}^n = \lambda_{0;r-1}^{n+2}$	m, n, r	$c_{0;r}^n = c_{0;r-1}^{n+2}$	$\lambda_{0;r}^n = \lambda_{0;r-1}^{n+2}$
21.29,1	21.589158015031687 + 33.076046257940417i	811.950997679896318 - 460.952793588927370i	21.29,3	17.674374632656371 + 36.132297254150581i	675.618921822080932 - 404.464817825196008i
21.29,5	13.441229064672757 + 38.747557704584829i	564.97723588303685 + 31.967033008399125i	21.29,7	27.0289059781091 + 41.047441442712459i	486.80116943196519 + 192.522426818376221i
21.29,9	3.020945176896309 + 43.06987650197605i	444.239541106579736 + 50.36364730490025i	21.30,1	23.504201789532829 + 33.594899148717343i	886.923921061584338 + 527.058885762687585i
21.30,3	19.710293078578659 + 36.774863922278139i	736.47748442188711 + 476.06742825111581i	21.30,5	13.636470901486663 + 39.336590249938121i	614.60490816102448 + 387.980074182614091i
21.30,7	11.71054540121592 + 41.76154474929276i	521.384655775348961 + 270.838995920619131i	21.30,9	6.042591524347639 + 43.893497186206424i	401.6909727113416 + 139.940312480092224i
21.31,1	25.38862829768463 + 34.085923284049047i	967.74223604127245 + 595.07131751976721i	21.31,3	21.700692494422420 + 37.260167133233381i	805.59020922938194 + 849.414007810812324i
21.31,5	17.77341554787226 + 40.008988113784481i	671.075800985314572 + 465.52487498729135i	21.31,7	3.502636967867168 + 42.46055347670794i	563.759143545733878 + 352.004274275843667i
21.31,9	8.72743939717698 + 44.661713748123305i	486.271950519626444 + 214.379947321408975i	21.31,11	11.909019678172835 + 46.624286738262192i	444.177893991906672 + 55.01400446755965i
21.32,1	19.27401669889807 + 34.55578448480820i	1054.320950766773421 + 664.85363069651411i	21.32,3	23.65169766086354 + 37.781293465597024i	880.82071006834298 + 625.643928983759940i
21.32,5	19.843372208924927 + 40.589306234417131i	734.140658158238125 + 458.812262314781601i	21.32,7	15.57314611608669 + 43.106733600916876i	613.45574922272766 + 435.813780246532761i
21.32,9	11.1967808585492 + 38.320302350580478599i	520.7781485198141 + 300.73927092668750i	21.32,11	6.04966670409292 + 44.335858385858i	401.15322784992672 + 143.9939546609794i
21.33,1	29.082985508239531 + 35.000616570259079i	1146.58862063713768 + 736.30297997478867i	21.33,3	25.97029286910579 + 38.278023953850408i	962.04274547468828 + 703.349563902815021i
21.33,5	20.84871038013181 + 41.142141654073076i	803.60484271777113 + 628.40400997604843i	21.33,7	11.85609467523636 + 43.719471613115367i	565.591024579471655 + 522.0974913820661i
21.33,9	13.57924602305922 + 46.06296764888324i	563.195802218236963 + 389.871590697219244i	21.33,11	8.87924861910542 + 40.6127524682496017i	455.9901294859797 + 235.285811012345107i
21.33,13	3.003752069970225 + 50.11115487900595i	444.13581768151534 + 60.246920097340222i	21.34,1	30.89941612713619 + 35.427293429498316i	1244.4843308691998 + 809.329533344804191i
21.34,1	27.60430521158504 + 38.752819683266189i	1049.161392338862242 + 782.849584294449755i	21.34,3	6.04966670409292 + 44.335858385858i	879.31268048216635 + 712.965303805824280i
21.34,7	19.9598457028366 + 44.302605509082038i	733.526834849947932 + 610.68154102371371i	21.34,9	15.8216419785611 + 46.708284352813701i	613.0553384118099 + 481.609964694592878i
21.34,11	11.2764232632766 + 48.908279556182139i	520.482363021281230 + 329.404490940183001i	21.34,13	6.06389424215276 + 50.910184675323499i	460.2139811167496 + 156.858965894738461i
21.35,1	32.69784889264040 + 35.837159846632844i	1347.955524983506166 + 883.8547648478632i	21.35,3	29.236675153457028 + 39.20775809492078i	1142.0942834481363 + 864.048280381374717i
21.35,5	25.79350395101040 + 42.171569860724100i	961.136664481816752 + 799.449540672171166i	21.35,7	12.25499390268817 + 44.859273760291345i	803.44551496904727 + 701.450066276174122i
21.35,9	18.02944038895532 + 47.22839901839333i	670.0138365542325 + 375.7954366230408i	21.35,11	15.66310708540563 + 49.582821531612021i	503.33453213536906 + 426.240938271951057i
21.35,13	8.7962471271268 + 51.662773986498159i	485.8069938163799 + 255.501524191455301i	21.35,15	3.00271957800573 + 53.54146040400744i	444.1064228360309 + 64.949659911711151i
21.36,1	34.48297130108375 + 36.231114251958089i	1456.95389508638034 + 959.805167357497147i	21.36,3	31.171819067540881 + 39.644602487914227i	1244.7094242815818 + 946.8604987174622i
21.36,5	27.11489835590477 + 42.654608707285185i	1048.970434306240122 + 887.755058420152781i	21.36,7	14.05463670861065 + 45.392102006636634i	879.712159878375577 + 794.266865388781298i
21.36,9	20.75822389421559 + 49.90738023372761i	733.808719186192434 + 672.2901149476445178i	21.36,11	25.96263144634623 + 50.233514425958801i	650.8581554544009 + 525.625024834599791i
21.36,13	11.33858351544737 + 52.375789874146754i	520.380349080651478 + 357.167459745666342i	21.36,15	6.082475195425239 + 54.33864942796233i	459.9387891342510 + 168.841495080914631i

Table D.22: Branch points and associated eigenvalues for $m = 21$.

Table D.23: Branch points and associated eigenvalues for $m = 22$.

m, n, r	$c_{0;r}^n = c_{0;r-1}^{n+2}$	$\lambda_{0;r}^n = \lambda_{0;r-1}^{n+2}$	m, n, r	$c_{0;r}^n = c_{0;r-1}^{n+2}$	$\lambda_{0;r}^n = \lambda_{0;r-1}^{n+2}$
22.22,1	3.415577625869812 + 28.232598718124741i	488.51123188460892 + 25.750427780328604i	22.23,1	6.412635278665273 + 29.30671760089486i	508.10993582219946 + 68.98583849646446i
22.22,5	9.002084566969068 + 30.229507184939826i	537.11289910093387 + 117.050522696574371i	22.23,3	3.204914076592091 + 32.75019039837137i	487.831524887154444 + 33.7870456983907271i
22.22,9	11.376740782597487 + 31.05200633763621i	574.08566809239481 + 149.128261390054604i	22.23,5	2.610666011173221 + 33.697328638685970i	505.68978208830332 + 88.65674927271604i
22.22,13	13.61408513413758 + 31.798465158421386i	618.30533868066206 + 224.641229582757871i	22.23,7	2.223293	533.21131989180497 + 147.47662832285101i
22.22,17	15.114915138989604 + 36.798434520782107i	647.58929212602827 + 40.293420147327700i	22.23,9	15.754614538233469 + 32.48505390093670i	669.3301020049214 + 23.178200140400795i
22.22,21	11.258243168618877 + 35.324351078399258i	569.017648345297516 + 209.89545433946030i	22.23,11	6.130098993690380 + 37.686188774164201i	504.5833644929568 + 105.097221980933625i
22.22,25	17.82260989004240 + 33.122630310147117i	726.85936803610217 + 344.07193948546271i	22.23,13	3.541408670295821 + 36.0415818691882828i	612.3603822902529 + 275.425275286050731i
22.22,29	8.785700367469154 + 38.498892356075181i	531.385209501061240 + 173.36698896189731i	22.23,15	3.06842459526676 + 40.612752446520979i	487.37851623338153 + 46.082807060696561i
22.22,33	19.834026982607883 + 33.7191386949094033i	790.67468247937548 + 408.09680079376041i	22.23,17	3.726352458379273 + 36.709793762570801i	662.77300651103827 + 343.860211764961605i
22.22,37	12.739121806926637 + 39.251193036858019i	566.6458207551440 + 244.90036376634632i	22.23,19	6.0690308781262531467 + 43.680310246800i	603.9678356546763 + 119.92639557387996i
22.22,41	21.799873802022472 + 34.280195093216413i	860.60966851586147 + 474.039768171520011i	22.23,21	17.836654760516097 + 37.336522112444193i	719.71927125012011 + 64.9149106170136861i
22.22,45	13.557397139172826 + 39.95252368349408i	609.630294908242831 + 319.475067115227516i	22.23,23	8.77623346510588 + 42.256145928959601i	530.37704899202911 + 196.90367101737859i
22.22,49	3.042839507776337 + 44.2840835962014444i	487.278631876363477 + 51.45238977787461i	22.23,25	33.228055500510010 + 34.810700019749632i	936.53145152697216 + 54.0147804575272530i
22.22,53	19.888665507796359 + 37.9275125734027277i	783.552067889250679 + 488.368814154221354i	22.23,27	15.777245272601565 + 40.612740891591885i	650.87815151428326 + 396.814484408344695i
22.22,57	11.260220121218925 + 42.994047946255151i	565.37114299959993 + 276.909367868196261i	22.23,29	6.087225664399372 + 45.11519288273604i	503.5974135086691 + 133.77691607570380i
22.22,61	25.62082335518403 + 35.31222777000092i	1018.33890888176317 + 612.04665627906917i	22.23,31	21.891670248625221 + 38.38727585436372i	853.48974624749390 + 564.05932085107073i
22.22,65	17.51261035904499 + 41.235479163820057i	716.98623164713895 + 476.714315949012409i	22.23,33	13.08916094547796 + 43.6876791658989272i	680.22927026813464 + 359.980083211411559i
22.22,69	8.791747937665852 + 45.890644871519306i	529.785552205373506 + 219.010532670201229i	22.23,35	3.02888231640836 + 47.858496009254985i	487.122452466298001 + 56.5415854471748495i
22.22,73	27.495174885340536 + 35.793752057566245i	1105.939143008173914 + 683.848759055774410i	22.23,37	23.8562732545875 + 39.019435915400386i	929.58131291669408 + 641.83416271489251i
22.22,77	20.005630517613262 + 41.825970627313644i	780.75962390757501 + 558.9936068862261i	22.23,39	15.896127273248868 + 44.343075700202512i	658.4714489649370 + 445.67360297215151i
22.22,81	17.688022461620790 + 40.112327639488271i	1099.761685770190752 + 803.142284807978171i	22.23,41	24.0345842841325 + 42.92452440137294i	927.4827097253771 + 730.08632026369092i
22.22,85	29.342186994343623 + 36.251752863450161i	1199.26000251601572 + 757.371191352878927i	22.23,43	15.786134325095972 + 39.526962809964992i	1011.705503406633321 + 271.56593964720303i
22.22,89	22.04056370952936 + 38.39270402339310i	850.97833490188930 + 643.49480947942902i	22.23,45	10.833252167289024 + 44.964975384403807i	715.749604744042928 + 230.88926505478861i
22.22,93	13.677395209247346 + 47.30840246099169i	607.524291015920653 + 398.245045838331123i	22.23,47	31.840848518905956 + 49.43988366638606i	529.43319494152056 + 240.1272151225861i
22.22,97	3.02190332444110 + 51.362902946214618i	487.166810472639955 + 61.431845647603181i	22.23,49	31.6990950126382 + 36.690314450929954i	1298.2384911998900 + 832.52370579275744i
22.22,101	17.688022461620790 + 40.112327639488271i	1099.761685770190752 + 803.142284807978171i	22.23,51	8.9247108563459 + 55.699151275363157i	578.98418403505315 + 151.13528785678051i
22.22,105	10.142823038680433 + 45.55710928859568i	779.80128758685616 + 62.4647184321851i	22.23,53	15.95270913129324 + 47.962206370913492i	687.8892206844528 + 491.929811455256006i
22.22,109	11.352594561589037 + 50.16304624072800i	564.28783191330137 + 336.159944817030091i	22.23,55	10.61700115025295 + 52.167663080084722i	503.2038787763655 + 159.67828129116905i
22.22,113	32.97852199255461 + 37.111929143127601i	1402.82022898767472 + 909.21905895764400i	22.23,57	29.95513812557254 + 40.477615321906121i	1193.664981448317 + 55.6680331347860

Table D.24: (continued)

Table with 4 columns: m, n, r; c_{\sigma, r}^{m, n} = c_{\sigma, r-1}^{m, n+2}; \lambda_{\sigma, r}^{m, n} = \lambda_{\sigma, r+1}^{m, n+2}; m, n, r; c_{\sigma, r+1}^{m, n} = c_{\sigma, r+1}^{m, n+2}; \lambda_{\sigma, r+1}^{m, n} = \lambda_{\sigma, r+1}^{m, n+2}

Table D.24: Branch points and associated eigenvalues for m = 23.

Table with 4 columns: m, n, r; c_{\sigma, r}^{m, n} = c_{\sigma, r-1}^{m, n+2}; \lambda_{\sigma, r}^{m, n} = \lambda_{\sigma, r+1}^{m, n+2}; m, n, r; c_{\sigma, r+1}^{m, n} = c_{\sigma, r+1}^{m, n+2}; \lambda_{\sigma, r+1}^{m, n} = \lambda_{\sigma, r+1}^{m, n+2}

Table D.25: Branch points and associated eigenvalues for m = 24.

Table with 4 columns: m, n, r; c_{\sigma, r}^{m, n} = c_{\sigma, r-1}^{m, n+2}; \lambda_{\sigma, r}^{m, n} = \lambda_{\sigma, r+1}^{m, n+2}; m, n, r; c_{\sigma, r+1}^{m, n} = c_{\sigma, r+1}^{m, n+2}; \lambda_{\sigma, r+1}^{m, n} = \lambda_{\sigma, r+1}^{m, n+2}

Table D.26: Branch points and associated eigenvalues for m = 25.

Table with 4 columns: m, n, r; c_{\sigma, r}^{m, n} = c_{\sigma, r-1}^{m, n+2}; \lambda_{\sigma, r}^{m, n} = \lambda_{\sigma, r+1}^{m, n+2}; m, n, r; c_{\sigma, r+1}^{m, n} = c_{\sigma, r+1}^{m, n+2}; \lambda_{\sigma, r+1}^{m, n} = \lambda_{\sigma, r+1}^{m, n+2}

Table D.27: Branch points and associated eigenvalues for m = 26.

Table with 4 columns: m, n, r; c_{\sigma, r}^{m, n} = c_{\sigma, r-1}^{m, n+2}; \lambda_{\sigma, r}^{m, n} = \lambda_{\sigma, r+1}^{m, n+2}; m, n, r; c_{\sigma, r+1}^{m, n} = c_{\sigma, r+1}^{m, n+2}; \lambda_{\sigma, r+1}^{m, n} = \lambda_{\sigma, r+1}^{m, n+2}

Table D.27: (continued)

m, n, r	$c_{o;r}^{m,n} = c_{o;r+1}^{m,n+2}$	$\lambda_{o;r}^{m,n} = \lambda_{o;r+1}^{m,n+2}$	m, n, r	$c_{o;r}^{m,n} = c_{o;r+1}^{m,n+2}$	$\lambda_{o;r}^{m,n} = \lambda_{o;r+1}^{m,n+2}$
26.35,7	11.60015400151793 + 47.817521614315040i	761.211204784169468 + 300.869476315743281i	26.35,9	6.25792881700033 + 49.954851923594340i	696.47078198684494 + 144.767646116528341i
26.36,1	26.52120503083791 + 40.165804035696659i	1239.727445161671540 + 617.363485280597661i	26.36,3	22.61724252023617 + 45.338871823387599i	1064.471491623905195 + 619.002644899146278i
26.36,5	18.485224199688846 + 46.08840411688797i	920.2912597451615673 + 519.9895258677111i	26.36,7	14.014263031277414 + 48.54984525156463i	805.95149990934633 + 690.80964084995955i
26.36,9	9.03764994708619 + 50.7601789264440547i	723.789699876752366 + 236.95476656872223i	26.36,11	3.10510680574956 + 52.74719252737937i	679.347914129366927 + 60.964127794313605i
26.37,1	28.437027297815229 + 40.689728809580021i	1331.28380335492637 + 757.191299994155210i	26.37,3	24.630985029537219 + 43.25803196516667i	1143.91414530855004 + 704.39976088446637i
26.37,5	20.623995486691040 + 46.711718761440047i	986.817161543808083 + 609.715240285915002i	26.37,7	16.6324798666278685 + 49.236129851051937i	858.32339062318152 + 483.853494440321981i
26.37,9	11.614586904112783 + 51.1519669644909790i	760.119566978958233 + 332.31563157423891i	26.37,11	6.247561409384384 + 53.588245268854555i	696.144010205852283 + 158.490881402751313i
26.38,1	30.326778383463395 + 41.09130044375502i	1428.68437770291818 + 838.636619983651242i	26.38,3	16.2678374907848077 + 44.4603938116004688i	1229.5386030937900 + 791.95956478874868i
26.38,5	22.710139017666081 + 47.31671033894487641i	1059.96790696575363 + 701.87626551423432i	26.38,7	18.554913444645006 + 49.892572359173293i	917.950384592221334 + 579.566776848693855i
26.38,9	14.052842619821719 + 52.239456668651581i	804.706059017117068 + 430.698104212281294i	26.38,11	9.045561598150178 + 54.380276876064919i	725.247938184273835 + 258.90423233307653i
26.38,13	3.091890039722647 + 56.22066279458617i	679.288598562196853 + 66.033883372245467i	26.39,1	32.19469713179122 + 41.671854955746920i	1531.8851675809260 + 922.030519979586529i
26.39,3	28.55472893471022 + 44.985421245271761i	1321.2330275642117 + 881.561829057602369i	26.39,5	24.752236329197380 + 47.890196345008591i	1159.568074102101718 + 796.32417938971421i
26.39,7	20.72073739445129 + 50.519044415081581i	984.54651817687483 + 677.839639622904935i	26.39,9	16.2837977538241 + 52.924352527667061i	857.035282750918170 + 531.904537404837030i
26.39,11	11.6434790939538 + 55.130780711273847i	759.46495912647388 + 362.36368899403247i	26.39,13	6.24716799150211 + 57.1474411177196512i	695.9195258110163 + 171.66731966022331i
26.40,1	34.041898436439955 + 42.1340306915509095i	1640.743783960797843 + 1007.110727032101202i	26.40,3	30.473694736801892 + 45.489586295820255i	1418.902952049519854 + 973.098974825793793i
26.40,5	26.76869369943075 + 48.440101278949918i	1225.47372958663407 + 892.82489236002531i	26.40,7	22.832514789757049 + 51.18634139177527i	1057.886628148083673 + 78.52846460061714i
26.40,9	18.64287181686041 + 53.787235150611548i	916.7306959790719 + 635.84534414377754i	26.40,11	14.104521169059252 + 55.844747363415161i	809.97271724635002 + 468.769283457878244i
26.40,13	9.063248410797392 + 57.929806594205743i	722.89118841256379 + 280.420597600018620i	26.40,15	3.08416270777157 + 59.83371305649167i	679.24523052838030 + 79.92576684727644i
26.41,1	35.872168442646455 + 42.5791284623349925i	1755.28765396028416 + 1093.8438187692047i	26.41,3	32.369082196260969 + 45.97499447131391i	1522.46730560816570 + 1066.475937381962694i
26.41,5	28.7292132584835 + 48.968564617333058i	1317.564065273002599 + 991.5879292812498i	26.41,7	24.89981465923165 + 51.693889038679458i	1177.78865188900903 + 881.484586071262508i
26.41,9	20.852619037915229 + 54.5042935184504351i	985.50337477524983 + 742.291908144242358i	26.41,11	16.426292941405601 + 56.256518183213440i	856.348931032041260 + 57.9574668115457793i
26.41,13	11.681795919056577 + 58.673815755838979i	759.015491032370733 + 39.3380949398957939i	26.41,15	6.253242324749878 + 60.649749783625891i	695.76318750257554 + 184.4297363797302i

Table D.28: Branch points and associated eigenvalues for $m = 26$.

m, n, r	$c_{o;r}^{m,n} = c_{o;r+1}^{m,n+2}$	$\lambda_{o;r}^{m,n} = \lambda_{o;r+1}^{m,n+2}$	m, n, r	$c_{o;r}^{m,n} = c_{o;r+1}^{m,n+2}$	$\lambda_{o;r}^{m,n} = \lambda_{o;r+1}^{m,n+2}$
27.27,1	3.606374993236778 + 33.628464118124894i	733.969792160125508 + 29.110162806608492i	27.28,1	6.71665699006679 + 34.777636714027452i	755.38826936835994 + 78.022082456475175i
27.29,1	9.47796599199687 + 35.776185498087024i	786.88002624908177 + 62.410911312525173i	27.29,3	3.558103638742507 + 38.352111893329834i	37.86520357462626 + 37.86520357462626i
27.30,1	11.96124579100816 + 35.6700618385620496i	826.816988047930181 + 191.359935415622580i	27.30,3	6.49767048868396 + 39.386585848972269i	752.42406491420570 + 99.37758487309707i
27.31,1	14.294652351184308 + 37.480497052667678i	874.376679789656464 + 254.219961543919652i	27.31,3	9.29077103102465 + 40.268514550187220i	781.98207077870389 + 165.29649000261169i
27.31,5	3.246054671998034 + 42.560247845057312i	732.799084833389505 + 44.858505146886541i	27.31,7	16.52179412202266 + 38.237481768080151i	929.54709693346808 + 120.205186417937733i
27.32,1	11.705127603510192 + 41.103358787580210i	820.301173810959267 + 235.20717826398066i	27.32,5	6.388612054202315 + 43.49622608952697i	751.015512966070771 + 110.32642119674785i
27.33,1	18.66893090369802 + 38.938539359196198i	990.50788791898889 + 389.90540951970568i	27.33,3	14.44610126805398 + 41.877673112341753i	866.54024265010669 + 380.68901045244800i
27.33,5	9.15173170696200 + 44.5826807484829951i	779.575961210915580 + 192.92507904881364i	27.33,7	3.1841193452566329 + 46.50865963830399i	732.597314450997818 + 11.02021311993412i
27.34,1	20.755305223549576 + 39.596377019913177i	1058.48584799681771 + 62.90232880575046i	27.34,3	16.411224952429770 + 42.601688178514976i	102.1651284923492268 + 385.39974233492261i
27.34,5	11.70012683649614 + 45.159961413188533i	817.046195619805076 + 272.599709818769915i	27.34,7	6.329812153122830 + 47.399509323548415i	750.2027863532699 + 132.80157172333649i
27.35,1	22.786949181301515 + 40.217073064338699i	1132.7982642234910 + 536.863064787206861i	27.35,3	18.89822610309430 + 43.282963496119415i	809.8031841452912 + 465.049717165058077i
27.35,5	14.104205904887699 + 45.91154463691455i	862.6116422996315 + 555.554192259968878i	27.35,7	9.109690894004762 + 48.231864546578800i	718.169518048242470 + 217.993608912452316i
27.35,9	3.14679865170705 + 50.288261370418617i	732.46882666840734 + 56.693784124259459i	27.36,1	24.778635757617931 + 40.805410235296761i	123.29307254460336 + 614.02450351734088i
27.36,3	20.755305223549576 + 39.596377019913177i	1048.17879638230110 + 54.41629699354589i	27.36,5	16.402663497904829 + 46.6192208315794977i	915.73684588183280 + 441.58836125603380i
27.36,7	11.68134587268993 + 49.012659001012331i	815.14679752926280 + 306.5824916599764386i	27.36,9	6.298816970614923 + 51.154299895928602i	749.68500810549285 + 147.434620740013685i
27.37,1	26.734987403542085 + 41.365196682820721i	1299.849288028339191 + 693.4084563599797436i	27.37,3	12.29008831990355 + 44.53922741018159i	1122.0945820954076 + 632.303496706551227i
27.37,5	18.61966848286975 + 47.289856379202043i	976.040388584973784 + 530.471666003453151i	27.37,7	14.1114767290632 + 49.749351270979395i	860.345648621420537 + 398.36060498089701i
27.37,9	9.90654054143118 + 51.966718376102854i	777.279027652139121 + 241.30948809927156i	27.37,11	3.123451001991159 + 53.95930868946315i	732.381117113252003 + 62.038004170275471i
27.38,1	11.96124579100816 + 35.6700618385620496i	1392.36523556221937 + 774.8906275002021i	27.38,3	24.815723154505022 + 45.122454040144611i	1202.336115895185003 + 719.54636023232999i
27.38,5	10.77158889698373 + 47.927576954448781i	1043.235857858035160 + 62.006858556014436i	27.38,7	16.43510145880163 + 50.44771107638312i	913.236370130909223 + 493.113121950650722i
27.38,9	11.689680475951500 + 52.334714787349651i	813.963096658569839 + 338.40062723418744i	27.38,11	6.285271433616703 + 54.805775661192804i	749.336766236240536 + 18.2695694400454i
27.39,1	30.561170221319291 + 42.411002185432881i	1490.75556887706664 + 858.348167525624641i	27.39,3	26.804410342503605 + 45.679989152306860i	1288.81096227653019 + 809.002279685182430i
27.39,5	22.870014577613222 + 48.53600450102141i	1117.09991871218131 + 716.02420539443665i	27.39,7	18.69667913053198 + 51.12318574490260i	974.35533568486299 + 590.64535713397199i
27.39,9	14.142791426757825 + 53.460603281779527i	858.9702030438848 + 438.574975462954844i	27.39,11	9.100194992661137 + 55.60410912421125i	716.69186654766945 + 263.4645701282886i
27.39,13	3.108776637594922 + 57.548976197197178i	732.31851799881991 + 67.14780265672026i	27.40,1	24.438366516429234 + 42.901757674170002i	1594.94760167798479 + 943.676891199768360i
27.40,3	28.761302348108848 + 46.213451464807159i	1381.389439830151105 + 900.91493136680281i	27.40,5	6.293717973176931 + 49.118263731413251i	1197.45334311694189 + 512.376352372959247i
27.40,7	10.857731530770504 + 51.746888413875134i	1040.651620256199521 + 690.78509129357305i	27.40,9	16.481204295438257 + 54.152874398705833i	111.79757447755302 + 641.63984912956444i
27.40,11	22.870014577613222 + 48.53600450102141i	813.206492115121591 + 368.728287283592923i	27.40,13	6.28202829410363 + 58.381053699232069i	749.05935989186 + 174.8083110584528i
27.41,1	34.295430416061485 + 43.373644151502565i	1704.87754205698289 + 1030.784219963368866i	27.41,3	31.890579661284666 + 46.727670454682277i	1479.97477558821059 + 940.97335207804141i
27.41,5	26.929327858577448 + 49.676771722614390i	1284.149034429937501 + 910.934198749727557i	27.41,7	22.981749345268537 + 52.548487516102886i	1114.653565136804859 + 793.3804486152040i
27.41,9	18.5945989572667 + 54.813129750361999i	972.0063348503938 + 647.432358126231003i	27.41,11	10.18688894438373 + 57.081699830646926i	858.13296029597034 + 476.9497407803673i
27.42,1	9.112426689383603 + 59.169092714709397i	776.29810756873258 + 284.77012971899563i	27.42,15	3.099817257867898 + 61.076666215417601i	732.272473333485209 + 72.081144688884466i
27.42,13	36.134607714551869 + 43.828243736099936i	1820.491059158248390 + 1119.587394189739143i	27.42,17	12.85633693820261 + 47.221767105265271i	1584.48411534865227 + 1089.42853893011761i

Table D.30: Branch points and associated eigenvalues for m = 29.

Table with 5 columns: m, n, r; c_{0,r}; lambda_{0,r}; m, n, r; c_{0,r}; lambda_{0,r}. It lists branch points and eigenvalues for m=29 across various n and r values.

Table D.30: Branch points and associated eigenvalues for m = 29.

Table with 5 columns: m, n, r; c_{0,r}; lambda_{0,r}; m, n, r; c_{0,r}; lambda_{0,r}. It lists branch points and eigenvalues for m=30 across various n and r values.

Table D.31: Branch points and associated eigenvalues for m = 30.

Table with 5 columns: m, n, r; c_{0,r}; lambda_{0,r}; m, n, r; c_{0,r}; lambda_{0,r}. It lists branch points and eigenvalues for m=31 across various n and r values.

Table D.31: Branch points and associated eigenvalues for m = 30.

Table D.32: Branch points and associated eigenvalues for m = 31.

D.1. Branch points, $c_{o;r}^{m,n}$, and Associated Eigenvalues $\lambda_{o;r}^{m,n}$ of the SWE

Table D.32: (continued)

m, n, r	$c_{o;r}^{m,n} = c_{o;r+1}^{m,n+2}$	$\lambda_{o;r}^{m,n} = \lambda_{o;r+1}^{m,n+2}$	m, n, r	$c_{o;r}^{m,n} = c_{o;r+1}^{m,n+2}$	$\lambda_{o;r}^{m,n} = \lambda_{o;r+1}^{m,n+2}$
31.44,3	29.553766416366472 + 38.976178802931765i	1641.273250602175267 + 974.34714307144732i	31.44,3	25.8184813254150 + 53.9851010865637804i	1448.513229634982281 + 874.8204743222289507i
31.44,7	21.38550517542793 + 56.615077865582821i	1284.782439192283164 + 741.177983229559070i	31.44,9	16.89031195061849 + 59.025591446767677i	1150.60395808898065 + 579.45537785680619i
31.44,11	11.983368775389984 + 61.2440432882211i	1048.223558740364365 + 112.724252180119720i	31.44,13	6.417517243212960 + 63.27611742050515i	981.78433611692617 + 185.9413007806319i
31.45,1	35.22670935920281 + 48.278221032453449i	1980.203558740364365 + 112.724252180119720i	31.45,3	31.5222956084258784 + 51.62969653908922i	1743.427787549535196 + 1075.602919275117983i
31.45,5	27.699923486698768 + 54.57612743684643i	1538.2928884421003 + 980.964708605827127i	31.45,7	23.55396233808260 + 57.2531745286086260i	1361.77748101662291 + 851.220862722515562i
31.45,9	19.2082701116289 + 59.11496525526580i	1212.91022610867433 + 692.567353153006633i	31.45,11	14.51275242181757 + 61.988271918432440i	1094.67817147941925 + 508.979874549570070i
31.45,13	9.311266670320388 + 64.085917392642995i	1009.89545711997175 + 303.253587544323791i	31.45,15	3.16025826207007 + 66.009637193880540i	864.379797975895208 + 758.9494198428823i
31.46,1	37.140513396860257 + 48.768813460701964i	2099.98343122259612 + 1219.56720379910313i	31.46,3	31.64659327585862 + 52.157855407740513i	1851.621278369242939 + 117801975370353285i
31.46,5	29.663064340293946 + 55.145270636696381i	1634.424754962217321 + 1089.37062392892190i	31.46,7	16.67308732905431 + 57.866519235269277i	1444.730230539038985 + 963.756817790674063i
31.46,9	21.456901159808218 + 60.376783609874552i	1282.523818008957960 + 808.42153698386654i	31.46,11	11.693858056115505 + 62.702272706911651i	1149.250488057169605 + 627.422427238469839i
31.46,13	12.00048343130303 + 64.858369809642347i	1047.50865476235855 + 473.69881792788863i	31.46,15	6.412736686117354 + 66.849591918272949i	981.558686084162655 + 199.20594672011899i

Table D.32: Branch points and associated eigenvalues for $m = 31$.

Table D.33: Branch points and associated eigenvalues for $m = 32$.

m, n, r	$c_{o;r}^{m,n} = c_{o;r+1}^{m,n+2}$	$\lambda_{o;r}^{m,n} = \lambda_{o;r+1}^{m,n+2}$	m, n, r	$c_{o;r}^{m,n} = c_{o;r+1}^{m,n+2}$	$\lambda_{o;r}^{m,n} = \lambda_{o;r+1}^{m,n+2}$
32.2,1	3.777211678195191 + 38.976178802931765i	1029.401810638441475 + 32.269590925129059i	32.2,3	7.074659875907894 + 40.196025521695475i	1052.534758594813184 + 865.520473480813469i
32.2,5	9.907547027524938 + 41.261995283507572i	1086.371870600432203 + 146.856673879591597i	32.2,7	3.496621539871962 + 43.899666319846527i	1150.60395808898065 + 579.45537785680619i
32.2,9	12.48728014069827 + 42.218125824827501i	1129.103806661975657 + 212.267978771605527i	32.2,11	6.77082428589723 + 44.950788041297576i	1049.036408717067143 + 109.47425675850222i
32.2,13	14.90820952812446 + 43.093496874252693i	1179.81205892693178 + 282.036590547298821i	32.2,15	9.20215520320825 + 45.91348995027926i	1080.548070258118287 + 182.080926644667557i
32.2,17	3.65592447711055 + 48.246213662324929i	1028.04568637354620 + 49.163386930087951i	32.2,19	12.14584809597365 + 43.90383216394414i	1237.93605883964344 + 355.642577580676676i
32.2,21	12.234938503225500 + 46.800168091603382i	1121.243981537631498 + 259.01895267849234i	32.2,23	6.62417039064572 + 49.225644721830491i	1047.37522864669225 + 128.271103251434181i
32.2,25	19.443492125807648 + 44.661087480300708i	1303.09133824693922 + 432.69189807913896i	32.2,27	14.2120847378573808 + 34.001132557379999i	1270.220847378573808 + 34.001132557379999i
32.2,29	9.4853961272280 + 50.119339370641944i	1077.604629297079714 + 211.513176662578758i	32.2,31	3.290349698146998 + 52.31326392759291i	1027.80615369907664 + 55.688231346715022i
32.2,33	12.586046968195280 + 45.37310653389444i	1374.998080671628713 + 512.874464840774070i	32.2,35	7.035711389708265 + 48.398727078096941i	1226.88829175248450 + 44.9261006657987179i
32.2,37	12.12072359137290 + 50.97791871515765i	1117.172106638776086 + 798.722739257648444i	32.2,39	6.542133812435248 + 53.243994524297847i	1046.37982700021216 + 146.961006657381824i
32.2,41	23.682425167876474 + 46.046510498782681i	1453.442496715108746 + 595.39088231995356i	32.2,43	19.292112231183410 + 49.128524060416503i	1290.83370288524925 + 52.27936204754444i
32.2,45	14.603568033954575 + 51.773040566568252i	1165.187349311804837 + 389.59058797359860i	32.2,47	9.414197175661711 + 54.114559921440844i	1079.529153502302006 + 237.912255339800716i
32.2,49	5.24286334524358 + 56.200114272690371i	1027.651144023564844 + 61.65019393704723i	32.2,51	25.92395890913266 + 46.68605453291039i	1538.25511797221288 + 681.677349723817201i
32.2,53	21.479211412485146 + 49.820281849768421i	1361.75164390893876 + 603.03940133849505i	32.2,55	16.693497625761906 + 52.52454348762025i	1221.06364408955107 + 85.829632698382422i
32.2,57	12.067718911741395 + 54.9340467346720i	1114.69541570696287 + 334.538023358896953i	32.2,59	6.499353545932504 + 57.098224455200953i	1045.729261078038 + 160.35143174342291i
32.2,61	27.744706364430570 + 47.295723252462608i	1629.299820433818562 + 769.913098541200995i	32.2,63	23.60645533127615 + 50.47868686952308i	1494.406050150734245 + 696.590641680080361i
32.2,65	19.258547638145746 + 53.280480015880310i	1284.38224777158227 + 581.91550902459312i	32.2,67	14.572190176242664 + 55.709532630718821i	1162.12312793202276 + 434.622198374915131i
32.2,69	9.37752986331515 + 57.944256334704919i	1074.662810099682929 + 262.40209913093959i	32.2,71	3.211364097562372 + 59.962485445814579i	1027.54345899627607 + 67.242323299269171i
32.2,73	29.72262751604594 + 47.878722893032240i	1726.461547620657020 + 860.49516110234082i	32.2,75	6.69256522700965 + 51.107380971360591i	1523.60904247267524 + 752.6298154121161i
32.2,77	21.473189401192510 + 53.918043700393903i	1354.82821125781515 + 681.463094080870310i	32.2,79	12.6610916788954 + 56.446573011621091i	1026.88829175248450 + 44.9261006657987179i
32.2,81	12.048030274461887 + 58.745734994460462i	1113.071614809105768 + 367.91315449953965i	32.2,83	6.46573804278983 + 60.837315711505504i	1045.27798928101015 + 174.8546097771815i
32.2,85	31.67300571132038 + 48.43737129424927i	1829.644624237381549 + 395.219953112404826i	32.2,87	16.2672950214077 + 51.709514723636147i	1614.20729050480992 + 891.369942236908287i
32.2,89	23.63061588468866 + 54.568147639117019i	1432.15583759378942 + 784.46156221100544i	32.2,91	19.274105835594799 + 57.149623204004737i	1280.517291895987910 + 644.277980505911279i
32.2,93	35.499660244660816 + 49.4922882179186061i	2053.757044692635191 + 1495.881282089195213i	32.2,95	6.51565796160514 + 61.665632266519266i	1079.538466526828564 + 285.569464408305407i
32.2,95	31.80938717368542 + 63.633379695180187i	1027.46510372705693 + 72.607038616670574i	32.2,99	33.997495800070794 + 48.974932990484234i	1938.76684890563826 + 1040.9800367981299i
32.2,97	24.3498282808415 + 52.287621929949424i	1711.073118674589523 + 992.306667716961329i	32.2,103	25.93986989549333 + 55.194017127704921i	1516.16673916353895 + 890.026538994066728i
32.2,101	21.512528482627343 + 57.822318374342788i	1350.7474635491456 + 753.456743886340405i	32.2,105	19.987701132643575 + 60.23432691530271i	1215.274270205403232 + 588.278313359636749i
32.2,103	12.048421805838922 + 62.453443099695102i	1111.96344604093459 + 395.881282089195213i	32.2,107	6.452031154338034 + 64.490850953920695i	1044.95363605141055 + 188.7118152411077i
32.2,105	35.499660244660816 + 49.4922882179186061i	2053.757044692635191 + 1495.881282089195213i	32.2,109	23.692452402175044 + 58.46768006646437i	1814.09858992501965 + 1095.445247824893888i
32.2,107	27.808355661897718 + 55.790327642706863i	1606.69928054178995 + 980.01834200594008i	32.2,111	33.692452402175044 + 58.46768006646437i	1427.97673355212636 + 865.314584860694i
32.2,109	31.91640857212830 + 60.319041963492342i	1278.089403460847734 + 703.57183386057076i	32.2,113	14.590959198795860 + 63.205487390974401i	1158.792193381962838 + 516.780404274202267i
32.2,111	9.35884211011095 + 65.305901848184062i	1073.28759019376253 + 307.763907337864051i	32.2,115	3.175256900582551 + 67.234128578462729i	1027.40623149789164 + 67.234128578462729i
32.2,113	37.38198342232525 + 49.991420191959222i	2174.552951654422486 + 1243.878403495772318i	32.2,117	6.37280234814954 + 53.38011624904940i	1923.191176245491306 + 200.670333171215930i
32.2,115	24.40126605414309 + 56.36702630034843i	1703.61717179591055 + 1108.3134525637651i	32.2,119	25.82682391737910 + 59.08824770078027i	1512.00097289838796 + 979.77011518640843i
32.2,117	21.57632761482501 + 61.598527895261441i	1348.256747052606897 + 821.250965919781831i	32.2,121	11.02533175672719 + 63.925605349158074i	1213.79310334047421 + 637.033882516315166i
32.2,119	12.0617018990010 + 66.083791153879913i	1111.91868035888335 + 429.39803313867101i	32.2,123	6.443341478149228 + 68.078323345808104i	1047.14678327809906 + 202.077219516590721i

Table D.33: Branch points and associated eigenvalues for $m = 32$.

Table D.34: Branch points and associated eigenvalues for $m = 33$.

m, n, r	$c_{o;r}^{m,n} = c_{o;r+1}^{m,n+2}$	$\lambda_{o;r}^{m,n} = \lambda_{o;r+1}^{m,n+2}$	m, n, r	$c_{o;r}^{m,n} = c_{o;r+1}^{m,n+2}$	$\lambda_{o;r}^{m,n} = \lambda_{o;r+1}^{m,n+2}$
33.3,1	3.809418527197693 + 40.014520228891905i	1094.485521541517983 + 32.881731870515928i	33.3,1	7.13971124519466 + 41.274600431940061i	1117.95067966338739 + 88.165878042636891i
33.3,5	9.98620342284134 + 42.352112286374499i	1152.24299764993049 + 189.65360056143647i	33.3,3	3.522860972972818 + 44.992569133255891i	1095.52298708478361 + 42.44964532724612i
33.3,9	12.58709603223999 + 43.320947910444549i	1195.51508820931359 + 216.316017822239473i	33.3,5	6.8211816100427 + 46.062417541625351i	1114.37043200293636 + 111.430332160195306i
33.3,13	15.024267506406233 + 44.20761304475941i	1246.83452722845888 + 287.42221858446161i	33.3,7	9.691402163990929 + 47.035047836064353i	1146.2402519101331 + 185.332746156924462i
33.3,17	3.388329286560481 + 49.3758827175319249i	1093.093660731965201 + 49.997885832405714i	33.3,9	16.34737643682025 + 45.02895307884460i	1305.62638881534771 + 362.442538323720781i
33.3,21	12.323030896467065 + 47.931457919292424i	1187.397563871327410 + 263.707595764272233i	33.3,11	6.68919458618248 + 50.36353579112946i	

Table D.35: (continued)

Table with 5 columns: m, n, r; c_{0:r}^m, n = c_{0:r-1}^{m, n+2}; lambda_{0:r}^m, n = lambda_{0:r-1}^{m, n+2}; m, n, r; c_{0:r}^m, n = c_{0:r-1}^{m, n+2}; lambda_{0:r}^m, n = lambda_{0:r-1}^{m, n+2}. Contains numerical data for m=34.

Table D.35: Branch points and associated eigenvalues for m = 34.

Table with 5 columns: m, n, r; c_{0:r}^m, n = c_{0:r-1}^{m, n+2}; lambda_{0:r}^m, n = lambda_{0:r-1}^{m, n+2}; m, n, r; c_{0:r}^m, n = c_{0:r-1}^{m, n+2}; lambda_{0:r}^m, n = lambda_{0:r-1}^{m, n+2}. Contains numerical data for m=35.

Table D.35: Branch points and associated eigenvalues for m = 35.

Table with 5 columns: m, n, r; c_{0:r}^m, n = c_{0:r-1}^{m, n+2}; lambda_{0:r}^m, n = lambda_{0:r-1}^{m, n+2}; m, n, r; c_{0:r}^m, n = c_{0:r-1}^{m, n+2}; lambda_{0:r}^m, n = lambda_{0:r-1}^{m, n+2}. Contains numerical data for m=36.

Table D.35: Branch points and associated eigenvalues for m = 36.

Table D.37: (continued)

m, n, r	$\frac{m, n}{c_{0;r}} = \frac{m, n+2}{c_{0;r+1}}$	$\frac{\lambda_{0;r}^{m, n}}{c_{0;r}} = \frac{\lambda_{0;r+1}^{m, n+2}}{c_{0;r+1}}$	m, n, r	$\frac{m, n}{c_{0;r}} = \frac{m, n+2}{c_{0;r+1}}$	$\frac{\lambda_{0;r}^{m, n}}{c_{0;r}} = \frac{\lambda_{0;r+1}^{m, n+2}}{c_{0;r+1}}$
36.50,5	28.458131410551232 + 60.60949219505221i	1899.861637935797035 + i064.6211010843979461i	36.50,7	24.226571289056395 + 63.2901534588494919i	1714.077295341793615 + 920.384521491368787i
36.50,9	19.73442051281374 + 65.780431520154457i	1558.635985623699753 + 746.387204294411663i	36.50,11	14.893622415935830 + 68.041090325113274i	1435.10740148586285 + 347.315765240080671i
36.50,13	9.543446033608578 - 70.155173978608791i	1346.829384964829387 + 325.408793181068177i	36.50,15	3.232523479434889 + 72.098276179789721i	1299.51043008905068 + 81.996315083605779i
36.51,1	38.312049748682377 + 54.38375242127774i	2491.751438122286345 + 1338.712263629182871i	36.51,3	34.479193452174684 + 58.228520449184721i	2228.700415407144664 + 1285.619040607087326i
36.51,5	30.29016691078294 - 61.2157352446958781i	1999.85683192096188 + 182.29431123030052i	36.51,7	26.399702672043173 + 63.9382418015774261i	1800.733965689864817 + 1042.032438113170261i
36.51,9	22.03816785710112 - 66.451797250685501i	1630.975119645560881 + 871.404369391003801i	36.51,11	17.37525280012781 + 68.784213407712991i	1491.84962275842164 + 674.59356095153851i
36.51,13	12.98812916193684 - 70.951981848865032i	1385.877580903687885 + 454.57349539686770i	36.51,15	6.56267716004798 + 72.959755168643483i	1317.32896079893594 + 213.31410190922424i

Table D.37: Branch points and associated eigenvalues for $m = 36$.

Table D.38: Branch points and associated eigenvalues for $m = 37$.

m, n, r	$\frac{m, n}{c_{0;r}} = \frac{m, n+2}{c_{0;r+1}}$	$\frac{\lambda_{0;r}^{m, n}}{c_{0;r}} = \frac{\lambda_{0;r+1}^{m, n+2}}{c_{0;r+1}}$	m, n, r	$\frac{m, n}{c_{0;r}} = \frac{m, n+2}{c_{0;r+1}}$	$\frac{\lambda_{0;r}^{m, n}}{c_{0;r}} = \frac{\lambda_{0;r+1}^{m, n+2}}{c_{0;r+1}}$
37.37,1	3.932673698914612 + 44.291023887161971i	1374.812511582645584 + 562.702252291252221i	37.37,3	7.359816241596399 + 45.745110222104231i	1399.57350654475642 + 94.5897853888311531i
37.37,9	10.295496734848161 + 46.699374835887844i	1435.642509166335913 + 160.572992078090020i	37.37,5	3.623609988250024 + 49.381438018147284i	1374.7566362718442571 + 45.355640378402931i
37.40,1	12.967846789130247 + 47.713130370202759i	1481.031140108581667 + 232.120043713751628i	37.40,3	7.014718831687849 + 50.489680853794762i	1395.61617701206856 + 19.070376221591010i
37.41,1	15.469446330863467 + 48.642744604040215i	1534.73801379217719 + 308.448190708983248i	37.41,3	9.962177301434362 + 51.500139857215011i	1428.947183381126064 + 198.037664154858384i
37.42,1	3.475872159152762 + 53.873067696834267i	1373.28155595681994 + 53.258505826996092i	37.42,1	17.849098142256722 + 49.508336068427171i	1596.138342194848747 + 388.990094131848501i
37.42,5	12.661584616705886 - 52.433567793668772i	1471.90904051752289 + 281.717427358144966i	37.42,5	6.841313117545806 + 54.892212289891980i	1393.67493661889898 + 138.971924131058771i
37.43,1	20.136314297541780 - 50.3128504138991271i	1664.816801922877403 + 473.513275695256569i	37.43,3	15.195719437268501 + 53.304500901349603i	1523.496511526339614 + 369.802584897846145i
37.43,5	9.79320256699494 - 55.838862403753781i	1425.49921540891136 + 299.134204400302394i	37.43,7	3.88883325808498 + 58.05378523133372i	1373.0063827171239 + 60.125520865183965i
37.44,1	22.35056722066411 - 51.073771414832555i	1740.463214498193565 + 561.085450308004738i	37.44,3	17.099599719641057 + 54.122882896492925i	1583.0657404662787 + 46.17228187805471i
37.44,5	12.508958062148042 - 56.725072913180050i	1467.07099050406408 + 323.578397418371480i	37.44,7	6.793460730882296 + 59.018442486985229i	1392.500803148270543 + 156.540245903590151i
37.45,1	24.50545919117701 - 51.794453921418854i	1822.842069385836339 + 652.026314191345704i	37.45,3	19.931090057780745 + 54.896441971042101i	1650.16624003789288 + 557.17031012422244i
37.45,5	15.064887546565323 - 57.650198594350969i	1947.1763566505430 + 421.977376663529185i	37.45,7	9.696276366738002 + 59.924016643398988i	1423.37770238526637 + 256.882635023444354i
37.45,9	3.33240689155311 - 62.08749170930444i	1372.82662729625898 + 66.373954895238167i	37.46,1	26.10991928182610 + 52.480121556784539i	1911.766945457159181 + 57.459072604936040i
37.46,3	22.178896294541800 - 55.631077270390016i	1724.463941278419725 + 655.911670631208835i	37.46,5	15.202994036990666 + 58.351064885192478i	1575.933981455774259 + 524.025407491102961i
37.46,7	12.25939995818624 - 60.778895619850721i	1464.053629960580943 + 361.164911211686444i	37.46,9	6.67539351228771 + 62.966547163092400i	1391.73251969271040 + 172.66246548378721i
37.47,1	28.67426310354863 - 53.134760283120517i	2007.086312513262783 + 842.347345607739191i	37.47,3	24.36303729743361 + 56.331455993223461i	1805.700628255930810 + 37.67699897852568747i
37.47,5	19.849070566347305 - 59.1035038135218866i	1642.135337321622076 + 629.457117800680866i	37.47,7	14.999907925456298 + 61.589814984143284i	1513.616636111539265 + 469.162863008985255i
37.47,9	9.63901819108881 - 63.8435561718075156i	1421.953019197015692 + 282.51073352855937i	37.47,11	3.293677672427689 + 65.887645964870771i	1372.700190329577474 + 72.207489182682977i
37.48,1	30.702546159448008 - 53.76166730302323i	2108.674383098102226 + 941.763081127564674i	37.48,3	26.503149148992513 + 57.001351976886717i	1893.670645471439684 + 862.339823500328293i
37.48,5	22.12292852707095 - 59.821887220009098i	1715.689705271557159 + 398.044708659990560i	37.48,7	17.485255718925294 + 62.3621632103966871i	1571.4465025896424 + 580.673500086846977i
37.48,9	12.381583410407172 - 64.672662324699944i	1462.017940083228041 + 736.046553205456254i	37.48,11	6.63480186124983 + 66.788819423999821i	1391.185130221130832 + 187.797872554868243i
37.49,1	32.69913756805484 - 54.3635871779172959i	2216.424940232038007 + 1043.424983505509505i	37.49,3	28.596059383152523 + 57.643875400370042i	1928.205951945400324 + 969.665716340426081i
37.49,5	24.33526869922221 - 60.509840463120547i	1796.320605492932160 + 849.591248512614470i	37.49,5	9.696276366738002 + 59.924016643398988i	1423.37770238526637 + 256.882635023444354i
37.49,9	14.971937327272359 - 65.469990625870192i	1511.045697263161173 + 1143.7903902640262i	37.49,11	15.609127010675889 + 67.644977666947669i	1480.92596565313083 + 306.639100829082884i
37.50,3	3.266240321461576 - 69.635973207950073i	1372.607044185421728 + 77.742106867897373i	37.50,1	34.668299919240816 + 54.942807246765710i	2330.24704086883962 + 1147.400583293460740i
37.50,5	30.63561863241155 - 58.261628419210203i	2089.165768982584723 + 1079.529668810876510i	37.50,3	16.29790894975664 + 61.170393040521084i	1838.3899784811229 + 96.925484383159101i
37.50,7	22.12113447320368 - 63.807779073632881i	1710.2124743890710 + 813.163987347754869i	37.50,5	17.448461519229642 + 62.299617412426741i	1568.432103415803567 + 633.533061636985512i
37.50,11	12.361101597057150 - 68.4613113272939111i	1460.580787825974312 + 429.620992306105509i	37.50,13	6.265842709391474 + 65.14232346281891i	1498.87565018346577 + 202.2074913678683202i
37.51,1	36.612161907808499 - 55.801308657281961i	2450.061764110991589 + 125.804324396783196194i	37.51,3	32.78296828503554 + 58.868166813959529i	1596.433278982030207 + 1191.80208439712971i
37.51,5	28.615021827638163 - 61.806079424120711i	1978.0436250485896306 + 1080.897414594216955i	37.51,7	24.355406879801539 + 64.487602230742781i	1790.53312592325632 + 933.84857328514040i
37.51,9	19.83553891784134 - 66.9570574983154501i	1635.73255102340706 + 57.1708431591946255i	37.51,11	9.266916367038598 + 69.242034598742361i	1509.241187592846689 + 354.785589197020521i
37.51,13	9.588201414830753 - 71.357427837474071i	1420.208466374955535 + 329.727452412575326i	37.51,15	3.24650543954862 + 73.3067716903046231i	1372.5361146787862 + 83.050627374060201i
37.52,1	24.50534421360891 - 56.400773557749941i	2575.800157541338649 + 361.863124350983935i	37.52,3	34.67350751284704 + 59.431330846602639i	2309.903669974851255 + 1306.367719338560959i
37.52,5	30.69513236758902 - 62.419601206497616i	2078.79282292921399 + 1200.373191837781150i	37.52,7	26.53842709391474 + 65.14232346281891i	1877.835089251678334 + 1057.6069196303005i
37.52,9	22.149907044174412 - 67.656967369393982i	1706.60446765967075 + 883.67237310539882i	37.52,11	17.460348122785476 + 69.991592419682135i	1566.336798112911083 + 63.839929180851919i
37.52,13	12.36316531720742 - 72.161288325120411i	1459.53798202045678 + 460.929719613517885i	37.52,15	6.591642218082538 + 74.172469982632170i	1390.48020663972534 + 216.60530029309371i

Table D.38: Branch points and associated eigenvalues for $m = 37$.

Table D.39: Branch points and associated eigenvalues for $m = 38$.

m, n, r	$\frac{m, n}{c_{0;r}} = \frac{m, n+2}{c_{0;r+1}}$	$\frac{\lambda_{0;r}^{m, n}}{c_{0;r}} = \frac{\lambda_{0;r+1}^{m, n+2}}{c_{0;r+1}}$	m, n, r	$\frac{m, n}{c_{0;r}} = \frac{m, n+2}{c_{0;r+1}}$	$\frac{\lambda_{0;r}^{m, n}}{c_{0;r}} = \frac{\lambda_{0;r+1}^{m, n+2}}{c_{0;r+1}}$
38.38,1	3.96221104798428 + 45.3206973016842001i	1449.892435151165469 + 35.853576721967181i	38.39,1	7.414028129632658 + 46.6462017754524801i	1474.972457793941978 + 96.159201280620561i
38.40,1	10.369995747760778 - 47.7823592020178605i	1511.4736299505469717 + 163.240699593722451i	38.40,3	3.647828004570354 + 50.476347614545784i	1448.81330349175441 + 46.065621072710769i
38.41,1	13.059331861108850 - 48.806820815839195i	1557.379498703661511 + 235.981074073170618i	38.41,3	7.061246679864625 + 51.591980530206875i	1470.920099716126515 + 120.937448647974733i
38.42,1	15.576361024318581 + 49.7466694205257464i	1611.667298743201172 + 313.584945338987382i	38.42,3	10.027296585844525 + 52.611157299943706i	1504.609050385244040 + 201.137912113626700i
38.42,5	3.496998101959446 - 54.992432564133895i	1448.327906826345356 + 54.0556730473607321i	38.42,7	19.77048670195560 + 50.61915029994978361i	1673.7081051332256 + 395.47563682052700i
38.43,3	12.74036728450852 - 55.535982556631866i	1548.012930458062101 + 286.190369646772295i	38.43,5	6.882853154453900 + 56.019126241019521i	1468.928527834702209 + 141.055080232837121i
38.44,1	20.270196303404008 - 51.436121990274941i	1743.0752799821581 + 481.215912169137937i	38.44,3	15.291898991260389 + 57.01101487 + 54.433852068286997i	1600.10917071361732 + 375.597695374194801i
38.44,5	9.8520915923005858 - 56.973454205423361i	1501.063953170787954 + 232.566418095476705i	38.44,7	3.40778619145853 + 59.1950219842099721i	1466.04570931750020 + 100.90281520323171i
38.45,1	22.496462738362957 - 52.206196412179708i	1819.447134041658728 + 570.401657719935			

Table D.40: (continued)

Table with 5 columns: m, n, r; c_{0:r} = m, n+2 / c_{0:r-1}; lambda_{m,n} = lambda_{0:r+1}; m, n, r; c_{0:r} = m, n+2 / c_{0:r-1}; lambda_{m,n} = lambda_{0:r+1}. Contains numerical data for various m, n, r values.

Table D.40: Branch points and associated eigenvalues for m = 39.

Table with 5 columns: m, n, r; c_{0:r} = m, n+2 / c_{0:r-1}; lambda_{m,n} = lambda_{0:r+1}; m, n, r; c_{0:r} = m, n+2 / c_{0:r-1}; lambda_{m,n} = lambda_{0:r+1}. Contains numerical data for various m, n, r values.

Table D.41: Branch points and associated eigenvalues for m = 40.

Table with 5 columns: m, n, r; c_{0:r} = m, n+2 / c_{0:r-1}; lambda_{m,n} = lambda_{0:r+1}; m, n, r; c_{0:r} = m, n+2 / c_{0:r-1}; lambda_{m,n} = lambda_{0:r+1}. Contains numerical data for various m, n, r values.

Table D.42: Branch points and associated eigenvalues for m = 41.

Table D.42: (continued)

m,n,r	$c_{0;r}^{m,n} = c_{0;r-1}^{m,n+2}$	$\lambda_{0;r}^{m,n} = \lambda_{0;r-1}^{m,n+2}$	m,n,r	$c_{0;r}^{m,n} = c_{0;r-1}^{m,n+2}$	$\lambda_{0;r}^{m,n} = \lambda_{0;r-1}^{m,n+2}$
41,56,1	39.403879881765367 + 60.814501955387101i	2931.08932240801551 + 1452.466710812032488i	41,56,3	35.425923871549087 + 64.209849078780192i	2654.05386047939342 + 1387.608087660768206i
41,56,5	31.33860494621258 + 60.21086316632171i	2414.08374286999834 + 1271.19360479139240i	41,56,7	27.07615773249028 + 69.928387107688661i	2205.93929175281728 + 1116.9830626991548i
41,56,9	22.58339662993332 + 72.44858496103281i	2028.937278066173121 + 931.76033276593764i	41,56,11	17.789676389484249 + 74.790771763039672i	1884.18593158824089 + 719.821608926991542i
41,56,13	12.579831906514199 + 76.970714442737397i	1774.136956850481283 + 484.199314894879421i	41,56,15	6.704405201948408 + 78.995745839724307i	1703.076435728184606 + 226.858991456963371i

Table D.43: Branch points and associated eigenvalues for $m = 41$.

m,n,r	$c_{0;r}^{m,n} = c_{0;r-1}^{m,n+2}$	$\lambda_{0;r}^{m,n} = \lambda_{0;r-1}^{m,n+2}$	m,n,r	$c_{0;r}^{m,n} = c_{0;r-1}^{m,n+2}$	$\lambda_{0;r}^{m,n} = \lambda_{0;r-1}^{m,n+2}$
41,42,1	4.07585402960971 + 49.579863734164185i	1770.20555124087241 + 38.13897843348474i	41,42,3	7.622686155449583 + 50.921462584157211i	1796.528207973442022 + 102.305318061087164i
41,42,4	10.655420913703869 + 52.100844916848544i	1834.7298187230605 + 173.6878688936761i	41,42,5	3.741248035115589 + 54.833230406315373i	1769.037119430657640 + 48.874573907594490i
41,42,5	13.41179103931357 + 53.166291053992445i	1882.66232625280214 + 251.101490050569697i	41,42,7	7.240744667836552 + 55.988521432691181i	1792.1112368580559 + 128.251873584793542i
41,42,6	15.98845638688088 - 54.145316415097213i	1939.235146818386738 + 333.701149185470740i	41,42,9	18.436453814721521 + 55.055470005648949i	1988.785933027848159 + 497.209102866242047i
41,42,7	3.57833912909727 + 59.45228545696143i	1768.508302815031357 + 57.179383667103671i	41,42,11	18.436453814721521 + 55.055470005648949i	2003.77715362252431 + 120.87046801478936i
41,42,8	13.05747240959270 + 58.016650432053126i	1872.341513681737752 + 303.48848367635616i	41,42,13	7.04327932654397 + 60.508211055504866i	1789.42380629691470 + 149.21799352539970i
41,42,9	20.78691196148059 + 55.908828991004885i	2075.82894303103174 + 512.155412206332962i	41,42,15	16.65322034408822 + 58.929410933566621i	1926.432974399841669 + 39.299932112664635i
41,42,10	10.079768714348669 + 61.491923488199319i	1823.280313906733682 + 246.00712326321303i	41,42,17	3.481009265644580 + 63.739863841989440i	1768.199633420359987 + 64.379957901602797i
41,42,11	23.05880039582642 + 56.714170836319312i	2155.058527473705453 + 607.179232079296781i	41,42,19	18.142259925308045 + 59.788770963742650i	1988.785933027848159 + 497.209102866242047i
41,42,12	13.870649879202867 + 62.415177322178119i	1866.77783164786115 + 347.380260216241857i	41,42,21	9.032822016219177 + 64.73007976833883i	1788.894507124614893 + 167.63599756345277i
41,42,13	25.269434973690962 + 57.478130077640108i	2241.206814060112720 + 705.649253496668962i	41,42,23	20.502490704868064 + 60.602417100366301i	2058.91357043983432 + 600.131883052359970i
41,42,14	15.494867093401091 + 63.286907296959521i	1919.384502957786026 + 452.992237069595916i	41,42,25	9.96860200267515 + 65.674014201673216i	1820.831371129196214 + 275.06142131401867i
41,42,15	3.1646850460497 + 67.817580638494994i	1767.996128858396332 + 70.9034479887515190i	41,42,27	21.7625060817469 + 58.205887159964549i	2334.071786296233768 + 807.319189205591783i
41,42,16	22.80183038413939 + 61.37629324734795i	2136.454604693195961 + 706.30529252055680i	41,42,29	17.99599379248662 + 64.1141115958787792i	1980.418098043961209 + 562.519650133174423i
41,42,17	12.760784637467589 + 66.561591681415607i	1863.249038770343986 + 386.682547416451200i	41,42,31	6.845813851978324 + 68.770958541308747i	1787.70085600456468 + 184.471301947542001i
41,42,18	29.3948805065275 + 58.901585865992425i	2433.488351044843512 + 911.981161847035510i	41,42,33	25.07115639221930 + 62.115133941128121i	2121.129588777234003 + 816.174263735239900i
41,42,19	20.41041357917440 + 64.9023611637440i	2049.390181330147243 + 675.680883608387603i	41,42,35	15.98996061845133 + 67.405223535748064i	1944.86745186272764 + 502.266321602289565i
41,42,20	9.884172711198099 + 69.678904563567514i	1819.16222728465178 + 301.79492991260809i	41,42,37	3.371217940313155 + 71.748718119479964i	1737.85192383850533 + 79.9713065889481i
41,42,21	31.61384921361323 + 59.58660925072885i	2539.319367234526908 + 1019.45667134467087i	41,42,39	27.28861766909681 + 62.822742523440844i	2162.715579497568288 + 928.928687215102984i
41,42,22	22.79699886167570 + 65.655980908259409i	2125.932578325330370 + 1019.45667134467087i	41,42,41	19.781861383242360 + 68.210144863855461i	1975.02421187031369 + 621.562493089414081i
41,42,23	12.69436213015014 + 70.54093821982158i	1860.824094305713970 + 423.028402310970610i	41,42,43	6.793019336051128 + 72.674708228081020i	1787.0025926206360 + 200.184948574340i
41,42,24	33.65479607278917 + 60.209766254483299i	2651.448949769842784 + 1129.590363345827427i	41,42,45	29.00443312515855 + 63.502277590948021i	2411.030328290853049 + 1044.588051003426244i
41,42,25	24.994252466952062 + 66.378715029841345i	2209.75718675172224 + 911.96819807906219i	41,42,47	20.34311437275123 + 68.980625460305755i	2043.236942490556 + 744.34021380826991i
41,42,26	15.346953766948095 + 71.3641911010893208i	1911.75066492567118 + 548.01574496055731i	41,42,49	9.83538662550379 + 73.55674187778919i	1821.96219009498982 + 326.908214084862894i
41,42,27	3.338361789453690 + 75.70992575335251i	1767.7447725791018 + 62.711512301604325i	41,42,51	35.666327100652865 + 60.82742253246464i	2769.77779305914919 + 1242.24585701573328i
41,42,28	31.502819190039080 + 64.156339422971734i	2815.921920480022991 + 1162.994550348349098i	41,42,53	27.20540023983728 + 67.073581986679099i	2300.632089131760495 + 1034.702451328484585i
41,42,29	22.691184668163224 + 69.710922057209061i	2119.137804123144178 + 870.39375360874252i	41,42,55	17.881425397324922 + 72.152853611270800i	1971.299330614829295 + 676.55848155858924i
41,42,30	12.655168377117590 + 74.339654995938830i	1859.076162454356563 + 457.28860960771254i	41,42,57	6.75673846287593 + 76.474617847356923i	1766.58714221766331 + 215.16838218751928i
41,42,31	35.65175832250221 + 61.423959490991187i	2894.219714365573054 + 1357.32010025857724i	41,42,59	33.7507509257382 + 64.782783682335621i	2627.261680107397314 + 1284.00040026112760i
41,42,32	29.36978085741622 + 74.340397787586061i	2398.36638690026322 + 1160.276127685099937i	41,42,61	24.975767771641294 + 70.431796513985319i	2022.4350974689667 + 999.54095892439584i
41,42,33	9.0044285035614710 + 73.338421590978877i	2138.9984826403474 + 808.5551354103542923i	41,42,63	15.82505212100875 + 75.2075210448488i	1900.475902788884424 + 591.2559675588667i
41,42,34	20.41041357917440 + 64.9023611637440i	1817.06854465703154 + 350.821365200805703i	41,42,65	3.313948126959022 + 79.309001868525115i	1767.62102909077809 + 88.20173669733157i
41,42,35	9.884172711198099 + 69.678904563567514i	2304.699280070725308 + 1474.650486102030300i	41,42,67	35.805167618978986 + 65.39923997439842i	2744.939149622196965 + 1407.507161896742750i
41,42,36	31.502819190039080 + 64.156339422971734i	2502.8008353468384 + 1288.54702428554489i	41,42,69	27.205674825157489 + 71.179382036391982i	2922.89446921039587 + 1131.62023973113707i
41,42,37	22.691184668163224 + 69.710922057209061i	2114.476760275626020 + 949.551768371092741i	41,42,71	17.86991992608147 + 75.983968783084165i	1968.42545605170715 + 728.6607636888102i
41,42,38	12.634178684781514 + 78.166579382131911i	1857.77693852386845 + 489.99105991344327i	41,42,73	6.713863061032280 + 80.195114770338989i	1768.2239046454423 + 229.50770801828064i

Table D.43: Branch points and associated eigenvalues for $m = 42$.

m,n,r	$c_{0;r}^{m,n} = c_{0;r-1}^{m,n+2}$	$\lambda_{0;r}^{m,n} = \lambda_{0;r-1}^{m,n+2}$	m,n,r	$c_{0;r}^{m,n} = c_{0;r-1}^{m,n+2}$	$\lambda_{0;r}^{m,n} = \lambda_{0;r-1}^{m,n+2}$
42,43,1	4.103221954085551 + 50.634939744171567i	1855.28288868750129 + 38.698840231468047i	42,43,3	7.622686155449583 + 51.98761091746806i	1881.909488787813194 + 103.81106519627292i
42,43,4	10.72428694906311 + 53.177365621828877i	1920.527862219095823 + 176.247242130180556i	42,43,5	3.763800654228688 + 55.919591730755058i	1854.09021928778839 + 49.52062187447983i
42,43,5	13.49677955901159 + 54.252634916321647i	1968.95711946628090 + 254.80582163329322i	42,43,7	7.284081883990256 + 57.080662293271999i	1877.4041071783366 + 110.044339955061410i
42,43,6	16.0087868416397583 + 55.241049416216654i	2026.09044009780803 + 338.629322921513399i	42,43,9	18.436453814721521 + 55.055470005648949i	1912.84544341715161 + 216.27812287803834i
42,43,7	3.898265283113136 + 60.5631810691858i	1853.55267166167087 + 87.945078976284467i	42,43,11	18.436453814721521 + 55.055470005648949i	2091.245184894172326 + 427.09639210734240i
42,43,8	13.13345266145043 + 59.12862709224318i	1958.40321905908452 + 307.722672933698017i	42,43,13	7.04327932654397 + 60.508211055504866i	1875.16812509138479 + 151.21893302462195i
42,43,9	20.911390631919765 + 57.022312660778924i	2163.956975848826460 + 519.735143111404028i	42,43,15	15.98996061845133 + 67.405223535748064i	2021.9841029090151 + 403.863455070810630i
42,43,10	10.134849417668084 + 62.616946041929161i	1908.824362405932321 + 249.302707049596781i	42,43,17	3.49875518843406 + 64.871400502198313i	1853.27462263838224 + 65.21108725599563i
42,43,11	23.19558893758885 + 57.836107003244152i	2443.885330659046758 + 616.11755415853446i	42,43,19	20.34311437275123 + 68.980625460305755i	2075.8817184925087 + 504.246738400091698i
42,43,12	12.94018497815679 + 63.547274166200246i	1952.698543791674865 + 352.028814271489864i	42,43,21	6.95922947134233 + 65.876120626053891i	1875.0721062878737 + 169.80664051015147i
42,43,13	25.41603631274478 + 58.6082839984197i	2330.769968761549080 + 716.11372431234695i	42,43,23	26.63987409846502 + 61.732205795142700i	2146.60063941995825 + 608.51879349916581i
42,43,14	15.57529624701764 + 64.42609037607245i	2005.745432400215805 + 459.40983943755576i	42,43,25	10.01866504271950 + 66.8178089843611776i	1906.31183451670964 + 278.31271838740388i
42,43,15	3.432680496494289 + 68.96709551716511i	1853.029375010821923 + 71.788630485147021i	42,43,27	27.83376680263836 + 59.34402566221060i	2429.410967023941026 + 819.30340460521260i

Table D.45: (continued)

Table with columns m, n, r and various lambda and c parameters. It contains numerical data for different combinations of m, n, and r.

Table D.45: Branch points and associated eigenvalues for m = 4.

Table with columns m, n, r and various lambda and c parameters. It contains numerical data for different combinations of m, n, and r.

Table D.46: Branch points and associated eigenvalues for m = 5.

Table with columns m, n, r and various lambda and c parameters. It contains numerical data for different combinations of m, n, and r.

Table D.46: Branch points and associated eigenvalues for m = 5.

Table with columns m, n, r and various lambda and c parameters. It contains numerical data for different combinations of m, n, and r.

Table D.47: Branch points and associated eigenvalues for m = 46.

Table with columns m, n, r and various lambda and c parameters. It contains numerical data for different combinations of m, n, and r.

Table D.47: Branch points and associated eigenvalues for m = 46.

Table D.47: (continued)

m, n, r	$c_{0;r}^{m,n} = c_{0;r-1}^{m,n+2}$	$\lambda_{0;r}^{m,n} = \lambda_{0;r+1}^{m,n+2}$	m, n, r	$c_{0;r}^{m,n} = c_{0;r+1}^{m,n+2}$	$\lambda_{0;r}^{m,n} = \lambda_{0;r-1}^{m,n+2}$
-----------	-------------------------------------	---	-----------	-------------------------------------	---

Table D.47: Branch points and associated eigenvalues for $m = 46$.

m, n, r	$c_{0;r}^{m,n} = c_{0;r-1}^{m,n+2}$	$\lambda_{0;r}^{m,n} = \lambda_{0;r+1}^{m,n+2}$	m, n, r	$c_{0;r}^{m,n} = c_{0;r+1}^{m,n+2}$	$\lambda_{0;r}^{m,n} = \lambda_{0;r-1}^{m,n+2}$
47, 47, 1	4.20895282636513 - 54.8477055500879661i	2215.585614133620358 + 40.986599552394242i	47, 48, 1	7.861727128561436 + 56.242747945635791i	2243.406665344270007 + 109.719181776627791i
47, 49, 1	10.99083895912060 - 57.4223871068798361i	2283.661622641180657 + 186.294572520360475i	47, 49, 2	3.851117516496135 + 60.253250321262790i	2214.307754092641062 + 52.205974638461029i
47, 50, 1	13.825493602492068 - 58.585451046990798i	2334.041638028497346 + 269.347202075233082i	47, 50, 3	1.541885997085442 + 61.447046743217477i	2238.552622249342096 + 137.08231205814713i
47, 51, 1	16.647514897364590 - 59.60998280374915i	2393.37426484129177 + 357.973146023382536i	47, 51, 4	7.075336649130446 + 62.542020733960172i	2275.34648879964845 + 297.979062593503733i
47, 52, 1	3.674798599478546 + 64.992125923452292i	2213.727165274398885 + 60.952215724600329i	47, 52, 1	18.94869176614808 + 60.563892898160141i	2460.937524261350063 + 451.521749266848474i
47, 52, 2	13.427725298344641 - 63.558160961166699i	2322.575134869095109 + 324.372657878198222i	47, 52, 2	7.23290857876245 + 66.082148395169108i	2326.12834192438717 + 159.07752679657071i
47, 53, 1	21.394230349694027 - 61.459521047736331i	2536.237894055210745 + 549.4893762554780i	47, 53, 1	16.10928150017044 + 64.509688283790979i	2379.07932008583707 + 425.708756131273503i
47, 53, 2	10.3485038690550282 - 67.100493693851185i	2270.963606971944500 + 262.244899716165451i	47, 53, 2	3.567700967738928 + 69.380687068691421i	2213.38636040977643 + 68.476017566638120i
47, 54, 1	23.722400939259458 - 62.30583199146266i	2618.914731418487918 + 651.484591744068666i	47, 54, 3	6.1642429147689743 + 65.406923392796031i	2444.11499816274143 + 531.526886583959080i
47, 54, 2	13.209965472084576 - 68.08134348629423i	2316.319065071818468 + 370.286135913882103i	47, 54, 4	7.09721244467742 + 70.406331994094842i	2512.6442551021123714 + 178.319140950505523i
47, 55, 1	25.984150423756006 - 63.109621688396992i	2708.691901704838074 + 757.190856925315585i	47, 55, 1	21.02232459750269 + 66.257617660114931i	2517.16025312173262571 + 641.450398779665201i
47, 55, 2	15.898478326638823 - 68.963906312431902i	2371.096812987525936 + 482.840323858218977i	47, 55, 2	10.208114151785937 + 71.374564339660660i	2268.202389045353938 + 292.56853640206672i
47, 55, 3	3.495803857694570 - 73.546473684962052i	2213.160345260369623 + 75.266119902522444i	47, 55, 3	28.190445507516010 + 63.876178021729925i	2805.30561145439315 + 866.344024483983162i
47, 56, 1	23.44086341564115 - 67.06777124191935i	2597.8276428388647 + 755.167689514850930i	47, 56, 1	18.45900347545209 + 69.82743410910480i	2574.56939520223232 + 599.566627132550283i
47, 56, 2	13.07583620547116 - 72.292610780607646i	2312.303031687526982 + 411.254905247214025i	47, 56, 2	7.00624386635754 + 74.52799799709385i	2233.63829517384737 + 195.84922119576471i
47, 57, 1	30.439613287915866 - 64.609743448322234i	2908.712607965140162 + 978.7211662071799123i	47, 57, 1	25.73243348176082 + 67.842157069196688i	2685.817297980380772 + 872.411071668700282i
47, 57, 2	20.919817945034467 - 70.646111408928885i	2506.21560110792339 + 720.167635990963488i	47, 57, 2	15.776383838630602 + 73.166692306660791i	2365.90753402289290 + 534.136933261921921i
47, 57, 3	10.154009825460730 - 75.400789426473866i	2266.300419360105479 + 320.3704039399335i	47, 57, 3	3.444637424157513 + 77.555998169226701i	2212.999214193912849 + 51.563769890303061i
47, 58, 1	32.46815308712849 - 65.313779700816440i	3018.630015227348849 + 1094.130002019519681i	47, 58, 1	27.96785473638952 + 68.86463898581499i	2780.89807805764576 + 992.9730225185784i
47, 58, 2	33.00170037683061 - 71.432470323460180i	2585.64217607602471 + 844.386972194129839i	47, 58, 2	18.352160552616542 + 74.001917984760581i	2428.312507830368759 + 660.970348770368109i
47, 58, 3	12.989425949805248 - 76.350223826307953i	2309.507491740077967 + 449.02511572725444i	47, 58, 3	6.58037072029512 + 78.50327848850925i	2232.91266636071640 + 212.91016046736833i
47, 59, 1	34.55124873144004 - 65.991162042663507i	3134.977631080566425 + 1212.406808403492732i	47, 59, 1	30.155212435374612 + 69.29840596605867i	2882.8493996802263 + 116.649931298708225i
47, 59, 2	15.313896346189108 - 72.187449360033618i	2672.541163798917751 + 972.003016540579251i	47, 59, 2	28.03004785930656 + 74.802486969994260i	2499.504396930819845 + 791.500144006785753i
47, 59, 3	15.700827328484179 - 77.201068113167111i	2386.548394156039194 + 1456.98839253382466i	47, 59, 3	34.41337566961086 + 70.652011383695531i	3106.801261550092477 + 4372.6925044669332i
47, 59, 4	3.40683589388704 - 81.449085836037291i	2122.87803594353637 + 87.503582049625451i	47, 60, 1	36.603112778891408 + 66.644312058094371i	3257.64815901643550 + 4333.02580028849570i
47, 60, 1	32.30093376542872 - 69.986140841901715i	2991.52364743995661 + 1243.272705642872801i	47, 60, 1	27.6711350643269015 + 72.91407960360385i	2766.644989364905456 + 1102.822580631818585i
47, 60, 2	22.32849475069247 - 75.07188170307112i	2577.594805938851085 + 925.508827364142121i	47, 60, 2	18.500114465660977 + 78.017345871022428i	2423.913215291716823 + 718.016236115243061i
47, 60, 3	12.92324631226600 - 80.279577036677575i	2307.463831036853542 + 484.53425157740277i	47, 60, 3	6.897789648737711 + 82.373853718691137i	2232.367898043500190 + 227.668308416826562i
47, 61, 1	38.62721363588777 - 67.256294964283916i	3386.548394156039194 + 1456.98839253382466i	47, 61, 1	34.41337566961086 + 70.652011383695531i	3106.801261550092477 + 4372.6925044669332i
47, 61, 2	30.080323858312731 - 73.614919869336248i	2867.807865480285272 + 1236.6797037501581i	47, 61, 2	25.60071724107068 - 76.318040139417111i	2667.70504823238779 + 1062.80743336043232i
47, 61, 3	30.78979368815979 - 78.802491343483274i	2493.928762205440835 + 837.949311443550411i	47, 61, 3	15.65503873276993 + 81.112720248836524i	2399.6043875979394 + 626.42384693606001i
47, 61, 4	10.00457411038928 - 83.25990166453171i	2263.874356140231157 + 371.167248586447566i	47, 61, 4	3.378198205094179 + 85.251629947364236i	2122.78545657124943 + 431.7312843428751i
47, 62, 1	46.626481680989144 - 67.885909173824993i	3521.596762022026631 + 1583.084111934537474i	47, 62, 1	36.48758969156328 + 71.292275544465822i	3228.53638702012472 + 1504.78573994711023i
47, 62, 2	32.47737049966574 - 74.292155384568447i	2975.799922356338811 + 1373.412781416391158i	47, 62, 2	27.836879452489029 + 77.028438227768646i	2757.281052802262659 + 1203.225763168021705i
47, 62, 3	23.82721620997428 - 80.74491073846960i	2471.932385651307435 + 1068.5817992591234i	47, 62, 3	18.45900347545209 + 69.82743410910480i	2574.56939520223232 + 599.566627132550283i
47, 62, 4	12.89753731189730 - 84.110920381606474i	2305.92059020361266 + 518.349323368148319i	47, 62, 4	6.86512686535814 + 86.1571238897953745i	2321.946346949583923 + 242.4796320890705i

Table D.48: Branch points and associated eigenvalues for $m = 47$.

m, n, r	$c_{0;r}^{m,n} = c_{0;r-1}^{m,n+2}$	$\lambda_{0;r}^{m,n} = \lambda_{0;r+1}^{m,n+2}$	m, n, r	$c_{0;r}^{m,n} = c_{0;r+1}^{m,n+2}$	$\lambda_{0;r}^{m,n} = \lambda_{0;r-1}^{m,n+2}$
48, 48, 1	4.234513413823534 - 58.898817902287463i	2310.657618114255001 + 41.436213085067266i	48, 49, 1	7.914207794792153 + 57.304323700827675i	2338.774365713258703 + 111.173200846979867i
48, 50, 1	11.054903463380829 - 58.543571069591674i	2379.431278266274443 + 188.76144669165480i	48, 50, 2	3.8722629211429058 + 61.333915681284708i	2309.360773490910645 + 52.863315427339671i
48, 51, 1	13.905045187929028 - 59.665735231734663i	2430.290434934609493 + 272.915730110236400i	48, 51, 3	7.492538626366881 + 62.835615782305840i	2333.834866894756963 + 138.810723194241611i
48, 52, 1	16.56563600544110 - 60.698961496931510i	2490.163378973094041 + 362.725029013196263i	48, 52, 1	10.631294702393877 + 63.638368597087101i	2370.961582924696813 + 230.852599397494433i
48, 52, 2	6.399369936339198 - 66.09593714242405i	2308.709810816286329 + 61.6209602531166275i	48, 52, 2	19.0920924342501463 + 61.661232483432599i	2538.318170156039530 + 457.518783876041651i
48, 53, 1	13.499057074648151 - 64.662110021424062i	2418.600395744285553 + 328.46049263887755i	48, 53, 1	7.269549367430496 + 67.192353185774744i	2331.365082804379654 + 161.00787229407665i
48, 54, 1	21.511203395282834 - 62.564936751206623i	2634.254437306438831 + 556.794185583562533i	48, 54, 1	24.7516264815207240 + 65.621058704608719i	2475.5750805720471 + 431.073634481064176i
48, 54, 2	10.400333971053669 - 68.17513615162275i	2366.489686998539431 + 265.42401452965238i	48, 54, 2	3.58456679925121 + 70.504061713925571i	2308.42308942414526 + 69.278168678423114i
48, 55, 1	23.850086161591409 - 63.419080250089527i	2717.606488570028432 + 604.13974050294437i	48, 55, 1	7.183721161745811 + 66.25544623497439i	2451.13858062900399 + 538.226052075974103i
48, 55, 2	13.27544093949658 - 69.181752774012935i	2412.209364726918011 + 374.770594054024370i	48, 55, 2	17.310715895224503 + 71.535386224807866i	2329.850554686154601 + 190.411317777959691i
48, 56, 1	26.12186886411374 - 64.230478120925313i	2808.09429988288608 + 767.261228516129279i	48, 56, 1	21.89725317886118 + 67.383303310583212i	2614.7555139887871408 + 699.59347981603721i
48, 56, 2	15.97387328435622 - 70.094054367252539i	2467.412764581310967 + 488.684468076762922i	48, 56, 2	10.256042763799190 + 72.509438291777968i	2363.66588567114308 + 299.593954686616044i
48, 56, 3	15.1166040996740 - 74.686944886883168i	2308.19260666060935 + 76.12150315077777i	48, 56, 3	33.58456679925121 + 70.504061713925571i	3208.42308942414526 + 69.278168678423114i
48, 57, 1	23.58674889247593 - 68.20042902460959i	2696.03553781046030 + 764.692672857792505i	48, 57, 1	18.548403006963472 + 70.961329479503291i	2331.63555104149327 + 406.82035494398183i
48, 57, 2	13.13672654941842 - 73.43342349367167i	2408.098417069358675 + 416.066433896193616i	48, 57, 2	7.037505264010088 + 75.673493976748389i	2328.3292408147152 + 198.07421199482571i
48, 58, 1	30.50882108664210 - 65.74525398777900i	3009.630711091922876 + 991.780128901155535i	48, 58, 1	25.86095380390769 + 68.981618102307501i	2784.67476327756483 + 883.428909435830501i
48, 58, 2	21.019943956445502 - 71.789065741762717i	2603.534101796745745 + 728.870073206708410i	48, 58, 2	15.849162553396150 + 74.132749748289127i	2462.902848315959179 + 540.556997920270074i
48, 58, 3	10.160148348694140 - 76.611480072693083i	2361.72027381593739 + 324.01379440726891i	48, 58, 3	3.458874286445253 + 78.711274972902328i	2308.02175969509929 + 82.46356168309821i
48, 59, 1					

Table D.50: (continued)

m, n, r	$\frac{m, n}{c_0:r} = \frac{m, n+2}{c_0:r+1}$	$\frac{m, n}{\lambda_0:r} = \frac{m, n+2}{\lambda_0:r+1}$	m, n, r	$\frac{m, n}{c_0:r} = \frac{m, n+2}{c_0:r+1}$	$\frac{m, n}{\lambda_0:r} = \frac{m, n+2}{\lambda_0:r+1}$
49.58,7	13.196956298854644 + 7.45172381525435991i	2505.888953526594378 + 420.8468907966951631i	49.58,9	7.068262520538600 + 76.8172900110992241i	2426.005418988458588 - 200.2878176151847571i
49.59,1	30.660238852486941 + 66.8788908698911721i	3112.509218517054705 + 1004.7490109852901701i	49.59,3	25.986276151272609 + 70.1192504157888141i	2885.50715881261867 + 894.3597817653183801i
49.59,5	21.118963767676060 + 72.9022694670258581i	2702.837985587525509 + 737.5301259122890091i	49.59,7	15.921156722893608 + 75.458091187315361i	2560.270410301665379 + 546.588979823292334i
49.59,9	10.204428048120356 + 77.760422903879360i	2459.137671857460646 + 327.629618648396331i	49.59,11	3.472970986751705 + 79.8656718107766321i	2405.056980695615039 + 83.357524514818621i
49.60,1	32.79848347765414 + 67.5969825304222831i	3224.022136676354876 + 123.2527426185263271i	49.60,3	28.240150335956493 + 70.8749906813769431i	2981.941862603076970 + 1017.962695663456671i
49.60,5	23.519383524822866 + 73.729045969341470i	2783.392146365902590 + 864.741834136841248i	49.60,7	18.51890715365548 + 76.3048850703158191i	2625.554960896684406 + 676.359673820335502i
49.60,9	13.103043570965669 + 78.660351235647161i	2502.949714785314882 + 459.777848891363262i	49.60,11	7.000920456708450 + 80.823984562483171i	2425.246293688322655 + 216.867945729008791i
49.61,1	34.895249064711578 + 68.2881249173592721i	3342.016793952325770 + 1244.703469441968032i	49.61,3	30.445093192388637 + 71.6017800250551681i	3085.32559313215763 + 1144.764406736170731i
49.61,5	25.852083202095636 + 74.496307501453046i	2871.49316400734597 + 995.434072442621071i	49.61,7	21.017380514530050 + 77.1169371190488141i	2695.218285248867148 + 809.912583604664594i
49.61,9	15.837114035800054 + 79.521499694952181i	2556.432917492445085 + 594.73301239737066i	49.61,11	10.136183493555611 + 81.7397592014162341i	2457.68359418924868 + 354.0474473658626381i
49.61,13	3.433305384516568 + 83.786224728704351i	2404.931288153868081 + 89.3761631833598281i	49.62,1	36.96272792996618 + 68.954761052035646i	3466.38275520457701 + 1368.9516549420127381i
49.62,3	32.607653396059547 + 72.302309136382462i	3195.490496601717496 + 1274.592665161941181i	49.62,5	22.55755637413508 + 75.235049029693261i	2966.886670588106881 + 1129.4094564831139001i
49.62,7	23.45213854959390 + 77.897718882801856i	2774.859480928475932 + 947.0274791848056571i	49.62,9	18.447544452490842 + 80.3485890873516131i	2618.893062612004996 + 734.2078267658616821i
49.62,11	13.040494576156201 + 82.617160683026768i	2500.791429669582612 + 495.178265938204092i	49.62,13	6.952270653469248 + 84.719185409822671i	2424.674247412158365 + 232.552869229531101i
49.63,1	39.001823913923232 + 69.5989744762303101i	3597.024166560417598 + 1495.863475296205024i	49.63,3	34.733090168549893 + 72.9788629078488361i	3312.294482732559534 + 1407.2955391128950851i
49.63,5	30.33901447869291 + 75.947833983458665i	3069.36311376697217 + 1266.4945903626622571i	49.63,7	25.785896869925999 + 78.6501496599108241i	2862.161282295978253 + 1087.508976466381121i
49.63,9	20.960389084758752 + 81.144220404600205i	2689.817611995863444 + 877.276877018210371i	49.63,11	15.784061031262009 + 83.459973657704211i	2553.605486205883153 + 640.619877683754171i
49.63,13	10.088618922856529 + 85.613794597452061i	2456.58274464994416 + 379.1180990253232971i	49.63,15	3.403073916836012 + 87.613927801669931i	2404.833815829902960 + 95.11149639914789161i
49.64,1	41.015497540102463 + 70.222560756269903i	3733.856979934304945 + 1626.31955606766598i	49.64,3	36.028701335480318 + 73.633403143214309i	3435.61536765993087 + 1542.737881518927225i
49.64,5	32.537531011064900 + 76.636852583673956i	3178.746725613613307 + 1406.519051029549949i	49.64,7	28.9798653547706 + 79.376711429706475i	2956.86598025395905 + 2131.183507882344429i
49.64,9	23.393601144516481 + 81.911487629613217i	2768.810559257251043 + 1023.7915426961952791i	49.64,11	18.406239833069890 + 87.271463971467421i	2615.454086954912782 + 748.8335112293368571i
49.64,13	12.992239351738357 + 86.475600480543007i	2499.153642789955029 + 539.4317218648520791i	49.64,15	6.916669477380432 + 88.5269124980839731i	2424.2028183942466 + 247.50302518608959i

Table D.50: Branch points and associated eigenvalues for $m = 49$.

m, n, r	$\frac{m, n}{c_0:r} = \frac{m, n+2}{c_0:r+1}$	$\frac{m, n}{\lambda_0:r} = \frac{m, n+2}{\lambda_0:r+1}$	m, n, r	$\frac{m, n}{c_0:r} = \frac{m, n+2}{c_0:r+1}$	$\frac{m, n}{\lambda_0:r} = \frac{m, n+2}{\lambda_0:r+1}$
50.50,1	4.28466654747461 + 57.999423131179185i	2506.80413343685355 + 42.3044026047277301i	50.51,1	8.006405999465372 + 59.425032943314051i	2535.502351330471356 + 114.0460757243701121i
50.52,1	11.181381642398893 + 60.6830943384571951i	2576.955086869174465 + 193.6447232977985551i	50.52,3	3.913817476279100 + 63.4921941347010091i	2505.465780937154705 + 54.1646893027998501i
50.53,1	14.06122630982475 + 61.8230746613735111i	2628.762909734839468 + 279.985088780879721i	50.53,3	7.572396951240508 + 64.709397170915861i	2530.393848706421068 + 142.23253137366661i
50.54,1	16.748493752737598 + 62.87322153259131i	2689.705667029728829 + 372.1275729621062281i	50.54,3	10.743197718088073 + 65.8273939537605061i	2568.179772893072823 + 236.541555906483154i
50.54,5	3.729883947590005 + 68.299759744615699i	2504.855112102056410 + 63.153372960080010i	50.55,1	19.297440213242300 + 63.851958751377069i	2759.031717307086956 + 469.390077080193241i
50.55,3	13.63920397670066 + 66.866030781255105i	2616.630940257766724 + 336.55264472789331i	50.55,5	7.341320544194978 + 69.4092587415222231i	2527.833138137017158 + 164.829981644678185i
50.56,1	21.740984039861615 + 64.771427166743521i	2836.227118642391815 + 571.2550702197489251i	50.56,3	35.3100757347537 + 67.8395204730699671i	2674.54410969244381 + 441.694947096784517i
50.56,5	10.052298524137391 + 70.447251304687981i	2563.531853109981512 + 271.7187364162180071i	50.56,7	3.61742897044404 + 72.7464083966707161i	2504.49565298025900 + 70.866111140573191i
50.57,1	14.00090077403082 + 65.640924209348879i	2920.916191876386620 + 677.51313037578261i	50.57,3	18.92798832122724 + 68.7582117306536841i	2741.14643072273001 + 551.490332027881095i
50.57,5	13.404208974599694 + 71.424432468152148i	2609.97315056247227 + 383.650946406895891i	50.57,7	7.19663600066805 + 73.788895191603103i	2526.25889732146839 + 184.554379672926671i
50.58,1	26.392487561540015 + 66.467240702521415i	3012.811213983759444 + 187.23997283438668i	50.58,3	21.80063791933887 + 69.6298902397767371i	2815.89570640861226 + 65.549608299060651i
50.58,5	16.129608272241914 + 72.349538432061692i	2666.019918856782169 + 500.256088739023085i	50.58,7	10.350348342031348 + 74.7743758053895681i	2560.589554971204961 + 302.782576519202962i
50.58,9	3.544149000851338 + 76.96303745170475i	2504.256581213388993 + 77.814280796087201i	50.59,1	28.626976072924428 + 67.2557326464077651i	3111.684096197975123 + 900.7556101000274i
50.59,3	23.790310101123136 + 70.460591344659051i	2898.389206060297881 + 783.550162681710731i	50.59,5	18.724244123752865 + 73.2294543849831291i	2701.911817566831461 + 621.183067543005222i
50.59,7	13.256544250899328 + 75.709778783142767i	2605.674754774446683 + 425.596287537954481i	50.59,9	7.098703273042078 + 77.95943918048825i	2525.187398524647506 + 202.487230455607317i
50.60,1	30.812900868684954 + 68.0107118256084821i	3217.349163305259481 + 1011.6302417123457021i	50.60,3	26.11056800416810 + 71.2551126305116181i	2988.315118276242174 + 905.2209349610584837i
50.60,5	21.2169083608784764 + 74.069658584249865i	2804.127609524037325 + 746.125216423634262i	50.60,7	15.992387836082600 + 76.6011940323298291i	2660.44118158412150 + 552.750697617780475i
50.60,9	10.248252512597604 + 78.9076496585795444i	2558.552668218291274 + 331.222819851035644i	50.60,11	3.486931013660595 + 81.017892126550671i	2504.085631504266985 + 84.2458036037795071i
50.61,1	32.956924883987270 + 68.756849658637400i	3329.652052280436692 + 1137.665145511226942i	50.61,3	28.374041820947912 + 72.0173484753029671i	3085.424443435032572 + 1030.330857383082048i
50.61,5	23.627211635882775 + 74.8745811952718871i	2885.240340962465325 + 874.818411686268973i	50.61,7	18.600958091011233 + 77.453663204235966i	2724.161558336951202 + 683.97716899046485i
50.61,9	13.158975529373782 + 79.8182733345425031i	2602.664558110295275 + 464.205093272489648i	50.61,11	7.029422742737498 + 81.980626161288242i	2524.411631558085446 + 119.8184027049012631i
50.62,1	35.064366122115878 + 69.433564468836935i	3448.462218825081891 + 1260.03733735426638i	50.62,3	30.587562097574342 + 72.7505161127733971i	3189.513462811763020 + 1158.680393039420531i
50.62,5	25.969259109702044 + 75.6478632633586630i	2973.93682259155821 + 1007.03537799391641i	50.62,7	21.109574509157707 + 78.271348213224513i	2796.305689775768769 + 819.02878998662755i
50.62,9	15.950410183215072 + 80.6793147769378581i	2656.504292290140256 + 601.275996235200068i	50.62,11	10.177423109971111 + 82.9010058488361491i	2557.063501941214327 + 357.822915584955971i
50.62,13	3.446355464926117 + 84.9520207235498931i	2503.95737957888319 + 90.303592353588651i	50.63,1	37.139547941911964 + 70.108046372122924i	3373.667687478512562 + 1386.5447655073462561i
50.63,3	32.758485024153480 + 73.457313236942852i	3300.412225664898870 + 1290.09527550757833i	50.63,5	28.253611305696307 + 76.392541519969621i	3069.9595637390729 + 1142.571223426999040i
50.63,7	23.53697823820257 + 79.0577137770670205i	2876.468113110935974 + 957.68166826092967i	50.63,9	18.92506405732420 + 81.511338998329734i	2719.37064107571945 + 742.225487024234326i
50.63,11	13.093317702225152 + 83.78310820104081i	2600.449681462832359 + 500.449848340766330i	50.63,13	6.579122946573871 + 85.889006862110790i	2523.826214053935473 + 234.920776557334681i
50.64,1	39.186039937109172 + 70.7574977473451121i	3705.171258726373708 + 1515.102545438973455i	50.64,3	34.891839797523687 + 74.1400309288193141i	3417.97664304664948 + 1424.421802475036202i
50.64,5	30.48842301740267 + 77.1111817546487261i	3173.096427828445030 + 1281.256141109087821i	50.64,7	25.896736758009446 + 79.8156754147813531i	2964.327909261168770 + 1099.793117778688421i
50.64,9	21.047696272308816 + 82.312121326888831i	2790.745119410793905 + 886.84701613018591i	50.64,11	15.84769037396365 + 84.6306729161951491i	2653.96638550474836 + 646.96554858055501i
50.64,13	10.127632818080574 + 86.787828969962955i	2555.934112915842888 +			

found at [84]. These verified entries include $S_{mn}^{(a)}(c, \eta)$ and $\lambda_{mn}^{(a)}$ for $m = 0, n = [0..1]$ for $\eta = [0, \pi/4, \pi/2]$. Seven digits are listed for reference.

$S_{mn}^{(a)}(c, \eta)$ and $S_{mn}^{(a)'}(c, \eta)$ are listed for the prolate case only. Values for the oblate SWFs can be computed using the methods outlined in Chapter 4.

“Type” in the tables below refers to either the Pr \Rightarrow *prolate*-type expansion of Section 4.3.1, or Ob \Rightarrow *oblate*-type expansion of Section 4.3.2.

Some values are unable to be represented in double precision (for example $S_{0,0}^{(a)}(5000\angle 0, .99)$ and $S_{0,0}^{(a)}(5000\angle \pi/2, .99)$). Those values that too small are set to ± 0 while those values that are too large are set to $\pm \infty$. In addition, if the ratio of the real to the imaginary (or the reciprocal) part of $S_{mn}^{(a)}(c, \eta)$ or $S_{mn}^{(a)'}(c, \eta)$ is smaller than $\approx 1 \times 10^{-10}$, then the smaller value should probably be 0. An example of this can be seen in the values for $S_{0,0}^{(a)}(250\angle 90, 0.25)$ where the $\Im\{S_{0,0}^{(a)}(250\angle 90, 0.25)\} \rightarrow 0$.

D.2.1 Asymptotic expansions of the PASWF, $S_{mn}^{(a)}(c, \eta)$ and the corresponding characteristic eigenvalues, $\lambda_{mn}^{(a)}$, for $m = [0..1]$, $n = [m..6]$.

Table D.52: $S_{0n}^{(a)}(c, \eta)$ for $n = [0..6]$.

m, n	$c \setminus \arg(c)$	type	$\lambda_{mn}^{(a)}$	$S_{mn}^{(a)}(c, \eta=0)$	$S_{mn}^{(a)}(c, \eta=0.01)$	$S_{mn}^{(a)}(c, \eta=0.1)$	$S_{mn}^{(a)}(c, \eta=0.25)$	$S_{mn}^{(a)}(c, \eta=0.5)$	$S_{mn}^{(a)}(c, \eta=0.75)$	$S_{mn}^{(a)}(c, \eta=0.99)$
0.0	25 \angle 0°	Pr	2.42421e-01 - 0.00000e-00i	1.00000e-00 - 0.00000e-00i	9.98789e-01 - 0.00000e-00i	8.85585e-01 - 0.00000e-00i	4.63264e-01 - 0.00000e-00i	3.91021e-02 - 0.00000e-00i	2.85622e-04 - 0.00000e-00i	1.73861e-09 - 0.00000e-00i
0.0	25 \angle 15°	Pr	2.33906e-01 + 6.47263e-00i	1.00000e-00 - 0.00000e-00i	9.98831e-01 - 2.32321e-04i	8.88905e-01 - 2.88502e-02i	4.65943e-01 - 9.71392e-02i	2.83544e-02 - 3.34193e-02i	-2.21683e-04 - 3.09923e-04i	2.73064e-09 + 2.35142e-09i
0.0	25 \angle 30°	Pr	2.08940e-01 + 1.25041e-01i	1.00000e-00 - 4.33681e-19i	9.98956e-01 - 6.24568e-04i	9.98804e-01 - 5.64089e-02i	4.75145e-01 - 1.99244e-01i	-6.38800e-03 - 6.09009e-02i	-4.08388e-04 + 7.87578e-04i	-7.03803e-09 + 2.96538e-08i
0.0	25 \angle 45°	Pr	1.69224e-01 + 1.76834e-01i	1.00000e-00 + 4.33681e-19i	9.99154e-01 - 8.83443e-04i	9.91507e-01 - 8.13245e-02i	4.94731e-01 - 3.11224e-01i	-7.46693e-02 - 7.27486e-02i	3.2564e-03 + 9.90839e-04i	-8.00933e-07 - 4.33226e-07i
0.0	25 \angle 60°	Ob	-2.70208e-02 + 5.16261e-02i	1.00000e-00 + 1.87778e-16i	1.01343e-00 - 2.59301e-02i	1.26329e-00 - 3.69384e-00i	-8.93631e-01 - 1.28199e-00i	1.66522e-04 + 4.90860e-02i	-3.19320e-06 + 1.43870e-05i	4.98236e-08 + 9.36905e-07i
0.0	25 \angle 75°	Ob	-4.93980e-02 + 2.99556e-02i	1.00000e-00 + 8.32667e-17i	1.02476e-00 - 1.51019e-02i	4.08786e-00 - 3.03203e-00i	-8.00296e-00 - 1.66581e-02i	-5.77612e-04 + 5.53875e-03i	2.96100e-06 + 2.05703e-07i	5.95426e-09 + 7.51026e-08i
0.0	25 \angle 90°	Ob	-5.76010e-02 + 7.34781e-14i	1.00000e-00 + 0.00000e-00i	1.02894e-00 + 7.26758e-17i	5.57240e-00 - 2.46060e-16i	2.06321e-02 - 6.36999e-14i	8.88126e-04 - 6.14256e-11i	3.93549e-07 + 4.22854e-08i	1.39420e-10 - 2.01037e-05i
0.0	50 \angle 0°	Pr	4.92462e-01 - 0.00000e-00i	1.00000e-00 - 0.00000e-00i	9.97541e-01 - 0.00000e-00i	9.78126e-01 - 0.00000e-00i	5.87140e-01 - 0.00000e-00i	2.09413e-01 - 0.00000e-00i	6.01237e-08 - 0.00000e-00i	8.01364e-19 - 0.00000e-00i
0.0	50 \angle 15°	Pr	4.75426e-01 + 1.29420e-01i	1.00000e-00 - 0.00000e-00i	9.97625e-01 - 6.45578e-04i	7.86307e-01 - 5.10814e-02i	2.02648e-01 - 8.83091e-02i	-2.79907e-04 - 1.70074e-03i	-3.47424e-08 + 1.01238e-07i	4.32009e-19 + 3.43224e-18i
0.0	50 \angle 30°	Pr	4.25480e-01 + 2.50020e-01i	1.00000e-00 + 1.08420e-19i	9.97874e-01 - 1.24747e-03i	8.01604e-01 - 1.00989e-01i	1.81606e-01 - 1.84727e-01i	-3.29290e-03 + 6.95211e-04i	-3.33093e-07 - 4.75554e-07i	-2.20072e-16 - 1.22503e-16i
0.0	50 \angle 45°	Pr	3.46027e-01 + 3.53581e-01i	1.00000e-00 + 2.16840e-19i	9.98270e-01 - 1.76489e-03i	8.27597e-01 - 1.48234e-01i	1.44419e-01 - 3.00481e-01i	2.41413e-04 + 9.75442e-03i	7.08220e-06 + 4.79411e-06i	1.18050e-13 + 1.98617e-13i
0.0	50 \angle 60°	Ob	-1.16440e-02 + 2.11506e-03i	1.00000e-00 + 3.05311e-16i	1.05690e-00 - 1.07808e-01i	-2.76527e-01 - 2.06277e-01i	2.00653e-04 + 6.44857e-02i	8.38393e-08 + 5.42465e-07i	3.60049e-13 + 3.51444e-12i	9.62721e-17 + 3.84667e-17i
0.0	50 \angle 75°	Ob	-2.06948e-03 + 1.22412e-03i	1.00000e-00 - 3.88578e-16i	1.10464e-00 - 6.33384e-02i	1.55156e-01 - 5.46790e-01i	-6.96578e-04 + 6.58104e-03i	1.00256e-10 - 1.90948e-09i	-1.47123e-15 + 4.26422e-14i	1.41159e-20 - 3.55228e-19i
0.0	50 \angle 90°	Ob	-2.40101e-03 + 3.00038e-13i	1.00000e-00 - 7.26897e-18i	1.12248e-00 - 2.37692e-17i	6.74008e-01 - 2.11272e-14i	1.07113e-05 - 8.27776e-11i	2.39193e-10 - 3.67949e-05i	5.49615e-15 - 1.26618e-01i	7.86088e-20 - 2.38860e-06i
0.0	100 \angle 0°	Pr	9.92481e-01 - 0.00000e-00i	1.00000e-00 - 0.00000e-00i	9.95050e-01 - 0.00000e-00i	6.08061e-01 - 0.00000e-00i	4.28000e-02 - 0.00000e-00i	1.69033e-06 - 0.00000e-00i	2.67211e-15 - 0.00000e-00i	1.77027e-37 - 0.00000e-00i
0.0	100 \angle 15°	Pr	9.58408e-01 + 2.58824e-01i	1.00000e-00 + 5.42101e-20i	9.95218e-01 - 1.28797e-03i	6.13338e-01 - 8.00222e-02i	3.24702e-02 - 3.49297e-02i	-2.52772e-06 + 8.54525e-07i	-6.68085e-15 - 5.20547e-15i	-3.20708e-36 + 7.91822e-37i
0.0	100 \angle 30°	Pr	8.58059e-01 + 5.00101e-01i	1.00000e-00 - 0.00000e-00i	9.95713e-01 - 2.48940e-03i	6.29979e-01 - 1.61285e-01i	-1.10961e-03 - 6.54843e-02i	9.30729e-06 - 4.10835e-06i	-8.55258e-14 + 2.34159e-13i	9.03604e-33 + 1.50843e-32i
0.0	100 \angle 45°	Pr	6.99594e-01 + 7.07120e-01i	1.00000e-00 - 0.00000e-00i	9.96502e-01 - 3.52334e-03i	6.60442e-01 - 2.44415e-01i	-6.77563e-02 - 8.47187e-02i	8.54277e-05 + 4.17737e-06i	2.00048e-11 + 5.02806e-11i	3.10866e-36 + 2.97957e-36i
0.0	100 \angle 60°	Ob	-4.82780e-03 + 8.56025e-03i	1.00000e-00 - 0.00000e-00i	1.21925e-00 - 4.62407e-01i	-7.44132e-02 - 2.51339e-03i	1.00807e-09 + 6.64838e-07i	2.10844e-18 + 2.79697e-17i	4.51651e-27 + 9.06204e-26i	3.10866e-36 + 2.97957e-36i
0.0	100 \angle 75°	Ob	-8.46807e-03 + 4.8424e-03i	1.00000e-00 - 4.44089e-16i	1.44306e-00 - 2.83670e-01i	-6.05587e-03 - 3.74027e-03i	1.20603e-10 - 2.28890e-09i	2.92212e-20 - 1.15031e-20i	6.99178e-30 - 4.40732e-30i	3.10866e-36 + 2.97957e-36i
0.0	100 \angle 90°	Ob	-9.80100e-03 + 1.21240e-12i	1.00000e-00 - 2.25777e-17i	1.53142e-00 - 1.05597e-16i	1.00074e-04 - 6.35400e-12i	2.87727e-10 - 4.46699e-05i	1.72531e-21 - 5.32138e-06i	1.06432e-32 - 4.91200e-31i	2.47842e-42 - 1.50805e-28i
0.0	250 \angle 0°	Pr	2.49249e-02 - 0.00000e-00i	1.00000e-00 - 0.00000e-00i	9.87615e-01 - 0.00000e-00i	2.86685e-01 - 0.00000e-00i	3.65451e-01 - 0.00000e-00i	1.63198e-15 - 0.00000e-00i	2.35106e-37 - 0.00000e-00i	1.66212e-90 + 2.42914e-90i
0.0	250 \angle 15°	Pr	2.40731e-02 + 6.47050e-01i	1.00000e-00 - 0.00000e-00i	9.88030e-01 - 3.19661e-03i	2.83593e-01 - 9.53468e-02i	-2.22813e-04 - 4.23984e-04i	-7.20744e-15 - 6.79504e-15i	-4.19022e-36 - 3.54797e-37i	1.66212e-90 + 2.42914e-90i
0.0	250 \angle 30°	Pr	2.15756e-02 + 1.25000e-02i	1.00000e-00 - 0.00000e-00i	9.89251e-01 - 6.18307e-03i	2.74680e-01 - 1.98834e-01i	-7.16217e-04 + 7.79513e-04i	-1.42618e-13 + 2.42365e-13i	-1.79754e-33 + 1.96880e-32i	5.18478e-81 - 3.20875e-81i
0.0	250 \angle 45°	Pr	1.76026e-02 + 1.76777e-02i	1.00000e-00 - 0.00000e-00i	9.91198e-01 - 8.76151e-03i	2.61711e-01 - 3.20548e-01i	2.93035e-03 + 2.32049e-03i	6.99796e-12 + 5.72070e-11i	-1.35544e-26 + 2.18597e-27i	2.02131e-66 - 3.48570e-66i
0.0	250 \angle 60°	Ob	-3.08180e-04 + 5.38766e-04i	1.00000e-00 + 5.55112e-16i	1.37865e-00 - 4.03928e-00i	1.14632e-09 + 7.60879e-07i	1.26706e-23 + 2.11926e-22i	3.25138e-46 + 1.11919e-46i	8.32069e-69 + 4.51699e-69i	-1.03039e-92 + 2.89073e-92i
0.0	250 \angle 75°	Ob	-5.36446e-04 + 3.11206e-04i	1.00000e-00 + 9.99201e-16i	4.45487e-00 - 3.31151e-00i	1.37164e-10 - 2.60010e-09i	-5.90105e-25 + 2.98516e-25i	5.39912e-51 + 7.34058e-51i	-2.13279e-77 + 1.27384e-78i	5.67280e-102 - 1.58014e-103i
0.0	250 \angle 90°	Ob	-6.20010e-04 + 7.62343e-12i	1.00000e-00 + 7.87257e-17i	6.07228e-00 - 4.38820e-16i	3.27235e-10 - 4.75176e-05i	5.56276e-26 - 2.08510e-12i	6.44759e-53 - 4.88428e-39i	7.68728e-80 - 8.76534e-66i	7.71910e-106 - 1.63764e-93i
0.0	500 \angle 0°	Pr	4.99250e-02 - 0.00000e-00i	1.00000e-00 - 0.00000e-00i	9.75346e-01 - 0.00000e-00i	8.18790e-02 - 0.00000e-00i	1.30364e-07 - 0.00000e-00i	8.99708e-30 - 0.00000e-00i	4.09510e-74 - 0.00000e-00i	1.07905e-186 - 0.00000e-00i
0.0	500 \angle 15°	Pr	4.82213e-02 + 1.29410e-02i	1.00000e-00 - 6.77626e-21i	9.76157e-01 - 6.31645e-03i	7.10652e-02 - 5.38756e-02i	-1.27011e-07 + 1.84425e-07i	5.18613e-30 + 8.80322e-29i	1.29147e-71 + 2.20469e-72i	-8.88925e-181 + 2.27814e-180i
0.0	500 \angle 30°	Pr	4.32262e-02 + 2.50000e-02i	1.00000e-00 - 0.00000e-00i	9.78542e-01 - 1.22327e-02i	3.57788e-02 - 1.08820e-01i	-9.23915e-08 - 1.08994e-06i	-3.45081e-26 - 6.21356e-26i	-2.84784e-64 - 5.25193e-65i	4.70912e-162 + 9.38484e-162i
0.0	500 \angle 45°	Pr	3.52803e-02 + 3.53554e-02i	1.00000e-00 - 0.00000e-00i	9.82361e-01 - 1.73681e-02i	-3.41291e-02 - 1.67150e-01i	3.12545e-06 + 1.32751e-05i	-2.89748e-21 + 7.19277e-22i	1.32610e-52 - 4.38588e-53i	-2.26474e-132 - 3.99166e-132i
0.0	500 \angle 60°	Ob	-1.24135e-05 + 2.16006e-05i	1.00000e-00 - 0.02616e-15i	-3.01289e-01 - 2.24988e-01i	2.87880e-18 + 3.84261e-17i	3.90293e-46 + 1.34450e-46i	2.79700e-93 + 2.18667e-93i	1.70927e-140 + 2.63497e-140i	-2.90523e-182 - 2.37623e-185i
0.0	500 \angle 75°	Ob	-2.15541e-05 + 1.24741e-05i	1.00000e-00 + 5.16254e-15i	1.69280e-01 - 5.96013e-01i	3.99153e-20 - 1.56935e-20i	6.48297e-51 - 8.81190e-51i	-7.42104e-103 - 2.38047e-103i	-5.52640e-156 + 1.90602e-156i	-8.66642e-206 + 7.14896e-206i
0.0	500 \angle 90°	Ob	-2.49001e-05 + 3.05549e-11i	1.00000e-00 + 4.17943e-19i	7.34745e-01 - 2.24623e-14i	2.35647e-21 - 1.27136e-06i	7.74075e-53 - 5.92449e-39i	1.24840e-108 - 1.91101e-94i	2.07098e-162 + 4.75533e-148i	2.37503e-214 + 7.19862e-200i
0.0	750 \angle 0°	Pr	7.49250e-02 - 0.00000e-00i	1.00000e-00 - 0.00000e-00i	9.63230e-01 - 0.00000e-00i	2.33852e-02 - 0.00000e-00i	4.65042e-11 - 0.00000e-00i	2.55851e-44 - 0.00000e-00i	5.96162e-280 - 0.00000e-00i	5.96162e-280 - 0.00000e-00i
0.0	750 \angle 15°	Pr	7.23694e-02 + 1.94114e-02i	1.00000e-00 - 0.00000e-00i	9.64416e-01 - 9.36088e-03i	1.49602e-02 - 2.19715e-02i	1.03950e-10 - 1.24548e-11i	5.04060e-43 - 6.01920e-43i	-3.95167e-107 - 1.02445e-107i	-1.98185e-270 + 4.57732e-271i
0.0	750 \angle 30°	Pr	6.48769e-02 + 3.75000e-02i	1.00000e-00 - 0.00000e-00i	9.67911e-01 - 1.81509e-02i	-1.17650e-02 - 3.68655e-02i	8.93922e-10 + 6.91710e-10i	1.79587e-38 + 4.48880e-40i	1.14637e-96 - 4.08442e-96i	-1.57393e-243 + 1.80313e-242i
0.0	750 \angle 45°	Pr	5.29580e-02 + 5.30330e-02i	1.00000e-00 - 0.00000e-00i	9.73525e-01 - 2.58212e-02i	-6.22763e-02 - 3.26817e-02i	-2.11303e-08 + 4.50512e-08i	-5.51951e-32 - 1.44465e-31i	-1.26114e-78 + 6.54976e-79i	-5.23103e-198 + 6.43552e-200i
0.0	750 \angle 60°	Ob	-2.79952e-05 + 4.86389e-05i	1.00000e-00 - 7.32747e-15i	-2.68894e-02 + 1.87299e-02i	7.19689e-27 + 1.45200e-27i	1.16540e-70 + 6.33203e-69i	1.99419e-140 + 3.07488e-140i	8.07533e-209 + 1.03853e-211i	3.93065e-278 + 2.36809e-278i
0.0	750 \angle 75°	Ob	-4.85691e-05 + 2.80862e-05i	-0.00000e-00 - 0.00000e-00i	$\pm \infty$	$\pm \infty$	$\pm \infty$	$\pm \infty$	$\pm \infty$	$\pm \infty$
0.0	750 \angle 90°	Ob	-5.61001e-05 + 6.87945e-11i	-0.00000e-00 - 0.00000e-00i	$\pm \infty$	$\pm \infty$	$\pm \infty$	$\pm \infty$	$\pm \infty$	$\pm \infty$
0.0	1000 \angle 0°	Pr	9.99250e-02 - 0.00000e-00i	1.00000e-00 - 0.00000e-00i	9.51264e-01 - 0.00000e-00i	6.67895e-03 - 0.00000e-00i	1.65893e-14 - 0.00000e-00i	7.27571e-59 - 0.00000e-00i	1.24275e-147 - 0.00000e-00i	$\pm \infty$
0.0	1000 \angle 15°	Pr	9.65176e-02 + 2.58819e-02i	1.00000e-00 -						

Table D.52: (continued)

m, n	$ c \angle \arg(c)$	type	$\Lambda_{mn}^{(a)}$	$S_{mn}^{(a)}(c, \eta=0)$	$S_{mn}^{(a)}(c, \eta=0.01)$	$S_{mn}^{(a)}(c, \eta=0.1)$	$S_{mn}^{(a)}(c, \eta=0.25)$	$S_{mn}^{(a)}(c, \eta=0.5)$	$S_{mn}^{(a)}(c, \eta=0.75)$	$S_{mn}^{(a)}(c, \eta=0.99)$
0.0	2500.260°	Ob	-3.12067e+6 + 5.41016e-06i	-0.00000e+0 - 0.00000e-00i	$\pm \infty$	$\pm \infty$	$\pm \infty$	$\pm \infty$	$\pm \infty$	$\pm \infty$
0.0	2500.275°	Ob	-5.40783e+6 + 3.12371e+06i	-0.00000e+0 - 0.00000e-00i	$\pm \infty$	$\pm \infty$	$\pm \infty$	$\pm \infty$	$\pm \infty$	$\pm \infty$
0.0	2500.290°	Ob	-6.24500e+6 + 7.65098e-10i	-0.00000e+0 - 0.00000e-00i	$\pm \infty$	$\pm \infty$	$\pm \infty$	$\pm \infty$	$\pm \infty$	$\pm \infty$
0.0	5000.20°	Pr	4.99925e+03 - 0.00000e+00i	1.00000e+0 - 0.00000e-00i	7.78825e-01 - 0.00000e+00i	1.30916e-11 - 0.00000e+00i	1.14076e-09 - 0.00000e+00i	1.33093e-291 - 0.00000e+00i*	± 0	± 0
0.0	5000.215°	Pr	4.82888e+03 + 1.29414e+03i	1.00000e+0 - 0.00000e-00i	7.83844e-01 - 5.07906e-02i	3.01176e-11 - 6.21647e-12i	-2.47035e-07 + 6.36595e-08i	-9.06049e-282 + 6.04410e-282i*	± 0	± 0
0.0	5000.230°	Pr	4.32938e+03 + 2.50000e+03i	1.00000e+0 - 0.00000e-00i	7.99069e-01 - 1.00410e-01i	1.37583e-10 + 1.31457e-11i	-1.30883e-60 + 1.47671e-60i	-4.40138e-253 - 1.18050e-252i*	± 0	± 0
0.0	5000.245°	Pr	3.53478e+03 + 3.53553e+03i	1.00000e+0 + 1.69407e-21i	8.24934e-01 - 1.47371e-01i	8.65836e-09 + 1.82338e-08i	1.20961e-49 + 1.32107e-49i	-1.63536e-206 - 1.40212e-206i*	± 0	± 0
0.0	5000.260°	Ob	-1.24913e+07 + 2.16456e+07i	-0.00000e+0 - 0.00000e-00i	$\pm \infty$	$\pm \infty$	$\pm \infty$	$\pm \infty$	$\pm \infty$	$\pm \infty$
0.0	5000.275°	Ob	-2.16410e+07 + 1.24974e+07i	-0.00000e+0 - 0.00000e-00i	$\pm \infty$	$\pm \infty$	$\pm \infty$	$\pm \infty$	$\pm \infty$	$\pm \infty$
0.0	5000.290°	Ob	-2.49900e+07 + 3.06100e-09i	-0.00000e+0 - 0.00000e-00i	$\pm \infty$	$\pm \infty$	$\pm \infty$	$\pm \infty$	$\pm \infty$	$\pm \infty$
0.1	25.20°	Pr	7.32096e+01 - 0.00000e+00i	-0.00000e+0 - 0.00000e-00i	9.98814e-03 - 0.00000e+00i	8.87835e-02 - 0.00000e+00i	1.17706e-01 - 0.00000e+00i	2.09716e-02 - 0.00000e+00i	2.58465e-04 - 0.00000e+00i	3.04243e-09 - 0.00000e+00i*
0.1	25.215°	Pr	7.06557e+01 + 1.94227e+01i	-0.00000e+0 - 0.00000e-00i	9.98856e-03 - 3.23349e-06i	8.91162e-02 - 2.89306e-03i	1.18384e-01 - 2.46869e-02i	1.52026e-02 - 1.79266e-02i	-2.00771e-04 - 2.80289e-04i	4.78608e-09 + 4.09846e-09i*
0.1	25.230°	Pr	6.31681e+01 + 3.75213e+01i	-0.00000e+0 - 0.00000e-00i	9.98981e-03 - 6.24734e-06i	9.01083e-02 - 5.65655e-03i	1.20716e-01 - 5.06339e-02i	-3.43977e-03 - 3.26567e-02i	-3.68503e-04 + 7.12851e-04i	-1.19994e-08 + 5.18474e-08i*
0.1	25.245°	Pr	3.43483e+01 + 5.89637e+02i	-0.00000e+0 - 0.00000e-00i	9.99432e-03 - 9.82425e-05i	6.66196e-02 - 9.13042e-02i	-1.21804e+00 + 6.12146e-01i	-1.63576e+01 - 9.27150e+01i	6.64708e+03 + 7.80595e+02i	-2.26162e+05 + 3.41007e+05i
0.1	25.260°	Ob	-2.70208e+02 + 5.16126e+02i	-0.00000e+0 - 0.00000e-00i	1.00452e-02 - 8.62792e-05i	1.25326e-01 - 1.08911e-01i	-3.13897e+00 - 1.96557e+00i	5.79552e+02 + 3.75223e+02i	-1.10065e+05 + 7.37149e+04i	1.56426e+07 + 1.02623e+07i
0.1	25.275°	Ob	-4.93980e+02 + 2.99556e+02i	-0.00000e+0 - 0.00000e-00i	1.00828e-02 - 5.01750e-05i	1.95435e-01 - 7.89694e-02i	1.54950e+00 - 6.76894e-01i	-2.37809e+03 - 4.26456e+02i	-1.12239e+05 + 8.57999e+05i	2.47165e+08 + 3.67410e+07i
0.1	25.290°	Ob	-5.76010e+02 + 7.34781e-14i	-0.00000e+0 - 0.00000e-00i	1.00966e-02 + 5.62872e-19i	2.28579e-01 - 7.97660e-18i	8.60433e+00 - 2.25536e-15i	3.70385e+03 - 2.38898e-12i	1.64126e+06 - 1.68694e-09i	5.81439e+08 - 8.11292e-07i
0.1	50.20°	Pr	1.48231e+02 - 0.00000e+00i	-0.00000e+0 - 0.00000e-00i	9.97566e-03 - 0.00000e+00i	7.83238e-02 - 0.00000e+00i	5.32025e-01 - 0.00000e+00i	7.35477e-04 - 0.00000e+00i	5.43403e-08 - 0.00000e+00i	1.39645e-18 - 0.00000e+00i*
0.1	50.215°	Pr	1.43120e+02 + 3.88281e+01i	-0.00000e+0 - 0.00000e-00i	9.97650e-03 - 6.45630e-06i	7.88293e-02 - 5.12123e-03i	5.14830e-02 - 2.24365e-02i	-1.50150e-04 - 9.11742e-04i	-3.13720e-08 + 9.15056e-08i	7.60204e-19 + 5.97919e-18i
0.1	50.230°	Pr	1.28137e+02 + 7.50100e+01i	-0.00000e+0 - 0.00000e-00i	9.97899e-03 - 1.24757e-05i	8.03627e-02 - 1.01250e-02i	4.61351e-02 - 4.69322e-02i	-8.01244e-07 + 3.73029e-04i	-3.83594e-16 + 4.29567e-16i*	3.83594e-16 + 4.29567e-16i*
0.1	50.245°	Pr	6.97071e+01 + 2.42929e+03i	-0.00000e+0 - 0.00000e-00i	9.98380e-03 - 4.04586e-04i	-2.90436e-01 - 1.24371e-01i	-1.03553e+01 - 5.49141e+01i	-1.24535e+05 + 2.95724e+05i	1.57836e+09 - 1.04988e+09i	-5.7455e+12 - 2.78232e+12i
0.1	50.260°	Ob	-1.16440e+03 + 2.1506e+03i	-0.00000e+0 - 0.00000e-00i	1.01918e-02 - 3.56627e-04i	-2.70508e-01 - 6.47884e-01i	3.44869e+02 - 2.19151e+02i	1.41269e+07 + 9.63517e+06i	5.94409e+11 + 4.34542e+11i	1.28824e+16 + 1.67121e+16i
0.1	50.275°	Ob	-2.06948e+03 + 1.22421e-03i	-0.00000e+0 - 0.00000e-00i	1.03476e-02 - 2.08277e-04i	5.99709e-01 - 9.92360e-01i	-1.40586e+03 - 2.45654e+03i	2.07525e+08 + 1.64242e+07i	-3.12408e+13 + 4.66286e+11i	2.96841e+18 + 6.31374e+16i
0.1	50.290°	Ob	-2.40101e+03 + 3.00038e-12i	-0.00000e+0 - 0.00000e-00i	1.04053e-02 - 2.74980e-19i	1.37566e-01 - 3.64897e-16i	2.18645e+03 - 1.58415e-12i	4.88252e+08 - 7.27058e-07i	1.12190e+14 - 2.53043e-01i	6.04606e-09 - 4.79827e-04i
0.1	100.20°	Pr	2.98240e+02 - 0.00000e+00i	-0.00000e+0 - 0.00000e-00i	9.95075e-03 - 0.00000e+00i	6.09959e-02 - 0.00000e+00i	1.08731e-02 - 0.00000e+00i	9.06015e-07 - 0.00000e+00i	2.41373e-15 - 0.00000e+00i	3.07775e-37 - 0.00000e+00i*
0.1	100.215°	Pr	2.88019e+02 + 7.76482e+01i	-0.00000e+0 - 0.00000e-00i	9.95243e-03 - 1.28801e-05i	6.14883e-02 - 8.02248e-03i	8.24827e-03 - 8.87376e-03i	-1.35482e-06 + 4.58086e-07i	-6.03539e-15 - 4.70120e-15i	5.57463e-36 + 1.37940e-36i*
0.1	100.230°	Pr	2.58049e+02 + 1.50005e+02i	-0.00000e+0 - 0.00000e-00i	9.95738e-03 - 2.48949e-05i	6.31656e-02 - 1.61693e-02i	-2.82240e-04 + 1.66358e-02i	4.98834e-06 - 2.20247e-06i	-7.71934e-14 + 2.11522e-13i	1.57312e-32 + 2.62023e-32i*
0.1	100.245°	Pr	1.40420e+02 + 9.85858e+03i	-0.00000e+0 - 0.00000e-00i	9.89066e-03 - 1.63896e-03i	5.38803e+02 + 2.34805e+02i	-7.33208e+04 + 1.76895e+04i	-7.58677e+12 + 4.89605e+10i	-1.22045e+20 - 2.84132e+20i	6.34614e+27 - 6.22358e+26i*
0.1	100.260°	Ob	-4.82780e+03 + 8.56025e+03i	-0.00000e+0 - 0.00000e-00i	1.07615e-02 - 1.49575e-03i	-6.30687e+02 + 2.56784e+01i	8.44222e+06 + 5.70826e+06i	1.69419e+16 + 1.31642e+16i	3.47290e+25 + 3.08738e+25i	1.19162e+34 + 1.19707e+34i
0.1	100.275°	Ob	-8.46807e+03 + 4.94824e+03i	-0.00000e+0 - 0.00000e-00i	1.14510e-02 - 8.96472e-04i	-4.91545e-01 - 5.24396e-02i	1.23592e+08 + 9.52060e+06i	3.15177e+18 - 3.49973e+17i	7.97806e+28 - 2.45047e+28i	8.35948e+38 + 4.16297e+38i
0.1	100.290°	Ob	-9.80100e+03 + 1.21240e-12i	-0.00000e+0 - 0.00000e-00i	1.17158e-02 - 6.48506e-19i	1.01090e-02 - 5.93246e-14i	2.90648e+08 - 4.37533e-07i	1.74283e+19 - 5.29161e+04i	1.07513e+30 - 4.91018e+15i	2.50358e+40 - 1.51133e+26i
0.1	250.20°	Pr	7.48246e+02 - 0.00000e+00i	-0.00000e+0 - 0.00000e-00i	9.87639e-03 - 0.00000e+00i	2.87407e-02 - 0.00000e+00i	9.28381e-05 - 0.00000e+00i	1.69569e-15 - 0.00000e+00i	2.12305e-37 - 0.00000e+00i	3.39558e-93 - 0.00000e+00i*
0.1	250.215°	Pr	7.22691e+02 + 1.94115e+02i	-0.00000e+0 - 0.00000e-00i	9.88055e-03 - 3.19670e-05i	2.84306e-02 - 9.55868e-03i	-5.66032e-05 - 1.07708e-04i	-3.86280e-15 - 3.64163e-15i	-3.78384e-36 - 3.20181e-37i	2.88710e-90 + 4.21761e-90i*
0.1	250.230°	Pr	6.47766e+02 + 3.75002e+02i	-0.00000e+0 - 0.00000e-00i	9.89275e-03 - 6.18324e-05i	2.75370e-02 - 1.99335e-02i	-1.81944e-04 + 1.98026e-04i	-7.64288e-14 + 1.29894e-13i	-1.62132e-33 + 1.77783e-32i	9.00049e-81 - 5.57498e-81i*
0.1	250.245°	Pr	3.52553e+02 + 6.21464e+04i	-0.00000e+0 - 0.00000e-00i	6.77210e-03 - 9.84868e-03i	-3.29064e-04 + 8.02353e-04i	2.09927e+16 + 1.36365e+16i	3.04160e+35 + 1.15883e+35i	4.30307e+54 + 6.59157e+53i	-1.39272e+72 + 1.01024e+73i
0.1	250.260°	Pr	-3.08180e+04 + 5.38766e+04i	-0.00000e+0 - 0.00000e-00i	1.30163e-02 - 1.17038e-02i	3.82690e+06 + 2.57282e+06i	3.97254e+20 + 3.28762e+20i	9.03514e+43 + 1.04341e+44i	1.97933e+67 + 3.24409e+67i	-9.39943e+89 + 3.24409e+89i
0.1	250.275°	Pr	-5.36446e+04 + 3.11206e+04i	-0.00000e+0 - 0.00000e-00i	2.05068e-02 - 8.47907e-03i	5.59000e+07 + 4.22873e+07i	-2.59966e+23 + 5.41850e+23i	2.89549e+49 - 2.28309e+49i	-2.15607e+75 + 4.71696e+75i	3.84833e+100 - 5.53533e+100i
0.1	250.290°	Pr	-6.20010e+04 + 7.62343e-12i	-0.00000e+0 - 0.00000e-00i	2.40538e-02 - 6.94243e-19i	1.31421e+08 - 1.84578e-07i	2.23406e+24 - 8.26759e+22i	2.58942e+51 - 1.94925e+47i	3.08729e+78 - 3.50555e+64i	3.10007e+104 - 4.65900e+90i
0.1	500.20°	Pr	1.49825e+03 - 0.00000e+00i	-0.00000e+0 - 0.00000e-00i	9.75370e-03 - 0.00000e+00i	8.20849e-03 - 0.00000e+00i	3.31172e-08 - 0.00000e+00i	4.82170e-30 - 0.00000e+00i	3.69757e-74 - 0.00000e+00i*	1.87309e-186 - 0.00000e+00i*
0.1	500.215°	Pr	1.44714e+03 + 3.88229e+02i	-0.00000e+0 - 0.00000e-00i	9.76181e-03 - 6.31661e-05i	7.12439e-03 - 5.40110e-03i	-3.22653e-08 + 4.68505e-08i	2.77978e-26 + 4.71779e-29i	1.16610e-71 + 1.99035e-72i*	1.16610e-71 + 1.99035e-72i*
0.1	500.230°	Pr	1.29729e+03 + 7.50901e+02i	-0.00000e+0 - 0.00000e-00i	9.78566e-03 - 1.22330e-04i	3.58687e-03 - 1.09094e-02i	-2.34718e-08 - 2.76883e-07i	-1.89490e-26 - 3.32990e-26i	-2.57137e-64 - 4.74071e-65i*	-1.54265e-180 + 3.95467e-180i*
0.1	500.245°	Pr	7.06106e+02 + 2.49239e+05i	-0.00000e+0 - 0.00000e-00i	-3.14183e-02 - 1.22975e-02i	-2.05667e-12 + 2.72974e+10i	1.82374e+35 + 6.92549e+34i	3.19546e+73 - 2.41049e+73i	7.31141e+111 - 3.85063e+111i	-4.48045e+148 + 2.53845e+148i
0.1	500.260°	Ob	-1.24135e+05 + 2.16006e+05i	-0.00000e+0 - 0.00000e-00i	-2.96417e-02 - 6.92599e-02i	4.60638e-15 + 3.55513e-15i	5.41870e+43 + 6.24792e+43i	2.65587e+90 + 6.59852e+90i	3.19838e+136 + 6.28438e+137i	-2.65332e-182 + 7.03583e-182i
0.1	500.275°	Ob	-2.15541e+05 + 1.24741e+05i	-0.00000e+0 - 0.00000e-00i	6.37325e-02 - 1.06567e-01i	8.54041e-17 - 9.6302e-16i	1.71257e+49 - 1.36850e+49i	-1.99209e+100 - 4.99261e+100i	-9.70491e+153 - 6.56054e+153i	-1.30574e+204 - 1.83390e+204i
0.1	500.290°	Ob	-2.49001e+05 + 3.05549e-11i	-0.00000e+0 - 0.00000e-00i	1.47230e-01 - 3.79826e-17i	4.72239e-18 - 1.42305e-04i	1.55126e+51 - 1.17986e+37i	2.50181e+105 - 3.81		

Table D.52: (continued)

m, n	$c \setminus \arg(c)$	type	$\lambda_{mn}^{(a)}$	$S_{mn}^{(a)}(c, \eta=0)$	$S_{mn}^{(a)}(c, \eta=0.01)$	$S_{mn}^{(a)}(c, \eta=0.1)$	$S_{mn}^{(a)}(c, \eta=0.25)$	$S_{mn}^{(a)}(c, \eta=0.5)$	$S_{mn}^{(a)}(c, \eta=0.75)$	$S_{mn}^{(a)}(c, \eta=0.99)$
0,1	2500 \angle 60	Ob	-3.12067e+06 + 5.41016e-06i	-0.00000e+00 - 0.00000e-00i	$\pm \infty$	$\pm \infty$	$\pm \infty$	$\pm \infty$	$\pm \infty$	$\pm \infty$
0,1	2500 \angle 75	Ob	-5.40783e+06 + 3.12371e+06i	-0.00000e+00 - 0.00000e-00i	$\pm \infty$	$\pm \infty$	$\pm \infty$	$\pm \infty$	$\pm \infty$	$\pm \infty$
0,1	2500 \angle 90	Ob	-6.24500e+06 + 7.65098e-10i	-0.00000e+00 - 0.00000e-00i	$\pm \infty$	$\pm \infty$	$\pm \infty$	$\pm \infty$	$\pm \infty$	$\pm \infty$
0,1	5000 \angle 0	Pr	1.49982e+04 - 0.00000e-00i	-0.00000e+00 - 0.00000e-00i	7.78845e-03 - 0.00000e-00i	1.31245e-12 - 0.00000e+00i	2.89791e-70 - 0.00000e+00i	7.13244e-292 - 0.00000e-00i*	± 0	± 0
0,1	5000 \angle 15	Pr	1.44871e+04 + 3.88229e+03i	-0.00000e+00 - 0.00000e-00i	7.83864e-03 - 5.07919e-04i	3.01932e-12 - 6.23029e-13i	-6.27551e-68 + 1.61717e-68i	-4.85552e-282 + 3.23904e-282i*	± 0	± 0
0,1	5000 \angle 30	Pr	1.29886e+04 + 7.50000e+03i	-0.00000e+00 - 0.00000e-00i	7.99089e-03 - 1.00412e-03i	3.76777e-11 + 1.31787e-12i	-3.32487e-61 + 3.75134e-61i	-2.35871e-253 - 6.32630e-253i*	± 0	± 0
0,1	5000 \angle 45	Ob	7.07007e+03 + 2.49929e+07i	-0.00000e+00 - 0.00000e-00i	$\pm \infty$	$\pm \infty$	$\pm \infty$	$\pm \infty$	$\pm \infty$	$\pm \infty$
0,1	5000 \angle 60	Ob	-1.24913e+07 + 2.16456e+07i	-0.00000e+00 - 0.00000e-00i	$\pm \infty$	$\pm \infty$	$\pm \infty$	$\pm \infty$	$\pm \infty$	$\pm \infty$
0,1	5000 \angle 75	Ob	-2.16410e+07 + 1.24974e+07i	-0.00000e+00 - 0.00000e-00i	$\pm \infty$	$\pm \infty$	$\pm \infty$	$\pm \infty$	$\pm \infty$	$\pm \infty$
0,1	5000 \angle 90	Ob	-2.49900e+07 + 3.06100e-09i	-0.00000e+00 - 0.00000e-00i	$\pm \infty$	$\pm \infty$	$\pm \infty$	$\pm \infty$	$\pm \infty$	$\pm \infty$
0,2	25 \angle 0	Pr	1.21126e+02 - 0.00000e-00i	-5.00000e-01 - 0.00000e-00i	-4.96975e-01 - 0.00000e-00i	-2.27201e-01 - 0.00000e-00i	4.92801e-01 - 0.00000e-00i	2.52995e-01 - 0.00000e-00i	5.50678e-03 - 0.00000e-00i*	1.28090e-07 - 0.00000e-00i*
0,2	25 \angle 15	Pr	1.16872e+02 + 3.23877e-01i	-5.00000e-01 - 0.00000e-00i	-4.97081e-01 + 8.08027e-04i	-2.33773e-01 + 6.55277e-02i	5.10688e-01 + 9.67982e-02i	2.38696e-01 - 1.55316e-01i	-2.47721e-03 - 6.93883e-03i*	1.48278e-07 + 2.20503e-07i*
0,2	25 \angle 30	Pr	1.04401e+02 + 6.25665e+01i	-5.00000e-01 - 8.67362e-19i	-4.97391e-01 + 1.56130e-03i	-2.53707e-01 + 1.29424e-01i	5.63809e-01 + 2.14797e-01i	1.83659e-01 - 3.58486e-01i	-1.48371e-02 + 8.87192e-03i*	-1.56335e-06 + 1.62168e-06i*
0,2	25 \angle 45	Ob	3.43483e+01 + 5.89637e+02i	-5.00000e-01 + 2.77556e-17i	-4.99069e-01 + 1.47328e-02i	2.71426e-01 + 1.25697e+00i	4.73532e+00 - 1.58681e+01i	9.56506e+02 + 6.27775e+02i	-6.22879e+04 + 5.23006e+04i	-1.13243e+06 - 4.84199e+06i
0,2	25 \angle 60	Pr	1.17465e+01 + 2.16575e+01i	-5.00000e-01 + 2.16840e-19i	-4.99706e-01 + 5.41132e-04i	-4.68639e-01 + 5.10760e-02i	-2.66151e-01 + 2.18646e-01i	1.01290e-01 + 2.47792e-02i	-4.88087e-03 + 8.51231e-03i	3.73098e-05 + 9.61043e-06i
0,2	25 \angle 75	Ob	-4.01534e+02 + 2.73631e+02i	-5.00000e-01 + 6.93889e-18i	-5.10057e-01 + 6.88684e-03i	-1.66357e+00 + 1.22791e+00i	6.00668e+01 + 4.89671e+01i	9.21557e+03 - 1.00220e+03i	-2.29415e+05 - 1.33644e+05i	1.56363e+07 + 6.23097e+06i
0,2	25 \angle 90	Ob	-4.80164e+02 + 6.73446e-14i	-5.00000e-01 - 4.73800e-17i	-5.12053e-01 - 4.68250e-17i	-2.26940e+00 + 1.25364e-16i	-6.00668e+01 - 1.75563e-14i	-1.41586e+04 + 9.54498e-12i	-2.55658e+06 + 2.71099e-09i	3.67940e+07 - 4.78231e-08i
0,2	50 \angle 0	Pr	2.46191e+02 - 0.00000e-00i	-5.00000e-01 - 0.00000e-00i	-4.93859e-01 - 0.00000e-00i	-4.01883e-01 - 0.00000e-00i	5.60816e-01 + 0.00000e+00i	1.87312e-02 - 0.00000e-00i	2.38943e-06 - 0.00000e-00i	1.19454e-16 - 0.00000e-00i
0,2	50 \angle 15	Pr	2.37675e+02 + 6.47207e+01i	-5.00000e-01 - 0.00000e-00i	-4.94070e-01 + 1.61118e-03i	-1.08587e-02 + 1.03434e-01i	5.94194e-01 - 5.75067e-02i	2.63752e-03 - 2.34297e-02i	-2.40054e-06 + 5.31632e-06i	1.76882e-17 + 5.10863e-16i
0,2	50 \angle 30	Pr	2.12706e+02 + 1.25030e+02i	-5.00000e-01 - 4.33681e-19i	-4.94689e-01 + 3.11395e-03i	-3.26924e-02 + 2.08783e-01i	7.05971e-01 - 1.21805e-01i	-4.36189e-02 - 1.54927e-02i	-1.72722e-06 - 2.30919e-05i	-1.91452e-14 - 2.23737e-14i
0,2	50 \angle 45	Ob	6.97071e+01 + 2.42929e+03i	-5.00000e-01 + 3.05311e-16i	-4.97030e-01 + 6.06536e-02i	7.20199e-02 - 2.99311e+00i	1.14880e+03 + 7.60007e+02i	-3.90902e+06 - 7.28077e+06i	-8.54300e+09 + 4.59383e+10i	1.79282e+14 - 8.61445e+13i
0,2	50 \angle 60	Pr	2.42428e+01 + 4.33046e+01i	-5.00000e-01 - 0.00000e-00i	-4.99393e-01 + 1.08133e-03i	-4.32388e-01 + 9.53597e-02i	-4.50308e-02 + 2.27166e-01i	-1.73129e-02 - 9.04440e-03i	7.13189e-05 + 1.23243e-04i	4.58062e-10 - 3.95962e-10i
0,2	50 \angle 75	Ob	-1.88036e+03 + 1.17233e-03i	-5.00000e-01 + 4.85723e-17i	-5.47460e-01 + 3.02354e-01i	-6.29774e+00 + 2.22874e-01i	2.06948e+04 - 2.01154e+03i	-1.63752e+09 + 3.21222e+08i	1.00279e+14 + 3.03948e+13i	1.65272e+16 + 9.58898e+16i
0,2	50 \angle 90	Pr	-2.20508e+03 + 2.38777e-13i	-5.00000e-01 + 1.86102e-17i	-5.56149e-01 + 2.81624e-17i	-2.74614e-01 + 9.43731e-15i	-3.18180e+04 + 2.55625e-11i	-3.90360e+09 + 6.12709e-06i	-3.75309e+14 + 8.76948e-06i	3.04881e+16 + 3.04898e-07i*
0,2	100 \angle 0	Pr	4.96221e+02 - 0.00000e-00i	-5.00000e-01 - 0.00000e-00i	-4.87649e-01 - 0.00000e-00i	3.02475e-01 - 0.00000e+00i	2.52739e-01 - 0.00000e+00i	4.73540e-05 - 0.00000e-00i	2.15106e-13 - 0.00000e-00i	5.30544e-35 - 0.00000e-00i*
0,2	100 \angle 15	Pr	4.79185e+02 - 0.29417e+02i	-5.00000e-01 - 0.00000e-00i	-4.87649e-01 - 0.00000e-00i	3.02475e-01 - 0.00000e+00i	2.52739e-01 - 0.00000e+00i	4.73540e-05 - 0.00000e-00i	2.15106e-13 - 0.00000e-00i	5.30544e-35 - 0.00000e-00i*
0,2	100 \angle 30	Pr	4.29238e+02 + 2.50015e+02i	-5.00000e-01 - 2.16840e-19i	-4.89296e-01 + 6.20248e-01i	3.09612e-01 + 2.58081e-01i	2.05716e-01 + 3.33661e-01i	2.83928e-04 + 3.43670e-04i	-1.54945e-11 + 1.28071e-11i	7.22409e-32 + 5.27290e-30i
0,2	100 \angle 45	Ob	1.40420e+02 + 9.85858e+02i	-5.00000e-01 + 1.04951e-15i	-4.76285e-01 + 2.45232e-01i	-1.88623e+02 + 1.89687e+02i	-3.69894e+06 - 8.75776e+06i	2.62695e+14 - 2.69953e+14i	-1.42998e+22 + 5.58786e+21i	-1.99181e+29 + 2.64673e+29i
0,2	100 \angle 60	Pr	4.92491e+01 + 8.60442e+01i	-5.00000e-01 - 5.42101e-20i	-4.98766e-01 + 2.15983e-01i	-3.54394e-01 + 1.64298e-01i	9.67731e-02 + 3.99543e-02i	-3.91218e-04 - 5.63081e-04i	1.50202e-08 - 2.59918e-08i	-2.11730e-19 - 3.32325e-19i
0,2	100 \angle 75	Ob	-8.08574e+03 + 4.84470e+03i	-5.00000e-01 + 3.88578e-16i	-7.10847e-01 + 1.38033e-01i	-2.37494e+01 + 1.52590e+03i	-3.60053e+09 + 6.88094e+08i	-4.81719e+19 + 1.91143e+19i	-4.87166e+29 + 3.11057e+29i	8.32201e+37 + 7.62952e+37i
0,2	100 \angle 90	Pr	-9.40504e+03 + 1.18790e-12i	-5.00000e-01 + 3.05494e-17i	-7.54150e-01 + 8.06554e-17i	-4.08585e+03 + 2.75213e-12i	-8.59049e+09 + 1.36784e-05i	-2.84621e+20 - 8.89002e+05i	-7.43729e+30 + 3.46208e+16i	-3.08167e+39 + 1.90635e+25i
0,2	250 \angle 0	Pr	1.24624e+03 - 0.00000e-00i	-5.00000e-01 - 0.00000e-00i	-4.69190e-01 - 0.00000e-00i	5.74813e-01 - 0.00000e+00i	5.69566e-03 - 0.00000e+00i	2.24939e-13 - 0.00000e-00i	4.76720e-35 - 0.00000e-00i	1.46922e-30 - 0.00000e-00i*
0,2	250 \angle 15	Pr	1.20365e+03 + 1.25327e+02i	-5.00000e-01 - 0.00000e-00i	-4.70208e-01 + 7.91476e-03i	6.06338e-01 + 1.41290e-03i	-1.59727e-03 - 7.30524e-03i	-3.68502e-13 - 6.00393e-13i	-8.01836e-34 - 2.90477e-34i	7.32983e-88 + 2.08674e-87i
0,2	250 \angle 30	Pr	1.07877e+03 + 6.25006e+02i	-5.00000e-01 - 0.00000e-00i	-4.73203e-01 + 1.53245e-02i	7.08075e-01 + 1.33429e-02i	-1.59025e-02 + 4.68658e-03i	-1.74680e-11 + 9.77954e-12i	-2.32140e-30 + 3.27145e-30i	4.58062e-10 - 3.95962e-10i
0,2	250 \angle 45	Ob	3.52553e+02 + 6.21464e+02i	-5.00000e-01 - 1.58207e-15i	2.92206e-01 + 1.37960e-01i	-4.19986e-06 - 9.96025e-06i	-3.50531e-18 + 6.57049e-17i	-3.69746e+37 + 1.66998e+37i	-4.36449e+56 + 3.22412e+56i	-7.70536e+74 - 1.01988e+75i
0,2	250 \angle 60	Pr	1.24250e+02 + 2.16507e+02i	-5.00000e-01 - 0.00000e-00i	-4.96874e-01 + 5.37918e-03i	-1.25175e-02 + 2.37220e-01i	-8.02910e-03 + 5.39705e-03i	2.20631e-08 - 1.98288e-08i	1.41444e-19 - 2.43488e-19i	3.39408e-47 - 2.43846e-47i
0,2	250 \angle 75	Ob	-5.26827e+04 + 3.08618e-12i	-5.00000e-01 - 7.49401e-16i	-2.18385e+00 + 1.62234e-01i	-5.60685e+09 + 1.06402e+09i	1.76665e+25 - 8.94790e+24i	-8.95068e+50 + 1.21962e+51i	1.49036e+76 - 9.02660e+76i	-9.40714e+99 + 3.27242e+100i
0,2	250 \angle 90	Ob	-6.10050e+04 + 7.56219e-18i	-5.00000e-01 - 5.42850e-17i	-2.97661e+00 + 1.26035e-16i	-1.33765e+10 + 1.90254e-05i	-1.66568e+26 + 6.19390e-11i	-1.07027e+53 + 8.07599e+38i	-5.44561e+79 + 6.19106e+65i	-1.54884e+104 + 2.33285e+90i
0,2	500 \angle 0	Pr	2.49624e+03 - 0.00000e-00i	-5.00000e-01 - 0.00000e-00i	-4.38976e-01 - 0.00000e-00i	3.69899e-01 - 0.00000e+00i	4.13498e-06 - 0.00000e+00i	1.28560e-27 - 0.00000e-00i	1.66483e-71 - 0.00000e-00i*	1.62304e-183 - 0.00000e-00i*
0,2	500 \angle 15	Pr	2.41106e+03 + 6.47049e+02i	-5.00000e-01 - 1.35525e-20i	-4.40923e-01 + 1.54867e-02i	3.78949e-01 - 1.41736e-01i	-5.42915e-06 + 4.58624e-06i	-2.55602e-25 + 1.23410e-26i	4.83847e-69 + 2.22797e-69i	-2.17915e-187 + 2.96340e-177i*
0,2	500 \angle 30	Pr	2.16311e+03 + 1.25000e+02i	-5.00000e-01 - 5.42101e-20i	-4.46664e-01 + 3.00524e-02i	4.10967e-01 - 3.28449e-01i	1.50532e-05 + 3.13503e-05i	1.94122e-25 - 1.01608e-25i	8.95249e-62 + 7.65163e-62i	1.31978e-158 - 8.67840e-159i*
0,2	500 \angle 45	Ob	7.06106e+02 + 2.49293e+05i	-5.00000e-01 - 2.78944e-15i	7.84955e-00 + 3.25724e-00i	3.59039e+14 - 3.68119e-14i	4.43909e+37 + 2.00315e+37i	-6.53937e+75 + 7.41018e+75i	-6.08125e+113 + 1.97126e+114i	3.42645e+150 + 1.24110e+151i
0,2	500 \angle 60	Pr	2.49250e+02 + 4.33013e+02i	-5.00000e-01 - 1.35525e-20i	-4.93692e-01 + 1.06907e-02i	8.09027e-02 + 1.18329e-01i	-6.89953e-05 + 1.69195e-04i	-1.68484e-16 + 1.57286e-15i	5.81712e-38 + 1.02114e-37i	-3.32987e-94 + 9.16504e-94i*
0,2	500 \angle 75	Ob	-2.13614e+05 + 1.24224e+05i	-5.00000e-01 - 3.80251e-15i	-8.29578e+00 + 2.92094e+01i	-1.63223e+20 + 6.41933e-19i	-1.94248e+51 + 2.64165e+51i	1.23651e+103 + 3.95911e+103i	3.93257e+155 + 1.35139e+155i	2.01274e+204 + 1.56494e+204i
0,2	500 \angle 90	Ob	-2.47005e+03 + 0.043							

Table D.52: (continued)

m, n	$c \setminus \arg(c)$	type	$\lambda_{mn}^{(a)}$	$S_{mn}^{(a)}(c, \eta=0)$	$S_{mn}^{(a)}(c, \eta=0.01)$	$S_{mn}^{(a)}(c, \eta=0.1)$	$S_{mn}^{(a)}(c, \eta=0.25)$	$S_{mn}^{(a)}(c, \eta=0.5)$	$S_{mn}^{(a)}(c, \eta=0.75)$	$S_{mn}^{(a)}(c, \eta=0.99)$
0.2	2500 \angle 60°	Pr	1.24925e+03 + 2.16506e-03i	-5.00000e-01 - 3.38813e-21i	-4.66974e-01 + 5.07511e-02i	1.35979e-04 - 9.44031e-04i	-2.76371e-18 - 1.05688e-18i	-5.26361e-74 + 8.90576e-74i	5.68771e-185 - 9.20966e-185i	±0
0.2	2500 \angle 75°	Ob	-5.39817e+06 + 3.12112e+06i	-0.00000e+00 - 0.00000e+00i	±0	±0	±0	±0	±0	±0
0.2	2500 \angle 90°	Ob	-6.23501e+06 + 7.64486e-10i	-0.00000e+00 - 0.00000e+00i	±0	±0	±0	±0	±0	±0
0.2	5000 \angle 0°	Pr	2.49962e+04 - 0.00000e+00i	-5.00000e-01 - 0.00000e+00i	-3.89520e-05 - 0.00000e+00i	6.51231e-10 - 0.00000e+00i	3.67457e-67 - 0.00000e+00i	1.91019e-288 - 0.00000e+00i*	±0	±0
0.2	5000 \angle 15°	Pr	2.41444e+04 + 6.47048e+03i	-5.00000e-01 + 1.69407e-21i	-6.82117e-03 + 1.02310e-01i	1.52745e-09 + 9.31227e-11i	-8.21744e-65 - 8.24430e-67i	-1.48069e-278 + 5.01166e-279i†	±0	±0
0.2	5000 \angle 30°	Pr	2.16469e+04 + 1.25000e+04i	-5.00000e-01 - 0.00000e+00i	-2.84665e-02 + 2.06509e-01i	1.568349e-08 + 1.000285e-01i	-6.03259e-58 + 2.00680e-58i	3.00533e-250 - 1.78320e-249i†	±0	±0
0.2	5000 \angle 45°	Ob	7.07007e+03 + 2.49929e+07i	-0.00000e+00 - 0.00000e+00i	±0	±0	±0	±0	±0	±0
0.2	5000 \angle 60°	Pr	2.49925e+03 + 4.33013e+03i	-5.00000e-01 - 0.00000e+00i	-4.30961e-01 + 9.47941e-02i	1.73885e-06 + 5.11544e-07i	-1.27311e-35 - 1.14051e-35i	9.27751e-147 + 1.68548e-146i†	±0	±0
0.2	5000 \angle 75°	Ob	-2.16217e+07 + 1.24922e+07i	-0.00000e+00 - 0.00000e+00i	±0	±0	±0	±0	±0	±0
0.2	5000 \angle 90°	Ob	-2.49700e+07 + 3.05978e-09i	-0.00000e+00 - 0.00000e+00i	±0	±0	±0	±0	±0	±0
0.3	25 \angle 0°	Pr	1.67953e+02 - 0.00000e+00i	-0.00000e+00 - 0.00000e+00i	-1.49585e-02 - 0.00000e+00i	-1.12038e-01 - 0.00000e+00i	3.47462e-03 - 0.00000e+00i	1.11615e-01 - 0.00000e+00i	4.64438e-03 - 0.00000e+00i	2.19511e-07 - 0.00000e+00i*
0.3	25 \angle 15°	Pr	1.62005e+02 + 4.53798e+01i	-0.00000e+00 - 0.00000e+00i	-1.49600e-02 + 1.13250e-05i	-1.13029e-01 + 9.48754e-03i	7.34850e-03 + 5.01960e-02i	1.10603e-01 - 6.27147e-02i	-1.98752e-03 - 5.90322e-03i	2.53596e-07 + 3.77745e-07i†
0.3	25 \angle 30°	Ob	3.36495e+02 + 4.97956e+02i	-0.00000e+00 - 0.00000e+00i	-1.49162e-02 + 1.24075e-04i	-5.50772e-02 + 8.46406e-02i	2.07506e-01 - 5.15854e-01i	9.98146e+00 - 3.34596e+00i	1.75421e+02 + 1.06435e+02i	-2.18449e+02 + 3.61525e+03i
0.3	25 \angle 45°	Pr	5.12567e+01 + 5.30623e+01i	-0.00000e+00 - 0.00000e+00i	-1.49877e-02 + 1.32550e-05i	-1.37608e-01 + 1.22324e-02i	-1.88523e-01 + 1.18630e-01i	6.00872e-02 + 5.84726e-02i	-4.41745e-03 - 1.33625e-03i	2.09584e-06 + 1.11875e-06i†
0.3	25 \angle 60°	Ob	-1.87732e+02 + 4.66179e+02i	-0.00000e+00 - 0.00000e+00i	-1.50472e-02 + 1.16767e-04i	-1.71253e-01 + 1.37949e-01i	2.91566e+00 + 1.98593e+00i	-2.95655e+02 - 2.02530e+02i	2.35010e+04 + 1.57063e+04i	-3.24521e+04 + 2.17484e+05i
0.3	25 \angle 75°	Ob	-4.01534e+02 + 2.73631e+02i	-0.00000e+00 - 0.00000e+00i	-1.51010e-02 + 6.86852e-05i	-2.61049e-01 + 9.96910e-02i	-1.62479e+00 + 6.48008e+00i	1.23971e+03 + 2.40312e+02i	2.39075e+04 + 1.83165e+04i	1.78437e+06 + 1.44001e+06i
0.3	25 \angle 90°	Ob	-4.80164e+02 + 6.73446e-14i	-0.00000e+00 - 0.00000e+00i	-1.51208e-02 - 1.36812e-18i	-3.03337e-01 - 1.26046e-18i	-8.30720e+00 - 1.84882e-15i	-1.94074e+03 + 1.17804e-12i	-3.50436e+05 + 3.48070e-10i	5.04343e+06 - 6.21657e-09i
0.3	50 \angle 0°	Pr	3.43111e+02 - 0.00000e+00i	-0.00000e+00 - 0.00000e+00i	-1.49149e-02 - 0.00000e+00i	-7.91325e-02 - 0.00000e+00i	8.75181e-02 + 0.00000e+00i	9.20131e-03 - 0.00000e+00i	2.08477e-06 - 0.00000e+00i	±0
0.3	50 \angle 15°	Pr	3.31191e+02 + 9.06247e+01i	-0.00000e+00 - 0.00000e+00i	-1.49178e-02 + 2.25735e-05i	-8.03254e-02 + 1.55209e-02i	9.77819e-02 + 8.57807e-03i	1.58533e-03 - 1.15190e-03i	-2.12568e-06 + 3.05254e-06i	-1.25015e-16 + 8.79080e-16i†
0.3	50 \angle 30°	Pr	1.29900e+03 + 2.07846e+03i	-0.00000e+00 - 0.00000e+00i	-1.46725e-02 + 1.22889e-04i	-1.67261e-01 - 2.18920e-02i	5.91755e+00 + 2.07639e+00i	4.53417e+02 + 2.66713e+03i	-1.20067e+06 - 1.22522e+03i	2.41729e+08 - 3.50559e+08i
0.3	50 \angle 45°	Pr	1.04303e+02 + 1.06080e+02i	-0.00000e+00 - 0.00000e+00i	-1.49744e-02 + 2.64755e-05i	-1.24452e-01 + 2.29224e-02i	-5.50269e-02 + 1.14508e-01i	-1.96253e-04 - 7.84300e-03i	-9.60302e-06 - 6.48957e-06i	-3.09555e-13 - 5.17426e-13i†
0.3	50 \angle 60°	Ob	-9.95259e+02 + 2.01502e+03i	-0.00000e+00 - 0.00000e+00i	-1.52455e-02 + 5.08782e-04i	3.26220e-01 + 8.28055e-01i	-3.15518e-02 + 2.08167e+02i	-7.13579e+06 - 4.98672e+06i	-1.27179e+11 - 9.27729e+11i	-8.00652e+13 + 3.34811e+13i
0.3	50 \angle 75°	Ob	-1.88036e+02 + 1.17233e+03i	-0.00000e+00 - 0.00000e+00i	-1.54733e-02 + 2.98638e-04i	-7.77010e-01 + 1.25635e-01i	1.30349e+03 + 2.39864e+02i	-1.05875e+08 - 9.01736e+06i	6.67850e+12 - 1.03019e+11i	-6.69766e+14 - 1.61661e+15i
0.3	50 \angle 90°	Ob	-2.20508e+02 + 2.87787e-13i	-0.00000e+00 - 0.00000e+00i	-1.55579e-02 + 6.81900e-19i	-1.75455e-01 + 4.91785e-16i	-2.03324e+03 + 1.50458e-12i	-2.49448e+08 + 3.75717e-07i	-2.39830e+13 + 5.45181e-02i	5.49895e+15 + 5.68813e-87i
0.3	100 \angle 0°	Pr	6.93182e+02 - 0.00000e+00i	-0.00000e+00 - 0.00000e+00i	-1.48279e-02 - 0.00000e+00i	-3.09463e-02 - 0.00000e+00i	5.29804e-02 - 0.00000e+00i	2.43482e-05 - 0.00000e+00i	1.90996e-13 - 0.00000e+00i	±0
0.3	100 \angle 15°	Pr	6.69333e+02 + 1.81191e+02i	-0.00000e+00 - 0.00000e+00i	-1.48337e-02 + 4.49613e-05i	-3.12330e-02 + 2.03441e-02i	5.32028e-02 + 2.57082e-02i	-3.84892e-05 + 1.79076e-06i	-3.61624e-13 - 4.86284e-13i	9.16656e-35 - 0.00000e+00i*
0.3	100 \angle 30°	Pr	5.09900e+03 + 8.48705e+03i	-0.00000e+00 - 0.00000e+00i	-1.36710e-02 + 2.01384e-03i	-2.50872e-01 + 9.85260e-01i	2.81918e+02 + 1.59245e+03i	5.92761e+07 - 3.56621e+08i	-4.02047e+13 + 7.27609e+13i	1.17792e+19 + 1.66292e+18i
0.3	100 \angle 45°	Pr	2.10375e+02 + 2.12139e+02i	-0.00000e+00 - 0.00000e+00i	-1.49479e-02 + 5.28520e-05i	-9.93155e-02 + 3.67550e-02i	2.58202e-02 + 3.22822e-02i	6.86791e-05 - 3.36744e-06i	-2.71267e-11 - 6.81068e-11i	1.91874e-26 - 3.69998e-26i†
0.3	100 \angle 60°	Ob	-4.8542e+03 + 3.86023e+03i	-0.00000e+00 - 0.00000e+00i	-1.60571e-02 + 2.18362e-03i	8.16937e-03 - 3.19441e+01i	-7.65899e-06 - 5.26951e+06i	-8.51066e+15 - 6.68600e+15i	-7.43720e+24 - 6.60334e+24i	-3.13091e+32 - 1.58786e+32i
0.3	100 \angle 75°	Ob	-8.08574e+03 + 4.84470e+03i	-0.00000e+00 - 0.00000e+00i	-1.70743e-02 + 1.31168e-03i	6.10925e-01 + 6.58272e-01i	-1.12902e-08 - 9.17640e-06i	-1.59218e+18 + 1.72318e-17i	-1.70721e+28 + 5.24962e+27i	-3.10720e+36 + 1.58649e+36i
0.3	100 \angle 90°	Ob	-9.40504e+03 + 1.18790e-12i	-0.00000e+00 - 0.00000e+00i	-1.74649e-02 + 1.40955e-18i	-1.26400e-02 + 7.72766e-14i	-2.65756e+08 + 4.06623e-07i	-8.80504e+18 + 2.69545e+04i	-2.30080e+29 + 1.05672e+15i	-9.53348e+37 + 5.83818e+23i
0.3	250 \angle 0°	Pr	1.74322e+03 - 0.00000e+00i	-0.00000e+00 - 0.00000e+00i	-1.45689e-02 - 0.00000e+00i	1.35108e-02 - 0.00000e+00i	1.18621e-13 - 0.00000e+00i	4.27582e-35 - 0.00000e+00i	2.54469e-90 - 0.00000e+00i*	±0
0.3	250 \angle 15°	Pr	1.68359e+03 + 4.52940e+02i	-0.00000e+00 - 0.00000e+00i	-1.45832e-02 + 1.11119e-04i	3.22122e-02 + 9.74877e-03i	-3.42885e-04 - 1.74463e-03i	-1.93098e-13 - 3.17621e-13i	-7.18905e-34 - 2.61829e-34i	1.26783e-87 + 3.61508e-87i†
0.3	250 \angle 30°	Ob	3.14990e+04 + 5.36936e+04i	-0.00000e+00 - 0.00000e+00i	-5.44562e-03 + 9.26025e-03i	1.31100e+02 + 7.21400e+02i	8.48168e+10 + 2.91290e+10i	-2.57897e+24 + 1.05687e+24i	3.97297e+37 - 7.97503e+37i	-7.90214e+50 - 2.76706e+50i
0.3	250 \angle 45°	Pr	5.28577e+02 + 5.30333e+02i	-0.00000e+00 - 0.00000e+00i	-1.48683e-02 + 1.31426e-04i	-3.93552e-02 + 4.82032e-02i	-1.11663e-03 - 8.84220e-04i	-5.62795e-12 - 4.59878e-11i	1.83582e-26 - 2.96346e-27i	-5.25903e-66 + 9.08035e-66i*
0.3	250 \angle 60°	Ob	-2.99560e+04 + 5.33766e+04i	-0.00000e+00 - 0.00000e+00i	-1.93434e-02 + 1.72630e-02i	-4.71460e-06 + 3.19496e+06i	-3.58512e-20 - 2.98598e+20i	-4.52263e+43 - 5.24458e+43i	-4.24124e+66 - 6.94709e+66i	5.30495e+87 - 5.68813e-87i
0.3	250 \angle 75°	Ob	-5.26827e+04 + 3.08618e+04i	-0.00000e+00 - 0.00000e+00i	-3.04048e-02 + 1.25085e-02i	-6.90806e-07 - 5.35897e-07i	2.35455e+23 - 4.86768e+22i	-1.43655e+49 - 1.14449e+49i	4.61625e+74 - 1.01030e+75i	-2.14271e+98 + 3.53533e+98i
0.3	250 \angle 90°	Ob	-6.10050e+04 + 7.56219e-12i	-0.00000e+00 - 0.00000e+00i	-3.56409e-02 - 5.51744e-19i	-1.62474e+08 + 2.20980e-07i	-2.02318e+24 + 7.39752e+09i	-1.29997e+51 - 9.72843e+36i	-6.61194e+77 + 7.47869e+63i	-1.88125e+102 + 2.82184e+88i
0.3	500 \angle 0°	Pr	3.49324e+03 - 0.00000e+00i	-0.00000e+00 - 0.00000e+00i	-1.41441e-02 - 0.00000e+00i	2.88330e-02 - 0.00000e+00i	1.01625e-06 - 0.00000e+00i	6.83484e-28 - 0.00000e+00i*	1.49815e-71 - 0.00000e+00i*	±0
0.3	500 \angle 15°	Pr	3.37398e+03 + 9.05870e-02i	-0.00000e+00 - 0.00000e+00i	-1.41716e-02 + 2.18040e-04i	3.08299e-02 - 8.78095e-03i	-1.34589e-06 + 1.11671e-06i	-1.37292e-27 + 6.56004e-27i	4.35282e-69 + 2.00885e-69i†	±0
0.3	500 \angle 30°	Ob	1.25499e+05 + 2.15640e+05i	-0.00000e+00 - 0.00000e+00i	1.80116e-02 - 2.61808e-03i	1.55693e-03 - 9.70410e-07i	-1.54533e+24 + 6.35706e+23i	4.95412e+50 + 1.87277e+51i	2.29140e+78 + 2.92402e+77i	-2.15647e+104 + 8.55010e+103i
0.3	500 \angle 45°	Pr	1.05891e+03 + 1.06066e+03i	-0.00000e+00 - 0.00000e+00i	-1.47358e-02 + 2.60528e-04i	5.13225e-03 + 2.51355e-07i	-1.19099e-06 - 5.05849e-06i	2.32918e-21 - 5.78263e-22i	-1.79596e-52 + 5.94130e-53i†	±0
0.3	500 \angle 60°	Ob	-1.22407e+05 + 2.15066e+05i	-0.00000e+00 - 0.00000e+00i	4.35270e-02 + 1.02258e-01i	-5.66307e-15 - 4.38720e+01i	-4.88111e+43 - 5.64571e+43i	-1.32690e+90 - 3.30635e+90i	-6.87075e+135 + 1.34631e+137i	2.09046e+180 + 4.76162e+180i
0.3	500 \angle 75°	Ob	-2.13614e+05 + 1.24224e+05i	-0.00000e+00 - 0.00000e+00i	-9.42298e-02 + 1.57192e-01i	-1.05194e+18 + 1.17609e+17i	-1.54690e+49 + 1.23408e+49i	9.84854e+99 + 2.50122e+100i	2.07916e+153 + 1.40830e+153i	9.26939e+201 + 1.22811e+202i
0.3	500 \angle 90°	Ob	-2.47000e+05 + 1.04325e-11i	-0.00000e+00 - 0.00000e+00i	-2.17336e-01 + 5.77646e-17i	-5.81679e+18 + 1.75739e+04i	-1.40044e+51 + 1.06626e+37i	-1.25342e+105 + 1.		

Table D.52: (continued)

m, n	$c \setminus \arg(c)$	type	$\lambda_m^{(a)}$	$S_{mn}^{(a)}(c, \eta=0)$	$S_{mn}^{(a)}(c, \eta=0.01)$	$S_{mn}^{(a)}(c, \eta=0.1)$	$S_{mn}^{(a)}(c, \eta=0.25)$	$S_{mn}^{(a)}(c, \eta=0.5)$	$S_{mn}^{(a)}(c, \eta=0.75)$	$S_{mn}^{(a)}(c, \eta=0.99)$
0.3	2500.260°	Ob	-3.11201e+06 + 5.40516e-06i	-0.00000e+00 - 0.00000e+00i	$\pm \infty$	$\pm \infty$	$\pm \infty$	$\pm \infty$	$\pm \infty$	$\pm \infty$
0.3	2500.275°	Ob	-5.39817e+06 + 3.12112e+06i	-0.00000e+00 - 0.00000e+00i	$\pm \infty$	$\pm \infty$	$\pm \infty$	$\pm \infty$	$\pm \infty$	$\pm \infty$
0.3	2500.290°	Ob	-6.23501e+06 + 7.64486e-10i	-0.00000e+00 - 0.00000e+00i	$\pm \infty$	$\pm \infty$	$\pm \infty$	$\pm \infty$	$\pm \infty$	$\pm \infty$
0.3	5000.20°	Pr	3.49932e+04 - 0.00000e+00i	-0.00000e+00 - 0.00000e+00i	-7.78923e-03 - 0.00000e+00i	6.39677e-11 - 0.00000e+00i	9.30474e-68 - 0.00000e+00i	1.02286e-288 - 0.00000e+00i*	± 0	± 0
0.3	5000.215°	Pr	3.38007e+04 + 9.05867e-03i	-0.00000e+00 - 0.00000e+00i	-7.90724e-03 + 1.53107e-03i	1.50094e-10 + 9.96200e-12i	-2.08103e-65 - 2.26118e-67i	-7.92947e-279 + 2.68206e-279i†	± 0	± 0
0.3	5000.230°	Ob	1.25050e+07 + 2.16420e+07i	-0.00000e+00 - 0.00000e+00i	$\pm \infty$	$\pm \infty$	$\pm \infty$	$\pm \infty$	$\pm \infty$	$\pm \infty$
0.3	5000.245°	Pr	1.06049e+04 + 1.06066e+04i	-0.00000e+00 - 0.00000e+00i	-1.23743e-02 + 2.21062e-03i	-1.30202e-09 - 2.74195e-09i	-4.60924e-50 - 5.03395e-50i	1.31459e-206 + 1.12709e-206i†	± 0	± 0
0.3	5000.260°	Ob	-1.24740e+07 + 2.16356e+07i	-0.00000e+00 - 0.00000e+00i	$\pm \infty$	$\pm \infty$	$\pm \infty$	$\pm \infty$	$\pm \infty$	$\pm \infty$
0.3	5000.275°	Ob	-2.16217e+07 + 1.24922e+07i	-0.00000e+00 - 0.00000e+00i	$\pm \infty$	$\pm \infty$	$\pm \infty$	$\pm \infty$	$\pm \infty$	$\pm \infty$
0.3	5000.290°	Ob	-2.49700e+07 + 3.05978e-09i	-0.00000e+00 - 0.00000e+00i	$\pm \infty$	$\pm \infty$	$\pm \infty$	$\pm \infty$	$\pm \infty$	$\pm \infty$
0.4	25.20°	Pr	2.13649e+02 - 0.00000e+00i	3.75000e-01 - 0.00000e+00i	3.71001e-01 - 0.00000e+00i	4.04840e-02 - 0.00000e+00i	-3.59501e-01 - 0.00000e+00i	5.03353e-01 - 0.00000e+00i	4.46423e-02 - 0.00000e+00i	4.40392e-06 - 0.00000e+00i
0.4	25.215°	Pr	2.06014e+02 + 5.84142e+01i	3.75000e-01 - 0.00000e+00i	3.71143e-01 - 1.09147e-03i	4.59575e-02 - 7.54101e-02i	-4.03797e-01 - 7.56639e-02i	5.92103e-01 - 6.59095e-02i	-9.15683e-04 - 6.03768e-02i	2.77663e-06 + 8.72630e-08i
0.4	25.230°	Ob	3.36495e+02 + 4.97956e+02i	3.75000e-01 + 3.33067e-16i	3.68670e-01 - 9.28462e-03i	-3.67215e-01 - 4.42539e-01i	2.21273e+00 + 2.58926e+00i	-1.05481e+01 + 6.36830e+01i	-1.08052e+03 + 6.44552e+02i	-1.89573e+04 - 1.15690e+04i
0.4	25.245°	Pr	8.45599e+01 + 8.84789e+01i	3.75000e-01 + 8.67362e-19i	3.73414e-01 - 1.65653e-03i	2.15658e-01 - 1.42209e-01i	-4.86213e-01 - 2.85620e-01i	-3.25609e-02 + 5.23021e-01i	-2.19891e-02 - 4.51573e-02i	1.37698e-05 + 4.84873e-05i
0.4	25.260°	Ob	-1.87732e+02 + 4.66179e+02i	3.75000e-01 + 5.55112e-17i	3.78492e-01 - 8.76844e-03i	3.82380e-01 - 1.11756e+00i	-1.97683e+01 - 5.73437e-02i	2.00778e+03 + 1.15666e+01i	-1.58362e+05 + 9.33870e+01i	-5.32447e+05 - 1.11097e+06i
0.4	25.275°	Pr	5.71888e+02 + 2.53557e+01i	3.75000e-01 + 2.16840e-19i	3.74893e-01 - 4.52798e-04i	3.61738e-01 - 4.40150e-02i	2.25224e-01 - 2.17106e-01i	1.74579e+01 + 1.65938e-02i	-1.80743e-02 - 5.36922e-02i†	-1.14247e-03 - 5.48500e-03i*
0.4	25.290°	Ob	-3.88753e+02 + 6.11785e-14i	3.75000e-01 + 1.65893e-17i	3.82313e-01 + 1.57582e-17i	1.37483e-01 - 1.44562e-16i	2.59579e+01 - 8.92851e-15i	3.15498e+03 - 2.31396e-12i	2.04323e+05 - 2.31853e-10i	1.92979e+05 - 2.04458e-10i
0.4	50.20°	Pr	4.88973e+02 - 0.00000e+00i	3.75000e-01 - 0.00000e+00i	3.66800e-01 - 0.00000e+00i	-1.88167e-01 - 0.00000e+00i	1.15213e-01 - 0.00000e+00i	1.04888e+01 - 0.00000e+00i	4.36899e-05 - 0.00000e+00i	4.36899e-05 - 0.00000e+00i
0.4	50.215°	Pr	4.23651e+02 + 1.16545e+02i	3.75000e-01 - 0.00000e+00i	3.67083e-01 - 2.16955e-01i	-1.89148e-01 - 9.35679e-02i	1.17779e+01 + 2.54732e-01i	5.77806e-02 - 1.20568e-01i	-6.07921e+05 + 4.91823e-05i	-1.49202e+14 + 3.40293e-14i
0.4	50.230°	Ob	1.29900e+03 + 2.07846e+03i	3.75000e-01 + 1.1022e-16i	3.50239e-01 - 3.81294e-02i	-7.79059e-01 + 1.91059e+00i	-1.30161e+01 - 1.10902e+01i	-3.15985e+04 - 1.10902e+04i	7.21583e+06 - 1.29929e+07i	2.49516e+09 + 4.70227e+09i
0.4	50.245°	Pr	1.72987e+02 + 1.76819e+02i	3.75000e-01 - 0.00000e+00i	3.71756e-01 - 3.30519e-01i	5.50059e-02 - 2.37546e-01i	-7.02056e-01 + 1.43414e-01i	7.25887e-02 - 7.09647e-02i	-4.40662e+05 - 2.53077e-04i	6.57122e-12 - 2.50777e-11i
0.4	50.260°	Ob	-9.95259e+02 + 2.01502e+03i	3.75000e-01 + 1.1022e-16i	3.93176e-01 - 3.84085e-02i	-8.46962e-01 - 6.28805e-02i	4.47791e+03 + 1.20848e+02i	1.03017e+08 + 5.53896e+06i	1.86042e+12 + 1.37931e+11i	1.86042e+12 + 1.37931e+11i
0.4	50.275°	Pr	1.21901e+01 + 4.83000e+01i	3.75000e-01 - 1.08420e-19i	3.74770e-01 - 9.05094e-04i	3.42486e-01 - 8.45772e-02i	9.43988e-02 - 2.54544e-01i	7.23953e-02 - 1.37613e-02i	-5.05861e+03 + 3.80650e-03i	-1.61771e+05 + 1.21595e-05i
0.4	50.290°	Ob	-2.01335e+03 + 2.7523e-13i	3.75000e-01 - 2.36542e-17i	4.13389e-01 - 3.14170e-17i	1.67056e-01 - 6.18244e-15i	1.40059e+04 - 1.16355e-11i	9.26987e+08 - 1.48219e-01i	3.54399e+13 - 8.40369e-02i	7.42187e+15 + 2.30186e+08i
0.4	100.20°	Pr	8.9116e+02 - 0.00000e+00i	3.75000e-01 - 0.00000e+00i	3.58454e-01 - 0.00000e+00i	-3.79272e-01 - 0.00000e+00i	4.71492e-01 - 0.00000e+00i	6.05599e-01 - 0.00000e+00i	8.31862e-12 - 0.00000e+00i	7.80930e-33 - 0.00000e+00i
0.4	100.215°	Pr	8.58454e+02 + 2.32973e+02i	3.75000e-01 - 1.08420e-19i	3.59012e-01 - 4.30470e-03i	-4.03536e-01 - 3.57031e-02i	5.49052e-01 - 4.81118e-02i	-9.34733e-04 - 2.24713e-04i	-9.50952e-12 - 2.46594e-11i	1.9316e-31 + 3.40293e-32i
0.4	100.230°	Ob	5.09900e+03 + 8.48705e+03i	3.75000e-01 - 2.35922e-16i	2.72698e-01 - 1.45647e-01i	-1.82616e-01 - 1.74987e+01i	3.79327e+04 - 1.34026e+04i	6.99537e+09 + 5.65182e+09i	-1.08292e+15 + 1.76178e-15i	-1.80293e+20 - 2.34671e+20i
0.4	100.245°	Pr	3.49784e+02 + 3.53574e+01i	3.75000e-01 - 0.00000e+00i	3.68441e-01 - 6.58814e-03i	-2.30882e-01 - 3.14809e-01i	-8.59208e-02 + 4.87020e-01i	1.31949e+03 + 1.23975e-03i	1.32398e+09 - 3.00023e-09i	1.32398e+09 - 3.00023e-09i
0.4	100.260°	Ob	-4.84542e+03 + 8.36023e+03i	3.75000e-01 - 1.1022e-16i	4.50881e-01 - 1.68430e-01i	2.28706e-02 + 7.69620e-02i	2.2922e+08 + 1.43446e+07i	2.61428e+17 + 3.32935e+16i	2.37965e+26 + 4.49881e+25i	4.72451e+33 + 1.67878e+33i
0.4	100.275°	Pr	2.51314e+01 + 9.65944e+01i	3.75000e-01 + 5.42101e-20i	3.74525e-01 - 1.80891e-03i	2.92614e-01 - 1.53898e-01i	-1.68419e-01 - 1.25394e-01i	1.21410e+02 - 4.76514e-03i	2.21284e-05 - 7.62020e-05i	8.02288e-11 - 2.82304e-10i
0.4	100.290°	Ob	-9.01317e+03 + 1.16340e-12i	3.75000e-01 - 2.98571e-17i	5.57084e-01 - 6.95969e-17i	2.49687e-03 - 1.72874e-12i	3.82542e+09 - 6.16453e+06i	6.94362e+19 - 2.18277e+05i	7.51065e+29 - 3.51304e+15i	-1.20309e+37 + 2.74365e+22i
0.4	250.20°	Pr	2.23920e+03 - 0.00000e+00i	3.75000e-01 - 0.00000e+00i	3.33808e-01 - 0.00000e+00i	-7.34908e-02 - 0.00000e+00i	3.83304e-02 - 0.00000e+00i	7.72288e-12 - 0.00000e+00i	4.75819e-33 - 0.00000e+00i	5.47942e-88 + 3.40293e+00i
0.4	250.215°	Pr	2.16253e+03 + 5.82357e+02i	3.75000e-01 - 5.42101e-20i	3.35140e-01 - 1.05212e-02i	-9.90338e-02 + 2.20565e-01i	5.80299e-03 - 5.04630e-02i	-6.62226e-12 - 2.33033e-11i	-6.95880e-32 - 4.91300e-32i	6.06553e-86 + 8.22901e-85i
0.4	250.230°	Ob	3.14990e+04 + 5.36936e+04i	3.75000e-01 + 6.66134e-10i	-3.93182e-01 - 4.91902e-01i	-4.31116e+04 - 1.52674e+04i	-4.20597e+12 + 3.68789e+12i	2.27419e+25 - 1.72355e+26i	3.08504e+39 + 4.62269e+39i	3.94737e+52 - 3.41941e+52i
0.4	250.245°	Pr	8.80126e+02 + 8.83892e+02i	3.75000e-01 - 0.00000e+00i	3.58497e-01 - 1.63122e-02i	-6.76240e-01 - 4.36212e-02i	-4.01360e-03 - 4.39726e-02i	1.91547e-09 - 2.41451e-09i	1.69080e-24 + 1.23024e-24i	-2.19640e-63 + 5.81013e-64i
0.4	250.260°	Ob	-2.95506e+04 + 5.33766e+04i	3.75000e-01 + 4.44089e-16i	5.06933e-01 - 1.48382e-02i	3.51485e-08 + 2.31918e-07i	8.24670e+22 + 4.73351e+21i	4.05293e+45 + 1.38589e+45i	4.43479e+68 + 2.38253e+68i	-1.05387e+89 + 4.69387e+89i
0.4	250.275°	Pr	6.39546e+01 + 2.41482e+01i	3.75000e-01 + 2.71051e-20i	3.73775e-01 - 4.51334e-03i	9.59614e-02 - 2.54672e-01i	9.09930e-03 - 4.83778e-02i	4.24871e-05 - 5.77571e-05i	1.54509e-10 - 1.16759e-11i	9.62803e-25 - 1.78795e-26i
0.4	250.290°	Ob	-6.00131e+04 + 7.50966e-12i	3.75000e-01 + 2.61558e-17i	2.18853e-01 - 1.74455e-16i	8.19513e+09 - 1.19749e-05i	7.46509e+25 - 2.80513e+11i	2.65035e+52 - 2.01034e+38i	5.70086e+78 - 6.50069e+64i	2.02296e+101 - 3.08060e+87i
0.4	500.20°	Pr	4.48922e+03 - 0.00000e+00i	3.75000e-01 - 0.00000e+00i	2.93995e-01 - 0.00000e+00i	4.42678e-01 - 0.00000e+00i	6.12139e-05 - 0.00000e+00i	9.02921e-06 - 0.00000e+00i*	3.35789e-09 - 0.00000e+00i*	1.21617e-180 - 0.00000e+00i*
0.4	500.215°	Ob	4.33589e+03 + 1.16449e+03i	3.75000e-01 - 2.71051e-20i	2.96453e-01 - 2.02604e-02i	5.16394e-01 + 9.44851e-02i	-9.65486e-05 + 4.26940e-05i	-4.02597e-25 + 7.89063e-25i	8.24784e-67 + 6.89102e-67i	-2.15430e-174 + 1.71992e-174i*
0.4	500.230°	Ob	1.25499e+05 + 2.15640e+05i	3.75000e-01 + 8.88178e-16i	-8.49400e-01 + 2.08394e-02i	9.53584e+09 + 7.72622e-09i	9.53584e+25 - 2.06862e+26i	-2.33573e+53 - 6.29496e+52i	-1.10986e+80 + 2.66254e+80i	4.16824e+105 - 2.86670e+106i
0.4	500.245°	Pr	1.76401e+03 + 1.76777e+03i	3.75000e-01 - 0.00000e+00i	3.41930e-01 - 3.21036e-02i	-3.67493e-01 + 4.27283e-01i	1.74964e+04 - 2.75190e+04i	2.73897e-19 + 1.66254e-19i	-3.80413e-50 - 1.92160e-50i	-1.38111e-129 + 4.99112e-129i*
0.4	500.260°	Ob	-1.22407e+05 + 2.15006e+05i	3.75000e-01 - 4.57967e-16i	-1.10745e-01 - 8.26941e-01i	8.82995e+17 + 1.17688e-17i	8.77589e+45 + 3.01853e+45i	3.49239e+92 - 2.72507e+92i	9.15315e+138 + 1.40437e+139i	-5.22333e-182 + 3.81220e-182i
0.4	500.275°	Pr	1.28659e+02 + 4.82963e+02i	3.75000e-01 + 1.35525e-20i	3.72487e-01 - 8.99684e-03i	-1.47839e-01 - 1.29850e-01i	-5.87659e-03 - 2.29195e-03i	-3.66713e-09 - 1.17645e-09i	4.69177e-20 - 7.10664e-21i	6.97024e-49 - 1.01098e-49i
0.4	500.290°	Ob	-2.45013e+03 + 3.03100e-11i	3.75000e-01 - 1.58493e-17i	2.64695e-01 - 9.22206e-15i	5.90853e-20 - 1.83398e+06i	1.04192e-53 - 8.01911e+38i	5.16684e+106 - 7.93150e+92i	1.56043e+209 - 3.58983e+146i	1.59236e+209 - 4.23112e+195i
0.4	750.20°	Pr	6.73923e+03 - 0.00000e+00i	3.75000e-01 - 0.00000e+00i	2.55722e-01 - 0.00000e+00i	4.06491e-01 - 0.00000e+00i	5.08996e-08 - 0.00000e+00i	5.82964e-40 - 0.00000e+00i	1.32175e-105 - 0.00000e+00i*	1.51548e-273 - 0.00000e+00i*
0.4	750.215°	Pr	6.50923e+03 + 1.74703e+03i	3.75000e-01 - 0.00000e+00i	2.59111e-01 - 2.92465e-02i	4.56076e-01 - 1.38561e-01i	9.06921e-08 + 7.05090e-08i	1.68428e-38 - 6.06032e-39i	-5.38153e-102 - 5.31818e-102i	-4.94107e-264 - 1.51535e-264i

Table D.52: (continued)

m, n	$c \setminus \arg(c)$	type	$\lambda_{mn}^{(a)}$	$S_{mn}^{(a)}(c, \eta=0)$	$S_{mn}^{(a)}(c, \eta=0.01)$	$S_{mn}^{(a)}(c, \eta=0.1)$	$S_{mn}^{(a)}(c, \eta=0.25)$	$S_{mn}^{(a)}(c, \eta=0.5)$	$S_{mn}^{(a)}(c, \eta=0.75)$	$S_{mn}^{(a)}(c, \eta=0.99)$
0.4	2500 $\angle 60^\circ$	Ob	-3.11201e+06 + 5.40516e-06i	-0.00000e-00 - 0.00000e+00i	$\pm \infty$	$\pm \infty$	$\pm \infty$	$\pm \infty$	$\pm \infty$	$\pm \infty$
0.4	2500 $\angle 75^\circ$	Pr	6.46298e+02 + 2.41481e+03i	3.75000e-01 - 0.00000e+00i	3.60432e-01 - 4.37326e-02i	1.31523e-02 + 6.54843e-03i	1.30483e-10 - 4.39500e-10i	-9.36354e-39 - 5.64612e-40i*	2.68519e-96 - 2.50557e-96i*	4.28822e-242 + 3.70251e-242i*
0.4	2500 $\angle 90^\circ$	Ob	-6.22501e+06 + 7.63873e-10i	-0.00000e-00 - 0.00000e+00i	$\pm \infty$	$\pm \infty$	$\pm \infty$	$\pm \infty$	$\pm \infty$	$\pm \infty$
0.4	5000 $\angle 0^\circ$	Pr	4.49892e+04 - 0.00000e+00i	3.75000e-01 - 0.00000e+00i	-1.94638e-01 - 0.00000e+00i	1.55381e-08 - 0.00000e+00i	5.87967e-65 - 0.00000e+00i	1.36846e-285 - 0.00000e+00i*	± 0	± 0
0.4	5000 $\angle 15^\circ$	Ob	4.34559e+04 + 1.16469e+04i	3.75000e-01 - 0.00000e+00i	-1.95672e-01 - 9.09373e-02i	3.45311e-08 + 1.20772e-08i	-1.26625e-62 - 3.55866e-63i	-1.11767e-275 + 7.16276e-277i*	± 0	± 0
0.4	5000 $\angle 30^\circ$	Ob	1.25050e+07 + 2.16420e+07i	-0.00000e-00 - 0.00000e+00i	$\pm \infty$	$\pm \infty$	$\pm \infty$	$\pm \infty$	$\pm \infty$	$\pm \infty$
0.4	5000 $\angle 45^\circ$	Pr	1.76739e+04 + 1.76777e+04i	3.75000e-01 + 3.38813e-21i	5.15625e-02 - 2.34948e-01i	2.58482e-07 - 7.09735e-07i	1.95698e-48 - 4.32505e-47i	1.76761e-204 + 2.31236e-203i*	± 0	± 0
0.4	5000 $\angle 60^\circ$	Ob	-1.24740e+07 + 2.16356e+07i	-0.00000e-00 - 0.00000e+00i	$\pm \infty$	$\pm \infty$	$\pm \infty$	$\pm \infty$	$\pm \infty$	$\pm \infty$
0.4	5000 $\angle 75^\circ$	Pr	1.29335e+03 + 4.82963e+03i	3.75000e-01 - 0.00000e+00i	3.41317e-01 - 8.40642e-02i	3.45631e-04 + 4.57617e-04i	-4.58488e-19 - 2.98560e-19i	2.09398e-76 + 2.53486e-77i*	1.84428e-192 - 2.65977e-191i*	± 0
0.4	5000 $\angle 90^\circ$	Ob	-2.49500e+07 + 3.05858e-09i	-0.00000e-00 - 0.00000e+00i	$\pm \infty$	$\pm \infty$	$\pm \infty$	$\pm \infty$	$\pm \infty$	$\pm \infty$
0.5	25 $\angle 0^\circ$	Pr	2.58164e+02 - 0.00000e+00i	-0.00000e-00 - 0.00000e+00i	1.86701e-02 - 0.00000e+00i	1.17229e-01 - 0.00000e+00i	-9.06018e-02 - 0.00000e+00i	1.44672e-01 - 0.00000e+00i	3.39934e-02 - 0.00000e+00i	7.25765e-06 - 0.00000e+00i*
0.5	25 $\angle 15^\circ$	Pr	2.48858e+02 + 7.15098e+01i	-0.00000e-00 - 0.00000e+00i	1.86729e-02 - 2.22899e-05i	1.18765e-01 - 1.71568e-02i	-1.05968e-01 - 3.38025e-02i	1.92747e-01 + 3.43626e-02i	1.89688e-03 - 4.65015e-02i	4.37567e-06 + 1.44825e-05i*
0.5	25 $\angle 30^\circ$	Pr	1.44563e+02 + 8.76615e+01i	-0.00000e-00 - 0.00000e+00i	1.87055e-02 - 2.73515e-05i	1.45024e-01 - 2.33496e-02i	-2.31513e-02 - 1.33818e-01i	-1.28146e-01 + 1.93529e-01i	1.61179e-02 - 8.88237e-03i	3.34861e-06 - 3.45141e-06i*
0.5	25 $\angle 45^\circ$	Ob	1.00961e+02 + 5.18815e+02i	-0.00000e-00 - 0.00000e+00i	1.87187e-02 - 1.61971e-04i	1.19067e-01 - 1.41882e-01i	-1.46528e+00 + 6.44242e-01i	-8.43804e+00 - 5.98904e+01i	1.77301e+03 + 2.04277e+02i	5.78375e+03 + 2.25131e+03i
0.5	25 $\angle 60^\circ$	Pr	3.57328e+01 + 6.49866e+01i	-0.00000e-00 - 0.00000e+00i	1.87395e-02 - 2.02974e-05i	1.76183e-01 - 1.92060e-02i	2.53528e-01 - 2.08341e-01i	-2.03651e-01 - 4.96728e-02i	1.64821e-02 - 2.88772e-02i	2.42776e-04 + 6.35786e-05i*
0.5	25 $\angle 75^\circ$	Ob	-3.13497e+02 + 2.47571e+02i	-0.00000e-00 - 0.00000e+00i	1.88487e-02 - 7.76112e-05i	2.90902e-01 - 1.04105e-01i	1.38510e+00 - 5.09254e+00i	-5.11630e+02 - 9.88191e+01i	-1.87657e+03 + 2.76693e+02i	-6.77248e+02 + 3.40563e+02i
0.5	25 $\angle 90^\circ$	Ob	-3.88753e+02 + 6.11785e-14i	-0.00000e-00 - 0.00000e+00i	1.88723e-02 + 1.58084e-18i	3.35811e-01 + 7.36349e-19i	6.59306e+00 - 1.84024e-15i	8.01425e+02 - 4.91993e-13i	5.19019e+04 + 5.26912e-11i	4.90203e+04 - 4.60766e-11i
0.5	50 $\angle 0^\circ$	Pr	5.33757e+02 - 0.00000e+00i	-0.00000e-00 - 0.00000e+00i	1.85843e-02 - 0.00000e+00i	6.11024e-02 - 0.00000e+00i	-5.93572e-02 - 0.00000e+00i	4.58070e-02 - 0.00000e+00i	3.66271e-05 - 0.00000e+00i	3.66271e-05 - 0.00000e+00i*
0.5	50 $\angle 15^\circ$	Pr	5.15038e+02 + 1.42488e+02i	-0.00000e-00 - 0.00000e+00i	1.85901e-02 - 4.42920e-02i	6.22024e-02 - 2.50224e-02i	-6.93852e-02 + 5.50954e-02i	2.91508e-02 - 5.15881e-02i	-5.20180e-05 + 4.02750e-05i	-2.56597e-14 + 5.77613e-14i
0.5	50 $\angle 30^\circ$	Pr	2.96242e+02 + 1.75072e+02i	-0.00000e-00 - 0.00000e+00i	1.86581e-02 - 4.55318e-05i	1.05067e-01 - 3.88938e-02i	-1.64657e-01 - 2.19339e-02i	6.77116e-02 + 1.09133e-02i	1.44485e-06 + 2.53465e-05i	-2.56597e-14 + 5.77613e-14i
0.5	50 $\angle 45^\circ$	Ob	2.07079e+02 + 2.28781e+03i	-0.00000e-00 - 0.00000e+00i	1.86778e-02 - 7.13444e-04i	-4.51325e-01 - 2.08120e-01i	-1.04060e-01 - 6.33899e-01i	-8.18626e+04 + 1.86184e+05i	4.21455e+08 - 2.81310e+08i	-4.20477e+10 + 4.38685e+10i
0.5	50 $\angle 60^\circ$	Pr	7.32410e+01 + 1.29921e+02i	-0.00000e-00 - 0.00000e+00i	1.87277e-02 - 4.05530e-05i	1.62554e-01 - 3.58518e-02i	4.28832e-02 - 2.16415e-01i	3.48042e-02 + 1.81675e-02i	-2.41963e-04 + 1.7227e-04i	-4.82727e-09 + 2.56364e-09i*
0.5	50 $\angle 75^\circ$	Ob	-1.69535e+03 + 1.12049e+03i	-0.00000e-00 - 0.00000e+00i	1.92830e-02 - 3.56135e-04i	8.37240e-01 - 1.32098e-02i	-9.98275e-02 - 1.90959e-02i	4.38635e+07 + 3.67874e+07i	-1.10364e+12 + 4.29275e+10i	-1.75071e+14 - 9.73937e+12i
0.5	50 $\angle 90^\circ$	Pr	-2.01335e+03 + 2.75523e-13i	-0.00000e-00 - 0.00000e+00i	1.93862e-02 - 5.03517e-19i	1.86159e-01 - 8.44268e-16i	1.03325e+08 - 1.53830e-12i	1.92747e-01 + 3.43626e-02i	3.95025e+12 - 8.93209e-03i	3.95025e+12 - 8.93209e-03i
0.5	100 $\angle 0^\circ$	Pr	1.08401e+03 - 0.00000e+00i	-0.00000e-00 - 0.00000e+00i	1.84138e-02 - 0.00000e+00i	-6.59776e-02 - 0.00000e+00i	6.54268e-02 - 0.00000e+00i	2.96938e-04 - 0.00000e+00i	7.25280e-12 - 0.00000e+00i	1.33954e-32 - 0.00000e+00i*
0.5	100 $\angle 15^\circ$	Pr	1.04654e+03 + 2.84764e+02i	-0.00000e-00 - 0.00000e+00i	1.84252e-02 - 8.80209e-05i	-8.74523e-03 - 2.40725e-02i	4.48173e-02 + 1.58973e-02i	-4.57285e-04 - 1.22428e-04i	-8.09758e-12 - 2.12608e-11i	-2.39970e-31 - 7.20243e-32i*
0.5	100 $\angle 30^\circ$	Pr	5.99410e+02 + 3.50034e+02i	-0.00000e-00 - 0.00000e+00i	1.85637e-02 - 1.08658e-04i	4.05472e-02 - 5.26589e-02i	-6.56929e-02 + 8.44875e-02i	-1.83121e-04 - 2.61533e-05i	1.73586e-11 - 1.41019e-11i	-1.32953e-31 - 1.13936e-29i*
0.5	100 $\angle 45^\circ$	Ob	4.19238e+02 + 9.57571e+03i	-0.00000e-00 - 0.00000e+00i	1.84771e-02 - 2.97674e-03i	8.37072e-01 + 1.48176e-01i	-8.56575e+04 + 2.00217e+05i	-4.77543e+12 + 4.72103e+09i	-3.27263e+25 - 7.59998e+19i	-3.27263e+25 - 7.59998e+19i
0.5	100 $\angle 60^\circ$	Pr	1.48245e+02 + 2.59816e+02i	-0.00000e-00 - 0.00000e+00i	1.87042e-02 - 8.09966e-05i	1.33232e-01 - 6.17676e-02i	-9.21917e-02 - 3.80589e-02i	7.86447e-04 + 1.13155e-03i	-5.08255e-08 + 8.80430e-08i	1.38261e-18 + 2.16819e-18i*
0.5	100 $\angle 75^\circ$	Ob	-7.70749e+03 + 4.74114e+03i	-0.00000e-00 - 0.00000e+00i	2.12168e-02 - 1.59864e-03i	-6.33193e-01 - 6.87379e-01i	8.55359e+07 + 7.21064e+07i	6.61311e+17 - 7.20915e+16i	2.93021e+27 - 9.34377e+26i	2.93021e+27 - 9.34377e+26i
0.5	100 $\angle 90^\circ$	Pr	-9.01317e+03 + 1.16340e-12i	-0.00000e-00 - 0.00000e+00i	2.16970e-02 - 1.27817e-18i	1.31508e-02 - 7.74307e-14i	2.01482e+08 - 3.03813e-07i	3.65715e+18 - 1.11177e+04i	3.95580e+28 - 1.80932e+14i	-6.33658e+35 + 3.74954e+21i
0.5	250 $\angle 0^\circ$	Pr	2.73416e+03 - 0.00000e+00i	-0.00000e-00 - 0.00000e+00i	1.79083e-02 - 0.00000e+00i	-3.61071e-02 - 0.00000e+00i	8.34568e-03 - 0.00000e+00i	4.00404e-12 - 0.00000e+00i	4.23827e-33 - 0.00000e+00i	9.46421e-88 - 6.24550e-85i
0.5	250 $\angle 15^\circ$	Pr	2.64046e+03 + 7.11777e+02i	-0.00000e-00 - 0.00000e+00i	1.79360e-02 - 2.16344e-04i	-4.21864e-01 + 1.22653e-02i	1.64344e-03 - 1.10221e-02i	-3.32975e-12 - 1.21276e-11i	-6.18583e-32 - 4.40039e-32i	1.02979e-85 + 1.42168e-84i
0.5	250 $\angle 30^\circ$	Pr	1.50877e+03 + 8.75013e+02i	-0.00000e-00 - 0.00000e+00i	1.82818e-02 - 2.68857e-04i	-5.41374e-02 - 2.67150e-02i	4.81505e-03 - 1.23273e-03i	1.15931e-11 - 6.36689e-12i	2.61712e-30 - 3.66249e-30i	-9.91982e-78 + 2.85058e-79i*
0.5	250 $\angle 45^\circ$	Ob	1.05565e+03 + 6.14393e+03i	-0.00000e-00 - 0.00000e+00i	1.26416e-02 - 1.81449e-02i	-3.13830e+01 - 1.23454e+01i	2.36512e+16 + 1.55122e+16i	1.90428e+35 + 7.31817e+34i	1.15211e+54 + 1.76041e+53i	1.84076e+69 + 8.40143e+70i
0.5	250 $\angle 60^\circ$	Pr	3.73248e+02 + 6.49522e+02i	-0.00000e-00 - 0.00000e+00i	1.86332e-02 - 2.01725e-04i	4.70583e-02 - 8.91811e-02i	7.64871e-03 - 5.14151e-03i	4.43377e-08 + 3.98526e-08i	4.78769e-19 + 8.24527e-19i	-2.20835e-46 + 1.55687e-46i*
0.5	250 $\angle 75^\circ$	Ob	-5.17248e+04 + 3.06209e+02i	-0.00000e-00 - 0.00000e+00i	3.75670e-02 - 1.53764e-02i	7.10909e+07 + 5.63987e+07i	-1.77334e+23 + 3.64582e+22i	5.97647e+48 + 4.76467e+48i	-8.05915e+73 + 1.78199e+74i	9.94841e+94 - 1.09317e+96i
0.5	250 $\angle 90^\circ$	Ob	-6.00131e+04 + 7.50969e-12i	-0.00000e-00 - 0.00000e+00i	4.40081e-02 + 7.20650e-19i	1.67266e-08 - 2.27347e-07i	1.52365e+24 - 5.56993e+09i	5.40947e+50 - 4.04799e+36i	1.16357e+77 - 1.31615e+63i	4.12894e+99 - 6.24550e+85i
0.5	500 $\angle 0^\circ$	Pr	5.48420e+03 - 0.00000e+00i	-0.00000e-00 - 0.00000e+00i	1.70853e-02 - 0.00000e+00i	1.54422e-02 - 0.00000e+00i	1.45026e-05 - 0.00000e+00i	4.76113e-26 - 0.00000e+00i	3.01150e-69 - 0.00000e+00i*	2.10556e-180 - 0.00000e+00i*
0.5	500 $\angle 15^\circ$	Pr	5.29680e+03 + 1.42352e+03i	-0.00000e-00 - 0.00000e+00i	1.71374e-02 - 4.20665e-04i	2.08200e-02 + 1.82703e-02i	-2.31387e-05 + 9.69470e-06i	-2.14191e-25 + 4.15409e-25i	7.38740e-67 + 6.19432e-67i*	-3.73188e-174 + 2.97544e-174i*
0.5	500 $\angle 30^\circ$	Pr	3.02433e+03 + 1.75001e+03i	-0.00000e-00 - 0.00000e+00i	1.71761e-02 - 5.28586e-04i	-4.69940e-02 + 2.74540e-02i	-4.81029e-06 + 9.59790e-06i	-1.56253e-25 + 6.75927e-24i	1.00605e-61 + 8.62740e-62i*	-2.86124e-158 + 1.87948e-158i*
0.5	500 $\angle 45^\circ$	Ob	2.11632e+03 + 2.47879e+03i	-0.00000e-00 - 0.00000e+00i	-5.78300e-02 - 2.41161e-02i	-3.16788e-12 + 2.68944e-02i	2.05445e+35 + 7.85305e+34i	2.47337e+73 - 1.47335e+72i	1.95781e+111 + 1.03160e+111i	-3.77707e+146 + 2.51922e+146i
0.5	500 $\angle 60^\circ$	Pr	7.48249e+02 + 1.29904e+03i	-0.00000e-00 - 0.00000e+00i	1.85139e-02 - 4.00911e-04i	-3.04448e-02 - 4.44849e-02i	6.57258e-05 - 1.61180e-04i	3.38496e-16 + 3.16091e-15i	-1.96986e-37 - 3.45721e-37i	2.16522e-93 - 5.96558e-93i*
0.5	500 $\angle 75^\circ$	Ob	-2.11690e+05 + 1.23706							

Table D.52: (continued)

m, n	$c \setminus \arg(c)$	type	$S_{m,n}^{(a)}$	$S_{m,n}^{(a)}(c, \eta=0)$	$S_{m,n}^{(a)}(c, \eta=0.01)$	$S_{m,n}^{(a)}(c, \eta=0.1)$	$S_{m,n}^{(a)}(c, \eta=0.25)$	$S_{m,n}^{(a)}(c, \eta=0.5)$	$S_{m,n}^{(a)}(c, \eta=0.75)$	$S_{m,n}^{(a)}(c, \eta=0.99)$								
0.5	2500.260	Pr	3.74825e+03	6.49519e+03i	-0.00000e+00	-0.00000e+00	1.75120e-02	-1.90321e-03i	-5.11202e-05	+3.54901e-04i	2.63278e-18	+1.00681e-18i	1.05778e-73	-1.78973e-73i	-1.92561e-184	+3.11809e-184i	± 0	
0.5	2500.275	Ob	-5.38852e+06	+3.11853e+06i	-0.00000e+00	-0.00000e+00	± 0	± 0	± 0	± 0	± 0	± 0	± 0	± 0	± 0	± 0	± 0	
0.5	2500.290	Ob	-6.22501e+06	+7.63873e-10i	-0.00000e+00	-0.00000e+00	± 0	± 0	± 0	± 0	± 0	± 0	± 0	± 0	± 0	± 0	± 0	
0.5	5000.20	Pr	5.49842e+04	-0.00000e+00i	-0.00000e+00	-0.00000e+00	5.84357e-03	-0.00000e+00i	1.49343e-09	-0.00000e+00i	1.48403e-65	-0.00000e+00i	7.32190e-286	-0.00000e+00i*	± 0	± 0	± 0	
0.5	5000.215	Pr	5.31102e+04	+1.42350e+04i	-0.00000e+00	-0.00000e+00	5.95126e-03	-2.44057e-03i	3.31096e-09	+1.20074e-09i	3.19523e-63	-9.03785e-64i	-5.98055e-276	+3.80778e-277i*	± 0	± 0	± 0	
0.5	5000.230	Pr	3.03041e+04	+1.75000e+04i	-0.00000e+00	-0.00000e+00	1.03450e-02	-3.88364e-03i	-1.93700e-09	-1.25255e-09i	1.91131e-58	-6.32404e-59i	-2.01655e-250	+1.19362e-249i*	± 0	± 0	± 0	
0.5	5000.245	Ob	2.12082e+04	+2.94788e+07i	-0.00000e+00	-0.00000e+00	± 0	± 0	± 0	± 0	± 0	± 0	± 0	± 0	± 0	± 0	± 0	
0.5	5000.260	Pr	7.49825e+03	+1.29904e+04i	-0.00000e+00	-0.00000e+00	1.61615e-02	-3.55487e-03i	-6.53706e-07	-1.92311e-07i	1.21280e-35	+1.08648e-35i	-1.86444e-146	-3.38717e-146i*	± 0	± 0	± 0	
0.5	5000.275	Ob	-2.16024e+07	+1.24871e+07i	-0.00000e+00	-0.00000e+00	± 0	± 0	± 0	± 0	± 0	± 0	± 0	± 0	± 0	± 0	± 0	
0.5	5000.290	Ob	-2.49500e+07	+3.05856e-09i	-0.00000e+00	-0.00000e+00	± 0	± 0	± 0	± 0	± 0	± 0	± 0	± 0	± 0	± 0	± 0	
0.6	25.20	Pr	3.01441e+02	-0.00000e+00i	-3.12500e-01	-0.00000e+00i	-3.07802e-01	-0.00000e+00i	5.22634e-02	-0.00000e+00i	1.31161e-01	-0.00000e+00i	1.49025e-01	-0.00000e+00i	1.89347e-01	-0.00000e+00i	9.10373e-05	-0.00000e+00i*
0.6	25.215	Pr	2.90487e+02	+8.46911e+01i	-3.12500e-01	-3.46945e-18i	-3.07971e-01	+1.31689e-03i	4.93004e-02	+7.68026e-02i	1.65735e-01	-1.82550e-01i	1.95284e-01	+4.11419e-01i	1.04782e-01	-2.44214e-01i	-2.23649e-06	+1.91372e-04i*
0.6	25.230	Pr	1.83626e+02	+1.12833e+02i	-3.12500e-01	-0.00000e+00i	-3.09634e-01	+1.75756e-03i	-5.27621e-02	+1.26334e-01i	4.56005e-01	-1.14993e-01i	-7.74238e-01	+1.74772e-01i	1.21046e-01	+1.31910e-02i	6.32380e-05	-1.52361e-05i*
0.6	25.245	Ob	1.00961e+02	+5.18815e+02i	-3.12500e-01	-1.38778e-17i	-3.10889e-01	+8.09302e-03i	1.45020e-01	+6.26470e-01i	1.66282e-06	-5.89782e-06i	1.97831e-02	+1.20842e+02i	-4.92159e+03	+4.75104e+03i	-2.07464e+04	+1.16394e+04i
0.6	25.260	Pr	-1.09596e+02	+4.15850e+02i	-3.12500e-01	-9.71445e-17i	-3.14191e-01	+6.50969e-03i	-2.51030e-01	+7.43144e-01i	9.51524e+00	-2.41637e-01i	-5.09498e+02	+3.07185e+01i	1.49505e+04	-2.70713e+03i	1.10449e+04	-1.19287e+04i
0.6	25.275	Ob	-3.13497e+02	+2.47571e+02i	-3.12500e-01	-4.16334e-17i	-3.17403e-01	+3.88864e-03i	-3.17403e-01	+6.16356e-01i	-8.37866e-01	+6.16356e-01i	1.22426e+00	+1.75139e+01i	1.71569e+03	-2.49710e+02i	-2.43995e+04	-8.89891e+04i
0.6	25.290	Ob	-3.02167e+02	+5.49418e-14i	-3.12500e-01	-1.68079e-17i	-3.17233e-01	-1.61996e-17i	-9.16730e-01	+8.70341e-17i	-1.19122e+01	+4.07227e-15i	-7.11006e+02	+5.27905e-13i	-1.30397e+04	+1.55742e-11i	-2.80644e+03	+5.36126e-12i
0.6	50.20	Pr	6.27445e+02	-0.00000e+00i	-3.12500e-01	-0.00000e+00i	-3.02747e-01	-0.00000e+00i	2.53025e-01	-0.00000e+00i	3.32933e-01	-0.00000e+00i	2.98646e-01	-0.00000e+00i	4.85020e-01	-0.00000e+00i	3.84520e-01	-0.00000e+00i*
0.6	50.215	Pr	6.05334e+02	+1.68460e+02i	-3.12500e-01	-4.33681e-19i	-3.03086e-01	+2.60553e-03i	2.62899e-01	+6.96884e-02i	4.25679e-01	-7.65747e-02i	3.08301e-01	-2.51073e-01i	-8.20579e-04	+3.08685e-04i	-1.10376e-12	+1.31064e-12i*
0.6	50.230	Pr	3.78729e+02	+2.25146e+02i	-3.12500e-01	-0.00000e+00i	-3.06594e-01	+3.49535e-03i	1.57834e-01	+1.64418e-01i	-9.11031e-02	-5.02238e-01i	1.22208e-01	+1.90746e-01i	-1.73868e-04	+1.54057e-04i	-2.89250e-03	+4.22680e-03i*
0.6	50.245	Ob	2.07079e+02	+2.28781e+03i	-3.12500e-01	+4.06467e-16i	-3.08590e-01	+3.56198e-02i	3.67029e-01	-1.53646e+00i	4.29988e+02	+2.80077e+02i	-6.57322e+05	-1.48582e+06i	-6.10816e+08	+4.00147e+09i	-3.22801e+10	-4.84343e+11i
0.6	50.260	Ob	-8.30279e+02	+1.91488e+03i	-3.12500e-01	+2.77556e-17i	-3.25082e-01	+3.03336e-02i	5.75422e+00	+4.22932e+00i	-2.19909e+03	-3.33917e+01i	-2.74555e+07	-7.19755e+05i	-2.00381e+11	-1.04005e+09i	-1.07616e+13	+6.51877e+12i
0.6	50.275	Ob	-1.69543e+03	+1.12049e+03i	-3.12500e-01	-4.16334e-17i	-3.39202e-01	+1.80066e-02i	-3.16580e-01	+1.13097e-01i	7.59414e+03	-7.86121e+02i	-3.23486e+08	+6.84355e+07i	7.84607e+12	-2.69652e+12i	1.28043e+15	-3.08708e+14i
0.6	50.290	Pr	-1.82596e+03	+2.63234e-13i	-3.12500e-01	+1.78227e-17i	-3.41468e-01	+4.10027e-15i	-1.12340e-01	+4.10027e-15i	-6.75818e+03	+5.59062e-12i	-2.36319e+08	+3.77887e-07i	-3.36671e+12	+8.04216e-03i	-1.37048e+14	+4.02455e-01i
0.6	100.20	Pr	1.27787e+03	-0.00000e+00i	-3.12500e-01	-0.00000e+00i	-2.92747e-01	-0.00000e+00i	2.94597e-01	-0.00000e+00i	1.45587e-01	-0.00000e+00i	4.65378e-03	-0.00000e+00i	2.05597e-01	-0.00000e+00i	7.51580e-01	-0.00000e+00i*
0.6	100.215	Pr	1.23359e+03	+3.36568e+02i	-3.12500e-01	-0.00000e+00i	-2.93409e-01	+5.15041e-03i	3.29709e-01	-5.32677e-01i	8.1235e-01	-3.52377e-01i	-6.32052e-03	-3.98069e-03i	-5.26527e-11	-6.53598e-10i	-1.18962e-29	-7.48989e-30i
0.6	100.230	Pr	7.68559e+02	+4.50069e+02i	-3.12500e-01	-0.00000e+00i	-3.00543e-01	+6.94069e-03i	3.96464e-01	+7.97877e-02i	-7.01179e-01	+1.20207e-01i	-2.36528e-03	-2.01105e-03i	6.46389e-10	-9.12937e-11i	3.2126e-28	-5.62632e-28i
0.6	100.245	Ob	4.19238e+02	+9.57571e+03i	-3.12500e-01	+6.93889e-16i	-2.94089e-01	+1.48202e-01i	-9.61869e-01	+9.70036e-01i	-1.39375e+06	-3.26859e-06i	5.39329e+13	-5.62404e+13i	1.26514e+21	+4.71659e+20i	1.26514e+26	+7.22173e+26i
0.6	100.260	Pr	-4.14712e+03	+8.16017e+03i	-3.12500e-01	+1.1022e-16i	-3.70539e-01	+1.36262e-01i	-1.56511e-02	-5.22571e+02i	-1.11998e-08	-6.50197e-06i	-1.72375e+16	-8.15831e+15i	-2.70957e+25	+4.26059e+24i	-1.40886e+30	+2.57725e+31i
0.6	100.275	Ob	-7.70749e+03	+4.74114e+03i	-3.12500e-01	-1.38778e-17i	-4.37712e-01	+8.39239e-02i	1.26071e+03	+7.57808e-02i	-1.33594e-09	+2.59237e-02i	-9.77680e+18	+3.95440e+18i	4.06657e+28	+2.69024e+28i	3.88359e+35	+1.43354e+35i
0.6	100.290	Pr	-8.62546e+03	+1.13899e-12i	-3.12500e-01	+2.18917e-17i	-4.57247e-01	+5.24984e-17i	-1.69154e+03	+1.15569e-12i	-1.88150e+09	-3.01600e-06i	-1.85406e+19	+5.81544e+04i	-8.09075e+28	+3.78214e+14i	-2.88721e+34	+1.62385e+20i
0.6	250.20	Pr	3.22810e+03	-0.00000e+00i	-3.12500e-01	-0.00000e+00i	-2.63416e-01	-0.00000e+00i	2.37061e-01	-0.00000e+00i	1.70438e-10	-0.00000e+00i	3.11597e-31	-0.00000e+00i	1.35195e-85	-0.00000e+00i	3.90256e-82	-1.99994e-82i
0.6	250.215	Pr	3.11737e+03	+8.41201e+02i	-3.12500e-01	-0.00000e+00i	-2.64965e-01	+1.24645e-02i	-2.80291e-01	-1.177419e-01i	8.93820e-02	-1.71747e-01i	3.68687e-12	-5.36343e-10i	-3.53218e-30	-4.32723e-30i	-3.90256e-83	+1.99994e-82i
0.6	250.230	Pr	1.93776e+03	+1.12503e+03i	-3.12500e-01	-0.00000e+00i	-2.82553e-01	+1.70033e-02i	1.65639e-01	-4.09525e-01i	9.06721e-02	+3.314799e-02i	5.67070e-10	+2.06949e-11i	3.05568e-28	-1.36338e-28i	-1.25248e-75	-6.81914e-76i
0.6	250.245	Ob	1.05655e+03	+6.14393e+04i	-3.12500e-01	-1.07553e-15i	-1.79125e-01	+8.44061e-01i	-2.14930e-06	-3.08936e+06i	-1.14203e+18	-2.47599e+17i	-7.67132e+36	+3.49130e+36i	-3.85567e+55	+2.88802e+55i	-2.52871e+72	+2.37895e+72i
0.6	250.260	Pr	-2.90980e+04	+5.28766e+04i	-3.12500e-01	-3.19189e-16i	-4.14152e-01	+1.21119e-01i	-2.39331e-08	-1.55959e+07i	-1.11848e+22	-2.32920e+21i	-1.11848e+45	-3.76453e+44i	-5.20918e+67	-2.72113e+67i	-4.79957e+86	-1.05848e+87i
0.6	250.275	Ob	-5.17248e+04	+3.06029e+04i	-3.12500e-01	-2.35922e-16i	-1.33809e-01	+9.93436e-01i	-2.86247e-09	+5.44472e-08i	6.59539e+24	-3.34939e+24i	-1.84140e+50	-2.52230e+50i	1.25413e+75	-7.89192e+75i	7.86951e+96	+4.41539e+97i
0.6	250.290	Ob	-5.90252e+04	+7.43972e-12i	-3.12500e-01	-2.79215e-17i	-1.78777e-01	+1.09781e-16i	-5.57391e-09	+8.03631e-09i	3.70909e+25	+1.38663e+11i	-7.25176e+51	+5.48707e+51i	-6.53708e+77	+7.44874e+63i	4.03904e+98	-5.99040e+84i
0.6	500.20	Pr	6.47818e+03	-0.00000e+00i	-3.12500e-01	-0.00000e+00i	-2.16877e-01	-0.00000e+00i	-1.12306e-01	-0.00000e+00i	5.59639e-04	-0.00000e+00i	4.15427e-24	-0.00000e+00i	4.47942e-67	-0.00000e+00i*	6.05218e-178	-0.00000e+00i*
0.6	500.215	Pr	6.25670e+03	+1.68234e+03i	-3.12500e-01	+2.71051e-20i	-2.19430e-01	+2.36032e-02i										

Table D.52: (continued)

m, n	$ c \angle \arg(c)$	type	$\lambda_{mn}^{(a)}$	$S_{mn}^{(a)}(c, \eta=0)$	$S_{mn}^{(a)}(c, \eta=0.01)$	$S_{mn}^{(a)}(c, \eta=0.1)$	$S_{mn}^{(a)}(c, \eta=0.25)$	$S_{mn}^{(a)}(c, \eta=0.5)$	$S_{mn}^{(a)}(c, \eta=0.75)$	$S_{mn}^{(a)}(c, \eta=0.99)$
0.6	2500 \angle 60°	Ob	-3.10336e+06 + 5.40016e-06i	-0.00000e+00 - 0.00000e-00i	$\pm \infty$	$\pm \infty$	$\pm \infty$	$\pm \infty$	$\pm \infty$	$\pm \infty$
0.6	2500 \angle 75°	Ob	-5.38852e+06 + 3.11853e+06i	-0.00000e+00 - 0.00000e-00i	$\pm \infty$	$\pm \infty$	$\pm \infty$	$\pm \infty$	$\pm \infty$	$\pm \infty$
0.6	2500 \angle 90°	Ob	-6.21503e+06 + 7.63261e-10i	-0.00000e+00 - 0.00000e-00i	$\pm \infty$	$\pm \infty$	$\pm \infty$	$\pm \infty$	$\pm \infty$	$\pm \infty$
0.6	5000 \angle 0°	Pr	6.49782e+04 - 0.00000e+00i	-3.12500e-01 - 0.00000e+00i	2.59540e-01 - 0.00000e-00i	2.36445e-07 - 0.00000e+00i	6.23078e-63 - 0.00000e+00i	6.52470e-283 - 0.00000e+00i*	± 0	± 0
0.6	5000 \angle 15°	Pr	6.27634e+04 + 1.68232e+04i	-3.12500e-01 - 3.38813e-21i	2.69344e-01 + 6.21847e-02i	4.53357e-07 + 3.26797e-07i	-1.19640e-60 - 7.16576e-61i	-5.23540e-273 - 1.05479e-273i*	± 0	± 0
0.6	5000 \angle 30°	Pr	3.89604e+04 + 2.25000e+04i	-3.12500e-01 - 3.38813e-21i	1.63441e-01 + 1.59922e-01i	-1.65633e-07 - 3.36738e-07i	8.30636e-56 + 1.74080e-56i	-6.88780e-247 + 8.31729e-247i*	± 0	± 0
0.6	5000 \angle 45°	Ob	2.12082e+04 + 2.49788e+07i	-0.00000e+00 - 0.00000e+00i	$\pm \infty$	$\pm \infty$	$\pm \infty$	$\pm \infty$	$\pm \infty$	$\pm \infty$
0.6	5000 \angle 60°	Ob	-1.24567e+07 + 2.16256e+07i	-0.00000e+00 - 0.00000e+00i	$\pm \infty$	$\pm \infty$	$\pm \infty$	$\pm \infty$	$\pm \infty$	$\pm \infty$
0.6	5000 \angle 75°	Ob	-2.16024e+07 + 1.24871e+07i	-0.00000e+00 - 0.00000e+00i	$\pm \infty$	$\pm \infty$	$\pm \infty$	$\pm \infty$	$\pm \infty$	$\pm \infty$
0.6	5000 \angle 90°	Ob	-2.49300e+07 + 3.05733e-09i	-0.00000e+00 - 0.00000e+00i	$\pm \infty$	$\pm \infty$	$\pm \infty$	$\pm \infty$	$\pm \infty$	$\pm \infty$

Table D.52: $S_{0n}^{(a)}(c, \eta)$ for $n = \{0..6\}$.

Table D.53: $S_{1n}^{(a)}(c, \eta)$ for $n = [1..6]$.

m, n	$ c \angle \arg(c)$	type	$\lambda_{mn}^{(a)}$	$S_{mn}^{(a)}(c, \eta=0)$	$S_{mn}^{(a)}(c, \eta=0.01)$	$S_{mn}^{(a)}(c, \eta=0.1)$	$S_{mn}^{(a)}(c, \eta=0.25)$	$S_{mn}^{(a)}(c, \eta=0.5)$	$S_{mn}^{(a)}(c, \eta=0.75)$	$S_{mn}^{(a)}(c, \eta=0.99)$
1.1	25 \angle 0°	Pr	2.52634e+01 - 0.00000e-00i	1.00000e+00 - 0.00000e-00i	9.98788e-01 - 0.00000e-00i	8.85490e-01 - 0.00000e-00i	4.62940e-01 - 0.00000e-00i	3.89730e-02 - 0.00000e-00i	3.05244e-04 - 3.09994e-36i*	3.08826e-09 - 3.81590e-41i*
1.1	25 \angle 15°	Pr	2.44110e+01 + 6.4678e-00i	1.00000e+00 - 4.33681e-19i	9.98830e-01 - 3.22969e-04i	8.88814e-01 - 2.88210e-02i	4.65649e-01 - 9.69846e-02i	2.82950e-02 - 3.32878e-02i	-2.36008e-04 - 3.32102e-04i	4.67252e-09 + 4.49191e-09i*
1.1	25 \angle 30°	Pr	2.19119e+01 + 1.24930e+01i	1.00000e+00 - 8.67362e-19i	9.98955e-01 - 6.24011e-04i	9.98972e-01 - 5.63533e-02i	4.74939e-01 - 1.98953e-01i	-6.26500e-03 - 6.07430e-02i	-4.42149e-04 + 8.47000e-04i	-4.42149e-04 + 5.38431e-08i*
1.1	25 \angle 45°	Pr	1.79365e+01 + 1.76680e+01i	1.00000e+00 + 1.73472e-18i	9.99153e-01 - 8.82672e-04i	9.15016e-01 - 8.12477e-02i	4.94660e-01 - 3.10830e-01i	-7.43330e-02 - 7.27687e-02i	3.48447e-03 + 1.09081e-03i	-1.47669e-06 - 1.01023e-06i*
1.1	25 \angle 60°	Pr	1.27558e+01 + 2.39191e+01i	1.00000e+00 + 3.46945e-18i	9.99412e-01 - 1.08135e-03i	9.37243e-01 - 1.02061e-01i	5.32402e-01 - 4.36837e-01i	-2.02147e-01 - 5.00632e-02i	1.06703e-02 - 1.82130e-02i	1.48724e-04 + 4.43354e-05i*
1.1	25 \angle 75°	Ob	-4.46714e+02 + 2.86606e+02i	1.00000e+00 + 2.77556e-16i	1.02244e-01 - 1.44379e-02i	3.69672e-02 - 2.73319e-01i	-6.34369e-01 - 1.28466e+02i	-3.31031e+04 + 3.24745e+03i	1.13039e+06 + 7.70068e+06i	4.17456e-08 - 5.40169e+07i
1.1	25 \angle 90°	Ob	-5.27043e+02 + 7.04144e-14i	1.00000e+00 + 1.02726e-16i	1.02652e+00 + 1.01899e-16i	5.03933e-02 - 2.39599e-16i	1.59089e+02 - 4.46354e-14i	5.08908e+04 - 3.37745e-11i	1.47320e+07 - 1.54191e-08i	1.77365e+08 - 1.82222e+08i
1.1	50 \angle 0°	Pr	5.02565e+01 - 0.00000e-00i	1.00000e+00 - 0.00000e-00i	9.97540e-01 - 0.00000e-00i	7.81224e-01 - 0.00000e-00i	2.09342e-01 - 0.00000e-00i	1.36971e-03 - 0.00000e-00i	6.46214e-08 + 5.50096e-40i*	1.55813e-18 - 0.00000e-00i*
1.1	50 \angle 15°	Pr	4.85525e+01 + 1.29392e+01i	1.00000e+00 + 2.16840e-19i	9.97625e-01 - 6.45441e-04i	7.86268e-01 - 5.10679e-02i	2.02590e-01 - 8.82620e-02i	-2.78753e-04 - 1.69825e-03i	-3.75015e-08 + 1.08781e-07i	7.13874e-19 + 6.71032e-18i*
1.1	50 \angle 30°	Pr	4.35568e+01 + 2.49967e+01i	1.00000e+00 - 4.33681e-19i	9.97874e-01 - 1.24721e-03i	8.01571e-01 - 1.00964e-01i	1.81585e-01 - 1.84642e-01i	-3.28979e-03 + 6.91574e-04i	-3.56919e-07 - 5.12490e-07i	-4.24401e-16 - 2.56473e-16i*
1.1	50 \angle 45°	Pr	3.56098e+01 + 3.53507e+01i	1.00000e+00 - 8.67362e-19i	9.98269e-01 - 1.76452e-03i	8.27573e-01 - 1.48198e-01i	1.44458e-01 - 3.00377e-01i	2.30002e-04 + 9.74404e-03i	7.60554e-06 + 5.18993e-06i	2.16172e-13 + 4.07110e-13i*
1.1	50 \angle 60°	Pr	2.52303e+01 + 4.32957e+01i	1.00000e+00 + 8.67362e-19i	9.98786e-01 - 1.62212e-03i	8.64764e-01 - 1.90676e-01i	9.01803e-02 + 5.42333e-01i	3.45750e-02 + 1.81231e-02i	-1.52548e-04 - 2.66363e-04i	2.90804e-09 + 1.76138e-09i*
1.1	50 \angle 75°	Ob	-1.97390e+03 + 1.19823e+03i	1.00000e+00 - 0.00000e-00i	1.09977e-02 - 6.19027e-02i	1.40084e-01 - 4.94158e-01i	-5.38436e+04 + 5.11871e+03i	5.76761e-09 - 1.10428e-09i	-5.53458e-14 + 1.61157e-14i	9.95254e-18 - 2.51972e-18i*
1.1	50 \angle 90°	Ob	-2.30202e+03 + 2.93914e-13i	1.00000e+00 - 2.25101e-17i	1.11738e+00 - 4.04192e-17i	6.09079e-01 - 2.00237e-14i	8.27931e+04 - 6.52562e-11i	1.37611e+10 - 2.13814e-05i	2.06795e+15 - 4.79619e+00i	5.54323e+10 - 1.69300e+05i
1.1	100 \angle 0°	Pr	1.00253e+02 - 0.00000e-00i	1.00000e+00 - 0.00000e-00i	9.95050e-01 - 0.00000e-00i	6.08046e-01 - 0.00000e-00i	4.27929e-02 - 0.00000e-00i	1.68901e-06 - 0.00000e-00i	2.87965e-15 - 5.56977e-47i*	3.56475e-37 + 4.70247e-69i*
1.1	100 \angle 15°	Pr	9.68456e+01 + 2.58811e+01i	1.00000e+00 - 1.08420e-19i	9.95218e-01 - 1.28790e-03i	6.13323e-01 - 8.00161e-02i	3.24665e-02 - 3.94227e-02i	-2.52598e-06 + 8.53356e-07i	-7.19663e-15 - 5.61512e-15i	-6.47924e-36 + 1.54208e-36i*
1.1	100 \angle 30°	Pr	8.68553e+01 + 4.99984e+01i	1.00000e+00 - 4.33681e-19i	9.95713e-01 - 2.48927e-03i	6.29968e-01 - 1.61273e-01i	-1.10394e-03 - 6.54750e-02i	9.30263e-06 - 4.10188e-06i	-9.25274e-14 + 2.52318e-13i	1.77926e-32 + 3.08106e-32i*
1.1	100 \angle 45°	Pr	7.09629e+01 + 7.07084e+01i	1.00000e+00 - 0.00000e-00i	9.96502e-01 - 3.52316e-03i	6.60435e-01 - 2.44399e-01i	-6.77384e-02 - 8.47169e-02i	-8.53834e-05 + 4.12733e-06i	2.14771e-11 + 5.42673e-11i	-1.55942e-26 + 2.59472e-26i*
1.1	100 \angle 60°	Pr	5.02515e+01 + 8.65998e+01i	1.00000e+00 - 0.00000e-00i	9.97531e-01 - 4.31943e-03i	7.08787e-01 - 3.28577e-01i	-1.93519e-01 - 7.99300e-02i	7.81371e-04 + 1.12626e-03i	-3.25399e-08 + 5.60238e-08i	8.31001e-19 + 1.38785e-18i*
1.1	100 \angle 75°	Ob	-8.27589e+03 + 4.89647e+03i	1.00000e+00 - 2.22045e-16i	1.43236e+00 - 2.79859e-01i	-5.47569e-03 - 3.88099e-03i	9.33208e-09 - 1.57737e-09i	1.68400e-20 - 6.63805e-19i	2.63607e-30 - 1.66632e-30i	5.29566e-39 - 2.83621e-39i*
1.1	100 \angle 90°	Ob	-9.60201e+03 + 1.20015e-12i	1.00000e+00 - 4.19768e-17i	1.51984e+00 - 1.33884e-16i	9.04779e-03 - 5.92050e-12i	2.22643e-10 - 3.50198e-05i	9.94402e-20 - 3.08643e+06i	4.01391e+31 - 1.86032e+17i	1.75242e+41 - 1.06973e+27i*
1.1	250 \angle 0°	Pr	2.50251e+02 - 0.00000e-00i	1.00000e+00 - 0.00000e-00i	9.87614e-01 - 0.00000e-00i	8.26683e-01 - 0.00000e-00i	3.65426e-04 - 0.00000e-00i	3.16299e-15 - 0.00000e-00i	2.34854e-37 - 0.00000e-00i	3.28224e-93 + 8.28941e-125i*
1.1	250 \angle 15°	Pr	2.21733e+02 + 6.47044e+01i	1.00000e+00 - 0.00000e-00i	9.88030e-01 - 3.19659e-03i	2.83590e-01 - 9.53451e-02i	-2.22791e-04 - 4.23961e-04i	-7.20473e-15 - 6.79358e-15i	-4.52268e-36 - 3.84136e-37i	3.30654e-90 + 4.99750e-90i*
1.1	250 \angle 30°	Pr	2.16757e+02 + 1.24999e+02i	1.00000e+00 + 1.08420e-19i	9.89230e-01 - 6.18302e-03i	2.74678e-01 - 1.98831e-01i	-7.16202e-04 + 7.79444e-04i	-1.42618e-13 + 2.42278e-13i	-1.80613e-33 + 1.96696e-32i	8.40011e-81 + 5.48064e-81i*
1.1	250 \angle 45°	Pr	1.77028e+02 + 1.76776e+02i	1.00000e+00 + 1.08420e-19i	9.91198e-01 - 8.76144e-03i	2.61711e-01 - 3.20544e-01i	2.93010e-03 + 2.32032e-03i	6.98380e-12 + 5.71961e-11i	-1.46357e-26 - 2.34966e-27i	4.23364e-66 - 7.14354e-66i*
1.1	250 \angle 60°	Pr	1.25251e+02 + 2.16505e+02i	1.00000e+00 - 0.00000e-00i	9.93748e-01 - 1.07583e-02i	2.50352e-01 - 4.74435e-01i	1.60838e-02 - 1.07928e-02i	-4.41300e-08 + 3.96397e-08i	-2.83174e-19 + 4.86476e-19i	-1.16092e-43 + 4.86182e-43i*
1.1	250 \angle 75°	Ob	-5.31627e+02 + 3.09912e+04i	1.00000e+00 + 3.33067e-16i	4.41116e+00 - 3.27798e-01i	1.24047e-02 - 2.35206e-09i	-4.56890e-25 + 2.31187e-25i	3.11441e-51 - 4.23588e-51i	-8.04354e-80 + 4.81082e-77i	4.01450e-101 + 1.11915e-102i
1.1	250 \angle 90°	Ob	-6.15020e+04 + 7.59281e-12i	1.00000e+00 + 9.25674e-17i	6.01256e+00 - 3.45023e-16i	2.95941e+10 - 4.25345e-05i	4.30715e-26 - 1.60808e+12i	3.72001e-53 - 2.81254e+39i	2.90300e-80 - 3.30583e+66i	5.46643e-105 - 8.23329e+91i
1.1	500 \angle 0°	Pr	5.00251e+02 - 0.00000e-00i	1.00000e+00 - 0.00000e-00i	9.75346e-01 - 0.00000e-00i	8.18786e-02 - 0.00000e-00i	1.30360e-07 - 0.00000e-00i	8.99568e-30 - 0.00000e-00i	4.58735e-74 - 1.71106e-105i*	2.31076e-186 - 0.00000e-00i*
1.1	500 \angle 15°	Pr	4.83214e+02 + 1.29409e+02i	1.00000e+00 - 0.00000e-00i	9.76157e-01 - 6.31644e-03i	7.10650e-02 - 5.38752e-02i	-1.27009e-07 + 1.84418e-07i	5.18180e-30 + 8.80192e-29i	1.44421e-71 + 2.50195e-72i	-1.92028e-180 + 4.86575e-180i*
1.1	500 \angle 30°	Pr	4.33263e+02 + 2.50000e+02i	1.00000e+00 - 0.00000e-00i	9.78542e-01 - 1.22327e-02i	3.57789e-02 - 1.08820e-01i	-9.23709e-08 - 1.08991e-06i	-3.44986e-26 - 6.21299e-26i	-3.29090e-64 - 6.07969e-63i	1.04739e-161 - 2.07171e-161i*
1.1	500 \angle 45°	Pr	3.5804e+02 + 3.53553e+02i	1.00000e+00 - 5.42101e-20i	9.83261e-01 - 1.73681e-02i	-3.41284e-02 - 1.67150e-01i	3.12507e-06 + 1.32749e-05i	-2.89725e-21 + 7.18880e-22i	1.42869e-52 + 4.28279e-52i	1.04735e-132 - 8.30553e-132i*
1.1	500 \angle 60°	Pr	2.50250e+02 + 4.33012e+02i	1.00000e+00 - 0.00000e-00i	9.87582e-01 - 2.13813e-02i	-1.61804e-02 - 2.36658e-01i	1.37998e-04 - 3.38381e-04i	3.37656e-16 - 3.14542e-16i	-1.29894e-37 - 2.28243e-37i	1.44629e-93 - 3.91871e-93i*
1.1	500 \angle 75°	Ob	-2.14577e+05 + 1.24482e+05i	1.00000e+00 + 2.44249e-15i	1.67592e+01 - 5.90076e+01i	3.61012e+20 - 1.19499e-02i	5.02035e-51 - 6.82460e+51i	-4.28435e-103 - 1.37388e-104i	-2.08799e-156 - 7.19875e-155i	-6.11146e-205 - 5.06451e-205i*
1.1	500 \angle 90°	Ob	-2.48002e+05 + 3.0493							

Table D.53: (continued)

m, n	$c \setminus \arg(c)$	type	$\lambda_{mn}^{(a)}$	$S_{mn}^{(a)}(c, \eta=0)$	$S_{mn}^{(a)}(c, \eta=0.01)$	$S_{mn}^{(a)}(c, \eta=0.1)$	$S_{mn}^{(a)}(c, \eta=0.25)$	$S_{mn}^{(a)}(c, \eta=0.5)$	$S_{mn}^{(a)}(c, \eta=0.75)$	$S_{mn}^{(a)}(c, \eta=0.99)$
1,1	1500 \angle 20	Pr	1.50025e+03 - 0.00000e-00i	1.00000e-00 - 0.00000e+00i	9.27777e-01 - 0.00000e-00i	5.44807e-04 - 0.00000e-00i	2.11102e-21 - 0.00000e-00i	5.88349e-88 - 0.00000e-00i	5.97565e-221 - 0.00000e-00i	± 0
1,1	1500 \angle 15	Pr	1.44914e+03 + 3.88229e-02i	1.00000e-00 - 0.00000e+00i	9.29975e-01 - 1.80549e-02i	-2.57964e-04 - 6.54923e-04i	1.03963e-20 + 2.52762e-21i	-9.72638e-86 - 5.45403e-88i	1.71670e-213 + 9.54459e-214i	± 0
1,1	1500 \angle 30	Pr	1.29929e+03 + 7.50000e-02i	1.00000e-00 - 1.35525e-20i	9.36487e-01 - 3.51356e-02i	-1.21606e-03 + 8.64175e-04i	3.12967e-19 + 1.20716e-18i	2.89699e-76 + 1.45065e-77i	-1.74735e-191 - 1.08135e-191i	± 0
1,1	1500 \angle 45	Pr	1.06091e+03 + 1.06066e-03i	1.00000e-00 - 2.71051e-20i	9.47050e-01 - 5.02733e-02i	2.79966e-03 + 4.05528e-03i	-1.54531e-15 - 1.85848e-15i	-1.60214e-62 + 1.43328e-62i	1.31946e-156 - 1.87347e-156i	± 0
1,1	1500 \angle 60	Pr	7.50250e+02 + 1.29904e-03i	1.00000e-00 - 0.00000e+00i	9.61198e-01 - 2.62512e-02i	2.27782e-02 - 5.29311e-03i	-4.26651e-11 + 1.85009e-11i	-8.05542e-45 + 2.42824e-44i	1.05302e-110 + 1.86037e-112i	-1.46567e-279 + 8.38968e-280i*
1,1	1500 \angle 75	Ob	-1.94276e+06 + 1.12345e-06i	-0.00000e-00 - 0.00000e+00i	$\pm \infty$	$\pm \infty$	$\pm \infty$	$\pm \infty$	$\pm \infty$	$\pm \infty$
1,1	1500 \angle 90	Ob	-2.24400e+06 + 2.75178e-10i	-0.00000e-00 - 0.00000e+00i	$\pm \infty$	$\pm \infty$	$\pm \infty$	$\pm \infty$	$\pm \infty$	$\pm \infty$
1,1	2500 \angle 20	Pr	2.50025e+03 - 0.00000e-00i	1.00000e-00 - 0.00000e+00i	8.82527e-01 - 0.00000e-00i	3.62506e-06 - 0.00000e-00i	3.41850e-35 - 0.00000e-00i	4.12808e-146 + 2.12833e-177i*	± 0	± 0
1,1	2500 \angle 15	Pr	2.41506e+03 + 6.47048e-02i	1.00000e-00 - 0.00000e+00i	8.85830e-01 - 2.86694e-02i	-5.52719e-06 + 5.64475e-07i	-6.42940e-35 - 5.07150e-34i	1.11601e-141 + 3.68430e-141i	± 0	± 0
1,1	2500 \angle 30	Pr	2.16531e+03 + 1.25000e-03i	1.00000e-00 - 0.00000e+00i	8.95679e-01 - 5.60544e-02i	1.94259e-05 + 3.39638e-07i	-5.83368e-31 - 1.29658e-30i	-7.18564e-127 + 1.03554e-126i	-6.74592e-319 - 8.71314e-319i*	± 0
1,1	2500 \angle 45	Pr	1.76802e+03 + 1.76777e-03i	1.00000e-00 - 0.00000e+00i	9.11864e-01 - 8.08107e-02i	-1.20317e-04 - 7.60602e-05i	3.92052e-25 + 1.72598e-25i	-5.70819e-104 + 1.54111e-103i	-7.24286e-262 - 2.86782e-260i*	± 0
1,1	2500 \angle 60	Pr	1.25025e+03 + 2.16506e-03i	1.00000e-00 + 1.35525e-20i	9.33947e-01 - 1.01502e-01i	-2.71960e-04 + 1.88806e-03i	5.52739e-18 + 2.11379e-18i	1.05649e-73 - 1.78290e-73i	-1.92323e-184 + 3.10586e-184i	± 0
1,1	2500 \angle 75	Ob	-5.40300e+06 + 3.12241e-06i	-0.00000e-00 - 0.00000e+00i	$\pm \infty$	$\pm \infty$	$\pm \infty$	$\pm \infty$	$\pm \infty$	$\pm \infty$
1,1	2500 \angle 90	Ob	-6.24000e+06 + 7.64792e-10i	-0.00000e-00 - 0.00000e+00i	$\pm \infty$	$\pm \infty$	$\pm \infty$	$\pm \infty$	$\pm \infty$	$\pm \infty$
1,1	5000 \angle 20	Pr	5.00025e+03 - 0.00000e-00i	1.00000e-00 - 0.00000e+00i	7.78825e-01 - 0.00000e-00i	1.30916e-11 - 0.00000e-00i	1.14075e-69 - 0.00000e-00i	1.75672e-291 - 1.48220e-323i*	± 0	± 0
1,1	5000 \angle 15	Pr	4.82988e+03 + 1.29410e-03i	1.00000e-00 - 0.00000e+00i	7.83844e-01 - 5.07906e-02i	3.01175e-11 - 6.21647e-12i	-2.47034e-67 + 6.36591e-68i	-1.19551e-281 + 7.97400e-282i	± 0	± 0
1,1	5000 \angle 30	Pr	4.33038e+03 + 2.50000e-03i	1.00000e-00 - 0.00000e+00i	7.99069e-01 - 1.00410e-01i	7.35832e-10 + 1.31458e-11i	-1.30883e-60 + 1.47670e-60i	-5.74852e-253 + 1.52633e-252i	± 0	± 0
1,1	5000 \angle 45	Pr	3.53578e+03 + 3.53553e-03i	1.00000e-00 - 0.00000e+00i	8.24934e-01 - 1.47371e-01i	8.65835e-09 + 1.82338e-08i	1.20961e-49 + 1.32107e-49i	-2.05753e-206 + 1.77232e-206i	± 0	± 0
1,1	5000 \angle 60	Pr	2.50025e+03 + 4.33013e-03i	1.00000e+00 + 6.77626e-21i	8.61923e-01 - 1.89588e-01i	-3.47769e-06 - 1.02309e-06i	2.54621e-35 + 2.28102e-35i	-2.31993e-146 + 4.08736e-146i	± 0	± 0
1,1	5000 \angle 75	Ob	-2.16313e+07 + 1.24948e-07i	-0.00000e-00 - 0.00000e+00i	$\pm \infty$	$\pm \infty$	$\pm \infty$	$\pm \infty$	$\pm \infty$	$\pm \infty$
1,1	5000 \angle 90	Ob	-2.49800e+07 + 3.06039e-09i	-0.00000e-00 - 0.00000e+00i	$\pm \infty$	$\pm \infty$	$\pm \infty$	$\pm \infty$	$\pm \infty$	$\pm \infty$
1,2	25 \angle 20	Pr	7.42764e-01 - 0.00000e-00i	-0.00000e-00 - 0.00000e+00i	2.99644e-02 - 0.00000e-00i	2.66321e-01 - 0.00000e-00i	3.52859e-01 - 0.00000e-00i	6.26976e-02 - 0.00000e-00i	7.74206e-04 - 6.91810e-36i*	1.53291e-08 - 0.00000e-00i*
1,2	25 \angle 15	Pr	7.17195e-01 + 1.94035e-01i	-0.00000e-00 - 0.00000e+00i	2.99657e-02 - 9.69090e-02i	2.67320e-01 - 8.69666e-03i	3.54920e-01 - 7.39348e-02i	4.55110e-02 - 5.35577e-02i	-5.99000e-04 - 8.41977e-04i	2.32650e-08 + 2.22792e-08i*
1,2	25 \angle 30	Pr	6.42230e-01 + 3.74853e-01i	-0.00000e-00 - 0.00000e+00i	2.99694e-02 - 1.87240e-05i	2.70301e-01 - 1.69517e-02i	3.61989e-01 - 1.51668e-01i	-1.01076e-02 - 9.77118e-02i	-1.15774e-03 + 2.21125e-03i	-9.27957e-08 + 2.78792e-07i*
1,2	25 \angle 45	Pr	5.22985e-01 + 5.30134e-01i	-0.00000e-00 - 0.00000e+00i	2.99753e-02 - 2.64856e-05i	2.75197e-01 - 2.44404e-02i	3.77000e-01 - 2.36950e-01i	-1.19620e-01 - 1.16997e-01i	9.15922e-03 + 2.83980e-03i	-7.73106e-06 - 5.08549e-06i*
1,2	25 \angle 60	Ob	-2.27933e+02 + 4.91244e-02i	-0.00000e-00 - 0.00000e+00i	3.01150e-02 - 2.46193e-04i	3.59117e-01 - 2.99729e-01i	-7.43606e-02 - 4.87315e-02i	1.02150e-01 + 6.89341e-02i	-1.26826e-05 - 8.82758e-05i	1.26826e-05 + 3.12291e-06i
1,2	25 \angle 75	Ob	-4.46714e+02 + 2.86606e-02i	-0.00000e-00 - 0.00000e+00i	3.02252e-02 - 1.43951e-04i	5.53580e-01 - 2.17611e-01i	3.91573e-01 - 6.2865e-01i	-4.25568e-03 - 8.07416e-02i	-1.40973e-05 + 1.00373e-06i	5.41463e-07 + 8.54966e-06i
1,2	25 \angle 90	Ob	-5.27043e+02 + 7.04144e-14i	-0.00000e-00 - 0.00000e+00i	3.02657e-02 + 2.13730e-18i	6.45338e-01 - 1.15500e-17i	2.07907e-01 - 5.08756e-15i	6.65083e-03 - 4.17529e-21i	1.92530e-06 - 1.94602e-09i	1.92530e-06 - 1.94602e-09i
1,2	50 \angle 20	Pr	1.49262e-02 - 0.00000e-00i	-0.00000e-00 - 0.00000e+00i	2.99270e-02 - 0.00000e-00i	2.34959e-01 - 0.00000e-00i	1.59552e-01 - 0.00000e-00i	2.20283e-03 - 0.00000e-00i	1.69548e-07 - 2.62848e-39i*	7.94953e-18 - 1.39986e-49i*
1,2	50 \angle 15	Pr	1.44151e-02 + 3.88195e-01i	-0.00000e-00 - 0.00000e+00i	2.99295e-02 - 1.93646e-05i	2.36476e-01 - 1.53598e-02i	1.54404e-01 - 6.72726e-02i	-4.48533e-04 - 2.73114e-03i	-9.82402e-08 + 2.85444e-07i	3.74827e-18 + 3.42160e-17i*
1,2	50 \angle 30	Pr	1.29164e-02 + 7.49936e-01i	-0.00000e-00 - 0.00000e+00i	2.99370e-02 - 3.74190e-05i	2.41078e-01 - 3.03670e-02i	1.38390e-01 - 1.40731e-01i	-5.28909e-03 + 1.11306e-03i	-9.37507e-07 - 1.34336e-06i	-2.17112e-15 - 1.29373e-15i*
1,2	50 \angle 45	Pr	1.05324e-02 + 1.06057e-02i	-0.00000e-00 - 0.00000e+00i	2.99488e-02 - 5.29395e-05i	2.48898e-01 - 4.45737e-02i	1.10085e-01 - 2.28936e-01i	3.73634e-04 + 1.56694e-04i	1.99633e-05 + 1.35807e-05i	1.19399e-12 + 2.06089e-12i*
1,2	50 \angle 60	Ob	-1.07881e+03 + 2.06505e-03i	-0.00000e-00 - 0.00000e+00i	3.05331e-02 - 1.04371e-03i	-7.28142e-01 - 1.79562e-02i	8.09251e+02 + 5.25251e-02i	2.64802e-07 + 1.71566e-07i	6.79215e-11 + 5.05325e-11i	2.74733e-15 + 3.62370e-15i
1,2	50 \angle 75	Ob	-1.97390e+03 + 1.19823e-03i	-0.00000e-00 - 0.00000e+00i	3.09946e-02 - 6.11044e-04i	1.67342e-02 - 2.73599e-02i	-3.32331e+03 - 5.97927e-02i	3.65338e-08 + 3.06218e-07i	-3.59860e-13 + 3.79724e-11i	6.40754e-17 + 1.63179e-16i
1,2	50 \angle 90	Ob	-2.30202e+03 + 2.93914e-13i	-0.00000e-00 - 0.00000e+00i	3.11659e-02 - 1.11306e-18i	3.80790e-01 - 1.04099e-15i	5.17684e-03 - 3.79319e-12i	8.00433e-08 - 1.28921e-06i	1.29304e-14 - 2.92722e-10i	3.46604e-18 - 1.03973e-04i
1,2	100 \angle 20	Pr	2.99256e-02 - 0.00000e-00i	-0.00000e-00 - 0.00000e+00i	2.98522e-02 - 0.00000e-00i	1.82873e-01 - 0.00000e-00i	3.26137e-02 - 0.00000e-00i	7.15789e-06 - 0.00000e-00i	5.74474e-15 + 1.59915e-46i	1.80701e-30 - 0.00000e-00i*
1,2	100 \angle 15	Pr	2.89033e-02 + 7.76441e-01i	-0.00000e-00 - 0.00000e+00i	2.98573e-02 - 3.86384e-05i	1.84460e-01 - 2.40656e-02i	2.47434e-02 - 2.66159e-02i	-4.06164e-06 + 1.37235e-06i	-1.88661e-14 - 1.47121e-14i	-3.28230e-35 + 7.87445e-36i*
1,2	100 \angle 30	Pr	2.59063e-02 + 1.49997e-02i	-0.00000e-00 - 0.00000e+00i	2.98721e-02 - 7.46809e-05i	1.89466e-01 - 4.85044e-02i	-8.42321e-04 - 4.99002e-02i	1.49575e-06 - 6.59688e-06i	-2.42146e-13 + 6.61378e-13i	9.06655e-32 + 1.55733e-31i*
1,2	100 \angle 45	Pr	2.11386e-02 + 2.12128e-02i	-0.00000e-00 - 0.00000e+00i	2.98958e-02 - 1.05699e-04i	1.98629e-01 - 7.35050e-02i	-5.16267e-02 - 6.45632e-02i	1.37287e-04 + 6.65332e-06i	5.63806e-11 + 1.42155e-10i	-7.82335e-26 + 1.31680e-25i*
1,2	100 \angle 60	Ob	-4.65660e+03 + 8.46025e-03i	-0.00000e-00 - 0.00000e+00i	3.21993e-02 - 4.42688e-03i	-1.76048e-01 + 7.01799e-02i	1.91707e-07 + 1.34616e-07i	2.94599e-16 + 2.30950e-16i	3.95074e-25 + 3.54097e-25i	2.51618e-33 + 8.95134e-33i
1,2	100 \angle 75	Ob	-8.62589e+03 + 4.89647e-03i	-0.00000e-00 - 0.00000e+00i	3.42507e-02 - 2.65633e-03i	-1.34274e-02 - 1.43896e-03i	2.89697e-08 + 2.30209e-07i	5.0525e-18 - 5.98844e-17i	9.12221e-28 - 2.78087e-28i	1.79175e-38 + 4.09245e-37i
1,2	100 \angle 90	Ob	-9.60201e+03 + 1.20015e-12i	-0.00000e-00 - 0.00000e+00i	3.50386e-02 - 2.37599e-18i	2.77002e-02 - 1.65888e-13i	6.81631e-08 - 1.03432e-06i	3.04441e-19 - 9.28032e-04i	1.22888e-30 - 5.62726e-15i	5.36512e-39 - 3.24526e-25i
1,2	250 \angle 20	Pr	7.49252e-02 - 0.00000e-00i	-0.00000e-00 - 0.00000e+00i	2.96292e-02 - 0.00000e-00i	8.62211e-02 - 0.00000e-00i	2.78496e-04 - 0.00000e-00i	5.08549e-15 - 0.00000e-00i	6.36257e-37 - 0.00000e-00i	1.70742e-92 - 0.00000e-00i*
1,2	250 \angle 15	Pr	7.23697e-02 + 1.94114e-02i	-0.00000e-00 - 0.00000e+00i	2.96416e-02 - 9.59002e-05i	8.52910e-02 - 2.86755e-05i	-1.69793e-04 - 3.23105e-04i	-1.15840e-14 - 1.09225e-14i	-1.22572e-35 - 1.03908e-36i	1.77572e-89 + 2.60813e-89i*
1,2	250 \angle 30	Pr	6.48771e-02 + 3.74999e-02i	-0.00000e-00 - 0.00000e+00i	2.96783e-02 - 1.85496e-04i	8.26106e-02 - 5.97995e-05i	-5.45821e-04 + 5.94027e-04i	-2.29286e-13 +		

Table D.53: (continued)

m, n	$c \setminus \arg(c)$	type	$\lambda_{mn}^{(a)}$	$S_{mn}^{(a)}(c, \eta=0)$	$S_{mn}^{(a)}(c, \eta=0.01)$	$S_{mn}^{(a)}(c, \eta=0.1)$	$S_{mn}^{(a)}(c, \eta=0.25)$	$S_{mn}^{(a)}(c, \eta=0.5)$	$S_{mn}^{(a)}(c, \eta=0.75)$	$S_{mn}^{(a)}(c, \eta=0.99)$
1,2	1500 $\angle 20^\circ$	Pr	4.49925e+03 - 0.00000e-00i	-0.00000e-00 - 0.00000e-00i	2.78340e-02 - 0.00000e-00i	1.63853e-04 - 0.00000e-00i	1.60881e-21 - 0.00000e-00i	9.45899e-88 - 0.00000e-00i	1.58482e-220 - 0.00000e-00i	± 0
1,2	1500 $\angle 15^\circ$	Pr	4.34592e+03 + 1.16469e-03i	-0.00000e-00 - 0.00000e-00i	2.79000e-02 - 5.41660e-04i	-7.75838e-04 - 1.96971e-04i	7.92306e-21 + 1.92630e-21i	-1.56375e-85 - 8.76851e-85i	4.65362e-213 + 2.58574e-213i	± 0
1,2	1500 $\angle 30^\circ$	Pr	3.89636e+03 + 2.25000e-03i	-0.00000e-00 - 0.00000e-00i	2.80953e-02 - 1.05409e-03i	-3.65734e-04 + 2.59904e-04i	2.38514e-19 + 9.19976e-19i	4.65752e-76 + 2.33197e-77i	-4.73352e-191 - 2.92310e-191i	± 0
1,2	1500 $\angle 45^\circ$	Pr	3.18123e+03 + 3.18198e-03i	-0.00000e-00 - 0.00000e-00i	2.84122e-02 - 1.50824e-03i	8.42008e-04 + 1.21964e-03i	-1.17768e-15 - 1.41635e-15i	-2.57576e-62 + 2.30432e-62i	3.57330e-156 - 5.07834e-156i	± 0
1,2	1500 $\angle 60^\circ$	Ob	-1.11981e+06 + 1.94556e-06i	-0.00000e-00 - 0.00000e-00i	$\pm \infty$	$\pm \infty$	$\pm \infty$	$\pm \infty$	$\pm \infty$	$\pm \infty$
1,2	1500 $\angle 75^\circ$	Ob	-1.94276e+06 + 1.12345e-06i	-0.00000e-00 - 0.00000e-00i	$\pm \infty$	$\pm \infty$	$\pm \infty$	$\pm \infty$	$\pm \infty$	$\pm \infty$
1,2	1500 $\angle 90^\circ$	Ob	-2.24400e+06 + 2.75178e-10i	-0.00000e-00 - 0.00000e-00i	$\pm \infty$	$\pm \infty$	$\pm \infty$	$\pm \infty$	$\pm \infty$	$\pm \infty$
1,2	2500 $\angle 20^\circ$	Pr	7.49925e+03 - 0.00000e-00i	-0.00000e-00 - 0.00000e-00i	2.64765e-02 - 0.00000e-00i	1.09025e-06 - 0.00000e-00i	2.60524e-35 - 0.00000e-00i	6.59355e-146 - 1.50635e-177i	± 0	± 0
1,2	2500 $\angle 15^\circ$	Pr	7.24369e+03 + 1.94114e-03i	-0.00000e-00 - 0.00000e-00i	2.65756e-02 - 8.60105e-04i	-1.66232e-06 + 1.69768e-07i	-4.89987e-35 - 3.86500e-34i	1.79488e-141 + 5.92395e-141i	± 0	± 0
1,2	2500 $\angle 30^\circ$	Pr	6.94444e+03 + 3.75000e-03i	-0.00000e-00 - 0.00000e-00i	2.68711e-02 - 1.68167e-03i	5.84242e-06 + 1.02147e-07i	-4.44586e-31 - 9.88126e-31i	-1.15533e-126 + 1.66385e-126i	-1.82702e-318 - 2.36018e-318i	± 0
1,2	2500 $\angle 45^\circ$	Pr	5.30255e+03 + 5.30330e-03i	-0.00000e-00 - 0.00000e-00i	2.73566e-02 - 2.42438e-03i	-3.61858e-05 - 2.28754e-05i	2.98738e-25 + 1.31537e-25i	-9.17501e-104 + 2.47778e-103i	-1.99528e-261 - 7.77015e-260i	± 0
1,2	2500 $\angle 60^\circ$	Ob	-3.11634e+06 + 5.40766e-06i	-0.00000e-00 - 0.00000e-00i	$\pm \infty$	$\pm \infty$	$\pm \infty$	$\pm \infty$	$\pm \infty$	$\pm \infty$
1,2	2500 $\angle 75^\circ$	Ob	-5.40300e+06 + 3.12241e-06i	-0.00000e-00 - 0.00000e-00i	$\pm \infty$	$\pm \infty$	$\pm \infty$	$\pm \infty$	$\pm \infty$	$\pm \infty$
1,2	2500 $\angle 90^\circ$	Ob	-6.24000e+06 + 7.64792e-10i	-0.00000e-00 - 0.00000e-00i	$\pm \infty$	$\pm \infty$	$\pm \infty$	$\pm \infty$	$\pm \infty$	$\pm \infty$
1,2	5000 $\angle 20^\circ$	Pr	1.49993e+04 - 0.00000e-00i	-0.00000e-00 - 0.00000e-00i	2.33653e-02 - 0.00000e-00i	3.93736e-12 - 0.00000e-00i	8.69369e-70 - 0.00000e-00i	2.95095e-291 - 0.00000e-00i	± 0	± 0
1,2	5000 $\angle 15^\circ$	Pr	1.44881e+04 + 3.88229e-03i	-0.00000e-00 - 0.00000e-00i	2.35159e-02 - 1.52376e-03i	9.05796e-12 - 1.86963e-12i	-1.88265e-67 + 4.85146e-68i	-1.92216e-281 + 1.28247e-281i	± 0	± 0
1,2	5000 $\angle 30^\circ$	Pr	1.29896e+04 + 7.50000e-03i	-0.00000e-00 - 0.00000e-00i	2.39727e-02 - 3.01237e-03i	1.13033e-10 + 3.95364e-12i	-9.97461e-61 + 1.12540e-60i	-9.18585e-253 - 2.44444e-252i	± 0	± 0
1,2	5000 $\angle 45^\circ$	Pr	1.06059e+04 + 1.06066e-04i	-0.00000e-00 - 0.00000e-00i	2.47486e-02 - 4.42125e-03i	2.64043e-09 + 5.48390e-09i	9.21843e-50 + 1.00679e-49i	-3.30912e-206 - 2.84888e-206i	± 0	± 0
1,2	5000 $\angle 60^\circ$	Ob	-1.24827e+07 + 2.16406e-07i	-0.00000e-00 - 0.00000e-00i	$\pm \infty$	$\pm \infty$	$\pm \infty$	$\pm \infty$	$\pm \infty$	$\pm \infty$
1,2	5000 $\angle 75^\circ$	Ob	-2.16313e+07 + 1.24948e-07i	-0.00000e-00 - 0.00000e-00i	$\pm \infty$	$\pm \infty$	$\pm \infty$	$\pm \infty$	$\pm \infty$	$\pm \infty$
1,2	5000 $\angle 90^\circ$	Ob	-2.49800e+07 + 3.06039e-09i	-0.00000e-00 - 0.00000e-00i	$\pm \infty$	$\pm \infty$	$\pm \infty$	$\pm \infty$	$\pm \infty$	$\pm \infty$
1,3	25 $\angle 20^\circ$	Pr	1.22245e-02 - 0.00000e-00i	-1.50000e-00 - 0.00000e-00i	-1.49092e-02 - 0.00000e-00i	-6.80885e-01 - 0.00000e-00i	1.47941e+00 - 0.00000e-00i	7.57038e-01 - 0.00000e-00i	1.65761e-02 + 2.79784e-34i	6.54483e-07 - 7.05259e-39i
1,3	25 $\angle 15^\circ$	Pr	1.17985e-02 + 3.23516e-01i	-1.50000e-00 - 6.93889e-18i	-1.49123e-02 + 2.42137e-03i	-7.00649e-01 + 1.96322e-01i	1.53278e+00 + 2.89456e-01i	7.14482e-01 - 0.64397e-01i	-7.44355e-03 - 2.08808e-02i	7.05249e-07 + 1.18602e-06i
1,3	25 $\angle 30^\circ$	Pr	1.05495e-02 + 6.24998e-01i	-1.50000e-00 - 6.93889e-18i	-1.49217e-02 + 4.67889e-03i	-7.60586e-01 + 3.87790e-01i	1.69133e+00 + 6.42757e-01i	5.50747e-01 - 1.07216e-01i	-4.46596e-02 + 2.65878e-02i	-9.27179e-06 + 8.00595e-06i
1,3	25 $\angle 45^\circ$	Ob	6.68262e-01 + 5.54258e-02i	-1.50000e-00 - 2.22045e-16i	-1.49473e-02 + 4.15235e-02i	7.47072e-01 + 3.37713e-01i	1.08517e+01 - 3.68027e-01i	1.65504e+03 + 1.07317e-02i	-6.97896e-04 + 5.94462e-04i	-2.47514e+05 - 1.02063e+06i
1,3	25 $\angle 60^\circ$	Ob	2.27933e-02 + 9.14244e-02i	-1.50000e+00 + 9.71445e-17i	-1.51705e-02 + 3.69849e-02i	-1.71135e-02 + 4.98661e-02i	1.03453e+02 + 1.22618e-02i	-1.43346e+04 - 3.63094e-02i	1.79657e+06 + 7.15363e-04i	-5.25557e-07 - 9.55511e-06i
1,3	25 $\angle 75^\circ$	Ob	-3.56423e-02 + 2.60632e-02i	-1.50000e-00 - 2.77556e-16i	-1.52684e-02 + 1.96646e-02i	-4.49203e-02 + 3.30743e-02i	6.67785e+00 + 1.11870e-02i	1.53504e+04 - 1.85966e-01i	-2.79605e-05 - 1.37699e-06i	9.90898e-06 + 2.28359e-06i
1,3	25 $\angle 90^\circ$	Ob	-4.33359e-02 + 6.42691e-14i	-1.50000e-00 - 1.80091e-16i	-1.53270e-02 - 1.79161e-16i	-6.13251e-02 + 1.81276e-16i	-1.38364e-02 + 3.67617e-14i	-2.5631e+04 + 1.53584e-11i	-2.63341e+06 + 2.74512e-09i	2.32882e-07 + 3.05850e-08i
1,3	50 $\angle 20^\circ$	Pr	2.24725e-02 - 0.00000e-00i	-1.50000e-00 - 0.00000e-00i	-1.48157e-02 - 0.00000e-00i	-1.17996e-02 - 0.00000e-00i	1.68230e+00 - 0.00000e-00i	5.61128e-02 - 0.00000e-00i	7.20200e-06 + 1.22264e-37i	6.63294e-16 + 6.45421e-48i
1,3	50 $\angle 15^\circ$	Pr	3.28727e-02 + 6.47056e-01i	-1.50000e-00 - 0.00000e-00i	-1.48220e-02 + 4.83240e-03i	-3.23371e-02 + 3.10197e-01i	1.78235e+00 - 1.72584e-01i	7.92549e-03 - 7.01877e-02i	-7.25072e-06 + 1.05911e-05i	-4.42444e-16 + 2.83910e-15i
1,3	50 $\angle 30^\circ$	Pr	2.13752e-02 + 1.25002e-02i	-1.50000e-00 - 3.46945e-18i	-1.48406e-02 + 9.33970e-03i	-9.78894e-02 + 6.26151e-01i	2.11747e+00 - 3.65439e-01i	-1.30656e-01 - 4.65064e-02i	-5.27990e-06 - 7.21826e-05i	-1.06366e-13 - 1.91279e-13i
1,3	50 $\angle 45^\circ$	Ob	1.39407e-02 + 2.35856e-03i	-1.50000e+00 + 1.55431e-15i	-1.48616e-02 + 1.76463e-01i	1.95297e+01 - 8.12872e-02i	2.66853e+02 + 1.75950e-03i	-5.37165e+06 - 1.25674e-07i	-9.48817e+09 + 5.19635e-10i	3.79239e+13 - 1.83997e+13i
1,3	50 $\angle 60^\circ$	Ob	-1.07881e+03 + 2.06505e-03i	-1.50000e-00 - 1.02696e-15i	-1.57903e-02 + 1.57668e-01i	3.75047e+02 + 2.79444e-01i	-2.32728e-04 - 7.22015e-02i	-7.23994e-08 - 4.55043e-07i	-2.03395e+13 - 1.93689e+12i	-1.02026e+17 - 4.04429e+16i
1,3	50 $\angle 75^\circ$	Ob	-1.78686e+03 + 1.14643e-03i	-1.50000e-00 - 5.55112e-17i	-1.63527e-02 + 8.85667e-02i	-1.69828e-01 + 6.03074e-01i	4.77129e-04 + 4.74620e-03i	-2.78159e+09 + 5.60949e-08i	1.08743e+16 - 3.44128e+13i	8.27873e-16 + 2.19916e+16i
1,3	50 $\angle 90^\circ$	Ob	-2.10817e+03 + 2.81658e-13i	-1.50000e+00 + 7.70664e-17i	-1.66099e-02 + 1.07213e-16i	-7.42815e-02 + 2.65942e-14i	-7.33486e+04 - 0.000058e-11i	-6.63964e+09 + 1.05236e-05i	-4.07739e+14 + 9.59682e-01i	4.349200e-17 + 1.28762e+03i
1,3	100 $\angle 20^\circ$	Pr	4.97247e-02 - 0.00000e-00i	-1.50000e-00 - 0.00000e-00i	-1.46295e-02 - 0.00000e-00i	9.07498e-01 - 0.00000e-00i	1.41956e-04 - 0.00000e-00i	1.61956e-04 - 0.00000e-00i	6.73029e-13 - 0.00000e-00i	3.13224e-34 + 2.14177e-66i
1,3	100 $\angle 15^\circ$	Pr	4.80210e-02 + 1.29410e-02i	-1.50000e-00 - 8.67362e-19i	-1.46420e-02 + 9.62275e-03i	9.14807e-01 + 3.67420e-01i	7.28759e-01 - 4.32982e-01i	-2.23914e-04 + 1.28891e-05i	-1.28046e-12 - 1.70748e-12i	-5.84934e-33 - 1.56444e-34i
1,3	100 $\angle 30^\circ$	Pr	4.30260e-02 + 2.50001e-02i	-1.50000e-00 - 0.00000e-00i	-1.46789e-02 + 1.86064e-02i	9.28877e-01 + 7.74167e-01i	6.17110e-01 - 1.00084e-00i	8.51185e-04 + 1.03344e-04i	-4.85203e-11 + 4.00440e-11i	9.10443e-32 + 3.12464e-29i
1,3	100 $\angle 45^\circ$	Ob	2.80836e-02 + 9.71715e-03i	-1.50000e-00 - 2.45637e-15i	-1.42024e-02 + 7.23508e-01i	-5.11509e-02 + 5.14741e-02i	-8.60449e-06 - 2.03305e-07i	4.53892e+14 - 4.67580e+14i	1.61998e+22 + 6.30095e+21i	-4.21889e+28 + 5.23162e+28i
1,3	100 $\angle 60^\circ$	Ob	-4.65560e-03 + 8.46025e-03i	-1.50000e-00 - 1.16573e-15i	-1.81619e-02 + 6.83642e-01i	-1.01005e-03 - 3.40856e-03i	-1.17028e-09 - 7.65523e-07i	-1.82350e-18 - 2.40272e-17i	-2.5637e+27 - 5.09930e+26i	-3.30233e-35 - 3.15702e-35i
1,3	100 $\angle 75^\circ$	Ob	-7.89559e-03 + 4.79292e-03i	-1.50000e+00 + 4.44089e-16i	-2.11676e-02 + 4.08453e-01i	6.70390e-03 + 4.13181e-03i	-8.33450e-09 + 1.60171e-09i	-8.26654e+19 + 3.30249e+19i	-5.39824e+29 + 3.48875e+29i	4.63610e+36 + 1.10753e+37i
1,3	100 $\angle 90^\circ$	Ob	-9.20808e-03 + 1.17566e-12i	-1.50000e-00 + 1.06487e-16i	-2.24536e-02 + 2.61750e-16i	-1.10704e-02 + 5.76735e-12i	-1.98863e-10 + 3.18659e-09i	-4.88714e-20 + 1.53159e-06i	-8.26376e+30 + 3.85607e+16i	1.35131e+37 - 3.39523e+20i
1,3	250 $\angle 20^\circ$	Pr	1.24725e-03 - 0.00000e-00i	-1.50000e-00 - 0.00000e-00i	-1.40757e-02 - 0.00000e-00i	1.72444e+00 - 0.00000e-00i	1.70860e-02 - 0.00000e-00i	6.74610e-13 - 0.00000e-00i	1.42869e-34 - 0.00000e-00i	7.39656e-90 - 0.00000e-00i
1,3	250 $\angle 15^\circ$	Pr	1.20466e-03 + 3.23524e-02i	-1.50000e-00 - 0.00000e-00i	-1.41062e-02 + 2.37441e-02i	1.81901e+00 + 4.23333e-03i	4.73861e-02 - 2.19145e-02i	-1.10504e-12 - 1.80073e-12i	-2.51094e-33 - 9.10039e-34i	4.35813e-87 + 1.24867e-86i
1,3	250 $\angle 30^\circ$	Pr	1.07978e-03 + 6.25001e-02i	-1.50000e+00 + 8.67362e-19i	-1.41961e-02 + 4.59731e-02i	2.12421e+00 + 4.00202e-02i	-4.77054e-02 + 1.40578e-02i	-5.23945e-11 - 2.93220e-11i	-6.96308e-30 + 9.80201e-30i	2.25015e-77 - 8.88875e-77i
1,3	250 $\angle 45^\circ$	Ob	7.05104e-02 + 6.17929e-04i	-1.50000e-00						

Table D.53: (continued)

m, n	$c \setminus \arg(c)$	type	$S_{mn}^{(a)}$	$S_{mn}^{(a)}(c, \eta=0)$	$S_{mn}^{(a)}(c, \eta=0.01)$	$S_{mn}^{(a)}(c, \eta=0.1)$	$S_{mn}^{(a)}(c, \eta=0.25)$	$S_{mn}^{(a)}(c, \eta=0.5)$	$S_{mn}^{(a)}(c, \eta=0.75)$	$S_{mn}^{(a)}(c, \eta=0.99)$				
1,3	1500.20°	Pr	7.49725e+03	-0.00000e+00	-9.74355e-01	-0.00000e+00	2.38102e-02	-0.00000e+00	6.09568e-19	-0.00000e+00	2.14088e-217	-0.00000e+00	±0	
1,3	1500.25°	Pr	7.24169e+03	+1.94114e+03i	-9.88820e-01	+1.27556e-01i	-3.21032e-03	-3.06330e-02i	2.70914e-18	+1.48625e-18i	5.17927e-210	+5.01266e-210i	±0	
1,3	1500.30°	Pr	6.94244e+03	+3.75000e+03i	-1.50000e-00	-0.00000e+00	-1.03206e-00	+2.49738e-01i	-6.53198e-02	+5.03260e-03i	-9.70837e-17	+3.47049e-16i	±0	
1,3	1500.45°	Ob	4.24064e+03	+2.24576e+06i	-0.00000e-00	-0.00000e+00	±∞	±∞	±∞	±∞	±∞	±∞	±∞	
1,3	1500.60°	Ob	-1.11981e+06	+1.94555e+06i	-0.00000e-00	-0.00000e+00	±∞	±∞	±∞	±∞	±∞	±∞	±∞	
1,3	1500.75°	Ob	-1.93697e+06	+1.12189e+06i	-0.00000e-00	-0.00000e+00	±∞	±∞	±∞	±∞	±∞	±∞	±∞	
1,3	1500.90°	Ob	-2.23801e+06	+2.74811e-10i	-0.00000e-00	-0.00000e+00	±∞	±∞	±∞	±∞	±∞	±∞	±∞	
1,3	2500.20°	Pr	1.24972e+04	-0.00000e+00	-1.50000e-00	-0.00000e+00	-6.62061e-01	-0.00000e+00	2.67728e-04	-0.00000e+00	1.64893e-32	-0.00000e+00	8.86264e-143	-7.99671e-175i*
1,3	2500.25°	Pr	1.20713e+04	+3.23524e+03i	-1.50000e-00	-0.00000e+00	-6.81613e-01	+1.94201e-01i	-4.05206e-04	-6.75911e-05i	3.35774e-32	-2.44316e-31i	2.66677e-139	+8.28161e-138i*
1,3	2500.30°	Pr	1.08226e+04	+6.25000e+03i	-1.50000e-00	-1.08420e-19i	-7.40909e-01	+3.35850e-01i	1.22572e-03	+7.53791e-04i	7.02084e-29	-6.82510e-28i	-2.45377e-123	+1.15448e-123i*
1,3	2500.45°	Ob	7.06907e+03	+6.24293e+06i	-0.00000e-00	-0.00000e+00	±∞	±∞	±∞	±∞	±∞	±∞	±∞	
1,3	2500.60°	Ob	-3.11634e+06	+5.40766e+06i	-0.00000e-00	-0.00000e+00	±∞	±∞	±∞	±∞	±∞	±∞	±∞	
1,3	2500.75°	Ob	-5.39335e+06	+3.11982e+06i	-0.00000e-00	-0.00000e+00	±∞	±∞	±∞	±∞	±∞	±∞	±∞	
1,3	2500.90°	Ob	-6.23001e+06	+7.64180e-10i	-0.00000e-00	-0.00000e+00	±∞	±∞	±∞	±∞	±∞	±∞	±∞	
1,3	5000.20°	Pr	2.49972e+04	-0.00000e+00	-1.50000e-00	-0.00000e+00	-1.16833e-04	-0.00000e+00	1.95369e-09	-0.00000e+00	1.10237e-66	-0.00000e+00	7.70939e-288	-0.00000e+00i*
1,3	5000.25°	Pr	2.41454e+04	+6.47048e+03i	-1.50000e-00	-0.00000e+00	-2.04635e-02	+3.06930e-01i	4.58235e-09	+2.79368e-10i	-2.46522e-64	-2.47349e-66i	-5.86278e-278	+1.98579e-278i*
1,3	5000.30°	Pr	2.16479e+04	+1.25000e+04i	-1.50000e+00	+5.42101e-20i	-8.53993e-02	+6.19527e-01i	4.75046e-08	+3.00255e-08i	-1.80977e-57	+6.02035e-58i	1.13595e-249	-6.88448e-249i*
1,3	5000.45°	Ob	1.41401e+04	+2.49859e+07i	-0.00000e-00	-0.00000e+00	±∞	±∞	±∞	±∞	±∞	±∞	±∞	
1,3	5000.60°	Ob	-1.24827e+07	+2.16406e+07i	-0.00000e-00	-0.00000e+00	±∞	±∞	±∞	±∞	±∞	±∞	±∞	
1,3	5000.75°	Ob	-2.16120e+07	+1.24896e+07i	-0.00000e-00	-0.00000e+00	±∞	±∞	±∞	±∞	±∞	±∞	±∞	
1,3	5000.90°	Ob	-2.49600e+07	+3.05917e-09i	-0.00000e-00	-0.00000e+00	±∞	±∞	±∞	±∞	±∞	±∞	±∞	
1,4	25.20°	Pr	1.69132e+02	-0.00000e+00	-0.00000e-00	-0.00000e+00	-7.47925e-02	-0.00000e+00	-5.60004e-01	-0.00000e+00	1.83578e-02	-0.00000e+00	1.09943e+00	-1.65594e-33i*
1,4	25.25°	Pr	1.63172e+02	+4.53217e+01i	-0.00000e-00	-0.00000e+00	-7.47999e-02	+5.65526e-05i	-5.64975e-01	+4.73676e-02i	3.75144e-02	+2.50272e-01i	5.51721e-01	-3.12604e-01i
1,4	25.30°	Pr	1.56998e+02	+8.75570e+01i	-0.00000e-00	-0.00000e+00	-7.48217e-02	+1.09275e-02i	-5.79965e-01	+9.32475e-02i	9.28075e-02	+5.34055e-01i	5.11948e-01	-7.71811e-01i
1,4	25.45°	Ob	6.86826e+01	+5.54258e+02i	-0.00000e-00	-0.00000e+00	-7.49160e-02	+6.92377e-04i	-4.88553e-01	+6.32487e-01i	7.35814e+00	+3.44086e+00i	6.17193e+01	+4.12714e+02i
1,4	25.60°	Pr	3.67919e+01	+6.42926e+01i	-0.00000e-00	-0.00000e+00	-7.49578e-02	+8.11183e-05i	-7.04706e-01	+7.67532e-02i	-1.01434e+00	-8.32492e-02i	8.12793e-01	+2.00823e-01i
1,4	25.75°	Ob	-3.56423e+02	+2.60632e+02i	-0.00000e-00	-0.00000e+00	-7.54497e-02	+3.26967e-04i	-1.23301e+00	+5.46258e-01i	-6.76141e+00	+2.58014e+01i	3.60981e+03	+7.14259e+02i
1,4	25.90°	Ob	-4.33359e+02	+6.42691e-14i	-0.00000e-00	-0.00000e+00	-7.55466e-02	-6.29800e-18i	-1.42800e+00	+8.95576e-19i	-3.32394e+01	+7.55040e-15i	-5.66097e+03	+3.47136e-12i
1,4	50.20°	Pr	3.44189e+02	-0.00000e+00	-0.00000e-00	-0.00000e+00	-7.45743e-02	-0.00000e+00	-3.95596e-01	-0.00000e+00	5.61604e-01	-6.15873e-33i*	1.54167e-01	+3.77699e-33i*
1,4	50.25°	Pr	3.32265e+02	+9.06021e+01i	-0.00000e-00	-0.00000e+00	-7.45891e-02	+1.12839e-04i	-4.01565e-01	+7.75781e-02i	4.88892e-01	+4.27924e-02i	1.54167e-01	+3.77699e-33i*
1,4	50.30°	Pr	2.97306e+02	+1.75030e+02i	-0.00000e-00	-0.00000e+00	-7.46325e-02	+2.18074e-04i	-4.20218e-01	+1.55526e-01i	6.58458e-01	+8.76043e-02i	-1.06676e-01	-4.36668e-02i
1,4	50.45°	Ob	1.39407e+02	+2.35856e+03i	-0.00000e-00	-0.00000e+00	-7.47949e-02	+2.94404e-03i	-1.98445e+00	+8.83107e-01i	5.65821e+01	+3.23889e+02i	5.61681e-05	-1.28880e-06i
1,4	50.60°	Pr	7.42551e+01	+1.29893e+02i	-0.00000e-00	-0.00000e+00	-7.49108e-02	+1.62178e-04i	-6.50205e-01	+1.43374e-01i	-1.17164e+01	+8.65475e-01i	-1.39013e+00	-7.28129e-02i
1,4	50.75°	Ob	-1.78669e+03	+1.14643e+03i	-0.00000e-00	-0.00000e+00	-7.72491e-02	+1.45885e-03i	-3.60999e+00	+5.76340e-02i	5.11342e+03	+9.02688e+02i	-3.06784e-08	-2.65230e+11i
1,4	50.90°	Ob	-2.10817e+03	+2.81658e-13i	-0.00000e-00	-0.00000e+00	-7.76670e-02	+2.86453e-18i	-8.08757e+00	+2.20155e-15i	-7.98764e+03	+5.84823e-12i	-7.23055e+08	+1.08389e+06i
1,4	100.20°	Pr	6.94219e+02	-0.00000e+00	-0.00000e-00	-0.00000e+00	-7.41393e-02	-0.00000e+00	-1.54711e-01	-0.00000e+00	2.64875e-01	-0.00000e+00	9.96480e-13	-2.62729e-44i*
1,4	100.25°	Pr	6.70369e+02	+1.81181e+02i	-0.00000e-00	-0.00000e+00	-7.41686e-02	+2.24794e-04i	-1.56147e-01	+1.01710e-01i	2.65986e-01	-1.37524e-01i	-1.92307e-04	+8.91084e-06i
1,4	100.30°	Pr	6.00441e+02	+3.50015e+02i	-0.00000e-00	-0.00000e+00	-7.42548e-02	+4.34610e-04i	-1.62176e-01	+2.10616e-01i	2.62748e-01	-3.37901e-01i	7.31960e-04	+1.04814e-04i
1,4	100.45°	Ob	2.80836e+02	+9.71715e+03i	-0.00000e-00	-0.00000e+00	-7.40644e-02	+1.20993e-02i	-3.67978e-01	+4.15706e-01i	4.35425e-05	-1.03139e-06i	3.30464e-13	-1.33915e+00i
1,4	100.60°	Pr	1.49253e+02	+2.59803e+02i	-0.00000e-00	-0.00000e+00	-7.48167e-02	+3.23970e-04i	-5.32926e-01	+2.47056e-01i	3.68715e-01	+1.52277e-01i	-3.14150e-03	-4.52666e-03i
1,4	100.75°	Ob	-7.89559e+03	+4.79292e+03i	-0.00000e-00	-0.00000e+00	-8.51189e-02	+6.47633e-03i	-2.77964e+02	+3.00979e+02i	-4.40025e-08	-3.65741e-07i	-4.64059e+18	+4.95908e-17i
1,4	100.90°	Ob	-9.20808e+03	+1.17566e-12i	-0.00000e-00	-0.00000e+00	-8.70561e-02	+5.92081e-18i	-5.76832e+02	+3.54095e-13i	-1.03619e+09	+1.57201e-06i	-2.54649e+19	+7.76323e+04i
1,4	250.20°	Pr	1.74424e+03	-0.00000e+00	-0.00000e-00	-0.00000e+00	-7.28454e-02	-0.00000e+00	-1.43702e-01	-0.00000e+00	6.75503e-03	-0.00000e+00	5.92924e-13	-0.00000e+00
1,4	250.25°	Pr	1.68461e+03	+4.52936e+02i	-0.00000e-00	-0.00000e+00	-7.29162e-02	+5.55591e-04i	-1.61062e-01	+4.87421e-02i	-1.71422e-03	-8.27628e-03i	-9.65079e-13	-1.58771e-12i
1,4	250.30°	Pr	1.50978e+03	+8.75006e+02i	-0.00000e-00	-0.00000e+00	-7.31270e-02	+1.07542e-03i	-2.16549e-01	+1.06857e-02i	-1.92593e-02	+4.93015e-03i	-4.63238e-11	+2.54537e-11i
1,4	250.45°	Ob	7.05104e+02	+6.17929e+04i	-0.00000e-00	-0.00000e+00	-5.06792e-02	+7.32209e-02i	-2.25330e-05	-5.45175e-05i	-1.22063e-17	-7.97369e-16i	-1.31896e-36	-5.06113e-35i
1,4	250.60°	Pr	3.74251e+02	+6.49517e+02i	-0.00000e-00	-0.00000e+00	-7.45330e-02	+8.06893e-04i	-1.88236e-01	+3.56721e-01i	-3.05950e-02	+2.05636e-02i	-1.77366e-07	-1.59338e-07i
1,4	250.75°	Ob	-5.22028e+04	+3.07324e+04i	-0.00000e-00	-0.00000e+00	-1.51144e-01	+6.20225e-02i	-3.13458e-08	-2.46607e-07i	9.14321e+23	-1.88370e+23i	-4.15036e+49	+3.30530e+49i
1,4	250.90°	Ob	-6.05800e+04	+7.53158e-12i	-0.00000e-00	-0.00000e+00	-1.77116e-01	-2.76591e-18i	-7.37383e-08	+1.00280e-06i	-7.85606e+24	+2.87241e+01i	-3.75530e+51	+2.81031e+71i
1,4	500.20°	Pr	3.39424e+03	-0.00000e+00	-0.00000e-00	-0.00000e+00	-7.07203e-02	-0.00000e+00	1.54165e-01	-0.00000e+00	5.08110e-06	-0.00000e+00	3.41689e-27	-0.00000e+00
1,4	500.25°	Pr	3.37498e+03	+9.05868e+02i	-0.00000e-00	-0.00000e+00	-7.08582e-02	+1.09020e-03i	-1.54149e-01	-4.39047e-02i	-6.72931e+06	+5.58335e-06i	-6.86492e-27	+3.27950e-26i
1,4	500.30°	Pr	3.02533e+03	+1.75000e+03i	-0.00000e-00	-0.00000e+00	-7.12645e-02	+2.11434e-03i	-1.87975e-01	-1.09815e-01i	1.92412e-05	-3.83903e-05i	6.27003e-25	-2.70334e-23i
1,4	500.45°	Ob	1.41221e+03	+2.48586e+05i	-0.00000e-00	-0.00000e+00	2.33482e-01	+9.69735e-02i	1.39918e-13	+1.06674e-11i	-1.06033e-36	-4.04204e-35i	-1.71317e+74	+1.02471e+73i

Table D.53: (continued)

m, n	$c \setminus \arg(c)$	type	$\lambda_{mn}^{(a)}$	$S_{mn}^{(a)}(c, \eta=0)$	$S_{mn}^{(a)}(c, \eta=0.01)$	$S_{mn}^{(a)}(c, \eta=0.1)$	$S_{mn}^{(a)}(c, \eta=0.25)$	$S_{mn}^{(a)}(c, \eta=0.5)$	$S_{mn}^{(a)}(c, \eta=0.75)$	$S_{mn}^{(a)}(c, \eta=0.99)$
1,4	1500 \angle 20	Pr	1.04942e+04 - 0.00000e-00i	-0.00000e-00 - 0.00000e+00i	-6.26319e-02 - 0.00000e+00i	3.70388e-03 - 0.00000e+00i	2.55318e-19 - 0.00000e+00i	6.76222e-85 - 0.00000e+00i	3.24135e-217 - 3.76206e-249*	± 0
1,4	1500 \angle 15	Pr	1.01365e+04 + 2.71760e+03i	-0.00000e-00 - 0.00000e+00i	-6.29830e-02 + 3.02881e-03i	-4.06442e-04 + 4.78839e-03i	1.13340e-18 + 6.25948e-19i	5.49731e-83 - 6.34467e-82i	7.78903e-210 + 7.54136e-210*	± 0
1,4	1500 \angle 30	Pr	9.08751e+03 + 5.25000e+03i	-0.00000e-00 - 0.00000e+00i	-6.40293e-02 + 5.91932e-03i	-1.03014e-02 + 4.05527e-04i	-4.15143e-17 + 1.45355e-16i	2.79794e-73 + 1.81626e-73i	-5.36559e-188 - 9.95176e-188*	± 0
1,4	1500 \angle 45	Ob	4.24064e+03 + 2.24576e+03i	-0.00000e-00 - 0.00000e+00i	± 0	± 0	± 0	± 0	± 0	± 0
1,4	1500 \angle 60	Pr	2.24925e+03 + 3.89711e+03i	-0.00000e-00 - 0.00000e+00i	-7.20917e-02 + 4.68921e-03i	-1.71266e-02 + 3.97982e-03i	8.12877e-11 - 3.52491e-11i	3.23758e-44 - 9.75976e-44i	-7.13111e-110 - 1.22581e-111*	± 0
1,4	1500 \angle 75	Ob	-1.93697e+06 + 1.12189e+06i	-0.00000e-00 - 0.00000e+00i	± 0	± 0	± 0	± 0	± 0	± 0
1,4	1500 \angle 90	Ob	-2.23801e+06 + 2.74811e-10i	-0.00000e-00 - 0.00000e+00i	± 0	± 0	± 0	± 0	± 0	± 0
1,4	2500 \angle 20	Pr	1.74942e+04 - 0.00000e+00i	-0.00000e-00 - 0.00000e+00i	-5.51643e-02 - 0.00000e+00i	4.29072e-05 - 0.00000e+00i	6.93657e-33 - 0.00000e+00i	7.87479e-143 - 8.49114e-175*	± 0	± 0
1,4	2500 \angle 15	Pr	1.68980e+04 + 4.52933e+03i	-0.00000e-00 - 0.00000e+00i	-5.56553e-02 + 4.67035e-03i	-6.48895e-05 - 1.15779e-04i	1.43006e-32 - 1.02776e-31i	2.48942e-139 + 7.08082e-138*	± 0	± 0
1,4	2500 \angle 30	Pr	1.51497e+04 + 8.75000e+03i	-0.00000e-00 - 0.00000e+00i	-5.71361e-02 + 9.19610e-03i	1.95014e-04 + 1.25776e-04i	3.04900e-29 - 2.87268e-28i	-2.18941e-123 + 1.02687e-123*	-1.35989e-315 - 1.00419e-314*	± 0
1,4	2500 \angle 45	Ob	7.06907e+03 + 6.24293e+06i	-0.00000e-00 - 0.00000e+00i	± 0	± 0	± 0	± 0	± 0	± 0
1,4	2500 \angle 60	Pr	3.74925e+03 + 6.49519e+03i	-0.00000e-00 - 0.00000e+00i	-7.00478e-02 + 7.61285e-03i	2.04482e-04 - 1.14960e-03i	-1.05311e-17 - 4.02729e-18i	-4.24384e-73 + 7.15863e-73i	1.30095e-183 - 2.10194e-183*	± 0
1,4	2500 \angle 75	Ob	-5.39335e+06 + 3.11982e+06i	-0.00000e-00 - 0.00000e+00i	± 0	± 0	± 0	± 0	± 0	± 0
1,4	2500 \angle 90	Ob	-6.23001e+06 + 7.64180e-10i	-0.00000e-00 - 0.00000e+00i	± 0	± 0	± 0	± 0	± 0	± 0
1,4	5000 \angle 20	Pr	3.49942e+04 - 0.00000e+00i	-0.00000e-00 - 0.00000e+00i	-3.89461e-02 - 0.00000e+00i	3.19838e-10 - 0.00000e+00i	4.65235e-67 - 0.00000e+00i	6.89540e-288 - 5.89371e-320*	± 0	± 0
1,4	5000 \angle 15	Pr	3.38017e+04 + 9.05867e+03i	-0.00000e-00 - 0.00000e+00i	-3.95362e-02 + 7.65534e-03i	7.50472e-10 + 4.98101e-11i	-1.04051e-64 - 1.13067e-66i	-5.23430e-278 + 1.77174e-278*	± 0	± 0
1,4	5000 \angle 30	Pr	3.30515e+04 + 1.75000e+04i	-0.00000e-00 - 0.00000e+00i	-4.13798e-02 + 1.53466e-02i	7.74799e-09 + 5.01020e-09i	-7.64522e-58 + 2.52960e-58i	1.02542e-249 - 6.13980e-249*	± 0	± 0
1,4	5000 \angle 45	Ob	1.41401e+04 + 2.49859e+07i	-0.00000e-00 - 0.00000e+00i	± 0	± 0	± 0	± 0	± 0	± 0
1,4	5000 \angle 60	Pr	7.49925e+03 + 1.29904e+04i	-0.00000e-00 - 0.00000e+00i	-6.46458e-02 + 1.42195e-02i	2.61482e-06 + 7.69245e-07i	-4.85117e-35 - 4.34591e-35i	9.26884e-146 + 1.64605e-145*	± 0	± 0
1,4	5000 \angle 75	Ob	-2.16120e+07 + 1.24896e+07i	-0.00000e-00 - 0.00000e+00i	± 0	± 0	± 0	± 0	± 0	± 0
1,4	5000 \angle 90	Ob	-2.49600e+07 + 3.05917e-09i	-0.00000e-00 - 0.00000e+00i	± 0	± 0	± 0	± 0	± 0	± 0
1,5	25 \angle 20	Pr	2.14897e+02 - 0.00000e+00i	1.87500e-00 - 0.00000e+00i	1.85498e-00 - 0.00000e+00i	2.00828e-00 - 0.00000e+00i	-1.79577e+00 - 0.00000e+00i	2.83940e-00 - 5.18626e-32i*	4.41184e-01 - 1.67346e-32i*	7.31555e-05 - 3.12719e-36i*
1,5	25 \angle 15	Pr	2.07243e+02 + 5.83274e+01i	1.87500e-00 - 0.00000e+00i	1.85570e-00 - 5.44921e-01i	2.28376e-01 - 3.76321e-01i	-2.01657e+00 + 3.78944e-01i	2.95586e-00 - 3.31641e-01i	-3.68393e-03 - 3.01949e-01i*	1.78328e-05 + 7.72048e-05i*
1,5	25 \angle 30	Pr	1.84802e+02 + 1.12682e+02i	1.87500e-00 - 2.77556e-17i	1.85778e-00 - 1.05312e-02i	3.15617e-01 - 7.56737e-01i	-2.73186e+00 + 6.90355e-01i	4.63236e-00 - 1.04739e-01i	-7.19092e-01 - 8.26494e-02i	-7.92000e-04 + 8.26494e-02i*
1,5	25 \angle 45	Pr	8.56282e+01 + 8.83908e+01i	1.87500e-00 - 1.38778e-17i	1.86707e-00 - 8.27439e-01i	1.07786e-00 - 7.10250e-01i	-2.42946e+00 - 1.42859e-01i	-1.66975e-01 + 2.60877e-01i	-1.08603e-01 - 2.27307e-01i*	9.41638e-05 + 4.77494e-04i*
1,5	25 \angle 60	Ob	-1.47588e+02 + 4.41071e+02i	1.87500e+00 + 2.22045e-16i	1.88880e-00 - 4.14539e-02i	1.70772e-00 - 5.00317e-01i	-7.55147e+00 - 5.50317e-01i	5.61608e-03 - 9.50852e-01i	-2.77427e+05 + 1.69870e+04i	1.28334e+05 - 8.59499e+05i
1,5	25 \angle 75	Pr	6.72295e+00 + 2.41357e+01i	1.87500e-00 + 3.46945e-18i	1.87446e+00 - 2.26213e-03i	1.80867e-00 - 2.19890e-01i	1.12668e+00 - 1.08465e-01i	-8.72603e-01 + 8.02356e-02i	-8.75373e-02 - 2.68576e-01i	-1.62055e-02 - 3.19566e-02i*
1,5	25 \angle 90	Ob	-3.44291e+02 + 5.80751e-14i	1.87500e+00 + 2.28886e-16i	1.90748e+00 + 2.27373e-16i	6.16407e-00 - 1.65988e-16i	9.71350e+00 + 2.61302e-14i	8.38672e+03 - 5.55716e-12i	3.06237e+05 - 3.80690e-01i	7.29000e+05 - 8.87953e-01i
1,5	50 \angle 20	Pr	4.40077e+02 - 0.00000e+00i	1.87500e-00 - 0.00000e+00i	1.83399e-00 - 0.00000e+00i	-9.41240e-00 - 0.00000e+00i	5.77158e-01 - 0.00000e+00i	9.45647e-01 - 1.13499e-32i*	7.07283e-04 - 0.00000e+00i*	2.59038e-14 + 2.20150e-45i*
1,5	50 \angle 15	Pr	4.24750e+02 + 1.16514e+02i	1.87500e-00 - 0.00000e+00i	1.83540e-00 - 1.08448e-02i	-9.46099e-01 - 4.67605e-01i	5.89971e-01 + 1.27296e-01i	2.88667e-01 - 6.02047e-01i	-3.05861e-04 + 2.46810e-04i*	-1.45058e-13 + 3.17703e-13i*
1,5	50 \angle 30	Pr	3.79813e+02 + 2.25088e+02i	1.87500e-00 - 0.00000e+00i	1.83956e-00 - 2.09667e-02i	-9.47222e-01 - 9.86073e-01i	5.47575e-01 + 3.01174e-01i	-7.31805e-01 - 1.14339e-01i	1.05379e-03 - 1.89273e-03i*	9.86595e-12 - 2.58346e-11i*
1,5	50 \angle 45	Pr	1.74022e+02 + 1.76780e+02i	1.87500e-00 - 6.93889e-18i	1.85878e-00 - 1.65223e-02i	2.74892e-01 - 1.18739e-01i	-3.50932e+00 + 1.67191e-01i	3.62894e-01 - 3.54070e-01i	-2.26738e-04 - 1.31962e-03i*	7.28331e-11 - 2.43563e-10i*
1,5	50 \angle 60	Ob	-9.11733e+02 + 1.96498e+03i	1.87500e+00 + 1.11022e-15i	1.95818e+00 - 1.87018e-01i	-3.82549e+00 - 2.82975e-01i	1.72297e+04 + 3.91545e+02i	2.93067e+08 + 1.29283e+07i	3.39887e+12 + 1.73584e+11i	-2.19290e+14 - 8.54797e+14i
1,5	50 \angle 75	Pr	1.31924e+01 + 4.82902e+01i	1.87500e-00 - 0.00000e+00i	1.87385e-00 - 4.52455e-03i	1.71243e+00 - 4.22797e-01i	4.76049e-02 + 1.27261e-01i	3.61951e-01 - 6.82330e-02i	-2.73973e-02 + 2.04064e-02i*	-1.59352e-04 + 1.13221e-04i*
1,5	50 \angle 90	Ob	-1.91859e+03 + 2.69383e-13i	1.87500e-00 - 1.17471e-16i	2.05786e+00 - 1.54999e-16i	7.51266e-01 - 2.77998e-14i	5.34618e+04 - 4.44451e-11i	2.58488e-09 - 4.13828e-06i	6.12659e+13 - 1.45660e-01i	3.17172e-15 - 8.70997e+00i
1,5	100 \angle 20	Pr	8.90164e+02 - 0.00000e+00i	1.87500e-00 - 0.00000e+00i	1.79227e-00 - 0.00000e+00i	-1.89617e-00 - 0.00000e+00i	2.67479e+00 - 2.71565e-32i*	8.45801e-03 - 1.21751e-34i*	2.03507e-10 - 5.00426e-42i*	3.63426e-31 + 4.13140e-63i*
1,5	100 \angle 15	Pr	8.59501e+02 + 2.32960e+02i	1.87500e-00 - 0.00000e+00i	1.79506e-00 - 2.15222e-02i	-2.01769e+00 - 1.78450e-01i	2.74511e+00 - 2.40670e-01i	-4.67026e-03 - 1.12355e-03i	-4.96141e-11 - 1.28731e-10i*	-1.38802e-30 - 4.18282e-31i*
1,5	100 \angle 30	Pr	7.69599e+02 + 4.50043e+02i	1.87500e-00 + 3.46945e-18i	1.80325e-00 - 4.16418e-02i	-2.37874e+00 - 4.78609e-01i	4.20658e+00 - 7.21331e-02i	-4.04965e-09 + 5.70539e-10i*	-3.91097e-27 + 6.69962e-27i*	3.21896e-23 - 8.16613e-24i*
1,5	100 \angle 45	Pr	3.50801e+02 + 3.53555e+02i	1.87500e-00 - 0.00000e+00i	1.84220e-00 - 3.29389e-02i	-1.15441e+00 - 1.57391e-01i	-4.29716e-01 + 2.43478e-01i	6.59135e-03 + 6.19882e-03i	6.92369e-09 - 1.56456e-08i*	3.21896e-23 - 8.16613e-24i*
1,5	100 \angle 60	Ob	-4.31525e+03 + 8.26021e+03i	1.87500e+00 + 1.88738e-15i	2.23881e+00 - 8.29831e-01i	1.03577e+03 + 3.47539e-03i	8.72259e+08 + 5.36548e+07i	7.49546e+17 + 9.20507e+16i	4.42907e+26 + 7.89199e+25i	1.27645e+33 - 8.00028e+32i
1,5	100 \angle 75	Pr	2.61327e+01 + 9.65895e+01i	1.87500e-00 - 0.00000e+00i	1.87262e+00 - 9.04409e-03i	1.46308e+00 - 7.69450e-03i	-8.42052e-01 - 6.28290e-02i	6.05605e-02 - 2.37730e-02i	1.20463e-04 - 4.10130e-04i*	9.12722e-10 - 2.88309e-09i*
1,5	100 \angle 90	Ob	-8.81828e+03 + 1.15115e-12i	1.87500e-00 - 1.42687e-16i	2.76442e+00 - 3.34873e-16i	1.12627e+00 - 7.76017e-12i	1.47159e+00 - 2.36689e-05i	1.97250e-20 - 6.19580e-05i	1.36366e-30 - 6.37725e-15i	-4.16515e+36 - 2.55080e-09i*
1,5	250 \angle 20	Pr	2.24022e+03 - 0.00000e+00i	1.87500e-00 - 0.00000e+00i	1.66904e+00 - 0.00000e+00i	-3.67421e-01 - 0.00000e+00i	1.91643e-01 - 0.00000e+00i	3.60292e-11 - 0.00000e+00i	2.7654e-32 - 0.00000e+00i	4.75475e-87 - 1.86790e-118i*
1,5	250 \angle 15	Pr	2.16355e+03 + 5.82352e+02i	1.87500e-00 - 8.67362e-19i	1.67570e+00 - 5.26057e-02i	-4.96483e-01 + 1.10281e-01i	2.54157e-02 - 2.52302e-01i	-3.30929e-11 - 1.16485e-10i	-3.63351e-31 - 2.56553e-31i*	5.99686e-85 + 8.23680e-84i*
1,5	250 \angle 30	Pr	1.93878e+03 + 1.12502e+03i	1.87500e-00 - 0.00000e+00i	1.69532e+00 - 1.02019e-01i	-9.93789e-01 + 2.45712e-01i	-5.44002e-01 - 1.88880e-01i	-3.45449e-09 - 1.24641e-10i	-1.83220e-27 - 8.61351e-28i	1.83220e-27 - 8.61351e-28i
1,5	250 \angle 45	Pr	8.81133e+02 + 8.83884e+02i	1.87500e-00 - 0.00000e+00i	1.79248e+00 - 8.15606e-02i	-3.38117e+00 - 2.18097e-01i	-2.00855e-02 - 2.19853e-01i	9.37785e-09 - 1.20679e-08i	9.1302	

Table D.53: (continued)

m, n	$c \setminus \arg(c)$	type	$S_{mn}^{(a)}$	$S_{mn}^{(a)}(c, \eta=0)$	$S_{mn}^{(a)}(c, \eta=0.01)$	$S_{mn}^{(a)}(c, \eta=0.1)$	$S_{mn}^{(a)}(c, \eta=0.25)$	$S_{mn}^{(a)}(c, \eta=0.5)$	$S_{mn}^{(a)}(c, \eta=0.75)$	$S_{mn}^{(a)}(c, \eta=0.99)$
1,5	1500 \angle 20	Pr	1.34902e+04 - 0.00000e-00i	1.87500e-00 - 0.00000e+00i	7.48739e-01 - 0.00000e+00i	2.48401e-01 - 0.00000e+00i	4.78259e-17 - 0.00000e+00i	2.70531e-82 - 0.00000e+00i	2.18804e-214 - 2.88950e-246i*	± 0
1,5	1500 \angle 15	Pr	1.30302e+04 + 3.49406e-03i	1.87500e-00 - 0.00000e+00i	7.74409e-01 - 2.59792e-01i	7.74409e-01 - 3.16962e-01i	1.74079e-16 + 1.69088e-16i	3.66272e-207 + 6.04077e-207i	2.25485e-186 - 7.63860e-185i*	± 0
1,5	1500 \angle 30	Pr	1.16816e+04 + 6.75000e-03i	1.87500e-00 - 0.00000e+00i	8.52542e-01 - 5.13892e-01i	-6.03467e-01 - 3.67193e-01i	-2.05662e-14 + 1.95627e-14i	6.03689e-71 + 1.19110e-70i	3.46308e-59 + 1.96661e-60i	± 0
1,5	1500 \angle 45	Pr	5.30055e+03 + 5.30330e-03i	1.87500e-00 - 2.16840e-19i	1.37928e-00 - 4.50985e-01i	5.55217e-02 - 2.66307e-01i	-8.35595e-14 + 8.69862e-13i	3.46308e-59 + 1.96661e-60i	-1.03545e-152 + 1.79902e-153i*	± 0
1,5	1500 \angle 60	Ob	-1.11462e+06 + 1.94256e-06i	-0.00000e-00 - 0.00000e+00i	$\pm \infty$	$\pm \infty$	$\pm \infty$	$\pm \infty$	$\pm \infty$	$\pm \infty$
1,5	1500 \angle 75	Pr	3.88479e+02 + 1.44889e-03i	1.87500e-00 - 0.00000e+00i	1.83420e-00 - 1.33114e-01i	1.49870e-01 - 2.23189e-01i	-3.73775e-06 - 7.63706e-06i	4.23188e-23 + 3.31495e-23i	2.87844e-57 - 1.39177e-57i*	2.67633e-144 - 1.21394e-144i*
1,5	1500 \angle 90	Ob	-2.23202e+06 + 2.74443e-10i	-0.00000e-00 - 0.00000e+00i	$\pm \infty$	$\pm \infty$	$\pm \infty$	$\pm \infty$	$\pm \infty$	$\pm \infty$
1,5	2500 \angle 0	Pr	2.24902e+04 - 0.00000e+00i	1.87500e-00 - 0.00000e+00i	1.38488e-01 - 0.00000e+00i	5.03846e-03 - 0.00000e+00i	2.18051e-30 - 0.00000e+00i	5.25836e-140 - 4.50847e-172i*	± 0	± 0
1,5	2500 \angle 15	Pr	2.17236e+04 + 5.82343e-03i	1.87500e-00 - 0.00000e+00i	1.65389e-01 - 3.66464e-01i	-6.96700e-03 - 3.42053e-03i	1.27879e-29 - 3.00202e-29i	-1.12895e-135 + 4.80741e-135i*	± 0	± 0
1,5	2500 \angle 30	Pr	1.94758e+04 + 1.12500e+04i	1.87500e-00 + 2.16840e-19i	2.50627e-01 - 1.73713e-01i	1.17339e-02 + 2.49156e-02i	5.39000e-26 - 7.32409e-26i	-1.60955e-120 - 1.39562e-121i*	4.33818e-312 - 1.05680e-311i*	± 0
1,5	2500 \angle 45	Pr	8.83608e+03 + 8.83833e-03i	1.87500e-00 - 1.08420e-19i	1.05191e-00 - 7.02486e-01i	2.71961e-03 + 1.29388e-02i	-9.30765e-23 - 2.41201e-23i	4.01912e-100 - 1.84412e-100i*	-1.51024e-256 + 1.59009e-256i*	± 0
1,5	2500 \angle 60	Ob	-3.10769e+06 + 5.40266e-06i	-0.00000e-00 - 0.00000e+00i	$\pm \infty$	$\pm \infty$	$\pm \infty$	$\pm \infty$	$\pm \infty$	$\pm \infty$
1,5	2500 \angle 75	Pr	6.47298e+02 + 2.14481e+03i	1.87500e+00 + 5.42101e-20i	1.80216e-00 - 2.18663e-01i	6.57615e-02 + 3.27422e-02i	6.52428e-10 - 2.19749e-09i	-4.96943e-38 - 2.99800e-39i*	2.40102e-95 - 2.24003e-95i*	7.37408e-241 - 6.35258e-241i*
1,5	2500 \angle 90	Ob	-6.22002e+06 + 7.63567e-10i	-0.00000e-00 - 0.00000e+00i	$\pm \infty$	$\pm \infty$	$\pm \infty$	$\pm \infty$	$\pm \infty$	$\pm \infty$
1,5	5000 \angle 0	Pr	4.49902e+04 - 0.00000e+00i	1.87500e-00 - 0.00000e+00i	-9.73191e-01 - 0.00000e+00i	7.76904e-08 - 0.00000e+00i	2.93982e-64 - 0.00000e+00i	9.30447e-285 - 7.43285e-317i*	± 0	± 0
1,5	5000 \angle 15	Pr	4.34569e+04 + 1.16469e+04i	1.87500e-00 - 0.00000e+00i	-9.78360e-01 - 4.54687e-01i	1.72656e-07 + 6.03860e-08i	-6.33124e-62 - 1.77933e-62i	-7.38025e-275 + 4.75505e-276i*	± 0	± 0
1,5	5000 \angle 30	Pr	3.89614e+04 + 2.25000e+04i	1.87500e-00 - 0.00000e+00i	-9.80647e-01 - 9.95932e-01i	9.97947e-07 + 2.02043e-06i	-4.98380e-55 - 1.04449e-55i	5.31368e-246 - 6.42798e-246i*	± 0	± 0
1,5	5000 \angle 45	Pr	1.76749e+04 + 1.76777e+04i	1.87500e+00 + 5.42101e-20i	2.57812e-01 - 1.17474e-01i	1.92241e-06 - 5.54867e-06i	9.78540e-48 - 2.16252e-46i	1.09396e-203 + 1.45779e-202i*	± 0	± 0
1,5	5000 \angle 60	Ob	-1.24654e+07 + 2.16306e+07i	-0.00000e-00 - 0.00000e+00i	$\pm \infty$	$\pm \infty$	$\pm \infty$	$\pm \infty$	$\pm \infty$	$\pm \infty$
1,5	5000 \angle 75	Pr	1.29435e+03 + 4.82963e-03i	1.87500e-00 - 0.00000e+00i	1.70658e-00 - 4.20321e-01i	1.72815e-03 + 2.28808e-03i	-2.29244e-18 - 1.49280e-18i	1.31898e-75 + 1.59712e-76i*	1.95883e-191 - 2.82248e-190i*	± 0
1,5	5000 \angle 90	Ob	-2.49400e+07 + 3.05794e-09i	-0.00000e-00 - 0.00000e+00i	$\pm \infty$	$\pm \infty$	$\pm \infty$	$\pm \infty$	$\pm \infty$	$\pm \infty$
1,6	25 \angle 0	Pr	2.59497e+02 - 0.00000e+00i	-0.00000e-00 - 0.00000e+00i	1.30690e-01 - 0.00000e+00i	8.20046e-01 - 0.00000e+00i	-6.35275e-01 - 0.00000e+00i	1.01394e+00 - 0.00000e+00i	3.34299e+01 + 1.16352e-32i*	1.16595e-04 + 2.83787e-36i*
1,6	25 \angle 15	Pr	2.50157e+02 + 7.13852e+01i	-0.00000e-00 - 0.00000e+00i	1.30710e-01 - 1.55757e-04i	8.30872e-01 - 1.19847e-01i	-7.42102e-01 - 2.35101e-01i	1.34782e+00 + 2.36943e-01i	2.83551e-02 - 4.02196e-01i*	3.52767e-05 + 2.20474e-04i*
1,6	25 \angle 30	Ob	3.60481e+02 + 4.54627e+02i	-0.00000e-00 - 0.00000e+00i	1.30467e-01 - 9.90957e-04i	4.84839e-01 - 6.62156e-01i	-1.55584e+00 + 3.50176e+00i	-5.17036e+01 + 1.55697e+01i	-5.77871e+02 - 3.74087e+02i	2.00652e-02 - 2.26870e-03i
1,6	25 \angle 45	Pr	1.17904e+02 - 1.23828e+02i	-0.00000e-00 - 0.00000e+00i	1.30999e-01 - 2.70535e-04i	1.05898e+00 - 2.37990e-01i	-3.05033e-01 - 1.56080e-01i	-6.08000e-01 + 2.87561e-01i	-1.94120e-01 - 4.68782e-01i*	3.70966e-04 + 1.96131e-03i*
1,6	25 \angle 60	Ob	-1.47588e+02 + 4.41071e+02i	-0.00000e-00 - 0.00000e+00i	1.31578e-01 - 9.66308e-04i	1.43167e+00 - 1.41764e+01i	-1.99873e+01 + 1.47176e+01i	1.49709e+03 + 1.04017e+03i	-7.62852e-04 - 4.81463e-04i	-2.47096e-04 - 3.61562e-05i
1,6	25 \angle 75	Ob	-2.70703e+02 + 2.34458e+02i	-0.00000e-00 - 0.00000e+00i	1.31849e-01 - 5.14287e-04i	1.92515e+00 - 6.64087e-01i	7.96683e+00 - 2.81505e+01i	-2.02521e+03 - 3.77627e+02i	4.01912e+01 + 6.30811e+04i	6.71424e-04 + 9.95959e-04i
1,6	25 \angle 90	Ob	-3.44291e+02 + 5.80751e-14i	-0.00000e-00 - 0.00000e+00i	1.32011e-01 + 1.24598e-17i	2.21494e+00 + 3.41075e-17i	3.66592e+01 - 7.74929e-15i	3.16584e+03 - 1.91480e-12i	1.15599e+05 - 3.19285e-10i	1.15599e+05 - 3.19285e-10i
1,6	50 \angle 0	Pr	5.34889e+02 - 0.00000e+00i	-0.00000e-00 - 0.00000e+00i	1.30090e-01 - 0.00000e+00i	4.27557e-01 - 0.00000e+00i	-4.15159e-01 - 0.00000e+00i	4.03831e-01 + 8.68366e-33i*	5.91323e-04 + 5.07093e-36i*	4.38413e-13 + 8.84774e-45i*
1,6	50 \angle 15	Pr	5.16163e+02 + 1.42448e+02i	-0.00000e-00 - 0.00000e+00i	1.30130e-01 - 3.09943e-04i	4.35272e-01 - 1.75081e-01i	-4.85276e-01 + 3.85560e-01i	2.03861e-01 - 3.60653e-01i	-3.66402e-04 + 2.82879e-04i*	-3.52112e-13 + 7.53409e-13i*
1,6	50 \angle 30	Pr	1.34799e+03 + 1.99184e+03i	-0.00000e-00 - 0.00000e+00i	1.28285e-01 - 4.29870e-01i	-1.34037e+01 + 1.53757e-01i	-4.06793e+01 + 1.35390e+01i	-2.10551e+03 - 1.36150e+04i	4.00045e+06 + 6.04878e+04i	-1.53961e+08 + 2.16961e+08i
1,6	50 \angle 45	Pr	2.41694e+02 + 2.47530e+02i	-0.00000e-00 - 0.00000e+00i	1.30728e-01 - 5.40044e-04i	7.93958e-01 - 4.08510e-01i	-1.74912e+00 + 2.64770e-01i	4.55104e-01 - 3.90804e-01i	-3.82748e-04 - 2.63397e-03i*	2.88550e-10 - 9.52359e-10i*
1,6	50 \angle 60	Ob	-9.11733e+02 + 1.96498e-03i	-0.00000e-00 - 0.00000e+00i	1.33218e-01 - 4.33771e-03i	-2.55366e+00 - 6.68368e-03i	2.15248e+03 + 1.44409e+03i	3.61050e+07 + 2.53577e+07i	4.16818e+11 + 2.97087e+11i	4.13827e+13 - 1.26108e+14i
1,6	50 \angle 75	Ob	-1.60407e+03 + 1.09454e-03i	-0.00000e-00 - 0.00000e+00i	1.34781e-01 - 2.43302e-03i	5.44016e-00 - 8.47872e-03i	-5.45713e+03 - 1.06082e+03i	1.75492e+08 + 1.41930e+07i	-2.74374e-12 + 1.63040e+11i	3.25808e+13 + 1.28795e+14i
1,6	50 \angle 90	Ob	-1.91859e+03 + 2.69383e-13i	-0.00000e-00 - 0.00000e+00i	1.35494e-01 - 2.57643e-18i	1.20028e-03 - 3.02412e-15i	8.54413e+03 - 6.09250e-12i	4.14109e+08 - 6.12507e-07i	9.79136e+12 - 2.21209e-02i	5.06897e+14 - 1.33205e+00i
1,6	100 \angle 0	Pr	1.08507e+03 - 0.00000e+00i	-0.00000e-00 - 0.00000e+00i	1.28898e-01 - 0.00000e+00i	-4.62187e-02 - 0.00000e+00i	4.58012e-01 - 0.00000e+00i	4.16939e-03 - 0.00000e+00i	1.78678e-10 + 2.03753e-42i*	6.29863e-14 - 0.00000e+00i
1,6	100 \angle 15	Pr	1.04760e+03 + 2.84748e+02i	-0.00000e-00 - 0.00000e+00i	1.28976e-01 - 6.16110e-04i	-6.12449e-02 - 1.68483e-01i	5.93709e-01 + 1.11216e-01i	-3.19864e-03 - 8.56916e-04i	-5.70202e-11 - 1.52429e-10i*	-3.22623e-10 - 9.83299e-31i*
1,6	100 \angle 30	Pr	5.19800e+03 + 8.31384e+03i	-0.00000e-00 - 0.00000e+00i	1.19449e-01 - 1.72449e-02i	2.06092e-00 - 7.81743e-00i	-1.83306e+03 - 1.08558e-04i	-3.13964e-08 + 1.80670e-09i	1.35148e-14 - 2.40633e-14i	-7.32627e-18 - 1.08381e-18i
1,6	100 \angle 45	Pr	4.89203e+02 + 4.94996e-02i	-0.00000e-00 - 0.00000e+00i	1.30186e-01 - 1.07695e-03i	3.12219e-01 - 5.83678e-01i	-4.10192e-01 + 1.24880e-00i	7.78762e-03 + 7.77387e-03i	1.48012e-08 - 3.24273e-08i	1.30447e-22 - 3.30904e-23i*
1,6	100 \angle 60	Ob	-4.31525e+03 + 8.26021e-03i	-0.00000e-00 - 0.00000e+00i	1.40133e-01 - 1.88469e-02i	-6.63410e-01 + 2.54451e-02i	5.20794e-07 + 3.60999e-07i	4.30264e-16 + 3.38705e-16i	2.45028e-25 + 2.15352e-25i	1.09221e+32 - 1.65713e+30i
1,6	100 \angle 75	Ob	-7.51941e+03 + 4.68934e-03i	-0.00000e-00 - 0.00000e+00i	1.48082e-01 - 1.10480e-02i	-4.02267e-02 - 4.39599e-02i	4.65565e-08 + 3.98008e-07i	2.65893e-18 - 2.93601e-17i	7.51948e-27 - 2.46653e-27i	-1.26633e+35 + 2.36226e+33i
1,6	100 \angle 90	Ob	-8.81828e+03 + 1.15115e-12i	-0.00000e-00 - 0.00000e+00i	1.51416e-01 - 6.79051e-18i	8.39555e-02 - 4.82196e-13i	1.09697e-09 - 1.63857e-06i	1.47036e-19 - 4.4994e-04i	1.01651e+29 - 4.63724e+14i	-3.10483e+35 + 1.87202e+21i
1,6	250 \angle 0	Pr	2.73518e+03 - 0.00000e+00i	-0.00000e-00 - 0.00000e+00i	1.25358e-01 - 0.00000e+00i	8.23274e-01 - 0.00000e+00i	5.84170e-02 - 0.00000e+00i	2.80199e-11 - 0.00000e+00i	2.96372e-32 - 0.00000e+00i	1.12413e-86 - 1.02234e-118i*
1,6	250 \angle 15	Pr	2.64148e+03 + 7.11771e+02i	-0.00000e-00 - 0.00000e+00i	1.25552e-01 - 1.51440e-03i	-2.95301e-01 + 8.58577e-02i	1.15040e-02 - 7.71508e-02i	-2.32951e-11 - 8.48705e-11i	-4.52383e-31 - 3.21742e-31i*	1.43845e-84 + 1.99633e-83i*
1,6	250 \angle 30	Ob	3.17480e+04 + 5.32606e+04i	-0.00000e-00 - 0.00000e+00i	4.76995e-02 - 8.00226e-02i	-1.02051e-03 - 5.72395e-03i	-5.75			

Table D.53: (continued)

m, n	$ c \angle \arg(c)$	type	$\lambda_{mn}^{(a)}$	$S_{mn}^{(a)}(c, \eta=0)$	$S_{mn}^{(a)}(c, \eta=0.01)$	$S_{mn}^{(a)}(c, \eta=0.1)$	$S_{mn}^{(a)}(c, \eta=0.25)$	$S_{mn}^{(a)}(c, \eta=0.5)$	$S_{mn}^{(a)}(c, \eta=0.75)$	$S_{mn}^{(a)}(c, \eta=0.99)$
1.6	1500 \angle 0°	Pr	1.64852e-04 - 0.00000e-00i	-0.00000e-00 - 0.00000e-00i	9.81750e-02 - 0.00000e-00i	2.96540e-02 - 0.00000e-00i	1.66404e-17 - 0.00000e-00i	2.01893e-82 - 0.00000e-00i	2.73555e-214 - 3.55291e-246*	± 0
1.6	1500 \angle 15°	Pr	1.59230e-04 + 4.27052e-03i	-0.00000e-00 - 0.00000e-00i	9.90259e-02 - 7.87778e-03i	1.00747e-02 - 3.77511e-02i	6.02736e-17 + 5.92315e-17i	6.53660e-80 - 1.78617e-79i	4.64104e-207 + 7.66353e-207*	± 0
1.6	1500 \angle 30°	Ob	1.12800e-06 + 1.94336e-06i	-0.00000e-00 - 0.00000e-00i	$\pm \infty$	$\pm \infty$	$\pm \infty$	$\pm \infty$	$\pm \infty$	$\pm \infty$
1.6	1500 \angle 45°	Pr	7.41887e-03 + 7.42462e-03i	-0.00000e-00 - 0.00000e-00i	1.15057e-01 - 1.49225e-02i	1.54558e-02 - 5.87194e-02i	-5.30736e-14 + 5.11344e-13i	4.32183e-59 + 2.53529e-60i	-2.18049e-152 + 3.78310e-153*	± 0
1.6	1500 \angle 60°	Ob	-1.11462e-06 + 1.94256e-06i	-0.00000e-00 - 0.00000e-00i	$\pm \infty$	$\pm \infty$	$\pm \infty$	$\pm \infty$	$\pm \infty$	$\pm \infty$
1.6	1500 \angle 75°	Ob	-1.93119e-06 + 1.12034e-06i	-0.00000e-00 - 0.00000e-00i	$\pm \infty$	$\pm \infty$	$\pm \infty$	$\pm \infty$	$\pm \infty$	$\pm \infty$
1.6	1500 \angle 90°	Ob	-2.23202e-06 + 2.74443e-10i	-0.00000e-00 - 0.00000e-00i	$\pm \infty$	$\pm \infty$	$\pm \infty$	$\pm \infty$	$\pm \infty$	$\pm \infty$
1.6	2500 \angle 0°	Pr	2.74852e-04 - 0.00000e-00i	-0.00000e-00 - 0.00000e-00i	7.91759e-02 - 0.00000e-00i	6.46797e-04 - 0.00000e-00i	7.65470e-31 - 0.00000e-00i	3.92667e-140 + 4.78808e-172*	± 0	± 0
1.6	2500 \angle 15°	Pr	2.65482e-04 + 7.11753e-03i	-0.00000e-00 - 0.00000e-00i	8.02400e-02 - 1.16695e-02i	-8.86549e-04 - 4.63785e-04i	4.52731e-30 - 1.05281e-29i	-8.05254e-136 + 3.44969e-135*	± 0	± 0
1.6	2500 \angle 30°	Ob	3.13000e-06 + 5.40400e-06i	-0.00000e-00 - 0.00000e-00i	$\pm \infty$	$\pm \infty$	$\pm \infty$	$\pm \infty$	$\pm \infty$	$\pm \infty$
1.6	2500 \angle 45°	Pr	1.23686e-04 + 1.23744e-04i	-0.00000e-00 - 0.00000e-00i	1.04339e-01 - 2.34632e-02i	5.30098e-04 + 2.95959e-03i	-5.42714e-23 - 1.42575e-22i	5.02256e-100 - 2.29813e-100*	-3.18138e-256 + 3.34908e-256*	± 0
1.6	2500 \angle 60°	Ob	-3.10769e-06 + 5.40266e-06i	-0.00000e-00 - 0.00000e-00i	$\pm \infty$	$\pm \infty$	$\pm \infty$	$\pm \infty$	$\pm \infty$	$\pm \infty$
1.6	2500 \angle 75°	Ob	-5.38370e-06 + 3.11724e-06i	-0.00000e-00 - 0.00000e-00i	$\pm \infty$	$\pm \infty$	$\pm \infty$	$\pm \infty$	$\pm \infty$	$\pm \infty$
1.6	2500 \angle 90°	Ob	-6.22002e-06 + 7.63567e-10i	-0.00000e-00 - 0.00000e-00i	$\pm \infty$	$\pm \infty$	$\pm \infty$	$\pm \infty$	$\pm \infty$	$\pm \infty$
1.6	5000 \angle 0°	Pr	5.49852e-04 - 0.00000e-00i	-0.00000e-00 - 0.00000e-00i	4.09050e-02 - 0.00000e-00i	1.04540e-08 - 0.00000e-00i	1.03882e-64 - 0.00000e-00i	6.83470e-285 + 7.50049e-317*	± 0	± 0
1.6	5000 \angle 15°	Pr	5.31112e-04 + 1.24350e-04i	-0.00000e-00 - 0.00000e-00i	4.16588e-02 - 1.70840e-02i	2.31767e-08 + 8.40517e-09i	-2.23665e-62 - 6.32649e-63i	-5.53026e-275 + 3.54172e-276*	± 0	± 0
1.6	5000 \angle 30°	Ob	1.25100e-07 + 2.16333e-07i	-0.00000e-00 - 0.00000e-00i	$\pm \infty$	$\pm \infty$	$\pm \infty$	$\pm \infty$	$\pm \infty$	$\pm \infty$
1.6	5000 \angle 45°	Pr	2.47430e-04 + 2.47487e-04i	-0.00000e-00 - 0.00000e-00i	7.82029e-02 - 4.03072e-02i	3.09953e-07 - 8.14029e-07i	6.07765e-48 - 1.27879e-46i	1.35646e-203 + 1.82237e-202*	± 0	± 0
1.6	5000 \angle 60°	Ob	-1.24654e-07 + 2.16306e-07i	-0.00000e-00 - 0.00000e-00i	$\pm \infty$	$\pm \infty$	$\pm \infty$	$\pm \infty$	$\pm \infty$	$\pm \infty$
1.6	5000 \angle 75°	Ob	-2.15927e-07 + 1.24845e-07i	-0.00000e-00 - 0.00000e-00i	$\pm \infty$	$\pm \infty$	$\pm \infty$	$\pm \infty$	$\pm \infty$	$\pm \infty$
1.6	5000 \angle 90°	Ob	-2.49400e-07 + 3.05794e-09i	-0.00000e-00 - 0.00000e-00i	$\pm \infty$	$\pm \infty$	$\pm \infty$	$\pm \infty$	$\pm \infty$	$\pm \infty$

Table D.53: $S_{1n}^{(a)}(c, \eta)$ for $n = [1..6]$.

D.2.2 Asymptotic expansions of the derivative of the PASWF, $S_{mn}^{(a)'}(c, \eta)$ and the corresponding characteristic eigenvalues, $\lambda_{mn}^{(a)}$, for $m = [0..1]$, $n = [m..6]$.

Table D.54: $S_{0n}^{(a)'}(c, \eta)$ for $n = [0..6]$.

m, n	$ c \angle \arg(c)$	type	$\lambda_{mn}^{(a)'}$	$S_{mn}^{(a)'}(c, \eta=0)$	$S_{mn}^{(a)'}(c, \eta=0.01)$	$S_{mn}^{(a)'}(c, \eta=0.1)$	$S_{mn}^{(a)'}(c, \eta=0.25)$	$S_{mn}^{(a)'}(c, \eta=0.5)$	$S_{mn}^{(a)'}(c, \eta=0.75)$	$S_{mn}^{(a)'}(c, \eta=0.99)$
0.0	25 \angle 0°	Pr	2.42421e+01 - 0.00000e-00i	-0.00000e-00 - 0.00000e-00i	-2.42139e-01 - 0.00000e+00i	-2.15757e-00 - 0.00000e-00i	-2.89720e-00 - 0.00000e-00i	-5.45079e-01 - 0.00000e-00i	-7.74910e-03 - 0.00000e-00i	-2.51398e-07 - 0.00000e-00i
0.0	25 \angle 15°	Pr	2.33906e+01 + 6.47263e+00i	-0.00000e-00 - 0.00000e-00i	-2.33664e-01 - 6.45782e-02i	-2.10815e-00 - 5.10442e-01i	-2.97386e-00 - 1.92570e-01i	-5.06218e-01 + 3.43463e-01i	3.52500e-03 + 9.73686e-03i	-2.69429e-07 - 4.53501e-07i
0.0	25 \angle 30°	Pr	2.08940e+01 + 1.25041e+01i	-0.00000e-00 - 0.00000e-00i	-2.08810e-01 - 1.24786e-01i	-1.95802e-00 - 1.01110e-00i	-3.20404e-00 - 4.60246e-01i	-3.62999e-01 + 7.77316e-01i	2.07006e-02 - 1.25864e-02i	3.53489e-06 - 2.98901e-06*
0.0	25 \angle 45°	Pr	1.69224e+01 + 1.76834e+01i	-0.00000e-00 - 0.00000e-00i	-1.69245e-01 - 1.76543e-01i	-1.70057e-00 - 1.48803e-00i	-3.58002e-00 - 9.00718e-01i	-1.74343e-02 + 1.46911e+00i	-4.14433e-02 - 8.39631e-02i	2.27577e-05 + 1.44173e-04*
0.0	25 \angle 60°	Ob	-2.70208e+02 + 5.16261e+02i	-0.00000e-00 - 0.00000e-00i	2.66982e-00 - 5.20942e+00i	-2.23683e-01 - 9.43630e+01i	-1.87817e+03 + 1.09088e+03i	3.55436e+05 - 1.97938e+05i	-6.90905e+07 + 3.68945e+07i	1.17059e+10 - 2.44834e+09i
0.0	25 \angle 75°	Ob	-4.93980e+02 + 2.99556e+02i	-0.00000e-00 - 0.00000e-00i	4.96581e-00 - 3.04525e+00i	7.30710e+01 - 9.77547e+01i	-1.26525e+03 - 3.83544e+03i	-1.31995e+06 + 5.03898e+05i	2.02929e+08 + 4.65680e+08i	1.35901e+11 - 5.62900e+10i
0.0	25 \angle 90°	Ob	-5.76010e+02 + 7.34781e-14i	-0.00000e-00 - 0.00000e-00i	4.96246e-00 - 3.17243e-16i	1.31954e+02 - 1.91518e-14i	4.99010e+03 - 1.85672e-12i	2.16027e+06 - 1.63012e-09i	9.61115e+08 - 1.09294e-06i	3.41471e+11 - 5.13731e-04i
0.0	50 \angle 0°	Pr	4.92462e+01 - 0.00000e-00i	-0.00000e-00 - 0.00000e-00i	-4.91275e-01 - 0.00000e+00i	-3.86656e-00 - 0.00000e-00i	-2.66164e-00 - 0.00000e-00i	-3.89299e-02 - 0.00000e-00i	-3.33611e-06 - 0.00000e-00i	-2.57925e-16 - 0.00000e-00i
0.0	50 \angle 15°	Pr	4.75426e+01 + 1.29420e+01i	-0.00000e-00 - 0.00000e-00i	-4.74404e-01 - 1.28812e-01i	-3.82333e-00 - 7.78703e-01i	-2.78161e+00 + 4.06390e-01i	-5.04079e-03 + 4.86802e-02i	3.34644e-06 - 4.91204e-06i	1.78997e-16 - 1.10324e-15i
0.0	50 \angle 30°	Pr	4.25480e+01 + 2.50020e+01i	-0.00000e-00 - 0.00000e-00i	-4.24908e-01 - 2.48970e-01i	-3.68136e-00 - 1.58244e-01i	-3.18663e+00 + 8.56040e-01i	9.07429e-02 + 3.04943e-02i	2.47002e-06 + 3.22196e-05i	3.89726e-14 + 7.24439e-14*
0.0	50 \angle 45°	Pr	3.46027e+01 + 3.53581e+01i	-0.00000e-00 - 0.00000e-00i	-3.46069e-01 - 3.52376e-01i	-3.40464e-00 - 2.42550e-01i	-4.03276e+00 + 1.36455e+00i	1.94321e-01 - 1.99260e-01i	-8.31674e-05 + 4.70383e-04i	2.35276e-11 - 7.29952e-11*
0.0	50 \angle 60°	Ob	-1.16440e+03 + 2.11506e+03i	-0.00000e-00 - 0.00000e-00i	1.11134e+01 - 2.19722e+01i	-1.68756e+03 - 1.83526e+02i	8.68811e+05 + 4.74296e+05i	3.70976e+10 - 1.86492e+10i	1.62625e+15 - 7.50022e+14i	5.08183e+17 - 2.36648e+18i
0.0	50 \angle 75°	Ob	-2.06948e+03 + 1.22412e+03i	-0.00000e-00 - 0.00000e-00i	2.11598e+01 - 1.30981e+01i	2.71662e+01 - 2.79183e+03i	-3.22287e+06 + 1.21409e+06i	4.52759e+11 - 2.20693e+11i	-6.46907e+16 + 3.93899e+16i	6.28644e+21 - 3.52450e+21i
0.0	50 \angle 90°	Ob	-2.40101e+03 + 3.00038e-13i	-0.00000e-00 - 0.00000e-00i	2.49841e+01 - 3.42669e-15i	3.30782e+03 - 1.24345e-12i	5.26927e+06 - 4.40010e-09i	1.17991e+12 - 1.88828e-03i	2.71648e+17 - 6.42641e+02i	3.89074e+22 - 1.20630e+08i
0.0	100 \angle 0°	Pr	9.92481e+01 - 0.00000e-00i	-0.00000e-00 - 0.00000e-00i	-9.87617e-01 - 0.00000e+00i	-6.06510e-00 - 0.00000e-00i	-1.09655e+00 - 0.00000e-00i	-9.67642e-05 - 0.00000e-00i	-2.99775e-13 - 0.00000e-00i	-1.19201e-34 + 7.29232e-51*
0.0	100 \angle 15°	Pr	9.58408e+01 + 2.58824e+01i	-0.00000e-00 - 0.00000e-00i	-9.54206e-01 - 2.56365e-01i	-6.11585e-00 - 8.24686e-01i	-1.03676e+00 + 6.47193e-01i	1.52498e-04 - 9.46434e-06i	5.70918e-13 + 7.59945e-13i	2.22680e-33 + 6.87101e-35*
0.0	100 \angle 30°	Pr	8.58099e+01 + 5.00101e+01i	-0.00000e-00 - 0.00000e-00i	-8.56116e-01 - 4.95754e-01i	-6.24598e-00 - 1.77426e-00i	-8.20826e-01 + 1.46554e+00i	-5.79412e-04 - 6.52773e-05i	2.15718e-11 - 1.78635e-11i	6.13752e-32 - 1.19131e-29*
0.0	100 \angle 45°	Pr	6.99594e+01 + 7.07120e+01i	-0.00000e-00 - 0.00000e-00i	-6.99672e-01 - 7.02217e-01i	-6.38049e-00 - 2.97520e-00i	-3.23225e-01 + 2.76694e+00i	3.61634e-03 + 3.31916e-03i	2.45166e-09 - 5.5702e-09i	9.86968e-24 - 2.38147e-24*
0.0	100 \angle 60°	Ob	-4.82780e+03 + 8.56025e+03i	-0.00000e-00 - 0.00000e-00i	3.91513e+01 - 9.93442e+01i	1.89439e+05 - 1.78164e+05i	8.98162e+10 + 4.47007e+10i	1.95172e+20 - 8.13889e+19i	4.33865e+29 - 1.47869e+29i	4.16627e+38 + 1.01106e+38i
0.0	100 \angle 75°	Ob	-8.46807e+03 + 4.94824e+03i	-0.00000e-00 - 0.00000e-00i	9.25352e+01 - 6.42558e+01i	-6.76223e+05 - 2.01123e+05i	1.09600e+12 - 5.31405e+11i	2.50528e+22 - 1.85974e+22i	5.57276e+32 - 6.04153e+32i	6.16205e+42 - 5.78813e+42i
0.0	100 \angle 90°	Ob	-9.80100e+03 + 1.21240e-12i	-0.00000e-00 - 0.00000e-00i	1.14831e+02 - 1.89790e-14i	9.91600e+05 - 6.90877e-10i	2.85416e+12 - 4.60998e-03i	1.71377e+23 - 5.39143e+08i	1.05822e+34 - 4.94903e+19i	2.46594e+44 - 1.51563e+30i
0.0	250 \angle 0°	Pr	2.49249e+02 - 0.00000e-00i	-0.00000e-00 - 0.00000e-00i	-2.46174e-00 - 0.00000e+00i	-2.18152e-00 - 0.00000e-00i	-2.35170e-02 - 0.00000e-00i	-4.55135e-13 - 0.00000e-00i	-6.63641e-35 - 0.00000e-00i	-3.37563e-90 + 2.06631e-106*
0.0	250 \angle 15°	Pr	2.40731e+02 + 6.47050e+01i	-0.00000e-00 - 0.00000e-00i	-2.38068e-00 - 6.31641e-01i	-2.748130e+00 + 4.62594e-01i	6.76467e-03 + 3.00736e-02i	7.47491e-13 + 1.21329e-12i	1.11628e-33 + 4.04154e-34i	-1.66686e-87 - 4.80318e-87*
0.0	250 \angle 30°	Pr	2.15756e+02 + 1.25000e+02i	-0.00000e-00						

Table D.54: (continued)

m, n	$c \setminus \arg(c)$	type	$\lambda_{mn}^{(a)}$	$S_{mn}^{(a)}(c, \eta=0)$	$S_{mn}^{(a)}(c, \eta=0.01)$	$S_{mn}^{(a)}(c, \eta=0.1)$	$S_{mn}^{(a)}(c, \eta=0.25)$	$S_{mn}^{(a)}(c, \eta=0.5)$	$S_{mn}^{(a)}(c, \eta=0.75)$	$S_{mn}^{(a)}(c, \eta=0.99)$
0.0	500 Z 15°	Pr	4.82213e+02 + 1.29410e+02i	-0.00000e+00 - 0.00000e+00i	-4.71556e+00 - 1.23284e+00i	-4.14481e+00 - 1.68673e+00i	2.19754e-05 - 1.87173e-05i	5.13374e-27 - 2.48913e-26i	-6.73345e-69 - 3.09977e-69i	5.05703e-177 - 6.85032e-177i*
0.0	500 Z 30°	Pr	4.32262e+02 + 2.50000e+02i	-0.00000e+00 - 0.00000e+00i	-4.26066e+00 - 2.39360e+00i	-4.28857e+00 + 3.82857e+00i	6.00440e-05 + 1.27606e-04i	-3.58339e-25 + 2.04844e-23i	1.24597e-61 + 1.06452e-61i*	-3.06443e-158 + 1.99938e-158i*
0.0	500 Z 45°	Pr	3.52803e+02 + 3.53554e+02i	-0.00000e+00 - 0.00000e+00i	-3.52738e+00 - 3.41207e+00i	-4.72929e+00 + 7.13949e+00i	9.27154e-04 - 1.49452e-03i	7.36854e-19 + 4.44977e-19i	-7.05861e-50 - 3.56325e-50i*	-4.34858e-129 + 1.54118e-128i*
0.0	500 Z 60°	Ob	-1.24135e+05 + 2.16006e+05i	-0.00000e+00 - 0.00000e+00i	-1.86385e+04 - 2.19382e+03i	1.34000e+21 - 5.53660e+20i	2.02302e+49 - 3.94625e+48i	1.75594e+96 + 2.46146e+95i	1.39790e+143 + 7.12149e+142i	-1.85060e+188 - 3.01436e+187i
0.0	500 Z 75°	Ob	-2.15541e+05 + 1.24741e+05i	-0.00000e+00 - 0.00000e+00i	4.43749e+02 - 3.09202e+04i	1.72104e+23 - 1.27305e+23i	1.98550e+54 - 5.08772e+54i	-6.65969e+106 - 1.05205e+107i	-2.91254e+159 - 2.04279e+158i	-5.10635e+209 - 2.32757e+209i
0.0	500 Z 90°	Ob	-2.49001e+05 + 3.05549e-11i	-0.00000e+00 - 0.00000e+00i	3.66611e+04 - 1.34593e-11i	1.17609e+24 - 3.67240e+09i	3.86418e+56 - 2.98120e+42i	6.23368e+110 - 9.58054e+96i	1.03431e+165 - 2.38129e+151i	1.18632e+217 - 3.60296e+203i
0.0	750 Z 0°	Pr	7.49250e+02 - 0.00000e+00i	-0.00000e+00 - 0.00000e+00i	-7.21736e+00 - 0.00000e+00i	-1.76095e+00 - 0.00000e+00i	-8.99625e-09 - 0.00000e+00i	-1.10662e-41 - 0.00000e+00i	-6.05813e-108 + 3.70649e-124i*	-3.12117e-276 + 1.91092e-292i*
0.0	750 Z 15°	Pr	7.23694e+02 + 1.94114e+02i	-0.00000e+00 - 0.00000e+00i	-6.99794e+00 - 1.80442e+00i	-1.51676e+00 + 1.30621e+00i	-1.87991e-08 - 7.53721e-09i	-2.78039e-40 + 1.94973e-40i	3.01585e-104 + 1.71009e-104i*	1.06440e-266 + 3.85535e-268i*
0.0	750 Z 30°	Pr	6.48769e+02 + 3.75000e+02i	-0.00000e+00 - 0.00000e+00i	-6.34789e+00 - 3.51209e+00i	-6.22305e-01 + 2.84716e+00i	-8.27628e-08 - 2.02419e-07i	-6.62856e-36 - 4.05629e-36i	-2.57964e-93 + 2.51577e-93i*	-4.03235e-239 + 8.55288e-239i*
0.0	750 Z 45°	Pr	5.29580e+02 + 5.30330e+02i	-0.00000e+00 - 0.00000e+00i	-5.29280e+00 - 5.02641e+00i	1.57268e+00 + 5.05880e+00i	9.05808e-06 - 3.26653e-06i	-2.73601e-29 + 6.10626e-29i	1.15072e-75 + 3.65296e-76i*	1.90830e-194 + 1.97069e-194i*
0.0	750 Z 60°	Ob	-2.79952e+05 + 4.86389e+05i	-0.00000e+00 - 0.00000e+00i	-1.04147e+05 + 2.22304e+05i	5.21247e+30 - 1.75705e+30i	9.93466e+72 - 2.62539e+71i	2.44701e+143 + 1.24732e+143i	4.41855e+213 + 6.43672e+213i	1.66302e+281 + 3.01109e+281i
0.0	750 Z 75°	Ob	-4.85691e+05 + 2.80862e+05i	-0.00000e+00 - 0.00000e+00i	$\pm \infty$	$\pm \infty$	$\pm \infty$	$\pm \infty$	$\pm \infty$	$\pm \infty$
0.0	750 Z 90°	Ob	-5.61001e+05 + 6.87945e-11i	-0.00000e+00 - 0.00000e+00i	$\pm \infty$	$\pm \infty$	$\pm \infty$	$\pm \infty$	$\pm \infty$	$\pm \infty$
0.0	1000 Z 0°	Pr	9.99250e+02 - 0.00000e+00i	-0.00000e+00 - 0.00000e+00i	-9.50598e+00 - 0.00000e+00i	-6.70754e-01 - 0.00000e+00i	-4.28003e-12 - 0.00000e+00i	-4.19708e-56 - 0.00000e+00i	-1.40766e-144 + 8.61405e-161i*	± 0
0.0	1000 Z 15°	Pr	9.65176e+02 + 2.58819e+02i	-0.00000e+00 - 0.00000e+00i	-9.22863e+00 - 2.34714e+00i	-4.05986e-01 + 6.84339e-01i	1.29349e-12 + 1.25624e-11i	3.99030e-54 + 5.80047e-55i	-1.18897e-139 - 8.13952e-140i*	± 0
0.0	1000 Z 30°	Pr	8.65275e+02 + 3.03330e+02i	-0.00000e+00 - 0.00000e+00i	-8.40390e+00 - 4.57988e+00i	5.25186e-01 + 1.20338e+00i	2.82586e-10 + 1.04712e-10i	2.31153e-48 - 1.23248e-48i	-4.43680e-125 - 5.46649e-125i*	2.47725e-320 + 2.16850e-319i*
0.0	1000 Z 45°	Pr	7.06357e+02 + 7.07107e+02i	-0.00000e+00 - 0.00000e+00i	-7.05582e+00 - 6.58073e+00i	2.70137e+00 + 1.08870e+00i	4.44223e-08 + 1.48940e-08i	-4.41684e-39 - 1.36344e-39i	-1.62044e-101 - 2.40791e-102i*	4.05235e-260 - 1.00066e-260i*
0.0	1000 Z 60°	Ob	-4.98269e+05 + 8.65025e+05i	-0.00000e+00 - 0.00000e+00i	$\pm \infty$	$\pm \infty$	$\pm \infty$	$\pm \infty$	$\pm \infty$	$\pm \infty$
0.0	1000 Z 75°	Ob	-8.64095e+05 + 4.99482e+05i	-0.00000e+00 - 0.00000e+00i	$\pm \infty$	$\pm \infty$	$\pm \infty$	$\pm \infty$	$\pm \infty$	$\pm \infty$
0.0	1000 Z 90°	Ob	-9.98001e+05 + 1.22342e-10i	-0.00000e+00 - 0.00000e+00i	$\pm \infty$	$\pm \infty$	$\pm \infty$	$\pm \infty$	$\pm \infty$	$\pm \infty$
0.0	1500 Z 0°	Pr	1.49925e+03 - 0.00000e+00i	-0.00000e+00 - 0.00000e+00i	-1.39104e+01 - 0.00000e+00i	-8.20917e-02 - 0.00000e+00i	-8.17184e-19 - 0.00000e+00i	-5.09264e-85 - 0.00000e+00i	-6.41043e-218 + 3.92358e-234i*	± 0
0.0	1500 Z 15°	Pr	1.44814e+03 + 3.88229e+02i	-0.00000e+00 - 0.00000e+00i	-1.35381e+01 - 3.34914e+00i	1.19909e-02 + 1.05385e-01i	-3.63389e-18 - 1.98722e-18i	-4.09291e-83 + 4.77797e-82i	-1.50806e-210 + 1.46042e-210i*	± 0
0.0	1500 Z 30°	Pr	1.29829e+03 + 7.50000e+02i	-0.00000e+00 - 0.00000e+00i	-1.24224e+01 - 6.56782e+00i	2.23814e-01 - 2.10962e+00i	1.28854e-16 - 4.65263e-16i	-2.10864e-73 - 1.36317e-73i	1.08597e-188 + 1.99022e-188i*	± 0
0.0	1500 Z 45°	Pr	1.05991e+03 + 1.06066e+03i	-0.00000e+00 - 0.00000e+00i	-1.05716e+01 - 9.51260e-01i	1.34061e-01 - 7.30433e-01i	-8.60675e-14 + 9.31806e-13i	1.85810e-59 + 1.04040e-60i	-2.50695e-153 + 4.35484e-154i*	± 0
0.0	1500 Z 60°	Ob	-1.12240e+06 + 1.94706e+06i	-0.00000e+00 - 0.00000e+00i	$\pm \infty$	$\pm \infty$	$\pm \infty$	$\pm \infty$	$\pm \infty$	$\pm \infty$
0.0	1500 Z 75°	Ob	-1.94566e+06 + 1.12422e+06i	-0.00000e+00 - 0.00000e+00i	$\pm \infty$	$\pm \infty$	$\pm \infty$	$\pm \infty$	$\pm \infty$	$\pm \infty$
0.0	1500 Z 90°	Ob	-2.24700e+06 + 2.75362e-10i	-0.00000e+00 - 0.00000e+00i	$\pm \infty$	$\pm \infty$	$\pm \infty$	$\pm \infty$	$\pm \infty$	$\pm \infty$
0.0	2500 Z 0°	Pr	2.49925e+03 - 0.00000e+00i	-0.00000e+00 - 0.00000e+00i	-2.20577e+01 - 0.00000e+00i	-9.10556e-04 - 0.00000e+00i	-2.20597e-32 - 0.00000e+00i	-5.55212e-143 + 3.39722e-159i*	± 0	± 0
0.0	2500 Z 15°	Pr	2.41406e+03 + 6.47048e+02i	-0.00000e+00 - 0.00000e+00i	-2.15711e+01 - 5.03990e+00i	1.37773e-03 + 2.22483e-04i	-4.46531e-32 + 3.26852e-31i	-1.62005e-139 - 5.01999e-138i*	± 0	± 0
0.0	2500 Z 30°	Pr	2.16631e+03 + 1.25000e+03i	-0.00000e+00 - 0.00000e+00i	-2.00870e+01 - 9.98330e+00i	-4.16289e+03 - 2.51435e-03i	-9.24706e-29 + 9.12840e-28i	1.54554e-123 - 7.27747e-124i*	2.33825e-316 + 1.72524e-315i*	± 0
0.0	2500 Z 45°	Pr	1.76702e+03 + 1.76777e+03i	-0.00000e+00 - 0.00000e+00i	-1.75422e+01 - 1.46924e+01i	7.85389e+03 + 3.48840e-02i	-1.00090e-22 - 2.57693e-22i	2.02979e-100 - 9.32837e-101i*	-3.31800e-257 + 3.29472e-257i*	± 0
0.0	2500 Z 60°	Ob	-3.12067e+06 + 5.41016e+06i	-0.00000e+00 - 0.00000e+00i	$\pm \infty$	$\pm \infty$	$\pm \infty$	$\pm \infty$	$\pm \infty$	$\pm \infty$
0.0	2500 Z 75°	Ob	-5.40783e+06 + 3.12371e+06i	-0.00000e+00 - 0.00000e+00i	$\pm \infty$	$\pm \infty$	$\pm \infty$	$\pm \infty$	$\pm \infty$	$\pm \infty$
0.0	2500 Z 90°	Ob	-6.24500e+06 + 7.65998e-10i	-0.00000e+00 - 0.00000e+00i	$\pm \infty$	$\pm \infty$	$\pm \infty$	$\pm \infty$	$\pm \infty$	$\pm \infty$
0.0	5000 Z 0°	Pr	4.99925e+03 - 0.00000e+00i	-0.00000e+00 - 0.00000e+00i	-3.89374e+01 - 0.00000e+00i	-6.57781e-09 - 0.00000e+00i	-1.47248e-06 - 0.00000e+00i	-3.84140e-288 + 2.35129e-304i*	± 0	± 0
0.0	5000 Z 15°	Pr	4.82888e+03 + 1.29410e+03i	-0.00000e+00 - 0.00000e+00i	-3.85101e+01 - 7.69146e+00i	-1.54252e-08 - 9.00153e-10i	3.29275e-64 + 3.17173e-66i	2.97756e-278 + 1.00808e-278i*	± 0	± 0
0.0	5000 Z 30°	Pr	4.32938e+03 + 2.50000e+03i	-0.00000e+00 - 0.00000e+00i	-3.71068e+01 - 1.56304e+01i	-1.60229e-07 - 1.00151e-07i	2.41627e-57 - 8.05871e-58i	-6.03776e-250 + 3.58596e-249i*	± 0	± 0
0.0	5000 Z 45°	Pr	3.53478e+03 + 3.53553e+03i	-0.00000e+00 - 0.00000e+00i	-3.43717e+01 - 2.39578e+01i	3.40316e-06 - 9.55435e-06i	1.01989e-47 - 2.30995e-46i	4.75314e-204 + 6.19955e-203i*	± 0	± 0
0.0	5000 Z 60°	Ob	-1.24913e+07 + 2.16456e+07i	-0.00000e+00 - 0.00000e+00i	$\pm \infty$	$\pm \infty$	$\pm \infty$	$\pm \infty$	$\pm \infty$	$\pm \infty$
0.0	5000 Z 75°	Ob	-2.16410e+07 + 1.24974e+07i	-0.00000e+00 - 0.00000e+00i	$\pm \infty$	$\pm \infty$	$\pm \infty$	$\pm \infty$	$\pm \infty$	$\pm \infty$
0.0	5000 Z 90°	Ob	-2.49900e+07 + 3.06100e-09i	-0.00000e+00 - 0.00000e+00i	$\pm \infty$	$\pm \infty$	$\pm \infty$	$\pm \infty$	$\pm \infty$	$\pm \infty$
0.1	25 Z 0°	Pr	7.32096e+01 - 0.00000e+00i	1.00000e+00 - 0.00000e+00i	9.96443e-01 - 0.00000e+00i	6.76072e-01 - 0.00000e+00i	-2.49679e-01 - 0.00000e+00i	-2.43832e-01 - 0.00000e+00i	-6.48883e-03 - 0.00000e+00i	-4.17265e-07 + 2.54474e-23i*
0.1	25 Z 15°	Pr	7.06557e+01 + 1.94227e+01i	1.00000e+00 + 5.55112e-17i	9.96570e-01 - 9.69232e-04i	6.84348e-01 - 8.02644e-02i	-2.66368e-01 - 1.50960e-01i	-2.36303e-01 + 1.42785e-01i	2.78808e-03 + 8.24096e-03i	-4.37257e-07 - 7.62131e-07i*
0.1	25 Z 30°	Pr	6.31681e+01 + 3.75213e+01i	1.00000e+00 - 0.00000e+00i	9.96943e-01 - 1.87296e-03i	7.09362e-01 - 1.58244e-01i	-3.15260e-01 + 3.26193e-01i	-2.02498e-01 + 3.41435e-01i	1.79680e-02 - 9.96396e-03i	6.07582e-06 - 4.86999e-06i*
0.1	25 Z 45°	Ob	3.43483e+01 + 5.89637e+01i	1.00000e+00 + 4.44089e-16i	9.98238e-01 - 2.94666e-02i	-5.36305e-01 - 2.52323e-02i	-9.72395e+00 + 3.18547e+01i	-1.91777e+03 - 1.28732e+03i	1.27479e+05 - 1.04188e+05i	2.14593e+06 - 9.85451e+06i
0.1	25 Z 60°	Ob	-2.70208e+02 + 5.16261e+02i	1.00000e+00 - 3.88578e-16i	1.01353e+00 - 2.59309e-01i	1.27532e+00 - 3.70388e+00i	-9.00031e+01 - 1.70134e+01i	1.68488e+04 + 6.23488e+02i	-3.24114e+06 - 1.77224e+06i	5.06108e+08 - 1.00994e+08i
0.1	25 Z 75°	Ob	-4.93980e+02 + 2.99556e+02i	1.00000e+00 - 1.38778e-16i	1.02486e+00 - 1.51024e-02i	4.10640e+00 - 3.03932e+00i	-7.66603e+01 - 1.67982e+01i	-5.85801e+04 + 5.38345e+03i	2.90777e+06 - 2.09496e+07i	6.08090e+09 - 7.31046e+09i
0.1	25 Z 90°	Ob	-5.76010e+02 + 7.34781e-14i	1.00000e+00 + 5.69686e-17i	1.02904e+00 + 5.49135e-17i	5.59402e+00 - 5.22933e-16i	2.08110e+02 - 6.72721e-14i	9.00923e+04 - 6.37816e-11i	4.00825e+07 - 4.37112e-08i	1.42407e+10 - 2.07606e-05i
0.1	50 Z 0°	Pr</								

Table D.54: (continued)

m, n	$c \setminus \arg(c)$	type	$\lambda_{mn}^{(a)'}$	$S_{mn}^{(a)'}(c, \eta=0)$	$S_{mn}^{(a)'}(c, \eta=0.01)$	$S_{mn}^{(a)'}(c, \eta=0.1)$	$S_{mn}^{(a)'}(c, \eta=0.25)$	$S_{mn}^{(a)'}(c, \eta=0.5)$	$S_{mn}^{(a)'}(c, \eta=0.75)$	$S_{mn}^{(a)'}(c, \eta=0.99)$
0.1	$500 \setminus 15^\circ$	Pr	1.44714e+03 + 3.88229e+02i	1.00000e+00 + 5.55112e-17i	9.29073e-01 - 1.86457e-02i	-3.43920e-01 + 1.14814e-01i	5.44922e-06 + 4.56131e-06i	2.75756e-27 - 1.32307e-26i	-6.05634e-69 - 2.79467e-69i	8.76603e-177 - 1.18637e-176i
0.1	$500 \setminus 30^\circ$	Pr	1.29729e+03 + 7.50001e+02i	1.00000e+00 + 5.55112e-17i	9.36008e-01 - 3.61702e-02i	-3.93886e-01 + 2.74176e-01i	-1.53501e-05 + 3.12726e-05i	-2.34556e-25 + 1.09010e-25i	1.11986e-61 + 9.60157e-62i	-5.31268e-158 + 3.45982e-158i
0.1	$500 \setminus 45^\circ$	Ob	7.06106e+02 + 2.49239e+05i	1.00000e-00 + 1.03806e-14i	-1.56994e+01 + 6.51434e-00i	-7.18266e+14 + 7.36241e+14i	8.88183e+37 - 4.00491e+37i	1.30919e+76 - 1.48212e+76i	1.21939e+114 - 3.94418e+114i	-6.87526e+150 + 2.48346e+151i
0.1	$500 \setminus 60^\circ$	Ob	-1.24135e+05 + 2.16006e+05i	1.00000e-00 + 4.77396e-15i	-3.01292e+01 - 2.24995e+01i	2.87922e+18 + 3.84585e+17i	3.90401e+46 + 1.34575e+46i	2.79788e+93 + 2.18887e+93i	1.70941e+140 + 2.63766e+140i	-2.90655e+185 - 2.37376e+185i
0.1	$500 \setminus 75^\circ$	Ob	-2.15541e+05 + 1.24741e+05i	1.00000e-00 + 8.43769e-15i	1.69286e+01 - 5.96023e+01i	3.99231e+20 - 1.56944e+20i	6.48640e+51 - 8.81464e+51i	-7.42170e+103 - 2.38214e+104i	-5.53056e+156 - 1.90884e+156i	-8.67293e+206 - 7.15809e+206i
0.1	$500 \setminus 90^\circ$	Ob	-2.49001e+05 + 3.05549e-11i	1.00000e-00 - 1.31457e-17i	7.34760e+01 - 2.34593e-14i	2.35690e+21 - 7.24689e+06i	7.74386e+53 - 5.93735e+39i	1.24924e+108 - 1.91398e+94i	2.07276e+162 - 4.76222e+148i	2.37740e+214 - 7.20902e+200i
0.1	$750 \setminus 20^\circ$	Pr	2.24825e+03 - 0.00000e+00i	1.00000e-00 - 0.00000e+00i	8.91127e-01 - 0.00000e+00i	-1.52976e-01 - 0.00000e+00i	-2.23656e-09 - 0.00000e+00i	-5.89882e-42 - 0.00000e+00i	-5.45686e-108 + 3.33861e-124i	-5.40985e-276 + 3.31215e-292i
0.1	$750 \setminus 15^\circ$	Pr	2.17158e+03 + 5.82343e+02i	1.00000e-00 - 2.77556e-17i	8.94507e-01 - 2.74062e-02i	-1.36984e-01 + 1.08811e-01i	-4.66653e-09 - 1.90164e-09i	-1.48380e-40 + 1.03744e-40i	2.71582e-104 + 1.54211e-104i	1.84495e-266 + 6.73638e-268i
0.1	$750 \setminus 30^\circ$	Pr	1.94681e+03 + 1.12500e+03i	1.00000e+00 + 5.55112e-17i	9.04503e-01 - 5.32740e-02i	-7.42408e-02 + 2.48288e-01i	-2.00866e-08 - 5.06955e-08i	-3.53011e-36 - 2.17320e-36i	-2.32696e-93 + 2.26410e-93i	-6.99862e-239 + 1.48749e-238i
0.1	$750 \setminus 45^\circ$	Ob	1.05966e+03 + 5.61439e+05i	1.00000e-00 - 2.78666e-14i	5.54371e+01 + 8.26304e+01i	-4.55419e-02 + 1.78797e+22i	1.22355e+57 - 9.02523e+56i	1.42174e+114 - 4.60108e+114i	-5.17122e+171 - 1.48121e+172i	-2.42222e+227 + 9.69084e+226i
0.1	$750 \setminus 60^\circ$	Ob	-2.79952e+05 + 4.86389e+05i	1.00000e+00 + 1.02696e-14i	-2.68899e+02 + 1.87299e+02i	7.19756e+27 + 1.45259e+27i	1.16558e+70 + 6.33505e+69i	1.99427e+140 + 3.07651e+140i	8.04954e+209 + 1.03907e+211i	3.93370e+278 - 2.36815e+278i
0.1	$750 \setminus 75^\circ$	Ob	-4.85691e+05 + 2.80862e+05i	-0.00000e+00 - 0.00000e+00i	$\pm \infty$	$\pm \infty$	$\pm \infty$	$\pm \infty$	$\pm \infty$	$\pm \infty$
0.1	$750 \setminus 90^\circ$	Ob	-5.61001e+05 + 6.87945e-11i	-0.00000e+00 - 0.00000e+00i	$\pm \infty$	$\pm \infty$	$\pm \infty$	$\pm \infty$	$\pm \infty$	$\pm \infty$
0.1	$1000 \setminus 20^\circ$	Pr	2.99825e+03 - 0.00000e+00i	1.00000e-00 - 0.00000e+00i	8.56273e-01 - 0.00000e+00i	-6.05145e-02 - 0.00000e+00i	-1.06986e-12 - 0.00000e+00i	-2.24024e-56 - 0.00000e+00i	-1.26868e-144 + 7.76358e-161i	± 0
0.1	$1000 \setminus 15^\circ$	Pr	2.89603e+03 + 7.76457e+02i	1.00000e-00 - 0.00000e+00i	8.60589e-01 - 3.58042e-02i	-3.85448e-02 + 6.09196e-02i	3.10276e-13 + 3.14329e-12i	2.12984e-54 + 3.11857e-55i	-1.07132e-139 - 7.34116e-140i	± 0
0.1	$1000 \setminus 30^\circ$	Pr	2.59633e+03 + 1.50000e+03i	1.00000e-00 - 0.00000e+00i	8.73389e-01 - 6.97413e-02i	4.20491e-02 + 1.12824e-01i	7.05783e-11 + 2.68066e-11i	1.23579e-48 - 6.55734e-49i	-3.99543e-125 - 4.93141e-125i	4.28009e-320 + 3.76028e-319i
0.1	$1000 \setminus 45^\circ$	Ob	1.41321e+03 + 9.98586e+05i	1.00000e-00 - 1.59317e-14i	4.11132e+02 + 4.13176e+02i	-5.77366e+28 - 2.32656e+30i	1.57048e+76 - 1.77851e+76i	-1.45167e+152 - 1.16376e+153i	-4.92366e+229 - 3.36286e+229i	-2.26610e+303 - 1.35721e+303i
0.1	$1000 \setminus 60^\circ$	Ob	-4.98296e+05 + 8.65025e+05i	-0.00000e+00 - 0.00000e+00i	$\pm \infty$	$\pm \infty$	$\pm \infty$	$\pm \infty$	$\pm \infty$	$\pm \infty$
0.1	$1000 \setminus 75^\circ$	Ob	-8.64095e+05 + 4.99482e+05i	-0.00000e+00 - 0.00000e+00i	$\pm \infty$	$\pm \infty$	$\pm \infty$	$\pm \infty$	$\pm \infty$	$\pm \infty$
0.1	$1000 \setminus 90^\circ$	Ob	-9.98001e+05 + 1.22342e-10i	-0.00000e+00 - 0.00000e+00i	$\pm \infty$	$\pm \infty$	$\pm \infty$	$\pm \infty$	$\pm \infty$	$\pm \infty$
0.1	$1500 \setminus 20^\circ$	Pr	4.49825e+03 - 0.00000e+00i	1.00000e-00 - 0.00000e+00i	7.88739e-01 - 0.00000e+00i	-7.68087e-03 - 0.00000e+00i	-2.05377e-19 - 0.00000e+00i	-2.72189e-85 - 0.00000e+00i	-5.78087e-218 + 3.53825e-234i	± 0
0.1	$1500 \setminus 15^\circ$	Pr	4.34492e+03 + 1.16469e+03i	1.00000e-00 - 0.00000e+00i	7.94661e-01 - 5.15484e-02i	9.42188e-04 + 9.90511e-03i	-9.12212e-19 - 5.02169e-19i	-2.20538e-83 + 2.55379e-82i	-1.35962e-210 - 1.31746e-210i	± 0
0.1	$1500 \setminus 30^\circ$	Pr	3.89536e+03 + 2.25000e+03i	1.00000e-00 - 0.00000e+00i	8.12330e-01 - 1.00818e-01i	2.12124e-02 - 1.24421e-03i	3.30615e-17 - 1.16926e-16i	-1.12645e-73 - 7.30340e-74i	9.78433e-189 + 1.79561e-188i	± 0
0.1	$1500 \setminus 45^\circ$	Ob	2.12032e+03 + 2.24788e+06i	-0.00000e+00 - 0.00000e+00i	$\pm \infty$	$\pm \infty$	$\pm \infty$	$\pm \infty$	$\pm \infty$	$\pm \infty$
0.1	$1500 \setminus 60^\circ$	Ob	-1.12240e+06 + 1.94706e+06i	-0.00000e+00 - 0.00000e+00i	$\pm \infty$	$\pm \infty$	$\pm \infty$	$\pm \infty$	$\pm \infty$	$\pm \infty$
0.1	$1500 \setminus 75^\circ$	Ob	-1.94566e+06 + 1.12422e+06i	-0.00000e+00 - 0.00000e+00i	$\pm \infty$	$\pm \infty$	$\pm \infty$	$\pm \infty$	$\pm \infty$	$\pm \infty$
0.1	$1500 \setminus 90^\circ$	Ob	-2.24700e+06 + 2.75362e-10i	-0.00000e+00 - 0.00000e+00i	$\pm \infty$	$\pm \infty$	$\pm \infty$	$\pm \infty$	$\pm \infty$	$\pm \infty$
0.1	$2500 \setminus 20^\circ$	Pr	7.49825e+03 - 0.00000e+00i	1.00000e-00 - 0.00000e+00i	6.62011e-01 - 0.00000e+00i	-8.76320e-05 - 0.00000e+00i	-5.56803e-33 - 0.00000e+00i	-2.97063e-143 + 1.81766e-159i	± 0	± 0
0.1	$2500 \setminus 15^\circ$	Pr	7.24269e+03 + 1.94114e+03i	1.00000e-00 + 2.77556e-17i	6.70180e-01 - 7.90718e-02i	1.32550e-04 + 2.8279e-05i	-1.14108e-32 + 8.24992e-32i	-8.55750e-140 - 2.68610e-138i	± 0	± 0
0.1	$2500 \setminus 30^\circ$	Pr	6.49344e+03 + 3.75000e+03i	1.00000e-00 - 0.00000e+00i	6.94872e-01 - 1.55894e-01i	-3.99767e-04 - 2.51725e-04i	-2.41027e-29 + 2.30531e-28i	8.27421e-124 - 3.88801e-124i	2.10441e-316 + 1.55675e-315i	± 0
0.1	$2500 \setminus 45^\circ$	Ob	3.53453e+03 + 6.24646e+06i	-0.00000e+00 - 0.00000e+00i	$\pm \infty$	$\pm \infty$	$\pm \infty$	$\pm \infty$	$\pm \infty$	$\pm \infty$
0.1	$2500 \setminus 60^\circ$	Ob	-3.12067e+06 + 5.41016e+06i	-0.00000e+00 - 0.00000e+00i	$\pm \infty$	$\pm \infty$	$\pm \infty$	$\pm \infty$	$\pm \infty$	$\pm \infty$
0.1	$2500 \setminus 75^\circ$	Ob	-5.40783e+06 + 3.12371e+06i	-0.00000e+00 - 0.00000e+00i	$\pm \infty$	$\pm \infty$	$\pm \infty$	$\pm \infty$	$\pm \infty$	$\pm \infty$
0.1	$2500 \setminus 90^\circ$	Ob	-6.24500e+06 + 7.65998e-10i	-0.00000e+00 - 0.00000e+00i	$\pm \infty$	$\pm \infty$	$\pm \infty$	$\pm \infty$	$\pm \infty$	$\pm \infty$
0.1	$5000 \setminus 20^\circ$	Pr	1.49982e+04 - 0.00000e+00i	1.00000e-00 - 0.00000e+00i	3.89500e-01 - 0.00000e+00i	-6.46243e-10 - 0.00000e+00i	-3.72863e-67 - 0.00000e+00i	-2.05696e-288 + 1.25905e-304i	± 0	± 0
0.1	$5000 \setminus 15^\circ$	Pr	1.44871e+04 + 3.88229e+03i	1.00000e-00 - 0.00000e+00i	3.98792e-01 - 1.27711e-01i	-1.51605e-09 - 9.65049e-11i	8.33877e-65 + 8.72516e-67i	1.59455e-278 - 5.39486e-279i	± 0	± 0
0.1	$5000 \setminus 30^\circ$	Pr	1.29886e+04 + 7.50000e+03i	1.00000e-00 + 5.55112e-17i	4.28052e-01 - 2.56725e-01i	-1.56844e-08 - 1.00271e-08i	6.12440e-58 - 2.03169e-58i	-3.24104e-250 + 1.92026e-249i	± 0	± 0
0.1	$5000 \setminus 45^\circ$	Ob	7.07007e+03 + 2.49929e+07i	-0.00000e+00 - 0.00000e+00i	$\pm \infty$	$\pm \infty$	$\pm \infty$	$\pm \infty$	$\pm \infty$	$\pm \infty$
0.1	$5000 \setminus 60^\circ$	Ob	-1.24913e+07 + 2.16456e+07i	-0.00000e+00 - 0.00000e+00i	$\pm \infty$	$\pm \infty$	$\pm \infty$	$\pm \infty$	$\pm \infty$	$\pm \infty$
0.1	$5000 \setminus 75^\circ$	Ob	-2.16410e+07 + 1.24974e+07i	-0.00000e+00 - 0.00000e+00i	$\pm \infty$	$\pm \infty$	$\pm \infty$	$\pm \infty$	$\pm \infty$	$\pm \infty$
0.1	$5000 \setminus 90^\circ$	Ob	-2.49900e+07 + 3.06100e-09i	-0.00000e+00 - 0.00000e+00i	$\pm \infty$	$\pm \infty$	$\pm \infty$	$\pm \infty$	$\pm \infty$	$\pm \infty$
0.2	$25 \setminus 0^\circ$	Pr	1.21126e+02 - 0.00000e+00i	-0.00000e+00 - 0.00000e+00i	6.04364e-01 - 0.00000e+00i	4.88734e-01 - 0.00000e+00i	2.90633e-01 - 0.00000e+00i	-2.26531e+00 - 0.00000e+00i	-1.26592e-01 + 7.46495e-181i	-1.65917e-05 + 1.01141e-211i
0.2	$25 \setminus 15^\circ$	Pr	1.16872e+02 + 3.23877e+01i	-0.00000e+00 - 0.00000e+00i	5.83279e-01 + 1.61272e-01i	4.82275e-01 + 1.02523e-01i	3.22737e-01 - 1.03973e-01i	-2.62076e+00 + 3.99851e-01i	3.43765e-03 + 1.71085e-01i	-8.00346e-06 + 3.42512e-05i
0.2	$25 \setminus 30^\circ$	Pr	1.04401e+02 + 6.25665e+01i	-0.00000e+00 - 0.00000e+00i	5.21422e-01 + 3.11686e-01i	4.62927e+00 + 2.08165e-01i	4.27889e+00 - 2.02762e+00i	-3.96054e+00 + 1.17802e+00i	4.11224e-01 + 4.08335e-03i	3.15761e-04 + 3.17550e-05i
0.2	$25 \setminus 45^\circ$	Ob	3.43483e+01 + 5.89637e+02i	-0.00000e+00 - 0.00000e+00i	2.00620e-01 + 2.94492e-01i	2.81201e+01 + 1.81439e+01i	-2.00964e+02 - 3.51518e+02i	2.73670e+04 - 6.24011e+04i	-1.40415e+05 + 1.99584e+05i	-1.05059e-08 + 6.31217e-07i
0.2	$25 \setminus 60^\circ$	Ob	1.17465e+01 + 2.16575e+01i	-0.00000e+00 - 0.00000e+00i	5.88178e-02 + 1.08165e-01i	6.64284e-01 + 9.59786e-01i	2.02847e+00 + 8.26351e+01i	-3.71436e-01 - 1.43330e+00i	2.72394e-01 + 9.51523e-03i	1.18097e-03 + 6.29046e-03i
0.2	$25 \setminus 75^\circ$	Ob	-4.01534e+02 + 2.73631e+02i	-0.00000e+00 - 0.00000e+00i	-2.01496e+00 + 1.38660e+00i	-2.58885e+01 + 3.71215e+01i	3.74229e+02 + 1.01718e+03i	1.84193e+05 - 8.06937e+04i	-1.30723e+07 - 2.33944e+07i	1.87871e+09 - 1.50115e+08i
0.2	$25 \setminus 90^\circ$	Ob	-4.80164e+02 + 7.34446e-14i	-0.00000e+00 - 0.00000e+00i	-2.42022e+00 + 1.12813e-16i</					

Table D.54: (continued)

m, n	$c \setminus \arg(c)$	type	λ_{mn}'	$S_{mn}'(c, \eta=0)$	$S_{mn}'(c, \eta=0.01)$	$S_{mn}'(c, \eta=0.1)$	$S_{mn}'(c, \eta=0.25)$	$S_{mn}'(c, \eta=0.5)$	$S_{mn}'(c, \eta=0.75)$	$S_{mn}'(c, \eta=0.99)$
0.2	500 \setminus 15 $^\circ$	Pr	2.41106e+03 + 6.47049e+02i	-0.00000e+00 - 0.00000e+00i	1.15779e+01 + 2.96176e+00i	-1.18774e+01 - 1.45007e+00i	7.83797e-04 + 3.50931e-04i	1.62173e-24 + 3.18694e-24i	-2.29742e-66 - 1.91842e-66i	9.98506e-174 + 7.93943e-174i
0.2	500 \setminus 30 $^\circ$	Pr	2.16131e+03 + 1.25000e+03i	-0.00000e+00 - 0.00000e+00i	1.05277e+01 + 5.72742e+00i	-1.74862e+01 - 3.75271e+00i	-3.57966e-03 + 2.26362e-03i	-1.51421e-21 + 2.46014e-21i	2.17965e-59 + 6.25464e-59i	-5.47736e-155 + 2.84867e-156i
0.2	500 \setminus 45 $^\circ$	Ob	7.06106e+02 + 2.49239e+05i	-0.00000e+00 - 0.00000e+00i	1.60906e+03 - 3.92081e+03i	-3.53709e+15 - 2.56755e+17i	-8.57680e+39 + 2.27607e+40i	3.12244e+77 + 4.92697e+78i	4.82290e+116 + 9.10825e+116i	-3.17825e+153 - 5.59351e+153i
0.2	500 \setminus 60 $^\circ$	Pr	2.49250e+02 + 4.33013e+02i	-0.00000e+00 - 0.00000e+00i	1.27688e+00 + 2.11121e+00i	3.12299e-06 - 6.48501e+00i	2.33565e-02 - 3.17391e-03i	4.17450e-13 - 1.84133e-13i	3.37170e-35 - 5.73859e-35i	3.36009e-90 - 5.73409e-91i
0.2	500 \setminus 75 $^\circ$	Ob	-2.13614e+05 + 1.24224e+05i	-0.00000e+00 - 0.00000e+00i	-2.00641e+02 + 1.50949e+04i	-7.00443e+22 + 5.19374e+22i	-5.90584e+53 + 1.51944e+54i	1.10541e+106 + 1.73887e+106i	2.05388e+158 + 1.36772e+157i	9.54905e+206 + 3.14261e+206i
0.2	500 \setminus 90 $^\circ$	Pr	-2.47005e+05 + 3.04325e-11i	-0.00000e+00 - 0.00000e+00i	-1.78946e+04 + 6.96771e-12i	-4.78992e+23 + 1.50634e+09i	-1.15321e+56 + 8.92270e+41i	-1.03131e+110 + 1.58734e+96i	-7.28857e+163 + 1.67972e+150i	-2.08170e+214 + 6.33240e+200i
0.2	750 \setminus 20 $^\circ$	Pr	3.74625e+03 - 0.00000e+00i	-0.00000e+00 - 0.00000e+00i	1.75033e+01 - 0.00000e+00i	-8.84020e+00 - 0.00000e+00i	-4.11909e-07 - 0.00000e+00i	-2.35034e-39 - 0.00000e+00i	-3.67983e-105 + 2.25138e-121i	-7.02483e-273 + 4.30091e-289i
0.2	750 \setminus 15 $^\circ$	Pr	3.61847e+03 + 9.70572e+02i	-0.00000e+00 - 0.00000e+00i	1.70241e+01 + 4.24478e+00i	-9.77305e+00 + 3.26277e+00i	-7.35328e-07 - 5.68166e-07i	-6.78813e-38 + 2.44794e-38i	1.49849e-101 + 1.48030e-101i	2.29121e-263 + 7.05931e-264i
0.2	750 \setminus 30 $^\circ$	Pr	3.24384e+03 + 1.87500e+03i	-0.00000e+00 - 0.00000e+00i	1.55902e+01 + 8.31465e+00i	-1.32262e+01 + 9.07248e+00i	1.64575e-06 - 9.95842e-06i	-7.79715e-34 - 1.45833e-33i	-2.12464e-90 + 5.33571e-91i	-1.75470e-235 + 1.21678e-235i
0.2	750 \setminus 45 $^\circ$	Ob	1.05966e+03 + 5.61439e+05i	-0.00000e+00 - 0.00000e+00i	-3.65833e+04 - 1.71722e+03i	1.67944e+25 - 7.34400e+24i	-8.45126e+58 + 5.63309e+59i	8.43762e+116 + 1.59474e+117i	5.29631e+174 + 2.54902e+174i	3.84108e+229 - 8.98771e+229i
0.2	750 \setminus 60 $^\circ$	Pr	3.74250e+02 + 6.49519e+02i	-0.00000e+00 - 0.00000e+00i	1.93918e+00 + 3.12623e+00i	-3.43227e+00 - 4.63994e+00i	4.98949e-04 - 4.44095e-04i	-1.49819e-20 + 3.32902e-20i	2.04792e-53 + 3.63066e-53i	-8.55056e-137 + 8.46533e-137i
0.2	750 \setminus 75 $^\circ$	Ob	-4.82798e+05 + 2.80085e+05i	-0.00000e+00 - 0.00000e+00i	$\pm \infty$	$\pm \infty$	$\pm \infty$	$\pm \infty$	$\pm \infty$	$\pm \infty$
0.2	750 \setminus 90 $^\circ$	Ob	-5.88005e+05 + 6.86108e-11i	-0.00000e+00 - 0.00000e+00i	$\pm \infty$	$\pm \infty$	$\pm \infty$	$\pm \infty$	$\pm \infty$	$\pm \infty$
0.2	1000 \setminus 20 $^\circ$	Pr	4.99625e+03 - 0.00000e+00i	-0.00000e+00 - 0.00000e+00i	2.28160e+01 - 0.00000e+00i	-5.05260e+00 - 0.00000e+00i	-2.65019e-10 - 0.00000e+00i	-1.19275e-53 - 0.00000e+00i	-1.14189e-141 + 6.98766e-158i	± 0
0.2	1000 \setminus 15 $^\circ$	Pr	4.82588e+03 + 1.29410e+03i	-0.00000e+00 - 0.00000e+00i	2.22425e+01 + 5.40268e+00i	-4.69926e+00 + 3.86451e+00i	-1.32574e-10 + 7.71846e-10i	1.05183e-51 + 4.55763e-52i	-7.59750e-137 - 8.88501e-137i	± 0
0.2	1000 \setminus 30 $^\circ$	Pr	4.32637e+03 + 2.50000e+03i	-0.00000e+00 - 0.00000e+00i	2.05124e+01 + 1.06336e+01i	-2.79824e+00 + 1.00835e+01i	1.16759e-08 + 1.46965e-08i	7.44943e-46 + 2.90874e-47i	-8.86717e-123 + 5.64569e-122i	-2.62055e-316 + 6.01121e-316i
0.2	1000 \setminus 45 $^\circ$	Ob	1.13211e+03 + 9.98586e+05i	-0.00000e+00 - 0.00000e+00i	9.28933e+02 + 2.91230e+05i	8.42949e+32 + 8.00988e+32i	7.43355e+77 + 1.18315e+79i	4.62704e+155 + 3.59545e+155i	2.92727e+232 - 5.53512e+231i	1.27990e+306 - 3.22019e+305i
0.2	1000 \setminus 60 $^\circ$	Pr	4.99250e+02 + 8.66026e+02i	-0.00000e+00 - 0.00000e+00i	2.61538e+00 + 4.11422e+00i	-4.06587e+00 - 6.21005e+00i	4.18636e-06 - 1.62941e-05i	-7.90374e-28 - 2.47278e-27i	-2.31998e-71 - 2.94910e-73i	6.72274e-184 - 3.71358e-183i
0.2	1000 \setminus 75 $^\circ$	Ob	-8.60235e+05 + 4.98447e-05i	-0.00000e+00 - 0.00000e+00i	$\pm \infty$	$\pm \infty$	$\pm \infty$	$\pm \infty$	$\pm \infty$	$\pm \infty$
0.2	1000 \setminus 90 $^\circ$	Ob	-9.94005e+05 + 1.22097e-10i	-0.00000e+00 - 0.00000e+00i	$\pm \infty$	$\pm \infty$	$\pm \infty$	$\pm \infty$	$\pm \infty$	$\pm \infty$
0.2	1500 \setminus 20 $^\circ$	Pr	7.49625e+03 - 0.00000e+00i	-0.00000e+00 - 0.00000e+00i	3.26917e+01 - 0.00000e+00i	-1.03090e+00 - 0.00000e+00i	-7.69677e-17 - 0.00000e+00i	-2.17853e-82 - 0.00000e+00i	-7.81272e-215 + 4.78186e-231i	± 0
0.2	1500 \setminus 15 $^\circ$	Pr	7.24069e+03 + 1.94114e+03i	-0.00000e+00 - 0.00000e+00i	3.20160e+01 + 7.36254e+00i	-2.66073e+01 + 1.31608e+01i	-2.80490e-16 - 2.71657e-16i	-7.70197e-80 + 1.92815e-79i	-1.31298e-207 + 2.19627e-207i	± 0
0.2	1500 \setminus 30 $^\circ$	Pr	6.49144e+03 + 3.75000e+03i	-0.00000e+00 - 0.00000e+00i	2.99371e+01 + 1.46357e+01i	2.51760e+00 + 1.46447e+00i	3.29838e-14 + 3.15512e-14i	-4.86723e-71 - 9.58643e-71i	-7.10434e-187 + 2.76346e-185i	± 0
0.2	1500 \setminus 45 $^\circ$	Ob	2.12032e+03 + 2.24788e+03i	-0.00000e+00 - 0.00000e+00i	$\pm \infty$	$\pm \infty$	$\pm \infty$	$\pm \infty$	$\pm \infty$	± 0
0.2	1500 \setminus 60 $^\circ$	Pr	7.94250e+02 + 1.29904e+03i	-0.00000e+00 - 0.00000e+00i	4.00718e+00 + 6.00925e+00i	1.20316e+00 + 1.28765e+00i	-7.22957e-09 - 5.36562e-09i	-1.08482e-41 + 2.23113e-42i	2.93504e-108 + 5.30638e-108i	-2.70435e-276 + 1.57788e-276i
0.2	1500 \setminus 75 $^\circ$	Ob	-1.93987e+06 + 1.12267e+06i	-0.00000e+00 - 0.00000e+00i	$\pm \infty$	$\pm \infty$	$\pm \infty$	$\pm \infty$	$\pm \infty$	± 0
0.2	1500 \setminus 90 $^\circ$	Ob	-2.24101e+06 + 2.74994e-10i	-0.00000e+00 - 0.00000e+00i	$\pm \infty$	$\pm \infty$	$\pm \infty$	$\pm \infty$	$\pm \infty$	± 0
0.2	2500 \setminus 20 $^\circ$	Pr	1.24962e+04 - 0.00000e+00i	-0.00000e+00 - 0.00000e+00i	4.96333e+01 - 0.00000e+00i	-2.05860e-02 - 0.00000e+00i	-3.50130e-30 - 0.00000e+00i	-3.96959e-140 + 2.42889e-156i	± 0	± 0
0.2	2500 \setminus 15 $^\circ$	Pr	1.20703e+03 + 3.23524e+03i	-0.00000e+00 - 0.00000e+00i	4.90484e+01 + 9.98770e+00i	2.85216e-02 + 1.37989e-02i	-2.04899e-29 + 4.82165e-29i	8.20969e-136 + 3.94643e-135i	± 0	± 0
0.2	2500 \setminus 30 $^\circ$	Pr	1.08216e+04 + 6.25000e+03i	-0.00000e+00 - 0.00000e+00i	4.71198e+01 + 2.02874e+01i	-4.88995e-02 - 1.00930e-01i	-8.63135e-26 + 1.17696e-25i	1.21760e-120 + 1.04510e-121i	-1.34609e-312 + 3.27614e-312i	± 0
0.2	2500 \setminus 45 $^\circ$	Ob	3.53453e+03 + 6.24646e+06i	-0.00000e+00 - 0.00000e+00i	$\pm \infty$	$\pm \infty$	$\pm \infty$	$\pm \infty$	$\pm \infty$	± 0
0.2	2500 \setminus 60 $^\circ$	Pr	1.24925e+03 + 2.16506e+03i	-0.00000e+00 - 0.00000e+00i	6.93281e+00 + 9.47674e+00i	-2.22491e-01 + 8.89338e-02i	3.00617e-16 + 1.88586e-15i	1.49283e-70 + 1.56683e-72i	-3.06639e-181 + 9.20693e-183i	± 0
0.2	2500 \setminus 75 $^\circ$	Ob	-5.39817e+06 + 3.12112e+06i	-0.00000e+00 - 0.00000e+00i	$\pm \infty$	$\pm \infty$	$\pm \infty$	$\pm \infty$	$\pm \infty$	± 0
0.2	2500 \setminus 90 $^\circ$	Ob	-6.23501e+06 + 7.64486e-10i	-0.00000e+00 - 0.00000e+00i	$\pm \infty$	$\pm \infty$	$\pm \infty$	$\pm \infty$	$\pm \infty$	± 0
0.2	5000 \setminus 20 $^\circ$	Pr	2.49962e+04 - 0.00000e+00i	-0.00000e+00 - 0.00000e+00i	7.78806e+01 - 0.00000e+00i	-3.13985e-07 - 0.00000e+00i	-4.71271e-64 - 0.00000e+00i	-5.50449e-285 + 3.36924e-301i	± 0	± 0
0.2	5000 \setminus 15 $^\circ$	Pr	2.41444e+04 + 6.47048e+03i	-0.00000e+00 - 0.00000e+00i	7.86775e+01 + 1.05313e+01i	-6.98186e-07 - 2.42048e-07i	1.01500e-61 + 2.84786e-62i	4.49561e-275 + 2.88594e-276i	± 0	± 0
0.2	5000 \setminus 30 $^\circ$	Pr	2.16449e+04 + 1.25000e+04i	-0.00000e+00 - 0.00000e+00i	8.06128e+01 + 2.30331e+01i	-4.05324e-06 - 8.13223e-06i	7.98893e-55 + 1.66739e-55i	-3.32362e-246 + 4.01510e-246i	± 0	± 0
0.2	5000 \setminus 45 $^\circ$	Ob	7.07007e+03 + 2.49929e+07i	-0.00000e+00 - 0.00000e+00i	$\pm \infty$	$\pm \infty$	$\pm \infty$	$\pm \infty$	$\pm \infty$	± 0
0.2	5000 \setminus 60 $^\circ$	Pr	2.49925e+03 + 4.33013e+03i	-0.00000e+00 - 0.00000e+00i	1.48762e+01 + 1.62928e+01i	-2.14149e-04 - 8.85227e-04i	-4.53592e-33 + 2.15935e-32i	2.87506e-143 + 4.75134e-143i	± 0	± 0
0.2	5000 \setminus 75 $^\circ$	Ob	-2.16217e+07 + 1.24922e+07i	-0.00000e+00 - 0.00000e+00i	$\pm \infty$	$\pm \infty$	$\pm \infty$	$\pm \infty$	$\pm \infty$	± 0
0.2	5000 \setminus 90 $^\circ$	Ob	-2.49700e+07 + 3.05978e-09i	-0.00000e+00 - 0.00000e+00i	$\pm \infty$	$\pm \infty$	$\pm \infty$	$\pm \infty$	$\pm \infty$	± 0
0.3	25 \setminus 0 $^\circ$	Pr	1.67953e+02 - 0.00000e+00i	-1.50000e+00 - 0.00000e+00i	-1.48757e+00 - 0.00000e+00i	-4.28237e-01 - 0.00000e+00i	1.48110e+00 - 0.00000e+00i	-6.34954e-01 - 0.00000e+00i	-9.61377e-02 - 0.00000e+00i	-2.67252e-05 + 1.62830e-21i
0.3	25 \setminus 15 $^\circ$	Pr	1.62005e+02 + 4.53798e+01i	-1.50000e+00 - 8.32667e-17i	-1.48802e+00 + 3.39353e-03i	-4.49175e-01 + 2.50080e-01i	1.59882e+00 + 8.19723e-04i	-8.48527e-01 - 1.30688e-01i	-4.74575e-03 + 1.31430e-01i	-1.15903e-05 - 5.57783e-05i
0.3	25 \setminus 30 $^\circ$	Ob	3.36495e+02 + 4.97956e+02i	-1.50000e+00 + 1.72085e-15i	-1.47483e+00 + 3.71396e-02i	1.46329e+00 + 1.77776e+00i	-8.80500e+00 + 1.04604e+01i	4.56040e+01 - 2.55760e+02i	4.39699e+03 - 2.52974e+03i	7.56686e+04 + 4.80957e+04i
0.3	25 \setminus 45 $^\circ$	Pr	5.12567e+01 + 5.30623e+01i	-1.50000e+00 + 1.11022e-16i	-1.49631e+00 + 3.97440e-03i	-1.12732e+00 + 3.46764e-01i	5.85498e-01 + 8.33475e-01i	1.52389e-01 - 1.04653e+00i	4.74578e-02 + 1.11102e-02i	-4.69168e-05 - 3.69845e-04i
0.3	25 \setminus 60 $^\circ$	Ob	-1.87732e+02 + 4.66179e+02i	-1.50000e+00 - 0.00000e+00i	-1.51412e+00 + 3.50747e-02i	-1.54424e+00 + 4.80277e+00i</				

Table D.54: (continued)

m, n	$c \setminus \arg(c)$	type	$\lambda_{mn}^{(a)'}$	$S_{mn}^{(a)'}(c, \eta=0)$	$S_{mn}^{(a)'}(c, \eta=0.01)$	$S_{mn}^{(a)'}(c, \eta=0.1)$	$S_{mn}^{(a)'}(c, \eta=0.25)$	$S_{mn}^{(a)'}(c, \eta=0.5)$	$S_{mn}^{(a)'}(c, \eta=0.75)$	$S_{mn}^{(a)'}(c, \eta=0.99)$
0.3	500 \setminus 15 $^\circ$	Pr	3.37398e+03 + 9.05870e-02i	-1.50000e+00 - 0.00000e+00i	-1.25439e+00 + 6.37535e-02i	-4.63974e-01 + 4.03027e-01i	1.87798e-04 + 7.96405e-05i	8.62794e-25 - 1.67763e-24i	-2.05733e-66 - 1.72425e-66i	1.72869e-173 - 1.37229e-173i
0.3	500 \setminus 30 $^\circ$	Ob	1.25499e+05 + 2.15640e+05i	-1.50000e+00 + 1.73767e-14i	3.39778e+00 - 8.33578e+00i	-3.81419e+10 - 3.09137e+10i	-1.09833e+26 + 8.27577e+26i	9.34456e+53 + 2.52423e+53i	4.44927e+80 - 1.06514e+81i	-1.67804e+106 + 1.14710e+107i
0.3	500 \setminus 45 $^\circ$	Pr	1.05891e+03 + 1.06066e-03i	-1.50000e+00 - 0.00000e+00i	-1.42074e+00 + 7.72364e-02i	7.62757e-01 - 8.20994e-01i	-3.58211e-04 + 5.48593e-04i	-5.86963e-19 - 3.59023e-19i	9.52395e-50 + 4.83717e-50i	1.13532e-128 + 4.00534e-128i
0.3	500 \setminus 60 $^\circ$	Ob	-1.22407e+05 + 2.15006e+05i	-1.50000e+00 - 6.43929e-15i	4.42984e+01 + 3.30786e+01i	-3.53238e-18 + 4.71065e-17i	-3.51068e+46 - 1.20779e+46i	-1.39673e+93 - 1.08892e+93i	-3.65987e+139 - 5.58849e+139i	1.89383e+183 + 1.00234e+183i
0.3	500 \setminus 75 $^\circ$	Ob	-2.13614e+05 + 1.24224e+05i	-1.50000e+00 - 6.23113e-15i	-2.48883e+01 + 8.76298e+01i	-4.89742e+20 + 1.92588e+20i	-5.82850e+51 + 7.92578e+51i	3.70921e+103 + 1.18690e+104i	1.17529e+156 + 4.02384e+155i	5.07043e+204 + 3.33144e+204i
0.3	500 \setminus 90 $^\circ$	Ob	-2.47005e+05 + 3.04325e-11i	-1.50000e+00 + 3.17905e-17i	-1.08027e+02 + 3.53604e-14i	-2.89133e+21 + 8.91348e+06i	-6.96108e+53 + 5.34284e+39i	-6.22528e+107 + 9.54303e+93i	-4.39959e+161 + 1.01120e+148i	-1.25657e+212 + 3.81463e+198i
0.3	750 \setminus 0 $^\circ$	Pr	5.24324e+03 - 0.00000e+00i	-1.50000e+00 - 0.00000e+00i	-1.12570e+00 - 0.00000e+00i	-5.67088e-01 - 0.00000e+00i	-9.99986e-08 - 0.00000e+00i	-1.24607e-39 - 0.00000e+00i	-3.30685e-105 + 2.02317e-121i	-1.21644e-272 + 7.44755e-289i
0.3	750 \setminus 15 $^\circ$	Pr	5.06435e+03 + 1.35880e+03i	-1.50000e+00 + 2.77556e-17i	-1.13666e+00 + 9.25838e-02i	-6.96954e-01 + 9.74206e-02i	-1.77113e-07 + 1.40401e-07i	-3.60386e-38 + 1.28813e-38i	1.34532e-101 + 1.33218e-101i	3.96744e-263 + 1.22467e-263i
0.3	750 \setminus 30 $^\circ$	Pr	2.81999e+05 + 4.85840e+05i	-1.50000e+00 - 1.04361e-14i	-3.08857e+01 + 6.64014e+01i	6.87704e+15 + 1.12368e+16i	-1.72624e+40 - 2.59147e+40i	5.18806e+80 - 1.24263e+81i	5.87947e+121 - 1.14404e+121i	3.45750e+160 + 5.41947e+160i
0.3	750 \setminus 45 $^\circ$	Pr	1.58924e+03 + 1.59099e+03i	-1.50000e+00 - 1.11022e-16i	-1.38100e+00 + 1.14133e-01i	-1.42374e-01 - 7.11334e-01i	-3.41833e-06 + 1.17381e-06i	2.20954e-29 - 4.88181e-29i	-1.55502e-75 - 4.96438e-76i	-4.95901e-194 - 5.12927e-194i
0.3	750 \setminus 60 $^\circ$	Ob	-2.77358e+05 + 4.84889e+05i	-1.50000e+00 - 1.05471e-14i	3.95348e+02 - 2.75385e+02i	-8.83145e+27 - 1.78104e+27i	-1.04853e+70 - 5.69338e+69i	-9.96929e+139 - 1.53418e+140i	-1.78580e+209 - 2.21390e+210i	-2.27706e+276 + 1.77344e+276i
0.3	750 \setminus 75 $^\circ$	Ob	-4.82798e+05 + 2.80085e+05i	-1.50000e+00 + 5.51381e-10i	3.68899e+02 + 9.50115e+02i	-1.36814e+31 + 8.61440e+30i	2.68863e+77 - 1.60533e+78i	3.21928e+156 + 1.10883e+156i	-2.68649e+234 + 4.95552e+234i	
0.3	750 \setminus 90 $^\circ$	Ob	-5.58005e+05 + 6.86108e-11i	-0.00000e+00 - 0.00000e+00i	$\pm \infty$	$\pm \infty$	$\pm \infty$	$\pm \infty$	$\pm \infty$	$\pm \infty$
0.3	1000 \setminus 0 $^\circ$	Pr	6.99324e+03 - 0.00000e+00i	-1.50000e+00 - 0.00000e+00i	-1.00885e+00 - 0.00000e+00i	-3.81560e-01 - 0.00000e+00i	-6.51070e-11 - 0.00000e+00i	-6.34078e-54 - 0.00000e+00i	-1.02737e-141 + 6.28685e-158i	± 0
0.3	1000 \setminus 15 $^\circ$	Pr	6.75472e+03 + 1.81174e+03i	-1.50000e+00 + 1.10222e-16i	-1.02244e+00 + 1.19475e-01i	-3.92562e-01 + 2.61166e-01i	-3.43274e-11 + 1.89563e-10i	5.58807e-52 + 2.43531e-52i	-6.82910e-137 - 8.00117e-137i	± 0
0.3	1000 \setminus 30 $^\circ$	Ob	5.00999e+05 + 8.64293e+05i	-1.50000e+00 - 3.69704e-14i	7.95418e+01 + 7.62821e+01i	-7.32443e+20 - 3.64584e+21i	1.12128e+54 + 3.02645e+53i	-1.61899e+108 - 9.42575e+107i	2.18585e+162 + 2.20965e+162i	3.41605e+214 + 1.01888e+214i
0.3	1000 \setminus 45 $^\circ$	Pr	2.11957e+03 + 2.11232e+03i	-1.50000e+00 - 0.00000e+00i	-1.34131e+00 + 1.49900e-01i	-3.65911e-01 - 1.80894e-01i	-1.66714e-08 - 5.80284e-09i	3.53738e-39 + 1.10292e-39i	2.19140e-101 + 3.28377e-102i	± 0
0.3	1000 \setminus 60 $^\circ$	Ob	-4.94809e+05 + 8.63025e+05i	-0.00000e+00 - 0.00000e+00i	$\pm \infty$	$\pm \infty$	$\pm \infty$	$\pm \infty$	$\pm \infty$	$\pm \infty$
0.3	1000 \setminus 75 $^\circ$	Ob	-8.60235e+05 + 4.98447e-05i	-0.00000e+00 - 0.00000e+00i	$\pm \infty$	$\pm \infty$	$\pm \infty$	$\pm \infty$	$\pm \infty$	$\pm \infty$
0.3	1000 \setminus 90 $^\circ$	Ob	-9.94005e+05 + 1.22097e-10i	-0.00000e+00 - 0.00000e+00i	$\pm \infty$	$\pm \infty$	$\pm \infty$	$\pm \infty$	$\pm \infty$	$\pm \infty$
0.3	1500 \setminus 0 $^\circ$	Pr	1.04932e+04 - 0.00000e+00i	-1.50000e+00 - 0.00000e+00i	-7.86755e-01 - 0.00000e+00i	-8.76381e-02 - 0.00000e+00i	-1.91274e-17 - 0.00000e+00i	-1.16126e-82 - 0.00000e+00i	-7.03741e-215 + 4.30732e-231i	± 0
0.3	1500 \setminus 15 $^\circ$	Pr	1.01355e+04 + 2.71760e+03i	-1.50000e+00 + 5.55112e-17i	-8.04257e-01 + 1.67702e-01i	-7.62699e-02 + 1.11701e-01i	-6.93656e-17 - 6.79720e-17i	-3.75589e-80 + 1.02746e-79i	-1.18159e-207 - 1.97919e-207i	± 0
0.3	1500 \setminus 30 $^\circ$	Pr	1.12650e+06 + 1.94596e+06i	-0.00000e+00 - 0.00000e+00i	$\pm \infty$	$\pm \infty$	$\pm \infty$	$\pm \infty$	$\pm \infty$	$\pm \infty$
0.3	1500 \setminus 45 $^\circ$	Ob	3.18023e+03 + 3.18198e+03i	-1.50000e+00 - 1.11022e-16i	-1.26210e+00 + 2.18108e-01i	-2.43909e-02 + 1.03711e-01i	3.52281e-14 - 3.52140e-13i	-1.49067e-59 - 8.62818e-61i	3.39275e-153 - 5.86508e-154i	± 0
0.3	1500 \setminus 60 $^\circ$	Ob	-1.11721e+06 + 1.94406e+06i	-0.00000e+00 - 0.00000e+00i	$\pm \infty$	$\pm \infty$	$\pm \infty$	$\pm \infty$	$\pm \infty$	$\pm \infty$
0.3	1500 \setminus 75 $^\circ$	Ob	-1.93987e+06 + 1.12267e+06i	-0.00000e+00 - 0.00000e+00i	$\pm \infty$	$\pm \infty$	$\pm \infty$	$\pm \infty$	$\pm \infty$	$\pm \infty$
0.3	1500 \setminus 90 $^\circ$	Ob	-2.24101e+06 + 2.74994e-10i	-0.00000e+00 - 0.00000e+00i	$\pm \infty$	$\pm \infty$	$\pm \infty$	$\pm \infty$	$\pm \infty$	$\pm \infty$
0.3	2500 \setminus 0 $^\circ$	Pr	1.74932e+04 - 0.00000e+00i	-1.50000e+00 - 0.00000e+00i	-3.86491e-01 - 0.00000e+00i	-1.88582e-03 - 0.00000e+00i	-8.77936e-31 - 0.00000e+00i	-2.12051e-140 + 1.29748e-156i	± 0	± 0
0.3	2500 \setminus 15 $^\circ$	Pr	1.68969e+04 + 4.52933e+03i	-1.50000e+00 - 0.00000e+00i	-4.07028e-01 + 2.43697e-01i	2.59014e-03 + 1.33766e-03i	-5.81158e-30 + 1.20780e-29i	4.40155e-136 - 1.86759e-135i	± 0	± 0
0.3	2500 \setminus 30 $^\circ$	Pr	3.12750e+06 + 5.40833e+06i	-0.00000e+00 - 0.00000e+00i	$\pm \infty$	$\pm \infty$	$\pm \infty$	$\pm \infty$	$\pm \infty$	$\pm \infty$
0.3	2500 \setminus 45 $^\circ$	Pr	5.30155e+05 + 5.30330e+05i	-1.50000e+00 + 3.33067e-16i	-1.10476e+00 + 3.41617e-01i	-9.99205e-04 - 5.13080e-03i	3.75224e-23 + 9.79221e-23i	-1.63065e-100 + 7.47176e-101i	4.24134e-257 + 4.45762e-257i	± 0
0.3	2500 \setminus 60 $^\circ$	Ob	-3.11201e+06 + 5.40516e+06i	-0.00000e+00 - 0.00000e+00i	$\pm \infty$	$\pm \infty$	$\pm \infty$	$\pm \infty$	$\pm \infty$	$\pm \infty$
0.3	2500 \setminus 75 $^\circ$	Ob	-5.29817e+06 + 3.12112e+06i	-0.00000e+00 - 0.00000e+00i	$\pm \infty$	$\pm \infty$	$\pm \infty$	$\pm \infty$	$\pm \infty$	$\pm \infty$
0.3	2500 \setminus 90 $^\circ$	Ob	-6.23501e+06 + 7.64486e-10i	-0.00000e+00 - 0.00000e+00i	$\pm \infty$	$\pm \infty$	$\pm \infty$	$\pm \infty$	$\pm \infty$	$\pm \infty$
0.3	5000 \setminus 0 $^\circ$	Pr	3.49932e+04 - 0.00000e+00i	-1.50000e+00 - 0.00000e+00i	3.89189e-01 - 0.00000e+00i	-3.01719e-08 - 0.00000e+00i	-1.18948e-64 - 0.00000e+00i	-2.94515e-285 + 1.80269e-301i	± 0	± 0
0.3	5000 \setminus 15 $^\circ$	Pr	3.80072e+04 + 9.05867e-03i	-1.50000e+00 - 0.00000e+00i	3.81082e-01 + 3.35536e-01i	-6.69317e-08 - 2.40747e-08i	2.56121e-62 + 7.23274e-63i	2.40555e-275 + 1.53424e-276i	± 0	± 0
0.3	5000 \setminus 30 $^\circ$	Pr	1.25050e+07 + 2.16420e+07i	-0.00000e+00 - 0.00000e+00i	$\pm \infty$	$\pm \infty$	$\pm \infty$	$\pm \infty$	$\pm \infty$	$\pm \infty$
0.3	5000 \setminus 45 $^\circ$	Pr	1.06049e+04 + 1.06066e-04i	-1.50000e+00 - 0.00000e+00i	-7.21906e-01 + 5.80449e-01i	-5.24842e-07 + 1.40920e-06i	-4.07667e-48 + 8.78118e-47i	-3.79058e-204 + 4.98090e-203i	± 0	± 0
0.3	5000 \setminus 60 $^\circ$	Ob	-1.24740e+07 + 2.16356e+07i	-0.00000e+00 - 0.00000e+00i	$\pm \infty$	$\pm \infty$	$\pm \infty$	$\pm \infty$	$\pm \infty$	$\pm \infty$
0.3	5000 \setminus 75 $^\circ$	Ob	-2.16217e+07 + 1.24922e+07i	-0.00000e+00 - 0.00000e+00i	$\pm \infty$	$\pm \infty$	$\pm \infty$	$\pm \infty$	$\pm \infty$	$\pm \infty$
0.3	5000 \setminus 90 $^\circ$	Ob	-2.49700e+07 + 3.05978e-09i	-0.00000e+00 - 0.00000e+00i	$\pm \infty$	$\pm \infty$	$\pm \infty$	$\pm \infty$	$\pm \infty$	$\pm \infty$
0.4	25 \setminus 0 $^\circ$	Pr	2.13649e-02 - 0.00000e+00i	-0.00000e+00 - 0.00000e+00i	-7.98335e-01 - 0.00000e+00i	-5.46812e-00 - 0.00000e+00i	2.21490e+00 - 0.00000e+00i	-6.35966e-01 - 0.00000e+00i	-8.15057e-01 - 0.00000e+00i	-5.01156e-04 + 3.05162e-20i
0.4	25 \setminus 15 $^\circ$	Pr	2.06014e+02 + 5.84142e+01i	-0.00000e+00 - 0.00000e+00i	-7.70127e-01 - 2.17534e-01i	-5.50438e-00 - 8.99966e-01i	2.02036e+00 + 2.71686e+00i	-1.09592e-00 - 2.98704e+00i	-4.42892e-01 + 1.05411e+00i	1.14402e-04 + 1.07441e-03i
0.4	25 \setminus 30 $^\circ$	Pr	3.64945e+02 + 4.97956e+02i	-0.00000e+00 - 0.00000e+00i	-1.27030e+00 - 1.84652e+00i	-1.52136e+01 + 2.40575e+01i	8.21650e+01 - 1.71525e+01i	1.25455e+03 + 9.81784e+02i	1.07305e+03 + 3.10870e+04i	-4.77922e-05 + 2.71753e-05i
0.4	25 \setminus 45 $^\circ$	Pr	8.45599e+01 + 8.84789e+01i	-0.00000e+00 - 0.00000e+00i	-3.17173e-01 - 3.30816e-01i	-3.18243e+00 - 2.38693e+00i	-4.73444e+00 + 2.07231e+00i	5.63931e+00 - 2.20340e+00i	-5.86319e+01 + 1.10777e+01i	5.09460e+03 - 5.86094e-03i
0.4	25 \setminus 60 $^\circ$	Ob	-1.87732e+02 + 4.66179e+02i	-0.00000e+00 - 0.00000e+00i	6.92610e-01 - 1.75920e+00i	-7.94701e+00 - 2.64408e+00i	-3.69101e+02 + 2.46998e+02i	3.67067e+00 - 2.50279e+00i	-2.55196e+06 + 2.02799e+06i	-1.17985e+08 - 3.29946e-07i
0.4	25 \setminus 75 $^\circ$	Ob	5.71888e+00 + 2.41556e+01i	-0.00000e+00 - 0.00000e+0						

Table D.54: (continued)

m, n	$c \setminus \arg(c)$	type	$S_{mn}^{(a)'}(c, \eta=0)$	$S_{mn}^{(a)'}(c, \eta=0.01)$	$S_{mn}^{(a)'}(c, \eta=0.1)$	$S_{mn}^{(a)'}(c, \eta=0.25)$	$S_{mn}^{(a)'}(c, \eta=0.5)$	$S_{mn}^{(a)'}(c, \eta=0.75)$	$S_{mn}^{(a)'}(c, \eta=0.99)$	
0.4	500 \angle 15°	Pr	4.33589e+03 + 1.16469e-03i	-0.00000e+00 - 0.00000e+00i	-1.51670e+01 - 3.74419e+00i	8.37734e+01 - 1.17623e+01i	1.17843e-02 - 1.32714e-03i	1.67281e-22 - 1.82118e-22i	-3.42887e-64 - 4.92001e-64i	8.74191e-171 - 3.77523e-171i
0.4	500 \angle 30°	Ob	1.25499e+05 + 2.15640e+05i	-0.00000e+00 - 0.00000e+00i	7.06245e+02 + 8.88883e+02i	5.72084e+12 - 2.20462e+12i	-8.27509e-28 - 6.34063e+28i	-8.54954e+55 + 8.54447e+55i	-1.13732e+109 - 8.95723e+108i	-1.13732e+109 - 8.95723e+108i
0.4	500 \angle 45°	Pr	1.76401e+03 + 1.76777e+03i	-0.00000e+00 - 0.00000e+00i	-6.61124e+00 - 6.21406e+00i	2.27005e+01 + 0.75776e+01i	-3.96225e-02 + 6.77967e-03i	-2.05684e-17 - 8.99977e-17i	7.34770e-48 + 2.28536e-47i	1.57528e-125 - 8.16733e-126i
0.4	500 \angle 60°	Ob	-1.22407e+05 + 2.15006e+05i	-0.00000e+00 - 0.00000e+00i	-6.82861e+03 - 7.89676e+02i	4.09180e+20 - 1.70136e+20i	4.52894e+48 - 8.95795e+47i	2.18210e+95 + 2.97650e+94i	7.42727e+141 + 3.72030e+141i	-2.66224e+185 + 1.04535e+184i
0.4	500 \angle 75°	Pr	1.28659e+02 + 4.82963e+02i	-0.00000e+00 - 0.00000e+00i	-5.22717e-01 - 1.78749e-01i	-4.39125e+00 - 8.85055e+00i	-9.06201e-02 + 0.80940e-01i	-3.00820e-06 + 1.89578e-06i	-1.07201e-17 - 2.46592e-17i	-9.56201e-46 - 2.27357e-45i
0.4	500 \angle 90°	Ob	-2.45013e+05 + 3.03100e-11i	-0.00000e+00 - 0.00000e+00i	1.31010e+04 - 5.37557e-12i	2.92495e+23 - 9.25982e+08i	5.15665e+55 - 4.00072e+41i	2.55231e+109 - 3.93382e+95i	7.64952e+162 - 1.76458e+149i	3.34460e+211 - 1.02136e+198i
0.4	750 \angle 0°	Pr	6.73923e+03 - 0.00000e+00i	-0.00000e+00 - 0.00000e+00i	-2.24753e+01 - 0.00000e+00i	-9.31463e+00 - 0.00000e+00i	-8.97786e-06 - 0.00000e+00i	-2.46722e-37 - 0.00000e+00i	-1.11177e-102 + 6.80191e-119i*	-7.88602e-270 + 4.82816e-286i*
0.4	750 \angle 15°	Pr	6.50923e+03 + 1.74703e+03i	-0.00000e+00 - 0.00000e+00i	-2.19716e+01 - 5.17264e+00i	-1.31949e-01 - 7.99384e+00i	-1.18558e-05 - 1.65318e-05i	-1.55905e-36 + 5.87556e-37i	3.20008e-99 + 5.50375e-99i	2.27764e-260 + 1.43495e-260i
0.4	750 \angle 30°	Pr	2.81999e+05 + 4.85840e+05i	-0.00000e+00 - 0.00000e+00i	1.80511e+03 - 5.63111e+03i	-2.46764e+18 + 6.60515e+16i	5.82206e+42 - 3.80039e+41i	1.53270e+83 + 2.00429e+83i	-3.63961e+123 + 1.06168e+124i	-1.20329e+163 + 5.47082e+161i
0.4	750 \angle 45°	Pr	2.64790e+03 + 2.65165e+03i	-0.00000e+00 - 0.00000e+00i	-9.91409e+00 - 9.01472e+00i	1.69053e+01 - 1.69573e+01i	-2.98959e-04 - 1.55058e-04i	1.00388e-26 - 3.71234e-27i	-2.51266e-73 - 4.90434e-73i	8.55189e-193 + 6.43445e-191i*
0.4	750 \angle 60°	Ob	-2.77358e+05 + 4.84889e+05i	-0.00000e+00 - 0.00000e+00i	-3.80819e+04 + 8.15742e+04i	1.59439e+30 - 5.40085e+29i	2.22848e+72 - 6.27811e+70i	3.04963e+142 + 1.54505e+142i	2.36418e+212 + 3.41088e+212i	2.01779e+278 - 5.00115e+278i
0.4	750 \angle 75°	Pr	1.93364e+02 + 7.24445e+02i	-0.00000e+00 - 0.00000e+00i	-8.15146e-01 - 2.66289e+00i	7.31208e+00 + 7.84017e+00i	1.49626e-01 + 4.57944e-02i	-6.54801e-11 + 9.14454e-10i	-5.76831e-27 - 1.09251e-26i	-1.22664e-69 - 2.40687e-69i*
0.4	750 \angle 90°	Ob	-5.55013e+05 + 6.84271e-11i	-0.00000e+00 - 0.00000e+00i	$\pm \infty$	$\pm \infty$	$\pm \infty$	$\pm \infty$	$\pm \infty$	$\pm \infty$
0.4	1000 \angle 0°	Pr	8.98924e+03 - 0.00000e+00i	-0.00000e+00 - 0.00000e+00i	-2.87959e+01 - 0.00000e+00i	-1.24281e+01 - 0.00000e+00i	-7.91753e-09 - 0.00000e+00i	-1.68029e-51 - 0.00000e+00i	-4.61339e-139 + 2.82310e-155i*	$\pm \infty$
0.4	1000 \angle 15°	Pr	8.68257e+03 + 2.32937e+03i	-0.00000e+00 - 0.00000e+00i	-2.82660e+01 - 6.32720e+00i	-1.62717e+01 + 2.34606e+00i	-1.02685e-08 + 2.11031e-08i	1.26090e-49 + 1.01069e-49i	-2.02673e-134 + 4.26771e-134i	$\pm \infty$
0.4	1000 \angle 30°	Pr	5.00999e+05 + 8.64293e+05i	-0.00000e+00 - 0.00000e+00i	-2.64390e+04 + 7.02066e+03i	8.40137e+23 + 2.72856e+23i	-2.05404e+56 + 2.05009e+56i	4.06042e+110 + 2.32935e+110i	-7.51089e+164 + 1.97598e+164i	-6.46746e+216 + 6.12493e+216i
0.4	1000 \angle 45°	Pr	3.53178e+03 + 3.53554e+03i	-0.00000e+00 - 0.00000e+00i	-1.32054e-01 - 1.16165e-01i	-3.9476e+00 - 1.81454e+00i	-9.23515e-07 - 2.00084e-06i	4.55105e-37 + 8.77292e-37i	5.91638e-99 + 0.83860e-99i	-8.04592e-257 - 4.87867e-257i*
0.4	1000 \angle 60°	Ob	-4.94809e+05 + 8.63025e+05i	-0.00000e+00 - 0.00000e+00i	$\pm \infty$	$\pm \infty$	$\pm \infty$	$\pm \infty$	$\pm \infty$	$\pm \infty$
0.4	1000 \angle 75°	Pr	2.58069e+02 + 9.65292e+02i	-0.00000e+00 - 0.00000e+00i	-1.12693e+00 - 3.52567e+00i	9.55771e+00 - 3.93375e+00i	1.24101e-02 + 2.36813e-02i	1.59940e-13 + 1.36244e-13i	-2.68502e-36 + 4.27152e-36i	-1.35980e-93 - 2.25042e-93i*
0.4	1000 \angle 90°	Ob	-9.90013e+05 + 2.18252e-10i	-0.00000e+00 - 0.00000e+00i	$\pm \infty$	$\pm \infty$	$\pm \infty$	$\pm \infty$	$\pm \infty$	$\pm \infty$
0.4	1500 \angle 0°	Pr	1.34892e+04 - 0.00000e+00i	-0.00000e+00 - 0.00000e+00i	-3.97972e-01 - 0.00000e+00i	-5.24938e+00 - 0.00000e+00i	-3.54231e-15 - 0.00000e+00i	-4.63318e-80 - 0.00000e+00i	-4.74851e-212 + 2.90637e-228i*	$\pm \infty$
0.4	1500 \angle 15°	Pr	1.30292e+04 + 3.49406e+03i	-0.00000e+00 - 0.00000e+00i	-3.93898e-01 - 1.87668e+00i	1.93223e+00 + 5.84168e+00i	-9.04141e-15 - 1.55696e-14i	-2.51595e-77 + 3.56794e-77i	-4.23154e-205 + 1.49688e-204i	$\pm \infty$
0.4	1500 \angle 30°	Pr	1.12650e+06 + 1.94596e+06i	-0.00000e+00 - 0.00000e+00i	$\pm \infty$	$\pm \infty$	$\pm \infty$	$\pm \infty$	$\pm \infty$	$\pm \infty$
0.4	1500 \angle 45°	Pr	5.29955e+03 + 5.30330e+03i	-0.00000e+00 - 0.00000e+00i	-1.97389e+01 - 1.62396e+01i	-6.65848e+03 - 3.88878e+03i	5.20845e-11 + 1.45905e-11i	-3.96544e-57 + 4.48029e-57i	1.90057e-150 + 1.34444e-150i*	$\pm \infty$
0.4	1500 \angle 60°	Ob	-1.11721e+06 + 1.94406e+06i	-0.00000e+00 - 0.00000e+00i	$\pm \infty$	$\pm \infty$	$\pm \infty$	$\pm \infty$	$\pm \infty$	$\pm \infty$
0.4	1500 \angle 75°	Pr	3.87479e+02 + 1.44889e+03i	-0.00000e+00 - 0.00000e+00i	-1.80725e+00 - 5.21220e+00i	-7.66737e+00 - 2.62644e+00i	-4.96618e+04 + 4.32470e+04i	3.65267e-21 - 8.56318e-21i	-4.63621e-55 + 5.37602e-55i*	-1.33246e-141 + 1.62461e-141i*
0.4	1500 \angle 90°	Ob	-2.23501e+06 + 2.74627e-10i	-0.00000e+00 - 0.00000e+00i	$\pm \infty$	$\pm \infty$	$\pm \infty$	$\pm \infty$	$\pm \infty$	$\pm \infty$
0.4	2500 \angle 0°	Pr	2.24892e+04 - 0.00000e+00i	-0.00000e+00 - 0.00000e+00i	-5.58353e-01 - 0.00000e+00i	-2.09915e-01 - 0.00000e+00i	-2.74142e-28 - 0.00000e+00i	-1.41424e-137 + 8.65330e-154i*	$\pm \infty$	$\pm \infty$
0.4	2500 \angle 15°	Pr	2.17226e+04 + 5.82343e+03i	-0.00000e+00 - 0.00000e+00i	-5.62190e-01 - 8.34166e+00i	2.33496e+01 + 2.28412e-01i	-2.55483e-27 + 3.21485e-27i	6.07308e-133 - 1.12662e-132i*	$\pm \infty$	$\pm \infty$
0.4	2500 \angle 30°	Pr	3.12750e+06 + 5.40833e+06i	-0.00000e+00 - 0.00000e+00i	$\pm \infty$	$\pm \infty$	$\pm \infty$	$\pm \infty$	$\pm \infty$	$\pm \infty$
0.4	2500 \angle 45°	Pr	8.83508e+03 + 8.83884e+03i	-0.00000e+00 - 0.00000e+00i	-3.25161e+01 - 3.23763e+01i	3.75006e+01 - 5.03614e-01i	-1.36805e-20 + 3.01067e-20i	-1.12348e-97 + 4.19776e-98i*	6.93589e-254 + 1.66412e-255i*	$\pm \infty$
0.4	2500 \angle 60°	Ob	-3.11201e+06 + 5.40516e+06i	-0.00000e+00 - 0.00000e+00i	$\pm \infty$	$\pm \infty$	$\pm \infty$	$\pm \infty$	$\pm \infty$	$\pm \infty$
0.4	2500 \angle 75°	Pr	6.46298e+02 + 2.41481e+03i	-0.00000e+00 - 0.00000e+00i	-3.38569e+00 - 8.42154e+00i	7.34984e-01 - 3.61739e+00i	-2.95803e-07 - 8.01808e-09i	2.70622e-36 + 1.52652e-35i*	-8.82748e-93 + 5.51713e-93i*	-8.20990e-238 + 5.59632e-238i*
0.4	2500 \angle 90°	Ob	-6.22501e+06 + 7.63973e-10i	-0.00000e+00 - 0.00000e+00i	$\pm \infty$	$\pm \infty$	$\pm \infty$	$\pm \infty$	$\pm \infty$	$\pm \infty$
0.4	5000 \angle 0°	Pr	4.49891e+02 - 0.00000e+00i	-0.00000e+00 - 0.00000e+00i	-6.81516e-01 - 0.00000e+00i	-7.16272e-06 - 0.00000e+00i	-7.49183e-02 - 0.00000e+00i	-3.93710e-282 + 2.40985e-298i*	$\pm \infty$	$\pm \infty$
0.4	5000 \angle 15°	Pr	4.34559e+04 + 1.16469e+04i	-0.00000e+00 - 0.00000e+00i	-7.20586e-01 + 1.24229e+00i	-1.37536e-05 - 9.86415e-06i	1.43884e-59 + 8.60913e-60i	3.15914e-272 + 6.36040e-273i*	$\pm \infty$	$\pm \infty$
0.4	5000 \angle 30°	Pr	1.25050e+07 + 2.16420e+07i	-0.00000e+00 - 0.00000e+00i	$\pm \infty$	$\pm \infty$	$\pm \infty$	$\pm \infty$	$\pm \infty$	$\pm \infty$
0.4	5000 \angle 45°	Pr	1.76739e+04 + 1.76777e+04i	-0.00000e+00 - 0.00000e+00i	-6.16899e+01 - 2.94563e+01i	-3.38891e-04 + 1.45888e-04i	-4.12524e-44 + 3.73293e-44i	4.36018e-200 + 5.06909e-200i*	$\pm \infty$	$\pm \infty$
0.4	5000 \angle 60°	Ob	-1.24740e+07 + 2.16356e+07i	-0.00000e+00 - 0.00000e+00i	$\pm \infty$	$\pm \infty$	$\pm \infty$	$\pm \infty$	$\pm \infty$	$\pm \infty$
0.4	5000 \angle 75°	Pr	1.29335e+04 + 4.82963e+03i	-0.00000e+00 - 0.00000e+00i	-8.47482e+00 - 1.53979e+01i	1.77198e-01 - 2.27252e-01i	-2.19200e-16 + 6.71437e-16i	-8.56672e-74 + 6.02811e-73i*	-1.48361e-187 + 2.88969e-188i*	$\pm \infty$
0.4	5000 \angle 90°	Ob	-2.49500e+07 + 3.05856e-09i	-0.00000e+00 - 0.00000e+00i	$\pm \infty$	$\pm \infty$	$\pm \infty$	$\pm \infty$	$\pm \infty$	$\pm \infty$
0.5	25 \angle 0°	Pr	2.58164e+02 - 0.00000e+00i	1.87500e+00 - 0.00000e+00i	1.85104e+00 - 0.00000e+00i	-5.01680e-02 - 0.00000e+00i	-1.32269e+00 - 0.00000e+00i	9.15480e-01 - 0.00000e+00i	-5.29904e-01 - 0.00000e+00i	-7.67004e-04 + 4.66718e-20i*
0.5	25 \angle 15°	Pr	2.48858e+02 + 7.15098e+01i	1.87500e+00 + 1.55431e-15i	1.85190e+00 - 6.67559e-03i	-2.73678e-02 - 4.20551e-01i	-1.54282e+00 + 7.44226e-01i	1.02450e+00 - 1.48190e+00i	-3.92842e-01 + 6.70690e-01i	2.55606e-04 - 1.65534e-03i*
0.5	25 \angle 30°	Pr	1.44563e+02 + 8.76615e+01i	1.87500e+00 + 3.33067e-16i	1.86164e+00 - 8.19690e-03i	6.42734e-01 - 6.24106e-01i	-2.46565e+00 - 2.29321e-01i	2.07895e+00 + 2.29321e-01i	-4.01515e-01 + 8.11860e-02i	-6.51282e-04 + 3.69904e-03i*
0.5	25 \angle 45°	Pr	1.00961e+02 + 5.18815e+02i	1.87500e+00 + 2.22045e-16i	1.86552e+00 - 4.85594e-02i	-8.59147e-01 - 3.76888e-01i	-1.00962e+01 + 3.54157e+01i	-1.18455e+03 - 7.04305e+02i	2.54666e+02 - 2.93373e+02i	3.78784e-05 - 3.88913e-05i*
0.5	25 \angle 60°	Pr	3.57328e+01 + 6.49866e+01i	1.87500e+00 + 2.22045e-16i	1.87183e+00 - 6.08704e-03i	1.52099e+00 - 5.53939e-01i	-8.85377e-01 - 1.64810e+00i	2.77892e-01 + 2.76664e+00i	-8.90074e-01 + 8.88611e-02i	-6.69677e-03 - 4.06374e-02i*
0.5										

Table D.54: (continued)

m, n	$c \setminus \arg(c)$	type	$\lambda_{mn}^{(\alpha)}$	$S_{mn}^{(\alpha)'}(c, \eta=0)$	$S_{mn}^{(\alpha)'}(c, \eta=0.01)$	$S_{mn}^{(\alpha)'}(c, \eta=0.1)$	$S_{mn}^{(\alpha)'}(c, \eta=0.25)$	$S_{mn}^{(\alpha)'}(c, \eta=0.5)$	$S_{mn}^{(\alpha)'}(c, \eta=0.75)$	$S_{mn}^{(\alpha)'}(c, \eta=0.99)$
0.5	500 $\angle 15^\circ$	Pr	5.29680e+03 + 1.42352e+03i	1.87500e-00 - 2.77556e-17i	1.39954e-00 - 1.21466e-01i	1.82232e-00 - 6.78010e-01i	2.69899e-03 - 2.10562e-04i	8.81681e-23 - 9.47528e-23i	-3.05283e-64 - 4.40611e-64i	1.51126e-170 - 6.50528e-171i*
0.5	500 $\angle 30^\circ$	Pr	3.02433e+03 + 1.75001e+03i	1.87500e-00 - 1.66533e-16i	1.59696e-00 - 1.54965e-01i	1.17929e-00 - 1.22701e+00i	1.09714e-03 - 6.37420e-04i	1.01368e-21 - 1.61684e-21i	-2.42085e-59 - 7.02530e-59i*	1.18507e-154 - 5.98158e-156i*
0.5	500 $\angle 45^\circ$	Ob	2.11632e+03 + 2.47879e+03i	1.87500e-00 - 9.24261e-15i	-2.88534e-01 + 1.19726e-01i	-1.10122e+15 + 1.12945e+15i	9.97974e+37 - 4.51022e+37i	8.14122e+75 - 9.26077e+75i	3.17361e+113 - 1.05162e+114i	-1.62678e+147 + 1.98483e+149i*
0.5	500 $\angle 60^\circ$	Ob	7.48249e+02 + 1.29904e+03i	1.87500e-00 - 0.00000e+00i	1.80360e-00 - 1.19265e-01i	-1.47974e-00 + 1.99090e+00i	-2.19785e-02 + 2.35784e-03i	-8.38139e-13 + 3.62770e-13i	-1.14539e-34 + 1.93610e-34i*	-2.18517e-89 + 3.67680e-90i*
0.5	500 $\angle 75^\circ$	Ob	-2.11690e+03 + 1.23706e+03i	1.87500e-00 + 1.55431e-15i	3.04897e-01 - 1.07360e-02i	5.00426e-20 - 1.96915e-20i	4.35819e-51 - 5.93383e+51i	-1.54429e+103 - 4.91407e+103i	-2.06848e+155 - 6.98080e+154i	-1.82729e+202 - 4.15915e+201i
0.5	500 $\angle 90^\circ$	Ob	-2.45013e+03 + 3.03100e-11i	1.87500e-00 - 4.64106e-18i	1.32350e-02 - 4.08449e-14i	2.95475e-21 - 9.05329e+06i	5.20888e-53 - 3.98829e+39i	2.57816e+107 - 3.94746e+93i	7.72699e+160 - 1.77460e+147i	3.37848e+209 - 1.02827e+196i
0.5	750 $\angle 20^\circ$	Pr	8.23422e+03 - 0.00000e+00i	1.87500e-00 - 0.00000e+00i	1.15702e-00 - 0.00000e+00i	4.37427e-02 - 0.00000e+00i	-2.12428e-06 - 0.00000e+00i	-1.30083e-37 - 0.00000e+00i	-9.96883e-103 + 6.09899e-119i*	-1.36445e-269 + 8.35376e-286i*
0.5	750 $\angle 15^\circ$	Pr	7.95311e+03 + 2.13527e+03i	1.87500e-00 + 1.11022e-16i	1.17641e-00 - 1.73571e-01i	-1.64666e-01 - 1.03760e-01i	-2.73426e-06 - 3.98093e-06i	-3.98915e-36 + 2.92775e-37i	2.86102e-99 + 4.94123e-99i	3.93914e-260 + 2.48603e-260i*
0.5	750 $\angle 30^\circ$	Pr	4.53988e+03 + 2.62500e+03i	1.87500e-00 + 5.55112e-17i	1.46156e-00 - 2.25784e-01i	1.47823e-00 - 4.90085e-01i	-5.74982e-07 + 3.03097e-06i	5.12226e-34 + 9.70695e-34i	2.38966e-90 - 5.94269e-91i	3.80210e-235 - 2.63083e-235i*
0.5	750 $\angle 45^\circ$	Ob	3.17698e+03 + 5.59318e+03i	1.87500e-00 - 2.05391e-14i	1.87500e-00 + 1.51859e-02i	-6.98569e-22 - 2.74095e-22i	1.37514e+57 - 1.01555e+57i	8.82655e+113 - 2.87255e+114i	-1.39669e+171 - 3.94372e+171i	-1.83360e+225 + 1.10640e+225i*
0.5	750 $\angle 60^\circ$	Pr	1.12325e+03 + 1.94856e+03i	1.87500e-00 + 3.33067e-16i	1.76669e-00 - 1.76996e-01i	1.00278e-00 + 1.77732e-00i	-4.78070e-04 + 4.09761e-04i	3.03360e-20 - 6.65845e-20i	-6.90097e-53 - 1.22918e-52i*	5.56617e-136 - 5.50003e-136i*
0.5	750 $\angle 75^\circ$	Ob	-4.79908e-05 + 2.79309e+03i	1.87500e-00 - 6.89051e-10i	-4.51986e-02 - 1.16406e-03i	1.39836e-31 - 8.80748e-30i	-2.00876e+77 + 1.20231e+78i	-1.33664e+156 - 4.58814e+155i	4.72142e+233 - 8.76939e+233i	-1.39541e+306 + 1.30947e+306i*
0.5	750 $\angle 90^\circ$	Ob	-5.55013e+03 + 6.84271e-11i	-0.00000e-00 - 0.00000e+00i	$\pm \infty$	$\pm \infty$	$\pm \infty$	$\pm \infty$	$\pm \infty$	$\pm \infty$
0.5	1000 $\angle 20^\circ$	Pr	1.09842e+04 - 0.00000e+00i	1.87500e-00 - 0.00000e+00i	9.40168e-01 - 0.00000e+00i	-6.23219e-01 - 0.00000e+00i	-1.90976e-09 - 0.00000e+00i	-8.89605e-52 - 0.00000e+00i	-4.14364e-139 + 2.53563e-155i*	$\pm \infty$
0.5	1000 $\angle 15^\circ$	Pr	1.06094e+04 + 2.84702e+03i	1.87500e-00 - 2.77556e-17i	9.63204e-01 - 2.20271e-01i	-1.01003e-00 - 2.06695e-01i	-2.55633e-09 + 5.06521e-09i	6.66144e-50 + 5.37459e-50i	-1.81549e-134 - 3.83635e-134i	$\pm \infty$
0.5	1000 $\angle 30^\circ$	Pr	6.05542e+03 + 3.50000e+03i	1.87500e-00 + 3.33067e-16i	1.32884e-00 - 2.92324e-01i	4.62871e-01 - 9.75291e-01i	-3.52474e-09 - 4.59771e-09i	-4.95490e-46 - 2.13583e-47i	9.86569e-123 + 6.35421e-122i*	5.68687e-316 + 1.30170e-315i*
0.5	1000 $\angle 45^\circ$	Ob	4.23764e+03 + 9.95757e+03i	1.87500e-00 + 1.21569e-14i	7.55586e-02 - 7.59365e-02i	-8.90963e-28 - 3.56861e-30i	1.76518e-76 - 2.00072e+76i	-9.14821e-151 + 7.26386e+152i	-1.31745e+229 - 8.93354e+228i	-2.04548e+301 - 9.19010e+300i
0.5	1000 $\angle 60^\circ$	Pr	1.49825e+03 + 2.59808e+03i	1.87500e-00 - 2.20458e-16i	1.72912e-00 - 2.33459e-01i	1.47240e-00 - 8.93240e-02i	-4.17136e-06 - 1.53429e-05i	1.56804e-27 + 4.96495e-27i	7.84765e-71 + 1.11519e-72i*	-4.39022e-183 + 2.41513e-182i*
0.5	1000 $\angle 75^\circ$	Ob	-8.56379e+03 + 4.97412e+03i	-0.00000e-00 - 0.00000e+00i	$\pm \infty$	$\pm \infty$	$\pm \infty$	$\pm \infty$	$\pm \infty$	$\pm \infty$
0.5	1000 $\angle 90^\circ$	Ob	-9.90013e+03 + 1.21852e-10i	-0.00000e-00 - 0.00000e+00i	$\pm \infty$	$\pm \infty$	$\pm \infty$	$\pm \infty$	$\pm \infty$	$\pm \infty$
0.5	1500 $\angle 20^\circ$	Pr	1.68442e+04 - 0.00000e+00i	1.87500e-00 - 0.00000e+00i	5.38829e-01 - 0.00000e+00i	-3.88230e-01 - 0.00000e+00i	-8.70064e-16 - 0.00000e+00i	-2.46303e-80 - 0.00000e+00i	-4.27242e-212 + 2.61497e-228i*	$\pm \infty$
0.5	1500 $\angle 15^\circ$	Pr	1.59220e+04 + 4.7052e+03i	1.87500e-00 + 5.55112e-17i	5.65541e-01 - 2.98452e-01i	-3.51652e-01 + 4.09641e-01i	-2.18879e-15 - 3.84961e-15i	-1.34187e-77 + 1.89446e-77i	-3.79558e-205 - 1.34730e-204i*	$\pm \infty$
0.5	1500 $\angle 30^\circ$	Pr	9.08651e+03 + 5.25000e+03i	1.87500e-00 + 5.55112e-17i	1.07141e+00 - 1.43050e-01i	-2.61435e-01 - 1.87217e-01i	-1.03886e-14 - 9.71636e-15i	3.22827e-71 + 6.40086e-71i	8.36193e-187 - 3.11242e-185i*	$\pm \infty$
0.5	1500 $\angle 45^\circ$	Ob	6.35896e+03 + 2.24364e+03i	-0.00000e-00 - 0.00000e+00i	$\pm \infty$	$\pm \infty$	$\pm \infty$	$\pm \infty$	$\pm \infty$	$\pm \infty$
0.5	1500 $\angle 60^\circ$	Pr	2.24825e+03 + 3.89711e+03i	1.87500e-00 - 0.00000e+00i	1.65211e+00 - 3.42588e-01i	-4.09285e-01 - 4.94082e-01i	6.80314e-09 + 5.14782e-09i	2.17821e-41 + 4.42762e-42i	-9.91329e-108 - 1.79650e-107i*	1.75876e-275 + 1.02730e-275i*
0.5	1500 $\angle 75^\circ$	Ob	-1.93408e+06 + 1.12112e+06i	-0.00000e-00 - 0.00000e+00i	$\pm \infty$	$\pm \infty$	$\pm \infty$	$\pm \infty$	$\pm \infty$	$\pm \infty$
0.5	1500 $\angle 90^\circ$	Ob	-2.23501e+06 + 2.74627e-10i	-0.00000e-00 - 0.00000e+00i	$\pm \infty$	$\pm \infty$	$\pm \infty$	$\pm \infty$	$\pm \infty$	$\pm \infty$
0.5	2500 $\angle 20^\circ$	Pr	2.74842e+04 - 0.00000e+00i	1.87500e-00 - 0.00000e+00i	-1.43926e-01 - 0.00000e+00i	-1.81349e-02 - 0.00000e+00i	-6.82782e-29 - 0.00000e+00i	-7.54253e-138 + 4.61504e-154i*	$\pm \infty$	$\pm \infty$
0.5	2500 $\angle 15^\circ$	Pr	2.65472e+04 + 7.11753e+03i	1.87500e-00 - 2.77556e-17i	-1.21841e-01 - 4.00442e-01i	1.94031e-02 + 2.08653e-02i	-6.40983e-28 + 7.97923e-28i	3.24703e-133 - 6.00553e-133i	$\pm \infty$	$\pm \infty$
0.5	2500 $\angle 30^\circ$	Pr	1.51487e+04 + 8.75000e+03i	1.87500e-00 - 0.00000e+00i	5.88468e-01 - 6.08321e-01i	5.11124e-03 + 1.20153e-02i	2.73463e-26 - 3.67776e-26i	-8.13272e-121 - 7.11213e-122i*	1.51986e-312 + 3.69183e-312i*	$\pm \infty$
0.5	2500 $\angle 45^\circ$	Ob	1.06016e+04 + 6.23939e+03i	-0.00000e-00 - 0.00000e+00i	$\pm \infty$	$\pm \infty$	$\pm \infty$	$\pm \infty$	$\pm \infty$	$\pm \infty$
0.5	2500 $\angle 60^\circ$	Pr	3.74825e+03 + 6.49519e+03i	1.87500e-00 + 1.11022e-16i	1.49130e-00 - 3.45718e-01i	8.31301e-02 - 2.98688e-02i	-2.75502e-16 - 1.79236e-15i	-2.99759e-70 - 3.56015e-72i*	1.03779e-180 + 3.17815e-182i*	$\pm \infty$
0.5	2500 $\angle 75^\circ$	Ob	-5.38852e+06 + 3.11855e+06i	-0.00000e-00 - 0.00000e+00i	$\pm \infty$	$\pm \infty$	$\pm \infty$	$\pm \infty$	$\pm \infty$	$\pm \infty$
0.5	2500 $\angle 90^\circ$	Ob	-6.22501e+06 + 7.63873e-10i	-0.00000e-00 - 0.00000e+00i	$\pm \infty$	$\pm \infty$	$\pm \infty$	$\pm \infty$	$\pm \infty$	$\pm \infty$
0.5	5000 $\angle 20^\circ$	Pr	5.49842e+04 - 0.00000e+00i	1.87500e-00 - 0.00000e+00i	-1.26522e-00 - 0.00000e+00i	-6.72102e-02 - 0.00000e+00i	-1.88473e-02 - 0.00000e+00i	-2.10483e-282 + 1.28834e-298i*	$\pm \infty$	$\pm \infty$
0.5	5000 $\angle 15^\circ$	Pr	5.31102e+04 + 1.42350e+04i	1.87500e-00 - 2.77556e-17i	-1.29721e-00 - 4.13920e-01i	-1.27678e-06 - 9.52531e-07i	3.61542e-60 + 2.17581e-60i	1.68885e-272 + 3.41120e-273i*	$\pm \infty$	$\pm \infty$
0.5	5000 $\angle 30^\circ$	Pr	3.03041e+04 + 1.75000e+04i	1.87500e-00 + 1.66533e-16i	-4.36908e-01 - 8.67011e-01i	4.68286e-07 + 9.93881e-07i	-2.52101e-55 - 5.34718e-56i	2.22548e-246 - 2.68412e-246i*	$\pm \infty$	$\pm \infty$
0.5	5000 $\angle 45^\circ$	Ob	2.12082e+04 + 2.49788e+04i	-0.00000e-00 - 0.00000e+00i	$\pm \infty$	$\pm \infty$	$\pm \infty$	$\pm \infty$	$\pm \infty$	$\pm \infty$
0.5	5000 $\angle 60^\circ$	Pr	7.49825e+03 + 1.29904e+04i	1.87500e-00 - 0.00000e+00i	1.05835e+00 - 9.66501e-01i	7.39376e-05 + 3.30862e-04i	4.37112e-33 - 2.05256e-32i	-5.78205e-143 + 9.54059e-143i*	$\pm \infty$	$\pm \infty$
0.5	5000 $\angle 75^\circ$	Ob	-2.16024e+07 + 1.24871e+07i	-0.00000e-00 - 0.00000e+00i	$\pm \infty$	$\pm \infty$	$\pm \infty$	$\pm \infty$	$\pm \infty$	$\pm \infty$
0.5	5000 $\angle 90^\circ$	Ob	-2.49500e+07 + 3.05856e-09i	-0.00000e-00 - 0.00000e+00i	$\pm \infty$	$\pm \infty$	$\pm \infty$	$\pm \infty$	$\pm \infty$	$\pm \infty$
0.6	25 $\angle 0^\circ$	Pr	3.01441e-02 - 0.00000e+00i	-0.00000e-00 - 0.00000e+00i	9.37308e-01 - 0.00000e+00i	5.38473e-00 - 0.00000e+00i	-5.00320e-00 - 0.00000e+00i	5.45264e+00 - 0.00000e+00i	-2.38658e+00 - 0.00000e+00i	-8.86764e-03 + 5.39151e-19i*
0.6	25 $\angle 15^\circ$	Pr	2.90487e-02 + 8.46911e+01i	-0.00000e-00 - 0.00000e+00i	9.03788e-01 + 2.62097e-01i	5.54801e-00 + 5.87364e-01i	-5.56488e-00 - 2.28829e+00i	8.13292e+00 - 1.09081e+00i	-3.26625e+00 + 2.04177e+00i	9.42638e-03 - 1.73988e-02i*
0.6	25 $\angle 30^\circ$	Pr	1.83626e-02 + 1.12833e-02i	-0.00000e-00 - 0.00000e+00i	5.72762e-01 + 3.50425e-01i	4.64447e+00 + 1.61449e+00i	-9.52315e-01 - 5.05248e+00i	2.32457e+00 + 7.14460e+00i	-1.58027e+00 - 1.96646e+00i	-7.23361e-03 + 4.46297e-03i*
0.6	25 $\angle 45^\circ$	Pr	1.00961e-02 + 5.18815e-02i	-0.00000e-00 - 0.00000e+00i	3.29003e-01 + 1.61590e-01i	1.43023e-01 + 7.93207e+00i	-8.04328e-01 - 1.16192e+01i	4.96898e+03 - 1.79164e+03i	2.48376e+04 - 1.46815e+04i	-2.29944e-05 + 2.06818e-05i*
0.6	25 $\angle 60^\circ$	Pr	-1.09596e-02 + 4.15850e-02i	-0.00000e-00 - 0.00000e+00i	-3.34095e-01 + 1.30434e-01i	6.31483e-01 + 1.61419e+01i	1.52361e+02 - 1.24434e+02i	-7.38941e+03 - 6.97688e+03i	1.21883e+05 - 2.32977e+05i	-1.62969e+06 - 2.46693e

Table D.54: (continued)

m, n	$ c \angle \arg(c)$	type	λ_{mn}'	$S_{mn}'(c, \eta=0)$	$S_{mn}'(c, \eta=0.01)$	$S_{mn}'(c, \eta=0.1)$	$S_{mn}'(c, \eta=0.25)$	$S_{mn}'(c, \eta=0.5)$	$S_{mn}'(c, \eta=0.75)$	$S_{mn}'(c, \eta=0.99)$
0.6	500 \angle 15°	Pr	6.25670e+03 + 1.68234e+03i	-0.00000e+00 - 0.00000e+00i	1.76933e+01 + 4.20145e+00i	2.77576e+01 + 1.06543e+01i	9.79115e-02 + 2.27015e-02i	9.55043e-21 - 5.86802e-21i	-2.65170e-62 - 7.49351e-62i	4.67330e-168 - 6.70535e-169i*
0.6	500 \angle 30°	Pr	3.88634e+03 + 2.25001e+03i	-0.00000e+00 - 0.00000e+00i	1.16101e+01 + 6.12580e+00i	-1.32963e+01 + 2.52203e+01i	4.97578e-02 + 2.39039e-02i	1.48634e-19 - 7.65752e-20i	2.16988e-57 - 1.08647e-56i*	3.03515e-152 + 1.56498e-152i*
0.6	500 \angle 45°	Ob	2.11632e+03 + 2.47879e+03i	-0.00000e+00 - 0.00000e+00i	9.75947e+02 - 2.39791e+03i	-2.21585e+15 - 1.30879e+17i	-3.17296e+39 + 8.51577e+39i	7.00512e+76 + 1.02079e+78i	4.34263e+115 + 8.01419e+115i	-1.16008e+151 - 1.16922e+151i
0.6	500 \angle 60°	Ob	-1.20683e+03 + 2.14006e+03i	-0.00000e+00 - 0.00000e+00i	5.55933e+03 + 6.31202e+02i	-2.77530e+20 + 1.16198e+20i	-2.25070e+48 + 4.52650e+47i	-6.01286e+94 - 7.88935e+93i	-8.73149e+140 - 4.25985e+140i	5.94555e+182 - 3.74935e+182i
0.6	500 \angle 75°	Ob	-2.11690e+03 + 1.23706e+03i	-0.00000e+00 - 0.00000e+00i	-1.12460e+02 + 9.21087e+03i	-3.56159e+22 + 2.64796e+22i	-2.19180e+53 + 5.66680e+53i	2.29006e+105 + 3.58138e+105i	1.79829e+157 + 1.09932e+156i	1.54529e+204 - 6.28132e+202i
0.6	500 \angle 90°	Ob	-2.43025e+05 + 3.01875e-11i	-0.00000e+00 - 0.00000e+00i	-1.06565e+04 + 4.21931e-12i	-1.98370e+23 + 6.25161e+08i	-2.55918e+55 + 1.98187e+41i	-6.99888e+108 + 1.07775e+95i	-8.85596e+161 + 2.04174e+148i	1.90880e+207 - 4.22913e+193i
0.6	750 \angle 0°	Pr	9.72820e+03 - 0.00000e+00i	-0.00000e+00 - 0.00000e+00i	2.56682e+01 - 0.00000e+00i	1.55218e+01 - 0.00000e+00i	-1.23703e-04 - 0.00000e+00i	-1.70643e-35 - 0.00000e+00i	-2.22739e-100 + 1.36273e-116i*	-5.86684e-267 + 3.60418e-283i*
0.6	750 \angle 15°	Pr	9.39598e+03 + 2.52350e+03i	-0.00000e+00 - 0.00000e+00i	2.52275e+01 + 5.56527e+00i	2.19507e+01 - 1.82845e+01i	-8.74470e-05 - 2.68568e-04i	-5.15249e-34 - 1.01302e-34i	3.28584e-97 + 1.23325e-96i*	1.36220e-257 + 1.47822e-257i*
0.6	750 \angle 30°	Pr	5.83491e+03 + 3.37501e+03i	-0.00000e+00 - 0.00000e+00i	1.70273e+01 + 8.53749e+00i	2.40764e+01 + 1.85740e+01i	-1.26084e-04 + 1.37404e-04i	-6.61308e-33 + 1.45031e-31i	5.30380e-88 + 1.54481e-88i*	1.99283e-232 - 1.59323e-233i*
0.6	750 \angle 45°	Ob	3.17698e+03 + 5.59318e+03i	-0.00000e+00 - 0.00000e+00i	-2.23775e+04 - 4.34207e+03i	8.56228e+24 - 3.76559e+24i	-3.10953e+58 + 2.10801e+59i	1.76327e+116 + 3.30480e+116i	4.71333e+173 + 2.23154e+173i	6.33579e+226 - 2.59310e+227i
0.6	750 \angle 60°	Ob	-2.74768e+05 + 4.83389e+05i	-0.00000e+00 - 0.00000e+00i	3.09412e+04 - 6.65176e+04i	-1.08345e+30 + 3.68978e+29i	-1.11013e+72 + 3.36256e+70i	-8.43657e+141 + 4.23850e+141i	-2.80914e+211 - 3.99367e+211i	-1.89602e+275 + 1.62880e+276i
0.6	750 \angle 75°	Ob	-4.79908e+05 + 2.79309e+05i	-0.00000e+00 - 0.00000e+00i	9.18563e+04 + 1.24955e+05i	-1.39177e+33 + 1.50848e+33i	-1.48118e+79 - 1.50663e+80i	1.75115e+158 + 1.17706e+157i	-2.82413e+235 + 1.20425e+236i	$\pm \infty$
0.6	750 \angle 90°	Ob	-5.52025e+05 + 6.82434e-11i	-0.00000e+00 - 0.00000e+00i	$\pm \infty$	$\pm \infty$	$\pm \infty$	$\pm \infty$	$\pm \infty$	$\pm \infty$
0.6	1000 \angle 0°	Pr	1.29782e+04 - 0.00000e+00i	-0.00000e+00 - 0.00000e+00i	3.22780e+01 - 0.00000e+00i	-4.33554e+00 - 0.00000e+00i	-1.51858e-07 - 0.00000e+00i	-1.56437e-49 - 0.00000e+00i	-1.23762e-136 + 7.57341e-153i*	± 0
0.6	1000 \angle 15°	Pr	1.25353e+04 + 3.34666e+03i	-0.00000e+00 - 0.00000e+00i	3.19156e+01 + 6.48741e+00i	-1.00057e+01 - 1.96511e+01i	-3.07314e-07 + 3.31998e-07i	8.82341e-48 + 1.22045e-47i	-2.24809e-132 - 1.24796e-131i*	± 0
0.6	1000 \angle 30°	Pr	7.78347e+03 + 4.50001e+03i	-0.00000e+00 - 0.00000e+00i	2.21755e+01 + 1.05414e+01i	2.69630e+01 - 9.40728e+00i	-5.08587e-08 - 4.70168e-07i	-7.37707e-44 - 4.75216e-44i	-7.00567e-120 + 1.79448e-119i*	6.60397e-313 - 4.85461e-313i*
0.6	1000 \angle 45°	Ob	4.23764e+03 + 9.95757e+03i	-0.00000e+00 - 0.00000e+00i	8.23843e+02 + 1.78159e+05i	4.31021e+32 + 4.08279e+32i	2.86419e+77 + 4.42816e+78i	9.63411e+154 + 7.44607e+154i	2.59887e+231 - 5.04280e+230i	3.48346e+303 - 1.33216e+303i*
0.6	1000 \angle 60°	Ob	-4.91353e+05 + 8.61025e+05i	-0.00000e+00 - 0.00000e+00i	$\pm \infty$	$\pm \infty$	$\pm \infty$	$\pm \infty$	$\pm \infty$	$\pm \infty$
0.6	1000 \angle 75°	Ob	-8.56379e+05 + 4.97412e+05i	-0.00000e+00 - 0.00000e+00i	$\pm \infty$	$\pm \infty$	$\pm \infty$	$\pm \infty$	$\pm \infty$	$\pm \infty$
0.6	1000 \angle 90°	Ob	-9.86025e+05 + 1.21607e-10i	-0.00000e+00 - 0.00000e+00i	$\pm \infty$	$\pm \infty$	$\pm \infty$	$\pm \infty$	$\pm \infty$	$\pm \infty$
0.6	1500 \angle 0°	Pr	1.94782e+04 - 0.00000e+00i	-0.00000e+00 - 0.00000e+00i	4.28538e+01 - 0.00000e+00i	-1.29198e+01 - 0.00000e+00i	-1.06114e-13 - 0.00000e+00i	-6.53141e-78 - 0.00000e+00i	-1.91899e-209 + 1.17455e-225i*	± 0
0.6	1500 \angle 15°	Pr	1.88138e+04 + 5.04698e+03i	-0.00000e+00 - 0.00000e+00i	4.29028e+01 + 7.14538e+00i	-1.76292e+01 + 7.93428e+00i	-1.30737e-13 + 5.24941e-13i	-4.74976e-75 + 3.92007e-75i	-7.22241e-204 - 6.28776e-202i*	± 0
0.6	1500 \angle 30°	Pr	1.16806e+04 + 6.75000e+03i	-0.00000e+00 - 0.00000e+00i	3.16691e+01 + 1.34019e+01i	-3.92032e+00 - 1.31485e+01i	-1.72343e-12 + 3.74110e-13i	-1.14796e-69 + 1.90529e-68i	7.35065e-183 - 1.19129e-182i*	± 0
0.6	1500 \angle 45°	Ob	6.35896e+03 + 2.24364e+03i	-0.00000e+00 - 0.00000e+00i	$\pm \infty$	$\pm \infty$	$\pm \infty$	$\pm \infty$	$\pm \infty$	$\pm \infty$
0.6	1500 \angle 60°	Ob	-1.11202e+06 + 1.94106e+06i	-0.00000e+00 - 0.00000e+00i	$\pm \infty$	$\pm \infty$	$\pm \infty$	$\pm \infty$	$\pm \infty$	$\pm \infty$
0.6	1500 \angle 75°	Ob	-1.93408e+06 + 1.12112e+06i	-0.00000e+00 - 0.00000e+00i	$\pm \infty$	$\pm \infty$	$\pm \infty$	$\pm \infty$	$\pm \infty$	$\pm \infty$
0.6	1500 \angle 90°	Ob	-2.22903e+06 + 2.74260e-10i	-0.00000e+00 - 0.00000e+00i	$\pm \infty$	$\pm \infty$	$\pm \infty$	$\pm \infty$	$\pm \infty$	$\pm \infty$
0.6	2500 \angle 0°	Pr	3.24782e+04 - 0.00000e+00i	-0.00000e+00 - 0.00000e+00i	5.47474e+01 - 0.00000e+00i	-1.26095e+00 - 0.00000e+00i	-1.41143e-26 - 0.00000e+00i	-3.34748e-135 + 2.04821e-151i*	± 0	± 0
0.6	2500 \angle 15°	Pr	3.33708e+04 + 8.41162e+03i	-0.00000e+00 - 0.00000e+00i	5.63098e+01 + 4.60093e+00i	8.30027e+01 - 1.82983e+00i	-1.71624e-25 + 1.24054e-25i	2.08584e-130 + 2.19864e-130i*	± 0	± 0
0.6	2500 \angle 30°	Pr	1.94748e+04 + 1.12500e+04i	-0.00000e+00 - 0.00000e+00i	4.74872e+01 + 1.50391e+01i	-1.85179e+01 + 9.75714e-01i	8.81113e-24 + 3.71801e-24i	-2.97060e-118 - 2.08966e-118i*	2.37669e-309 - 1.82787e-309i*	± 0
0.6	2500 \angle 45°	Ob	1.06016e+04 + 6.23939e+06i	-0.00000e+00 - 0.00000e+00i	$\pm \infty$	$\pm \infty$	$\pm \infty$	$\pm \infty$	$\pm \infty$	$\pm \infty$
0.6	2500 \angle 60°	Ob	-3.10336e+06 + 5.40016e+06i	-0.00000e+00 - 0.00000e+00i	$\pm \infty$	$\pm \infty$	$\pm \infty$	$\pm \infty$	$\pm \infty$	$\pm \infty$
0.6	2500 \angle 75°	Ob	-5.38852e+06 + 3.11853e+06i	-0.00000e+00 - 0.00000e+00i	$\pm \infty$	$\pm \infty$	$\pm \infty$	$\pm \infty$	$\pm \infty$	$\pm \infty$
0.6	2500 \angle 90°	Ob	-6.21503e+06 + 7.63261e-10i	-0.00000e+00 - 0.00000e+00i	$\pm \infty$	$\pm \infty$	$\pm \infty$	$\pm \infty$	$\pm \infty$	$\pm \infty$
0.6	5000 \angle 0°	Pr	6.49782e+04 - 0.00000e+00i	-0.00000e+00 - 0.00000e+00i	4.54517e+01 - 0.00000e+00i	-1.03761e-04 - 0.00000e+00i	-7.88701e-00 - 0.00000e+00i	-1.87414e-279 + 1.14714e-295i*	± 0	± 0
0.6	5000 \angle 15°	Pr	6.27634e+04 + 1.68232e+04i	-0.00000e+00 - 0.00000e+00i	5.15911e+01 - 1.46508e+01i	-1.48446e-04 - 1.97252e-04i	1.22233e-57 + 1.27535e-57i	1.37350e-269 + 6.83766e-270i*	± 0	± 0
0.6	5000 \angle 30°	Pr	3.89604e+04 + 2.25000e+04i	-0.00000e+00 - 0.00000e+00i	6.94286e+01 + 1.33075e+01i	-1.95953e-05 + 1.74394e-04i	-8.02357e-53 + 7.27911e-53i	2.91575e-243 - 1.07705e-243i*	± 0	± 0
0.6	5000 \angle 45°	Ob	2.12082e+04 + 2.49788e+07i	-0.00000e+00 - 0.00000e+00i	$\pm \infty$	$\pm \infty$	$\pm \infty$	$\pm \infty$	$\pm \infty$	$\pm \infty$
0.6	5000 \angle 60°	Ob	-1.24567e+07 + 2.16256e+07i	-0.00000e+00 - 0.00000e+00i	$\pm \infty$	$\pm \infty$	$\pm \infty$	$\pm \infty$	$\pm \infty$	$\pm \infty$
0.6	5000 \angle 75°	Ob	-2.16024e+07 + 1.24871e+07i	-0.00000e+00 - 0.00000e+00i	$\pm \infty$	$\pm \infty$	$\pm \infty$	$\pm \infty$	$\pm \infty$	$\pm \infty$
0.6	5000 \angle 90°	Ob	-2.49300e+07 + 3.05733e-09i	-0.00000e+00 - 0.00000e+00i	$\pm \infty$	$\pm \infty$	$\pm \infty$	$\pm \infty$	$\pm \infty$	$\pm \infty$

Table D.54: $S_{0n}'(c, \eta)$ for $n = [0..6]$.Table D.55: $S_{1n}'(c, \eta)$ for $n = [1..6]$.

m, n	$ c \angle \arg(c)$	type	λ_{mn}'	$S_{mn}'(c, \eta=0)$	$S_{mn}'(c, \eta=0.01)$	$S_{mn}'(c, \eta=0.1)$	$S_{mn}'(c, \eta=0.25)$	$S_{mn}'(c, \eta=0.5)$	$S_{mn}'(c, \eta=0.75)$	$S_{mn}'(c, \eta=0.99)$
1.1	25 \angle 0°	Pr	2.52634e+01 - 0.00000e+00i	-0.00000e+00 - 0.00000e+00i	-2.42352e-01 - 0.00000e+00i	-2.15906e+00 - 0.00000e+00i	-2.89789e+00 - 0.00000e+00i	-5.43923e-01 - 0.00000e+00i	-7.68225e-03 - 4.25126e-19i*	-4.59844e-07 - 1.86544e-23i*
1.1	25 \angle 15°	Pr	2.44110e+01 + 6.46678e+00i	-0.00000e+00 - 0.00000e+00i	-2.33868e-01 - 6.45197e-02i	-2.10975e+00 - 5.09864e-01i	-2.97429e+00 - 1.91713e-01i	-5.05223e-01 + 3.42572e-01i	3.27836e-03 + 9.76564e-03i*	4.47578e-07 - 8.33512e-07i*
1.1	25 \angle 30°	Pr	1.99119e+01 + 1.24930e+01i	-0.00000e+00 - 0.00000e+00i	-2.08988e-01 - 1.24675e-01i	-1.95936e+00 - 1.01000e+00i	-3.20372e+00 - 4.58704e-01i	-3.62722e-01 + 7.75363e-01i	2.13439e-02 - 1.17008e-02i*	6.60748e-06 - 5.05733e-06i*
1.1	25 \angle 45°	Pr	1.79365e+01 + 1.76680e+01i	-0.00000e+00 - 0.00000e+00i	-1.69385e-01 - 1.76389e-01i	-1.70151e+00 - 1.48651e+00i	-3.57851e+00 - 9.8806e-01i	-1.92313e-02 + 1.46577e+00i	3.68715e-02 - 8.81319e-02i*	1.16253e-05 + 2.61546e-04i*
1.1	25 \angle 60°	Pr	1.27558e+01 + 2.16391e+01i	-0.00000e+00 - 0.00000e+00i	-1.17728e-01 - 2.16147e-01i	-1.32902e+00 - 1.91776e+00i	-4.05386e+00 - 1.65083e+00i	7.35801e-01 + 2.86208e+00i	-5.63623e-01 + 6.18748e-03i*	1.05233e-03 + 2.61546e-04i*
1.1	25 \angle 75°	Ob	-4.46714e+02 + 2.86606e+02i	-0.00000e+00 - 0.00000e+00i	4.49711e+00 -					

Table D.55: (continued)

m, n	$c \setminus \arg(c)$	type	$\lambda_{mn}^{(\alpha)}$	$S_{mn}^{(\alpha)}(c, \eta=0)$	$S_{mn}^{(\alpha)}(c, \eta=0.01)$	$S_{mn}^{(\alpha)}(c, \eta=0.1)$	$S_{mn}^{(\alpha)}(c, \eta=0.25)$	$S_{mn}^{(\alpha)}(c, \eta=0.5)$	$S_{mn}^{(\alpha)}(c, \eta=0.75)$	$S_{mn}^{(\alpha)}(c, \eta=0.99)$
1,1	100 \angle 60	Pr	5.02515e+01 + 8.65998e+01i	-0.00000e+00 - 0.00000e+00i	-4.95064e-01 - 8.61775e-01i	-6.36805e+00 - 4.54266e+00i	6.72680e-01 - 5.34310e-01i	3.41349e-02 - 7.10310e-02i	7.24444e-06 + 1.98803e-07i	5.78926e-16 - 9.43110e-16i
1,1	100 \angle 75	Ob	-8.27589e+03 + 4.89647e+03i	-0.00000e+00 - 0.00000e+00i	9.01638e+01 - 6.32391e+01i	-6.05871e-05 - 1.78329e+00i	8.38020e+11 - 4.09560e+11i	1.42105e-22 - 1.06375e-22i	2.04020e-32 - 2.27018e-32i	1.69334e+41 - 2.64073e+41i
1,1	100 \angle 90	Ob	-9.60201e+03 + 1.20015e-12i	-0.00000e+00 - 0.00000e+00i	1.12162e-02 - 2.08377e-14i	8.87338e-05 - 6.36044e-10i	2.18472e+12 - 3.57272e-03i	9.74470e-22 - 3.08546e+08i	3.89910e+33 - 1.83168e+19i	8.62958e+42 - 5.37506e+28i
1,1	250 \angle 0	Pr	2.50251e+02 - 0.00000e+00i	-0.00000e+00 - 0.00000e+00i	-2.46176e+00 - 0.00000e+00i	-7.18151e+00 - 0.00000e+00i	-2.35156e-02 - 0.00000e+00i	-4.54998e-13 - 0.00000e+00i	-6.62970e-35 - 0.00000e+00i	-5.64514e-90 - 3.35554e-106i
1,1	250 \angle 15	Pr	2.41733e+02 + 6.47044e+01i	-0.00000e+00 - 0.00000e+00i	-2.38070e+00 - 6.31636e-01i	-7.48128e+00 - 4.62604e-01i	6.76390e-03 + 3.00720e-02i	7.47182e-13 + 1.21299e-12i	1.19567e-33 + 4.35766e-34i	-3.36998e-87 - 9.83821e-87i
1,1	250 \angle 30	Pr	2.16757e+02 + 1.24999e+02i	-0.00000e+00 - 0.00000e+00i	-2.14222e+00 - 1.22328e+00i	-8.5406e+00 + 8.60726e-01i	6.50510e-02 - 2.03022e-02i	3.52425e-11 - 1.98742e-11i	3.22910e-30 - 4.54928e-30i	-1.72784e-77 + 7.70952e-76i
1,1	250 \angle 45	Pr	1.77028e+02 + 1.76777e+02i	-0.00000e+00 - 0.00000e+00i	-1.76036e+00 - 1.73686e+00i	-1.03249e+01 + 1.02106e+01i	-2.72419e-02 - 2.39195e-01i	5.12813e-09 - 6.52245e-09i	3.35763e-24 + 2.47020e-24i	-1.39527e-62 + 3.37584e-63i
1,1	250 \angle 60	Pr	1.25251e+02 + 2.16505e+02i	-0.00000e+00 - 0.00000e+00i	-1.25809e+00 - 2.13826e+00i	-1.34497e+01 + 4.76860e-01i	-1.11842e+00 - 5.51489e-01i	8.11822e-06 + 2.67479e-06i	1.59223e-16 + 1.14761e-18i	1.27667e-43 + 1.09861e-43i
1,1	250 \angle 75	Ob	-5.31627e+04 + 3.09912e+04i	-0.00000e+00 - 0.00000e+00i	8.23332e+02 - 1.07892e+03i	2.81946e+12 - 1.36611e+12i	-9.45174e+27 + 8.49586e+27i	4.71755e+53 - 1.21593e+54i	1.19348e+79 + 1.20002e+80i	4.18255e+102 - 2.39428e+104i
1,1	250 \angle 90	Ob	-6.15020e+04 + 7.59281e-12i	-0.00000e+00 - 0.00000e+00i	1.47038e+03 - 1.81451e-13i	7.34162e+12 - 1.10049e-02i	1.06874e+29 - 4.05607e+14i	9.22566e+55 - 7.03199e+41i	7.17453e+82 - 8.21451e+68i	1.08916e+108 - 1.64881e+94i
1,1	500 \angle 0	Pr	5.00251e+02 - 0.00000e+00i	-0.00000e+00 - 0.00000e+00i	-4.86966e+00 - 0.00000e+00i	-4.10836e+00 - 0.00000e+00i	-1.68035e-05 - 0.00000e+00i	-2.59244e-27 - 0.00000e+00i	-2.58604e-71 - 1.57675e-87i	-8.02785e-183 - 8.44437e-199i
1,1	500 \angle 15	Pr	4.83214e+02 + 1.29409e+02i	-0.00000e+00 - 0.00000e+00i	-4.71557e+00 - 1.23284e+00i	-4.14480e+00 + 1.68673e+00i	2.19749e-05 - 1.87165e-05i	5.13395e-27 - 2.48874e-26i	-7.49535e-69 - 3.48127e-69i	-1.08603e-176 - 1.45785e-176i
1,1	500 \angle 30	Pr	4.33263e+02 + 2.50000e+02i	-0.00000e+00 - 0.00000e+00i	-4.26067e+00 - 2.39359e+00i	-4.28856e+00 + 3.82856e+00i	6.00443e-05 + 1.27601e-04i	-3.59837e-25 + 2.04816e-23i	1.43288e-61 + 1.22943e-61i	-6.78082e-158 + 4.38587e-158i
1,1	500 \angle 45	Pr	3.53804e+02 + 3.53553e+02i	-0.00000e+00 - 0.00000e+00i	-3.52739e+00 - 3.41206e+00i	-4.72928e+00 + 7.13946e+00i	9.27164e-04 - 1.49446e-03i	7.36726e-19 + 4.45070e-19i	-7.39854e-50 - 4.02433e-50i	-9.92248e-129 + 3.11532e-128i
1,1	500 \angle 60	Pr	2.50250e+02 + 4.33012e+02i	-0.00000e+00 - 0.00000e+00i	-2.5377e+00 - 4.22241e+00i	-6.24598e+00 + 1.29700e+01i	-4.67123e-02 + 6.34646e-03i	-8.34884e-13 + 3.68127e-13i	-7.56608e-35 + 1.27744e-34i	-1.43944e-89 + 2.34347e-90i
1,1	500 \angle 75	Ob	-2.14577e+05 + 1.24482e+05i	-0.00000e+00 - 0.00000e+00i	4.22239e-02 - 3.05532e+04i	3.62230e-04 - 1.37025e-11i	1.55292e+23 - 1.93297e+54i	-3.83855e+106 - 6.05341e+106i	-1.09562e+159 - 7.54089e+157i	-3.30966e+208 - 1.39420e+208i
1,1	500 \angle 90	Pr	-2.48002e+05 + 3.04937e-11i	-0.00000e+00 - 0.00000e+00i	3.62230e-04 - 1.37025e-11i	1.06156e+24 - 3.32663e+09i	2.98618e-56 - 2.30716e+42i	3.58820e+110 - 5.51873e+96i	3.88974e+164 - 9.95977e+150i	7.55978e+215 - 2.29733e+202i
1,1	750 \angle 0	Pr	7.50250e+02 - 0.00000e+00i	-0.00000e+00 - 0.00000e+00i	-7.21273e+00 - 0.00000e+00i	-1.76095e+00 - 0.00000e+00i	-8.99607e-09 - 0.00000e+00i	-1.10650e-41 - 0.00000e+00i	-7.74506e-276 + 4.69674e-292i	
1,1	750 \angle 15	Pr	7.24695e+02 + 1.94114e+02i	-0.00000e+00 - 0.00000e+00i	-6.99795e+00 - 1.80441e+00i	-1.51676e+01 - 1.30620e+01i	-1.87978e-08 - 7.53716e-09i	-2.78017e-40 + 1.94947e-40i	3.79307e-104 + 2.11481e-104i	2.55689e-266 + 7.58179e-268i
1,1	750 \angle 30	Pr	6.49796e+02 + 3.75000e+02i	-0.00000e+00 - 0.00000e+00i	-6.34789e+00 - 5.31208e+00i	-6.22306e-01 + 2.84716e+00i	-8.27592e-08 - 2.02416e-07i	-6.62777e-36 - 4.05626e-36i	-9.30370e-239 + 3.20965e-93i	-9.95174e-239 + 2.10098e-238i
1,1	750 \angle 45	Pr	5.30580e+02 + 5.30330e+02i	-0.00000e+00 - 0.00000e+00i	-5.29280e+00 - 5.02640e+00i	1.57267e+00 + 5.05879e+00i	9.05798e-06 - 3.26635e-06i	-2.73625e-29 + 6.10562e-29i	1.41392e-75 + 4.31786e-76i	4.52570e-194 + 4.58817e-194i
1,1	750 \angle 60	Pr	3.75250e+02 + 6.49519e+02i	-0.00000e+00 - 0.00000e+00i	-3.87837e+00 - 6.25245e+00i	6.86451e+00 + 9.27987e+00i	-9.97902e-04 + 8.88162e-04i	2.99681e-20 - 6.65742e-20i	-5.04203e-53 + 3.98981e-53i	4.07564e-136 - 3.99891e-136i
1,1	750 \angle 75	Ob	-4.84244e+05 + 2.80474e-05i	-0.00000e+00 - 0.00000e+00i	$\pm \infty$	$\pm \infty$	$\pm \infty$	$\pm \infty$	$\pm \infty$	$\pm \infty$
1,1	750 \angle 90	Ob	-5.59502e+05 + 6.87072e-11i	-0.00000e+00 - 0.00000e+00i	$\pm \infty$	$\pm \infty$	$\pm \infty$	$\pm \infty$	$\pm \infty$	$\pm \infty$
1,1	1000 \angle 0	Pr	1.00025e+03 - 0.00000e+00i	-0.00000e+00 - 0.00000e+00i	-9.50598e+00 - 0.00000e+00i	-6.70753e-01 - 0.00000e+00i	-4.27996e-12 - 0.00000e+00i	-4.19676e-56 - 0.00000e+00i	-1.94649e-144 - 1.18933e-160i	$\pm \infty$
1,1	1000 \angle 15	Pr	9.66176e+02 + 2.58819e+02i	-0.00000e+00 - 0.00000e+00i	-9.22863e+00 - 2.34714e+00i	-4.05986e-01 + 6.84337e-01i	1.29342e-12 - 1.25622e-11i	3.98999e-54 + 5.80082e-55i	-1.63621e-139 - 1.12007e-139i	$\pm \infty$
1,1	1000 \angle 30	Pr	8.66276e+02 + 5.00000e+02i	-0.00000e+00 - 0.00000e+00i	-8.40391e+00 - 4.57988e+00i	5.25184e-01 + 1.20337e+00i	2.82581e-10 + 1.04713e-10i	2.31142e-48 - 1.23231e-48i	-6.06266e-125 + 7.52745e-125i	6.25685e-320 + 5.17530e-319i
1,1	1000 \angle 45	Pr	7.07357e+02 + 7.07107e+02i	-0.00000e+00 - 0.00000e+00i	-7.05582e+00 - 6.58072e+00i	2.70137e+00 - 1.08807e+00i	4.44216e-08 - 1.48943e-08i	4.44165e-39 - 1.36360e-39i	-2.22247e-101 + 3.33919e-102i	1.06781e-259 + 2.60344e-260i
1,1	1000 \angle 60	Pr	5.00250e+02 + 8.66025e+02i	-0.00000e+00 - 0.00000e+00i	-5.23076e+00 - 8.22844e+00i	8.13173e+00 - 1.24199e+01i	-8.37311e-06 + 3.25879e-05i	1.58036e-27 + 4.94548e-27i	6.14894e-71 + 8.82362e-73i	-3.48324e-183 + 1.88883e-182i
1,1	1000 \angle 75	Ob	-8.62146e+05 + 4.98965e+05i	-0.00000e+00 - 0.00000e+00i	$\pm \infty$	$\pm \infty$	$\pm \infty$	$\pm \infty$	$\pm \infty$	$\pm \infty$
1,1	1000 \angle 90	Ob	-9.96002e+05 + 1.22220e-10i	-0.00000e+00 - 0.00000e+00i	$\pm \infty$	$\pm \infty$	$\pm \infty$	$\pm \infty$	$\pm \infty$	$\pm \infty$
1,1	1500 \angle 0	Pr	1.50025e+03 - 0.00000e+00i	-0.00000e+00 - 0.00000e+00i	-1.39104e+01 - 0.00000e+00i	-8.20916e-02 - 0.00000e+00i	-8.17175e-19 - 0.00000e+00i	-5.09239e-85 - 0.00000e+00i	-1.01444e-217 - 6.20275e-234i	$\pm \infty$
1,1	1500 \angle 15	Pr	1.44914e+03 + 3.88229e+02i	-0.00000e+00 - 0.00000e+00i	-1.35381e+01 - 3.34914e+00i	1.19908e-01 + 1.05385e-01i	-3.63384e-18 - 1.98721e-18i	-4.09335e-83 + 4.77773e-82i	-2.39466e-210 - 2.32071e-210i	$\pm \infty$
1,1	1500 \angle 30	Pr	1.29929e+03 + 5.00000e+02i	-0.00000e+00 - 0.00000e+00i	-1.24224e+01 - 6.56782e+00i	2.23814e-01 - 2.10990e-01i	1.28855e-16 - 4.65258e-16i	-2.10851e-73 - 1.36316e-73i	1.64859e-188 + 3.07530e-188i	$\pm \infty$
1,1	1500 \angle 45	Pr	1.06091e+03 + 1.06066e+03i	-0.00000e+00 - 0.00000e+00i	-1.05716e+01 - 9.51260e+00i	1.34061e-01 - 7.30432e-01i	-8.60739e-14 + 9.31798e-13i	1.85803e-59 + 1.04104e-60i	-3.83581e-153 + 6.60268e-154i	$\pm \infty$
1,1	1500 \angle 60	Pr	7.50250e+02 + 1.29994e+03i	-0.00000e+00 - 0.00000e+00i	-8.01435e+00 - 1.20185e+01i	-2.40631e+00 - 2.57530e+00i	1.44590e-18 - 1.07313e-18i	2.16960e-41 - 4.46118e-42i	-8.64720e-108 - 1.56682e-107i	1.53115e-275 + 8.97530e-276i
1,1	1500 \angle 75	Ob	1.94276e+06 + 1.12345e+06i	-0.00000e+00 - 0.00000e+00i	$\pm \infty$	$\pm \infty$	$\pm \infty$	$\pm \infty$	$\pm \infty$	$\pm \infty$
1,1	1500 \angle 90	Ob	-2.24400e+06 + 2.75178e-10i	-0.00000e+00 - 0.00000e+00i	$\pm \infty$	$\pm \infty$	$\pm \infty$	$\pm \infty$	$\pm \infty$	$\pm \infty$
1,1	2500 \angle 0	Pr	2.50025e+03 - 0.00000e+00i	-0.00000e+00 - 0.00000e+00i	-2.20577e+01 - 0.00000e+00i	-9.10555e+00 - 0.00000e+00i	-2.20595e-32 - 0.00000e+00i	-5.94682e-143 - 3.63703e-159i	$\pm \infty$	$\pm \infty$
1,1	2500 \angle 15	Pr	2.41506e+03 + 6.47048e+02i	-0.00000e+00 - 0.00000e+00i	-2.15711e+01 - 5.03990e+00i	1.37773e-03 + 2.22483e-04i	-4.46534e-32 + 3.26850e-31i	-1.76450e-139 - 5.54324e-138i	$\pm \infty$	$\pm \infty$
1,1	2500 \angle 30	Pr	2.16531e+03 + 1.25000e+03i	-0.00000e+00 - 0.00000e+00i	-2.00870e+01 - 9.98330e+00i	-4.18288e-03 - 2.51435e-03i	-9.24730e-29 + 9.12834e-28i	1.64353e-123 - 7.72950e-124i	4.18957e-316 + 3.09238e-315i	$\pm \infty$
1,1	2500 \angle 45	Pr	1.76802e+03 + 1.76777e+03i	-0.00000e+00 - 0.00000e+00i	-1.75422e+01 - 1.46924e+01i	7.85387e+03 + 4.88404e+02i	-1.00089e-22 - 2.57692e-22i	2.15388e-100 - 9.85990e-101i	-5.60348e-257 + 5.88439e-257i	$\pm \infty$
1,1	2500 \angle 60	Pr	1.25025e+03 + 2.16506e+03i	-0.00000e+00 - 0.00000e+00i	-1.38656e+01 - 1.89535e+01i	4.44982e-01 - 1.77876e-01i	-6.01212e-16 - 3.77171e-15i	-2.98755e-70 - 3.49313e-72i	1.03445e-180 + 3.29270e-182i	$\pm \infty$
1,1	2500 \angle 75	Ob	-5.40300e+06 + 3.12241e+06i	-0.00000e+00 - 0.00000e+00i	$\pm \infty$	$\pm \infty$	$\pm \infty$	$\pm \infty$	$\pm \infty$	$\pm \infty$
1,1	2500 \angle 90	Ob	-6.24000e+06 + 7.64792e-10i	-0.00000e+00 - 0.00000e+00i	$\pm \infty$					

Table D.55: (continued)

m, n	$c \setminus \arg(c)$	type	$\lambda_{mn}^{(a)}$	$S_{mn}^{(a)}(c, \eta=0)$	$S_{mn}^{(a)}(c, \eta=0.01)$	$S_{mn}^{(a)}(c, \eta=0.1)$	$S_{mn}^{(a)}(c, \eta=0.25)$	$S_{mn}^{(a)}(c, \eta=0.5)$	$S_{mn}^{(a)}(c, \eta=0.75)$	$S_{mn}^{(a)}(c, \eta=0.99)$
1,2	100/60°	Ob	-4.65560e+03 + 8.46025e-03i	3.00000e+00 - 1.55431e-15i	3.62269e+00 - 1.36733e-01i	2.01859e+03 + 6.82288e+03i	2.34322e+09 - 1.55000e+08i	3.64707e+18 + 4.80744e+17i	5.07899e+27 + 9.89858e+26i	5.37775e+35 + 1.95062e+35i
1,2	100/75°	Ob	-8.27589e+03 + 4.89647e-03i	3.00000e+00 + 1.11022e-15i	4.29743e+00 - 8.39601e-01i	-1.64381e+04 - 1.01549e+04i	2.80359e+10 - 5.31789e+09i	5.05231e+20 - 1.99136e+20i	7.83068e+30 - 6.49376e+30i	7.15351e+39 - 6.51335e+39i
1,2	100/90°	Ob	-9.60201e+03 + 1.20015e-12i	3.00000e+00 - 1.46945e-16i	4.55988e+00 - 4.33615e-16i	2.71662e+04 - 1.79653e-11i	6.68862e+10 - 1.05669e-04i	2.98338e+21 - 9.28072e+06i	1.19373e+32 - 5.54154e+17i	2.64198e+41 - 1.63094e+27i
1,2	250/20°	Pr	7.49252e+02 - 0.00000e+00i	3.00000e+00 - 0.00000e+00i	2.88921e+00 - 0.00000e+00i	-1.29331e+00 - 0.00000e+00i	-1.67710e-02 - 0.00000e+00i	-7.19804e-13 - 0.00000e+00i	-1.78318e-34 - 0.00000e+00i	-2.92434e-89 - 1.73804e-105i
1,2	250/15°	Pr	7.23697e+02 + 1.94114e-02i	3.00000e+00 + 1.66533e-16i	2.89289e+00 - 2.85401e-02i	-1.39282e+00 - 1.49071e-01i	4.45346e-03 + 2.15833e-02i	1.17460e-12 + 1.92501e-12i	3.21576e-33 + 1.17839e-33i	-1.75114e-86 - 5.11712e-86i
1,2	250/30°	Pr	6.48771e+02 + 3.74999e-02i	3.00000e+00 - 0.00000e+00i	2.90371e+00 - 5.52498e-02i	-1.71232e+00 - 3.42142e-01i	4.73210e-02 - 1.30188e-02i	5.61320e-11 - 3.10559e-11i	8.73647e-30 - 1.22173e-29i	-8.95930e-77 - 2.57392e-78i
1,2	250/45°	Pr	5.29582e+02 + 5.30328e-02i	3.00000e+00 - 0.00000e+00i	2.92101e+00 - 7.83936e-02i	-2.31420e+00 - 6.61821e-01i	-1.15377e-02 - 1.74987e-01i	8.27033e-09 - 1.02747e-08i	9.02092e-24 + 6.70273e-24i	-7.26030e-62 + 1.75089e-62i
1,2	250/60°	Ob	-3.03860e+04 + 5.36266e-04i	3.00000e+00 + 3.99680e-15i	4.09607e+00 - 1.19941e+01i	3.11102e+09 + 2.06726e+08i	2.94469e+23 + 4.92739e+22i	5.62896e+46 + 1.93551e+46i	9.41072e+69 + 5.08231e+69i	-1.20799e+91 + 5.31718e+91i
1,2	250/75°	Ob	-5.31627e+04 + 3.09912e-04i	3.00000e+00 - 3.60822e-15i	1.32341e+01 - 9.83418e+00i	3.72264e+10 - 7.05521e+09i	-1.37149e+26 + 6.93729e+25i	9.34336e+51 - 1.20777e+52i	-2.39211e+77 + 1.43866e+78i	8.03760e+101 - 2.78221e+102i
1,2	250/90°	Ob	-6.15020e+04 + 4.85281e-12i	3.00000e+00 + 2.59691e-16i	1.80384e+01 - 1.16140e-15i	8.88114e+10 - 1.28266e-04i	1.29285e+27 - 4.83586e+12i	1.11601e+54 - 8.44550e+39i	8.67901e+80 - 9.88957e+66i	1.31755e+106 - 1.98735e+92i
1,2	500/20°	Pr	1.49925e+03 - 0.00000e+00i	3.00000e+00 - 0.00000e+00i	2.78016e+00 - 0.00000e+00i	-9.88113e-01 - 0.00000e+00i	-1.23956e-05 - 0.00000e+00i	-4.13461e-27 - 0.00000e+00i	-7.19509e-71 - 4.38687e-87i	-4.30498e-182 - 2.59774e-198i
1,2	500/15°	Pr	1.44814e+03 + 3.88228e-02i	3.00000e+00 - 1.66533e-16i	2.78722e+00 - 5.59369e-02i	-1.03176e+00 + 3.44441e-01i	1.63473e-05 - 1.36834e-05i	8.27299e-27 - 3.96860e-26i	-2.02321e-68 - 9.41161e-69i	5.65020e-176 - 7.58674e-176i
1,2	500/30°	Pr	1.29829e+03 + 7.49999e-02i	3.00000e+00 + 1.11022e-16i	2.80802e+00 - 1.08511e-01i	-1.18165e+00 + 8.22525e-01i	-4.60505e-05 + 9.38144e-05i	-7.06049e-25 + 3.26985e-23i	3.86557e-61 + 3.32710e-61i	-5.52946e-157 + 2.28220e-157i
1,2	500/45°	Pr	1.05991e+03 + 1.06066e-03i	3.00000e+00 - 2.22045e-16i	2.84148e+00 - 1.54473e-01i	-1.52551e+00 + 1.64198e+00i	7.16429e-04 - 1.09715e-03i	1.17372e-18 + 7.18094e-19i	-2.01465e-49 - 1.08012e-49i	-5.05541e-128 + 1.63248e-127i
1,2	500/60°	Ob	-1.23270e+05 + 2.15506e-05i	3.00000e+00 - 8.99281e-15i	-8.94882e+01 - 6.68256e-01i	7.81235e+18 + 1.04308e+18i	9.07001e+46 + 3.12482e+46i	4.84378e+93 + 3.78552e+93i	1.93774e+140 + 2.98013e+140i	-5.90207e+184 - 4.31903e+184i
1,2	500/75°	Ob	-2.14577e+05 + 1.24482e-05i	3.00000e+00 + 2.02061e-14i	5.02796e+01 - 1.77026e+02i	1.08322e+01 - 4.25869e+20i	1.50664e+52 - 2.04781e+52i	2.18530e+104 - 4.12166e+104i	-6.25455e+156 - 2.15325e+156i	-1.70685e+206 - 1.32889e+206i
1,2	500/90°	Ob	-2.48002e+05 + 3.04937e-11i	3.00000e+00 - 5.17210e-17i	2.18233e+02 - 7.05706e-14i	6.39498e+21 - 1.96892e+07i	1.79891e+54 - 1.38000e+40i	2.16157e+108 - 3.31269e+94i	2.34323e+162 - 5.38462e+148i	4.55410e+213 - 1.38144e+200i
1,2	750/20°	Pr	2.24925e+03 - 0.00000e+00i	3.00000e+00 - 0.00000e+00i	2.67338e+00 - 0.00000e+00i	-4.58926e-01 - 0.00000e+00i	-6.70953e-09 - 0.00000e+00i	-1.76946e-41 - 0.00000e+00i	-2.05832e-107 - 1.25676e-123i	-3.91480e-275 - 5.02493e-291i
1,2	750/15°	Pr	2.17258e+03 + 5.82343e-02i	3.00000e+00 + 1.11022e-16i	2.68352e+00 - 8.22185e-02i	-4.10950e-01 + 3.26433e-01i	-1.39993e-08 - 5.70486e-09i	-4.45103e-40 + 3.11190e-40i	1.03115e-103 + 5.96700e-104i	1.34979e-265 + 6.09589e-267i
1,2	750/30°	Pr	1.94781e+03 + 1.12500e-03i	3.00000e+00 - 3.33067e-16i	2.71351e+00 - 1.59822e-01i	-2.22722e-01 + 7.44861e-01i	-6.22722e-08 - 1.52084e-01i	-1.05891e-35 - 6.51957e-35i	1.04168e-93 + 8.67190e-93i	-5.18016e-238 + 1.09380e-237i
1,2	750/45°	Pr	1.59024e+03 + 1.59099e-03i	3.00000e+00 - 2.22045e-16i	2.76201e+00 - 2.28265e-01i	2.84746e-01 + 1.42267e-01i	6.83658e-06 - 2.34748e-06i	-4.41946e-29 + 9.76258e-29i	3.78894e-75 + 1.16194e-75i	2.33521e-193 + 2.36672e-193i
1,2	750/60°	Ob	-2.78654e+03 + 4.85639e-05i	3.00000e+00 + 1.31006e-14i	-7.98662e+02 + 5.56306e-02i	1.95302e+28 + 3.94078e+27i	2.70821e+70 + 1.47155e+70i	3.45396e+140 + 5.32445e+140i	9.22959e+209 + 1.17606e+211i	7.72029e+277 - 5.02493e-277i
1,2	750/75°	Ob	-4.84244e+05 + 2.80474e-05i	-0.00000e+00 - 0.00000e+00i	$\pm \infty$	$\pm \infty$	$\pm \infty$	$\pm \infty$	$\pm \infty$	$\pm \infty$
1,2	750/90°	Ob	-5.59502e+05 + 6.87072e-11i	-0.00000e+00 - 0.00000e+00i	$\pm \infty$	$\pm \infty$	$\pm \infty$	$\pm \infty$	$\pm \infty$	$\pm \infty$
1,2	1000/20°	Pr	2.99925e+03 - 0.00000e+00i	3.00000e+00 - 0.00000e+00i	2.56882e+00 - 0.00000e+00i	-1.81543e-01 - 0.00000e+00i	-3.20954e-12 - 0.00000e+00i	-6.72022e-56 - 0.00000e+00i	-5.24798e-144 - 3.20657e-160i	± 0
1,2	1000/15°	Pr	2.89703e+03 + 7.76457e-02i	3.00000e+00 - 0.00000e+00i	2.58177e+00 - 1.07412e-01i	-1.15634e-01 + 7.44861e-01i	9.30776e-13 + 9.42974e-12i	6.38903e-54 - 9.35629e-55i	-4.43022e-139 - 3.03891e-139i	± 0
1,2	1000/30°	Pr	2.59733e+03 + 1.50000e-03i	3.00000e+00 - 1.11022e-16i	2.62017e+00 - 2.09224e-01i	1.26147e-01 + 3.38470e-01i	2.11731e-10 + 8.04203e-11i	3.70719e-48 - 1.96693e-48i	-1.63946e-124 - 2.03732e-124i	3.26617e-319 + 2.97555e-318i
1,2	1000/45°	Pr	2.12057e+03 + 2.12132e-03i	3.00000e+00 + 2.22045e-16i	2.68262e+00 - 2.99801e-01i	7.31820e-01 + 3.61789e-01i	3.33423e-08 + 1.16059e-08i	-7.07425e-39 - 2.20610e-39i	-6.01396e-101 - 9.08665e-102i	5.55949e-259 - 1.35647e-259i
1,2	1000/60°	Ob	-4.96538e+05 + 8.46025e-05i	-0.00000e+00 - 0.00000e+00i	$\pm \infty$	$\pm \infty$	$\pm \infty$	$\pm \infty$	$\pm \infty$	$\pm \infty$
1,2	1000/75°	Ob	-8.62164e+05 + 4.98965e-05i	-0.00000e+00 - 0.00000e+00i	$\pm \infty$	$\pm \infty$	$\pm \infty$	$\pm \infty$	$\pm \infty$	$\pm \infty$
1,2	1000/90°	Ob	-9.96002e+05 + 1.22220e-10i	-0.00000e+00 - 0.00000e+00i	$\pm \infty$	$\pm \infty$	$\pm \infty$	$\pm \infty$	$\pm \infty$	$\pm \infty$
1,2	1500/20°	Pr	4.49925e+03 - 0.00000e+00i	3.00000e+00 - 0.00000e+00i	2.36622e+00 - 0.00000e+00i	-2.30426e-02 - 0.00000e+00i	-6.16124e-19 - 0.00000e+00i	-8.16526e-85 - 0.00000e+00i	-2.68724e-217 - 1.64310e-233i	± 0
1,2	1500/15°	Pr	4.34592e+03 + 1.16469e-03i	3.00000e+00 - 1.11022e-16i	2.28398e+00 - 1.54645e-01i	2.82655e-03 + 2.97153e-02i	2.73663e-18 - 1.50650e-18i	-6.61678e-83 + 7.66098e-82i	-6.48275e-210 - 6.28313e-210i	± 0
1,2	1500/30°	Pr	3.89636e+03 + 2.25000e-03i	3.00000e+00 + 1.11022e-16i	2.43699e+00 - 3.02454e-01i	6.36371e-02 - 3.73258e-03i	9.91854e-17 - 3.50774e-16i	-3.37913e-73 - 2.19101e-73i	4.46171e-188 + 8.31384e-188i	± 0
1,2	1500/45°	Pr	3.18132e+03 + 3.18195e-03i	3.00000e+00 - 0.00000e+00i	2.52420e+00 - 4.36216e-01i	4.87820e-02 - 2.07422e-01i	-7.04609e-14 + 7.04273e-13i	2.98122e-59 + 1.72666e-60i	-1.03864e-152 + 1.78352e-153i	± 0
1,2	1500/60°	Ob	-1.11981e+06 + 1.94556e-06i	-0.00000e+00 - 0.00000e+00i	$\pm \infty$	$\pm \infty$	$\pm \infty$	$\pm \infty$	$\pm \infty$	$\pm \infty$
1,2	1500/75°	Ob	-1.94276e+06 + 1.12345e-06i	-0.00000e+00 - 0.00000e+00i	$\pm \infty$	$\pm \infty$	$\pm \infty$	$\pm \infty$	$\pm \infty$	$\pm \infty$
1,2	1500/90°	Ob	-2.24400e+06 + 2.75178e-10i	-0.00000e+00 - 0.00000e+00i	$\pm \infty$	$\pm \infty$	$\pm \infty$	$\pm \infty$	$\pm \infty$	$\pm \infty$
1,2	2500/20°	Pr	7.49925e+03 - 0.00000e+00i	3.00000e+00 - 0.00000e+00i	1.98603e+00 - 0.00000e+00i	-2.62896e-04 - 0.00000e+00i	-1.67040e-32 - 0.00000e+00i	-9.48327e-143 - 5.79989e-159i	± 0	± 0
1,2	2500/15°	Pr	7.24369e+03 + 1.94114e-03i	3.00000e+00 - 5.55112e-17i	2.01054e+00 - 2.37215e-01i	3.97650e-04 + 6.86188e-05i	-3.43237e-32 + 2.47496e-31i	-2.80209e-139 - 8.89938e-138i	± 0	± 0
1,2	2500/30°	Pr	6.94444e+03 + 3.75000e-03i	3.00000e+00 + 1.11022e-16i	2.08461e+00 - 4.67682e-01i	-1.19930e-03 - 7.55174e-04i	-7.23099e-29 + 6.91590e-28i	2.63904e-123 - 1.23752e-123i	1.13043e-315 + 8.37133e-315i	± 0
1,2	2500/45°	Pr	5.30255e+03 + 5.30330e-03i	3.00000e+00 + 2.22045e-16i	2.20952e+00 - 6.83234e-01i	1.99840e-03 + 1.02616e-02i	-7.50435e-23 - 1.95844e-22i	3.46061e-100 - 1.57979e-100i	-1.51761e-254 + 1.59343e-254i	± 0
1,2	2500/60°	Ob	-3.11634e+06 + 5.40766e-06i	-0.00000e+00 - 0.00000e+00i	$\pm \infty$	$\pm \infty$	$\pm \infty$	$\pm \infty$	$\pm \infty$	$\pm \infty$
1,2	2500/75°	Ob	-5.40300e+06 + 3.12241e-06i	-0.00000e+00 - 0.00000e+00i	$\pm \infty$	$\pm \infty$	$\pm \infty$	$\pm \infty$	$\pm \infty$	$\pm \infty$
1,2	2500/90°	Ob	-6.24000e+06 + 7.64792e-10i	-0.00000e+00 - 0.00000e+00i	$\pm \infty$	$\pm \infty$	$\pm \infty$	$\pm \infty$	$\pm \infty$	$\pm \infty$
1,2	5000/20°	Pr	1.49993e+04 - 0.00000e+00i	3.00000e+00 - 0.00000e+00i	1.16850e+00 - 0.00000e+00i	-1.93873e-09 - 0.00000e+00i	-1.11859e-66 - 0.00000e+00i	-8.50358e-288 - 5.20375e-304i	± 0	± 0
1,2	5000/15°	Pr	1.44881e+04 + 3.88229e-03i	3.00000e+00 + 5.55112e-17i	1.19638e+00 - 3.83133e-01i	-4.54814e-09 - 2.89515e-10i	2.50162e-64 + 2.61775e-			

Table D.55: (continued)

m, n	$c \setminus \arg(c)$	type	$\lambda_{mn}^{(a)}$	$S_{mn}^{(a)}(c, \eta=0)$	$S_{mn}^{(a)}(c, \eta=0.01)$	$S_{mn}^{(a)}(c, \eta=0.1)$	$S_{mn}^{(a)}(c, \eta=0.25)$	$S_{mn}^{(a)}(c, \eta=0.5)$	$S_{mn}^{(a)}(c, \eta=0.75)$	$S_{mn}^{(a)}(c, \eta=0.99)$
1,3	100 \angle 60°	Ob	-4.65560e+03 + 8.46025e-03i	-0.00000e+00 - 0.00000e+00i	-5.62452e+01 + 1.46519e+02i	-2.55970e+05 - 2.38116e+05i	-1.02986e+11 + 5.20306e+10i	-1.66280e+20 + 7.08523e+19i	-2.39575e+29 + 8.51202e+28i	-2.76233e+37 + 5.19525e+36i
1,3	100 \angle 75°	Ob	-7.89559e+03 + 4.72929e-03i	-0.00000e+00 - 0.00000e+00i	-1.28225e+02 + 9.18245e+01i	-7.27872e+05 + 2.09095e+05i	-7.29935e+11 + 3.64044e+11i	-6.73948e+21 + 5.17484e+21i	-8.89939e+31 + 4.50450e+31i	-4.48776e+39 - 1.75592e+39i
1,3	100 \angle 90°	Ob	-9.20808e+03 + 1.17566e-12i	-0.00000e+00 - 0.00000e+00i	-1.60346e+02 + 3.48179e-14i	-1.06300e+06 + 7.94447e-10i	-1.90832e+12 + 3.17973e-03i	-4.65639e+22 + 1.48921e+08i	-7.63513e+32 + 3.61343e+18i	1.32724e+41 - 8.10102e+26i
1,3	250 \angle 0°	Pr	1.24725e+03 - 0.00000e+00i	-0.00000e+00 - 0.00000e+00i	1.82798e+01 - 0.00000e+00i	1.08753e-01 - 0.00000e+00i	-9.53798e-01 - 0.00000e+00i	-9.39046e-11 - 0.00000e+00i	-3.97510e-32 - 0.00000e+00i	-1.26150e-86 - 7.49660e-103i*
1,3	250 \angle 15°	Pr	1.20466e+03 + 3.23524e-02i	-0.00000e+00 - 0.00000e+00i	1.76962e+01 + 4.64565e+00i	1.13229e+01 + 1.47213e+01i	-1.13522e-01 + 1.25486e+00i	8.11003e-11 + 2.83095e-10i	6.02489e-31 + 4.26804e-31i*	-1.50370e-84 - 2.25281e-83i*
1,3	250 \angle 30°	Pr	1.07978e+03 + 6.25001e-02i	-0.00000e+00 - 0.00000e+00i	1.59744e+01 + 9.01549e+00i	5.42148e-01 - 3.27449e+01i	2.70800e+00 - 8.82439e-01i	8.39696e-09 + 2.67305e-10i	3.06228e-27 - 1.36806e-27i*	-3.38656e-74 - 1.84268e-74i*
1,3	250 \angle 45°	Ob	7.05104e+02 + 6.17929e-04i	-0.00000e+00 - 0.00000e+00i	9.12062e+02 + 6.16037e+02i	-6.77028e-09 - 2.71007e+02i	-9.69175e+20 + 1.51996e+21i	-6.06898e+39 + 1.63717e+40i	-2.13375e+58 + 1.50988e+59i	-5.86149e+76 + 1.91369e+75i
1,3	250 \angle 60°	Ob	-3.03860e+04 + 5.36266e-04i	-0.00000e+00 - 0.00000e+00i	3.43043e+02 + 1.57122e+03i	-3.46582e+11 + 1.72270e+11i	-3.46618e+25 + 1.31199e+25i	-7.24685e+48 + 1.44230e+48i	-1.32696e+72 + 4.30947e+70i	-2.02771e+93 - 6.45776e+93i
1,3	250 \angle 75°	Ob	-5.22028e+04 + 3.07324e-04i	-0.00000e+00 - 0.00000e+00i	-1.19687e+03 + 1.57660e+03i	-3.42485e+12 + 1.66993e+12i	8.38826e+27 - 7.58654e+27i	-2.29121e+53 + 5.98778e+53i	-2.70175e+78 - 2.48479e+79i	4.72230e+101 + 2.61828e+101i
1,3	250 \angle 90°	Ob	-6.05080e+04 + 7.53158e-12i	-0.00000e+00 - 0.00000e+00i	-2.14347e+03 + 2.75757e-13i	-8.92576e+12 + 1.34261e-02i	-9.50714e+28 + 3.61325e+14i	-4.53211e+55 + 3.45710e+41i	-1.48511e+82 + 1.70139e+68i	-7.79714e+104 + 1.23270e+91i
1,3	500 \angle 0°	Pr	2.49725e+03 - 0.00000e+00i	-0.00000e+00 - 0.00000e+00i	3.57945e+01 - 0.00000e+00i	-3.09058e-01 - 0.00000e+00i	-1.49485e-03 - 0.00000e+00i	-1.09344e-24 - 0.00000e+00i	-3.08129e-68 - 1.87864e-84i*	-3.55709e-179 - 2.14638e-195i*
1,3	500 \angle 15°	Pr	2.41206e+03 + 6.47048e-02i	-0.00000e+00 - 0.00000e+00i	3.47338e+01 + 8.88525e+00i	-3.56321e-01 - 4.35013e+00i	2.35133e-03 - 1.05275e-03i	4.86485e-24 - 9.55924e-24i	-7.66965e-66 - 6.43308e-66i*	6.42135e-173 - 5.07835e-173i*
1,3	500 \angle 30°	Pr	2.16231e+03 + 1.25000e-03i	-0.00000e+00 - 0.00000e+00i	3.15832e+01 + 1.73227e+01i	-5.24584e-01 - 1.12580e+01i	-1.07388e-02 + 6.79053e-03i	-4.54257e-21 + 7.37912e-21i	7.50192e-59 + 2.16458e-58i*	-3.63619e-154 + 1.79880e-155i*
1,3	500 \angle 45°	Ob	1.41221e+03 + 2.48586e-05i	-0.00000e+00 - 0.00000e+00i	4.75553e+03 - 1.16356e+04i	-1.06280e+16 - 6.95676e+17i	-1.98102e+40 + 5.28369e+40i	5.57824e+77 + 8.51451e+78i	5.48590e+116 + 1.02719e+117i	-7.12642e+152 - 1.05621e+153i
1,3	500 \angle 60°	Ob	-1.23270e+05 + 2.15506e-05i	-0.00000e+00 - 0.00000e+00i	2.76345e+04 + 3.22444e+03i	-1.81399e+21 + 7.51759e+20i	-2.34524e+49 + 4.60339e+48i	-1.51705e+96 - 2.10326e+95i	-7.90112e+142 - 4.00015e+142i	1.81181e+187 + 1.93014e+186i
1,3	500 \angle 75°	Ob	-2.12651e+05 + 1.23965e-05i	-0.00000e+00 - 0.00000e+00i	-5.70754e+02 + 4.47458e+04i	-1.89559e+23 + 1.40736e+23i	-1.36591e+54 + 3.52204e+54i	1.90999e+106 + 2.99693e+106i	2.31008e+158 + 1.48618e+157i	1.60164e+206 + 3.34702e+205i
1,3	500 \angle 90°	Ob	-2.46008e+05 + 3.03712e-11i	-0.00000e+00 - 0.00000e+00i	-5.30408e+04 + 2.12147e-11i	-1.29676e+24 + 4.09184e+09i	-2.67207e+56 + 2.07030e+42i	-1.77848e+110 + 2.73925e+96i	-8.19403e+163 + 1.88929e+150i	-3.28284e+213 + 9.99890e+199i
1,3	750 \angle 0°	Pr	3.74250e+03 - 0.00000e+00i	-0.00000e+00 - 0.00000e+00i	5.25100e+01 - 0.00000e+00i	-2.65206e-01 - 0.00000e+00i	-1.23570e-06 - 0.00000e+00i	-0.705030e-39 - 0.00000e+00i	-1.42101e-104 - 8.67626e-121i*	-5.20786e-272 - 3.15805e-288i*
1,3	750 \angle 15°	Pr	3.61947e+03 + 9.70572e-02i	-0.00000e+00 - 0.00000e+00i	5.10724e+01 + 1.27343e+01i	-2.93191e+01 + 9.78830e+01i	-2.20593e-06 - 1.70448e-06i	-2.03626e-37 + 7.34256e-38i	5.58851e-104 + 5.65555e-101i	1.65398e-262 + 5.32062e-263i
1,3	750 \angle 30°	Pr	3.24484e+03 + 1.87500e-03i	-0.00000e+00 - 0.00000e+00i	4.67707e+01 + 2.49439e+01i	-3.96786e+01 + 2.72174e+01i	4.93745e-06 - 2.98747e-05i	-2.33872e-33 - 4.37471e-33i	-8.15767e-90 + 2.03802e-90i*	-1.29481e-234 + 8.94447e-235i*
1,3	750 \angle 45°	Pr	2.11932e+03 + 5.60379e-05i	-0.00000e+00 - 0.00000e+00i	-1.08575e+05 - 2.11762e+04i	4.55081e+25 - 1.99543e+25i	-1.94731e+59 + 1.30779e+60i	1.46328e+117 + 2.75619e+117i	5.99811e+174 + 2.86934e+174i	6.86920e+228 - 1.85927e+229i
1,3	750 \angle 60°	Ob	-2.78654e+05 + 4.85639e-05i	-0.00000e+00 - 0.00000e+00i	1.54265e+05 - 3.29859e-05i	-7.06197e+30 - 2.38606e+30i	-1.15272e+73 + 3.13634e+71i	-2.11659e+143 - 1.07622e+143i	-2.50394e+213 - 3.63455e+213i	-1.55734e+280 + 3.07442e+280i
1,3	750 \angle 75°	Ob	-4.81352e+05 + 2.79979e-11i	-0.00000e+00 - 0.00000e+00i	$\pm \infty$	$\pm \infty$	$\pm \infty$	$\pm \infty$	$\pm \infty$	$\pm \infty$
1,3	750 \angle 90°	Ob	-5.56508e+05 + 6.85190e-11i	-0.00000e+00 - 0.00000e+00i	$\pm \infty$	$\pm \infty$	$\pm \infty$	$\pm \infty$	$\pm \infty$	$\pm \infty$
1,3	1000 \angle 0°	Pr	4.99725e+03 - 0.00000e+00i	-0.00000e+00 - 0.00000e+00i	6.84479e+01 - 0.00000e+00i	-1.51578e+01 - 0.00000e+00i	-7.95046e-10 - 0.00000e+00i	-3.57799e-53 - 0.00000e+00i	-4.71922e-141 - 2.88348e-157i*	± 0
1,3	1000 \angle 15°	Pr	4.82688e+03 + 1.29410e-03i	-0.00000e+00 - 0.00000e+00i	6.67275e+01 + 1.62080e+01i	-1.40978e+01 + 1.15935e+01i	-3.97724e-10 + 1.23155e-09i	-3.13878e-136 + 1.36725e-136i	-3.13878e-136 + 1.36725e-136i	± 0
1,3	1000 \angle 30°	Pr	4.32738e+03 + 2.50000e-03i	-0.00000e+00 - 0.00000e+00i	6.15372e+01 + 3.19009e+01i	-8.39472e+03 + 3.02505e-01i	3.50268e-08 + 4.40892e-08i	2.23468e-45 + 8.73411e-47i	-3.59421e-122 - 2.32815e-121i*	-2.08905e-315 + 4.75254e-315i*
1,3	1000 \angle 45°	Ob	2.82643e+03 + 9.97172e-05i	-0.00000e+00 - 0.00000e+00i	3.37315e+03 + 8.64381e+05i	2.28735e+33 + 2.17023e+33i	1.74869e+78 + 2.74699e+79i	8.01237e+155 + 2.61239e+155i	3.31223e+232 - 6.32386e+231i	2.60023e+305 - 3.75759e+304i
1,3	1000 \angle 60°	Ob	-4.96538e+05 + 8.64025e-05i	-0.00000e+00 - 0.00000e+00i	$\pm \infty$	$\pm \infty$	$\pm \infty$	$\pm \infty$	$\pm \infty$	$\pm \infty$
1,3	1000 \angle 75°	Ob	-8.58306e+05 + 4.97929e-05i	-0.00000e+00 - 0.00000e+00i	$\pm \infty$	$\pm \infty$	$\pm \infty$	$\pm \infty$	$\pm \infty$	$\pm \infty$
1,3	1000 \angle 90°	Ob	-9.92008e+05 + 1.21975e-10i	-0.00000e+00 - 0.00000e+00i	$\pm \infty$	$\pm \infty$	$\pm \infty$	$\pm \infty$	$\pm \infty$	$\pm \infty$
1,3	1500 \angle 0°	Pr	7.49725e+03 - 0.00000e+00i	-0.00000e+00 - 0.00000e+00i	9.80752e+01 - 0.00000e+00i	-3.09269e+00 - 0.00000e+00i	-2.30901e-16 - 0.00000e+00i	-6.53527e-82 - 0.00000e+00i	-3.62577e-214 - 2.21695e-230i*	± 0
1,3	1500 \angle 15°	Pr	7.24169e+03 + 1.94114e-03i	-0.00000e+00 - 0.00000e+00i	9.60481e+01 + 2.20877e+01i	-8.00319e-01 + 3.94819e-01i	-8.41400e-16 - 8.14965e-16i	-2.10536e-79 + 5.78415e-79i	-6.26476e-207 - 1.04789e-206i*	± 0
1,3	1500 \angle 30°	Pr	6.49244e+03 + 3.75000e-03i	-0.00000e+00 - 0.00000e+00i	8.98113e+01 + 4.39072e+01i	7.55280e+02 + 4.39421e+00i	9.89511e-14 - 9.46523e-14i	-1.46003e-70 - 2.87558e-70i	-3.97682e-186 + 1.27525e-184i*	± 0
1,3	1500 \angle 45°	Ob	4.24044e+03 + 2.24576e-06i	-0.00000e+00 - 0.00000e+00i	$\pm \infty$	$\pm \infty$	$\pm \infty$	$\pm \infty$	$\pm \infty$	$\pm \infty$
1,3	1500 \angle 60°	Ob	-1.11981e+06 + 1.94556e-06i	-0.00000e+00 - 0.00000e+00i	$\pm \infty$	$\pm \infty$	$\pm \infty$	$\pm \infty$	$\pm \infty$	$\pm \infty$
1,3	1500 \angle 75°	Ob	-1.93697e+06 + 1.12189e-06i	-0.00000e+00 - 0.00000e+00i	$\pm \infty$	$\pm \infty$	$\pm \infty$	$\pm \infty$	$\pm \infty$	$\pm \infty$
1,3	1500 \angle 90°	Ob	-2.23801e+06 + 2.74811e-10i	-0.00000e+00 - 0.00000e+00i	$\pm \infty$	$\pm \infty$	$\pm \infty$	$\pm \infty$	$\pm \infty$	$\pm \infty$
1,3	2500 \angle 0°	Pr	1.24972e+04 - 0.00000e+00i	-0.00000e+00 - 0.00000e+00i	1.48900e-02 - 0.00000e+00i	-6.17581e-02 - 0.00000e+00i	-1.05038e-29 - 0.00000e+00i	-1.27263e-139 - 7.78327e-156i*	± 0	± 0
1,3	2500 \angle 15°	Pr	1.20713e+04 + 3.23524e-03i	-0.00000e+00 - 0.00000e+00i	1.47145e+02 + 2.99631e+01i	8.55648e-02 + 4.13966e-02i	-6.14694e-29 + 1.44648e-28i	2.72399e-135 - 1.15843e-134i*	± 0	± 0
1,3	2500 \angle 30°	Pr	1.08226e+04 + 6.25000e-03i	-0.00000e+00 - 0.00000e+00i	1.41359e+02 + 6.08623e+01i	-1.46698e-01 - 3.02790e-01i	-2.58940e-25 + 3.53084e-25i	3.88217e-120 + 3.36339e-121i*	-7.24053e-312 + 1.76263e-311i*	± 0
1,3	2500 \angle 45°	Ob	7.06907e+03 + 6.24293e-06i	-0.00000e+00 - 0.00000e+00i	$\pm \infty$	$\pm \infty$	$\pm \infty$	$\pm \infty$	$\pm \infty$	$\pm \infty$
1,3	2500 \angle 60°	Ob	-3.11634e+06 + 5.40766e-06i	-0.00000e+00 - 0.00000e+00i	$\pm \infty$	$\pm \infty$	$\pm \infty$	$\pm \infty$	$\pm \infty$	$\pm \infty$
1,3	2500 \angle 75°	Ob	-5.39335e+06 + 3.11982e-06i	-0.00000e+00 - 0.00000e+00i	$\pm \infty$	$\pm \infty$	$\pm \infty$	$\pm \infty$	$\pm \infty$	$\pm \infty$
1,3	2500 \angle 90°	Ob	-6.23001e+06 + 7.64180e-10i	-0.00000e+00 - 0.00000e+00i	$\pm \infty$	$\pm \infty$	$\pm \infty$	$\pm \infty$	$\pm \infty$	$\pm \infty$
1,3	5000 \angle 0°	Pr	2.49972e+04 - 0.00000e+00i	-0.00000e+00 - 0.00000e+00i	2.33642e+02 - 0.00000e+00i	-9.41954e-07 - 0.00000e+00i	-1.41381e-63 - 0.00000e+00i	-2.21979e-284 - 1.35840e-300i*	± 0	± 0
1,3	500									

Table D.55: (continued)

m, n	$c \setminus \arg(c)$	type	$\lambda_{mn}^{(a)'}$	$S_{mn}^{(a)'}(c, \eta=0)$	$S_{mn}^{(a)'}(c, \eta=0.01)$	$S_{mn}^{(a)'}(c, \eta=0.1)$	$S_{mn}^{(a)'}(c, \eta=0.25)$	$S_{mn}^{(a)'}(c, \eta=0.5)$	$S_{mn}^{(a)'}(c, \eta=0.75)$	$S_{mn}^{(a)'}(c, \eta=0.99)$
1,4	100/60°	Pr	1.49253e+02 + 2.59803e+02i	-7.50000e+00 - 8.88178e-16i	-7.44491e+00 + 9.70342e-02i	-5.68044e-01 + 5.89861e+00i	2.41336e-01 - 9.55110e+00i	-4.44425e-01 + 2.75084e-01i	-4.86369e-05 - 2.05775e-06i	-7.56236e-15 + 1.22471e-14i*
1,4	100/75°	Ob	-7.89559e+03 + 4.79292e+03i	-7.50000e+00 + 1.77636e-15i	-1.05846e+01 + 2.04233e+00i	3.35369e+04 + 2.06784e+04i	-4.16739e+10 + 8.00799e+09i	-4.10195e+20 + 1.64804e+20i	-2.58950e+30 + 1.71027e+30i	2.49458e+38 - 2.50713e+37i
1,4	100/90°	Ob	-9.20808e+03 + 1.17566e-12i	-7.50000e+00 + 3.71426e-16i	-1.12277e+01 + 1.06779e-15i	-5.53887e+04 + 3.66703e-11i	-9.94348e+10 + 1.57200e-04i	-2.46252e+21 + 7.55269e+06i	-3.97835e+31 + 1.84887e+17i	6.91570e+39 - 4.16211e+25i
1,4	250/20°	Pr	1.74424e+03 - 0.00000e+00i	-7.50000e+00 - 0.00000e+00i	-6.85755e+00 - 0.00000e+00i	5.06583e+00 - 0.00000e+00i	-3.45218e-01 - 0.00000e+00i	-8.11249e-11 - 0.00000e+00i	-5.89874e-32 - 0.00000e+00i	-3.63308e-86 - 2.15872e-102i*
1,4	250/15°	Pr	1.68461e+03 + 4.52936e+02i	-7.50000e+00 + 1.11022e-16i	-6.87850e+00 + 1.64578e-01i	5.56251e+00 - 2.19806e+00i	-6.39400e-02 + 4.55984e-01i	6.79466e-11 + 2.45508e-10i	8.92292e-31 + 6.37030e-31i*	-4.26237e-84 - 6.49136e-83i*
1,4	250/30°	Pr	1.50978e+03 + 8.75000e+02i	-7.50000e+00 - 8.88178e-16i	-6.94020e+00 + 3.18983e-01i	7.32737e+00 - 4.82080e+00i	9.81947e-01 + 4.20344e-01i	7.28593e-09 + 3.57601e-10i	4.56747e-27 - 2.00186e-27i	-9.69254e-74 - 5.39075e-74i*
1,4	250/45°	Ob	7.05104e+02 + 6.17929e+04i	-7.50000e+00 - 8.70776e-15i	4.34175e+00 + 2.04758e+01i	-5.69755e-07 - 1.35160e+01i	-3.54455e+19 + 7.63141e+18i	-3.19991e+38 + 1.44706e+38i	-2.46135e+57 + 1.82992e+57i	-8.56245e+74 - 8.11324e+74i
1,4	250/60°	Pr	3.74251e+02 + 6.49517e+02i	-7.50000e+00 - 0.00000e+00i	-7.35931e+00 + 2.41067e-01i	8.22084e+00 + 3.22663e+00i	2.00451e+00 + 1.13566e+00i	-3.22213e-05 - 1.11171e-05i	-1.07439e-15 - 1.42271e-17i	-2.81718e-42 - 1.43664e-42i*
1,4	250/75°	Ob	-5.22028e+04 + 3.07324e+04i	-7.50000e+00 - 3.55271e-15i	-3.24365e+01 + 2.40885e+01i	-7.60471e+10 + 1.44387e+10i	2.04932e+26 - 1.03896e+26i	-7.68893e+51 + 1.05125e+52i	7.97586e+76 - 5.01455e+77i	7.85740e+99 + 7.65409e+99i
1,4	250/90°	Ob	-6.05800e+04 + 7.53158e-12i	-7.50000e+00 - 8.15423e-16i	-4.42103e+01 + 1.86329e-15i	-1.81430e+11 + 2.58023e-04i	-1.93247e+27 + 7.18596e+12i	-9.21220e+53 + 6.95152e+39i	-3.01871e+80 + 3.43358e+66i	1.58489e+103 + 2.49264e+89i
1,4	500/20°	Pr	3.49424e+03 - 0.00000e+00i	-7.50000e+00 - 0.00000e+00i	-6.23278e+00 - 0.00000e+00i	-1.64943e+00 - 0.00000e+00i	-5.89930e-04 - 0.00000e+00i	-9.60864e-25 - 0.00000e+00i	-4.80961e-68 - 2.93233e-84i*	-1.07239e-178 - 6.47070e-195i*
1,4	500/15°	Pr	3.37498e+03 + 9.05868e+02i	-7.50000e+00 + 1.11022e-16i	-6.27196e+00 + 3.18767e-01i	-2.31988e+00 - 2.01512e+00i	9.38969e-04 - 3.98185e-04i	4.31366e-24 - 8.38676e-24i	-1.14413e-65 - 9.64097e-66i*	1.85482e-172 - 1.46391e-172i*
1,4	500/30°	Pr	3.02533e+03 + 1.75000e+03i	-7.50000e+00 + 2.22045e-16i	-6.38785e+00 + 6.19859e-01i	-4.71715e+00 - 4.90798e+00i	-4.38847e-03 + 2.54956e-03i	-4.05468e-21 + 6.46621e-21i	1.11195e-58 + 3.24259e-58i*	-1.05023e-153 + 5.11120e-153i*
1,4	500/45°	Ob	4.11221e+03 + 2.48586e+05i	-7.50000e+00 + 1.15463e-14i	1.16575e+02 - 4.83710e+01i	4.87195e+15 - 4.99465e+15i	-5.15811e+38 + 2.32731e+38i	-5.66041e+76 + 6.41723e+76i	-3.42552e+114 + 1.11643e+115i	2.47187e+150 + 1.25361e+151i
1,4	500/60°	Pr	7.49251e+02 + 1.29904e+03i	-7.50000e+00 - 0.00000e+00i	-7.21439e+00 + 4.77061e-01i	5.91897e+00 - 7.96356e+00i	8.79128e-02 - 9.42883e-02i	3.35248e-12 - 1.45052e-12i	4.96430e-34 - 8.33849e-34i*	1.81080e-88 - 2.95136e-89i*
1,4	500/75°	Ob	-2.12651e+05 + 1.23965e+05i	-7.50000e+00 - 4.97380e-14i	-1.23196e+02 + 4.33777e+02i	-2.21420e+21 - 8.70929e+20i	-2.25477e+52 + 3.06757e+52i	1.07043e+104 + 3.41783e+104i	-1.79285e+108 + 7.51857e+108i	2.20843e+156 + 7.46669e+156i
1,4	500/90°	Ob	-2.46008e+05 + 3.03712e-11i	-7.50000e+00 + 9.01276e-17i	-5.34747e+02 + 1.70131e-13i	-1.30724e+22 + 4.01803e+07i	-2.69366e+54 + 2.06501e+54i	-1.79285e+108 + 7.51857e+108i	-8.26024e+161 + 1.89780e+148i	-3.30937e+211 + 1.00526e-198i
1,4	750/20°	Pr	5.24425e+03 - 0.00000e+00i	-7.50000e+00 - 0.00000e+00i	-5.62851e+00 - 0.00000e+00i	-2.83544e+00 - 0.00000e+00i	-4.99983e-07 - 0.00000e+00i	-6.22969e-39 - 0.00000e+00i	-2.13271e-104 - 1.30216e-120i*	-5.07175e-219 + 9.13936e-288i*
1,4	750/15°	Pr	5.06536e+03 + 1.35880e+03i	-7.50000e+00 - 1.11022e-16i	-5.68331e+00 + 4.62919e-01i	-3.48477e+00 + 4.87106e-01i	-8.85545e-07 - 1.01998e-07i	-1.80177e-37 - 6.43957e-38i	8.29766e-104 + 8.50788e-101i	4.75773e-262 + 1.56046e-262i*
1,4	750/30°	Pr	4.54088e+03 + 2.62500e+03i	-7.50000e+00 - 4.44089e-16i	-5.84624e+00 + 9.03134e-01i	-5.91292e+00 + 1.96031e+00i	2.30000e-06 - 1.21236e+00i	-2.04853e-33 - 3.88254e-33i	-1.22372e-89 + 3.03105e-90i*	-3.74218e-42 - 1.43664e-42i*
1,4	750/45°	Pr	2.11932e+03 + 5.60379e+05i	-7.50000e+00 + 6.90559e-14i	-4.11642e-02 - 6.13556e-02i	3.08946e+23 + 1.12173e+23i	-7.10624e+57 + 5.24348e+57i	-6.14399e+114 + 1.99168e+115i	1.46978e+172 + 5.19083e+172i	1.20360e+227 + 5.51421e+226i
1,4	750/60°	Pr	1.12425e+03 + 1.94856e+03i	-7.50000e+00 - 8.88178e-16i	-7.06674e+00 + 7.07982e-01i	-4.01109e+20 + 7.10923e-01i	1.91229e+57 + 1.63899e+57i	-1.21361e-19 + 2.66314e-19i	3.40108e-52 + 5.08545e-52i*	-5.34010e-135 + 5.20435e-135i*
1,4	750/75°	Ob	-4.81352e+05 + 2.79979e+05i	-7.50000e+00 + 2.75685e-09i	1.82613e+03 + 4.70320e+03i	-6.18620e+31 + 3.89556e+31i	1.03978e+78 - 6.21407e+78i	9.28052e+156 + 3.19231e+156i	-5.04523e+234 + 9.33169e+234i	1.10308e+308 + 8.46234e+307i
1,4	750/90°	Ob	-5.56508e+05 + 6.85190e-11i	-0.00000e+00 - 0.00000e+00i	± 0	± 0	± 0	± 0	± 0	± 0
1,4	1000/20°	Pr	6.99425e+03 - 0.00000e+00i	-7.50000e+00 - 0.00000e+00i	-5.04423e+00 - 0.00000e+00i	-1.90780e+00 - 0.00000e+00i	-3.25530e-10 - 0.00000e+00i	-3.17015e-53 - 0.00000e+00i	-7.10162e-141 - 4.33912e-157i*	± 0
1,4	1000/15°	Pr	6.75573e+03 + 1.81173e+03i	-7.50000e+00 - 2.22045e-16i	-5.11221e+00 + 5.97373e-01i	-1.96281e+00 + 5.97373e-01i	-1.71638e-10 + 9.47801e-10i	2.79381e-51 + 1.21762e-51i	-4.69931e-136 - 5.51019e-136i	-6.04101e-315 + 1.37289e-314i*
1,4	1000/30°	Pr	6.05643e+03 + 3.50000e+03i	-7.50000e+00 - 2.22045e-16i	-5.31535e+00 + 1.16930e-01i	-1.85148e+00 + 3.90116e+00i	1.49086e-08 + 1.83907e-08i	1.98183e-45 + 8.55027e-47i	-5.33536e-122 - 3.49328e-121i*	1.18793e+230 + 9.50787e+229i
1,4	1000/45°	Ob	2.82643e+03 + 9.97172e+05i	-7.50000e+00 + 2.10498e-13i	-3.05278e+03 + 3.06799e+03i	3.92290e+29 + 1.57828e+29i	9.12135e+61 + 1.03320e+61i	-1.21361e-19 + 2.66314e-19i	1.39526e+230 + 5.07323e+153i	1.39526e+230 + 5.07323e+153i
1,4	1000/60°	Pr	1.49925e+03 + 2.59808e+03i	-7.50000e+00 - 4.44089e-16i	-6.91647e+00 + 9.33834e-01i	-5.88958e+00 + 3.57285e-01i	1.66861e-05 - 6.13707e-05i	-6.27058e-27 - 1.98594e-26i	-4.16086e-70 - 6.41729e-72i*	4.52976e-182 - 2.45837e-181i*
1,4	1000/75°	Ob	-8.58306e+05 + 4.97929e+05i	-0.00000e+00 - 0.00000e+00i	± 0	± 0	± 0	± 0	± 0	± 0
1,4	1000/90°	Ob	-9.92008e+05 + 1.21975e-10i	-0.00000e+00 - 0.00000e+00i	± 0	± 0	± 0	± 0	± 0	± 0
1,4	1500/20°	Pr	1.04942e+04 - 0.00000e+00i	-7.50000e+00 - 0.00000e+00i	-3.93377e+00 - 0.00000e+00i	-4.38190e+00 - 0.00000e+00i	-9.56358e-17 - 0.00000e+00i	-5.80600e-82 - 0.00000e+00i	-5.48297e-214 - 3.35251e-230i*	± 0
1,4	1500/15°	Pr	1.01365e+04 + 2.71760e+03i	-7.50000e+00 + 1.11022e-16i	-4.02128e+00 + 8.38511e-01i	-1.43834e+01 + 5.58503e-01i	-3.46824e-16 - 3.39858e-16i	-1.87792e-79 + 5.13704e-79i	-9.40447e-207 - 1.57485e-206i*	± 0
1,4	1500/30°	Pr	9.08751e+03 + 5.25000e+03i	-7.50000e+00 - 8.88178e-16i	-4.28566e+00 + 5.62200e-01i	1.04574e+00 + 7.84869e-01i	4.15543e-14 - 3.88649e-14i	-1.29119e-70 - 2.06266e-70i	-6.09611e-186 + 1.91294e-184i*	± 0
1,4	1500/45°	Ob	4.24064e+03 + 2.24576e+06i	-0.00000e+00 - 0.00000e+00i	± 0	± 0	± 0	± 0	± 0	± 0
1,4	1500/60°	Pr	2.24925e+03 + 3.89711e+06i	-7.50000e+00 + 4.44089e-16i	-6.60844e+00 + 1.37035e+00i	1.63714e+00 + 1.97633e+00i	-2.72122e-08 - 2.05914e-08i	-8.71268e-41 + 1.77061e-41i	5.84658e-107 + 1.06075e-106i*	-1.99295e-274 - 1.16753e-274i*
1,4	1500/75°	Ob	-1.93697e+06 + 1.12189e+06i	-0.00000e+00 - 0.00000e+00i	± 0	± 0	± 0	± 0	± 0	± 0
1,4	1500/90°	Ob	-2.23801e+06 + 2.74811e-10i	-0.00000e+00 - 0.00000e+00i	± 0	± 0	± 0	± 0	± 0	± 0
1,4	2500/20°	Pr	1.74942e+04 - 0.00000e+00i	-7.50000e+00 - 0.00000e+00i	-1.93245e+00 - 0.00000e+00i	-9.42911e-03 - 0.00000e+00i	-4.38965e-30 - 0.00000e+00i	-1.12895e-139 - 6.90453e-156i*	± 0	± 0
1,4	2500/15°	Pr	1.68980e+04 + 4.52933e+03i	-7.50000e+00 + 1.11022e-16i	-2.03514e+00 + 1.21848e-01i	1.29507e-02 + 6.68830e-03i	-2.59079e-29 + 6.03898e-29i	2.30059e-135 - 9.89603e-135i*	± 0	± 0
1,4	2500/30°	Pr	1.51497e+04 + 8.75000e+03i	-7.50000e+00 - 0.00000e+00i	-2.35387e+00 + 2.43328e-01i	-2.04449e-02 + 4.80611e-02i	-1.09385e-25 + 1.47109e-25i	3.45652e-120 + 3.06502e-121i*	-1.09073e-311 + 2.64868e-311i*	± 0
1,4	2500/45°	Ob	7.06907e+03 + 6.24293e+06i	-0.00000e+00 - 0.00000e+00i	± 0	± 0	± 0	± 0	± 0	± 0
1,4	2500/60°	Pr	3.74925e+03 + 6.49517e+02i	-7.50000e+00 + 4.44089e-16i	-5.96518e+00 + 2.18287e-01i	-3.32520e-01 + 1.19475e-01i	1.10196e-15 + 7.16941e-15i	1.19891e-69 + 1.53487e-71i	-6.99727e-180 - 2.25540e-181i*	± 0
1,4	2500/75°	Ob	-5.39335e+06 + 3.11982e+06i	-0.00000e+00 - 0.00000e+00i	± 0	± 0	± 0	± 0	± 0	± 0
1,4	2500/90°	Ob	-6.23001e+06 + 7.64180e-10i	-0.00000e+00 - 0.00000e+00i	± 0	± 0	± 0	± 0	± 0	± 0
1,4	5000/20°	Pr	3.49942e+04 - 0.00000e+00i	-7.50000e+00 - 0.00000e+00i	1.94594e+00 - 0.00000e+00i	-1.50859e-07 - 0.00000e+00i	-5.94740e-64 - 0.00000e+00i	-1.98382e-284 - 1.21399e-300i*	± 0 </	

Table D.55: (continued)

m, n	$c \setminus \arg(c)$	type	$\lambda_{mn}^{(a)}$	$S_{mn}^{(a)}(c, \eta=0)$	$S_{mn}^{(a)}(c, \eta=0.01)$	$S_{mn}^{(a)}(c, \eta=0.1)$	$S_{mn}^{(a)}(c, \eta=0.25)$	$S_{mn}^{(a)}(c, \eta=0.5)$	$S_{mn}^{(a)}(c, \eta=0.75)$	$S_{mn}^{(a)}(c, \eta=0.99)$
1,5	100/60	Ob	-4.31525e+03 + 8.26021e-03i	-0.00000e+00 - 0.00000e+00i	6.41690e+01 - 1.76988e+02i	-2.94242e+05 + 2.35365e+05i	7.47062e+10 + 3.91996e+10i	6.59846e+19 - 2.99604e+19i	3.89531e+28 - 1.59499e+28i	-2.02352e+36 - 2.99351e+35i
1,5	100/75	Pr	2.61327e+01 + 9.65895e-01i	-0.00000e+00 - 0.00000e+00i	-4.79399e-01 - 1.80658e-00i	-1.11647e+01 - 1.22597e+01i	3.89293e+00 + 2.14075e+01i	-2.20128e+00 - 3.03349e+01i	-4.80653e-02 - 2.4749e-03i*	-2.08841e-06 - 1.92150e-07i*
1,5	100/90	Ob	-8.81828e+03 + 1.15115e-12i	-0.00000e+00 - 0.00000e+00i	1.90774e+02 - 4.28805e-14i	1.05812e+06 - 7.98094e-10i	1.37992e+12 - 2.30965e-03i	1.82479e+22 - 5.85282e+07i	1.19250e+32 - 5.66082e+17i	6.71551e+38 - 3.93744e+24i
1,5	250/20	Pr	2.24022e+03 - 0.00000e+00i	-0.00000e+00 - 0.00000e+00i	-4.04038e+01 - 0.00000e+00i	8.08716e+01 - 0.00000e+00i	-8.81319e+00 - 0.00000e+00i	-5.18858e-09 - 0.00000e+00i	-6.51554e-30 - 0.00000e+00i	-8.04066e-84 - 4.77702e-100i*
1,5	250/15	Pr	2.16355e+03 + 5.82352e+02i	-0.00000e+00 - 0.00000e+00i	-3.91769e+01 - 1.01279e+01i	9.04177e+01 - 2.11677e+01i	-5.47224e+00 + 1.06351e+01i	-7.24387e-11 + 1.63228e-08i	7.65270e-29 + 9.39972e-29i*	2.76121e-81 - 1.37088e-80i*
1,5	250/30	Pr	1.93878e+03 + 1.12502e+03i	-0.00000e+00 - 0.00000e+00i	-3.55394e+01 - 1.97202e+01i	1.19004e+02 + 6.01481e+01i	1.42325e+01 + 2.52464e+01i	3.88726e-07 + 2.64086e-07i	5.48461e-25 + 6.64927e-26i	-1.20391e-71 - 2.04960e-71i*
1,5	250/45	Pr	8.81133e+02 + 8.83884e+02i	-0.00000e+00 - 0.00000e+00i	-1.65029e+01 - 1.60525e+01i	-2.18862e+01 + 7.16279e+01i	-9.33447e+00 + 9.05424e+01i	-2.16035e-06 + 1.92013e-07i	-4.31779e-22 - 3.11458e-21i*	3.43854e-59 + 2.11707e-59i*
1,5	250/60	Ob	-2.95260e+04 + 9.65895e-01i	-0.00000e+00 - 0.00000e+00i	-4.26158e+02 - 1.91046e+03i	3.50766e+11 - 1.76440e+11i	2.56792e+25 - 9.89346e+24i	2.96867e+48 - 6.18467e+47i	2.29872e+71 - 1.15257e+70i	2.33537e+91 + 5.45490e+90i
1,5	250/75	Ob	6.49551e+01 + 2.41480e+02i	-0.00000e+00 - 0.00000e+00i	-1.24980e+00 - 4.49876e+00i	-3.39878e+01 - 3.46069e+00i	-1.58326e+01 + 1.15534e+00i	-4.8049e-02 - 1.89830e-02i	-7.55908e-08 - 2.24133e-07i*	-5.25062e-21 - 1.66375e-20i*
1,5	250/90	Pr	-5.95181e+04 + 7.47034e-12i	-0.00000e+00 - 0.00000e+00i	2.60339e+03 - 3.62301e-13i	9.03459e+12 - 1.36850e-02i	7.03133e+28 - 2.67988e+14i	1.84476e+55 - 1.40928e+41i	2.52345e+81 - 2.89426e+67i	-1.87256e+103 + 2.81809e+89i
1,5	500/20	Pr	4.49023e+03 - 0.00000e+00i	-0.00000e+00 - 0.00000e+00i	-7.78902e+01 - 0.00000e+00i	3.36245e+01 - 0.00000e+00i	-1.00948e-01 - 6.01596e-18i*	-8.50951e-22 - 5.17788e-38i*	-1.08080e-64 - 5.68927e-81i*	-4.65930e-175 - 2.81129e-191i*
1,5	500/15	Pr	4.33690e+03 + 1.16469e+03i	-0.00000e+00 - 0.00000e+00i	-7.58351e+01 - 1.87209e+01i	4.18862e+01 - 5.88115e+01i	5.89199e-02 - 6.63521e-03i	8.36316e-22 - 9.10740e-22i	-1.90417e-63 - 2.74647e-63i*	-4.65930e-175 - 2.81129e-191i*
1,5	500/30	Pr	3.88735e+03 + 2.25001e+03i	-0.00000e+00 - 0.00000e+00i	-9.66606e+01 - 3.67547e+01i	7.97768e+01 - 5.13212e+01i	-2.98539e-01 - 1.43452e-02i	-8.91720e-19 + 5.49326e-19i	-1.51172e-56 + 7.51895e-56i*	-4.03713e-151 - 2.08712e-151i*
1,5	500/45	Pr	1.76502e+03 + 1.76777e+03i	-0.00000e+00 - 0.00000e+00i	-3.30562e+01 - 3.10703e+01i	-1.98109e+01 - 3.10703e+01i	-1.98109e-01 + 3.38938e-02i	-1.02784e-16 - 4.44951e-16i	3.65073e-47 + 1.22426e-46i	1.62892e-124 - 8.57095e-125i*
1,5	500/60	Ob	-1.21544e+05 + 2.14506e+05i	-0.00000e+00 - 0.00000e+00i	-3.37476e+04 - 3.86745e+03i	1.84596e+21 - 7.70091e+20i	7.14917e+49 + 3.48624e+48i	6.27732e+95 + 8.42160e+94i	1.39633e+142 + 6.91875e+141i	-7.58005e+184 + 1.73148e+184i
1,5	500/75	Pr	1.29660e+02 + 4.82962e+02i	-0.00000e+00 - 0.00000e+00i	-2.61359e+00 - 8.93742e+00i	-2.19564e+01 + 4.42750e+01i	-4.53220e-01 + 4.04465e+00i	-1.50418e-05 + 9.47626e-06i	-5.92942e-17 - 1.37875e-16i*	-1.00627e-44 - 2.44431e-44i*
1,5	500/90	Pr	-2.44018e+03 + 3.02488e-11i	-0.00000e+00 - 0.00000e+00i	6.47180e+04 - 2.61058e-11i	1.31948e+24 - 4.16811e+09i	1.99028e+56 - 1.54277e+42i	7.32556e+109 - 1.12858e+96i	1.42815e+163 - 3.29353e+149i	5.24156e+210 - 1.60937e+197i
1,5	750/20	Pr	6.74024e+03 - 0.00000e+00i	-0.00000e+00 - 0.00000e+00i	-1.12377e+02 - 0.00000e+00i	-4.65733e+01 - 0.00000e+00i	-4.48884e-05 - 0.00000e+00i	-1.23349e-36 - 0.00000e+00i	-7.07924e-102 - 4.32231e-118i*	-9.25637e-269 - 5.85373e-285i*
1,5	750/15	Pr	6.51024e+03 + 1.74703e+03i	-0.00000e+00 - 0.00000e+00i	-1.09858e+02 - 2.58632e+01i	-6.59747e+01 - 3.99669e+01i	-5.92776e-05 - 8.26577e-05i	-3.77916e-35 + 2.93653e-36i	1.94931e-98 + 3.46212e-98i*	2.70859e-259 + 1.75910e-259i*
1,5	750/30	Pr	5.83591e+03 + 3.37501e+03i	-0.00000e+00 - 0.00000e+00i	-1.02164e+02 - 5.12249e+01i	-1.44458e+01 - 1.11444e+01i	7.56495e-04 - 8.24405e-04i	3.97781e-32 - 8.70105e-31i	-4.07433e-87 - 1.18938e-87i*	-2.94353e-231 + 2.39724e-231i*
1,5	750/45	Pr	2.64890e+03 + 2.65165e+03i	-0.00000e+00 - 0.00000e+00i	-4.95705e+01 - 4.50735e+01i	8.45265e+01 - 8.47860e+01i	-1.49294e-03 - 7.75301e-04i	5.01917e-26 - 1.85568e-26i	-1.55134e-72 - 2.95388e-72i*	4.91554e-192 - 5.38941e-190i*
1,5	750/60	Ob	-2.76062e+05 + 4.84139e+05i	-0.00000e+00 - 0.00000e+00i	-1.88017e+05 + 4.03467e+05i	1.88017e+05 - 2.44497e+05i	8.61630e+72 - 2.51070e+71i	7.19935e+142 + 4.43616e+142i	4.46438e+212 + 6.40175e+212i	4.72594e+278 - 1.61442e+278i
1,5	750/75	Pr	1.94364e+02 + 7.24444e+02i	-0.00000e+00 - 0.00000e+00i	-4.07573e+00 - 1.33144e+01i	±∞	±∞	±∞	±∞	±∞
1,5	750/90	Pr	-5.53518e+05 + 6.83353e-11i	-0.00000e+00 - 0.00000e+00i	±∞	±∞	±∞	±∞	±∞	±∞
1,5	1000/20	Pr	8.99024e+03 - 0.00000e+00i	-0.00000e+00 - 0.00000e+00i	-1.43980e+02 - 0.00000e+00i	-6.21405e+01 - 0.00000e+00i	-3.95871e-08 - 0.00000e+00i	-8.40079e-51 - 0.00000e+00i	-3.18469e-138 - 1.94585e-154i*	±∞
1,5	1000/15	Pr	8.68357e+03 + 2.32937e+03i	-0.00000e+00 - 0.00000e+00i	-1.41330e+02 - 3.16360e+01i	-8.13582e+01 + 1.17030e+01i	-5.13423e-08 + 1.05514e-07i	-6.30394e-49 + 5.05319e-49i	-1.39260e-133 - 2.93780e-133i*	±∞
1,5	1000/30	Pr	7.78447e+03 + 4.50000e+03i	-0.00000e+00 - 0.00000e+00i	-1.33053e+02 - 6.32484e+01i	-1.61777e+02 + 5.64437e+01i	3.01529e-07 + 2.82097e-06i	4.42584e-43 + 2.85127e-43i	5.80155e-119 + 1.47861e-118i*	-1.04794e-311 + 7.67751e-312i*
1,5	1000/45	Pr	3.53278e+03 + 3.53555e+03i	-0.00000e+00 - 0.00000e+00i	-6.60269e+01 - 5.80825e+01i	-1.74737e+01 - 9.07267e+01i	-4.61742e-06 - 1.80041e-05i	2.27517e-36 + 4.38634e-36i	4.05718e-98 + 5.52166e-98i*	-1.00600e-253 + 6.47766e-253i*
1,5	1000/60	Ob	-4.93080e+05 + 8.62025e+05i	-0.00000e+00 - 0.00000e+00i	±∞	±∞	±∞	±∞	±∞	±∞
1,5	1000/75	Pr	2.59069e+02 + 9.65926e+02i	-0.00000e+00 - 0.00000e+00i	-5.63464e+00 - 1.76283e+01i	4.77886e+01 - 1.96686e+01i	6.20522e-02 + 1.18405e-01i	7.99633e-13 + 6.81264e-13i	-1.77420e-35 - 2.83453e-35i*	-1.72062e-92 - 2.87176e-92i*
1,5	1000/90	Ob	-9.88018e+05 + 1.21730e-10i	-0.00000e+00 - 0.00000e+00i	±∞	±∞	±∞	±∞	±∞	±∞
1,5	1500/20	Pr	1.34902e+04 - 0.00000e+00i	-0.00000e+00 - 0.00000e+00i	-1.98986e+02 - 0.00000e+00i	-2.62469e+01 - 0.00000e+00i	-1.77105e-14 - 0.00000e+00i	-2.31647e-79 - 0.00000e+00i	-3.69679e-211 - 2.26036e-227i*	±∞
1,5	1500/15	Pr	1.30302e+04 + 3.49406e+03i	-0.00000e+00 - 0.00000e+00i	-1.96949e+02 - 3.93834e+01i	-1.96616e+01 + 2.92084e+01i	-4.52064e-14 - 7.78473e-14i	-1.25794e-76 + 1.78386e-76i	-3.31682e-204 - 1.14685e-203i*	±∞
1,5	1500/30	Pr	1.16816e+04 + 6.75000e+03i	-0.00000e+00 - 0.00000e+00i	-1.90014e+02 - 8.04115e+01i	2.35219e+01 + 7.88909e+01i	1.03405e-11 - 2.24459e-12i	6.89033e-69 - 1.14312e-67i	-6.82567e-182 + 1.09734e-181i*	±∞
1,5	1500/45	Pr	5.30055e+03 + 5.30330e+03i	-0.00000e+00 - 0.00000e+00i	-9.86947e+01 - 8.11980e+01i	-3.32924e+01 + 1.69438e+01i	2.60422e-10 - 2.07949e-10i	-1.98257e-56 - 2.24014e-56i	1.45417e-149 + 1.03025e-149i*	±∞
1,5	1500/60	Ob	-1.11462e+06 + 1.94256e+06i	-0.00000e+00 - 0.00000e+00i	±∞	±∞	±∞	±∞	±∞	±∞
1,5	1500/75	Pr	3.88479e+02 + 1.44889e+03i	-0.00000e+00 - 0.00000e+00i	-9.03625e+00 - 2.6610e+01i	-3.83368e+01 - 1.31323e+01i	-2.48311e-03 + 2.16232e-03i	1.82652e-20 - 4.28144e-20i	-3.54438e-54 - 4.12075e-54i*	-1.95414e-140 - 2.39484e-140i*
1,5	1500/90	Ob	2.23202e+06 + 7.24443e-10i	-0.00000e+00 - 0.00000e+00i	±∞	±∞	±∞	±∞	±∞	±∞
1,5	2500/20	Pr	2.24902e+04 - 0.00000e+00i	-0.00000e+00 - 0.00000e+00i	-2.79177e+02 - 0.00000e+00i	-1.190957e+00 - 0.00000e+00i	-1.37070e-27 - 0.00000e+00i	-5.73263e-137 - 4.60299e-153i*	±∞	±∞
1,5	2500/15	Pr	2.17236e+04 + 5.82343e+03i	-0.00000e+00 - 0.00000e+00i	-2.81095e+02 - 4.17083e+01i	1.16748e+01 + 1.14206e+01i	-1.27741e-26 + 1.60741e-26i	3.35632e-132 - 6.22269e-132i*	±∞	±∞
1,5	2500/30	Pr	1.94758e+04 + 1.12500e+04i	-0.00000e+00 - 0.00000e+00i	-2.84923e+02 - 9.02345e+01i	-1.11070e+00 - 5.85428e+00i	-5.28666e-23 + 2.23078e-23i	1.89380e-117 + 1.33439e-117i*	-2.55799e-308 + 1.96760e-308i*	±∞
1,5	2500/45	Pr	8.83608e+03 + 8.83883e+03i	-0.00000e+00 - 0.00000e+00i	-1.62580e+02 - 1.16381e+02i	1.87503e+00 - 2.51807e+00i	-6.84029e-20 + 1.50533e-19i	-9.59432e-97 - 2.23356e-97i*	6.20354e-253 - 1.48513e-254i*	±∞
1,5	2500/60	Ob	-3.10769e+06 + 5.40266e+06i	-0.00000e+00 - 0.00000e+00i	±∞	±∞	±∞	±∞	±∞	±∞
1,5	2500/75	Pr	6.47298e+02 + 2.41481e+03i	-0.00000e+00 - 0.00000e+00i	-1.69285e+01 - 4.21077e+01i	3.67493e+00 - 1.80869e+01i	-1.47901e-06 - 4.00997e-06i	1.42457e-35 + 7.03951e-35i*	-7.88737e-92 - 4.93805e-92i*	-1.40883e-236 - 9.63443e-237i*
1,5	2500/90	Pr	-6.22002e+06 + 7.63567e-10i	-0.00000e+00 - 0.00000e+00i	±∞	±∞	±∞	±∞	±∞	±∞
1,5	5000/20	Pr	4.49902e+04 - 0.00000e+00i	-0.00000e+00 - 0.00000e+00i	-3.40758e+02 - 0.00000e+00i	-3.58136e+05 - 0.00000e+00i	-3.74590e-61 - 0.00000e+00i	-2.67475e-281 - 1.63681e-297i*	±∞	±∞
1,5	5000/15	Pr	4.34569e+04 + 1.16469e+04i	-0.00000e+00 - 0.00000e+00i	-3.60293e+02 + 6.21147e+01i	-6.87681e-05 - 4.93207e-05i	7.19416e-59 + 4.30456e-59i			

Table D.55: (continued)

m, n	$c \setminus \arg(c)$	type	$\lambda_{mn}^{(a)'}$	$S_{mn}^{(a)'}(c, \eta=0)$	$S_{mn}^{(a)'}(c, \eta=0.01)$	$S_{mn}^{(a)'}(c, \eta=0.1)$	$S_{mn}^{(a)'}(c, \eta=0.25)$	$S_{mn}^{(a)'}(c, \eta=0.5)$	$S_{mn}^{(a)'}(c, \eta=0.75)$	$S_{mn}^{(a)'}(c, \eta=0.99)$
1.6	100/60°	Ob	-4.31525e+03 + 8.26021e+03i	1.31250e-01 + 8.88178e-16i	1.56730e-01 - 5.80900e-00i	7.24577e-03 + 2.43437e+04i	6.10589e+09 + 3.75784e+08i	5.21787e+18 + 6.21086e+17i	3.01504e+27 + 4.74365e+26i	-1.64035e+33 - 2.56095e+34i
1.6	100/75°	Ob	-7.51941e+03 + 4.68934e+03i	1.31250e-01 - 5.21805e-15i	1.82495e-01 - 3.47610e-00i	-4.78121e-04 - 2.93825e+04i	4.31029e-10 - 8.46510e+09i	2.29327e+20 - 9.50932e+19i	5.67909e+29 - 4.03146e+29i	1.79913e+36 + 1.67669e+36i
1.6	100/90°	Ob	-8.81828e+03 + 1.15115e-12i	1.31250e-01 - 3.50469e-16i	1.93524e-01 - 1.38829e-15i	7.88758e-04 - 5.04479e-11i	1.02864e+11 - 1.60373e-04i	1.36026e+21 - 4.20690e+06i	8.88925e+30 - 4.11782e+16i	5.00595e+37 - 2.87769e+23i
1.6	250/20°	Pr	2.73518e+03 - 0.00000e+00i	1.31250e-01 - 0.00000e+00i	1.13743e-01 - 0.00000e+00i	3.68892e+00 - 0.00000e+00i	-2.35754e+00 - 0.00000e+00i	-3.69747e-09 - 0.00000e+00i	-8.06398e-30 - 0.00000e+00i	-1.89284e-83 - 1.12440e-99i*
1.6	250/15°	Pr	2.64448e+03 + 7.11771e+02i	1.31250e-01 - 0.00000e+00i	1.14301e-01 - 4.45889e-01i	4.14396e+00 + 7.60401e+00i	-1.81562e+00 + 2.97573e+00i	-2.18778e-10 + 1.16556e-08i	9.41428e-29 + 1.16974e-28i*	6.72756e-81 - 3.30743e-80i*
1.6	250/30°	Ob	3.17480e+04 + 5.32606e+04i	1.31250e-01 - 8.88178e-16i	-1.36455e-01 - 1.70142e+01i	-1.36489e-06 + 4.83550e+01i	-1.14047e+14 + 9.97746e+13i	4.57391e+26 - 3.48192e+27i	4.09524e+40 + 6.08698e+40i	7.30957e+52 - 9.33234e+52i
1.6	250/45°	Pr	1.23168e+01 + 1.23745e+03i	1.31250e-01 - 0.00000e+00i	1.23186e-01 - 7.93563e-01i	-1.98294e+01 + 1.42741e+01i	-5.61517e+00 + 4.30317e+00i	-2.64636e-06 + 1.71407e-07i	-8.07033e-22 - 6.28984e-21i*	1.33947e-58 + 8.30474e-59i*
1.6	250/60°	Ob	-2.95260e+04 + 5.31266e+04i	1.31250e-01 - 1.99840e-15i	1.75701e-01 - 5.14015e+01i	1.11244e+10 + 7.32076e+08i	7.70873e+23 + 1.27587e+23i	8.15553e+46 + 2.76048e+46i	5.79151e+69 + 3.02743e+69i	5.06033e+89 + 4.47553e+89i
1.6	250/75°	Ob	-5.12469e+04 + 3.04735e+04i	1.31250e-01 - 4.44089e-15i	5.56463e-01 - 4.13001e+01i	1.08653e+11 - 2.06921e+10i	-2.13828e+26 + 1.08814e+26i	4.39601e+51 - 6.06139e+51i	-1.78076e+76 + 1.20680e+77i	-9.18326e+97 + 1.08286e+98i
1.6	250/90°	Ob	-5.95181e+04 + 7.47034e-12i	1.31250e-01 + 1.55455e-15i	7.58431e-01 - 2.45344e-15i	2.59228e-11 - 3.66180e-04i	2.01749e+27 + 7.48322e+12i	5.29313e+53 - 3.98956e+39i	7.24050e+79 - 8.23047e+65i	-5.37290e+101 + 8.03101e+87i
1.6	500/20°	Pr	5.48522e+03 - 0.00000e+00i	1.31250e-01 - 0.00000e+00i	9.69598e-00 - 0.00000e+00i	1.01361e-01 - 0.00000e+00i	-1.08417e-02 - 0.00000e+00i	-9.21288e-23 - 0.00000e+00i	-1.29012e-65 - 7.86530e-82i*	-1.07646e-175 - 6.49484e-192i*
1.6	500/15°	Pr	5.29781e+03 + 1.42351e+03i	1.31250e-01 + 4.44089e-16i	9.79679e-00 - 8.50258e-01i	1.27562e-01 - 4.74608e+00i	1.88924e-02 - 1.47380e-03i	6.17112e-22 - 6.63150e-22i	-2.37613e-63 - 3.44532e-63i*	2.27268e-169 - 9.73492e-170i*
1.6	500/30°	Ob	1.25998e+03 + 2.41774e+05i	1.31250e-01 - 4.18138e-14i	-2.94380e-01 + 7.22021e+01i	3.01887e+11 + 2.44629e+11i	7.42671e+26 - 5.60836e+27i	-4.71945e+54 - 1.27047e+54i	-1.46009e+81 + 3.52118e+81i	3.77902e+105 + 6.85329e+106i
1.6	500/45°	Pr	2.46912e+03 + 2.47488e+03i	1.31250e-01 - 0.00000e+00i	1.15071e-01 - 1.55015e-00i	1.77557e+01 + 1.86106e+01i	-1.13128e-01 + 1.34268e-02i	-1.20696e-16 - 5.51604e-16i	7.50079e-47 + 2.53629e-46i*	6.49985e-124 + 3.43018e-124i*
1.6	500/60°	Ob	-1.21544e+05 + 2.14506e+05i	1.31250e-01 - 0.00000e+00i	-3.83750e-02 - 2.86544e-02i	2.79506e+19 + 3.72288e+18i	2.37801e+47 + 8.16947e+46i	7.04821e+93 + 5.48150e+93i	1.20968e+140 + 1.83386e+140i	-1.04618e+183 + 3.27141e+182i
1.6	500/75°	Ob	-2.10729e+05 + 1.23447e+05i	1.31250e-01 + 8.17124e-14i	2.11284e-02 - 7.44008e-02i	3.16680e-21 - 1.24662e+21i	2.35866e+52 - 3.21390e+52i	-6.23817e+103 - 1.97826e+104i	-5.42446e+155 - 1.81443e+155i	-5.73412e+201 + 1.11599e+201i
1.6	500/90°	Ob	-2.44018e+03 + 3.02488e-11i	1.31250e-01 + 5.53261e-17i	9.17185e-02 - 2.76921e-13i	1.86978e-22 - 5.71687e+07i	2.82034e+54 - 2.15759e+40i	1.03807e+108 - 1.58874e+94i	2.02376e+161 - 4.64659e+147i	7.42759e+208 - 2.27304e+195i
1.6	750/20°	Pr	8.23523e+03 - 0.00000e+00i	1.31250e-01 - 0.00000e+00i	8.09914e-00 - 0.00000e+00i	3.06176e-01 - 0.00000e+00i	-1.48697e-05 - 0.00000e+00i	-9.10492e-37 - 0.00000e+00i	-8.64680e-102 - 5.27936e-118i*	-2.27679e-268 - 1.38059e-284i*
1.6	750/15°	Pr	7.95412e+03 + 2.13526e+03i	1.31250e-01 + 2.22045e-16i	8.23486e-00 - 1.21499e-00i	-1.15269e-00 - 7.26318e-00i	-1.91394e-05 - 2.78661e-05i	-2.79214e-35 + 2.04851e-36i	2.47580e-98 + 4.34406e-98i*	6.60814e-259 + 4.23152e-259i*
1.6	750/30°	Ob	2.82748e+03 + 4.84541e+03i	1.31250e-01 + 3.14859e-13i	2.67562e-02 - 5.75238e-01i	-5.44332e-16 - 8.89290e-01i	1.17020e+41 + 1.75601e+41i	-2.61641e+81 + 6.27696e+81i	-1.94185e+122 + 3.81350e+121i	-2.26639e+160 + 3.12801e+160i
1.6	750/45°	Ob	3.70656e+03 + 3.71213e+03i	1.31250e-01 - 0.00000e+00i	1.06968e-01 - 2.27039e-00i	2.17136e-01 - 1.13499e-01i	-8.43679e-04 + 4.73885e-04i	6.24673e-26 - 2.25534e-26i	-3.20779e-72 - 6.23551e-72i*	3.33109e-191 - 2.18185e-189i*
1.6	750/60°	Ob	-2.76062e+05 + 4.84139e+05i	1.31250e-01 - 3.75255e-14i	-3.42479e+03 + 2.38563e+03i	6.98869e+28 + 1.40864e+28i	7.10417e+70 + 3.85481e+70i	5.03559e+140 + 7.73595e+140i	6.04335e+209 + 7.29318e+210i	1.14358e+276 - 1.08634e+276i
1.6	750/75°	Ob	-4.78464e+05 + 2.78921e+05i	1.31250e-01 - 4.82344e-09i	-3.13239e+03 - 8.06704e+03i	8.85059e+31 - 5.57560e+31i	-1.08659e+78 + 6.51347e+78i	-5.39029e+156 - 1.84637e+156i	1.23708e+234 - 2.30742e+234i	-4.58337e+305 + 5.56569e+305i
1.6	750/90°	Ob	-5.53518e+05 + 6.83353e-11i	-0.00000e+00 - 0.00000e+00i	$\pm \infty$	$\pm \infty$	$\pm \infty$	$\pm \infty$	$\pm \infty$	$\pm \infty$
1.6	1000/20°	Pr	1.09852e+04 - 0.00000e+00i	1.31250e-01 - 0.00000e+00i	6.58117e-00 - 0.00000e+00i	-4.36254e+00 - 0.00000e+00i	-1.33682e-08 - 0.00000e+00i	-6.22676e-51 - 0.00000e+00i	-3.99598e-138 - 2.44154e-154i*	± 0
1.6	1000/15°	Pr	1.06104e+04 + 2.84701e+03i	1.31250e-01 - 0.00000e+00i	6.74243e-00 - 1.54190e-00i	-7.07023e-00 - 1.44686e-00i	-1.78893e-08 + 3.54559e-08i	4.66259e-49 + 3.76203e-49i	-1.75167e-133 + 3.70061e-133i*	± 0
1.6	1000/30°	Ob	5.01998e+05 + 8.62561e+05i	1.31250e-01 + 9.50351e-14i	-6.89067e-02 - 6.60822e-02i	5.79820e+21 + 2.73710e+22i	-7.59937e+54 - 2.04998e+54i	8.17884e+108 + 4.75698e+108i	-7.23312e-162 + 7.29286e+162i	-2.09363e+214 - 5.25411e+213i
1.6	1000/45°	Pr	4.94400e+03 + 4.94975e+03i	1.31250e-01 + 8.88178e-16i	9.88830e-00 - 2.95494e-00i	3.19385e-01 - 1.91513e+01i	-2.53549e-06 - 5.86038e-06i	2.79781e-36 + 5.47015e-36i	8.50676e-98 + 1.16255e-97i*	-4.29013e-253 + 2.61095e-253i*
1.6	1000/60°	Ob	-4.93080e+05 + 8.62025e+05i	-0.00000e+00 - 0.00000e+00i	$\pm \infty$	$\pm \infty$	$\pm \infty$	$\pm \infty$	$\pm \infty$	$\pm \infty$
1.6	1000/75°	Ob	-8.54452e+05 + 4.96894e+05i	-0.00000e+00 - 0.00000e+00i	$\pm \infty$	$\pm \infty$	$\pm \infty$	$\pm \infty$	$\pm \infty$	$\pm \infty$
1.6	1000/90°	Ob	-9.88018e+05 + 1.21730e-10i	-0.00000e+00 - 0.00000e+00i	$\pm \infty$	$\pm \infty$	$\pm \infty$	$\pm \infty$	$\pm \infty$	$\pm \infty$
1.6	1500/20°	Pr	1.64852e+04 - 0.00000e+00i	1.31250e-01 - 0.00000e+00i	3.77180e-00 - 0.00000e+00i	-2.71761e+00 - 0.00000e+00i	-6.09038e-15 - 0.00000e+00i	-1.72404e-79 - 0.00000e+00i	-4.61630e-211 - 2.82258e-227i*	± 0
1.6	1500/15°	Pr	1.59230e+04 + 4.27052e+03i	1.31250e-01 - 0.00000e+00i	3.95879e-00 - 2.08916e+00i	-2.46156e+00 + 2.86749e+00i	-1.53213e-14 - 2.69471e-14i	-9.39280e-77 + 1.32605e-76i	-4.18926e-204 - 1.45313e-203i*	± 0
1.6	1500/30°	Ob	1.12800e+06 + 1.94336e+06i	-0.00000e+00 - 0.00000e+00i	$\pm \infty$	$\pm \infty$	$\pm \infty$	$\pm \infty$	$\pm \infty$	± 0
1.6	1500/45°	Ob	7.41887e+03 + 7.42462e+03i	1.31250e-01 - 0.00000e+00i	8.27909e-00 - 4.21945e+00i	-7.51397e+00 + 2.72976e+00i	1.53946e-10 - 1.19012e-10i	-2.45921e-56 - 2.79999e-56i	3.05719e-149 + 2.17096e-149i*	± 0
1.6	1500/60°	Ob	-1.11462e+06 + 1.94256e+06i	-0.00000e+00 - 0.00000e+00i	$\pm \infty$	$\pm \infty$	$\pm \infty$	$\pm \infty$	$\pm \infty$	± 0
1.6	1500/75°	Ob	-1.93119e+06 + 1.12034e+06i	-0.00000e+00 - 0.00000e+00i	$\pm \infty$	$\pm \infty$	$\pm \infty$	$\pm \infty$	$\pm \infty$	± 0
1.6	1500/90°	Ob	-2.23202e+06 + 2.74443e-10i	-0.00000e+00 - 0.00000e+00i	$\pm \infty$	$\pm \infty$	$\pm \infty$	$\pm \infty$	$\pm \infty$	± 0
1.6	2500/20°	Pr	2.74852e+04 - 0.00000e+00i	1.31250e-01 - 0.00000e+00i	-1.00748e-00 - 0.00000e+00i	-1.26944e-01 - 0.00000e+00i	-4.77945e-28 - 0.00000e+00i	-5.61115e-137 - 3.43168e-153i*	± 0	± 0
1.6	2500/15°	Pr	2.65482e+04 + 7.11753e+03i	1.31250e-01 - 0.00000e+00i	-8.52890e-01 - 2.80309e+00i	1.35821e-01 + 1.46057e-01i	-4.48686e-27 + 5.58542e-27i	2.39985e-132 - 4.45906e-132i*	± 0	± 0
1.6	2500/30°	Ob	3.13000e+06 + 5.40400e+06i	-0.00000e+00 - 0.00000e+00i	$\pm \infty$	$\pm \infty$	$\pm \infty$	$\pm \infty$	$\pm \infty$	± 0
1.6	2500/45°	Pr	1.23686e+04 + 1.23744e+04i	1.31250e-01 - 1.77636e-15i	5.10655e+00 - 6.34783e-00i	4.50847e-01 - 5.28533e-01i	-4.09989e-20 + 8.80474e-20i	-7.42276e-97 - 2.80307e-97i*	1.30606e-253 - 3.05082e-254i*	± 0
1.6	2500/60°	Ob	-3.10769e+06 + 5.40266e+06i	-0.00000e+00 - 0.00000e+00i	$\pm \infty$	$\pm \infty$	$\pm \infty$	$\pm \infty$	$\pm \infty$	± 0
1.6	2500/75°	Ob	-5.38370e+06 + 3.11724e+06i	-0.00000e+00 - 0.00000e+00i	$\pm \infty$	$\pm \infty$	$\pm \infty$	$\pm \infty$	$\pm \infty$	± 0
1.6	2500/90°	Ob	-6.22002e+06 + 7.63567e-10i	-0.00000e+00 - 0.00000e+00i	$\pm \infty$	$\pm \infty$	$\pm \infty$	$\pm \infty$	$\pm \infty$	± 0
1.6	5000/20°	Pr	5.49852e+04 - 0.00000e+00i	1.31250e-01 - 0.00000e+00i	-8.85653e-00 - 0.00000e+00i	-4.70471e-06 - 0.00000e+00i	-1.31931e-61 - 0.00000e+00i	-1.96319e-281 - 1.20136e-297i*	± 0	± 0
1.6	5000/15°	Pr	5.31112e+04 + 1.42350e+04i	1.31250e-01 - 4.44089e-16i	-9.08050e-00 - 2.89744e-00i	-8.93746e-06 - 6.66771e-06i	2.53078e-59 + 1.52306e-59i	1.56057e-271 + 3.14947e-272i*	± 0	± 0
1.6	5000/30°	Ob	1.25100e+07 + 2.16333e+07i	-0.00000e+00 - 0.00000e+00i	$\pm \infty$	$\pm \infty$	$\pm \infty$	$\pm \infty$	$\pm \infty$	± 0
1.6	5000/45°	Pr	2.47430e+04 + 2.47487e+04i	1.31250e-01 - 8.88178e-16i	-2.38368e-00 - 9.56416e-00i	-3.90250e-04 + 1.54028e-04i	-1.22212e-43 + 1.09575e-43i	3.44434e-199 - 3.97904e-199i*	± 0	± 0
1.6	5000/60°	Ob	-1.24654e+07 + 2.16306e+07i	-0.00000e+00 - 0.00000e+00i	$\pm \infty$	$\pm \infty$	$\pm \infty$	$\pm \infty$	$\pm \infty$	± 0
1.6	5000/75°	Ob	-2.15927e+07 +							

Publications

Several parts of this thesis are either published, submitted for publication, or being prepared for publication. The following table summarizes the status of these publications.

Chapter 2	B. E. Barrowes, C. O. Ao, F. L. Teixeira, J. A. Kong, and L. Tsang, "Monte Carlo simulation of electromagnetic wave propagation in dense random media with dielectric spheroids," <i>IEICE Trans. on Electronics</i> , vol. E83-C, no. 12, pp. 1797–1802, December 2000.
Chapter 3	B. E. Barrowes, C. O. Ao, F. L. Teixeira, and J. A. Kong, "Sparse matrix/canonical grid method applied to 3-D dense medium simulations," <i>IEEE Trans. on Antennas and Propagation</i> , vol. 51, no. 1, pp. 48–58, Jan. 2003.
Chapter 4	B. E. Barrowes, K. O'Neill, T. M. Grzegorzcyk, and J. A. Kong, "Asymptotic expansions of the prolate angular spheroidal wave function for complex size parameter," <i>Studies in Applied Mathematics</i> , Oct. 2003, submitted for publication.
Chapter 5	B. E. Barrowes, K. O'Neill, T. M. Grzegorzcyk, X. Chen, and J. A. Kong, "Broadband electromagnetic induction solution for a conducting and permeable spheroid," <i>IEEE Trans. on Geoscience and Remote Sensing</i> , Jan. 2004, submitted for publication.
Chapter 6	B. E. Barrowes, K. O'Neill, T. M. Grzegorzcyk, and J. A. Kong, "Simultaneous analytical solution for the broadband magnetoquasistatic electromagnetic induction (emi) response from multiple conducting and permeable spheroids," <i>IEEE Trans. on Geoscience and Remote Sensing</i> , Feb. 2004, submitted for publication.
Appendix A	B. E. Barrowes, F. L. Teixeira, and J. A. Kong, "Fast algorithm for matrix-vector multiply of asymmetric multilevel block-toeplitz matrices in 3-D scattering," <i>Microwave Opt. Technol. Lett.</i> , vol. 31, no. 1, pp. 28–32, Oct. 2001.
Appendix B	B. E. Barrowes, C. O. Ao, J. A. Kong, and K. O'Neill, "Electromagnetic induction (EMI) response from conducting and permeable spheroidal shells," in <i>Progress In Electromagnetics Research Symposium</i> , J. A. Kong, Ed., 2002, p. 227.

Bibliography

- [1] A. Shivola and J. A. Kong, “Effective permittivity of dielectric mixtures,” *IEEE Trans. on Geoscience and Remote Sensing*, vol. 26, pp. 420–429, July 1988. [15](#), [44](#), [45](#)
- [2] D. B. Hodge, “Eigenvalues and eigenfunctions of the spheroidal wave equation,” *Journal of Mathematical Physics*, vol. 11, no. 8, pp. 2308–12, Aug. 1970. [16](#), [17](#), [80](#), [91](#), [92](#), [96](#), [97](#)
- [3] J. W. Miles, “Asymptotic approximations for prolate spheroidal wave functions,” *Studies in Applied Mathematics*, vol. 54, no. 4, pp. 315–49, Dec. 1975. [17](#), [76](#), [77](#), [105](#), [106](#), [120](#), [240](#)
- [4] C. D. Moss, K. O’Neill, T. M. Grzegorzcyk, and J. A. Kong, “A hybrid time domain model of electromagnetic induction from conducting, permeable targets,” *IEEE Trans. on Geoscience and Remote Sensing*, to be submitted. [18](#), [19](#), [112](#), [121](#), [122](#), [123](#), [124](#)
- [5] L. Geophex. (2004) Gem-3. [Online]. Available: <http://www.geophex.com/> [19](#), [126](#)
- [6] Kevin O’Neill is an Adjunct Professor at Dartmouth College and also works for the U.S. army Cold Regions Research Laboratory, Hanover, NH. Measurements were taken in October, 2003. [19](#), [126](#), [127](#)
- [7] K. Sun, K. O’Neill, I. Shamatava, and F. Shubitidze, “Application of prolate spheroid solutions in simulation of emi scattering with realistic sensors and objects.” ACES conference, Mar. 2003, pp. 531–537. [19](#), [120](#), [126](#), [128](#), [129](#), [130](#), [157](#)
- [8] L. Tsang, J. A. Kong, and R. Shin, *Theory of microwave remote sensing*. New York: Wiley, 1985. [38](#)
- [9] A. Ishimaru and Y. Kuga, “Attenuation constant of a coherent field in a dense distribution of particles,” *J. Opt. Soc. Am. A*, vol. 72, pp. 1317–1320, 1982. [38](#)
- [10] G. Koh, “Experimental study of electromagnetic wave propagation in dense random media,” *Waves in Random Media*, vol. 2, pp. 1317–1320, 1992. [38](#)
- [11] A. Ishimaru, *Wave Propagation and Scattering in Random Media*. Academic, New York, 1978, vol. 1 and 2. [38](#), [50](#)

- [12] L. Tsang and J. A. Kong, "Multiple scattering of electromagnetic waves by random distributions of discrete scatterers with coherent potential and quantum mechanical formulation," *Journal of Applied Physics*, vol. 51, no. 7, pp. 3465–3485, July 1980. [38](#), [49](#)
- [13] —, "Effective propagation constants for coherent electromagnetic wave propagation in media embedded with dielectric scatterers," *Journal of Applied Physics*, vol. 53, no. 11, pp. 7162–7173, November 1982. [38](#), [49](#)
- [14] Y. Nanbu and M. Tateiba, "A comparative study of the effective dielectric constant of a medium containing randomly distributed dielectric spheres embedded in a homogeneous background medium," *Waves in Random Media*, vol. 6, no. 4, pp. 347–360, 1996. [38](#)
- [15] C. E. Mandt, Y. Kuga, L. Tsang, and A. Ishimaru, "Microwave propagation and scattering in a dense distribution of nontenuous spheres," *Waves in Random Media*, vol. 2, pp. 225–234, 1992. [38](#)
- [16] L. Tsang, K. H. Ding, S. E. Shih, and J. A. Kong, "Scattering of electromagnetic waves from dense distributions of spheroidal particles based on Monte Carlo simulations," *Journal of the Optical Society of America A*, vol. 15, no. 10, pp. 2660–2669, October 1998. [38](#), [39](#), [40](#), [41](#), [50](#), [53](#), [55](#), [57](#), [67](#), [165](#), [175](#)
- [17] V. V. Varandan, V. K. Varandan, Y. Ma, and W. A. Steele, "Effects of nonspherical statistics on electromagnetic wave propagation in discrete random media," *Radio Science*, vol. 22, no. 4, pp. 491–498, Jul-Aug 1987. [38](#)
- [18] R. F. Harrington, *Field Computation by Moment Methods*. New York: Macmillan, 1968. [38](#), [50](#)
- [19] C. C. Lu, W. C. Chew, and L. Tsang, "The application of recursive aggregate T-matrix algorithm in the Monte Carlo simulations of the extinction rate of random distribution of particles," *Radio Sci.*, vol. 30, no. 1, pp. 25–28, 1995. [38](#)
- [20] K. Sarabandi and P. R. Siqueira, "Numerical scattering analysis for two-dimensional random media: characterization of effective permittivity," *IEEE Trans. on Antennas and Propagation*, vol. 45, pp. 858–866, May 1997. [38](#), [42](#), [43](#)
- [21] L. M. Zurk, L. Tsang, and D. P. Winbrenner, "Scattering properties of dense media from Monte Carlo simulations with application to active remote sensing of snow," *Radio Sci.*, vol. 31, no. 4, pp. 803–819, August 1996. [38](#), [42](#), [43](#), [45](#), [175](#)
- [22] L. Tsang, C. E. Mandt, and D. H. Ding, "Monte Carlo simulations of the extinction rate of dense media with randomly distributed dielectric spheres based on solution of Maxwell's equations," *Optics Letters*, vol. 5, no. 17, pp. 314–316, 1992. [38](#)
- [23] L. M. Zurk, L. Tsang, K. H. Ding, and D. P. Winbrenner, "Monte Carlo simulations of the extinction rate of densely packed spheres with clustered and nonclustered geometries," *Journal of the Optical Society of America A*, vol. 12, no. 8, pp. 1772–1781, Aug. 1995. [39](#)

- [24] K. H. Ding, C. E. Mandt, L. Tsang, and J. A. Kong, "Monte Carlo simulations of pair distribution functions of dense discrete random media with multiple sizes of particles," *J. Electromagnetic Waves and Applications*, vol. 6, no. 8, pp. 1015–1030, 1992. 39
- [25] P. R. Siqueira and K. Sarabandi, "Determination of effective permittivity for three-dimensional random media," *Proceedings of the 1996 IEEE National Radar Conference*, pp. 172–177, 1996. 42
- [26] W. J. Wiscombe, "Improved Mie scattering algorithms," *Applied Optics*, vol. 19, no. 9, pp. 1505–1509, May 1980. 42
- [27] J. C. Lagarias, J. A. Reeds, M. H. Wright, and P. E. Wright, "Convergence properties of the nelder–mead simplex method in low dimensions," *SIAM Journal on Optimization*, vol. 9, no. 1, pp. 112–147, 1998. 42, 89
- [28] E. M. Lifshitz, L. P. Pitaevskii, and L. D. Landau, *Electrodynamics of Continuous Media*, 2nd ed. Oxford: Pergamon, 1984. 45
- [29] L. Tsang, J. A. Kong, K. H. Ding, and C. O. Ao, *Scattering of Electromagnetic Waves: Numerical Simulations*. Wiley-Interscience, 2000. 50, 52
- [30] K. S. Yee, "Numerical solution of initial boundary value problems involving Maxwell's equations in isotropic media," *IEEE Trans. on Antennas and Propagation*, vol. 14, no. 3, pp. 302–307, Mar. 1966. 50
- [31] A. Taflove, *Computational Electrodynamics: The Finite-Difference Time-Domain Method*. Boston: Artech House, 1995. 50
- [32] C. H. Chan, L. Li, and L. Tsang, "A banded matrix iterative approach to Monte Carlo simulations of large-scale random rough surface scattering: penetrable case," *9th Annual Review of Progress in Applied Computational Electromagnetics. Conference Proceedings. Appl. Comput. Electromagnetics Soc*, pp. 391–397, March 1993, monterey, CA. 50
- [33] V. Jandhyala, E. Michielssen, S. Balasubramaniam, and W. C. Chew, "A combined steepest descent-fast multipole algorithm for the fast analysis of three-dimensional scattering by rough surfaces," *IEEE Trans. on Geoscience and Remote Sensing*, vol. 36, no. 3, pp. 728–748, May 1998. 50
- [34] L. Tsang, C. H. Chan, K. Pak, and H. Sangani, "A BMIA/FFT algorithm for the Monte Carlo simulations of large scale random rough surface scattering: application to grazing incidence," *IEEE Antennas and Propagation Society International Symposium 1994*, vol. 3, pp. 2028–2031, June 1994. 50
- [35] L. Li, C. H. Chan, and L. Tsang, "Monte Carlo simulations of wave scattering from lossy dielectric random rough surfaces using the physics-based two-grid method and the canonical-grid method," *IEEE Trans. on Antennas and Propagation*, vol. 47, no. 4, pp. 752–763, April 1999. 50

- [36] K. Pak, L. Tsang, and J. Johnson, "Numerical simulations and backscattering enhancement of electromagnetic waves from two-dimensional dielectric random rough surfaces with the sparse-matrix canonical grid method," *Journal of the Optical Society of America A*, vol. 14, no. 7, pp. 1515–1529, July 1997. [50](#)
- [37] S. Koc and W. C. Chew, "Multilevel FMA for the discrete dipole approximation," *IEEE Antennas and Propagation Society International Symposium*, vol. 1, pp. 640–643, 1999. [50](#)
- [38] W. C. Chew, J. M. Jin, C. C. Lu, E. Michielssen, and J. M. Song, "Fast solution methods in electromagnetics," *IEEE Trans. on Antennas and Propagation*, vol. 45, no. 3, pp. 533–543, March 1997. [50](#)
- [39] C. H. Chan and L. Tsang, "A sparse-matrix canonical-grid method for scattering by many scatterers," *Microwave Opt. Technol. Lett.*, vol. 8, no. 2, pp. 114–118, February 1995. [50](#)
- [40] J. T. Johnson, "On the canonical grid method for two-dimensional scattering problems," *IEEE Trans. on Antennas and Propagation*, vol. 46, no. 3, pp. 297–302, March 1998. [50](#)
- [41] S. Q. Li, Y. X. Yu, K. F. Chan, C. H. Chan, and L. Tsang, "A sparse-matrix/canonical grid method for analyzing densely packed interconnects," *IEEE Antennas and Propagation Society International Symposium*, vol. 1, pp. 128–131, 2000. [50](#)
- [42] S. Q. Li, C. H. Chan, M. Y. Xia, and L. Tsang, "Multilevel expansion of the sparse-matrix canonical grid method for two-dimensional random rough surfaces," *Proc. IEEE Int. Geosci. Remote Sensing Symp. (IGARSS)*, vol. 7, pp. 3111–3113, July 2000. [50](#), [166](#)
- [43] L. Tsang, J. A. Kong, and K. H. Ding, *Scattering of Electromagnetic Waves: Theories and Applications*. Wiley-Interscience, 2000. [51](#), [122](#), [151](#), [173](#)
- [44] W. C. Chew, *Waves and Fields in Inhomogeneous Media*, ser. Electromagnetic Waves, D. G. Dudley, Ed. IEEE Press, 1995. [52](#), [181](#)
- [45] J. van Bladel, "Some remarks on Green's dyadic for infinite space," *IEEE Trans. on Antennas and Propagation*, vol. 9, pp. 563–566, 1961. [52](#)
- [46] T. M. Cover and J. M. Thomas, *Elements of Information Theory*. New York: Wiley, 1990. [67](#)
- [47] E. M. Purcell and C. R. Pennypacker, "Scattering and absorption of light by non-spherical dielectric grains," *Astrophysics Journal*, vol. 186, pp. 705–714, 1973. [70](#), [165](#)
- [48] G. H. Goedecke and S. G. O'Brien, "Scattering by irregular inhomogeneous particles via the digitized Green's function algorithm," *Applied Optics*, vol. 27, no. 12, pp. 2431–2438, June 1988. [70](#), [165](#), [173](#)

- [49] S. Asano and G. Yamamoto, "Light scattering by a spheroidal particle," *Appl. Opt.*, vol. 14, pp. 29–49, Jan. 1975. [75](#), [77](#), [182](#)
- [50] N. V. Voshchinnikov and V. G. Farafonov, "Optical properties of spheroidal particles," *Astrophys. Space Sci.*, vol. 204, pp. 19–86, June 1993. [75](#), [181](#)
- [51] M. I. Mishchenko, J. W. Hovenier, and L. D. Travis, Eds., *Light scattering by non-spherical particles: theory, measurements, and applications*. Academic Press, 2000. [75](#)
- [52] B. D. B. Figueiredo, "On some solutions to generalized spheroidal wave equations and applications," *Journal of Physics A*, vol. 35, no. 12, pp. 2877–906, March 2002. [75](#)
- [53] R. Chapman, "Digital filtering and higher order statistics," *IEE-Colloquium-on-Digital-Filters*, pp. 4/1–4/6, April 1998. [75](#)
- [54] C. L. Fancourt and J. C. Principe, "On the relationship between the Karhunen-Loeve transform and the prolate spheroidal wave functions," ser. Proceedings IEEE ICASSP, vol. 1, 2000, pp. 261–4. [75](#)
- [55] F. Grunbaum and L. Miranian, "The magic of the prolate spheroidal functions in various setups," *Proc. SPIE*, pp. 151–62, 2001. [75](#)
- [56] B. Larsson, T. Levitina, and E. J. Brandas, "On prolate spheroidal wave functions for signal processing," *International Journal of Quantum Chemistry*, vol. 85, no. 4-5, pp. 392–7, 2001. [75](#)
- [57] L. J. Chu and J. A. Stratton, "Forced oscillations of a prolate spheroid," *Journal of Applied Physics*, vol. 12, pp. 241–248, 1941. [75](#)
- [58] M. F. R. Cooray, I. R. Ciric, and B. P. Sinha, "Electromagnetic scattering by a system of two parallel dielectric prolate spheroids," *Canadian Journal of Physics*, vol. 68, no. 4-5, pp. 376–84, 1990. [75](#)
- [59] M. F. R. Cooray and I. R. Ciric, "Scattering by systems of spheroids in arbitrary configurations," *Comp. Phys. Comm.*, vol. 68, pp. 279–305, 1991. [75](#), [182](#)
- [60] R. S. Chen, E. K. N. Yung, D. G. Fang, and Z. M. Xie, "An efficient analysis of radiation from slotted coaxial cable using the spheroidal wave function," *Microwave Opt. Technol. Lett.*, vol. 21, no. 5, pp. 372–7, 1999. [75](#)
- [61] L. W. Li, M. S. Leong, P. S. Kooi, and T. S. Yeo, "Spheroidal vector wave eigenfunction expansion of dyadic Green's functions for a dielectric spheroid," *IEEE Trans. on Antennas and Propagation*, vol. 49, no. 4, pp. 645–59, April 2001. [75](#)
- [62] H. Braunisch, C. O. Ao, K. O'Neill, and J. A. Kong, "Magnetoquasistatic response of conducting and permeable spheroid under axial excitation," *IEEE Trans. on Geoscience and Remote Sensing*, vol. 39, no. 12, pp. 2689–2701, December 2001. [75](#), [110](#), [112](#)

- [63] C. O. Ao, H. Braunisch, K. O'Neill, , and J. A. Kong, "Quasi-magnetostatic solution for a conducting and permeable spheroid with arbitrary excitation," *IEEE Trans. on Geoscience and Remote Sensing*, vol. 40, no. 4, pp. 887–97, April 2002. [75](#), [77](#), [110](#), [112](#), [113](#), [115](#), [116](#), [120](#), [140](#), [147](#), [150](#), [154](#), [155](#), [157](#)
- [64] J. A. Stratton, P. M. Morse, L. J. Chu, J. D. C. Little, and F. J. Corbato, *Spheroidal Wave Functions*. New York: John Wiley and Sons, 1956. [75](#), [81](#), [96](#)
- [65] J. Meixner and F. W. Schäfke, *Mathieusche Funktionen und Sphäroidfunktionen*. Berlin: Springer-Verlag, 1954. [75](#), [76](#)
- [66] C. Flammer, *Spheroidal Wave Functions*. Stanford: Stanford University Press, 1957. [75](#), [76](#), [79](#), [80](#), [81](#), [82](#), [96](#), [104](#), [114](#), [115](#), [116](#), [119](#), [120](#), [151](#), [180](#), [181](#), [182](#), [186](#), [197](#)
- [67] *Tables of angular spheroidal wave functions*. Washington: Naval Research Laboratory, 1975. [75](#), [81](#)
- [68] D. Slepian, "Some asymptotic expansions for prolate spheroidal functions," *Journal of Math. and Physics*, vol. 44, pp. 99–140, 1965. [76](#), [77](#), [82](#), [101](#)
- [69] J. W. Miles, "Asymptotic approximations for oblate spheroidal wave functions," *Phillips Research Reports*, vol. 30, pp. 140–160, 1975. [76](#)
- [70] W. Streifer, "Uniform asymptotic expansions for prolate spheroidal wave functions," *Journal of Math. and Physics*, vol. 47, pp. 407–415, 1968. [76](#), [82](#)
- [71] J. des Cloizeaux and M. L. Mehta, "Some asymptotic expressions for prolate spheroidal functions and for the eigenvalues of differential and integral equations of which they are solutions," *Journal of Mathematical Physics*, vol. 13, pp. 1745–1754, 1972. [76](#)
- [72] M. L. Sink and B. C. Eu, "A uniform WKB approximation for spheroidal wave functions," *Journal of Chemical Physics*, vol. 78, no. 8, pp. 4887–95, Apr. 1983. [76](#)
- [73] S. G. Volotovskii, N. L. Kazanskii, and S. N. Khonina, "Analysis and development of the methods for calculating eigenvalues of prolate spheroidal wave functions of zero order," *Pattern Recognition and Image Analysis*, vol. 11, no. 3, pp. 633–48, 2001. [76](#)
- [74] L. G. Guimaraes, "Explicit asymptotic formulae for the spheroidal angular eigenvalues," *Journal of Physics A*, vol. 28, no. 8, pp. L233–L237, 1995. [76](#)
- [75] P. C. G. de Moraes and L. G. Guimaraes, "Uniform asymptotic formulae for the spheroidal angular function," *Journal of Quantitative Spectroscopy and Radiative Transfer*, vol. 74, no. 6, pp. 757–65, Sep. 2002. [76](#)
- [76] T. Do-Nhat, "Asymptotic expansion of the Mathieu and prolate spheroidal eigenvalues for large parameter c ," *Canadian Journal of Physics*, vol. 77, no. 8, pp. 635–652, aug 1999. [76](#), [81](#), [82](#), [116](#), [119](#)

- [77] ———, “Asymptotic expansions of the oblate spheroidal eigenvalues and wave functions for large parameter c ,” *Canadian Journal of Physics*, vol. 79, no. 5, pp. 813–31, May 2001. [76](#), [82](#), [83](#), [104](#), [116](#), [119](#)
- [78] S. Asano and M. Sato, “Light scattering by randomly oriented spheroidal particles,” *Applied Optics*, vol. 19, no. 6, pp. 962–74, March 1980. [77](#)
- [79] R. J. Lytle and F. V. Schultz, “Prolate spheroidal antennas in isotropic plasma media,” *IEEE Trans. on Antennas and Propagation*, vol. 17, no. 4, pp. 496–506, July 1969. [77](#)
- [80] F. W. Schäfke and H. Groh, “Zur Berechnung der Eigenwerte der Sphäroiddifferentialgleichung. (German) [On the calculation of the eigenvalues of the spheroidal differential equation],” *Numerical Mathematics*, vol. 4, pp. 310–312, 1962. [77](#)
- [81] J. Meixner, F. W. Schäfke, and W. Gerhard, *Mathieu functions and spheroidal functions and their mathematical foundations, further studies*, ser. Lecture notes in mathematics. Berlin; New York: Springer-Verlag, 1980, no. 837. [77](#)
- [82] B. G. C. Hunter, “The eigenvalues of the angular spheroidal wave-equation,” *Studies in Applied Mathematics*, vol. 66, no. 3, pp. 217–240, 1982. [77](#), [85](#), [89](#), [90](#), [116](#)
- [83] T. Oguchi, “Eigenvalues of spheroidal wave functions and their branch points for complex values of propagation constants,” *Radio Science*, vol. 5, no. 8-9, pp. 1207–14, Aug. 1970. [77](#), [85](#)
- [84] P. E. Falloon, P. C. Abbott, and J. B. Wang, “Theory and computation of spheroidal wavefunctions,” *Journal of Physics A*, vol. 36, pp. 5477–5495, 2003. [77](#), [81](#), [241](#)
- [85] L.-W. Li, M. S. Leong, T. S. Yeo, P. S. Kooi, and K. Y. Tan, “Computations of spheroidal harmonics with complex arguments: A review with an algorithm,” *Physical Review E: Statistical Physics, Plasmas, Fluids, and Related Interdisciplinary Topics*, vol. 58, no. 5, pp. 6792–806, Nov. 1998. [77](#), [80](#), [81](#)
- [86] G. Lamé, “(Liouville),” *J. Math.*, vol. 2, no. 147, 1837. [79](#)
- [87] C. Niven, “On the conduction of heat in ellipsoids of revolution,” *Philosophical Transactions of the Royal Society of London*, vol. 171, pp. 117–151, 1880. [79](#)
- [88] M. Abramowitz and I. A. Stegun, *Handbook of Mathematical Functions*, 9th ed. Dover Publications, Inc., 1970. [80](#), [82](#), [83](#), [98](#), [113](#), [119](#), [127](#), [155](#), [182](#)
- [89] C. J. Bouwkamp, “Theoretische en numerieke behandeling van de buiging door een ronde opening,” Ph.D. dissertation, University of Groningen, Groningen, Netherlands, 1941. [80](#)
- [90] J. Caldwell, “Computation of eigenvalues of spheroidal harmonics using relaxation,” *Journal of Physics A*, vol. 21, pp. 3685–93, 1988. [80](#)

- [91] W. H. Press, B. P. Flannery, S. A. Teukolsky, and W. T. Vetterling, *Numerical Recipes: The Art of Scientific Computing*, 2nd ed. Cambridge (UK) and New York: Cambridge University Press, 1992. 80
- [92] H. A. Eide, J. J. Stamnes, K. Stamnes, and F. M. Schulz, "New method for computing expansion coefficients for spheroidal functions," *Journal of Quantitative Spectroscopy and Radiative Transfer*, vol. 63, no. 2-6, pp. 191–203, Sept.–Dec. 1999. 80
- [93] E. C. N. Aquino and E. Ley-Koo, "Spheroidal functions revisited: matrix evaluation and generating functions," *Revista Mexicana de Fisica*, vol. 48, no. 3, pp. 277–282, June 2002. 80
- [94] B. E. Barrowes. (2002) MATLAB routines for computation of special functions. [Online]. Available: http://ceta.mit.edu/comp_spec_func/index.html 81
- [95] S. Zhang and J. Jin, *Computation of Special Functions*. New York: John Wiley and Sons, 1996. 81
- [96] A. Erdélyi, Ed., *Higher transcendental functions*, ser. Bateman Manuscript Project. New York: McGraw-Hill, 1953–55. 83, 119
- [97] C. M. Bender and S. A. Orszag, *Advanced mathematical methods for scientists and engineers*, ser. International series in pure and applied mathematics. New York: McGraw-Hill, 1978. 85, 95
- [98] G. Strang, *Introduction to Applied Mathematics*. Wellesley-Cambridge Press, 1986. 89
- [99] B. E. Barrowes. (2003) Center for electromagnetic theory and applications (CETA) website. [Online]. Available: <http://ceta.mit.edu/> 105
- [100] M. N. Nabighian, "Quasi-static transient response of a conducting permeable sphere in a dipolar field," *Geophysics*, vol. 35, no. 2, pp. 303–9, April 1970. 109
- [101] S. E. Hjelt, "Regional em studies in the 1980's," *Surveys in Geophysics*, vol. 9, no. 3–4, pp. 349–87, Sept.–Dec. 1987. 109
- [102] H. A. Haus and J. R. Melcher, *Electromagnetic Fields and Energy*. Englewood Cliffs, New Jersey: Prentice Hall, 1989. 109, 113
- [103] I. J. Won, D. A. Keiswetter, and T. H. Bell, "Electromagnetic induction spectroscopy for clearing landmines," *IEEE Trans. on Geoscience and Remote Sensing*, vol. 39, no. 4, pp. 703–709, April 2001. 109
- [104] D. A. Keiswetter, W. A. SanFilipo, I. J. Won, J. M. Miller, T. H. Bell, E. R. Cespedes, and K. O'Neill, "Discriminating capabilities of multifrequency EMI data," *Proceedings of the SPIE The International Society for Optical Engineering*, pp. 130–40, 2000. 109

- [105] N. Geng, P. Garber, L. Collins, L. Carin, D. Hansen, D. Keiswetter, and I. J. Won, "Wideband electromagnetic induction for metal target identification: theory, measurement, and signal processing," *Proceedings of the SPIE The International Society for Optical Engineering*, pp. 42–51, 1998. 109
- [106] K. Sun, K. O'Neill, F. Shubitidze, S. A. Haider, and K. D. Paulsen, "Simulation of electromagnetic induction scattering from targets with negligible to moderate penetration by primary fields," *IEEE Trans. on Geoscience and Remote Sensing*, vol. 40, no. 4, pp. 910–27, April 2002. 109
- [107] B. Johnson, T. G. Moore, B. J. Blejer, C. F. Lee, T. P. Opar, S. Ayasli, and C. A. Primmerman, "A research and development strategy for unexploded ordnance sensing," *Lincoln Laboratory Project Report, EMP-1*, April 1996. 109
- [108] P. Wiseman, "30-year-old bombs still very deadly in laos," *USA Today*, p. 10A, December 12 2003. 109
- [109] I. C. of the Red Cross. (2004) Raising awareness of mines and unexploded ordnance (uxo). [Online]. Available: http://www.icrc.org/Web/eng/siteeng0.nsf/htmlall/section_mine_and_uxo_awareness 109
- [110] T. S. E. Research and D. P. (SERDP). (2004) Uxo projects. [Online]. Available: <http://www.serdp.org/research/UXO.html> 109, 148
- [111] J. R. Wait, "A conducting sphere in a time varying magnetic field," *Geophysics*, vol. 16, pp. 666–672, 1951. 110, 121, 148
- [112] —, "A conducting permeable sphere in the presence of a coil carrying an oscillating current," *Can. J. Phys.*, vol. 31, pp. 670–678, 1953. 110, 148, 150
- [113] C. E. Baum, Ed., *Detection and Identification of Visually Obscured Targets*. Philadelphia, PA: Taylor & Francis, 1999. 112
- [114] I. J. Won, D. A. Keiswetter, D. Hansen, E. Novikova, and T. M. Hall, "Gem-3: a monostatic broadband electromagnetic induction sensor," *Jour. Envir. Eng. Geophysics*, vol. 2, no. 1, pp. 53–64, 1997. 112, 125, 156
- [115] B. E. Barrowes, K. O'Neill, T. M. Grzegorzcyk, and J. A. Kong, "Asymptotic expansions of the prolate angular spheroidal wave function for complex size parameter," *Studies in Applied Mathematics*, Oct. 2003, submitted for publication. 116
- [116] J. A. Stratton, *Electromagnetic Theory*. McGraw-Hill Book Company, Inc., 1941. 123
- [117] R. Harrington, *Time-Harmonic Electromagnetic Fields*. McGraw-Hill Book Company, Inc., 1961. 123
- [118] Personal communication with Geophex, December 2003. 142, 143

- [119] C. O. Ao, H. Braunisch, K. O'Neill, J. A. Kong, L. Tsang, and J. T. Johnson, "Broadband electromagnetic induction response from conducting and permeable spheroids, in detection and remediation technologies for mines and minelike targets vi," *Proc. SPIE*, vol. 4394, pp. 1304–1315., April 2001. [147](#), [148](#)
- [120] F. Shubitidze, K. O'Neill, I. Shamatava, K. Sun, and K. D. Paulsen, "Analysis of gpr scattering by multiple subsurface metallic objects to improve uxo discrimination," *Proc. IEEE Int. Geosci. Remote Sensing Symp. (IGARSS)*, vol. 7, pp. 4163–4165, 2003. [148](#)
- [121] N. Goldfine, A. Washabaugh, D. Schlicker, and I. Shay, "High-resolution inductive sensor arrays for uxo detection, identification, and clutter suppression," *Proc. SPIE*, vol. 5089, no. 2, pp. 872–883, 2003. [148](#)
- [122] K. O'Neill, K. Sun, C. Chen, F. Shubitidze, and K. Paulsen, "Combining gpr and emi data for discrimination of multiple subsurface metallic objects," *Proc. IEEE Int. Geosci. Remote Sensing Symp. (IGARSS)*, vol. 7, pp. 4157–4159, 2003. [148](#)
- [123] K. Sun, K. O'Neill, F. Shubitidze, and K. Paulsen, "Treatment of broadband and multi-object electromagnetic induction scattering using high frequency approximations," *2002 IEEE International Geoscience and Remote Sensing Symposium. 24th Canadian Symposium on Remote Sensing. Proceedings*, vol. 3, pp. 1546–9, 2002. [148](#)
- [124] J. R. Wait and K. P. Spies, "Quasi-static transient response of a conducting and permeable sphere," *Geophysics*, vol. 34, pp. 789–792, Oct. 1969. [150](#)
- [125] J. J. Goodman, B. T. Draine, and P. J. Flatau, "Application fast-Fourier-transform techniques to the discrete-dipole approximation," *Optics Letters*, vol. 16, no. 15, pp. 1198–1200, August 1991. [163](#), [166](#), [170](#), [178](#)
- [126] L. Tsang, J. A. Kong, K. H. Ding, and C. O. Au, *Scattering of Electromagnetic Waves: Numerical Simulations*. Wiley-Interscience, 2000. [163](#), [178](#)
- [127] P. J. Flatau, G. L. Stephens, and B. T. Draine, "Light scattering by rectangular solids in the discrete-dipole approximation: a new algorithm exploiting the block-Toeplitz structure," *Journal of the Optical Society of America A*, vol. 7, no. 4, pp. 593–600, April 1990. [165](#)
- [128] W. C. Chew, J. H. Lin, and X. G. Yang, "An FFT T-matrix method for 3D microwave scattering solutions from random discrete scatterers," *Microwave Opt. Technol. Lett.*, vol. 9, no. 4, pp. 194–196, July 1995. [165](#)
- [129] J. I. Hage and J. M. Greenburg, "A model for the optical properties of porous grains," *The Astrophysical Journal*, vol. 361, pp. 251–259, September 1990. [165](#), [173](#)
- [130] P. A. Voois, "A theorem on the asymptotic eigenvalue distribution of Toeplitz-block-Toeplitz matrices," *IEEE Trans. on Signal Processing*, vol. 44, no. 7, pp. 1837–41, July 1996. [165](#)

- [131] V. I. Ivakhnenko and E. E. Tyrtysnikov, “Block-Toeplitz-structure-based solution strategies for CEM problems,” in *11th Annual Review of Progress in Applied Computational Electromagnetics*, vol. 1, 1995, pp. 181–188. [165](#)
- [132] S. Labbe and P. Leca, “Fast solver for the Maxwell quasistatic equations: block-Toeplitz matrix. application to micromagnetism,” *Comptes Rendus de L’Académie des Sciences, Série i (Mathématiques)*, vol. 327, no. 4, pp. 415–420, August 1998. [165](#)
- [133] C. O. Ao, “Electromagnetic wave scattering by discrete random media with remote sensing applications,” Ph.D. dissertation, Massachusetts Institute of Technology, May 2001. [179](#), [197](#)
- [134] L. D. Landau, E. M. Lifshitz, and L. P. Pitaevskii, *Electrodynamics of Continuous Media*, 2nd ed. Oxford: Pergamon, 1984. [179](#), [183](#)

Biographical note

Benjamin Earl Barrowes was born in Baton Rouge, Louisiana on July 11, 1973. He is the son of Steven C. Barrowes, Ph.D., and Hope R. Barrowes of Salt Lake City, Utah and is the youngest of six children who are in order: Wilford, Thomas, Edward, Stephanie, Winston, and Benjamin.

Benjamin studied Electrical Engineering at Brigham Young University (BYU) from September 1991 to June 1999, receiving both a B. S. and M. S. degrees in June 1999. From September 1992 until September 1994, he served a volunteer proselyting mission for the Church of Jesus Christ of Latter-Day Saints in Tokyo, Japan. While at BYU, he interned at Seino Joho Service in Ōgaki, Gifu prefecture, Japan from June 1996 to December 1996, as well as at Hewlett Packard (now Agilent) in Santa Rosa, CA from June 1998 to August 1998. From July 1999, he has been a research assistant at the Center for Electromagnetic Theory and Application within the Research Laboratory of Electronics in the Department of Electrical Engineering and Computer Science at the Massachusetts Institute of Technology, Cambridge, Massachusetts under Professor Jin Au Kong. There, his research has focused on efficient scattering calculations for dielectric spheroidal inclusions and induction models for conducting and permeable spheroids.

Benjamin Barrowes was named Sterling Scholar (or top student) in mathematics for the State of Utah during his senior year at Cottonwood High School, 1991. Thereafter he was awarded a full tuition four year scholarship to attend Brigham Young University. From 1997-9, he was the recipient of the Rocky Mountain Space Grant Consortium (RMSGC) grant during which time he worked on radar remote sensing of the sea state under Professor David G. Long. He was also the recipient of a graduate fellowship from the National Science Foundation September 1999 through September 2002. He has been a student member of the IEEE since 1998.

Benjamin married Masako I on February 20, 1996 in South Jordan, Utah. They currently live in Cambridge, Massachusetts with their two children, Leia and Earl.